Inhibition of Glycosidases in Breast Cancer Cell Lines: Observations from 2D and 3D Cell Culture Systems

Diego Reyes Sarria

A thesis submitted in partial fulfilment of the requirements of the University of Westminster for the degree of Doctor of Philosophy

May 2026

Abstract:

Breast cancer presents a significant challenge in oncology due to its diverse nature and varying treatment responses among subtypes, particularly in triple-negative breast cancer (TNBC). A growing body of research highlights the role of glycosidases in the aberrant glycosylation associated with breast cancer progression.

This study assessed iminosugar glycosidase inhibitors for their effect on breast cancer behaviour *in vitro*. TNBC cells (MDA-MB-231 and BT-549), oestrogen receptor-positive (MCF-7) and HER2-positive cells (SKBR3) were assessed both in 2D and in 3D cell cultures.

As expected, alterations in glycosylation were observed using lectin fluorescence microscopy following treatment of the cancer cells with the inhibitor compounds 1-Deoxynojirimycin (DNJ), 255, 42, and 44, iminosugars provided in collaboration with the Phytoquest company. After glycosidase inhibitor treatment, a significant decrease in the cancer cell metabolic activity was assessed by Alamar Blue Assay. This was accompanied by a reduction in the cell count and reduced cell migration across both 2D and 3D cell culture. An additive effect was observed when doxorubicin was combined with the inhibitors in 2D. Additionally, this study assessed CIN in BC in *vitro* models using the CBMN assay. Higher rates of CIN were observed in 2D cultures compared to 3D. Given the known impact of glycosidase inhibition on oxidative stress and DNA damage, and on glycoproteins involved in cell cycle regulation, an effect of glycosidase inhibition on genomic instability could be expected. However, in this study, while treatment of the cells with glycosidase inhibitors was shown to influence cell viability and apoptosis, the effect on CIN was not statistically significant, warranting further investigation into the relationship between cytotoxicity and genomic stability. The observed differences between 2D and 3D cultures highlight the importance of incorporating extracellular matrix and biophysical cues when studying breast cancer behaviour. The observed additive effects of glycosidase inhibition alongside doxorubicin suggest this approach may enhance breast cancer responsiveness to chemotherapeutic drugs. This thesis contributes to understanding the potential role of glycosidase inhibitor compounds in modulating breast cancer behaviour. It sets the stage for future research concerned with improving breast cancer outcomes.

Dedicated

To

"God Almighty"

and my lovely family

Acknowledgments

I want to express my deepest gratitude to my supervisors, Professor Miriam Dwek and Professor Emanuela Volpi, for their huge, valuable support and guidance throughout my PhD journey. Their expertise, encouragement, and insightful feedback have been invaluable in shaping my research and academic development.

Professor Dwek's vast knowledge in the field of glycobiology and her meticulous approach to research have inspired me to strive for excellence. Her ability to foster critical thinking and innovation has greatly enriched my understanding of the subject matter.

Professor Volpi has been equally influential, providing constant support and encouragement during challenging times. Her dedication to mentoring and her keen insights into scientific inquiry have helped me navigate the complexities of my research with confidence.
I am genuinely grateful for their patience, guidance, and the countless hours they have invested in my academic growth. This thesis would not have been possible without their mentorship. Thank you for believing in me and for pushing me to reach my full potential.

List of abbreviations

αSMA	smooth muscle actin
ACM	artificial cancer mass
ADCC	antibody-dependent cell-mediated cytotoxicity
ALI	air-liquid interface culture
ALL	acute lymphoblastic leukemia
ATCC	American Type Culture Collection
ATM	ataxia telangiectasia-mutated protein
ATR	rad3-related kinases
BAF	barrier-to-autointegration factor
BC	breast cancer
BCL2	b-cell lymphoma
BLBC	basal-like breast cancer
BER	base excision repair
BM	basement membrane
BN	binucleated
BSA	bovine serum albumin
BVDV	bovine viral diarrhoea virus
CAFs	cancer-associated fibroblasts
CAM	cell adhesion molecule
CASP3	caspase-3
CAZy	carbohydrate-active enzymes
CBMN	cytokinesis-block micronucleus
CCN1	cellular communication network factor 1
cDNA	complementary DNA
CDG	congenital disorders of glycosylation
CEA	carcinoembryonic antigen
CIN	chromosomal instability
CGH	comparative genomic hybridisation
Con A	concanavalin a

CRC	colorectal cancer
CSCs	cancer stem cells
Ct	cycle threshold
Cyt-B	cytochalasin-B
ΔCt	delta Ct
DAPI	4',6-diamidino-2-phenylindole
DDR	DNA damage response
dH2O	deionised water
DNJ	deoxynojirimycin
DPX	phthalate-free
eNOS	nitric oxide synthase
EC	endothelial cells
ECM	extracellular matrix
EGFR	epidermal growth factor receptor
EHS	engelbreth-Holm-Swarm
EMT	epithelial-mesenchymal transition
ENMs	engineered nanomaterials
ER	estrogen receptor
ER	endoplasmic reticulum
ESCs	embryonic stem cells
FAP	fibroblast activating protein
FAK	focal adhesion kinase
FBS	fetal bovine serum
FISH	fluorescent *in situ* hybridisation
FGF	fibroblast growth factor
5-FU	fluorouracil
FSP-1	fibroblast-specific protein-1
IL-6	interleukin-6
ILKI	integrin-linked kinase
IGF-1	insulin-like growth factor 1
ITH	Intra-tumoral heterogeneity

GalNAc	N-acetyl galactosamine
GALNTs	GalNac transferases
GBA1	glucosylceramidase β-1
GERL	Golgi-endoplasmic reticulum-lysosome
GH	glycoside hydrolases
GlcNAc	N-acetylglucosamine
GLUTs	glucose transporters
GNTs	N-acetylglucosaminyltransferase
GTase	glycosyltransferases
GTPase	guanosine triphosphatase
HER2	human epidermal growth factor receptor 2
HDfs	human dermal fibroblasts
HR	homologous recombination repair
H&E	haematoxylin and eosin
IHC	immunohistochemistry
iPSC	induced pluripotent stem cells
KCL	potassium chloride
MCAM	melanoma cell adhesion molecule
MDC1	mediators of DNA damage checkpoint 1
MCs	mesenchymal stem cells
MGAT5	n-acetylglucosaminyltransferase
MMR	mismatch repair
MN	micronuclei
MSI	microsatellite instability
MSS	microsatellite stability
NBUD	nuclear buds
NE	nuclear envelope
NER	nucleotide excision repair
NHDF	neonatal normal human fibroblast
NHEJ	non-homologous end joining
NJ	nojirimycin

NLG	N-linked glycosylation
NN-DNJ	N-(n-Nonyl)deoxynojirimycin
NPBs	nucleoplasmic bridges
OLG	O-linked glycosylation
OT	O-GlcNAc transferase
PBS	phosphate buffer saline
PDGFR	platelet-derived growth factor receptor
PDO	patient derived organoid
PDT	Photo dynamic therapy
PDTX	patient-derived tumour xenografts
PFS	progression-free survival
P4HA1	prolyl-4 hydroxylase subunit alpha-1
PTM	post-translational modifications
PR	progesterone receptor
pRb	retinoblastoma tumour suppressor
PSA	prostate-specific antigen
qRT-PCR	real-time reverse transcriptase polymerase chain reaction
RhoA	ras homolog Family member A
ROS	reactive oxygen species
RPII	RNase polymerase II
RTK	receptor tyrosine kinases
STRs	Short-tandem repeats
SSC	saline sodium citrate
TRAIL	tumor necrosis nactor related apoptosis- inducing ligand
TBN-DNJ	2,3,4,6-tetra-O-benzyl-(+)-1-deoxynojirimycin
TGF-β	tumour growth factor β
TGF-β	transforming growth factor β
TM	tunicamycin
TME	tumor microenvironment
TNF-α	tumour necrosis factor
TNBC	triple negative breast cancer

TLS	translesion DNA synthesis
TOPB1	topoisomerase 1 binding protein
UDP	uridine diphosphate
UEA-I	*Ulex europaeus agglutinin*
UGGT	UDP-glucose glycoprotein glucosyltransferase
HIV	human immunodeficiency virus
VSMCs	vascular network smooth muscle cells
WGA	wheat germ agglutinin

Table of Contents Page numbers

Abstract: i

Acknowledgments iii

List of abbreviations iv

List of figures xv

List of tables xxx

Chapter 1 1

Introduction 1

1. 3D Models in Drug Discovery and Cancer Resistance 2

1.1. Breast Cancer 3

1.2. Breast cancer subtypes 3

1.2.1. Triple negative breast cancer 4

1.3. Hallmarks of cancer 5

1.4. The tumour microenvironment in cancer progression. 6

1.5. Epithelial-mesenchymal transition 7

1.6. Hypoxia 9

1.7. Genomic instability 9

1.7.1. DNA damage checkpoint 11

1.7.2. Increased frequencies of base pair mutations 12

1.7.3. Microsatellites instability 13

1.7.4. Chromosomal instability 13

1.7.4.1. Cytochalasin-B mechanisms of action 18

1.7.5. DNA repair pathway 20

1.7.6. Nucleotide excision repair 20

1.7.7. Base excision repair 21

1.7.8. Mismatch repair 22
1.8. Apoptosis 23
1.9. The process of metastasis 27
1.10. Glycosylation 28
1.10.1. N-linked glycosylation 32
1.10.2. O-Linked glycosylation 37
1.10.3. Glycosidases 39
1.10.4. Glycosidases in cancer. 41
1.10.5. Glycosidase inhibition. 42
1.10.6. Iminosugars 44
1.10.7. Lectins 48
1.10.8. Doxorubicin 52
1.11. 2D model systems 54
1.11.1. In-vivo models 55
1.12. 3D models in cancer research 56
1.12.1. Spheroids 56
1.12.2. Organoids 57
1.12.3. Limitations of organoids 59
1.12.4. Difference between spheroids and organoids 59
1.12.5. Tumoroids 60
1.12.6. In vitro models of breast cancer 61
1.12.7. Matrigel 63
1.12.8. ECM scaffolds 64
1.12.9. Alginate constructs 65
1.13. Chitosan constructs 65
1.13.1. RAFT 3D culture systems 65

1.14. Aims and objectives 68

Chapter 2 69

Materials and methods 69

2. Materials and equipment 70

2.1. Methods 73

2.1.2 Cell culture in 2D 73

2.1.3 3D culture 74

2.1.4. 3D Tumoroid assembly and optimisation. 75

2.1.5. Chemotherapy Drug and glycosidase inhibition treatment in 2 and 3D 78

2.1.6. Alamar Blue assay in 2D and 3D 79

2.1.7. Lectin and DAPI (4',6-diamidino-2-phenylindole) assay in 2D and 3D 81

2.1.8. Imaging of 3D tumoroids 82

2.1.9. Image J analysis in 2D and 3D 82

2.1.10. Particle analysis 83

2.1.11. Wound healing assay 85

2.2. Gene expression analysis 86

2.2.1. RNA Extraction 87

2.2.2. cDNA Synthesis 87

2.2.3. Quantitative real-time polymerase chain reaction qPCR 89

2.2.4. Calculating Cycle threshold values from amplified genes 89

2.3. Cytokinesis block micronucleus 90

2.3.1 Giemsa Staining 91

2.3.2. CIN Imaging 91

2.4. CIN scoring 92

2.5. CIN studies in 3D models 94

2.6. Cytokinesis block micronucleus assay in 3D 95

2.6.1. Stock preparation of collagenase type I before cell retrieval..... 95

2.6.2. Cell retrieval after tissue dissociation from 3D constructs for CIN studies 95

2.7. Fluorescence In-Situ Hybridisation (FISH) 97

2.8. Imaging 98

2.9. Statistical analysis 98

Chapter 3 99

Glycosidase inhibition of breast cancer cells grown in 2D..... 99

3. Introduction..... 100

3.1. Lectin staining with Con A, UEA-1 and WGA following treatment with glycosidase inhibitors 101

3.2. Assessing the metabolic activity of breast cancer following glycosidase inhibition. . 110

3.3. Nucleic particle analysis measurement..... 124

3.4. Wound healing assay 133

3.5. Expression analysis of BCL2 and CASP9 in MDA-MB-231..... 147

3.6. Discussion 149

3.6.1. Exposure of breast cancer cells to doxorubicin 150

3.6.2. Synergistic effect of breast cancer cells 150

3.6.3. Imino sugars alter cell metabolism 152

3.6.4. Cellular growth decrease through exposure to a glycosidase inhibitor..... 153

3.6.5. Increase in lectin labelling as a result of glycosidase inhibition. 153

3.6.6. Glycosidase inhibition affects cell motility..... 155

3.6.7. Gene expression analysis 156

3.7. Summary..... 158

3. 8. Summary of findings and novelty 158

Chapter 4 ..... **160**

Glycosidase inhibition on 3D breast cancer tumoroid culture models **160**

4. Introduction **161**

4.1. Tumoroid optimisation studies **163**

4.2. Tumoroid metabolic activity **166**

4.3. 3D Tumoroid invasive front analysis **167**

4.4. Cell motility measurement **170**

4.5. 3D tumoroid glycosidase inhibition treatment **172**

4.6. Metabolic activity of the glycosidase inhibition treatment **172**

4.7. MDA-MB-231 3D Tumoroids DAPI count particle analysis **174**

4.8. MDA-MB-231 tumoroids validation studies **181**

4.9. Discussion **183**

4.9.1. Glycosidase inhibitors reduced metabolic activity **187**

4.9.2. Cell motility reduction **188**

4.10. Summary **190**

4.11. Summary of findings and novelty **191**

Chapter 5 ..... **192**

Comparative studies of CIN in 2D and 3D models **192**

5. Introduction **193**

5.1. Evaluation of CIN in culture models **194**

5.1.1. CIN in 2D **194**

5.2. Adaptation of CBMN in 3D **198**

5.2.1. Comparative studies of CIN in 2D and 3D culture models **198**

5.2.2. Pancentromeric FISH to differentiate between clastogenic and aneugenic CIN events **202**

5.3 The glycosidase inhibition and CIN **205**

5.4. Discussion 209

5.4.1. CIN in 2D 209

5.4.2. CIN in 2D vs 3D 212

5.4.3. Clastogenic and Aneugenic Effects in CIN 217

5.5. CIN associated with glycosidase inhibition 218

5.6 Summary 221

5.7. Findings and novelty 222

Chapter 6 223

Discussion 223

6. Discussion 224

6.1 Glycosidase inhibition in 2D and 3D 224

6.1. 2D limitations 241

6.2. 3D limitations 241

6.3. CIN Limitations 242

6.4 Future directions 242

Conclusion 245

Novel contributions 246

References 247

Appendices 319

List of figures Page number

Figure 1.1. MN formation and NPBs due to chromosome missegregation, due to DNA strand break misrepair and incomplete chromatid separation or telomere end fusion from the cytokinesis block using cyt-B (Fenech, 2020, a)..... 18

Figure 1.2. The mechanisms of action of cyt-B and D are known to bind to the barbed (+) end of microfilament, inhibiting polymerisation (Trendowski, 2015). 20

Figure 1.3. Representation of glycoproteins and their type. O-linked glycoproteins attach to serine and threonine residues through oxygen atoms, while N-linked glycoproteins attach to a nitrogen atom through asparagine residues. The major types of N-glycans result from the cleavage by glycosidases to form high mannose glycoproteins, and to further facilitate the synthesis of carbohydrate-modifying enzymes such as glycosyltransferase to form hybrid and complex glycoproteins (Reily et al., 2019)..... 32

Figure 1.4. N-glycan synthesis begins in the ER with the transfer of a lipid-glycan precursor to an aspartic acid residue by oligosaccharyltransferase (OST). Sequential removal of glucose residues occurs via α-glucosidases, followed by the removal of a mannose residue by ER α-mannosidase. After passing a quality-control checkpoint as the calnexin, calreticulin cycle, the glycoprotein moves to the Golgi apparatus for further trimming and modifications by various glycosyltransferases, including α-mannosidases and sialyltransferases. This process creates a variety of N-glycoforms, often terminating in sialic acid. Glycosyltransferase expression levels influence the final N-glycan composition, the accessibility of glycosylation sites, and the duration the glycoprotein spends in the ER and Golgi apparatus (Reily et al., 2019). 36

Figure 1.5. The T-synthase catalyses the addition of Gal from UDP-α-D-GAL to α-D-GalNAc on peptides, forming the T-antigen (core 1). This structure is then modified into core 2 by C2GnT1-3, which adds β1,6-linked GlcNAc from UDP-α-D-GlcNAc. The core 3 structure is created by C3GnT6, adding β1,3-GlcNAc to the GalNAc. Core 4 is formed from core 3 via C2GnT2, which adds β1,6-GlcNAc. Sialic acid can be added to cores 1-3 by ST6GalNAc1 at the 6-position or by ST3Gal1 at the 3-position of terminal GAL. Additionally, GlcNAc residues in core 2/3 can be extended with β1,4-linked GAL and capped by ST3Gal4/6 sialyltransferases (Thompson & Wakarchuk, 2022)..... 38

Figure 1.6. Glucosidase-mediated steps in the NLG pathway interact with calnexin to facilitate protein folding and subsequent glycan processing. However, inhibition of β-glucosidase results in protein misfolding, ER retention and degradation (Chang et al., 2013). 43
Figure 1.7. DNJ, a piperidine alkaloid, is a polyhydroxylated iminosugar. It is an analogue of D-glucose, with the oxygen in the ring substituted by a nitrogen atom. 48
Figure 1.8.The morphology of a spheroid and an organoid is represented when cultured with different cell types (Fitzgerald et al., 2021). 60
Figure 1.9. Schematic representation of different culture systems from 2D cultures to 3D complex tumoroids. Cancer cells are seeded in plates as monolayers and incubated to mimic the conditions required for cell proliferation. 1) 3D simple tumoroids consisting of collagen, laminin, fibronectin, and collagen IV as the ECM are surrounded by endothelial cells and cancer cells. 2) RAFT^{TM} absorbers absorb interstitial fluid; the tumoroid is treated with drugs. 3) Cancer cells treated with drugs. 4) 3D complex tumoroids are transferred into a hydrogel containing human dermal fibroblasts (HDfs) and human umbilical vein endothelial cells (HUVECs) in 24-well plates and compressed with RAFT^{TM} absorbers to produce a more complex tumoroid. 5) Cultures are then treated with drugs and analysed using flow cytometry, fluorescence imaging, cell viability, ELISA and cell cycle analysis (Stamati *et al*., 2020)..... 67

Figure 2.1. Schematic representation of an example of the fabrication of tumoroids. Upper panel: collagen compression using RAFT^{TM} absorbers, followed by medium and incubation. Lower panel: Methodology of tumoroids fabricated from immortalised cell lines embedded in compressed collagen, assembled, and treated with glycosidase inhibitors to allow studies of breast cancer cells following glycosidase inhibition. 77
Figure 2.2. Particle analysis of stained cells with DAPI grown in 2D. Cells were imaged at 40x magnification using an EVOS microscope, with the bar representing 500 µm. In the left image, DAPI-stained cells are shown, while in the right image, ImageJ particle analysis highlights the results of counted cells. 83
Figure 2.3. A brightfield image of the whole tumoroid is shown on the left side, and on the right side, the results of the ImageJ binary mask particle analysis are displayed, indicating that, despite some folded collagen areas in the tumoroid, the algorithm can accurately predict cell

growth. The entire tumoroid image was captured at 100X magnification, resulting from 176 multiple captured using Evos fluorescent/brightfield microscopy. 84
Figure 2.4. A brightfield image of the whole tumoroid is shown on the left side. On the right side, the DAPI-stained tumoroid is highlighted by a square to facilitate measurement of cell density, which can also be indicated in the whole image, despite some folded collagen areas in the tumoroid; the algorithm can accurately predict cell growth. The entire tumoroid image was captured at 100X magnification, resulting from 176 multiple images stitched together using Evos microscopy. 85
Figure 2.5. Images of the CBMN method applied to breast cancer cells revealed various nuclear abnormalities, which were analysed to assess the rate of CIN among the cells. The cells were observed using light microscopy at a 400X magnification with a scale bar of 10 µm. The upper panel displayed mononucleated cells, both with and without nuclear abnormalities, including nuclear buds (NBUD) and MN, as well as multilobar and multinucleated cells. The lower panel featured BN cells, presenting both with and without nuclear abnormalities, such as BN with MN, nuclear buds, and NPBs. 92
Figure 2.6. The image is an example of the CMBN assay from breast cancer cells grown in 2D, as the scoring count of annotated BN cells with and without abnormalities was subsequently processed in Excel for tabulation and data analysis. 93
Figure 2.7. MDA-MB-231 cells grown in 2D showed the Data analysis of the CBMN assay scoring count in experiment 1. A range of 14 images was captured in this experiment to display the BN with and without abnormalities, which resulted in the calculation of the CIN percentage. The MNi, NBUDS and NPBs were also calculated. 94

Figure 3.1. Schematic workflow representation of the glycosidase inhibition treatment involving different techniques to evaluate the effect of breast cancer cells. 101
Figure 3.2. Con A lectin binding of untreated cells. The image J analysis of the example shows how the cellular fluorescence of each cell line was assessed. A square was drawn to mark the area of lectin staining to be evaluated, followed by a small square used to measure the background. This approach was carried out for all four breast cancer cell lines exposed to glycosidase inhibitors. The microscope was set to a total magnification of 100X, with a scale bar representing 500 µm. 103

Figure 3.3. Fluorescence lectin microscopy of MCF-7 cells with/without exposure to glycosidase inhibitor compounds. Changes in lectin binding were observed, consistent with an accumulation of N-linked structures, increased (Con A, UEA-1, and WGA binding) following exposure of the cells to glycosidase inhibitor compounds at 0.5 mM for 24 hours. Left panel: Fluorescence microscopy images of MCF-7 cells stained with Con A (column 1), UEA-1 (column 2), and WGA (column 3), either untreated or treated (DNJ, 255, 42, and 44). The microscope was set to a total magnification of 100X, with a scale bar representing 500 µm. Right panel: Histogram depiction of the Image J data following analysis of the CTCF. The data were presented as mean values ± SE with N = 9. One-way ANOVA statistical analysis was performed. No significant difference was shown. 105

Figure 3.4. Fluorescence lectin microscopy of SKBR3 cells with/without exposure to glycosidase inhibitor compounds. Changes in lectin binding were observed, consistent with the accumulation of N-linked structures (increased Con A, UEA-1, and WGA binding) following exposure of the cells to a glycosidase inhibitor compound at 0.5 mM for 24 hours. Left panel: Fluorescence microscopy images of SKBR3 cells stained with Con A (column 1), UEA-1 (column 2), and WGA (column 3), either untreated or treated (DNJ, 255, 42, and 44), The microscope was set to a toal magnification of 100X, with a scale bar representing 500 µm. Right panel: Histogram depiction of the Image J data following analysis of the results CTCF. The data were presented as mean values ± SE, with N = 9. One-way ANOVA statistical analysis was performed. There was a significant difference on Con A * (DNJ, *p=<0.05) and UEA (42 inhibitor compound *p=<0.05), no significant difference in UEA. 106

Figure 3.5. Fluorescence lectin microscopy of BT-549 cells with/without exposure to glycosidase inhibitor compounds. Changes in lectin binding were observed, consistent with an accumulation of N-linked structures (increased Con A, UEA-1 and WGA binding) following exposure of the cells to glycosidase inhibitor compound at 0.5 mM for 24 hours. Left panel: Fluorescence microscopy images of BT-549 cells stained with Con A (column 1), UEA-1 (column 2), and WGA (column 3), either untreated or treated (DNJ, 255, 42, and 44),), The microscope was set to a total magnification of 100X, with a scale bar representing 500 µm. Right panel: Histogram depiction of the Image J data following analysis of the results of CTCF. The data were presented as mean values ± SE, with N = 9. One-way ANOVA statistical analysis

was performed. A significant difference was shown in Con A for all the compound inhibitors *P=<0.05. No significant difference in UEA and WGA was shown. 108
Figure 3.6. Fluorescence lectin microscopy of MDA-MB-231 cells with/without exposure to glycosidase inhibitor compounds. Changes in lectin binding were observed, consistent with an accumulation of N-linked structures (increased Con A, UEA-1 and WGA binding) following exposure of the cells to glycosidase inhibitor compound at 0.5 mM for 24 hours. Left panel: Fluorescence microscopy images of MDA-MB-231 cells stained with Con A (column 1), UEA-1 (column 2), and WGA (column 3), either untreated or treated (DNJ, 255, 42, and 44). The microscope was set to a total magnification of 100X, with a scale bar representing 500 µm. Right panel: Histogram depiction of the Image J data following analysis of the results of CTCF. The data were presented as mean values ± SE, with N = 9. One-way ANOVA statistical analysis was performed. No significant differences were shown. 109
Figure 3.7. Cell viability results for MCF-7 cells subjected to 24-hour treatments with glycosidase inhibitors at concentrations of 0.5 mM (top panel) and 1 mM (bottom panel), with or without the addition of doxorubicin at 5 µM, are presented for each biological replicate. Each treatment involving glycosidase inhibitors was conducted in triplicate, resulting in a total of n = 9 for cell viability, which will be detailed in the following section. The data were presented as mean values ± SE, with N = 3. A one-way ANOVA statistical analysis was performed. 112
Figure 3.8. The cytotoxic effects on the MCF-7 ER+ breast cancer cell line were evaluated, focusing on glycosidase inhibitors with doxorubicin exposure, and compared to doxorubicin alone as a control at 5 µM. The left panel illustrates the reduction percentage at a concentration of 0.5 mM, while the right panel shows the reduction percentage at 1 mM. The data were presented as mean values ± standard error, with N=9. A one-way ANOVA statistical analysis was performed to assess the significance of the results. No significant differences were shown. 113
Figure 3.9. The cytotoxic effects on the MCF-7 ER+ breast cancer cell line were evaluated, focusing on glycosidase inhibitors with and without exposure to doxorubicin. The left panel illustrates the reduction percentage at a concentration of 0.5 mM, while the right panel shows the reduction percentage at 1 mM. Untreated (UT) MCF-7 cells were compared with those treated with glycosidase inhibitors. The data were presented as mean values ± standard error,

with N=9. A one-way ANOVA statistical analysis was performed to assess the significance of the results. No significant differences were shown at 0.5 mM, while at 1 mM, it showed significant differences *p =< 0.050 (DNJ), **p =< 0.050 (255). 114

Figure 3.10. Cell viability results for SKBR3 HER2^{+} were subjected to 24-hour treatments with glycosidase inhibitors at concentrations of 0.5 mM (top panel) and 1 mM (bottom panel), with or without the addition of doxorubicin at 5 µM. They are presented for each biological replicate. Each treatment involving glycosidase inhibitors was conducted in triplicate, resulting in a total of N = 9 for cell viability, which will be detailed in the following section. The data are presented as mean values ± SE with N=3. A one-way ANOVA statistical analysis was performed. 115

Figure 3.11. The cytotoxic effects on the SKBR3 HER^{+} breast cancer cell line were evaluated, focusing on glycosidase inhibitors with doxorubicin exposure compared to doxorubicin alone as a control at 5 µM. The left panel illustrates the reduction percentage at a concentration of 0.5 mM, while the right panel shows the reduction percentage at 1 mM. The data were presented as mean values ± standard error, with N=9. A one-way ANOVA statistical analysis was performed to assess the significance of the results. No significant differences were shown. 116

Figure 3.12. The cytotoxic effects on the SKBR3 HER2^{+} breast cancer cell line were evaluated, focusing on glycosidase inhibitor exposure. The left panel illustrates the reduction percentage at a concentration of 0.5 mM, while the right panel shows the reduction percentage at 1 mM. Untreated SKBR3 cells were compared with those treated with glycosidase inhibitors. The data were presented as mean values ± standard error, with N = 9. A one-way ANOVA statistical analysis was performed to assess the significance of the results. No significant differences were shown. 117

Figure 3.13. Cell viability results for the BT-549 TNBC line were subjected to 24-hour treatments with glycosidase inhibitors at concentrations of 0.5 mM (top panel) and 1 mM (bottom panel), with or without the addition of doxorubicin at 5 µM. They were presented for each biological replicate. Each treatment involving glycosidase inhibitors was conducted in triplicate, resulting in a total of n = 9 for cell viability, which will be detailed in the following section. The data were presented as mean values ± SE, with N = 3. A one-way ANOVA statistical analysis was performed. 118

Figure 3.14. The cytotoxic effects on the BT-549 TNBC cell line were evaluated, focusing on glycosidase inhibitors with doxorubicin exposure compared to doxorubicin alone as a control at 5 µM. The left panel illustrates the reduction percentage at a concentration of 0.5 mM, while the right panel shows the reduction percentage at 1 mM. The data were presented as mean values ± standard error, with N=9. A one-way ANOVA statistical analysis was performed to assess the significance of the results. No significant differences were shown. 119
Figure 3.15. The cytotoxic effects on the BT-549 TNBC line were evaluated, focusing on the exposure to glycosidase inhibitors. The left panel illustrates the reduction percentage at a concentration of 0.5 mM, while the right panel shows the reduction percentage at 1 mM. Untreated BT-549 cells were compared with those treated with glycosidase inhibitors. The data were presented as mean values ± standard error, with N=9. A one-way ANOVA statistical analysis was performed to assess the significance of the results. Significant differences at 0.5 mM and 1mM were shown (DNJ) *p =< 0.050 , (44) * p =< 0.050. 120
Figure 3.16. Cell viability results for the MDA-MB-231 TNBC line were subjected to 24-hour treatments with glycosidase inhibitors at concentrations of 0.5 mM (top panel) and 1 mM (bottom panel), with or without the addition of doxorubicin at 5 µM and are presented for each biological replicate. Each treatment involving glycosidase inhibitors was conducted in triplicate, resulting in a total of n = 9 for cell viability, which will be detailed in the following section. The data were presented as mean values ± SE, with N = 3. A one-way ANOVA statistical analysis was performed..... 121
Figure 3.17. The cytotoxic effects on the BT-549 TNBC cell line were evaluated, focusing on glycosidase inhibitors with doxorubicin exposure compared to doxorubicin alone as a control at 5 µM. The left panel illustrates the reduction percentage at a concentration of 0.5 mM, while the right panel shows the reduction percentage at 1 mM. The data were presented as mean values ± standard error, with N = 9. A one-way ANOVA statistical analysis was performed to assess the significance of the results. No statistical differences were shown. 122
Figure 3.18. The cytotoxic effects on the MDA-MB-231 TNBC line were evaluated, focusing on the exposure to glycosidase inhibitors. The left panel illustrates the reduction percentage at a concentration of 0.5 mM, while the right panel shows the reduction percentage at 1 mM. Untreated MDA-MB-231 cells were compared with those treated with glycosidase inhibitors.

The data were presented as mean values ± standard error, with N = 9. A one-way ANOVA statistical analysis was performed to assess the significance of the results. Statistical differences were shown at 0.5 mM and 1 mM concentrations, (255) **p =< 0.050, (DNJ) *p =< 0.050. 123

Figure 3.19. An example of applied image measurement, taken at 100X total magnification and scale bar representing 500 µm, in the particle analysis of the DNJ compound utilises ImageJ through a binary process of masking thresholds and the watershed tool to effectively separate cells that appear merged. Without this methodology, manually counting individual cells would be difficult and inaccurate. 124

Figure 3.20. Upper Panel: Visualisation of DAPI fluorescence representing the nuclei of MCF-7 ER^+ breast cancer cells treated for 24 hours with glycosidase inhibitors, including DNJ and Phytoquest compounds (42, 44, and 255) at a concentration of 0.5 mM. Lower Panel: A histogram displaying particle analysis data from the glycosidase inhibition treatment using the ImageJ particle analysis program, with median values presented as ± SE with N = 27. The microscope was set to a total magnification of 100X, with a scale bar representing 500 µm. A one-way ANOVA statistical analysis was conducted on the non-parametric data to compare untreated and treated cells. No significant differences were shown in terms of reductions. It showed a statistical difference in the increase in cell numbers instead. 126

Figure 3.21. Upper Panel: Visualisation of DAPI fluorescence representing the nuclei of SKBR3 $HER2^+$ breast cancer cells treated for 24 hours with glycosidase inhibitors, including DNJ and Phytoquest compounds (42, 44, and 255) at a concentration of 0.5 mM. Lower Panel: A histogram displaying particle analysis data from the glycosidase inhibition treatment using the ImageJ particle analysis program, with median values presented as ± SE with N = 27. The microscope was set to a total magnification of 100X, with a scale bar representing 500 µm. A one-way ANOVA statistical analysis was conducted on the non-parametric data to compare untreated and treated cells. A significant difference was shown on (DNJ) *p= < 0.050, and (255) *p =< 0.050. 44 and 44 compounds did not show significant differences. 128

Figure 3.22. Upper Panel: Visualisation of DAPI fluorescence representing the nuclei of BT-549 TNBC cells treated for 24 hours with glycosidase inhibitors, including DNJ and Phytoquest compounds (42, 44, and 255) at a concentration of 0.5 mM. Lower Panel: A histogram displaying particle analysis data from the glycosidase inhibition treatment using the ImageJ

particle analysis program, with median values presented as ± SE with N = 27. The microscope was set to a total magnification of 100X, with a scale bar representing 500 µm. A one-way ANOVA statistical analysis was conducted on the non-parametric data to compare untreated and treated cells. No significant differences were shown..... 130
Figure 3.23. Upper Panel: Visualisation of DAPI fluorescence representing the nuclei of MDA-MB-231 TNBC cells treated for 24 hours with glycosidase inhibitors, including DNJ and Phytoquest compounds (42, 44, and 255) at a concentration of 0.5 mM. Lower Panel: A histogram displaying particle analysis data from the glycosidase inhibition treatment using the ImageJ particle analysis program, with median values presented as ± SE with N = 27. The microscope was set to a total magnification of 100X, with a scale bar representing 500 µm. A one-way ANOVA statistical analysis was conducted on the non-parametric data to compare untreated and treated cells. A significant difference was show on (DNJ) *p=< 0.050. No significant difference was shown in the ither compounds..... 132
Figure 3.24. Time-course of wound healing in MCF-7 ER^+ breast cancer cells treated with glycosidase inhibitors at 0.5 mM for 24 hours. The upper panel illustrates images of MCF-7 cells in a scratch assay treated with DNJ, 42,44, and 255 inhibitor compounds at different time points, measured at 0, 6, 12, and 24 hours. Total magnification of X100, with a scale bar representing 650 µm. The lower panel shows the percentage gap wound closure at various time points of untreated vs treated cells with glycosidase inhibitors. The data are presented as mean values ± standard error, with a sample size of N = 12. A one-way ANOVA statistical analysis was performed. No significant differences were shown. 135
Figure 3.25. Time-course of wound healing in SKBR3 $HER2^+$ breast cancer cells treated with glycosidase inhibitors at 0.5 mM for 24 hours. The upper panel illustrates images of SKBR3 cells in a scratch assay treated with DNJ, 42, 44, and 255 inhibitor compounds at different time points, measured at 0, 6, 12, and 24 hours. Total magnification of X100, with a scale bar representing 650 µm. The lower panel shows the percentage gap wound closure at various time points of untreated vs treated cells with glycosidase inhibitors. The data are presented as mean values ± standard error, with a sample size of N = 12. A one-way ANOVA statistical analysis was performed to assess the significance of the results. A significance difference was shown on (255) *p=< 0.050 after 24 hours. 138

Figure 3.26. Time-course of wound healing in BT-549 TNBC cells treated with glycosidase inhibitors at 0.5 mM for 24 hours. The upper panel illustrates images of a BT-549 cell scratch assay treated with DNJ, 42, 44, and 255 inhibitor compounds at different time points, measured at 0, 6, 12, and 24 hours. Total magnification of X100, with a scale bar representing 650 µm. The lower panel shows the percentage gap wound closure at various time points of untreated vs treated cells with glycosidase inhibitors. The data are presented as mean values ± standard error, with a sample size of N = 12. A one-way ANOVA statistical analysis was performed to assess the significance of the results. No significant differences were shown. 141

Figure 3.27. Time-course of wound healing in MDA-MB-231 TNBC cells treated with glycosidase inhibitors at 0.5 mM for 24 hours. The upper panel illustrates images of MDA-MB-231 cells in a scratch assay treated with DNJ, 42, 44, and 255 inhibitor compounds at different time points, measured at 0, 6, 12, and 24 hours. Total magnification of X100, with a scale bar representing 650 µm. The lower panel shows the percentage gap wound closure at various time points of untreated vs treated cells with glycosidase inhibitors. The data were presented as mean values ± standard error, with a sample size of N = 12. A one-way ANOVA statistical analysis was performed to assess the significance of the results. A significant difference was shown on (255) ****p=< 0.050. 144

Figure 3.28. A summary of the glycosidase inhibition treatment at 0.5 mM for 24 hours showed the course of wound healing in the MCF-7, SKBR3 (upper panel), BT-549, and MDA-MB-231 (lower panel) breast cancer cell lines. The data were presented as mean values ± standard error, with a sample size of N = 12. A one-way ANOVA statistical analysis was performed to assess the significance of the results. 146

Figure 4.1. Schematic representation of A 3D RAFT^{TM} system fabrication of tumoroids with breast cancer cells exposed to inhibitors at 0.5mM, a collaboration with prof Marilena Loizidou, University College London. Below, a 24-well plate tumoroid can be observed through bright-field images, stained with DAPI using EVOS fluorescence at a 100x magnification with a bar scale representing 2 cm. With 2 × 10^4 cells seeded per 96-well plate. 176 images were completely stitched together using automated settings to have a view of the whole tumoroid and were established at the University of Westminster. 163

Figure 4.2. A total magnification of 100X with a scale bar representing 2 cm of brightfield images of MCF-7 cells (left panel) and MDA-231 tumoroids (right panel) were captured over 11 days, with the cells fixed accordingly. 164
Figure 4.3. MCF-7 is shown in the left panel, while MDA-MB-231 tumoroids are depicted in the right panel Total magnification of X100, with a scale bar representing 2 cm DAPI-stained images in a 24-well plate, following an eleven-day incubation, the results from 176 multiple captures using Evos microscopy illustrate that an ACM (middle mass) nucleic stain indicates increased cell density at day 11, which is surrounded by a non-cellular compartment (Dark background): growth optimisation profiles for days 3, 5, 3,5,7, and 11. 165
Figure 4.4. Alamar blue assay histogram of MCF-7 and MDA-MB-231 tumoroids cell viability measurements at days 3,5,7, and 11. Both showed an increase in cell proliferation at day 3. On days 5 and 7, cell viability decreased and increased on day 11. One tumoroid was deployed for each day with a total of 4 tumoroids for each cell line. 166
Figure 4.5. MCF-7 and MDA-MB-231 tumoroids were captured at with total magnification of X100, and a scale bar representing 2 cm brightfield images in a 24-well plate after a ten-day incubation, resulting from 176 multiple captures using Evos microscopy. This showed an ACM (middle mass) and a non-cellular compartment (external surrounding areas) on days 3, 5, 7, and 11, representing the growth optimisation profile. 167
Figure 4. 6. In the upper panel, three images of the same tumoroids are displayed. The image on the left is stained with DAPI, while the middle image has undergone binary processing and converted into a mask. The DAPI image was captured at a total magnification of 100X, with a scale bar representing 2 cm. The image on the right illustrates the measurements taken from a yellow circle encircling the central cancer cell mass. The analysis results reveal the invasive front measurements of the cell protrusions that extend from the original ACM into the surrounding non-cellular collagen compartments. Lower panel: MDA-MB-231 tumoroids had a more significant overall outgrowth from the original ACM than MCF-7 tumoroids. One tumoroid for each day was produced with a total of 4 for each cell line. No significant differences were shown on MCF-7 tumoroid but in MDA-MB-231 tumoroids ****p=< 0.05. 169
Figure 4.7. Upper panel: Example of an image J analysis of MCF-7 tumoroids captured at a total magnification of 100X, with a scale bar of 2 cm. DAPI stained images in a 24 well plate,

following a ten-day incubation, resulted from 176 multiple captures using Evos microscopy shows an ACM (middle mass) image J analysis of nucleic stain DAPI analysis results show the distance migrated measurement and the number of invasive bodies from the original ACM into the non-cellular collagen compartments. Lower panel: MDA-MB-231 tumoroids indicated exponential growth from day 3 to day 7, and a decrease in several clumps was seen by day 11. MCF-7 tumoroids number of invasive bodies from day 3 to day 5 showed an increase, but again, it decreased by day 11—median values ± SE. One tumoroid was deployed for each day with a total of four tumoroids for each cell line. No significant differences were shown. . 170

Figure 4.8. The histograms depicting the migration distances of MCF-7 and MDA-MB-231 tumoroids were analysed over an 11-day optimisation period. MCF-7 tumoroids exhibited a marked increase in migration distance between days 5 and 7; however, by day 11, no cell clumps were detected. In contrast, MDA-MB-231 tumoroids experienced the most significant increase in migration distance on day 7, followed by a decrease by day 11. Median values ± SE. One-way ANOVA performed. No significant differences were shown. One tumoroid was deployed for each day with a total of 4 tumoroids for each cell line. 171

Figure 4.9. A histogram of MDA-MB-231 tumoroids cell viability measurements at day 11. This shows the percentage reduction of Alamar blue in the tumoroids after exposure to glycosidase inhibitor compounds DNJ, 255, 42, and 44 at days 2, 4, 6, 8, and 10. Tumoroids treated with *c*ompound 255 indicated the highest percentage reduction compared to the untreated tumoroid. Median values ± SE and *a t*-test was carried out. There was a significant difference in all treated groups (DNJ) **p=< 0.05, (255) ***p=< 0.05, (42) *p=< 0.05, (44) *p=< 0.05. N=3 technical replicates were deployed. 173

Figure 4.10. A brightfield image on the left, particle analysis measurements in the middle, and a whole tumoroid with DAPI-stained central cancer cell mass on the right, showing a selected area to be analysed. An example of an image J analysis of MDA-MB-231 tumoroids captured at a total magnification of 100X DAPI stained images, with a scale bar representing 2 cm. The images resulted from 176 multiple captures using Evos microscopy, analysis of nucleic stain DAPI results shows particle analysis through binary processing, picture threshold RPG/B&W mask, watershed, particle analysis of tumoroids by choosing areas of 500 µm at high cell density to avoid folded collagen areas to interfere with the particle analysis. Data analysis was presented as median values ± SE. 174

Figure 4.11. The MDA-MB-231 tumoroid histogram of particle analysis cell count, using ImageJ, showed a significant difference in all treated compounds, DNJ, 255, 42, and 44, compared to the untreated. The data were presented as median values ± standard error. A one-way ANOVA statistical analysis was performed to assess the significance of the results. A significant difference was shown in all treated cells. (DNJ) ****p= < 0.05, (255) ****p= < 0.05, (42) ****p= < 0.05, (44) ****p= < 0.05. N=3 was deployed. 176

Figure 4.12. Visualisation of DAPI fluorescence of the MDA-MB-231 3D tumoroid nucleic particle analysis captured at total magnification of 200X, with a scale bar representing 500 µm. EVOS fluorescence microscopy showed a reduction in the cell numbers of the treated tumoroids, as the untreated tumoroid cell density is higher. Median values ± SE. These visualised images were sectioned and cut similarly to all 3D tumoroids, without interfering with folded collagen areas. An example is illustrated in Figure 4.10. A significant difference was shown in all treated cells **** p =< 0.05. N=3 was deployed. 178

Figure 4.13. Histogram analysis of MDA-MB-231 3D tumoroid, the invasive front (left panel), and the invasive bodies count (right panel). The data were presented as median values ± standard error. A one-way ANOVA statistical analysis was performed to assess the significance of the results. N=3 technical replicates were deployed. 180

Figure 4.14. Visualisation of DAPI fluorescence of the MDA-MB-231 3D tumoroid nuclei representation following a ten-day incubation resulted from 176 multiple captures using Evos fluorescence microscopy at a total magnification of 100X, with a scale bar representing 2 cm. Data analysis was presented as median values ± SE. One-way ANOVA statistical analysis. Treatment of glycosidase inhibition on MDA-MB-231 tumoroids consisted of 3 tumoroids to generate technical triplicates for each treatment. 181

Figure 4.15. Upper panel: Visualisation of DAPI fluorescence of the MDA-MB-231 3D tumoroid nuclei representation following a ten-day incubation, resulting from 176 multiple captures using Evos fluorescence microscopy at a total magnification of X40, with a scale bar representing 2 cm. Lower panel: Statistical analysis from the particle analysis, measurement of invasive bodies and outgrowth. Data analysis was presented as Median values ± SE. One-way ANOVA statistical analysis. A significant difference was shown with both DNJ and 255 for particle analysis, *** p= < 0.05. No significant difference was shown on the number of invasive bodies and outgrowth. N=3 technical replicates were deployed. 183

Figure 5.1. A schematic representation of the workflow for the evaluation of CIN in breast cancer cells cultured as 2D compared to 3D culture models. CIN levels were also assessed when the cells were exposed to glycosidase inhibitors in a 2D environment. 194
Figure 5.2. Cumulative CIN of BN cells with and without biomarkers from the four breast cancer cell lines grown in 2D. The top panel: BT-549 cells compared with MCF-7 and MDA-MB-231 cells. Middle panel: BT-549 cells were compared to SKBR3 cells and MDA-MB-231 to MCF-7 cells. Lower panel: MDA-MB-231 cells were compared to SKBR3 cells, and MCF-7 to SKBR3 cells. Data were presented as values from two replicate biological experiments. Data analysis was done using the pairwise Chi-square test. There was a significant difference on (BT-549 vs MCF-7) ****p= < 0.05, (BT-549 vs SKBR3) ****p= < 0.05, (BT-549 vs MDA-MB-231) ***p= < 0.05. There was no significant difference in the other comparisons. 197
Figure 5.3. CIN Comparative studies in 2D and 3D showed the statistical analysis of CBMN assay scores from normal BN cells, and abnormalities such as MN, NBPs and NBUDs are indicators of chromosomal aberrations in CIN. Top panel: BT-549 and MDA-MB-231 were compared in 2D and 3D culture models. In the lower panel, MCF-7 and SKBR3 were compared between 2D and 3D conditions. Data were presented as two biological repeats, as data analysis was done using a pairwise Chi-square test. There was a significant difference on (BT-549) ****p= < 0.05, (MCF-7) *p= < 0.05 and, (SKBR3) *p= < 0.05. There was no significant difference on MDA-MB-231 cells. 200
Figure 5.4. MN rates in 2D and 3D show the statistical analysis of CBMN assay scores as indicators of chromosomal aberrations in CIN. Top panel: BT-549 and MDA-MB-231 were compared in 2D and 3D culture models. In the lower panel, MCF-7 and SKBR3 were compared between 2D and 3D conditions. Data were presented as two biological repeats, as data analysis was done using a pairwise Chi-square test. There was a significant difference on (BT-549) ****p= < 0.05, (MCF-7) ****p= < 0.05 and, (SKBR3) *p= < 0.05. There was no significant difference on MDA-MB-231 cells. 201
Figure 5.5. Examples of MN with and without centromeric signals: a) The DAPI channel shows a BN cell with an MN (arrow). B) In green, the pancentromeric sequences on nuclei. c) The merged image shows no green, fluorescent signal in the micronucleus, suggesting a lack of centromeric target DNA, which implies the content of the micronucleus is a fragment of a

chromosome, not an entire chromosome (clastogenic event). d) A BN cell with MN stained with DAPI. f) The green channel showed BN cells, indicating pancentromeric signals in the MN. g) DAPI and green channels confirmed aneugenic characteristics. h) BN cells with MN DAPI channel. i) Red signals detected the presence of HER2 signals on the BN cell, and the arrow also indicated the presence of multiple copies of HER2 in the MNi. j) HER2 and PAN-C copies were detected in the MN, describing it as an eugenic event. Total magnification of X400, with a scale bar representing 10 µm. 204

Figure 5.6. The level of CIN in treated MDA-MB-231 cells with glycosidase inhibitors at 0.5 mM for 24 hours showed that the statistical analysis of CBMN assay scores from normal BN cells and abnormalities such as MN (Fragmented chromosomes), NBPs(mis-repaired DNA or end-to-end chromosome fusions), and nuclear buds (amplified DNA or DNA complexes being eliminated) are indicators of chromosomal aberrations in CIN. The top panel showed the untreated cells compared to those treated with DNJ and compound inhibitor 255. The lower panel showed the untreated cells compared to the compound inhibitor 42. Data were presented as two biological repeats. Data analysis was done using a pairwise Chi-square test. No significant difference resulted. 207

Figure 5.7. The level of CIN in treated MDA-MB-231 cells with glycosidase inhibitors at 0.5 mM for 24 hours was assessed using statistical analysis of CBMN assay scores, which included MN, serving as indicators of chromosomal aberrations in CIN. The top panel showed the untreated cells compared to those treated with DNJ and compound inhibitor 255. The lower panel showed the untreated cells compared to the compound inhibitor 42. Data were presented as two biological repeats. Data analysis was done using a pairwise Chi-square test. No significant difference resulted. 208

Figure 6.1. At the upper site, mannosidase trims the high-mannose glycoprotein, which then becomes a hybrid glycoprotein. At the lower site, Inhibition of Golgi α1,2-mannosidase I occurs with DNJ and a compound inhibitor (255, 42), potentially resulting in unfolded glycans being sent to the UPR and eventually leading to apoptosis……237

List of tables

Page number

Table 1.1. Breast cancer molecular subtypes..... 4

Table 1.2. Summary of the lectin recognition sites in N-linked and O-linked pathways..... 52

Table 2. 1. List of reagents..... 70

Table 2. 2. Equipment, kits and software..... 71

Table 2. 3. Immortalised breast cancer cells deployed in this study..... 72

Table 2. 4. The concentration of the reagents used to prepare the RAFT™ system..... 75

Table 3.1. Corrected total cell fluorescence (CTCF) from the average of the integrated density percentage of the untreated vs cells treated with glycosidase inhibitors..... 104

Table 3. 2. Metabolic activity of breast cancer cells treated with glycosidase inhibition at concentrations of 0.5 mM and 1 mM by the compound inhibitors, DNJ, 42 44 and 255, as well as by doxorubicin at 5 µM in combination and used alone. The measurement employed was the percentage reduction in the Alamar Blue reagent. The values are the mean average of triplicates..... 111

Table 3. 3. One-way ANOVA statistical analysis of particle analyses of the four breast cancer cell lines used in this study..... 133

Table 3. 4. Scratch assay from One-way ANOVA statistical analysis of MCF-7 cells treated with glycosidase inhibitors..... 136

Table 3. 5. Scratch assay results from One-way ANOVA statistical analysis of SKBR3 cells treated with glycosidase inhibitors..... 139

Table 3. 6. Scratch assay results from the One-way ANOVA test statistical analysis of BT-549 cells treated with glycosidase inhibitors..... 142

Table 3. 7. Scratch assay results from One-way ANOVA statistical analysis of MDA-MB-231 cells treated with glycosidase inhibitors..... 145

Table 3. 8. One-way ANOVA statistical analysis of the level of gene expression of BCL2 and CASP3 fold-rate of MDA-MB-231 cells after glycosidase inhibition treatment over 24 hours. 149

Table 4. 1. One-way ANOVA test statistical analysis comparing the untreated and treated 3D tumoroids, as analysed by particle analysis using ImageJ..... 177

Table 4. 2. Dunnett's multiple comparisons test between treated and untreated MDA-MB-231 tumoroids with glycosidase inhibitors DNJ, compounds 25, 42, and 44 from the Phytoquest company. 179
Table 5. 1. The data analysis from a Chi-square test reveals the differences between BN cells with and without CIN, based on a minimum of 300 BN cells grown in 2D. 195
Table 5. 2. The pairwise Chi-square test compares CIN in the breast cancer cell lines..... 196
Table 5. 3. A Chi-square test shows the differences between BN cells with and without CIN, based on cells grown in 3D. 199
Table 5. 4. The pairwise Chi-square test on the four breast cancer cell lines to compare cumulative CIN in 2D and 3D culture models. 199
Table 5. 5. MN centromere testing on all four cell lines in 2D and 3D. 202
Table 5. 6. The MN centromere test across all four cell lines in 2D and 3D. 203
Table 5. 7. A Chi-square test was carried out on MDA-MB-231 between untreated cells and those treated with glycosidase inhibitors. 206
Table 5. 8. A pairwise Chi-square test on MDA-MB-231 cells to show the cumulative CIN between untreated cells and those treated with glycosidase inhibitors. 206

Chapter 1

Introduction

1. 3D Models in Drug Discovery and Cancer Resistance

Cancer is one of the significant causes of mortality worldwide (World Health Organisation, 2025), with nearly 10 million people succumbing to the disease in 2020, and breast cancer, the most common type of cancer, was diagnosed in 2.26 million cases (Ferlay *et al.*, 2020). Conventional therapeutic techniques include surgery, radiotherapy and chemotherapy and therapeutic strategies are selected depending on the type of tumour and the stage of cancer at diagnosis. However, these treatments can fail when a tumour is detected at an advanced stage because cancer metastasis has spread to secondary organs (Tredan *et al.*, 2007). Approaches have been developed to identify new molecular targets, leading to targeted therapies to eliminate tumour cells and complement conventional treatment modalities. The primary purpose of functional models is to assess cancer evolution and clonal selection of tumour cells when exposed to anticancer drugs. Over the last two decades, 3D culture system models, including tumoroids, spheroids, and organoids, have enabled the functional analysis of solid tumours and have been utilised to determine drug efficacy. This has led to improvements in personalised approaches for predicting sensitivity and resistance to treating various types of cancer (Swain *et al*., 2015). This biomarker-based approach has been developed from a fundamental science experiment perspective and moved to clinical validation, guiding therapy choice(s). Companion diagnostics aligned to treatments have begun to shift clinical diagnostics away from assessing where the tumour originates, which was previously used to treat cancer patients with a single targeted drug, to biomarker-based approaches. For instance, the first precision medicine model involving biomarker evaluation was the use of endocrine therapy for oestrogen receptor-positive breast cancer (Harbeck *et al*., 2019). A notable feature of such approaches is that many targeted treatments are successful in only a low percentage of patients (Ayyar *et al*., 2016). However, despite advances in targeted therapies, the development of resistance to treatment (often following an initial response) remains an issue. It is widely accepted that a better understanding of the tumour microenvironment and the mechanisms involved in tumour therapeutic resistance are crucial to the success of cancer research and drug discovery. There is significant potential for using

improved *in vitro* methods, such as 3D models, to better understand the processes underlying cancer cell resistance to therapy and to assess potential novel treatment modalities.

1.1. Breast Cancer

Breast cancer is the principal cause of mortality in women and the most commonly detected malignant growth (Bray *et al.*, 2018). It is the fifth leading cause of cancer-related deaths, and according to GLOBOCAN 2020 data, 2.3 million women were diagnosed with breast cancer worldwide (Sung *et al*., 2021). Breast cancer is a heterogeneous disease that consists of different subtypes characterised by specific epidemiological patterns (Wu *et al*., 2022). The most common cause of mortality in breast cancer patients is the spread of malignant cells from the primary tumour into other organs; this process, known as metastasis, is the principal cause of the recurrence of the illness. The organs to which breast cancer tends to metastasise are the brain, lung, bone, and liver.

1.2. Breast cancer subtypes

The majority of breast cancers are categorised into in situ carcinoma, where cancer cells stay within the ducts or lobules, and invasive carcinoma, which can spread to surrounding tissues and beyond. Over 80% of invasive breast cancers are invasive ductal carcinomas, and the vast majority of the remaining are invasive lobular carcinomas (Makky, 2015). In breast cancer, immunohistochemistry markers are used to detect tumours expressing oestrogen receptors (ER) and progesterone receptors (PR), which are typically used for breast tumour subtyping (Fulford *et al.*, 2006) and classically known as hormone receptor-positive (HR^+) tumours, human epidermal growth factor receptor 2 (HER2), HER2 amplified breast cancer and a type of breast cancer that does not express ER, PR and, HER2 known as triple-negative breast cancer (TNBC).

A new categorisation of breast cancer molecular subtypes was proposed in 2013 (Goldhirsch *et al*., 2013): luminal A, luminal B, basal-like or triple-negative breast cancer, and HER2-positive. The breast cancer molecular subtypes are (shown in Table 1.1).

Table 1.1. Breast cancer molecular subtypes

Subtype	ER Status	PR Status	HER2 Status	Ki-67 Status	Prognosis / Survival	Reference
Luminal A	Positive (+)	Positive (+)	Negative (-)	Low (< 20%)	Highest median survival; best prognosis.	(Fan *et al., 2006)(Hu et al., 2006),*
Luminal B	Positive (+)	Low (< 20%)	Negative (-)	High (+)	Intermediate; higher recurrence than Luminal A.	(Goldhirsch *et al.*, 2013)
HER2-positive	Negative (-)	Negative (-)	Positive (+)	Variable	Historically aggressive; poor without targeted therapy.	(Goldhirsch *et al.*, 2013)
Basal-like (TNBC)	Negative (-)	Negative (-)	Negative (-)	Variable	Higher recurrence rate; generally poorer prognosis.	(Goldhirsch *et al.*, 2013)

1.2.1. Triple negative breast cancer

TNBC is a type of breast cancer that does not express ER, PR or HER2 (Wolff *et al.*, 2013). TNBC is categorised by gene expression analysis as a basal-like breast cancer (BLBC) (Yin *et al.*, 2020). TNBC is the most common breast cancer diagnosis in women under 40 years of age and represents 10% to 20% of all breast cancer diagnoses (Morris *et al.*, 2007). TNBC is the most aggressive type of cancer when compared to other types of breast cancer. It is associated with increased recurrence rates and decreased time between treatment and recurrence, for instance, shortening progression-free survival (PFS). TNBC does not express hormone receptors and therefore does not respond to hormonal therapies. Also, it does not express HER2 receptors or respond to anti-HER2 therapy (Lehmann, 2011). Thus, for TNBC, the primary treatment modality following surgery and radiotherapy is chemotherapy. One of the most effective chemotherapeutic drugs and one of the most potent anthracycline drugs used in the treatment of patients with TNBC is doxorubicin (see section 1.10.8 for detailed information (Gupta *et al*., 2020; Obidiro *et al*., 2023). However, patients with HER2-positive cancers can achieve favourable outcomes with chemotherapy and trastuzumab-based treatments that do not include anthracyclines (Slamon *et al*., 2011; Schneeweiss *et al*., 2013; Tolaney *et al*., 2023). Patients with Luminal A breast cancer do not experience substantial benefits from doxorubicin-based chemotherapy, whereas individuals with higher-risk Luminal B subtypes exhibit better outcomes when treated with anthracyclines (Goldhirsch *et al*.,2011).

The recurrence rate of TNBC is within 3 to 5 years, and therefore, TNBC is an aggressive illness compared with other forms of breast cancer (Ovcaricek *et al*., 2011). The proliferation of TNBC cells is faster than that of different breast cancer cells, particularly those with a high nuclear grade (Jitariu *et al*., 2017).

1.3. Hallmarks of cancer

In the complex landscape of oncology, understanding the fundamental mechanisms behind cancer development and progression is vital. The concept of the "hallmarks of cancer" provides a comprehensive framework that outlines the core capabilities acquired during the multi-step development of human tumours (Hanahan & Weinberg, 2011). These hallmarks represent distinct and interconnected biological capabilities that enable cancer cells to thrive, invade, and metastasise. They include sustaining proliferative signalling, evading growth suppressors, resisting cell death, enabling replicative immortality, inducing angiogenesis, activating invasion and metastasis, deregulating cellular energetics, and avoiding immune destruction. Each hallmark contributes to the malignant phenotype, enhancing our understanding of cancer's complexity and highlighting potential therapeutic targets. By examining these hallmarks, researchers and clinicians can gain insight into the challenges of cancer treatment and explore innovative strategies to improve patient outcomes (Hanahan and Weinberg, 2011).

The evolving landscape of cancer research has introduced new dimensions to the traditional hallmarks of cancer, emphasising the complexity and adaptability of tumour cells. A crucial aspect of this is phenotypic plasticity, which allows cancer cells to change their characteristics in response to environmental pressures. This plasticity is supported by processes such as epithelial-mesenchymal transition (EMT) (see section 1.5 for more details) and the presence of cancer stem cells (CSCs). CSCs are self-renewing, stem-like cells characterised by their unique ability to seed new tumours (Mani *et al*., 2008). This term arises from a study that identified a rare subpopulation of leukemic cells that could initiate leukaemia when transplanted into immunodeficient mice. This provided the first solid evidence supporting the cancer stem cell theory, which suggests that tumours are organised hierarchically and sustained by a select group of self-renewing cells. Consequently, CSCs are central to understanding how cancers initiate, persist, and return (Bonnet & Dick, 1997). CSCs have also been found in solid tumours, such as those originating in the breast, colon, and brain (Al-hajj *et al*., 2003; Obrien *et al*., 2007; Ricci *et al*., 2007; Singh *et al*., 2004).

EMT and CSC enhance the cells' ability to metastasise and resist treatment. The capacity for transcriptional reprogramming further enables cancer cells to adapt quickly, presenting significant challenges for treatment, as these cells can evade standard therapies and contribute to tumour recurrence. Therefore, targeting the pathways that regulate EMT and CSCs could provide new therapeutic avenues, potentially reduce metastasis and improve patient outcomes (Hanahan, 2022).

Another critical aspect is the role of non-mutational epigenetic reprogramming and the microbiome in cancer development and treatment response. Epigenetic changes, such as DNA methylation and histone modification, can activate oncogenes or silence tumour suppressor genes without altering the DNA sequence, offering reversible targets for therapeutic intervention. The microbiome's influence on inflammation, immune modulation, and drug metabolism also highlights its potential role in shaping cancer progression and treatment efficacy. By modulating the microbiome, the effectiveness of existing therapies may improve, suggesting a compelling area for future research. These insights highlight the importance of a complete approach to cancer treatment, integrating genetic, epigenetic, and environmental factors to combat this multifaceted disease more effectively (Hananan, 2022).

1.4. The tumour microenvironment in cancer progression.

Cancer development is influenced by the tumour microenvironment (TME), which comprises various cell types, extracellular matrix (ECM) proteins, and glycosaminoglycans, among other components. The cells of the TME secrete growth factors, cytokines, and chemokines, which have been shown to alter the structure of the ECM. Tumour progression is promoted by stimulating factors produced by the cancer cells and also by cells of the TME (Chang *et al.*, 2015). Cancer-associated fibroblasts (CAF) are the main cellular constituent of the TME; these stromal cells surround the tumour cells and secrete proteins such as collagen, which is essential for mechanical maintenance, control of cancer cell proliferation, survival, promoting the development of new blood vessels (angiogenesis), metastasis, stimulate the immune response (immunogenicity) and influence therapy resistance (Ishii *et al.*, 2016). CAFs

differentiate into and activate fibroblasts of various subtypes and phenotypes (Augsten, 2014). For instance, resting fibroblasts in the healthy cells of the colon connect to the *lamina propria* adjacent to the epithelium. In contrast, a class of myofibroblasts known as pre-cryptal fibroblasts contributes to the regeneration and repair of physiological processes in the walls of the colonic crypt (Tommelein *et al.*, 2015).

Additionally, local fibroblasts may be the origin of some subtypes of CAFs, which are likely to line the edges of the tumour, whereas other types migrate from the bone marrow (BM). Other fibroblast subtypes are thought to differentiate into CAFs during the endothelial/epithelial-EMT (Augsten, 2014; Tommelein *et al*., 2015). Mesenchymal stem cells have been shown to differentiate into CAFs and promote the growth of endothelial cells (ECs) (Shiga *et al*., 2015). Tumour growth is stimulated by CAFs (Attieh & Vignjevic, 2016) through the overexpression of growth factors, important cell signalling proteins such as cytokines, peptides/proteins produced by cells to stimulate the immune system (chemokines), and changes in the ECM. Consequently, this increases tumour stiffness (Kalluri, 2016), a feature of the TME that has been shown to promote cancer proliferation. Studies have described the effect of tumour stiffness on the regulation of cellular communication network factor 1 (CCN1) in endothelial cells, where increased interactions between melanoma cells and the endothelium have stimulated the spread of cancer cells over the vasculature (Reid *et al*., 2017).

1.5. Epithelial-mesenchymal transition

EMT is a biological process associated with the initiation of metastasis, causing epithelial cells to lose their polarity and develop a mesenchymal phenotype (Thiery *et al*., 2009). A decrease in the expression of epithelial-specific genes, such as *E-cadherin*, and an increase in the expression of mesenchymal-specific genes, including N-cadherin and vimentin, are correlated with EMT (Takeichi, 1991; Thiery *et al*., 2009). EMT stimulates CSCs and provides tumour cells with migratory and invasive characteristics by transforming regular tumour cells into master cells capable of self-renewal and initiating tumour growth, thereby establishing a connection between their migration and tumour regeneration (Thiery *et al*., 2008; Mani *et al*., 2008). Research showed that forcing cells through the EMT using transcription factors like *Snail* or *Twist* reprogrammes them into CSCs. This transition causes cells to adopt a specific CD44-^{high,}

CD24-^{low} molecular surface marker profile and significantly enhances their ability to initiate new tumours (Mani *et al*., 2008). Once a mesenchymal phenotype has been completed, tumour cells gain an increased ability to migrate and invade, develop resistance to apoptosis and increase the production of components of the ECM (Kallury & Weinberg, 2009). The main events associated with EMT are the loss of epithelial markers, enhanced expression of mesenchymal markers, and reorganisation of the cytoskeleton. Studies showed that the transcriptional repressors S1P1, *Snail, Slug*, and *Twist* silence the CDH1 gene (which encodes E-cadherin), destroy epithelial structure and promote an invasive mesenchymal phenotype (Thiery et al., 2008; Kang & Massague, 2004).

A transforming protein, RhoA (Ras homolog Family member A), a guanosine triphosphatase (GTPase) that regulates actin cytoskeleton restructuring, is activated by signalling pathways that associate with *S1P1*, *Snail, Slug* and *Twist,* which are transcription factors that regulate the expression of tumour suppressors such as *E-cadherin* (Yu *et al*., 2010), induce an EMT (Yilmaz & Cristofori, 2009). In breast cancer, there is evidence that indicates that tumour cells undergo EMT to become active as cells lose their cell-cell adhesion, gain mobility, and develop the invasive properties required, particularly in the most aggressive subtype, TNBC, which does not express ER, PR, or HER2. Furthermore, it was revealed that circulating tumour cells in breast cancer patients show markers of EMT, particularly highlighting this activation in aggressive subtypes of TNBC. The findings proved that EMT, which facilitates cell detachment and metastasis, occurs in human patients. This process enables these cells to avoid standard detection methods by losing their epithelial markers (Mostert *et al*., 2009).

Melanoma cell adhesion molecule (MCAM), also known as CD146 and MUC18, is an internal membrane glycoprotein that was identified as a melanoma-specific cell adhesion molecule (Lehman *et al*., 1989) and as a marker for tumour progression (Yan *et al*., 2003). Other studies demonstrated an association with TNBC, as CD146 is the primary activator of EMT. Overexpression of CD146 in tumour cells resulted in the downregulation of epithelial markers and the upregulation of mesenchymal markers, leading to increased cell migration, invasion, and cancer stem cell properties (Zeng *et al*., 2012). Changes in molecular processes associated with EMT have led to the identification of biomarkers, providing insight into the TME. The ability of epithelial cells to lose their polarity during EMT could increase if CD146

overexpression were inhibited. This could be crucial in reversing EMT and reducing this aggressive tumour phenotype. For example, MDA-MB-231 is a TNBC human cell line with a mixed population of epithelial and mesenchymal-like cells due to the cancer cell heterogeneity; other TNBC cell lines often also include cells with a mesenchymal phenotype. The importance of EMT in TNBC is a subject that warrants further investigation (Li *et al.*, 2020). They demonstrated a correlation between 77 serum metabolites and aggressive, metastatic TNBC in Asian patients, but further investigation was needed to establish the direct, causal molecular mechanisms linking these metabolites to the induction of EMT. The study further established a metabolite prognostic panel that strongly correlates with patient 5-year survival rates, offering a potential clinical biomarker for risk stratification.

1.6. Hypoxia

Hypoxia is the lack of oxygen at the tissue level to maintain proper homeostasis and occurs as a feature of tumour growth, accompanied by inflammation in the reactive stroma and tumour macrophage polarisation, promoted by CAFs with increased levels of tumour-activated macrophages of the M2 phenotype reported (Mantovani *et al*., 2017). CAFs produce interleukin-6 (IL-6), which promotes the inflammatory phenotype (Cirri & Chiarugi, 2012). The overexpression of smooth muscle actin (αSMA) is a characteristic of CAFs (Darby *et al*., 2014). To distinguish between normal fibroblasts and CAFs, a range of "CAFs markers" is used; these include fibroblast-specific protein-1 (FSP-1/s100A4), fibroblast activating protein (FAP), platelet-derived growth factor receptor (PDGFR) and prolyl-4 hydroxylase subunit alpha-1 (P4HA1). Nonetheless, it is particularly challenging to categorise CAFs because they have a range of activation profiles and are an extremely heterogeneous population (Shiga *et al.*, 2015; Kalluri, 2016).

1.7. Genomic instability

Genomic instability is a defining characteristic of cancer, referring to various alterations in the genome that are commonly observed in cancers. These alterations include an increased frequency of base pair mutations, microsatellite instability (MSI), and changes in the number

and structure of chromosomes, known as chromosomal instability (CIN) (Al-Sohaily *et al*., 2010; Roschke & Kirsch, 2010).

Genome instability is inherent to human malignant growth; this process increases during the development of a tumour and results in the heterogeneous cellular populations within solid tumours, which enables tumours to adapt and evolve (Greaves, 2015; Davis *et al*., 2017; Swanton, 2012). Intra-tumoral heterogeneity (ITH) poses a significant challenge, as it is a primary reason for the failure of cancer treatments and is associated with poor clinical outcomes (Landau, 2015; Kreso *et al*., 2013).

Variations across the cancer genome, including genetic mutations and gene copy number changes, have been reported in many investigations concerned with genome-wide sequencing of tumours as well as the single-cell level; this has highlighted the extent to which genomic instability is intrinsic to cancer development (Navin, 2014; Gerlinger, 2012; Wang *et al.*, 2014). However, research into genome instability has failed to demonstrate the rate of genomic change in late-stage cancer. Unstable genomes and ITH are widely accepted to have a different effect on cancer evolution response than stable genomes; this is likely to be critical in helping unravel our understanding of the development of tumour genomes (Van and Kops, 2016).

Preserving genomic stability is a crucial aspect of homeostasis to maintain cellular integrity, avoid errors during DNA replication, endogenous genotoxic stress such as that caused by reactive oxygen species (ROS) from cellular metabolism, and exogenous carcinogen insults, for instance, exposure to ultraviolet light, ionising radiation or mutagenic chemicals or chemicals that can damage DNA. It is understood that a tumour's initiation and development are caused by acquired alterations in the genome of healthy cells and the selection of more destructive subclones (Nowell, 1976). Many studies of genomic instability have been conducted to understand and manipulate the mechanisms that control tumour initiation and progression. These aim to maintain and modify these mechanisms, as well as identify specific cell cycle checkpoints. Genomic instability can originate from impaired functioning and decreased DNA damage response pathways, where particular genes, such as *TP53*, *Ataxia telangiectasia mutated* (*ATM*), and Rad3-related (*ATR)* kinases, play a crucial role. These tumour-suppressor genes play a pivotal role in safeguarding the integrity of the genome

(Motoyama & Naka, 2004). Additionally, tumours showing genomic instability can develop due to acquired deficiencies in six DNA repair or damage tolerance pathways, which include base excision repair (BER), nucleotide excision repair (NER), DNA mismatch repair (MMR), homologous recombination repair (HR), non-homologous end joining (NHEJ), and translesion DNA synthesis (TLS) (Broustas & Lieberman, 2014).

1.7.1. DNA damage checkpoint

Cells have developed complex DNA repair systems to address various DNA lesions, allowing them to identify and eliminate specific DNA changes. However, the repair process is integrated into a larger DNA damage response that impacts the entire cell. The initial discovery of how cells respond to DNA damage came from studies on yeast. Researchers found that certain mutant strains of yeast, such as *Saccharomyces cerevisiae* with defects in specific genes (like rad9) or *Schizosaccharomyces pombe* that lacked a functioning protein called wee1, could not stop their cell cycle when DNA damage occurred. This suggests that these mutants are unable to respond correctly to DNA damage, underscoring the significance of these genes and proteins in the process (Weinert & Harwell, 1980; Rowley *et al.*, 1992). The research findings from these studies indicate that the process of cell cycle arrest plays a pivotal role in allowing sufficient time for DNA repair. As a result, DNA damage checkpoints were identified as crucial response mechanisms. Following the initial discovery of DNA damage checkpoints, the number of genes associated with the connection between DNA lesion recognition and cell cycle termination increased. This expansion in understanding provided valuable insights into the intricate mechanisms involved in DNA damage response and cell cycle regulation (Harper & Bartek, 2009). Research has made the maintenance of checkpoint mechanisms from yeast to humans increasingly evident. In metazoans, these mechanisms are complemented by additional DNA damage checkpoint yields, which work in cycles with transient cell cycle termination. The metazoan DNA damage response (DDR) can also lead to programmed cell death and cellular senescence (Jackson & Bartek, 2009). The cellular DNA damage response (DDR) is often affected by mutations in human cancers. The tumour suppressor gene *p53* is the "guardian of the genome" (Lane 1992).

Inactivating mutations in this gene, commonly found in human cancer cells, can significantly disrupt the DNA damage checkpoint response (Lane 1992; Lane & Levine, 2010)

Lane described p53 as the "guardian of the genome". *P53,* a tumour suppressor gene, is the main protection barrier against malignant cell growth (Lane, 1992). *P53* acts as a central node in the *p53* signal transduction pathway, identifying distinct types of oncogenic stress through effector molecules and resulting in appropriate cellular responses that reduce malignant growth. Cell proliferation activities are controlled via *TP53*, which prevents further DNA damage and directly delivers genomic and cellular repair in response to stress. Apoptosis is induced when *p53* is activated. However, when the damage is too severe for repair, an activated *p53* induces senescence to prevent malignant transformation (Efeyan *et al., 2006; Zhang et al.*, 2011). The *ATM* mediates the cellular response to DNA damage through its serine/threonine kinase activity (Bhatti *et al.*, 2011). In response to DNA damage, the *ATM* becomes an active phosphorylated molecule at Ser-1981. Several substrates, including *TP53*, γH2AX, and Chk2, are phosphorylated by an activated *ATM* (Smith *et al*., 2011). For instance, *TP53* is activated by an *ATM*-mediated phosphorylation on serine 15 (Zhang *et al.*, 2011).

1.7.2. Increased frequencies of base pair mutations

Studies on hereditary cancers have shown that a loss of DNA repair genes leads to an increased frequency of base pair mutations. For instance, in a hereditary condition known as MYH-associated polyposis, a mutation in a DNA, the BER gene resulted in an increase in G-C to T-A point mutations or single-nucleotide changes (Al-Tassan *et al*., 2002). This has shown, along with MSI in other types of hereditary DNA damage repair gene mutation, that the loss of genomic integrity can lead to genomic instability and the initiation of tumour growth. It has been suggested that an early step in the development of cancer cells is the expression of a mutator phenotype, characterised by an increase in mutation rates that causes changes in genes contributing to the maintenance of genetic stability (Loeb, 2001).

1.7.3. Microsatellites instability

Microsatellites, also known as Short Tandem Repeats (STRs), are short sequences of DNA consisting of 1-6 base pairs that repeat multiple times and are present throughout the human genome, both in coding and non-coding regions, accounting for approximately 3% of the human genome. Due to their repetitive nature, microsatellites are susceptible to a high mutation rate (Ellegren, 2004). When there is instability in the length of these repetitive DNA sequences in tumour DNA compared to the corresponding germline DNA, it is called MSI. This instability is a molecular phenotype resulting from a defective DNA MMR system. MSI is found in various types of cancers, including sporadic colon, gastric (90% sporadic and 10% hereditary), and endometrial cancer, (both sporadic and inherited forms) (reviewed by: Yamamoto & Imai, 2015). Determining MSI status in colorectal cancer (CRC) has significant implications for prognosis and treatment, as it can help diagnose tumours and reveal their classification (Setaffy and Langner, 2015). MSI has been linked to a better prognosis at each stage of the disease, showing that the high immunogenicity of unstable microsatellites can lead to remarkable effects on tumours through immune system-activating therapies. This has prompted discussions about developing tumour vaccines and converting MSS (microsatellite stability) tumours into MSI to enhance their immunogenicity (Nouri *et al.,* 2018).

1.7.4. Chromosomal instability

CIN is a specific type of genomic instability. CIN can be defined as an increase in the error rate during chromosome separation when the cell is dividing, which causes changes in chromosome number or aneuploidies (Duijf *et al*., 2013; Mitelman *et al*., 2018). In other words, CIN is the faulty segregation of chromosomes during mitosis, resulting in abnormal chromosome numbers (Rao *et al*., 2009). CIN is increasingly recognised as a hallmark of cancer, yet the precise role it plays in cancer development remains unclear. Researchers are actively investigating whether CIN serves as an initiating factor that precedes cancer formation or as a consequence that manifests in later stages of tumour progression. During the critical process of cell division, known as mitosis, chromosomes must be accurately and identically distributed to the daughter cells to preserve genomic stability. This meticulous segregation is pivotal for normal cellular function and organismal health. However, the

consequences can be severe when errors occur during this process, resulting in faulty chromosome segregation. Cells may enter programmed cell death pathways (apoptosis) due to the detection of chromosomal anomalies, or they may escape these pathways and develop malignant characteristics. This aberrant behaviour can lead to tumorigenesis, characterised by uncontrolled cell proliferation and further genomic instability, thereby creating a vicious cycle that complicates the landscape of cancer biology. Understanding the nuances of CIN is crucial for developing effective strategies to target cancers with CIN (Bakhoum *et al*., 2018).

Various techniques can be employed to track CIN and detect the outcomes associated with it. One notable method is fluorescent in situ hybridisation (FISH). This molecular cytogenetic technique allows for the detection of chromosome number abnormalities at the single-cell level (Torres-Ruiz *et al*., 2021). Alternative methods encompass karyotyping, array comparative genomic hybridisation (Array-CGH) (Veltman *et al*., 2002; Shaw-Smith *et al*., 2004), flow cytometry (Arkesteijn et al., 1995), and single-cell sequencing (Vitale *et al*., 2024) to identify alterations in chromosome number or structure, as well as specific tests like the Micronuclei (MN) assay that measure chromosome mis-segregation events over time or among cell groups (Fenech *et al*., 2003). The MN assay will be elaborated upon in the upcoming sections.

Metaphase analysis involves examining chromosomes during the metaphase stage of cell division, allowing researchers to identify structural anomalies and numerical chromosome changes. Conversely, interphase cytogenetic techniques focus on analysing the DNA content and morphological characteristics of interphase nuclei, providing insights into chromosomal abnormalities without requiring cells to be in mitosis. A particularly significant type of nuclear aberration identified in this context is the formation of MN. First discovered over a century ago, MN are small, nucleus-like structures that arise when the nuclear envelope (NE) surrounds lagging chromosomes or chromosome fragments during cell division. These structures typically form when the chromosomes do not properly segregate and are left behind after the cell has completed mitosis or meiosis. As a result, MN persists in the interphase of the cell cycle, as it has failed to be reincorporated into the main nucleus. (Fenech, 2020). As such, the presence of MN in cell cultures provides visual, easily quantifiable evidence of CIN. MN often have defects in their NE, which serves as a barrier to protect the

genome from the cytoplasmic environment and to facilitate proper nucleocytoplasmic transport. When the NE is ruptured, it can lead to damage in the DNA within the MN due to disruptions in DNA replication and repair, as well as exposure of interphase DNA and chromatin to the cytoplasm (Crasta *et al*., 2012; Hatch *et al*., 2013; Zhang *et al.,* 2015).

Factors contributing to chromosome lagging during cell division include defects in centromeres and kinetochores, which play crucial roles in the proper segregation of chromosomes. Additionally, abnormal attachments between kinetochores and microtubule structural filaments that help pull chromosomes apart can disrupt the alignment process. Defects in the assembly of the mitotic spindle, the apparatus responsible for separating sister chromatids, can also lead to complications in chromosome distribution. A recent study has shed light on this issue by investigating human somatic cells and mice that lack a functional kinesin motor protein known as KIF18A. This protein is essential for properly aligning chromosomes along the metaphase plate during mitosis. The study found that in the absence of KIF18A, both human and mouse cells exhibited significant misalignment of chromosomes, which persisted even after mitosis was completed. This misalignment can result in chromosome lagging, ultimately leading to genetic instability and potential developmental issues (Fonseca *et al*., 2019). KIF18A is identified as a promising anticancer target due to its role in mitotic arrest and cell death when knocked down. Volastra Therapeutics, founded in 2020, conducted drug discovery efforts, validating KIF18A through genetic knockdown and pharmacological inhibition. High-throughput screening led to the discovery of an ATP-non-competitive inhibitor, which was optimised for potency and selectivity. Efficacy studies have shown that these lead candidates bind to KIF18A with sub-nm. Potency, exhibit a long drug-target interaction for an extended period, and are selective without off-target effects. Preclinical studies demonstrated oral bioavailability, good tolerance, and tumour regression in mouse models, leaving normal proliferating cells unaffected. The inhibitors show effectiveness across various cancer types, including high-grade serous ovarian, breast, and lung cancers. The research indicates that Volastra has developed potent, selective KIF18A inhibitors as candidates for further clinical development (Zhang *et al*., 2022).

Acentric chromosome fragments are produced when DNA double-strand breaks go unrepaired, which can occur during DNA replication. These fragments lack a centromere and are unstable, compromising genomic integrity. The deregulation of various factors involved in DNA replication and repair has been associated with the formation of MN. An example is the ribonuclease RNase H2, which removes RNA-DNA hybrids. These hybrids can accumulate when dysfunctional, further destabilising the genome and increasing the risk of double-strand breaks. This underscores the complex interplay between DNA replication, repair mechanisms, and chromosomal integrity (Mackenzie *et al.*, 2017; Bartsch *et al.,* 2017). DNA damage response mediator proteins, including mediator of DNA damage checkpoint 1 (MDC1) and topoisomerase 1 binding protein (TOPB1) (Leeimbacher *et al*., 2019).

Improper assembly of nuclei and NE during mitotic exit contributes to MN formation. A recent study has demonstrated that the DNA-binding protein barrier-to-autointegration factor (BAF) plays a crucial role in nuclear formation. BAF organises and maintains a cluster of chromosomes into a single mass, enabling the formation of a single nucleus and preventing or inhibiting micronucleation (Samwer *et al*., 2017).

The presence of MN serves as a valuable biomarker for assessing genotoxic effects and the overall integrity of the genome. As research continues, understanding the mechanisms behind chromosomal aberrations and the role of MN can provide valuable insights into various diseases, including cancer, and contribute to advancements in genetic and epigenetic studies (Fenech, 2020).

The expression of chromosome abnormalities, indicated as MN, requires that nuclear division be completed. However, standard *in vivo* and *in vitro* micronucleus assays do not differentiate between non-dividing and dividing cells and thus become unreliable. This is because the proportion of cells that complete nuclear division is therefore capable of expressing MNi, varying based on factors such as culture conditions, the biological age of the cells, and the cytostatic or proliferative effects of the cytotoxic or genotoxic agent being studied. These factors can delay mitotic progression or induce apoptotic cell death, further complicating the results (Fenech, 2000; Fenech and Morley, 1986). Various methods were attempted to

achieve the MN to be scored efficiently, but the most reliable and widely adopted was the cytokinesis-block technique (Fenech & Morley, 1986)

In the cytokinesis block micronucleus (CBMN) assay, cells that have successfully undergone nuclear division are identified by their binucleated (BN) appearance, following the inhibition of the actin microfilament ring necessary for cytokinesis. This blockade of cytokinesis and the subsequent accumulation of BN cells is typically achieved by treating cell cultures with 3.0–6.0 μg/mL of cyt-B for 24 to 30 hours (Fenech, 2020 a). It is evident that, apart from measuring MN, using CBMN had other advantages, such as blocking cells at the BN stage, which proved to be an effective method for measuring the formation of nucleoplasmic bridges (NPBs). These bridges arise from dicentric chromosomes, which are formed due to several factors, including telomere end fusions, erroneous repair of DNA breaks, or the failure of complete chromatid separation during cell division. By focusing on this specific cell stage, researchers can gain deeper insights into the mechanisms underlying these genetic anomalies and their implications for cellular stability and potentially oncogenesis. (Fenech, 2007; Fenech, 2010; Fenech *et al.*, 2011; Thomas *et al*., 2003; Bull *et al*., 2012).

In BN cells, nuclei exhibit the formation of nuclear buds (NBUDs), which serve as a significant indicator of CIN by which nuclei can actively eliminate amplified genes and unresolved DNA repair complexes. The emergence of NBUDs suggests a response to genomic stress, allowing cells to manage excessive genetic material and facilitate the resolution of DNA damage. By removing these nuclear buds, cells may enhance their viability and maintain genomic stability, thereby playing a crucial role in their overall health and functionality. Understanding the dynamics of NBUD formation can provide valuable insights into the cellular strategies employed to cope with genetic abnormalities and the implications for various diseases, including cancer (Utani *et al*., 2011; Oobatake and Shimizu, 2020; Haaf *et al*, 1999). The MN and NPBs formation due to chromosome missegregation and DNA strand break misrepair are illustrated below in (Figure 1.1) (adapted from Fenech, 2020, a).

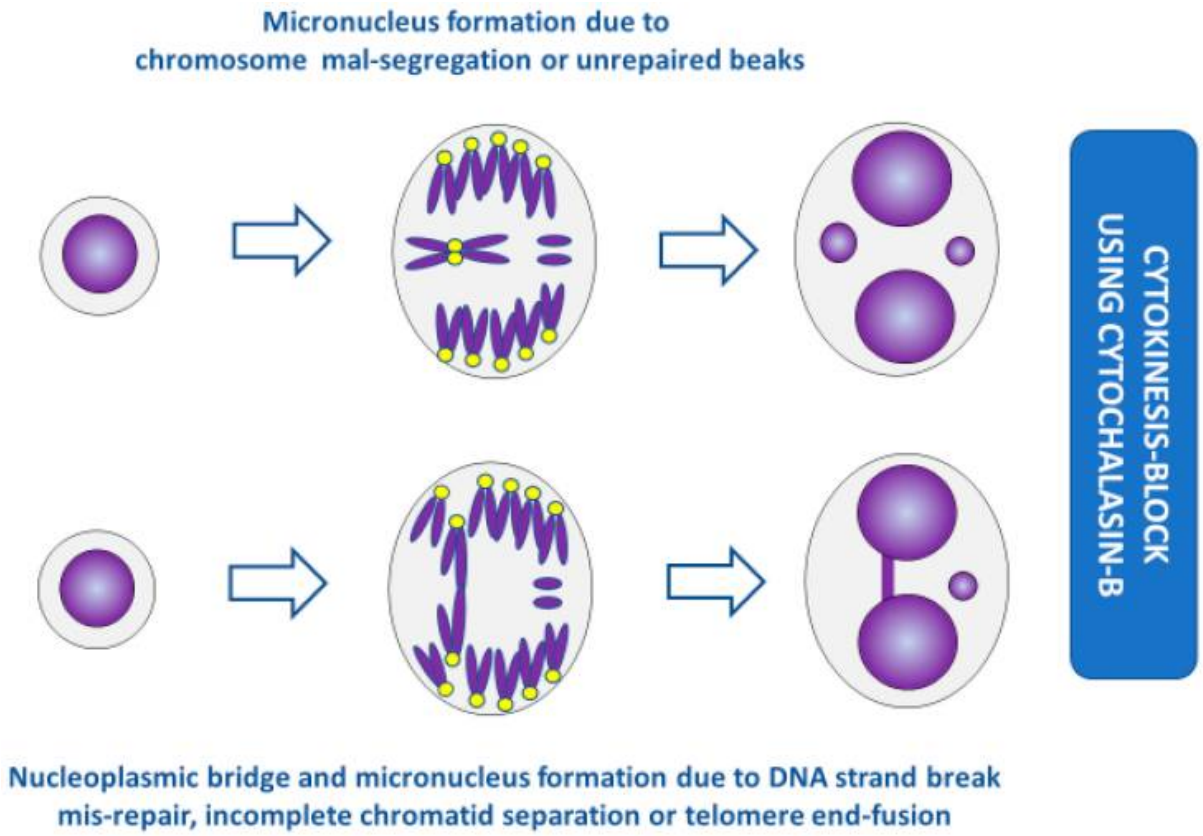

Figure 1.1. MN formation and NPBs due to chromosome missegregation, due to DNA strand break misrepair and incomplete chromatid separation or telomere end fusion from the cytokinesis block using cyt-B (Fenech, 2020, a).

1.7.4.1. Cytochalasin-B mechanisms of action

Derived from the metabolic processes of *Helminthosporium dematioideum* and other fungi (Maclean and Pollard, 1980), cyt-B is the most extensively studied compound in the cytochalasin family regarding its potential use in chemotherapy. Structurally, cyt-B features several highly polar keto and hydroxyl groups and a single hydrophobic benzyl unit positioned peripherally.

Cyt-B has been proposed to function as an inhibitor of actin polymerisation by selectively binding to the fast-growing, or barbed end, of filamentous actin (F-actin). This binding prevents the addition of actin monomers, thereby disrupting the dynamic equilibrium essential for maintaining cytoskeletal integrity and cellular function. Furthermore, cyt-B is known to interact with specific capping proteins, including CAPZA1, which belong to the α-

subunit family of F-actin capping proteins (Maclean and Pollard,1980; Theodoropoulos *et al*., 1994; Flanagan & Lin, 1980; Nishida *et al*., 1983). By inhibiting subsequent processes that follow actin polymerisation, cyt-B disrupts microfilament formation. This inhibition affects all three primary stages of actin polymerisation: nucleation, elongation, and the steady state/annealing phase. Nucleation is crucial for microfilament formation, as this initial oligomerisation acts as the rate-determining step in the polymerisation reaction. Once the processive response is initiated, it continues until the physiological maximum polymerisation rate is reached (Maclean and Pollard, 1980). Cyt-B can inhibit nucleation, preventing any possibility of microfilament formation. Once polymerisation begins, elongation occurs primarily at the barbed end of the growing filament (Kuhn & Pollard, 2025).

The final step in polymerisation is annealing, but cytochalasin potency is reduced compared to its high effectiveness in nucleation and elongation (Maclean and Pollard, 1980; Flanagan & Lin, 1980).

Cyt-B is an inhibitor of cytokinesis that disrupts the actin cytoskeleton and interferes with the formation of the contractile ring and the development of the cleavage furrow. As a result, the cell is unable to divide, leading to the formation of a weakened cytoskeletal network. Furthermore, the cells form nuclei, resulting in an enlarged and multinucleated state. (Trendowski, 2015). Another potent inhibitor is cytochalasin D, which is more effective. However, cyt-B was chosen for this study due to its higher toxicity, and it is a safer option for *in vitro* studies. The mechanisms of action of Cyt-B are illustrated below in (Figure 1.2) (adapted from Trendowski, 2015).

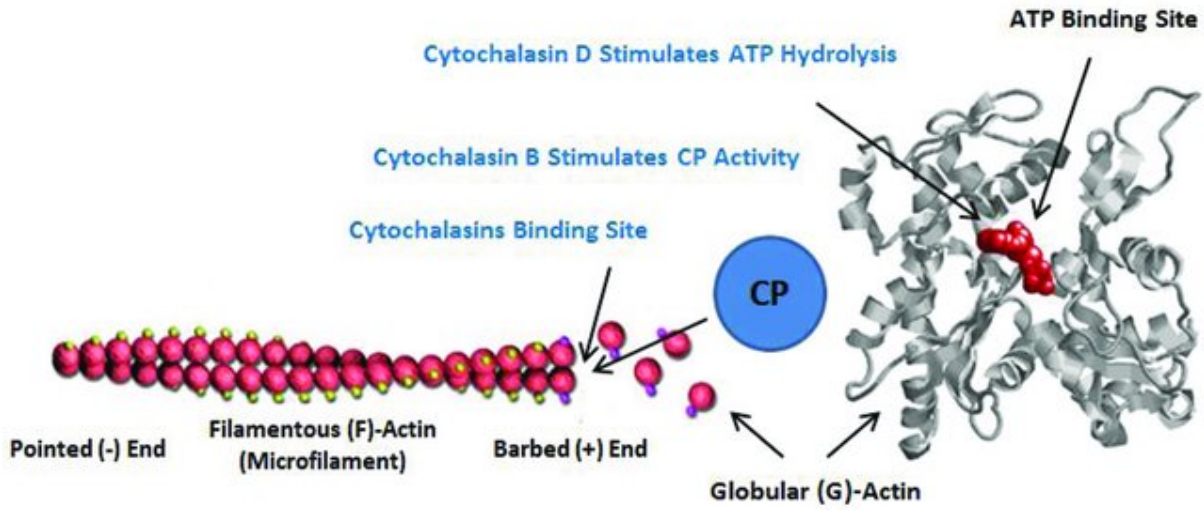

Figure 1.2. The mechanisms of action of cyt-B and D are known to bind to the barbed (+) end of microfilament, inhibiting polymerisation (Trendowski, 2015).

1.7.5. DNA repair pathway

Multiple pathways are activated in response to errors in DNA replication, many of which initiate DNA repair mechanisms. Different processes, such as DNA damage response (DDR) and DNA repair, are linked to recruit and localise different nuclear concentrations of DNA damage, sensors, mediators, transducers, and effector proteins (Polo & Jackson, 2011). DNA damage repair mechanisms such as NER, BER, MMR, and DNA double-strand break repair (DSBR) are activated intracellularly in response to DNA damage.

1.7.6. Nucleotide excision repair

The NER comprises more than 25 proteins that interplay to substitute incorrect nucleotides with the correct ones (Mitchel *et al*., 2003). The NER system repairs DNA damage caused by environmental insults, such as ultraviolet (UV) radiation, exogenous chemicals like benzopyrene and aflatoxin B1, and chemotherapeutic compounds like cisplatin. The first step in the NER process is the recognition of the damaged site on the DNA, followed by the excision of the damaged DNA strand, synthesis of the new DNA, and the separation of the sides, which are then ligated via specific ligase enzymes (Mitchel *et al.*, 2003). Three different NER pathways are also known, such as global genomic repair (GGR), transcription-coupled repair

(TCR), and differentiation-associated repair (DAR) (Nouspikel *et al*., 2006). The GGR's role is to repair all damaged sites in the whole genome. The TCR removes the damage that inhibits the transcription process of expressed genes (Tornaletti & Hanawalt, 1999). All these NER pathways are significantly crucial for repairing DNA damage. It has been found that NER-associated proteins are correlated with disorders such as xeroderma pigmentosum, Cockayne's syndrome, trichothiodystrophy, and other types of cancer (Lindahl, 1974; de Boer & Hoeijmakers, 2000).

1.7.7. Base excision repair

The BER pathway is a crucial cellular mechanism that functions to rectify damaged DNA by specifically replacing modified bases. These modifications can arise from various biochemical processes, including deamination, methylation, and oxidation, all of which compromise the integrity of the genetic material (Lindah, 1974). The repair begins with recognising the altered bases by specialised enzymes known as DNA glycosylases. These glycosylases are adapted to identify and bind to the damaged site, and they catalyse the removal of the modified base, resulting in the creation of apurinic or apyrimidinic sites—locations within the DNA where the base is missing.

Once the damaged base has been excised, the BER pathway's next step involves synthesising the correct nucleotide to fill the gap. This is achieved by polymerase delta or epsilon, which synthesises new DNA strands by incorporating the appropriate nucleotide complementary to the undamaged DNA strand.

Finally, to restore the continuity of the DNA strand, the free ends created by synthesising the new nucleotide are joined together by ligase enzymes. These ligases catalyse the formation of phosphodiester bonds between adjacent nucleotides, thereby sealing the repair and ensuring the stability of the DNA molecule (Jaroudi & Sengupta, 2007). This intricate process highlights the precision and efficiency with which cells can maintain genomic integrity in the face of various types of DNA damage.

1.7.8. Mismatch repair

The DNA MMR system is a critical biological process responsible for identifying and correcting errors in DNA that occur during the complex processes of replication and recombination. These errors can manifest as incorrect insertions, deletions, or mismatched nucleotide bases, which may escape detection during the initial proofreading phase carried out by DNA polymerases (Jiricny, 2006). If left uncorrected, these errors can lead to mutations that compromise the genome's integrity and stability, potentially resulting in diseases, including cancer.

The MMR system is conserved across various species, highlighting its fundamental importance in cellular biology. In prokaryotes, such as bacteria, the primary proteins facilitating this repair process are Mutator S and L (MutS and MutL). MutS functions by recognising and binding to mismatched bases in the DNA, effectively identifying the error. Once the mismatch is recognised, MutL is recruited to direct the repair process, which involves excising the section of DNA containing the error and synthesising the correct sequence using the complementary strand as a template.

The MMR system operates through analogous mechanisms in eukaryotic organisms, including humans. Still, it involves a different set of proteins, such as MLH1, MSH2, MSH6, and PMS2—essential players that ensure the fidelity of DNA replication. The presence of these repair mechanisms underscores the MMR system's evolutionary significance in preserving genome stability and preventing the accumulation of potentially harmful mutations (Hsieh and Yamane, 2008). The DNA MMR system is indispensable for safeguarding genetic information and maintaining organismal health across diverse life forms.

The analysis of gene expression profiles in human cancers has provided a significant understanding of the abnormal expression patterns of genes involved in various tumour-related functions such as cell adhesion, migration, angiogenesis, and kinase activation. It is well established that DNA repair genes play a crucial role in initiating tumorigenesis and that deficiencies in these genes can lead to cancer. However, the direct involvement of DNA repair and cell cycle checkpoint proteins in metastasis development remains inconclusive. The

association of DNA repair genes with metastasis has been primarily suggested through DNA gene expression microarray analyses, serving as proxies for *in vivo* metastasis phenotypes.

As tumours develop, specific genes are downregulated while others are upregulated, influencing the ability of cancer cells to spread to other parts of the body.

1.8. Apoptosis

The concept that apoptosis serves as a protective mechanism against cancer was first proposed in 1972. It indicates that apoptosis occurs in rapidly growing cells and hormone-dependent tumours following the withdrawal of hormones (Kerr *et al*., 1972). Their observations highlighted the potential role of programmed cell death in regulating cell populations and preventing the accumulation of damaged cells that could contribute to cancer development.

The identification of the B-cell lymphoma *(BCL-2)* oncogene, first observed through its upregulation resulting from chromosomal translocation in cases of follicular lymphoma (Korsmeyer 1992), marked a significant turning point in the exploration of apoptosis in cancer biology. Subsequent studies revealed that the *BCL-2* gene possesses intrinsic antiapoptotic properties (Vaux *et al*., 1988). This crucial finding initiated a deeper investigation into how apoptosis operates at the molecular level in cancer.

The growth of tumour cells depends on how quickly they divide and how many die. One major significance of cell death is through a process known as programmed cell death, also called apoptosis. Research from mouse studies, lab-grown cells, and analysis of human biopsies shows that the ability to resist apoptosis is a characteristic of most types of cancer (Hanahan and Weinberg, 2000). This process results from a series of physiological signals, revealing the disruption of cellular membranes, damage to cytoplasmic and nuclear scaffolds, extrusion of the cytosol, degradation of chromosomes, and fragmentation within 2 hours. Within 24 hours, these broken cells are engulfed by nearby cells in a tissue and disappear (Wyllie *et al.,* 1987).

The mechanisms involved in apoptosis are known as sensors and effectors. Sensors play a crucial role in assessing the extracellular and intracellular environments to determine whether a cell should live or die. These sensors regulate the second category of components, which act as the effectors of apoptotic death. These sensors are cell-surface receptors that interact with survival or death factors. Notable examples of these ligand-receptor interactions include the survival signals transmitted by IGF-1 and IGF-2 through their receptor, IGF-1R, as well as signals from IL-3 and its corresponding receptor, IL-3R (Lotem and Sachs, 1996; Butt *et a*l., 1999). Cell death is activated when FAS ligands, also known as CD95 or APO-1, interact with their receptors, and by tumour necrosis factor (TNF-α) binding to TNF-R1 (Ashkenazi and Dixit, 1999). Intracellular sensors determine the health of a cell, which can identify and activate death pathways when DNA is damaged, compromising genetic integrity.

Additionally, imbalances in cellular signalling pathways can be caused by the activation of oncogenes that drive uncontrolled cell proliferation, insufficient survival factors that support cell growth and maintenance, and hypoxia. By initiating cell death in these scenarios, the body can eliminate potentially damaged or dysfunctional cells, thereby maintaining overall cellular homeostasis and preventing the development of diseases such as cancer (Evan & Littlewood, 1998). Apoptosis is triggered by responding to proapoptotic signals in the mitochondria, which involves the release of cytochrome C, a potent catalyst of apoptosis (Green and Reed 1998).

The *BCL-2* family of proteins includes both proapoptotic members (such as BAX, BAK, BID, and BIM) and antiapoptotic members (like *BCL-2, BCL-XL*, and *BCL*-W), which cooperatively regulate apoptosis. Proapoptotic proteins promote cell death by facilitating the release of cytochrome C from the mitochondria, while antiapoptotic proteins help prevent this process. The tumour suppressor protein *p53* is critical in responding to DNA damage by upregulating Bax. Increased Bax levels enhance mitochondrial membrane permeability, leading to the release of cytochrome c. This event activates caspases, a family of proteases that serve as the final effectors of apoptosis. These caspases, once activated, orchestrate the dismantling of cellular components, ensuring a regulated process of cell death that maintains tissue homeostasis (Thornberry and Lazebnik, 1998). *Caspase-8* is activated through death receptors, such as FAS, located on the cell surface. In contrast, *caspase-9* is activated by

cytochrome C released from the mitochondria, as these proximal caspases initiate a cascade that activates various effector caspases. These effector caspases execute the cell death program by dismantling critical subcellular structures, organelles, and genome components.

In transgenic mouse models engineered to co-express the *BCL-2* gene alongside the MYC oncogene, it was observed that the *BCL-2* gene played a crucial role in facilitating the development of *BCL2*. This was achieved not by promoting the proliferation of lymphocytes, which was primarily driven by the MYC oncogene, but rather by enhancing the survival rates of these cells. By prolonging the lifespan of lymphocytes, the *BCL-2* gene effectively contributed to the accumulation of these cells, leading to the emergence of lymphomas. This interaction between *BCL-2* and *MYC* emphasises the complex regulatory mechanisms involved in tumorigenesis and the progression of haematological malignancies. (Strasser *et al*., 1990). Among the limited cases of lymphoma observed in *BCL-2* single transgenic mice, 50% exhibited somatic translocations that led to the exchange of genetic material and chromosomes. Notably, these translocations activated the c-MYC oncogene. This indicates that there is selective pressure favouring their evolution during the lymphomagenesis process to upregulate both *BCL-2* and c-MYC (McDonnell & Korsmeyer, 1991).

A more detailed exploration of the complex interaction between the *MYC* and *BCL-2* oncogenes has been clarified by research focusing on fibroblasts cultured under low-serum conditions. In these specific experimental settings, fibroblasts that express the *MYC* oncogene are subject to significant levels of apoptosis. This apoptotic response can be effectively contradicted by introducing various extrinsic survival factors. For example, the addition of insulin-like growth factor 1 (IGF-1), which is known to promote cell survival and growth, has been shown to prevent cell death in these MYC-expressing fibroblasts. The forced overexpression of *BCL-2* or its homolog *BCL-XL* can protect these cells from undergoing apoptosis.

Furthermore, disruptions to the death-signalling pathways typically activated by the FAS receptor can reduce the apoptotic response observed in MYC-expressing cells under low serum conditions. These findings highlight the crucial role of both MYC and *BCL-2* in regulating cell survival and apoptosis in fibroblast populations (Hueber *et al*. 1997).

This concept is further reinforced by additional research demonstrating that apoptosis is a formidable barrier to cancer development. For instance, in a transgenic mouse model where the retinoblastoma tumour suppressor, also known as pRb, was functionally inactivated in the choroid plexus—a network of blood vessels in the brain—the resultant slow-growing microscopic tumours exhibited significantly high apoptotic rates. However, when the *p53* tumour suppressor, another key regulator of apoptotic signalling, was also inactivated, the tumours grew more rapidly and displayed markedly fewer apoptotic cells (Symonds *et al*. 1994). Furthermore, studies on transgenic mice influenced by pancreatic islet tumours illustrated the role of extracellular survival signals. Knockout of the Insulin-like Growth Factor (IGF-2) gene, which is implicated in this tumorigenic pathway, reduced tumour growth and progression. The tumours that did arise were comparatively small, benign, and exhibited high apoptotic rates, reinforcing IGF-2's classification as an antiapoptotic survival factor (Christofori *et al*. 1994).

Cancer cells can develop resistance to apoptosis through various mechanisms, with one of the most prevalent being the mutation-induced loss of proapoptotic regulators, particularly the *p53* tumour suppressor gene. The functional inactivation of *p53*, occurring in more than 50% of human cancers, removes a crucial component of the cellular DNA damage response that can initiate the apoptotic cascade (Harris, 1996). Additionally, other cellular stress signals, such as hypoxia and oncogene hyperexpression, are partly mediated through *p53* to activate apoptotic pathways; therefore, loss of *p53* function disrupts the cell's ability to respond effectively (Levine, 1997). Furthermore, the PI3K–AKT/PKB signalling pathway has emerged as another critical player in resistance to apoptosis in many cancers. This pathway transmits antiapoptotic signals and can be stimulated by external factors, including IGF-1/2 or interleukin-3 (IL-3) (Evan & Littlewood, 1998), or by signals generated from Ras (Downward, 1998).

Almost all cancer cells exhibit specific adaptations that enable them to evade programmed cell death, or apoptosis, presenting significant challenges for effective cancer treatment. As research advances, scientists gain a deeper understanding of the intricate and often incomplete apoptotic signalling network that regulates cell death. This network comprises multiple components, many of which exist in redundant forms, meaning alternative pathways

can be activated when one route is disrupted. These redundancies have essential implications for developing novel antitumor therapies, as they suggest that tumour cells, which may have lost specific pro-apoptotic proteins, can still rely on others that serve similar functions to maintain specific apoptotic processes. For example, if a tumour cell loses a key protein that typically promotes apoptosis, it may still possess other proteins that can compensate for that loss, thereby allowing the cell to survive and proliferate. As technology evolves, scientists can more precisely map out the operative apoptotic pathways in different cancer types. This capability would enable researchers to identify which components of the apoptotic machinery are still functional in various cancers. By restoring the ability of cancer cells to undergo apoptosis, these new interventions could significantly improve treatment outcomes and efficacy in combating this complex disease (Hananan & Weinberg, 2000).

1.9. The process of metastasis

Metastasis is a hallmark of cancer that involves numerous interactions within the tumour microenvironment, including the transient transformation of epithelial cellular characteristics into those of migratory and invasive cells through the process of EMT described above (Kallury & Weinberg, 2009). Invasion through the ECM is followed by trans-endothelial migration of cancer cells through the basement membrane and into the lymphatics and blood vessels, in a process known as intravasation. Additionally, metastasis involves the detachment of tumour cells, invasion or intravasation through circulation, survival in the circulatory system, extravasation, and consequent proliferation in organs at distant sites (Eger & Mikulits, 2005). The mechanism of cell invasion in tumour cells into surrounding tissues is achieved by migrating sheets of detached tumour cells or as single cells, via mesenchymal or amoeboid cell types (Fried & Wolf, 2003). During cancer development, morphological and phenotypic alterations occur, including changes in the plasticity of tumour cells, such as EMT (Thiery *et al.*, 2009). Collective cell invasion, characterised by cell-cell interactions, remains intact during cellular movement (Fried *et al*., 2004). Cellular migration involves remodelling the ECM and restructuring the basement membrane (Wolf *et al*., 2007). About 90% of patient deaths occur due to circumstances from recurrent or metastatic disease (Chaffer & Weinberg, 2011). Metastatic organotropism refers to the distribution of distant metastases to other organs (Lu & Kang, 2007). Cancer subtypes, as well as the molecular characteristics of tumour cells, the

host immune microenvironment, and cell-cell communication, are implicated in metastatic processes (Chen *et al*., 2018). In breast cancer, the organs that are most likely to metastasise distantly are the bone, brain, liver, lung, and distant lymph nodes (Yates *et al.*, 2017). Different cell adhesion molecules that play a role in metastasis include selectins and integrins, two crucial families (Witz, 2008; Desgrosellier & Cheresh, 2010). In selectin-mediated tumour cells, adhesion molecules play a role in metastasis, while integrins contribute further to tumour development by interacting with both tumour cells and surrounding tissue (Bendas & Borsig, 2012). It is vital to develop 3D multicellular culture models and to understand how this early invasive process works, thereby providing more answers for cancer research.

1.10. Glycosylation

Glycosylation is the most common post-translational modification (PTM) in eukaryotic proteins (Apweiler *et al*., 1999). Compared to glycation, a non-enzymatic process, glycosylation is an enzymatic attachment and removal of carbohydrate (sugar) residues from proteins, most commonly N-linked and O-linked (Lis and Sharon, 1993; Markiv, Rambaruth and Dwek, 2012). The role of glycosylation includes regulating protein folding (Walsh *et al*., 1990) and cell-to-cell communication (Lasky, 1992). Glycosylated proteins are protected from enzymatic degradation (Homans & Dwek, 1987), and glycosylation is also a mechanism by which signals are conducted through cells, the signal transduction pathways (Haltiwanger & Stanley, 2002). Significantly, protein glycosylation is regulated depending on the species, tissue and cell type. There is much potential for treating various cancers due to observing disrupted glycosylation pathways or targeting glycan moieties themselves (Markiv *et al*., 2012).

Glycan structures can influence the biology of a cell, even though small changes in structure (Varki, 2017). Tumour development is correlated with changes in glycosylation, making glycoproteins useful as serological cancer biomarkers; these are used in clinical applications, such as cancer antigens (e.g., CA19-9 and CA72-4), which serve as tumour markers. Many cancer biomarkers are glycoproteins (Adamczyk *et al*., 2013), and some in clinical use include CA125, CA15-3, carcinoembryonic antigen (CEA), prostate-specific antigen (PSA), and a fucosylated form of α-fetoprotein used in hepatocellular carcinoma screening (Korekane *et*

al., 2012). These biomarkers are specific glycoproteins that have been used extensively over the last decade in cancer research. Incorporating cancer biomarkers into cancer care has transformed treatment approaches, leading to significant advances in cancer therapies and improved patient outcomes (reviewed by Passaro *et al*., 2024). Specific biomarkers such as CEA, CA-125 and PSA continue to have clinical application, commonly used to evaluate cancer prognosis, monitor treatment response, and detect disease recurrence (reviewed by Pal *et al*., 2022).

Cancer-associated glycoforms and glycosyltransferase/glycosidase activities involved in glycan synthesis offer significant potential for breast cancer drug discovery. Recent developments in methodologies for studying breast cancer and glycosylation offer potential for drug discovery, such as the development of specific inhibitors (Lavanya *et al*., 2014) and monoclonal antibodies (MBAs) (Sharkey & Goldenberg, 2006). An example is immunotherapy such as Pembrolizumab, a checkpoint inhibitor that blocks PD-1 on T cells, targeting tumours with a biomarker known as MSI-H. Regardless of whether the cancer is in the colon, uterus, or stomach, these drugs unmask the cancer cells so the body's immune system can destroy them (Brlek *et al*., 2025). There is more room to discover and develop biomarkers that can improve the detection and diagnosis of breast cancer by delivering increased specificity and sensitivity, and thus determining a specific treatment for precision medicine. Current treatment methods offer advantages for cancer patients; however, they also have limitations, such as applicability only to specific patient groups or the development of therapy resistance (Costa *et al*., 2020). Researchers examined the parent compound, kifunensine, alongside novel hydrophobic acylated derivatives designed to enhance cellular uptake. They treated primary mouse and human B cells with kifunensine and its newly developed acylated derivatives, such as JDW-II-004 and JDW-II-010. These targeted inhibitors effectively blocked Type I mannosidases, resulting in a dose-dependent increase in the formation of high-mannose N-glycans. Notably, the acylated derivatives demonstrated greater potency than the parent drug. Treatment with these inhibitors significantly impaired B-cell receptor signalling in primary mouse B cells. This impairment was accompanied by observable changes in surface receptors, including increased levels of CD79b and decreased levels of CD19 (Huang *et al*., 2022). Kifunensine is utilised to stimulate cells to generate uniformly high-mannose N-glycans. In the field of oncology, it is extensively employed in glycoengineering to create

afucosylated monoclonal antibodies (such as rituximab) that possess significantly improved abilities to kill cancer cells (Huang *et al*., 2022). A study investigated the effects of kifunensine on primary human NK cells and cultured YTS-CD16a cells. Kifunensine is a compound that interrupts the normal maturation of N-glycans, causing the cells to retain simpler, oligomannose-type N-glycans on their surface. The researchers then assessed the treated NK cells to evaluate changes in their antibody-binding affinity and their ability to trigger Antibody-Dependent Cell-Mediated Cytotoxicity (ADCC). Inhibition of N-glycan processing increased the antibody-binding affinity of the CD16a receptor on the NK cell surface. Additionally, the treated NK cells demonstrated a twofold increase in their ADCC effector function (Rodriguez Benavente *et al*., 2023).

There is also information on castanospermine in this section that mentions recent research study revealing that a synthetic analogue C-2 fluorinated used on castanospermine, which is originally an indolizidine alkaloid that was initially extracted from the seeds of Castanospermum australe (Hohenschutz *et al*., 1981). It is a potent inhibitor of α- and β-glucosidase (Saul *et al*., 1985). By introducing a fluorine atom at the C-2 position, researchers solved a major drawback of natural castanospermine, which is its lack of selectivity, meaning it blocks different glucosidase enzymes rather than targeting just one specific type, which limit its clinical use. Castanospermine also inhibits β-glucosidases; the C-2 fluorinated versions successfully narrowed this down to targeting α-glucosidases. Molecular docking revealed that C-2 fluorination maintains active site binding, whereas C-1 and 1-epi modifications disrupt crucial hydrogen bonding with residues such as Arg-526 and Asp-327 (Li *et al*., 2025). Castanospermine, an inhibitor of α-glucosidase, was categorised as a lysosomal storage disorder, characterised by the buildup of glycogen, particularly in muscle tissue, and this effect was reproduced in rats treated with castanospermine at 1.5–2.0 mg/g body weight (Saul *et al*., 1985).

The antibiotic Tunicamycin (TM) is a nucleoside antibiotic inhibitor that targets N-linked glycosylation and has been shown to have potential for delaying tumour growth and overcoming multidrug resistance. TM obstructs the transfer of UDP-N-acetylglucosamine (GlcNAc) to dolichol phosphate within the endoplasmic reticulum (ER), thus interfering with protein maturation by halting the biosynthesis of oligosaccharides (Wu *et al*., 2018). The

inhibition of this process leads to an unfolded protein response (UPR) and cellular stress, which can ultimately cause cell death or apoptosis through various signalling pathways which may involve the activation of the kinase activity of mTORC1, which mainly regulates cell growth and metabolism by the presence of high levels of gene nitric oxide synthase (eNOS) through the RagC pathway (Guha *et al*., 2017), and tumor necrosis nactor related apoptosis-inducing ligand (TRAIL)-induced pathway leading to cell death or apoptosis (Jung *et al*., 2012). Researchers studying dolichyl-phosphate N-acetylglucosamine-phosphotransferase 1 (DPAGT1) targeted inhibition with Tunicamycin, an antibiotic, identified that selective nucleoside-based compounds can inhibit N-glycan biosynthesis, offering a potent, low-toxicity approach against solid cancer cells. This study indicates that targeting this specific enzyme provides a new therapeutic window to treat solid tumours without the severe, non-selective damage caused by broader glycosylation inhibitors (Kurosu, 2018)

The therapeutic potential of TM in breast cancer treatment is significant. Various preclinical studies indicate that TM may serve as an effective drug for managing metastatic breast cancer, as it has been found to inhibit the growth and spread of breast cancer by regulating the Akt/NF-kB signalling pathway, which is involved in regulating cell survival, proliferation, and inflammation (Wang, 2018). Additionally, TM appears to enhance the antitumour effects of trastuzumab, also known as Herceptin, highlighting the potential benefits of combining TM with trastuzumab to boost the clinical effectiveness of trastuzumab in breast cancer treatment (Han *et al*., 2015). In other studies, it was shown that inhibition of protein glycosylation reversed the multidrug resistance (MDR) phenotype in cancer cell lines as a result of TM blocking the first step of glycoprotein P and breast cancer resistance protein, NLG by allowing more absorption of anticancer drugs such as doxorubicin, Paclitaxel, and topotecan. Thus, the cytotoxicity effect of cancer cells increases (Wojtowicz *et al*., 2015).

Despite TM efficacy *in vitro*, inhibiting NLG is not specific to particular cell types. Using this approach in cancer therapy could be risky, as it may lead to harmful effects on adjacent healthy tissues or organs, potentially exacerbating the disease. However, nanocarriers could offer a promising solution to reduce the cytotoxic effects of this drug (Banerjee *et a*l., 2024). This will be discussed in more detail in the glycosidase inhibition (section 1.10.5), as well as the use of TM with other inhibitor compounds such as 1-Deoxynojirimycin (DNJ) on

iminosugars (Section 1.10.6) and swainsonine. The representation of N-linked and O-linked glycan structures is attached to nitrogen and oxygen, respectively, and the three major types of N-glycans that arise from NLG are illustrated below in (Figure 1.3) (adapted from Reily *et al*., 2019).

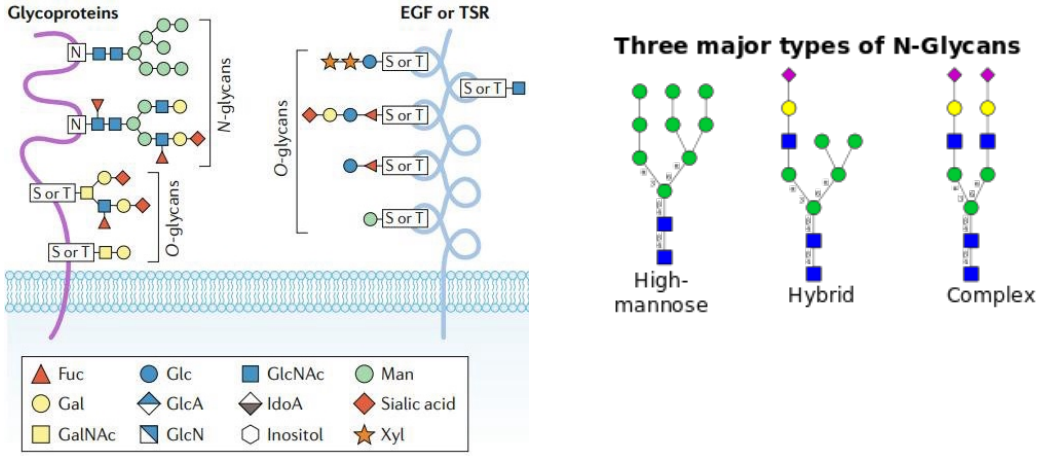

Figure 1.3. Representation of glycoproteins and their type. O-linked glycoproteins attach to serine and threonine residues through oxygen atoms, while N-linked glycoproteins attach to a nitrogen atom through asparagine residues. The major types of N-glycans result from the cleavage by glycosidases to form high mannose glycoproteins, and to further facilitate the synthesis of carbohydrate-modifying enzymes such as glycosyltransferase to form hybrid and complex glycoproteins (Reily *et al*., 2019).

1.10.1. N-linked glycosylation

The glycosylation process for N-linked glycans commences in the endoplasmic reticulum/Golgi apparatus, the organelles in which the carbohydrate structures are formed by glycosyltransferase and glycosidase enzymes (Pinho & Reis, 2015; Varki, 2017). NLG is a process that has been extensively investigated; it involves the attachment of monosaccharides to the polypeptide chain via a β linkage between GlcNAc and asparagine at the sequon Asn-X-Ser/Thr. The NLG process commences in the endoplasmic reticulum, where the role of chaperone molecules, calnexin and calreticulin, is to achieve protein folding. This process is known as protein transport during translation (a co-translational event). Subsequently, specific glycosidases cleave the glycan chain, and proteins that achieve correct

folding are delivered to the Golgi apparatus for additional PTMs (reviewed by Markiv *et al*., 2012). The biosynthesis of glycans is primarily determined by the glycosyltransferases (GTase) that assemble monosaccharide moieties into linear and branched glycan chains (Rini *et al*., 2022). In the context of glycan processing, information about galactosyltransferases is important, as they are part of the glycosyltransferases (GTases) that do not degrade glycans like glycosidases but instead synthesize them. GTases are enzymes that catalyse the formation of a covalent bond, known as glycosidic linkages, between a sugar molecule and another group by transferring a monosaccharide from a donor substrate to an acceptor substrate (Lairson *et al*., 2008; Weadge & Palcic, 2008). Acceptors can include other saccharides, proteins, lipids, nucleic acids, natural products, and synthetic products, making GTase the most chemically diverse enzyme class in terms of substrates and products (Palcic, 2011).

Glycosyltransferases catalyse their reactions with either inversion or retention of stereochemistry at the anomeric carbon of the donor substrate. For instance, β1–4 galactosyltransferase, an inverting glycosyltransferase, transfers galactose from UDP-α-Gal (with the exception of cytidine monophosphate-sialic acid and cytidine monophosphate-3-deoxy-D-manno-octulosonic acid, naturally occurring nucleotide sugars are typically α-linked) to produce a β1-4-linked galactose-containing product. The inversion of stereochemistry occurs because the enzyme employs an S_N2 (substitution nucleophilic bimolecular) reaction mechanism, in which an acceptor hydroxyl group attacks the anomeric carbon atom from one side while UDP departs from the opposite side. GTase reactions are typically stereospecific and regiospecific, allowing them to transfer the sugar with either retention or inversion of configuration at the anomeric carbon (Rini *et al*., 2022). A retaining galactosyltransferase is an enzyme that transfers a galactose sugar from an activated donor to an acceptor molecule while retaining the original anomeric (spatial) configuration of the bond, thus retaining the linked structures (Persson *et al*., 2001).

There are different types of galactosyltransferases, which include inverting galactosyltransferases such as β1-4- (β4Gal-T), β1-3- (β3Gal-T), and β1-6- (β6Gal-T), as well as retaining galactosyltransferases like α1-3- (α3-Gal-T) and α1-4-(α4Gal-T). These enzymes use UDP-α-D-Gal as the sugar donor and create β1-4-, β1-3-, β1-6-, α1-3-, and α1-4-linkages,

respectively. Each type of galactosyltransferase has several members. For example, the β4Gal-T group comprises at least seven members, designated as Gal-T1 to Gal-T7. Enzyme classification is based on the donor used, the position, and the stereochemistry of transfer (Palcic, 2011; Amado *et al*., 1999; Hennet, 2002). The most used and commercially available for over thirty years as a biocatalyst is bovine milk β1,4-galactosyltransferase (β1,4-GalT), which catalyses the transfer of galactose (Gal) from uridine diphosphate α-D galactose (UDP-Gal) to the 4-OH group of terminal GlcNAc acceptors, resulting in the formation of Galβ1-4GlcNAc-R (N-acetyl galactosamine, LacNAc) structures found on mammalian cell surfaces (Vasiliu *et al*., 2006).

Several investigations into the β1-6 branching of NLG have been conducted in breast and colon cancer (Dennis *et al*., 1999). This alteration is associated with the uncontrolled growth and invasion of cancer cells. A decrease in cancer cell metastasis *in vivo* was observed when mannosidase was inhibited with swainsonine. Clinical investigations for metastatic cancer were carried out to study swainsonine as a treatment for late-stage cancer patients, but this showed toxicity, and improved techniques have been proposed since (Markiv *et al*., 2012). The enzymatic action of α-1,6-mannosyltransferase creates the β1-6 branched oligosaccharide structure. This process involves the activity of the β-6 N-acetylglucosaminyltransferase (MGAT5) (Dennis *et al*., 1999). Significantly, the activity of MGAT5 is regulated by the RAS-RAF-MAPK kinase cell signalling pathway. An experimental study utilised tunicamycin to suppress NLG, decreasing cell surface receptor tyrosine kinases (RTKs) EGFR (ErbB2/ErbB3), IGFR-1, and MET. This observation, as reported by Contessa *et al*. in 2010, indicated that NLG plays a role in modulating various cancer-associated glycoproteins.

Tumour cells can induce both structural and functional changes across various cellular compartments. Modifications in glycosidase processing enzymes in other recent studies have shown that SKBR-3 and MCF-7 cell lines, when subjected to tunicamycin treatment, resulted in enhanced sensitivity to Herceptin (Peiris *et al*., 2017). This increased responsiveness was associated with greater cell cycle arrest and heightened levels of cellular apoptosis (Han *et al*., 2015). Furthermore, tunicamycin treatment of SKBR-3 cells resulted in a diminished response to the growth factor IGF-1, both independently and in conjunction with EGF (Peiris

et al., 2017). This reduction may be attributed to impaired IGFR-R1 functionality following deglycosylation, as documented in previous research (Girnita *et al*., 2000).

Additionally, it was observed that treating SKBR-3 cells with tunicamycin increased their sensitivity to the cancer drug doxorubicin. This study suggested that targeting glycosylation could be a strategy to make cancer cells more responsive to treatment (Peiris *et al.,* 2017). Recent research has revealed that SGK196, an O-mannose kinase responsible for phosphorylation, plays a significant role in altering N-glycosylation in breast cancer cells. Moreover, both gain and loss-of-function analyses indicated that N-glycosylated SGK196 inhibits cell migration, invasion, and metastasis in BC, especially in the basal-like breast cancer subtype. BT-549 and MDA-MB-231 cells were deployed in this study. It was discovered that N-glycosylation of SGK196 exerts regulatory effects via the PI3K/AKT/GSK3β signalling pathway. Thus, N-glycosylated SGK196 has a suppressive effect on basal-like breast cancer metastasis, offering new insights into its role in breast cancer (Xu *et al.,* 2020).

During synthesis of N-linked glycoproteins, the initial sugars are linked to a dolichol intermediate, which transfers them as a complete unit to the protein (Struck & Lennarz, 1980). The oligosaccharide chains consist of multiple glucose units that are either removed or processed by membrane-bound neutral glucosidases in the ER. The core mannose residues may be phosphorylated, removed, or extended with additional sugars depending on the specific protein. Phosphorylated core mannose residues serve as recognition signals that direct acid hydrolases to lysosomes (Kaplan *et al*., 1977; Gonzalez-Noriega *et al*., 1980; Farquhar, 1983).

Research shows that a membrane-associated mannose-6-phosphate (mannose-6-P) lectin attaches to newly formed lysosomal enzymes that possess mannose-6-P. This complex subsequently branches off from the Golgi-endoplasmic reticulum-lysosome (GERL) membrane system to create vesicles that transport hydrolases to lysosomes. Additionally, membrane-bound mannosidases can eliminate mannose residues from other glycoproteins. The oligosaccharide chains of these glycoproteins can also be lengthened by incorporating GlcNAc, GAL, and sialic acid, facilitated by glycosyltransferases in the Golgi apparatus, before these proteins are either integrated into the plasma membrane or released into the

extracellular environment (Schachter & Roseman, 1980). The N-linked glycosylation pathway is illustrated below in (Figure 1.4) (adapted from Reily *et al*., (2019).

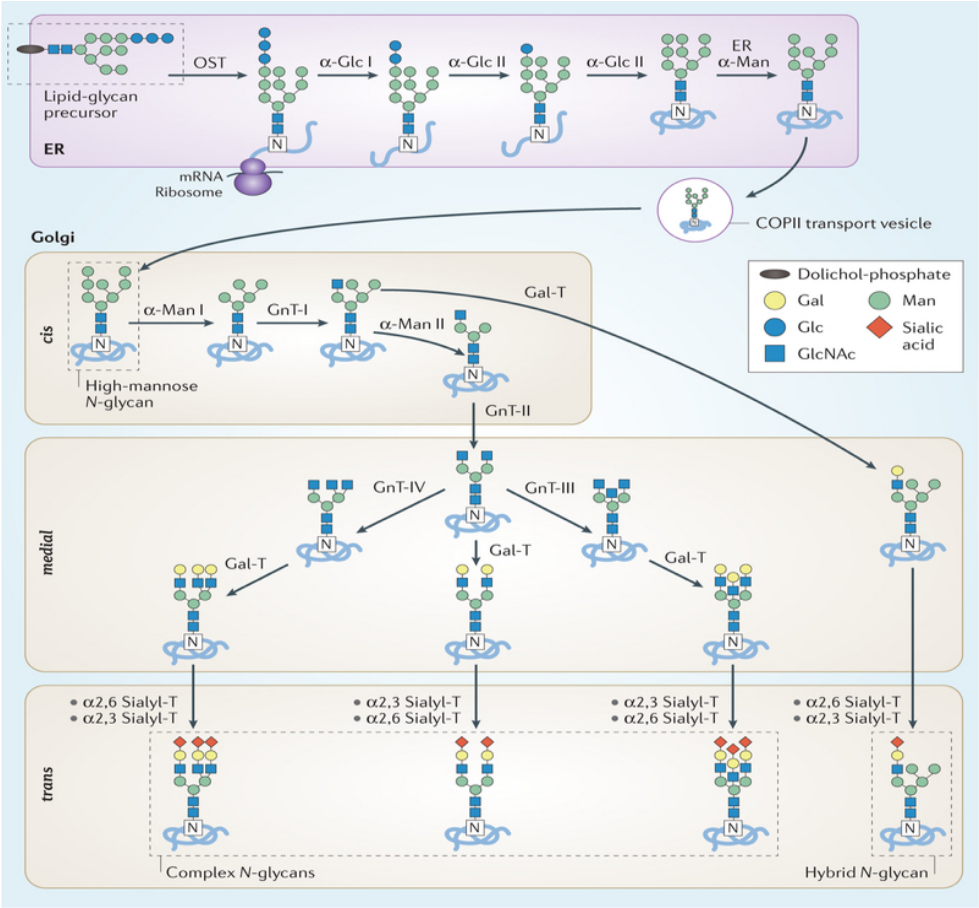

Figure 1.4. N-glycan synthesis begins in the ER with the transfer of a lipid-glycan precursor to an aspartic acid residue by oligosaccharyltransferase (OST). Sequential removal of glucose residues occurs via α-glucosidases, followed by the removal of a mannose residue by ER α-mannosidase. After passing a quality-control checkpoint as the calnexin, calreticulin cycle, the glycoprotein moves to the Golgi apparatus for further trimming and modifications by various glycosyltransferases, including α-mannosidases and sialyltransferases. This process creates a variety of N-glycoforms, often terminating in sialic acid. Glycosyltransferase expression levels influence the final N-glycan composition, the accessibility of glycosylation sites, and the duration the glycoprotein spends in the ER and Golgi apparatus (Reily *et al*., 2019).

1.10.2. O-Linked glycosylation

The most dominant form of O-linked (OLG) glycosylation is also known as mucin-type glycosylation; in this type of glycosylation, monosaccharides are attached to the protein in the Golgi apparatus in a post-translational event via the action of GTases. The first step in this process involves linkage via the hydroxyl group of Ser/Thr of N-acetylgalactosamine (GalNAc). This glycosylation occurs at Ser/Thr residues at a β-turn site in the peptide chains around charged amino acids. However, no consensus sequence has been acknowledged. GalNAc-linked glycans, or mucin-type O glycan, are synthesised by the action of polypeptide GalNAc transferases (GALNTs) (Brockhausen & Stanley, 2017). The specificity of GALNTs varies depending on the different amino acid sequences. Different from other glycosyltransferases that elongate sugars downstream, GALNTs specifically bind to the protein backbone to add the first sugar. They also contain a lectin domain that determines specificity based on nearby amino acid characteristics (Varki et al., 1999).This process is initiated by polypeptide N-acetylglucosaminyltransferase (GNTs), of which 20 homologous members have been described (Bennet et al., 2011). OLG is associated with a broad range of carbohydrate structures produced in a non-template-driven, sequential process involving the addition of glycans. OLG is an enzymatically catalysed process that involves a wide range of enzymes, which may play significant roles in regulating other cellular processes. GalNAc-linked glycans are a specific type of glycan structure that plays a crucial role in various biological processes. These glycans are prominently found in mucins, a family of high-molecular-weight glycoproteins abundant in mucus. Mucins are essential for providing a protective barrier on the surface of epithelial cells. They are particularly plentiful in the mucosal linings of organs such as the respiratory, gastrointestinal, and reproductive tracts. The presence of mucins on extracellular and secreted glycoproteins contributes significantly to their overall structural and functional properties, impacting a wide range of physiological processes, including cell signalling, immune response, and barrier function (Bennett et al., 2012; Vasudevan & Haltiwanger, 2014). Mucins contain many sites of O-glycosylation created by multiple tandem peptide repeats with a high Pro, Ser, and Thr content. Generally, these O-glycosylation sites have extended O-glycan core structures, which produce a substance in saliva that protects glycoproteins and cellular surfaces from external stress and bacterial infection and is recognised by the immune system. O-glycans comprise eight core structures. They are

essential for categorising blood group (H, A, and B) antigens alongside other O-linked glycoconjugates Tn antigen is the simplest form, consisting only of the initial GalNAc sugar attached to the protein. These sugar molecules are typically clustered on specific glycoproteins, such as mucin and human immunoglobulin A1 (IgA1). They are subsequently added throughout the cis, medial, and trans-Golgi compartments as the protein is transported. In contrast to NLG, carbohydrate structure cleavage does not occur as a co-translational process. Instead, the O-glycan chains are attached in a post-translational process by the sequential expansion of the structure with GAL, GlcNAc, sialic acid, and sometimes fucose (Brockhausen & Stanley, 2017). Figure 1.5, shown below, illustrates the mucin-type O-glycan core structures (adapted from Thompson & Wakarchuk, 2022).

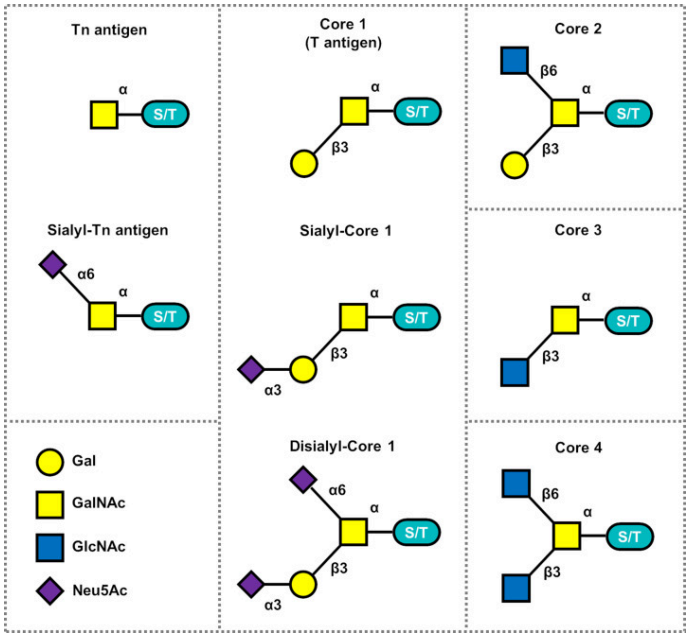

Figure 1.5. The T-synthase catalyses the addition of Gal from UDP-α-D-GAL to α-D-GalNAc on peptides, forming the T-antigen. This structure is then modified into core 2 by C2GnT1-3, which adds β1,6-linked GlcNAc from UDP-α-D-GlcNAc. The core 3 structure is created by C3GnT6, adding β1,3-GlcNAc to the GalNAc. Core 4 is formed from core 3 via C2GnT2, which adds β1,6-GlcNAc. Sialic acid can be added to cores 1-3 by ST6GalNAc1 at the 6-position or by ST3Gal1 at the 3-position of terminal GAL. Additionally, GlcNAc residues in core 2/3 can be

extended with β1,4-linked GAL and capped by ST3Gal4/6 sialyltransferases (Thompson & Wakarchuk, 2022)

1.10.3. Glycosidases

Glycosidases, also known as glycoside hydrolases (GH), are grouped into approximately 170 families of glycosidases within the Carbohydrate-Active Enzymes (CAZy) database (Terrapon *et al*., 2022). Most GHs share the same catalytic mechanism: acid/base catalysis that results in either retention or inversion of the anomeric configuration (Koshland, 1953).

The enzymatic reaction involves a proton donor and a nucleophile, often glutamate or aspartate. Inverting enzymes operate via a single nucleophilic substitution, in which a nucleophile directly displaces a leaving group, resulting in the inversion of configuration at the carbon atom undergoing the reaction. In contrast, retaining GHs utilise a more complex mechanism known as double displacement, characterised by the formation of a covalent glycosyl-enzyme intermediate. Initially, the enzyme covalently binds to the sugar molecule (glycosylation), creating this intermediate. Subsequently, this intermediate undergoes hydrolysis, releasing the product and regenerating the enzyme in its original state (deglycosylation). This dual-step mechanism enables retaining GHs to maintain the substrate's configuration during the reaction, thereby ensuring a specific outcome in carbohydrate metabolism (Zechel & Withers, 2000). GHs can be categorised according to the specificity of their substrates and the types of glycosidic bonds they break (Amin *et al.*, 2021).

Exoglycosidases cleave terminal sugar units from the ends of glycan chains; this category includes sialidases, which eliminate sialic acid residues, and galactosidases, which break down GAL from glycoproteins or glycolipids (Freeze and Krans, 2010; Chojnowska *et al.,* 2011). In contrast, endoglycosidases break glycosidic bonds within glycan chains, such as endo-β-N-acetylglucosaminidase, which targets N-glycans at particular locations (Freez and Krans, 2010).

GHs are enzymes that facilitate the degradation of di-, oligo-, and polysaccharides and glyconjugates. Enzymes that process carbohydrates, including glycosidases and GTases, transfer saccharides to other saccharides, small molecules, lipids, or proteins, and represent

approximately 1 to 3% of the genome in most organisms (Davies *et al*., 2005). GHs are a category of hydrolytic enzymes that use water to breakdown larger molecules into smaller fragments are typically found in cellular lysosomes, which facilitate the breakdown of carbohydrate components from a wide range of substrates, including polysaccharides, complex carbohydrates (such as glycoproteins, glycolipids, and glycosaminoglycans), nucleosides, and compounds that contain Thio sugars, a type of iminosugar where one or more oxygen atoms are replaced by sulphur. GHs can also transfer glycosyl groups to oligosaccharides, polysaccharides, and other hydroxyl acceptors. GHs are also divided into enzymes that hydrolyse O-glycosyl-, N-glycosyl-, and S-glycosyl-compounds, classified as enzyme classification (EC) EC 3.2.1, EC 3.2.2, and EC 3.2.3, respectively. Polysaccharide lyases (EC 4.2.2-) catalyse the cleavage of carbon-oxygen bonds between sugars, eliminating alcohol (Pigman, 1944; Florkin & Stots, 1973).

GHs, unlike GTases that primarily transfer sugar moieties, have evolved through various independent pathways, resulting in diverse three-dimensional (3D) structures. This diversity reflects their extensive functional roles, which are crucial for degrading glycan structures and supporting cellular energy and homeostasis. They are essential for the turnover of glycoconjugates involved in processes such as signalling, cell recognition, and the immune response. GHs also generate key intermediates for GTases, which synthesise complex glycans. For example, in the biosynthesis of N-glycan-containing glycoproteins in advanced eukaryotes, initial glycopeptides like $Glc_3Man_9GlcNAc_2$-Asn are trimmed by glucosidases and mannosidases in the ER and Golgi apparatus, preparing them for GTase action in creating complex N-glycans (Stanley *et al*., 2022).

Among the various enzymes involved in glycoprotein maturation, β-glucosidase II is a key enzyme. This enzyme is one of the two resident glucosidases in the ER and is essential for the proper folding and maturation of glycoproteins as it acts on N-linked glycans only. This process will be explored in more detail in (Section 1.10.5). Glucosidase II operates in concert with a molecular chaperone, UDP-glucose glycoprotein glucosyltransferase (UGGT). Together, they facilitate the intricate folding processes of glycoproteins, ensuring they acquire the correct 3D structure necessary for their biological functions. This is part of a critical quality control mechanism called the calnexin/calreticulin cycle. Within this cycle, glycoproteins

undergo repeated cycles of deglucosylation (removing glucose residues) and reglucosylation (adding glucose residues). This dynamic process is crucial for assuring that only properly folded glycoproteins can exit the ER, thus maintaining cellular integrity and function (Suzuki *et al*., 2022). In addition to these processes, a complex interplay between glycosylation and deglucosylation regulates the presence of the O-GlcNAc moiety on many nuclear and cytoplasmic proteins. This specific modification is mediated by the enzyme O-GlcNAc transferase (OT), which adds GlcNAc to target proteins (Zachara *et al*., 2022). Conversely, the removal of the O-GlcNAc moiety is catalysed by O-GlcNAcase, a glycosidase that plays a crucial role in modulating O-GlcNAcylation levels. This internal cellular regulatory modulates various cellular processes, including signal transduction, transcriptional regulation, and cellular stress responses. The influence of glycosidases extends beyond mere glycan metabolism, highlighting their pivotal role in broader cellular signalling pathways and overall cellular homeostasis. By orchestrating these modifications, glycosidases significantly contribute to the fine-tuning of cellular functions and the adaptation of cells to varying physiological conditions.

1.10.4. Glycosidases in cancer.

Glycosidases are present in higher levels in the interstitial fluid of tumours, in the serum of animals and patients with tumours, and in some tumour tissues compared to adjacent normal tissues. The most frequently observed increases in serum beta-N-acetylglucosaminidase and beta-glucuronidase have been identified, and these enzymes have been demonstrated to be released into the extracellular medium by various tumour cell types *in vitro* (Bernacki *et al.,* 1985). The process by which these hydrolytic enzymes are released by cells likely involves the exocytosis of lysosomes in tumours. Elevated levels of glycosidases in tumours could lead to increased shedding of tumour cells from the primary sites and local invasion, potentially causing structural alterations in the glycoconjugates present on tumour cell surfaces, either directly or indirectly. These modifications on the cell surface may promote the formation of thrombi by tumour cells and facilitate their implantation at secondary sites, as well as their attachment to endothelial cells or components of the subendothelial basement membrane in the microcirculation (Bernacki *et al.,* 1985).

The rapid increase in cancer cell proliferation creates a significant need for energy, which cancer cells meet by having an elevated expression of glucose transporters (GLUTs), allowing them to absorb glucose at a much higher rate than normal cells. This phenomenon is known as the "Warburg effect" (Warburg, 1956). It has been widely documented that numerous glycosidase enzymes show increased expression in various types of cancer. For instance, β-glucosidase is elevated in several cancers, including breast cancer (Zhou *et al*.,2017), gastric cancer (Li *et al*., 2021) and liver cancer (Zhang *et al*., 2016).

1.10.5. Glycosidase inhibition.

In recent decades, compounds have been identified as effective inhibitors of GHs. GHs are the first of a series of four critical enzymes involved in NLG processing. Some of the discovered inhibitors alter the structures of oligosaccharides attached to these glycoproteins, thereby altering their functional properties (Elbein, 1991). These alterations may affect the interactions of these proteins and biological systems, potentially altering their stability and activity (Pan and Elbein, 1995). For example, TM suppresses NLG, can lead to ER stress due to unfolded proteins, and restricts UDP-Gal uptake into the Golgi apparatus, causing cellular dysfunction (Vocadlo *et al*., 2022). By specifically inhibiting GHs, these new compounds offer a more nuanced approach, allowing for modifications to glycoprotein structure without completely halting glycosylation (Pan and Elbein, 1995). This distinction is crucial, as it opens the door to targeted therapeutic strategies that could fine-tune glycoprotein function rather than eliminate it. Understanding these inhibitors and their mechanisms may lead to novel treatments for diseases related to glycoprotein misfolding and dysfunction (Elbein, 1991).

The process of NLG at the asparagine residue of newly formed polypeptides is illustrated in (Figure 1.6) (adapted from Chang *et al*., 2013). Polypeptides produced during translation in the ER are depicted as an unfolded ribbon line, featuring an unprocessed oligosaccharide structure with three glucose terminals resembling a 'lollipop', attached to an asparagine. The ER-resident, membrane-bound enzymes glucosidases I and II systematically remove this oligosaccharide's terminal and second-to-last glucose. Interestingly, cultured cells can withstand the total termination of these ER α-glucosidases (Block *et al*., 1983; Stanley, 1984; Stanley, 1975; Hammond *et al.*, 1994a; Herbert *et al*., 1995).

After these glucose units are eliminated, the protein chaperone calnexin facilitates the folding of the polypeptide, which is then transported to the Golgi for further modification before secretion. Blocking the activity of ER glucosidases disrupts the interaction between the polypeptide and calnexin, leading to polypeptide misfolding, retention, and/or degradation (Anderson and Cresswell, 1994; Bergeron *et al*., 1994; Hammon and Helenius, 1994a; Hammond & Helenius, 1994b; Jackson *et al.,* 1994; Rajogapalan *et al*., 1994).

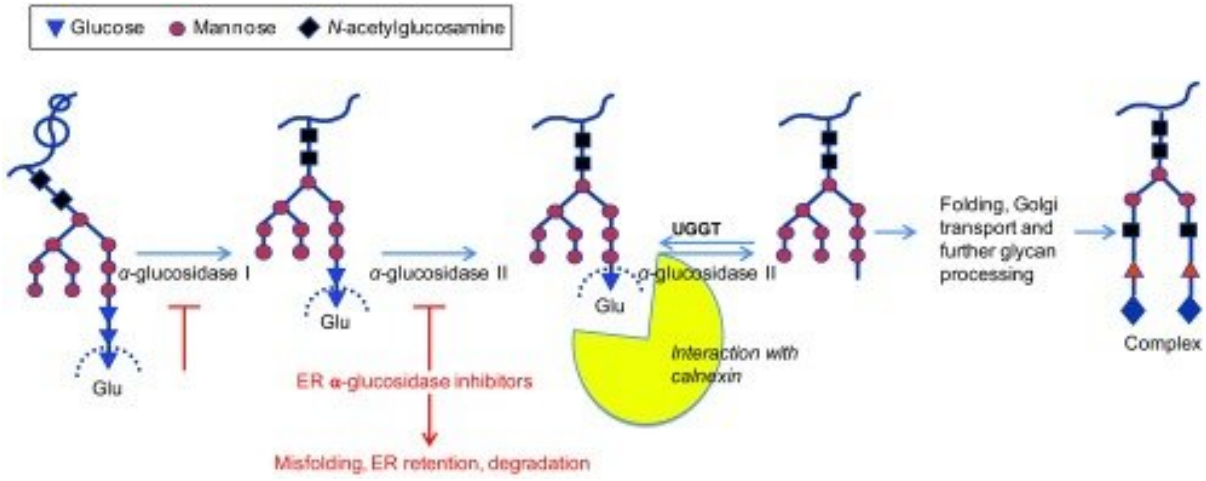

Figure 1.6. Glucosidase-mediated steps in the NLG pathway interact with calnexin to facilitate protein folding and subsequent glycan processing. However, inhibition of β-glucosidase results in protein misfolding, ER retention and degradation (Chang *et al*., 2013).

β-glucosidase, an enzyme coded by the glucosylceramidase β-1 (*GBA1)* gene, works in the lysosome of cells to break down a substance called glucosylceramide. When it does this, it splits it into ceramide and glucose, which are critical for the body (Kitatani *et al*., 2009; Dinur *et al*., 1986; Aureli *et al*., 2009).

Genetic research and functional studies found that there are similar and overlapping pathways linking neurodegenerative diseases and cancer. Several genes associated with Parkinson's disease, including *PARK2, PINK1*, and *GBA1*, have been found in cancer (Devine *et al*., 2011). *GBA1* plays a role in the development of breast cancer. When *GBA1* is inhibited, breast cancer cells become more sensitive to chemotherapy. This suggests that targeting *GBA1* could be a useful strategy to improve cancer treatment (Zhou *et al*., 2017). Other studies indicated that high expression of *GBA1* can be associated with poor prognosis in gastric cancer (Ma *et al*., 2019).

A recent investigation into the function of *GBA1* in gastric cancer resistance to chemotherapy assessed both GBA1 expression and activity in gastric cancer cells following 180 days of long-term exposure to fluorouracil (5-FU), a chemotherapy drug, as well as in gastric cancer tissues from patients undergoing chemotherapy. It has been demonstrated that *GBA1* activation is a characteristic response observed in patients with gastric cancer undergoing chemotherapy. Furthermore, GBA1 knockdown via siRNA has shown effectiveness against both chemotherapy-sensitive and chemotherapy-resistant gastric cancer cells, thereby enhancing 5-FU efficacy by inducing lysosomal dysfunction (Li *et al*., 2021). Other potential glycosidase inhibitors, such as iminosugars, serve as drug candidates.

1.10.6. Iminosugars

Iminosugars are polyhydroxylated compounds characterised by multiple hydroxyl (OH) groups attached to carbon atoms and an NH group. They are a unique class of compounds, structurally related to traditional sugars, characterised by substituting the ring oxygen atom with a nitrogen atom. This structural modification allows iminosugars to effectively mimic the transition state of glycosidic bond formation and hydrolysis, thereby interfering with the activity of carbohydrate-processing enzymes (Compain & Martin, 2007). Recent research reinforces the significant therapeutic potential of iminosugars. As competitive inhibitors of carbohydrate-processing enzymes, these glycomimetics are widely recognised for their antidiabetic, antiviral, and anticancer properties, acting through various host-targeted and metabolic regulatory mechanisms (reviewed by Tricase *et al*., 2025).

Iminosugars are recognised for inhibiting the ER glycosylation pathway by targeting and inhibiting α-glucosidase I and α-glucosidase II. They represent the most extensive class of α-glucosidase inhibitors under development (Simone *et al*., 2018). For instance, nojirimycin (NJ) is primarily derived from specific strains of *Streptomyces* bacteria and is also present in various plant sources and bacterial cultures (Lillelund *et al*., 2002). NJ has been extensively studied for its ability to inhibit both α- and β-glucosidase enzymes (Asano, 2003), which play a crucial role in carbohydrate metabolism. However, due to its hemiacetal structure (an

alcohol and ether attached to the same carbon) and a hydroxyl group at the C-1 position, NJ is considered an unstable compound with limited efficacy (Krishna *et al.*, 2023).

In contrast, its 1-deoxy analogue, DNJ, has become a significant medicinal compound, which is a naturally occurring iminosugar first isolated from the leaves of *Morus bombycis*, commonly known as the white mulberry (Niwa, 2009). The derivatives of DNJ have demonstrated strong inhibitory effects on the enzymes involved in modification and processing, making them valuable in managing various metabolic disorders (Brien and Murphy, 2011). DNJ has been recognised for its antiviral properties, showing effectiveness against a range of viral pathogens, including the human immunodeficiency virus (HIV), hepatitis B virus (HBV), woodchuck hepatitis virus, bovine viral diarrhoea virus (BVDV), and dengue virus (Chapel *et al*., 2007). This broad spectrum of activity highlights DNJ's potential as a therapeutic agent for viral infections, positioning it as a compound of interest for further research in antiviral drug development.

DNJ and its derivatives (such as N-butyl-DNJ or Miglustat) are potent inhibitors of ER α-glucosidases I and II. By blocking these enzymes, DNJ halts the very first steps of N-glycan processing, resulting in truncated, improperly folded glycoproteins (Elbein, 1987) and preventing them from interacting with quality-control chaperones like calnexin (Helenius & Aebi, 2001).

Research studies have shown that DNJ reduced the viability and survival of cancer cells, with a greater effect on glioblastoma cells than on gastric adenocarcinoma cells. The most critical finding was that DNJ did not cause significant cytotoxic damage to the healthy MRC5 cells, demonstrating a promising therapeutic window (Fonseca *et al*., 2024). The cytotoxic and antiproliferative properties of DNJ were consistent with earlier research on natural products, such as N-alkyl-1,5-dideoxy-1,5-imino-l-fucitols and N-(8-(3-ethynylphenoxy) octyl-1-deoxynojirimycin, which have exhibited similar effects across various cancer cell lines (Zhao *et al*., 2010; zhou *et al*., 2019; Tang *et al*., 2020).

Recent studies in 2025 by Montebugnoli *et al* have shown that two natural glycosidase inhibitors, iminosugars, D-fagomine (FGM) and DNJ, and their synthetic products, DNJ derivative, 2,3,4,6-tetra-O-benzyl-(+)-1-deoxynojirimycin (TBN-DNJ) and N-(n-

Nonyl)deoxynojirimycin (NN-DNJ), were screened for potential anticancer properties using Caco-2 and HCT-116 cells to evaluate early and late stages of colon cancer, respectively. It was found that metabolic activity decreased and glycolysis increased, a process cells use to oxidise glucose to generate energy in the form of ATP (Dashty, 2013). These effects varied based on the type of iminosugar, cell type, growth conditions, glucose concentration, exposure time (1-13 days), and in 2D and 3D spheroid models. Advanced methods, such as IncuCyte live cell imaging and Seahorse real-time cellular metabolic analysis, are automated and non-invasive techniques employed in biological research to observe living cells in real-time, delivering kinetic information (how cells function over time) instead of static, end-point data. Complementing microscopy analysis after staining cells with fluorescence probes allowed scientists to observe changes in energy metabolism substrates, including increased glycolysis and altered lipid and glycogen stores. The findings that iminosugars, both natural and synthetic, influence cellular bioenergetics pave the way for their potential use in various applications, including cancer therapy (Montebugnoli *et al*., 2025). Other recent studies indicated that when DNJ is combined with natural compounds like theaflavins or chemotherapy drugs, it effectively decreases the levels of proteins linked to metastasis, such as PTGS2 and MMP9, while also lowering systemic inflammation (Wang *et al*., 2025). Furthermore, another study indicates that modified DNJ derivatives, particularly those with C-6 structures containing specific groups such as tegafur, a chemotherapy drug, exhibit significant lipophilicity and anticancer properties. These compounds effectively lowered mitochondrial membrane potential selectively kills HCT-116 colorectal cancer cells. Compound C-6 exhibited significant toxicity against HCT-116 cells, inhibited cell migration and colony formation, and arrested the cell cycle at the S phase. C-6 caused DNA damage and triggered oxidative stress via the nuclear factor erythroid 2-related factor 2 signalling pathway, elevating malondialdehyde and nitric oxide levels while depleting protective antioxidant enzymes, such as glutathione and superoxide dismutase (Tang *et al*., 2024).

Recent studies from kifunensine and castanospermine are described in glycosylation (Section 1.10) are also naturally occurring, potent polyhydroxylated indolizidine alkaloids that act as powerful inhibitors of specific enzymes. Kifunensine has been demonstrated to block the Man I enzyme located in the ER and Golgi apparatus (Hering *et al*., 2005). As a result, the disruption of the N-glycosylation biosynthetic pathway caused by kifunensine leads to a higher rate of

high-mannose N-glycans and a decrease in the production of hybrid- and complex-type N-glycans (Kommineni *et al*., 2019; Xion *et al*., 2018). While castanospermine primarily functions as a potent, competitive inhibitor of α-glucosidase and β-glucosidase enzymes (Saul *et al*., 1983).

Additionally, research has been conducted testing swainsonine, an inhibitor of Golgi α-mannosidase II (GManII) that reversibly blocks complex N-glycan synthesis. Swainsonine, a hydrochloride salt produced by GLYCODesign, based in Toronto, Canada, is identified by the product code GD0039 (Tulsiani *et al*., 1982). Inhibition of GManII Golgi α-mannosidase II by swainsonine can prevent the formation of β(1→6)-branched complex type N-glycans in human cancer cells. Following this discovery, a phase I trial was conducted to evaluate the effectiveness of glycoprotein processing iminosugars and swainsonine hydrochloride (GD0039) as anti-cancer agents. This was followed by phase II clinical trials conducted in Canada around 2002 (Wrodnigg *et al*., 2008). The phase II trial involved 40 patients with advanced renal cell carcinoma or advanced colorectal cancer resistant to 5-FU, yielding promising results; however, during the pharmacokinetics and pharmacodynamics investigations of oral GD0039, all patients with advanced cancer discontinued treatment due to disease progression or toxicity. Despite this, GD0039 demonstrated the ability to prevent metastasis, inhibit tumour cell growth, activate lymphocyte proliferation, and enhance T-cell stimulation (Hossain & Andreana, 2019).

In a more recent study, researchers successfully reconstructed the swainsonine biosynthetic pathway, uncovering a distinct oxidation-reduction sequence catalysed by the tailoring enzymes SwnH2, SwnH1, and SwnN. By employing a removable O-acetyl group to regulate enzyme selectivity, the team developed unnatural polyhydroxylated indolizidine alkaloids. This work has established a biocatalytic framework for creating complex glycosidase inhibitors (Liu *et al*., 2026)

On the other hand, two drugs derived from iminosugars, Glyset™ and Zavesca™, have been approved for the clinical management of diabetes and type 1 Gaucher disease. Iminosugars have also been identified as competitive inhibitors, which are compounds that resemble the substrate of an enzyme, bind to the active site, and prevent the substrate from attaching,

thus inhibiting the enzyme function in processing N-glycans by α-glucosidase in the ER; they have also demonstrated efficacy against various envelope viruses (Boldescu *et al*., 2017). In summary, glycoprocessing enzymes play a crucial role in modifying and processing glycoproteins. These enzymes, which include GHs and GTases, facilitate essential biochemical reactions involving the addition, removal, or alteration of sugar chains. Structure of DNJ is shown below in (Figure 1.7)

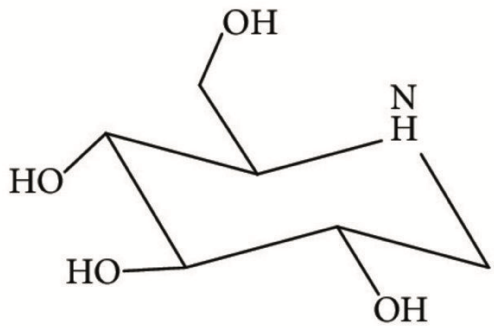

Figure 1.7. DNJ, a piperidine alkaloid, is a polyhydroxylated iminosugar. It is an analogue of D-glucose, with the oxygen in the ring substituted by a nitrogen atom.

1.10.7. Lectins

Lectins are a diverse group of proteins with the unique ability to bind selectively to specific carbohydrate structures, known as glycans, that are found on the surface of various cells. This binding plays a critical role in different biological processes, including cell signalling, cell adhesion, and the modulation of immune responses (Mishra *et al*., 2019). Lectins bind specific sugar residues on glycoproteins and glycolipids, making them valuable tools in various biomedical applications, including cancer research (Hamid *et al*., 2013). Different lectins have been deployed over the last few decades, exhibiting numerous antitumor activities. These lectins include legume lectin, Concanavalin A (Con A), Phytohemagglutinin (PHA) and mistletoe lectins (Liu *et al*., 2010). Furthermore, alterations in cell-surface glycans, such as increased fucosylation and sialylation, have been employed as cancer diagnostics (Pinho & Reis, 2015). These glycan modifications, including changes in N-linked glycan branching, are

frequently observed in cancerous glycoproteins and have been utilised as biomarkers for cancer diagnosis (Lin &Lubman, 2024)

Advances in glycoscience, genomics, proteomics, and mass spectrometry now enable precise identification of glycan structural differences and distinctions between diseased and normal cells (Pallar *et al.*, 2025). Particularly, cancer exhibits well-documented alterations in cell surface glycosylation during malignant transformation, tumour cell differentiation, and metastasis, reflecting the significant role of glycosylation changes in cancer progression (Mody *et al*., 1995; Tucillo *et al.*, 2014). The lectins used for this study were concanavalin A (Con A), wheat germ agglutinin (WGA) and *ulex europaeus* agglutinin (UEA-I).

Con A is a well-characterised lectin derived from the Jack bean (*Canavalia ensiformis*), which has been the subject of extensive research since its initial discovery (Jones & John, 1916). Jack bean salt extract is mainly utilised in scientific studies to isolate proteins such as urease and Con A. Jack bean extract is a concentrated solution derived from jack bean seeds. The extraction process typically includes purification with salts such as ammonium sulfate or sodium chloride. This extract is particularly recognised for its elevated levels of the enzyme urease (Pawar *et al*., 2022).

The jack bean is high in protein content (23–34%) and serves as an important source of these enzymes and lectins, which are typically extracted through methods involving salt, acid, or organic solvents. When salt bean jack extracts undergo ammonium sulphate precipitation followed by dialysis, the predominant protein isolated in the globulin fraction is canavalin. Associated with canavalin was a minor amount of a second globulin that was less soluble and contained a significantly higher amount of sulphur than canavalin and thus named this globulin concanavalin (Jones & John, 1916).

Con A recognises the linkages Manα 1-2Man, Manα1-3Man, and Manα 1-6Man. It strongly binds to high-mannose (Man3–Man9) and hybrid-type N-glycans (Mega & Hase, 1991). Con A demonstrates a specific affinity for carbohydrate structures with glucose and mannose, such as α -D-glucosyl and α -D-mannosyl residues of glycoproteins, making it a valuable tool in biological research. Its ability to bind to these sugars has facilitated the exploration of various cellular processes, particularly regarding the dynamics of cell surface receptors. Studies have

shown that Con A can be used to monitor changes in the quantity, distribution, and mobility of these receptors, which play crucial roles in regulating cell proliferation and mediating cell-cell interactions (Cohen, 1974; Wang *et al*., 1971).

Structurally, Con A is a tetramer composed of four identical monomers that intricately assemble to create a stable and functional structure resulting from a series of interactions, including polar interactions, hydrogen bonds, and electrostatic attractions (Hardman and Ainsworth, 1972; Reeke *et al*., 1975). These interactions are crucial for maintaining the protein structure and facilitating biological functions within the cellular environment.

Con A was the first lectin for which the chemical composition and the 3D structure were elucidated, setting a benchmark for subsequent studies in carbohydrate-binding proteins (Edelman *et al.,* 1972). This laid the foundation for our understanding of interactions and underscored the importance of structural biology in unravelling the complexities of biomolecular function.

Triticum vulgaris agglutinin, also known as WGA, exhibits a strong binding for GlcNAc and N-acetylneuraminic acid (sialic acid) residues, which are membrane-associated glycoproteins that are expressed on cancer cells and their corresponding stem cells. This characteristic makes WGA an invaluable targeting ligand for immunohistochemical analysis of brain tumours (Fisher & Kissel, 2001). The detailed linkage specificity for WGA is the highest affinity for chitobiose (GlcNAc β1-4GlcNAc) and terminal non-reducing GlcNAc β1-4GlcNAc. It also binds to sialic acid in α2,3- or α2,6-linkages (Allen *et al*., 1973). WGA has been thoroughly investigated in cancer research for its possible applications in treatment, diagnostics, and targeted drug delivery. Its strong affinity for the altered glycosylation patterns frequently present on the surfaces of cancer cells allows WGA to selectively bind to and inhibit the growth of different cancers, including leukemia in which even low doses showed maximum toxicity toward acute myeloid leukaemia cells (Ryva *et al*., 2019) and, cervical cancer in which WGA induced paraptosis (a type of program cell death) without caspase activation, cytoplasmic vacuolation, ER dilation and increased ER stress, and the unfolded protein response in WGA-treated cervical carcinoma cells (Tsai *et al*., 2017).

UEA-I, a lectin isolated from the seeds of the gorse (*Ulex europaeus*), exhibits a specific binding affinity for L-fucose, a sugar molecule commonly found on the surfaces of many glycoproteins and glycolipids (Fenlon *et al*., 1987). This unique characteristic has led to exploring UEA-I in various pathological contexts, particularly oncology. Research indicates that alterations in glycoconjugates associated with cancer cells often involve changes in fucose expression, and UEA-I is a valuable tool for studying these modifications. The detailed linkage specificity is that it strongly binds towards Fucα1-2Galβ1-3/4GlcNAc (H-type 1 or H-type 2 disaccharides) (Pereira *et al*., 1978).

For instance, several studies have stablish a correlation between UEA-I binding in glycoconjugates and poorer patient survival rates in various cancers (Ambros & Kurman, 1993). Specifically, in endometrial carcinoma, the elevated binding affinity of UEA-I to cancerous tissue has been linked to adverse clinical outcomes, suggesting that fucosylation patterns may play a critical role in tumour progression and patient prognosis (Ambros & Kurman, 1993). These findings highlight the potential of UEA-I not only as a research tool and a marker for cancer aggressiveness but also underscore its significance in understanding tumour biology and potential for patient management.

On the other hand, one example of a lectin frequently used in studies of OLG is *helix pomatia agglutinin* (HPA). This lectin specifically recognises truncated O-linked glycans that contain α-GalNAc, such as the Tn antigen (α-GalNAc-O-Ser/Thr). HPA is also known to be an essential indicator of metastatic potential in breast cancer (Brooks, 2000; Brooks & Leathem, 1991; Leathem & Brooks, 1987; Mitchel & Schumacher, 1999).

In this study these specific lectins (Con A, UEA-1 and WGA) were selected because their unique binding profiles serve as diagnostic probes for the various structural checkpoints in the N-linked glycan biosynthetic pathway. By combining them with glycosidase inhibitors, researchers can pinpoint which step in the processing pathway has been blocked.

Con A has a strong binding for these immature high-mannose and hybrid structures. An increase in Con A binding demonstrates that an inhibitor has successfully blocked early trimming (Elbein, 1987). UEA-1 specificity for terminal α1,2-fucose. If an inhibitor prevents a glycan from reaching the trans-Golgi, UEA-I binding will be absent or significantly reduced,

serving as a marker for complete maturation (Yonezawa *et al*., 1982). WGA recognises terminal or internal GlcNAc and sialic acid. WGA binding increases when processing reaches the medial-Golgi, signalling the transition toward complex maturation (Gallagher *et al*.,1985). While these lectins are useful for studying N-linked pathways, their carbohydrate specificity means they often recognise O-linked structures as well, as shown below in (Table 1.2)

Table 1.2. Summary of the lectin recognition sites in N-linked and O-linked pathways.

Lectin	N-linked recognition	O-linked recognition	Primary diagnostic use	Reference
Con A	**Yes** (Strong)	**No**	Identifies early-stage high-mannose blocks.	Cummings & Etzler,2009
WGA	**Yes**	**Yes**	Identifies transition to medial-Golgi maturation.	Gallagher, 1985
UEA-I	**Yes**	**Yes**	Identifies successful terminal trans-Golgi capping.	Arenas *et al* ., 2001

1.10.8. Doxorubicin

Doxorubicin is a chemotherapeutic agent with a molecular weight of 543 g/mol, first extracted from the bacterium *Streptomyces peucetius* var. *caesius* in the 1960s (Arcamone *et al*., 1969). Doxorubicin is an anthracycline antibiotic that intercalates DNA, disrupting the double helix and interfering with DNA replication and transcription. It inhibits topoisomerase II, a key enzyme essential for replication and chromosome segregation. It also forms free radicals (Tacar *et al,* 2013). Doxorubicin was approved by the FDA in 1974 (Sun *et al*., 2017). Doxorubicin, either alone or in combination with other drugs, has been prioritised for a range of solid tumours and metastatic cancers. It has been used in the treatment of soft tissue and bone sarcomas, along with cancers of the breast, ovary, bladder, and thyroid. Additionally, it is effective for treating acute lymphoblastic leukemia (ALL), acute myeloblastic leukemia, lymphoma, and small-cell lung cancer (Sinha *et al*., 2025). For instance, TNBC is one of the breast cancer subtypes in which doxorubicin is used for treatment (Furlanetto & Loibl, 2020; Medhi *et al*., 2020). Doxorubicin is also used to treat HER2-positive breast cancers (Savage & Widener, 2008). While doxorubicin can be highly effective, it also carries a considerable risk of cardiac toxicity, which restricts its long-term application. Doxorubicin is recognised as the most cardiotoxic drug in the anthracycline category of chemotherapy agents (Wu *et al*., 2022).

Nano-formulations of doxorubicin have received FDA approval for therapeutic use, such as Doxil, which is employed in treating Kaposi's syndrome (James *et al*., 1994), ovarian cancer

(Muggia *et al*., 1997), and breast cancer (Sparano *et al*., 2001). Cancer cells can develop resistance to therapy through a complex interplay of genetic and environmental factors. This resistance often arises from the accumulation of mutations that occur over time and the sequential genetic changes associated with cancer progression. Acquired resistance typically emerges in cancer cells that are non-responsive, enabling them to survive initial treatment and adapt to the specific therapeutic regimen. In contrast, specific resistance is linked to intrinsic characteristics of the cancer cells themselves, such as pre-existing mutations or alterations in cellular signalling pathways that render them less susceptible to treatment.

Additionally, the tumour microenvironment plays a significant role in resistance mechanisms. The attachment of cancer cells to the ECM can provide them with crucial survival signals, facilitating their ability to withstand therapy. This interaction may help the cells evade the effects of drugs by promoting structural changes or activating survival pathways. Understanding these multifaceted resistance mechanisms is essential for developing more effective treatment strategies and overcoming therapeutic challenges in cancer management (Dittmer and Leyh, 2015). Culturing breast cancer cell lines, specifically MCF-7 and MDA-MB-231, within a 3D ECM-based model has been demonstrated to notably diminish the efficacy of doxorubicin, a commonly used chemotherapeutic agent. This reduction in drug effectiveness highlights the challenges the tumour microenvironment poses in cancer treatment. Interestingly, when a β1-integrin blocking antibody is applied to the MDA-MB231 cells before the introduction of doxorubicin in the ECM (Matrigel), there is a remarkable increase in the sensitivity of these cells to the drug. This enhanced sensitivity is observed in a dose-dependent manner, suggesting that inhibiting β1-integrin may alter the cellular signalling pathways or microenvironment interactions that typically contribute to drug resistance, thereby offering a potential strategy for improving the effectiveness of doxorubicin in treating aggressive breast cancer phenotypes (Lovitt *et al*., 2018). This demonstrates the importance of understanding how tumour cells interact with their surroundings at a molecular level. It also suggests how cancer cells might become resistant to treatment. This is particularly relevant for chemotherapy drugs when patients do not respond to treatment.

In other recent studies, MDA-MB-231 and SKBR3 cells were treated with doxorubicin, and cell proliferation was measured using the Alamar Blue assay. When grown as two-dimensional (2D), MDA-MB-231 cells showed a significant decrease in viability after treatment with doxorubicin at 5 μM and 10 μM. However, in 3D cultures, they exhibited decreased sensitivity to doxorubicin. In contrast, SKBR3 cells exhibited a notable reduction in viability when exposed to doxorubicin at concentrations of 0.5 μM or higher in 2D cultures and at concentrations of 1 μM or higher in 3D cultures (Azimi *et al*., 2020).

1.11. 2D model systems

Cancer research and drug discovery investigations in 2-dimensional cell (2D) culture models have been extensively used. Early work in this field was undertaken by a scientist at Johns Hopkins University who propagated cervical cancer cells from Henrietta Lacks; these were taken without her consent, preceding the principles of informed consent in 1951 (Hudson & Collins, 2013). These immortalised cells are known as cancer cell lines and gave rise to "HeLa" cells; their unlimited proliferation ability has changed research in cancer. Additionally, BT20 is the first breast cancer cell line that was established in 1958 from an invasive ductal carcinoma (Lasfargues & Zzello, 1958). Subsequently, various cancer cell lines have been established and used extensively *in vitro* cell cultures in the last 50 years, as well as animal experiments using tissue grafts from different species (xenografts). Established cell lines, immune cells and even primary human cells can be maintained in tissue culture conditions.

A technique developed by Liu *et al.* (2012), known as conditional reprogramming, enables the initiation of 2D cultures from ordinary to epithelial cells with high efficiency, involving the presence of RHO kinase and fibroblast feeder cells. Further investigations reveal that 2D cell culture significantly alters cellular phenotypes and physiological characteristics, leading to variations that can misrepresent *in vivo* conditions. This shift in cellular behaviour emphasises the limitations of 2D systems in accurately modelling complex biological environments. Thus, only 16% of drugs developed were successful in clinical trials (phases II and III) when 2D culture models were used, indicating that cancer therapies had significant failures (Arrowsmith & Miller, 2013; Mestas & Hughes, 2004). 2D cultures have several advantages. For instance, human cells used in disease studies are cost-effective and have high-throughput

capabilities. However, these methods still require the proliferation of cells on stiff, rigid, and plastic surface environments since physiological conditions are promoted by cell growth in the tumour microenvironment.

Additionally, the tumour microenvironment comprises a heterogeneous and complex mix of cell types and ECM, which is not found in 2D cell culture. As a result, this prevents researchers from studying interactions in the tumour microenvironment with immune system cells and human cancer cells (Fitzgerald *et al*., 2021). 2D culture systems, such as 2D monolayer cultures, have contributed to understanding molecular mechanisms in the tumour microenvironment. However, murine models have delivered a better outcome because they more closely mimic the characteristics of a human tumour than 2D tissue culture.

1.11.1. *In-vivo* models

Physiological conditions of a tumour are better recapitulated in murine models than in 2D culture models. Tumours can be effectively cultivated by tail injection of cells into mice, allowing researchers to study the development and progression of cancer in a controlled environment. These mouse models may be genetically engineered to develop tumours at predetermined stages, enabling scientists to induce specific responses and observe the effects of various treatments or interventions at different points in the tumour's lifecycle. This method provides valuable insights into tumour biology and helps test the efficacy of new therapies before they are considered for human trials. Rodents share similar anatomical, cellular, and molecular characteristics with humans, which have been identified as critical properties and functions in cancer (Lamprecht *et al*., 2018). Tumours that develop in mice are embedded within a complex tumour microenvironment, which encompasses various cellular components, ECM, and signalling molecules that interact dynamically. This microenvironment plays a crucial role in tumour growth, progression, and response to treatment.

In contrast, traditional 2D cell cultures fail to replicate this intricate setting, stripping away essential factors such as cell-to-cell interactions, mechanical cues, and the biochemical landscape, which are vital for accurately modelling tumour behaviour and studying therapeutic responses. As a result, insights gained from 2D cultures may not fully reflect the

complexities of tumour biology observed *in vivo* (Mestas & Hughes, 2004). Human cancer cells can be transplanted and grown in immunodeficient mice using a patient-derived xenograft *in vivo* system, which maintains the immunodeficient characteristic of the murine system, thereby preventing rejection of the human cancer cells. However, this type of *in vivo* model is quite expensive, raises ethical concerns, requires several steps such as implantation, propagation, and drug screening, and prevents the delivery of a more effective treatment to the patient. This concerns the issue of patient mortality being reported before the initiation of initial therapy (Malaney *et al*., 2014).

1.12. 3D models in cancer research

3D models have revolutionised cancer research in the last decade, aiming to avoid using animals for experimentation, and invasive techniques, such as the extraction of biopsy samples from cancer patients. Medical professionals can analyse tissue samples from tumours to understand the genetic makeup and molecular profile of cancer cells. This provides personalised treatment strategies and potential biomarkers to predict patient responses to therapies, ultimately improving outcomes and reducing side effects. Different types of 3D culture systems, such as spheroids, tumoroids and organoids, are often used in cancer research. Although they share similarities in self-organisation, what differentiates them is the type of cells used to grow a tumour; for example, the use of patient-derived cells in organoid cultures is required to produce a tumour. Cancer cell lines can be established into 3D models, such as tumoroids.

1.12.1. Spheroids

Spheroids are multicellular aggregates of cancer cells cultivated on specialised low-attachment tissue culture plates. This method promotes the growth of cancer cells in a 3D configuration, allowing them to cluster closely together in a spherical formation. The 3D architecture of spheroids closely mimics the *in vivo* tumour microenvironment, facilitating more accurate studies of tumour behaviour and drug response. As these cancer cells aggregate, they generate and accumulate collagen, creating a fibrous matrix that supports the spheroid's structural integrity and mimics the extracellular matrix found in actual

tumours. This collagen deposition plays a crucial role in cell signalling. It can influence the cells' phenotypic characteristics, making spheroids an essential model in cancer research for understanding tumour progression and treatment efficacy (De Angelis *et al*., 2018). For instance, by implanting cell lines into a 3D matrix, spheroids can be generated, similar to organoids, with respect to cell proliferation and differentiation (Nyga *et al.,* 2013; Magdeldin *et al*., 2017). Spheroids prepared from the MCF-7 cell line displayed increased drug resistance compared with MCF-7 2D monolayer culture and demonstrated the role and importance of the TME in cellular invasion, an essential early step in metastasis, when these cell lines were grown in 3D spheroids (Brancato *et al*., 2018).

Additionally, hypoxia, resulting from a lack of blood supply, occurs in developing aggressive tumours associated with the acquisition of new blood vessels (angiogenesis), gene regulation, and signal transduction pathways. (Huang *et al.*, 2020). A spheroid typically comprises a central area of dead cells (necrotic area), a dormant area towards the central necrotic region, and proliferating cells surrounding it. Due to the lack of oxygen and nutrients in the interior, necrotic and quiescent zones developed, and the spheroid surface area is where cell proliferation takes place (Brancato et al., 2018; Han *et al*., 2009). Huang (2020) demonstrated that, in MDA-MB-231 spheroids examined following haematoxylin and eosin (H&E) staining and immunohistochemistry (IHC), the necrotic cavities were identified because of hypoxia. Previous investigations have shown that cancer spheroids exhibit slower proliferation compared to monolayer cultures.

1.12.2. Organoids

In the last two decades, a new technology known as 3D organoid culture has transformed translational cancer research. Organoids are multicellular structures comprising epithelial cells cultured in semisolid matrices, surrounded by pathway modulators and mitogens that induce cell division. Organoids that aim to resemble the 3D environment differ from spheroids, 3D cultures of established 2D monolayer cell lines. (Tsai *et al.*, 2018). Organoids are different from other culture systems in terms of their proliferative continuity and generation of various cell types that differentiate in a layer of cells bound to each other that forms the outer layer of a body surface known as epithelium. Organoids have enabled the

discovery of paracrine processes in the intratumor environment through the use of cocultures comprising immune cells and primary stromal fibroblasts within 3D organoids. As a result, this can have a significant impact on medical applications (Clevers & Tuveson, 2019). 3D organoids can be cultured using various methodologies, for instance, static suspensions, hanging drops, magnetic levitation, spinner bioreactor, rotating bioreactor, microfluidic system, and gel embedding procedures (Lv *et al*., 2017). 3D culture systems can be achieved using hydrogel matrices that contain extracellular matrix mixtures such as laminin, collagen, and proteoglycans. Adding growth factors, such as transforming growth factor β (TGF-β) and fibroblast growth factor (FGF), is also possible. When cultured organoids enable interactions between cells and the matrix, as well as cell-to-cell communication, to be elucidated (Kim *et al.*, 2019).

3D organoids can be grown with different types of cells, such as embryonic stem cells (ESCs), which have the capacity for unlimited cell proliferation; induced pluripotent stem cells(iPSC) are a type of pluripotent stem cell produced by adult cells; somatic stem cells also known as adult stem cells with limited differentiation, regenerating and repairing tissue damage and cancer cells lines (Xu *et al*., 2018). Organoids aim to resemble the *in vivo* environment, but they require careful handling and procedures for preparation and maintenance compared to spheroids (Lo & Karlsson, 2020). Organoids can be cultured using patient-derived organoids because they mimic the features of a human tumour. 3D organoids are widely used; whilst it is a recent technology, it has disrupted the field and provided scientists with more complex biological systems, for example, by incorporating extracellular matrix proteins that mimic the characteristics of a human tumour, providing more answers in cancer research investigations on the tumour microenvironment. Human tissue is developed by using different cell types with cell-to-cell signalling or targeted cells, which are combined with growth factors and other molecules that respond to a stimulus. A method known as colocalization determines if the targeted cells are in the same area using fluorescent labels. Step 2: An ECM must be created to serve as a 3D construct to allow biological conditions to thrive, such as the mechanical stability of cells and cell function regulation. Step 3 is the cell's differentiation and maturation by synthesising interstitial fluid containing proteins and nutrients that bind to other molecules to regulate their biological activity, such as biological effectors (Jong, 2005).

1.12.3. Limitations of organoids

It has been shown that organoids resemble tissues from which they were isolated due to their self-organising ability. Still, they cannot guarantee the exact replication of organ morphology in terms of size, shape, molecular features, and cellular structures (Cantore *et al*., 2016). However, existing methodologies and procedures are insufficient for generating sufficiently complex organoids to allow the formation of vascular smooth muscle cells (VSMCs). Thus, the main problem is using effective organoid techniques that investigate inflammatory disorders, since vascularisation is required in tissue inflammation to recall in situ immune cells. This primary concern has been attempted to be resolved by researchers using spinning bioreactors to generate organoids to promote the vascularisation process by co-culturing muscle cells with endothelial cells to produce vascular networks (Tatullo *et al.*, 2020). ECM complexity is another limitation since organoids require ECM, like the primary organ from which they are isolated. A reduced immunological response may result from an ineffective ECM mimicking the *in vivo* scenario. Thus, this may lead to limitations in research regarding tumour infiltration and drug penetration (Liu *et al.*, 2016).

1.12.4. Difference between spheroids and organoids

Spheroids and organoids are multicellular cultures prepared from cells obtained from diverse starting materials, including organ biopsies or tumour samples, suspended in microwells or droplets. Spheroids are recognised as simpler because constructs or scaffolding are not required to generate their phenotype. However, spheroids lack self-organisation and cellular polarity, and often lack the characteristics of the more complex *in vivo* environment. While spheroids are not as complex as organoids, they have the advantage that, predominantly for drug screening, their 3D structure is superior to that of 2D cell culture systems. Furthermore, in the investigation of TME on drug screening responses, spheroids can play an important role (Abraham *et al*., 2020). The difference between spheroids and organoids is illustrated below in (Figure 1.8), (adapted from Fitzgerald *et al*., 2021).

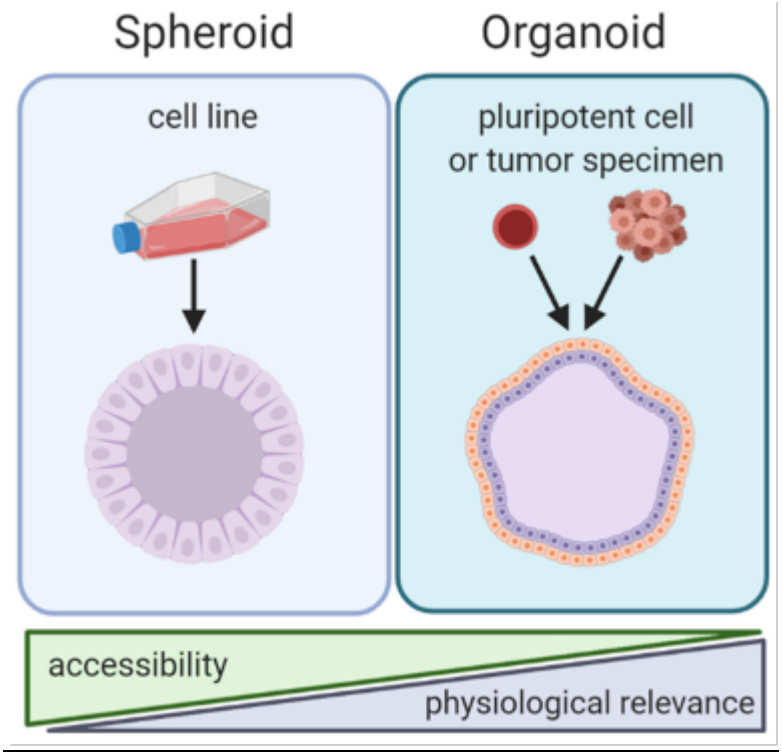

Figure 1.8.The morphology of a spheroid and an organoid is represented when cultured with different cell types (Fitzgerald *et al*., 2021).

1.12.5. Tumoroids

Tumoroids are usually prepared using immortalised cancer cell lines and are 3D organotypic models cultured *in vitro* with cellular self-organisation capabilities. This 3D culture model can be formed into 3D organoids when growing primary cells from cancer patients, rather than immortalised cell lines (Tsai *et al.*, 2018). Tumoroids resemble organoids more closely in the TME but are also cost-effective in research in drug discovery for use in precision medicine (Phelan *et al*.,2018). Furthermore, 3D tumoroids *in vitro*, after being cultured, can be allowed to expand, and their genome can be manipulated using CRISPR-Cas9 technology (Ohta & Sato, 2014). This offers considerably greater value compared to 2D cultures and organoids, as their genomes can be manipulated as well, but tumoroids are the only system that enables researchers to connect particular genetic changes to physiological behaviours that occur solely within the TME (Hank *et al*., 2020). This is because tumoroids maintain the genetic and phenotypic characteristics of the original tumour, which makes them essential for cancer

research (Kalla *et al*.,2025). Tumoroids *in vitro* play a crucial role in identifying potential therapeutic targets and new compounds (Xu *et al*., 2022).

Creating tumour sample models *in vivo* containing stromal and immune cells significantly modifies tumour progression and immune evasion (Hanahan & Coussens, 2012; Pancione *et al*., 2014). Different *in vitro* culture techniques, such as air-liquid interface culture (ALI), have been used to add fragments to maintain the heterogeneous tumour microenvironment and thus keep polarised epithelial cell layers near stromal cells. This technique showed that cystic structures were expanded from the neonatal small intestine for up to 350 days in culture (Ootani *et al*., 2009).

1.12.6. *In vitro* models of breast cancer

A recent study utilised a sophisticated fluidic device designed to facilitate the long-term 3D growth and invasion of cancer cells, which allowed researchers to identify 305 target genes exhibiting altered expression levels in invasive cancer cells compared to non-invasive tumoroid cells. The primary objective of the study was to explore tumour heterogeneity by isolating and analysing the gene expression profiles of specific invasive tumour cell subpopulations. To achieve this, researchers employed four triple-negative breast cancer (TNBC) cell lines, SUM149, MDA-MB-231, BT-549, and HCC1937, alongside three patient-derived xenografts (PDXs) designated as PDX1 (9040), PDX2 (vari004), and PDX3 (vari068). These cell lines and PDXs were meticulously seeded and cultured within the fluidic device, enabling an environment conducive to studying their invasive behaviours. Subsequent bioinformatic analyses revealed significant alterations in various biological functions, including ECM reorganisation, changes in immune response, and variations in the Rho signalling pathway (Yong *et al*., 2020).

In a complementary investigation, researchers adopted microwell arrays to facilitate the formation of MDA-MB-231 spheroids. A series of techniques, such as H&E staining, IHC, cell viability assays, and flow cytometry, were rigorously employed to study the structural characteristics and growth dynamics of these spheroids. Findings indicated that the growth rate of MDA-MB-231 spheroids was notably slower compared to their counterparts cultured as monolayers. Additionally, the spheroids exhibited differential zones of proliferation, and

upon transfer to 2D adherent culture systems, the migration ability of these cells significantly increased. Importantly, the spheroids exhibited heightened drug resistance and were found to correlate with an increased incidence of EMT, highlighting their enhanced resilience to toxicological responses relative to 2D (Huang and Tang, 2020).

Other contemporary research has highlighted the efficacy of poly (ADP-ribose) polymerase (PARP) inhibitors, such as Lynparza, which have received approval for treating advanced-stage HER2-negative breast cancer in patients harbouring BRCA1 or BRCA2 mutations. The administration of PARP inhibitors strategically exploits the vulnerabilities associated with these mutations, making the cancer cells more susceptible to DNA damage. This is predicated on the role of PARP as a critical enzyme responsible for repairing DNA damage in both healthy and malignant cells. Consequently, when Lynparza is used in the context of *BRCA1* and *BRCA2* mutations, the ability of these cancer cells to repair their DNA is significantly compromised, thereby decreasing their chances of survival following DNA damage (Breast *et al*., 2020). Functional genomics was screened on 200 breast cancer mutated genes, using spheroid culture systems to resemble a human tumour. Histone acetyltransferase CREBBP was identified as a novel tumour suppressor in triple-negative breast cancer. CREBBP alterations were associated with increased genomic heterogeneity and poorer patient survival, leading to upregulation and dependency on a *FOXM1* gene proliferative program. Targeting *FOXM1*-driven proliferation with CDK4/6 inhibitors (CDK4/6i) impaired growth in spheroids, cell line xenografts, and patient-derived models from multiple tumour types with CREBBP mutations or loss of protein expression (Peck *et al*, 2021).

Recent advances in 3D culture techniques have successfully developed patient-derived tumour organoid (PDO) models sourced from primary human cancer tissues. These PDOs are particularly valuable because they preserve the inherent heterogeneity of the original tumours, which is crucial for accurately identifying potential therapeutic targets and assessing drug responses. This fidelity to the patient's tumour characteristics allows for more personalised and effective treatment strategies.

In addition to PDOs, significant progress has been made in 3D co-culture assays. These assays are designed to study the complex interactions between different cell types, providing

insights into cell-cell communications that influence tumour behaviour and responses to therapy. This is essential for understanding the tumour microenvironment's role in cancer progression and treatment resistance. Moreover, integrating microfluidic technology into 3D culture systems represents a groundbreaking shift in preclinical cancer research. By mimicking the architecture and dynamics of real vasculature and blood flow, these systems enable a more accurate simulation of the physiological conditions within a tumour. This technology allows researchers to study how drugs circulate, their efficacy in various microenvironments, and how tumours adapt to therapeutic pressures over time (Xu *et al*., 2020). Together, these advancements pave the way for improved cancer research methodologies and more effective treatment paradigms.

1.12.7. Matrigel

Matrigel, also known as Engelbreth-Holm-Swarm (EHS) extract, is a reconstituted basement membrane matrix derived from tumour tissues (Kleinman & Martin, 2005). This extracellular protein mixture is often recognised by its commercial form, Cultrex, and is renowned for its ability to form a stable 3D gel at physiological temperature (37°C). The composition of Matrigel closely resembles the natural extracellular matrix, providing a conducive environment that supports various biological processes such as morphological development (morphogenesis), cellular differentiation, and proliferation, particularly in cancer cells.

The basement membrane, from which Matrigel is derived, is rich in essential components such as collagen, specifically type IV collagen, and variously arranged sulphated macromolecules and glycosylated molecules. These constituents play critical roles in cell adhesion, migration, and signalling, fundamentally influencing cell behaviour (Kleinman & Martin, 2005). Matrigel is a supportive substrate for cultivating various cell types in practical applications. Researchers can either culture primary cells on the surface of the gel or mix them within the matrix itself before the gel solidifies. Unlike many other cell lines, primary cells tend to differentiate rather than proliferate in the presence of this matrix, highlighting its unique ability to guide cellular fate.

For instance, Sertoli cells, which are specialised epithelial cells crucial for testicular function, display different morphological characteristics depending on their culture conditions. When seeded on top of the Matrigel, these cells tend to develop into a columnar structure, resembling their natural organisation *in vivo*. Conversely, when Sertoli cells are embedded within the gel matrix, they transform into glandular structures, complete with lumens, mimicking functional aspects of tissue architecture (Hadley *et al*., 1985). This plasticity in cellular behaviour emphasises the importance of Matrigel as a tool in both *in vitro* studies and biomedical research, particularly in tissue engineering and regenerative medicine. However, the differentiation in the Matrigel depends on the type of cell added. Thus, a 3D structure is formed when all the cells are added to this matrix and become like the tissue of origin. Often, epithelial cells become polarised once they are added to the Matrigel, which differs from the mechanisms in other growing environments. Many growth factors and the development of new vessels, released by proteases from malignant cells and other cells, are characterised by Matrigel, basement membranes, and matrix proteins such as laminin 1 and collagen IV that induce growth and angiogenesis (Enbring & Kleinman, 2003). Studies have demonstrated that short sequences of amino acids or fragments of laminin-1 peptides increase the development of new vessels (angiogenesis), tumour growth, metastasis, and protease activity (Enbring & Kleinman, 2003; Stack *et al.*, 2004). The remarkable ability to mimic the features of a human tumour in a Matrigel has delivered significant potential, transitioning from 2D to 3D, and promises important answers to cancer research.

1.12.8. ECM scaffolds

ECM scaffolds are composed of different components, altering stiffness, which is essential for studying cellular dissemination and migration in metastasis. (Nicolas *et al.*, 2020). A change in tumour stiffness can occur in the tumour microenvironment as gene expression is altered during metastasis; typically, stiffness is associated with various stages of cancer. For instance, dissemination and malignant cell migration are affected by porous hydrogel (Beri *et al.*, 2018). However, there is insufficient data available in cancer research to determine the effectiveness of biomaterials in understanding the complex process by which cancer initiates and progresses. This involves the migration of individual cells that detach from a primary tumour and invade other organs through the bloodstream, as well as their interaction with drug

resistance. Various types of biological constructs, including biodegradable scaffolds, can facilitate the proliferation and differentiation of tumour cells.

1.12.9. Alginate constructs

Different scaffolds have been investigated for their potential application as ECM materials. An alginate scaffold is an engineered biomaterial construct that can specify hypoxia levels in metastasis. This 3D scaffold was combined with Matrigel and gelatin *in vitro* to investigate the behaviour of breast cancer cells, such as MDA-MB-231 cells. When a scaffold comprising 50% alginate and 50% Matrigel increased the size and the shape of tumour cells (Cavo *et al*., 2018; Jian *et al*., 2019). However, different concentrations of alginate (1%) and gelatine (7%, 9%) contributed to soft ECMs with high cell adhesion, growth, and accumulation.

1.13. Chitosan constructs

Chitosan constructs have been used in investigations on cancer metastasis. A component of the ECM, chondroitin sulphate, was used to design chitosan-chondroitin sulphate scaffolds to promote EMT in the prostate cancer model. Chitosan-based scaffolds have attracted numerous technologists studying cancer metastasis. On the other hand, chondroitin sulphate is present in tumour tissue as a component of the extracellular matrix. It creates chitosan-chondroitin sulphate-based scaffolds as an ECM construct, thereby stimulating EMT in prostate cancer (Xu *et al.*, 2020).

1.13.1. RAFT 3D culture systems

Real architecture for tissue (RAFT$^{TM)}$), a commercially available technology used to create high-density, physiologically relevant 3D cell environments, primarily for drug discovery and cancer research. RAFT$^{TM)}$ is a culture *in vitro* 3D culture system in which epithelial cells are grown and placed into a collagen gel (Meyers *et al*., 1992; Andrei, 2006). For instance, immortalised cell lines, explanted epithelial cells, and dispersed primary keratinocyte cells are used in RAFT^{TM} cultures (Andrei *et al.,* 2010). The organotypic RAFT^{TM} culture system was developed to resemble the structure and biological features of the epidermis (Asselineau & Prunieras, 1984; Meyers *et al.*, 1992). Furthermore, RAFT^{TM} 3D culture has delivered

significant potential to researchers in investigating epitheliotropic viruses (Chow, 2015). Its system ranges from 30 µm to 140 µm in thickness. For instance, RAFT^{TM} models utilise thin layers to achieve higher cell viability, thereby increasing oxygen and nutrient supply to cells with rapid proliferation. However, increased thickness in tumour models provides the tumoroids more space to proliferate into 3D. Different cell types, such as neonatal normal human fibroblast (NHDF neo) and HCT 116 colon cancer cell line, can be grown using RAFT^{TM} layers. This shows that more complex tissue models can be developed for experimental purposes. For instance, bigger blood vessels are surrounded by smooth muscle cells and fibroblasts (Schermuly, 2011). A RAFT^{TM} system was used in an investigation to absorb the liquid from the cell culture collagen combination, resulting in the formation of a dense cancer mass. This was achieved by embedding the RAFT^{TM} gel in a cell-free, looser rat tail type I collagen matrix as the liquid was removed, resulting in a thick artificial cancer mass ACM) of 100 micrometres, as per the protocol (Nyga *et al.*, 2013). Illustration of the various culture systems, ranging from 2D cultures to more complex 3D tumoroids, is shown below in (Figure 1.9). (adapted from Stamati *et al*., 2020).

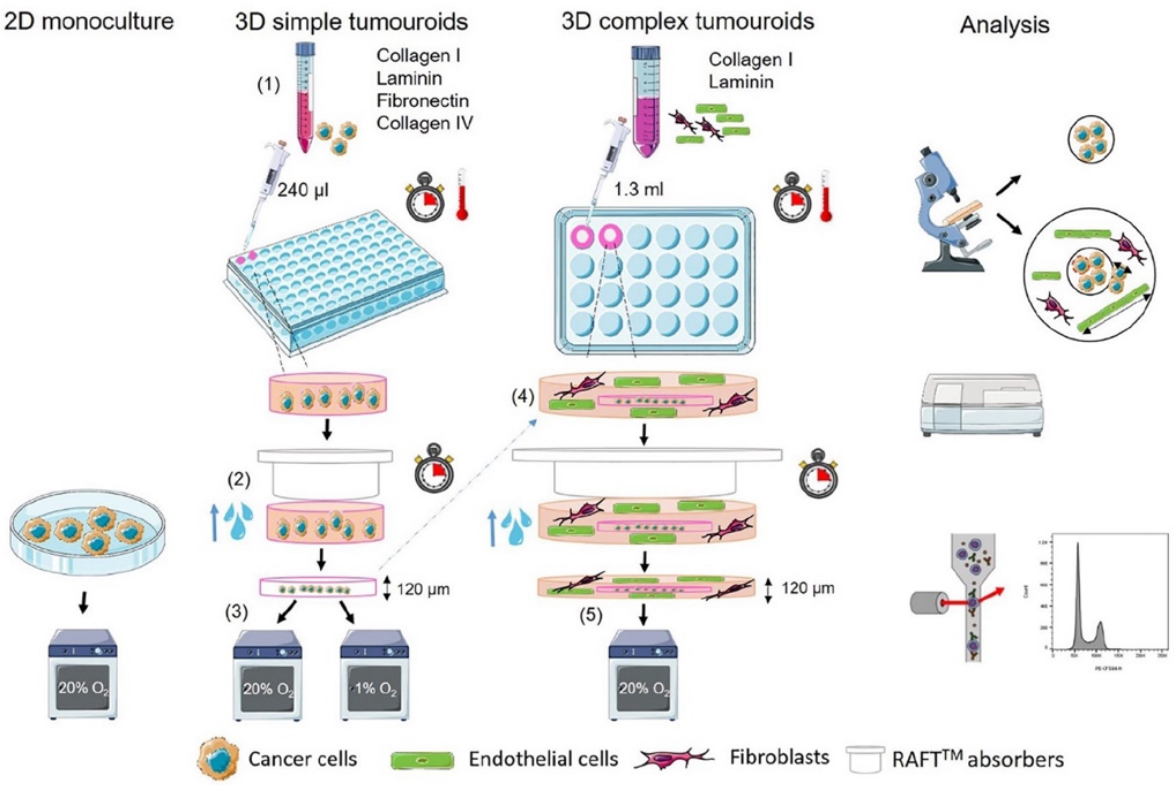

Figure 1.9. Schematic representation of different culture systems from 2D cultures to 3D complex tumoroids. Cancer cells are seeded in plates as monolayers and incubated to mimic the conditions required for cell proliferation. 1) 3D simple tumoroids consisting of collagen, laminin, fibronectin, and collagen IV as the ECM are surrounded by endothelial cells and cancer cells. 2) RAFT^{TM} absorbers absorb interstitial fluid; the tumoroid is treated with drugs. 3) Cancer cells treated with drugs. 4) 3D complex tumoroids are transferred into a hydrogel containing human dermal fibroblasts (HDfs) and human umbilical vein endothelial cells (HUVECs) in 24-well plates and compressed with RAFT^{TM} absorbers to produce a more complex tumoroid. 5) Cultures are then treated with drugs and analysed using flow cytometry, fluorescence imaging, cell viability, ELISA and cell cycle analysis (Stamati *et al*., 2020).

The next section (1.14) focuses on the aims and objectives of this study, which is based on different underlying hypotheses. One hypothesis suggests that altering the glycocalyx in cancer cells will enhance the penetration of chemotherapeutic agents. Another hypothesis proposes that glycosidase inhibition will impact cell motility, reduce cell numbers, and affect the metabolic activity of breast cancer cells. Additionally, it is hypothesised that 3D cell cultures demonstrate lower levels of CIN compared to 2D systems. Another hypothesis is that there is an association between glycosidase inhibition and CIN, and inhibition of glycosidase activity in MDA-MB-231 cells will increase CIN levels. The research questions in this study are: To what extent does inhibiting glycosidase enzymes sensitise breast cancer cells to doxorubicin? Is there a synergistic effect when doxorubicin is combined with iminosugars, including DNJ? Does this inhibition have a greater effect on breast cancer cells if there is a synergistic effect? Does the inhibition of NLG trimming differentially suppress breast cancer cell proliferation, migration, and invasion in 2D and 3D tumoroid models? and what is the relationship between glycosidase inhibition and CIN.

1.14. Aims and objectives

This study aimed to evaluate the effect on cell behaviour of inhibiting enzymes responsible for NLG trimming using breast cancer cells grown in 2D and 3D culture models.

Specific objectives were:

1) Assessment of the impact of glycosidase inhibition on the effectiveness of the chemotherapeutic drug, doxorubicin.
2) Assessment of the impact of glycosidase inhibition on cancer cell proliferation, migration and invasion in 2D and 3D.
3) Comparative assessment of CIN in 2D and 3D models and evaluation of the impact of glycosidase inhibitors on CIN.

Chapter 2

Materials and methods

2. Materials and equipment

The chemical reagents used in the experimental procedures are detailed in (Table 2.1.)

Table 2. 1. List of reagents

Reagents	Supplier / Source	Catalogue number
High glucose (4.5 g/L) DMEM	Thermofisher, UK	11965092
Foetal bovine serum (FBS)	Gibco, UK	16000044
Trypsin-EDTA Solution 10X	Sigma-Aldrich, UK	T4049
Rat Tail Collagen Type-I (>2 mg/mL, Chloroform Treate	First Link Ltd, UK	C3867
Phosphate-Buffered Saline (PBS)	Gibco, UK	D8537
Minimum Essential Medium (MEM)	Thermofisher, UK	11095080
Antibiotic Antimycotic Solution 100X	Sigma-Aldrich, UK	A5955
Neutralising buffer (1.6 M NaOH in 840 mM HEPES)	Sigma-Aldrich, UK	H3375
RAFT™ absorbers (96-welll)	Lonza, UK	016-1R17
RAFT™ absorbers (24-well)	Lonza, UK	016-1R16
Collagenase type-I	Gibco, UK	11500536
Hanks' Balanced Salt solution (HBSS)	Thermofisher, UK	14025092
HEPES buffer	Thermofisher Scientific, USA	J67485
Trypsin/EDTA, 0.5%	Thermofisher Scientific, UK	15400054
Dimethyl sulfoxide (DMSO)	Thermofisher Scientific, UK	20688
Cytochalasin-B (25 mg)	Thermofisher Scientific, UK	228090250
4',6-diamidino-2-phenylindole (DAPI -10mg)	Thermofisher Scientific, UK	D3571
Doxorubicin 50 mg	Thermofisher Scientific, UK	J64000
Alamar Blue 25 mL	invitrogen	Y00-025
Concanavalin A Flourescein Lectin	Vectors lab	FL-1001-25
Ulex Europaeus Agglutinin I flourescein	Vectors lab	FL-1061-2
Wheat Germ Agglutinin flourescein	Vectors lab	FL-1021-5
RNA extraction kit	Qiagen, RNeasy Kit	74104
QuantiTect SYBR Green PCR Kit (200)	Qiagen	204143
Ethanol 1 L	Thermofisher, UK	445740010
Methanol 2.5 L	Thermofisher, UK	325740025
Giemsa staining 100ml	Gibco, Life Technologies, Germany	10092013
Penicilline-streptomycin 10,000 units/mL	Thermofisher Scientific, UK	15140122
4 % v/v formaldehyde solution	Sigma-Aldrich, UK	R37814
DPX (phthalate-free) medium	Cell Path, UK	EA-1300-00A
DNJ	Phytoquest company	request
42	Phytoquest company	request
44	Phytoquest company	request
255	Phytoquest company	request
Formamide	Sigma-Aldrich, UK	F7503
0.1% Tween 20	sigma-Aldrich, UK	655204
SSC Buffer 20× Concentrate	Sigma-Aldrich, UK	S6639
VECTASHIELD antifade mounting medium with DAPI	Vectors lab	H-1500-10
Fixogum glue	(Marabu, U.K.).	Amazon
Potassium chloride at 0.075	Thermofisher Scientific, UK	042695-AP
Pan-centromeric probe AHC; KreatechTM	Leica Biosystems, Netherlands	KBI-20000G,

All the equipment, kits and software used are listed below in (Table 2.2).

Table 2. 2. Equipment, kits and software

Category	Item name	Manufacturer	Purpose
Kit	RNA extraction kit	Qiagen, RNeasy Kit	RNA extraction
Kit	QuantiTect SYBR Green PCR Kit (200)	Qiagen, RNeasy Kit	RT-qPCR
Equipment	Manual hemacytometer (Neubauer chamber)	Thermofisher	Cell counter
Equipment	DeNovix cell drop FL cell counter	Thermofisher	Cell counter
Equipment	Vios™ iDx and 255 L Tri-Gas CO_2 Incubator	Thermofisher	Incubator
Equipment	Gibson 1000,200,100,10 pipette	Thermofisher	Transfer volumes
Equipment	NSF 49 Certified A2 Biological Safety Cabinet	Lorderan	Sterilty control
Equipment	EVOS M7000 Imaging System w/ Onstage Incubator	Thermofisher	Flourescence microscopy
Equipment	Digital rocker platform	Thermofisher	Cell staining, agitation
Equipment	mpus BX51 Upright Brightfield/Darkfield Materials Microsco	Olympus	Cell counter, cell check
Equipment	Nanodrop spectrophotometer ND300	Thermofisher	Quantify RNA
Equipment	Spectrophotometer	BMG, Labtech, UK	Measure cell metabolic activity
Software	PRISM graphpad	Graphpad	Statistical analysis
Software	Image J	lational Institutes of Health	Processing and analysing scientific images
Equipment	light microscopy	Zeiss Axioskop 2, UK	Check quality of CIN images
Equipment	Zeiss 3000 automated scanner	Zeiss	Scanning multiple slides
Equipment	Fluorescence microscope magnification model BX41TF	Olympus	Captured flourescent images
Software	Cytocam software v2	Olympus	visualise the images through a camera
Software	QUPATH	QUPATH	Processing CIN images
Equipment	Megafuge™ 8 Small Benchtop Centrifuge Series	Thermofisher	Spin samples
Equipment	Real-Time PCR Instrument	Thermofisher	Gene expression

Table below (Table 2.3) presents four different breast cancer cell lines used to study glycosidase inhibition and CIN. These cell lines were specifically chosen because of their distinct subtypes and key characteristics, making them strategically important for this research. The goal is to determine whether glycosidase inhibitors affect the cell surface in all evaluated breast cancer cell lines, potentially allowing for better penetration of chemotherapeutic drugs. To assess whether these cell lines exhibit higher CIN when grown in 2D and 3D cultures.

Table 2. 3. Immortalised breast cancer cells deployed in this study.

Cell line	Type/subtype	Source details	Key characteristics
MCF-7	ER+ (Luminal A) (Koshkina *et al* ., 2011)	Pleural effusion, 69-year-old woman (Soule *et al* ., 1973)	Epithelial ductal adenocarcinoma; expresses ER, PR, and glucocorticoid receptors (Koshkina *et al* ., 2011); non-invasive; highly responsive to chemotherapy (Paclitaxel) (Holliday & Speirs, 2011; Abu Samaan *et al* ., 2019); used to study estrogen-dependent growth and hormonal therapy (tamoxifen) resistance (Moon *et al* ., 2020; Hegde *et al* ., 2016).
SKBR3	HER2+ (Peiris *et al* ., 2017)	Preural effusion from 43-year-old Caucasian woman (Trempe & Old, 1970).	Epithelial adenocarcinoma (Trempe & Old, 1970); overexpresses HER2 (Neu/Erb-2) gene product; evaluated for Herceptin binding and sensitivity to doxorubicin, EGF, and IGF (Peiris *et al* ., 2017).
BT-549	TNBC (Basal-like) (Cytion, 2025)	Isolated in 1978 from 72-year-old female (Lasfargues *et al.* , 1978).	Invasive epithelial ductal carcinoma (Lasfargues et al., 1978); negative for ER and PR; no HER2 amplification; Results in a poorer prognosis because the cancer cells have spread beyond the mammary ducts, indicating metastatic behaviour (Perou *et al* ., 2000; Sorlie *et al* ., 2001); used for drug resistance and evaluating new chemotherapeutic agents (Cytion, 2025).
MDA-MB-231	TNBC (Claudin-low) (Holliday & Speirs, 2011)	Preural effusion 40-year-old woman.Cailleau *et al* ., 1974)	Epithelial adenocarcinoma cell line; (cailleau *et al* ., 1974); highly aggressive; lacks ER, PR, and HER2 amplification (Liu *et al* ., 2003; Chavez *et al* ., 2011); Results in a poorer prognosis because the cancer cells have spread beyond the mammary ducts, indicating metastatic behaviour (Perou *et al* ., 2000; Sorlie *et al* ., 2001); invasive via proteolytic breakdown of ECM; claudin-low features include downregulated claudin-3/4, low Ki-67, and CD44+CD24-/low phenotype (Holliday & Speirs, 2011).

2.1. Methods

2.1.2 Cell culture in 2D

BT-549, SKBR3, MCF-7, and MDA-MB-231 breast cancer cell lines were obtained from the American Type Culture Collection (ATCC, VA, USA). Cells were cultured under sterile conditions using a containment level 2 hood cabinet. RPMI-1640 medium was used as the culture medium for BT-549 and MDA-MB-231, while Dulbecco's Modified Eagle Medium (DMEM) medium was used for MCF-7 and SKBR3. All cell lines were grown with 10% v/v foetal bovine serum (FBS), 1% v/v penicillin/streptomycin at 37°C and 5% $C0_2$. The penicillin reagent was not added before the treatments were deployed to avoid interfering with the drugs added to the cells. Most of the time, when the cells were taken from the liquid nitrogen tank and thawed accordingly, no penicillin was added to check for contamination or any signs of infection. Cells were cultured per ATCC Cell Culture guidelines (ATCC, CRM-HTB-26TM, 2021; ATCC, HTB-122TM, 2021). Stocks of cells were constantly grown from passage 1 to passage 10 to avoid alterations in morphology, response to stimuli and growth rates. All experiments were carried out within this range of passages, ideally at passage 4.

Usually, cells were allowed to reach 70-80% confluency before being passaged one day before cells were seeded into the 96- and 24-well plates. The same protocols were used for all other experiments, including those on CIN and glycobiology. When the cells reached a 70-80% confluence, the medium was discarded and washed with phosphate buffer saline (PBS) (3 mL), then discarded. The cells were required to be detached from the flask as 3 mL of Trypsin/EDTA X1 was added and incubated at 37°C and 5% $C0_2$ for 3 minutes. The cells were checked under the microscope to see if they were fully detached from the surface. About 3ml of medium was added to the cells, and the cells were counted by transferring 10 µL of Medium/cells into a manual hemacytometer (Neubauer chamber) covered by a cover slip to allow the cells to spread into the four grids. The cells were counted using a microscope. The cells were counted inside the four grids. The number of cells was calculated by adding the total number of cells in the four grids multiplied by 10,000 and divided by 4. Then, 100 µL of medium containing 10,000 cells was added to each 96-well plate, and the cells were allowed to adhere to the surface for 24 hours before glycosidase drug treatment (see section 2.1.5 for

detailed protocol). An automated DeNovix cell drop FL cell counter at the 501 TC laboratory at the University of Westminster was also used to double-check the accuracy of the cell numbers. This protocol followed the same cell culture procedure used for CIN studies in 2D, except that the cells were not seeded into plates. Experiments were deployed in the T25 and T75 flasks instead.

For the CIN studies (see section 2.4 CBMN), for the detailed protocol. The cells reached 70-80% confluency before all experiments, including glycosidase inhibition and CIN studies, were deployed.

2.1.3 3D culture

Cancer cells were embedded in collagen type-1 (rat tail) using the RAFT™, a commercially available 3D cell culture system deployed in 24-well plates. The protocol was carried out according to the manufacturer's instructions and as described (Magdelin *et al*., 2017). In brief, the reagents were prepared and then left in ice-cold water to maintain the rat tail collagen in a gel state. The amount of reagent added varied due to the number of wells in the cell culture plates used. In Table 2.4, all the reagent concentrations were described. 10X MEM was added to a 50 mL Falcon tube, and the collagen was carefully transferred to avoid air bubble formation. Then, it swirled slowly, drop by drop, until the solution turned a light pink colour. The neutralising reagent was prepared as a stock solution by adding 4.165 mL HEPES and 0.825 mL NaOH (10 M NaOH + 1 mM HEPES), and 0.493 mL was added to the Falcon tube. The cell stock was added last, after the cell count was performed using both the hemacytometer and the automated hemacytometer machine, to ensure the accuracy of the cell count. After centrifugation, a fresh medium containing 10% v/v FBS and 1% v/v penicillin/streptomycin was added to the desired amount of 500,000 cells. 1.2 mL of solution was added to each well (using a Gibson 1000 pipette) and incubated at 37°C and 5% CO_2 for 15-20 min to allow the collagen-embedded cells to dry. The RAFT™ absorbers were carefully added to each well and left at room temperature for 20 minutes.

All reagent liquid was absorbed using the RAFT™ absorbers in this step. Then, 1 mL of fresh growth medium was added, and the gels were placed in the tissue culture incubator. Initially, the 3D constructs were allowed to grow for between 18 and 28 days. Every 2 days, 500 µL of medium was removed, and an equal volume of fresh medium was added. After compressing

the collagen, the construct achieved a thickness of 100 µm (Nyga *et al.,* 2013). This protocol was modified from the original method; instead of adding 100,000 cells into the collagen in a 24-well plate, 500,000 cells were added.

Additionally, the 3D models instead of allowing to grow for 28 days; they had grown for 7 days before conducting CIN studies (see Section 2.6 CIN studies in 3D models) for detailed protocol. The reason why this protocol was required to be modified is that in the CIN studies in the four cell lines, insufficient cells were retrieved and visualised once fixed and set in the slides. Thus, several experimental repetitions were required, which increased the number of consumables, RAFT absorbers, and medium with 10% v/v FBS. The concentration of the reagents used to prepare the cells embedded in collagen (is shown in table 2.4).

Table 2. 4. The concentration of the reagents used to prepare the RAFT^{TM} system.

Plate	Number of wells	10X MEM (mL)	2mg/mL collagen (mL)	Neutralising solution (mL)	Cells seeded (mL) 500,000 cells/well
24 well plate	5	0.85	6.8	0.493	0.357 mL

2.1.4. 3D Tumoroid assembly and optimisation.

Tumoroids are a 3D model derived from immortalised cell lines and prepared in high-density collagen constructs (RAFT™ 3D model systems) under sterile conditions. Cells were prepared as in Section 2.2.2 and surrounded with collagen to create an ACM. In this study, MDA-MB-231 and MCF-7 breast cancer cell lines were deployed to fabricate tumoroids. Tumoroids consisted of a dense central ACM that contained the cancer cells and were generally prepared in a 96-well plate at a 2mg/ml collagen density, as plastic compression was applied. Then, a 24-well plate-sized model containing only collagen, termed an acellular compartment, was also prepared and assembled for breast cancer tumoroid models in glycobiology studies. The assembling architecture of the tumoroid “sandwich procedure” used by the University College London (Pape et al., 2019) was adapted in this study. In the protocol from the

"sandwich procedure", the tumoroids were generally allowed to grow for 21 days until experiments were deployed and 50,000 cells were seeded into the ACMs; however, for the glycosidase inhibition studies, this protocol was modified to optimise the growth of MCF-7 and MDA-MB-231 tumoroids. Over 10 days, tumoroids consisting of 20,000 cells each were seeded within collagen in a 96-well plate and compressed to create the ACMs and acellular compartments, which were monitored for optimisation studies. This resulted in metabolic activity assessments indicating optimal conditions for the tumoroids to undergo glycosidase inhibition treatment and testing from day 2.

A total of 240 µL of the collagen mixture was added to each 96-well plate containing 20,000 cells/ well and incubated at 37°C for 15 minutes to allow the gel to dry correctly. Non-cross-linked collagen was prepared simultaneously by repeating the RAFT^{TM} protocol, containing 1.3 mL in each 24-well plate for 15 minutes at 37°C. This was the first layer before the ACMs were added in the middle. Once the cast collagen hydrogels containing cancer cells were dried, 96-well plate-sized RAFT^{TM} absorbers were added to compress the collagen for 15 minutes at room temperature. This is how an ACM was created. Then, the ACM was carefully detached using sterile equipment and transferred into a 24-well plate containing non-compressed collagen. A final 1.3 mL layer of collagen/non-embedded cells was added to the 24-well plate and incubated for 15 minutes at 37°C and 5% CO_2 to allow cross-linking. The tumoroid was then compressed using a 24-well plate RAFT^{TM} for 15 minutes at room temperature. Then, 1 mL of DMEM with 10% v/v FBS was added, and every two days, half the volume was removed and replaced with 500 µL of fresh medium.

MDA-MB-231 and MCF-7 tumoroids were constructed, and their growth and metabolic activity were assessed at days 3, 5, 7, and 9. At day 2, MDA-MB-231 and MCF-7 tumoroids were incubated with 10% v/v Alamar Blue reagents at day 2 for 24 hours at 37°C, 5% CO_2. The next day, the supernatant was transferred from each tumoroid into a new plate to deploy spectrophotometry and measure its metabolic activity. The tumoroids from day 3 and the subsequent cell viability time points were washed several times with PBS and fixed with a 4% v/v formalin solution for 20 minutes at room temperature in a rocker. The protocol used for the DAPI staining procedure was adapted from the 2D cellular staining to 3D tumoroids for nuclei count analysis. Image analyses were developed at the University of Westminster by

generating a complete image of tumoroids from 176 stitched images captured at 40x total magnification using an Evos microscope, which is a digital inverted imaging system designed by Thermo Fisher Scientific for cell culture and fluorescence imaging.

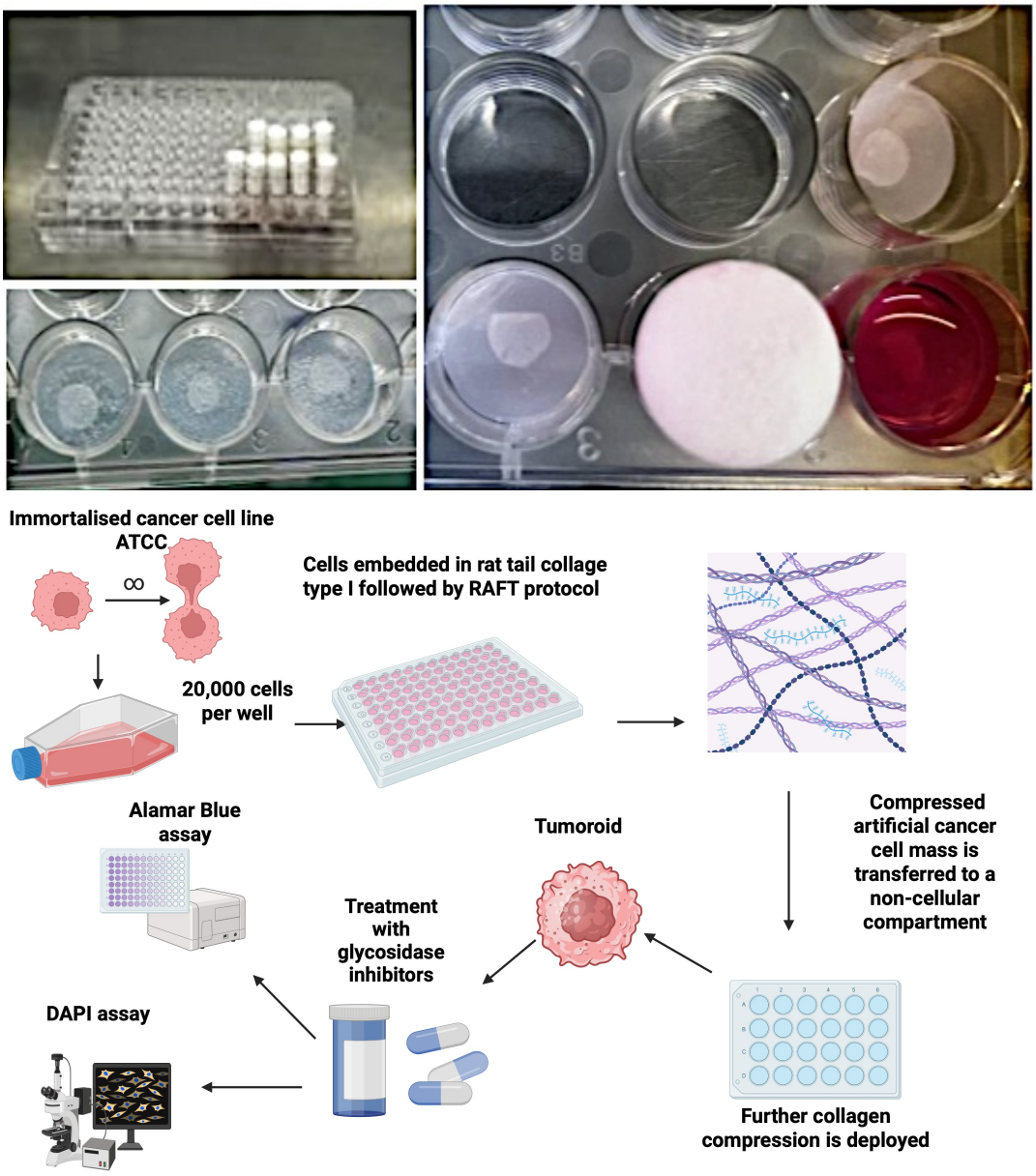

Figure 2.1. Schematic representation of an example of the fabrication of tumoroids. Upper panel: collagen compression using RAFT^{TM} absorbers, followed by medium and incubation. Lower panel: Methodology of tumoroids fabricated from immortalised cell lines embedded in compressed collagen, assembled, and treated with glycosidase inhibitors to allow studies of breast cancer cells following glycosidase inhibition.

2.1.5. Chemotherapy Drug and glycosidase inhibition treatment in 2 and 3D

In 2D cultures, concentrations of DNJ at 0.5 mM and 1 mM, along with the chemotherapeutic agent doxorubicin at 0.5 µM, have been previously utilised in other studies (Peiris *et al*., 2017; Azimi *et al*., 2020). Therefore, iminosugars obtained from Phytoquest (42, 44, and 255) were administered at the same concentrations as DNJ (0.5 mM and 1 mM) for glycosidase inhibition treatment on breast cancer cells. These compound inhibitors, which were provided in collaboration with the Phytoquest company by Dr Robert Nash, specialise in discovering and isolating iminosugars, a class of natural plant-based compounds that function as potent glycosidase inhibitors for therapeutic use and were kindly provided to study the effects these iminosugars may have in breast cancer cells. Iminosugars are a diverse group of compounds found in plants and microbes that have been of interest as potential therapeutic agents due to their ability to interact with human glycosidases, various proteins, and sugar receptors (Nash et al., 2011). These specific compounds have been highlighted in research and analytical contexts for their unique properties: Compound 255: Commonly used as a reference in the evaluation of glycosidase inhibition, this compound is recognised for its excellent water solubility and stability, often used to explore the regulation of postprandial hyperglycaemia because it can influence carbohydrate metabolism. Compound 42: This compound has been noted in research focusing on cationic peptides and polycations. In certain patent applications linked to Phytoquest investigations, it is described as a polyhydroxylated alkaloid, which may act as a precursor or structural element for synthetic derivatives such as 1-deoxynojirimycin. Compound 44: Typically identified as a targeting moiety within complex formulations, this compound is distinguished by its ability to selectively attach to cell surface molecules and positions it as a potential candidate for chaperoning roles, where the iminosugar is required to stabilise specific mutant enzymes, such as in therapies for Fabry disease. These compounds belong to a broader library of over 200 reported natural isolated iminosugars.

This experiment was conducted on 2D cultures, where the cells were exposed to the inhibitor compounds for 24 hours once they reached 70-80% confluency in 96-well plates. The breast cancer cells were treated with the inhibitor compounds, combined with and without

doxorubicin. Likewise, for the 3D experiments, the 3D models and tumoroids were subjected to glycosidase inhibitors at 0.5 mM without doxorubicin for 10 days. At days 2, 4, 6, 8, and 10, the cells were exposed to the compound inhibitors.

2.1.6. Alamar Blue assay in 2D and 3D

The Alamar Blue assay is a metabolism-based method that has been widely used since its introduction in 1993. This assay is employed to investigate the cytotoxicity of various test compounds *in vitro* and assess the proliferation of cell lines, bacteria, and fungi (Fields & Lancaster, 1993; Ahmed *et al*., 1994).

Alamar blue assays measure the metabolic activity or proliferation of living cells. The blue reagent is a non-fluorescent blue dye indicator, non-toxic and cell membrane permeable, known as resazurin (7-hydroxy-10-oxido phenoxazin-10-ium-3-one) in its oxidised form.

The oxidised state of the reagent, which appears blue, has its highest light absorption at a wavelength of 570 nm. In contrast, the pink reduced form exhibits a different absorbance spectrum when cells metabolise the reagent. To measure the extent of reduction of Alamar Blue, absorbance is generally recorded at 570 nm, employing 600 nm as a reference wavelength for normalisation. The absorbance values were measured at 600 and 570 nm using a spectrophotometer microplate reader.

The reduced form, resorufin (7-hydroxy-3H-phenoxazin-3-one), is a fluorescent pink dye that indicates the number of living cells, depending on the intensity of fluorescence generated. The conversion of resazurin to resorufin occurs in the cytosol, a reducing cell environment. This process is mediated by intracellular diaphorases, which are enzymes that facilitate the transfer of electrons, utilising NADPH or NADH as reductants (O'Brien *et al*., 2000).

This study used Alamar blue to determine the cytotoxic effect of the glycosidase inhibitors and doxorubicin on the four breast cancer cell lines *in vitro*. The protocol was deployed using the manufacturer's protocol (Invitrogen), which involved incubation times ranging from 1 to 4 hours. Still, for the 2D, the cells were exposed to the glycosidase inhibitors, and the protocol had to be optimised as the reduced form (pink colour) was obtained from 6 to 8 hours.

For the 2D monolayer cultures, SKBR3, BT-549, MDA-MB-231, and MCF-7 breast cancer cells were seeded into 96-well plates one day before treatment, allowing them to adhere to the surface for at least 24 hours before treatment with the glycosidase inhibitor combined with

doxorubicin. The seeding density of cells was 10,000 cells/well (96-well plates). Each treatment, for instance, DNJ, was analysed in triplicate on the 96-well plate. All the cells were treated with glycosidase inhibitors at 0.5 mM and 1 mM and doxorubicin (5 μM) for 24 hours. When the glycosidase inhibitor doxorubicin treatment commenced, the serum was adjusted to 5% v/v FBS and DMEM.

After 24 hours, the cells were incubated with 10% v/v Alamar Blue reagent for 6 - 8 hours at 37°C and 5% C02. The cells containing the medium and the reduced pink resorufin were transferred carefully into a new 96-well plate.

As previously described in the tumoroid optimisation (section 2.2.3), the MDA-MB-231 and MCF-7 tumoroids were constructed, and each of their growth and metabolic activity was measured at days 3, 5,7 and 11. At day 2, MDA-MB-231 and MCF-7 tumoroids were incubated with 10% v/v Alamar Blue reagent for 24 hours at 37°C and 5% CO_2. The next day, the supernatant was transferred from each tumoroid into a new plate to deploy spectrophotometry and measure its metabolic activity. For the glycosidase inhibition treatment on MDA-MB-231 optimised tumoroids, the metabolic activity was measured at day 11 after 24 hours with 10% v/v Alamar blue reagent.

The application of collagen matrices as 3D cell culture systems has significantly risen in recent years. Numerous publications in the literature indicate that when cells are grown in a 3D environment, observable modifications occur in their phenotype, metabolism, or composition compared to traditional two-dimensional monolayer cultures (Lupanova *et al*., 2010; Wu *et al*., 2009). This is why the incubation time for Alamar blue reagent was increased to 24 hours, as it requires a longer duration to penetrate the collagen and complete a reduced form compared to conventional monolayer cultures.

The following formula was used to calculate the percentage difference in reduction between treated and untreated cells in these experiments:

O1 = molar extinction coefficient (E) of oxidised Alamar Blue (blue) at 570 nm*

O2 = E of oxidised Alamar Blue at 600 nm*

A1 = absorbance of test wells at 570 nm

A2 = absorbance of test wells at 600 nm

P1 = absorbance of positive growth control well (cells plus Alamar Blue but no test agent) at 570 nm

P2 = absorbance of positive growth control well (cells plus Alamar Blue but no test agent) at 600 nm

$$\textbf{Percentage difference in reduction\%} = \frac{(O2 \times A1) - (O1 \times A2)}{(O2 \times P1) - (O1 \times P2)} \times 100$$

2.1.7. Lectin and DAPI (4',6-diamidino-2-phenylindole) assay in 2D and 3D

This protocol followed the method used in other 2D studies (Peiris *et al*., 2017). Once the cells had been treated with glycosidase inhibitors for 24 hours, they were washed with PBS for 5 minutes. Then, 100 µL of 4% v/v formaldehyde was added carefully to fix the cells at room temperature for 30 minutes. The formaldehyde was disposed of carefully by tilting the plate and extracting the liquid from the edges of the well to prevent damage to the fixed cells. This technique was employed throughout the entire procedure. The cells were then washed carefully with PBS for 5 minutes on a rocker platform at a gentle speed. This step was repeated twice. They can be stored overnight or proceed to the next steps right away. The PBS was discarded, and a blocking solution containing 5% v/v bovine serum albumin (BSA) was added. Surface blocking was necessary to reduce the non-specific interactions by blocking remaining spaces over the solid surface. The plate was left on the rocker platform at room temperature for 30 minutes. Next, the cells were washed twice with PBS for 5 minutes each. After this, all steps must be carried out in the dark. Aluminium foil was wrapped around the plate to prevent quenching the fluorescence. Lectins (Con A, UEA-I and, WGA) were prepared with a concentration of 5-10 mg/ml. The volume of each 96-well plate is 1 µL of lectin per 100 µL of PBS.

Generally, a stock of 15 µL in 1.5 mL PBS stock was made to increase the accuracy of smaller volumes when they are transferred into the mix preparation. The cells were left in the rocker platform at room temperature for 1 hour. The lectin preparation was disposed of, and cells were washed with PBS. This step was repeated. A 100 µL of DAPI-prepared solution was

added, consisting of 2 µL of DAPI in 10 mL of PBS (1 µg/mL). The cells were incubated for 10 minutes at room temperature on a rocker platform. The cells were washed twice with PBS, and 100 µL of the solution was added to each well. They were stored overnight. The image capture analysis must be completed within 5 days to maintain fluorescence at optimal quality. 3D tumoroids were stained with DAPI. For the DAPI incubation step, 1 mL of DAPI solution (1 µg/mL) was uniformly added to each well of the 24-well plate. This step was extended to 30 minutes, in contrast to the original protocol's 10-minute incubation time, allowing for better nuclear staining and visualisation.

In the 3D protocol, the tumoroids were washed with 1 ml of PBS, which was added to each well of the 24-well plate to maintain the tumoroids in a suitable environment. This was repeated twice. Then, the tumoroids were fixed with 4% v/v formaldehyde for 30 minutes at room temperature. Then the formaldehyde was removed, and the tumoroids were washed with PBS for 5 minutes. The tumoroids were stained with DAPI for 30 minutes. At this point, the tumoroids were either stored at the appropriate temperature for future analysis or immediately processed for imaging to ensure optimal preservation of structural and functional integrity.

2.1.8. Imaging of 3D tumoroids

After the tumoroids were fixed and stained with DAPI, the images were captured at 100X in both DAPI fluorescence-stained and brightfield channels for 24-well plate size resolution. These resulted from 176 multiple captures stitched together from an automated setting using Evos fluorescent microscopy. In previous studies and published articles, images of 3D models and tumoroids were captured sequentially (clockwise), allowing only ¼ of the images to be seen. Now, with the automated settings, a whole tumoroid can be seen, resulting in more accuracy for cell migration studies.

2.1.9. Image J analysis in 2D and 3D

Cancer cell images were captured in 2D using an Olympus inverted microscope and an Evos fluorescent microscope. The analysis of the microscopy-captured images was conducted using ImageJ (http://imagej.nih.gov/ij/download.html). The selected images were edited and captured using the same light intensity as all others. The magnification used to capture the

images was 100X. Following this section, measurements of the images were categorised depending on the type of analysis, such as:

2.1.10. Particle analysis

The particle analysis of the 2D and 3D images was performed by adjusting the threshold HBS, which converted the images into a binary process/mask/watershed, followed by particle analysis measurement. The DAPI assay was used to stain the nuclei of the cells as an alternative method for counting cell numbers and to analyse the various images captured, including those treated with glycosidase inhibitors, for comparison with untreated cells to assess any reduction in cell numbers. The particle analysis of the cells stained with DAPI is illustrated below in (Figure 2.2). The left image showed the DAPI-stained cells and the right one showed the detection and automated count of cells after the measurement was deployed.

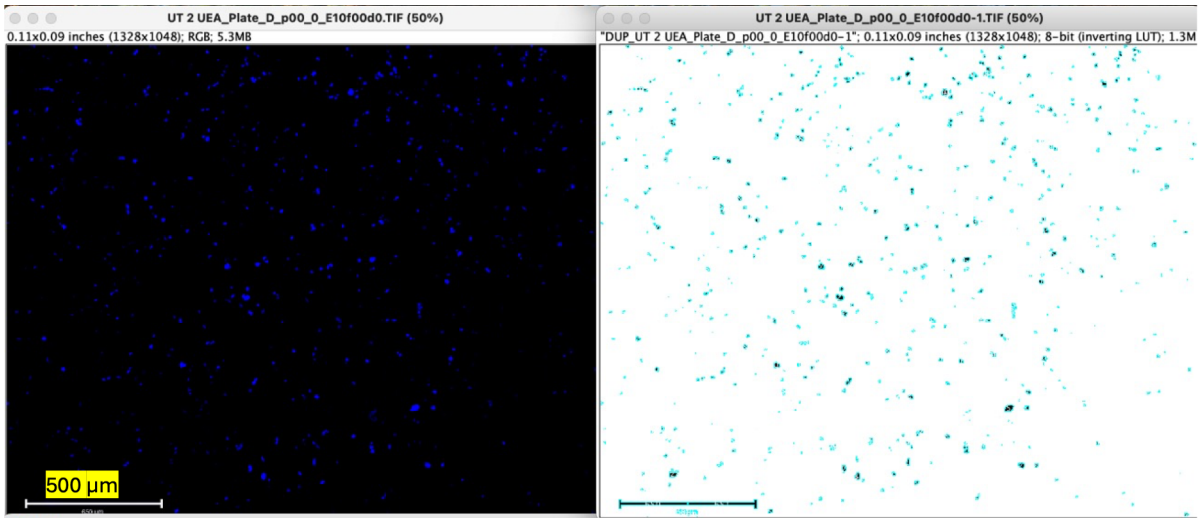

Figure 2.2. Particle analysis of stained cells with DAPI grown in 2D. Cells were imaged at 40x magnification using an EVOS microscope, with a scale bar representing 500 µm. In the left image, DAPI-stained cells are shown, while in the right image, ImageJ particle analysis highlights the results of counted cells.

In the tools section for the lectin staining assay, the fluorescence measurement is performed by drawing a square of the main area and a small square for the black background. More details of this measurement are described in Chapter 3 (Section 3.2). The image data was processed for further statistical analysis using Excel and GraphPad.

To carry out particle analysis in the 3D models, the tumoroid cell count of the whole tumoroid was initially measured. However, some folded collagen areas could have interfered with the cell count. Therefore, a non-folded collagen area of 250 µm was selected for each tumoroid measurement to minimise this interference. This ensured that the measurement was more accurate and that the results were reliable. This study utilised different measurement parameters and techniques to obtain precise and meaningful data, such as using the combination of the brightfield and DAPI settings in order to have clearer areas for cell count to deploy particle analysis. See chapter 4 (Section 4.10) for a more detailed description.

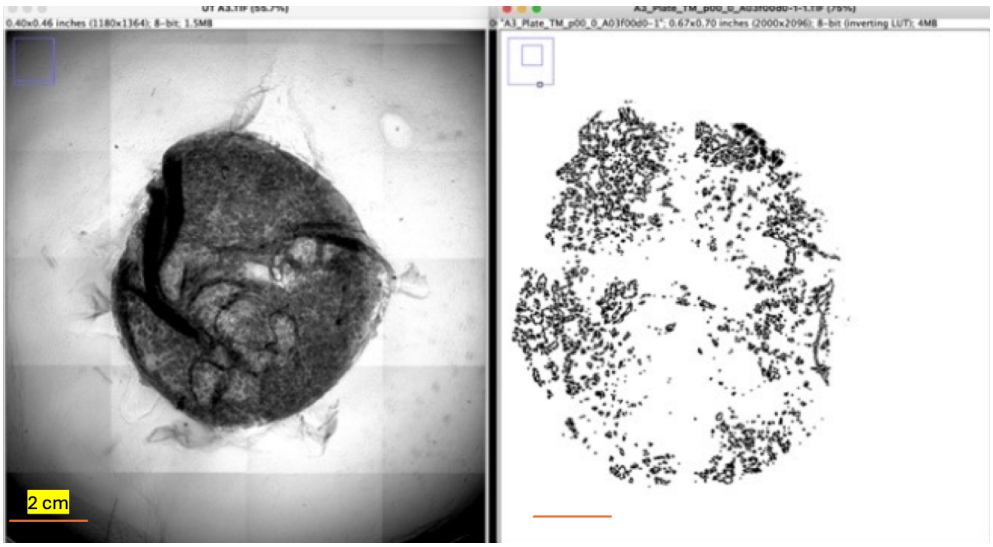

Figure 2.3. A brightfield image of the whole tumoroid is shown on the left side, and on the right side, the results of the ImageJ binary mask particle analysis are displayed, indicating that, despite some folded collagen areas in the tumoroid, the algorithm can accurately predict cell growth. The entire tumoroid image was captured at 100X magnification, with a scale bar representing 2 cm, resulting from 176 multiple captured using Evos fluorescent/brightfield microscopy.

The study set various parameters to measure the outgrowth, cell count, and invasive bodies of 3D tumoroids. Different parameters were used to obtain accurate measurements, including particle analysis to count the targeted areas in binary or threshold images. For instance, to analyse the DAPI images, all images were processed by setting them in process/binary/mask/count edges/maximise count/watershed. This was done to improve the accuracy of areas that were difficult to count, such as those with a high density of cell clumps within the compressed collagen. An example of how the measurement for each parameter of

outgrowth and cell migration of invasive bodies into the acellular compartment was explained in more detail is in Chapter 4 (see Section 4.2 and 4.3).

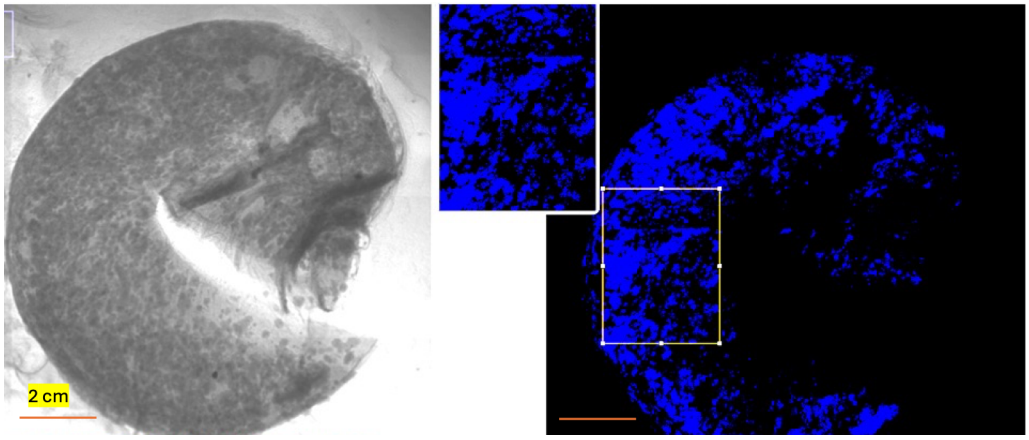

Figure 2.4. A brightfield image of the whole tumoroid is shown on the left side. On the right side, the DAPI-stained tumoroid is highlighted by a square to facilitate measurement of cell density, which can also be indicated in the whole image, despite some folded collagen areas in the tumoroid; the algorithm can accurately predict cell growth. The entire tumoroid image was captured at 100X magnification, with a scale bar representing 2 cm, resulting from 176 multiple images stitched together using Evos microscopy.

2.1.11. Wound healing assay

The wound healing (or scratch) assay is a widely utilised experimental technique designed to quantify 2D cell migration. This method is a standard, efficient, and simple *in vitro* approach for researching cell migration, resembling the way cells move during the wound healing process *in vivo* (Rodriguez *et al*., 2005). In this assay, an artificial gap is created on a confluent monolayer of cells, enabling researchers to observe and measure the cells' migratory response over time. To conduct the assay, breast cancer cells were seeded in 24-well plates at a density of 0.5 × 10^5 cells/mL and incubated for 24 to 48 hours until they achieved 90-100% confluence. Once confluence was reached, a standardised scratch was meticulously created using a sterile 1 mL micropipette tip. A ruler was placed on the wells to ensure accuracy and make a straight, uniform line across the cell layer.

Following the creation of the scratch, the culture medium within the wells were removed, and the cells were gently washed twice with 500 µL of PBS to eliminate any floating cells and debris that could interfere with the results. For the treatment conditions, 1 mL of complete DMEM supplemented with 10% FBS containing specific inhibitor compounds was added to each well while maintaining a control group of untreated cells for comparison.

Time-lapse imaging was initiated immediately after the medium replacement (designated as T = 0), with subsequent images captured at 6, 12, and 24 hours using a multi-mode plate reader at a magnification of 40X. Each plate was taken one by one, very carefully, and wrapped with parafilm to maintain sterile conditions. Images were taken straightaway by minimising the time outside the incubator. Additionally, an area of the well plate was marked at time 0 to maintain consistency in the exact location across all time points. This allows for real-time observation of the wound closure process.

Once the imaging was completed, wound areas were analysed using ImageJ software. A polygon selection tool was used to accurately outline the wound area, which was then quantified by selecting the "Measure" option from the analysis menu. The extent of cell migration and wound closure was calculated at each time point (T6, T12, and T24) by subtracting the wound area at the respective time from the initial wound area at T0. The percentage of wound closure is subsequently determined by normalising the difference in area to the initial area at T0, providing clear insights into the effects of treatments and the migratory capacity of the cells. % gap closure: (remaining area at any given point x100)/0hr area, then the result is subtracted from 100.

2.2. Gene expression analysis

To determine the impact of glycosidase inhibitors on treated cells, the following markers of apoptosis: *BCL-2*, *CASP-3*, and *CASP-9* were analysed through reverse transcriptase real-time polymerase chain reaction (RT-qPCR).

BT-549 and MDA-MB-231 cell lines cultured in T25 flasks were grown to 80% confluency and exposed to glycosidase inhibitors DNJ and Phytoquest compounds (42 and 255) for 24 hours. The glycosidase inhibitor concentration was 0.5 mM for both DNJ and Phytoquest inhibitors. Control was untreated cells. Following treatment, Trypsin/EDTA (X1) was added to the cells and incubated at 37°C for 3 minutes to allow cell detachment. This was followed by the

addition of medium and centrifugation at 1100 rpm for 5 minutes at 24°C. The yield of each sample varied between 400,000 and 500,000 cells and was then processed for RNA extraction.

2.2.1. RNA Extraction

The method used for extracting total RNA from MDA-MB-231 and BT-549 cells treated with glycosidase inhibitors in 2D involved several steps. Initially, the samples were homogenised by adding 0.35 mL of lysis buffer (RLT) to the cell pellet and resuspending it. The samples were mixed with 70% v/v ethanol and transferred to a RNeasy MinElute spin column. The column was centrifuged for 15 seconds at 13,000 rpm, and the flow-through was discarded. Next, 0.35 mL of buffer RW1 was added to the column and spun for 15 seconds at 13,000 RPM. The flow-through was again discarded, and 10 µL DNase I stock solution and 70 µL of buffer RDD were added directly to the RNeasy MinElute spin column membrane. The column was left to incubate for 15 min at room temperature. After that, 0.35 mL of the RW1 buffer solution was added to the column and centrifuged for 15 seconds at 13,000 rpm. The flow-through was discarded, and 0.5 mL buffer RPE was added to the column and centrifuged. The flow-through was again discarded, and 0.5 mL of 70% ethanol was added to the column, followed by centrifugation at 13,000 rpm for 2 minutes. The column was transferred to a new 2 mL collection tube and centrifuged for 5 minutes to dry the membrane. The column was then transferred to a 1.5 mL collection tube, and 20 µL RNase-free water was added to the middle of the spin column membrane. The spin column was centrifuged for 1 min at 13,000 rpm to obtain the total RNA. RNA purity and quantity were assessed using a Nanodrop spectrophotometer at 260/280nm.

2.2.2. cDNA Synthesis

Creating complementary DNA (cDNA) involves using the Quanti-Tec Reverse Transcription kit, manufactured by Qiagen in Germany. The primers used in this study were taken from the base pair sequences in Azimi *et al*. (2020). All the primers were subsequently verified using the NCBI platform and BLASTN to ensure they are 100% specific and identical (Azimi *et al*., 2020). Dr Nadege Presneau kindly provided the RNase polymerase II (RPII) at the University of Westminster. In practice, 1 µg RNA from the cells treated with glycosidase inhibitors was used to prepare the cDNA library. To eliminate genomic DNA (gDNA), 2 µL of DNase I wipe-

out buffer enzyme was added to the RNA template (concentration: 100 ng) and RNase-free water to create a master mix of 14 µL, which was then incubated for 2 minutes at 42°C. Next, 1 µL of reverse transcriptase (RT) enzyme, 4 µL of buffer, and 1 µL of primer mix were added to the samples containing RNA(entire genomic elimination reaction of 14 µL) to make a 20 µL reaction. The mixture was then resuspended and incubated at 52°C for 14 minutes. Finally, the sample was incubated at 95°C for 3 minutes to deactivate the RT enzyme. The resulting samples were stored at -80 °C for future use.

Primers used
BCL2
forward 5′ TCGCCCTGTGGATGACTGA 3′,
reverse 5′ CAGAGACAGCCAGGAGAAATCA 3′;
CASP3
forward 5′ CAGCAAACCTCAGGGAAAC 3′,
reverse 5′ TCACCCAACCACCCTGGTCTT 3′;
CASP9
forward 5′ GCTCTTCCTTTGTTCATCTCC 3′,
Reverse 5′ GCTGCTTGCCTGTTAGTTC 3′;
Reference genes:
GAPDH
forward 5′ GACAGTCAGCCGCATCTTCT 3′,
reverse 5′ TTAAAAGCAGCCCTGGTGAC 3′.
RPII
forward 5′GCACCACGTCCAATGACAT
reverse 5′GTGCGGCTGCTTCCATAA ‘3

Primer efficiency (linearity) was assessed before sample analysis, and qRT-PCR reactions were prepared using the QuantiNova SYBR Green kit (Qiagen, Germany) according to the manufacturer’s instructions.

2.2.3. Quantitative real-time polymerase chain reaction qPCR

The cDNA from cells treated with glycosidase inhibitors was used to quantify the expression of *BCL2, CASP3, CASP9*, and RNA polymerase II (RPII) as an endogenous control for quantitative qPCR. After obtaining the cDNA, a two-step reverse transcriptase SYBR Green qPCR (Applied Biosystems, Qiagen) was performed. The apoptotic markers and reference genes GAPDH and RPII were integrated into a 96-well plate specific for the Biosystem 7500 qPCR machine. All steps were followed according to the protocol provided (QuantiNova SYBR Green RT-qPCR kit) for 20 µL per reaction, including the volume of primers, RNase-free water, cDNA, ROX diluted to 1:200, and SYBR Green master mix. For this experiment, 2 biological repeats were deployed in triplicate. In total (N=6).

2.2.4. Calculating Cycle threshold values from amplified genes

CT average values were calculated in triplicate for each sample and then averaged. The next step was to calculate the delta Ct (**ΔCt),** which represents the difference in Ct values between the gene of interest and the housekeeping gene. RNA polymerase II(RPII) was used as the most reliable reference gene in this case.

ΔCt = Ct (gene of interest) – Ct (reference gene)

to calculate the **ΔCt** for the '**Untreated 1**' sample:

For example**: ΔCt Untreated 1** = 30.55 – 17.18

Then, a sample or a group of samples was used as a calibrator/reference to calculate the delta-delta Ct (ΔΔ**Ct**) values for all the samples.

For example: **ΔCt reference average** = (13.40 + 13.60 + 13.80)/3

To calculate *ΔΔ*Ct values, they were relative to the untreated/control group. This method explains the relative fold gene expression of samples in qPCR.

ΔΔCt = ΔCt (Sample) – ΔCt (reference average)

For example, to calculate the **ΔΔCt** for the Treated 1 sample:

ΔΔCt Treated 1 = 7.83 – 13.55

The last step was to calculate fold gene expression values with 2 to the power of negative ***ΔΔ*Ct:**

Fold gene expression = 2^-(ΔΔCt)

2.3. Cytokinesis block micronucleus

The CBMN protocol was employed as previously described (Fenech, 2007). Once the cell cultures reached 70-80% confluence, cyt-B was added to the cells in their flasks at a final concentration of 5 μg/mL and incubated at 37°C and 5% CO_2 for 24 hours. Cells were trypsinised and counted using a manual hemacytometer (for more detail, see Section 2.2.1), with a range of 500,000 to 1 million cells. Hypotonic treatment was performed by adding potassium chloride (KCL) at 0.075 M dropwise and gently swirling the sample to prevent cell bursting. A volume between 5 and 7 mL was added. KCL was used as a hypotonic solution due to its lower solute concentration than the cytoplasm of a cell, resulting in water rushing into the cell through osmosis, which causes the cell to swell and improve visualisation of cells. Then, the cells were incubated for 7 minutes at 37°C and pelleted by centrifugation for 5 minutes at 1100 rpm. The supernatant was discarded, and the pellet resuspended. A fixative solution (cold or kept on ice) was added to the resuspended cells using a 3:1 ratio of methanol to acetic acid. This was added dropwise for the first 2 mL, carefully swirling to achieve a final volume of 5 to 7 mL. Cells were pelleted and resuspended as before, then centrifuged for 5 min at 1100 rpm. This step was repeated twice. A sample was taken by adding a drop to a microscope slide and viewed using light microscopy. Another volume of fixative solution was added and stored at -20°C. It was suggested that the fixed cells be centrifuged before being added to the slide for staining.

2.3.1 Giemsa Staining

A drop of fixative was added to the cells from the deployed cyt-B treatment, and the slides were allowed to dry for at least 24 hours. The cells were then stained accordingly using a 5% v/v Giemsa solution (Giemsa stain improves R66 solution), as suggested. The solution was prepared by dissolving 5 mL of Giemsa solution in 95 mL of PBS. The slides were incubated for 10 minutes in a 5% v/v Giemsa solution at room temperature and then washed several times with deionised water (dH2O), allowing them to air-dry. DPX (phthalate-free) medium was added carefully, along with a coverslip (22mm x 50mm). All slides were labelled accordingly to the date, cell type, and treatment type. Quality control was assessed with light microscopy to determine whether all the treated cells with cyt-B had been effectively stained and had clear image quality before being captured with the scanner. They were stored at 4°C. Note: Optimal conditions were maintained for the duration of staining at 30 minutes to enhance the visualisation of the cytoplasm of fixed cells under the Zeiss 3000 scanner.

2.3.2. CIN Imaging

The quality of the images on the slides was assessed using light microscopy at a magnification of 400X. All the cells in the slides were stained with Giemsa staining (described in section 2.4.1). The Zeiss 3000 automated scanner was also deployed to visualise and capture a bigger population of cells with better resolution using fine-tuning and an adapted protocol for cells instead of tissues. Multiple slides were scanned, as the Images taken ranged from 50 µm to 100 µm. Images were also processed using QUPATH software.

Example of mononucleated, BN, and multinucleated cells, both with and without abnormalities, are shown in (Figure 2.5)

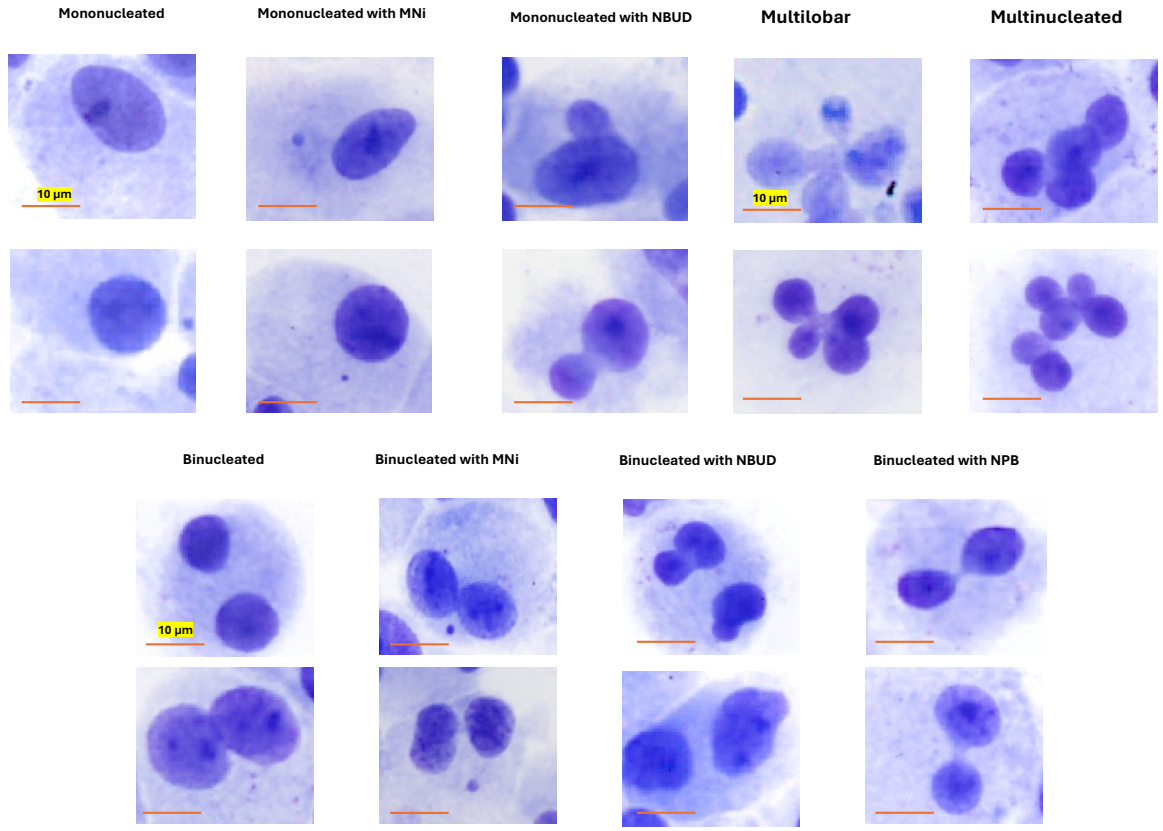

Figure 2.5. Images of the CBMN method applied to breast cancer cells revealed various nuclear abnormalities, which were analysed to assess the rate of CIN among the cells. The cells were observed using light microscopy at a 400X magnification with a scale bar of 10 µm. The upper panel displayed mononucleated cells, both with and without nuclear abnormalities, including nuclear buds (NBUD) and MN, as well as multilobar and multinucleated cells. The lower panel featured BN cells, presenting both with and without nuclear abnormalities, such as BN with MN, nuclear buds, and NPBs.

2.4. CIN scoring

CIN levels were measured using a scoring system whereby an average of 300 BN cells per experiment were analysed for the presence of MN, BN with NPBs, and BN with NBUDs. In this study, the number of captured cells in Image 1 (Fig. 2.6) was annotated based on their morphology. The objective was to detect the presence of (MN), NPBs, and NBUDs as

indicators of DNA damage, which signifies evidence of CIN among the four cell lines investigated. This protocol follows the guidelines set forth by Fenech (2007).

The CIN levels of the breast cancer studied in this investigation were accurately counted and annotated according to their morphological results, and the data were tabulated in Excel for further statistical analysis. An example of annotated CIN data is shown below (Figure 2.6).

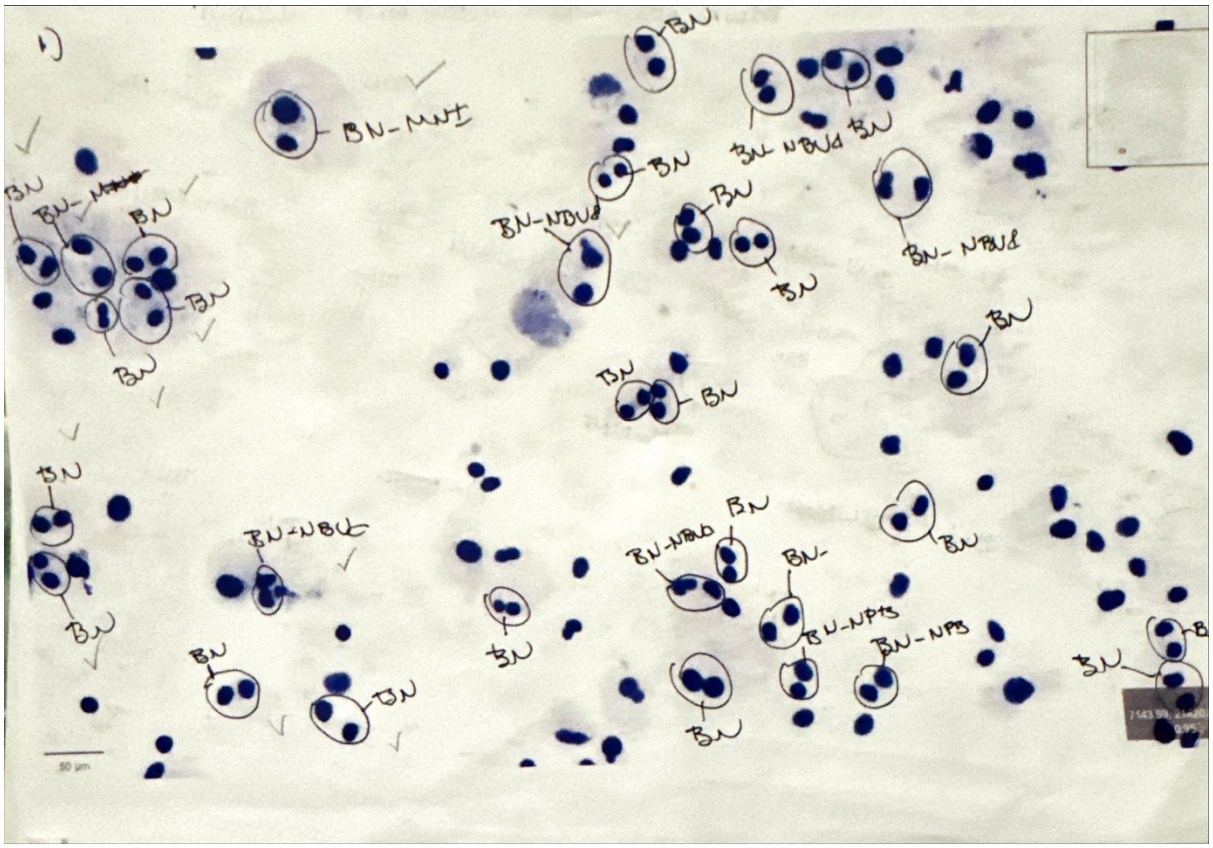

Figure 2.6. The image is an example of the CMBN assay from breast cancer cells grown in 2D, as the scoring count of annotated BN cells with and without abnormalities was subsequently processed in Excel for tabulation and data analysis.

This methodology was consistently applied to the other cell lines grown under identical and varied culture conditions.

The tabulated data was compiled (shown in Figure 2.7) to track every annotated image accurately, total all the scoring in Excel, and calculate the scoring for each experiment accordingly.

MDA-MB-231	EXP 1	2D		BN	BN Mni	BN NBUD	BN NPB		EXP 2
			Image 1	22	1	5	2		
			Image 2	19	2	3	1		
			Image 3	19	1	7	3		
			Image 4	18	1	5	2		
			Image 5	19	2	4	0		
			Image 6	10	2	6	1		
			Image 7	21	2	7	0		
			Image 8	14	3	1	0		
			Image 9	11	2	4	0		
			Image 10	14	3	6	1		
			Image 11	13	2	2	0		
			Image 12	17	2	4	0		
			Image 13	21	2	8	1		
			Image 14	20	2	4	1		
								TOTAL CIN	CIN %
			TOTAL	238	27	66	12	105	30.6122449
					7.87172012	19.2419825	3.49854227		

Figure 2.7. MDA-MB-231 cells grown in 2D showed the Data analysis of the CBMN assay scoring count in experiment 1. A range of 14 images was captured in this experiment to display the BN with and without abnormalities, which resulted in the calculation of the CIN percentage. The MNi, NBUDS and NPBs were also calculated.

2.5. CIN studies in 3D models

The RAFT^{TM} system protocol was carried out according to the manufacturer's instructions and as described (Magdelin *et al*., 2017). This protocol was then modified to increase the yield of cells fixed with hypotonic treatment and harvested after the cytokinesis block nucleus assay. The number of seeded cells increased to 5 × 10^5 cells embedded in rat tail I collagen per 24-well plate and grown for 7 days instead of 28 days, resulting in higher cell numbers.

2.6. Cytokinesis block micronucleus assay in 3D

The CMBN assay was adapted at the University of Westminster to be deployed in 3D model cultures. This adaptation was based on a RAFT™ protocol for nuclei retrieval for flow cytometry analysis based on 3D tissue disassociation by collagenase.

2.6.1. Stock preparation of collagenase type I before cell retrieval

Cells were harvested using collagenase type I at a working solution concentration of 202 U. After cell disassociation, the cells were harvested using collagenase type I. The cells were then counted after retrieval to determine the cell number and viability. To prepare collagenase type I, 1 mL of Hank's Balanced Salt Solution (HBSS) with calcium and magnesium was added to a 1 g vial of collagenase and vortexed gently to ensure complete dissolution. The volume of HBSS with calcium and magnesium was determined by diluting the collagenase solution to 100 U/µL (1000X stock solution). For example, 1 µL is equivalent to one working solution when the solution has been diluted to 1000X. The vial was rinsed with one volume of HBSS containing calcium and magnesium, and then the contents were combined. The 1000x stock working solution was filtered through a 0.2 µm low-protein-binding filtration unit. The collagenase was dispensed into aliquots and stored at –20°C to –5°C, protected from light. For a concentration of collagenase of 220 U/mg, equivalent to 220,000 U/g, a solution of 1 g/mL was prepared, yielding a concentration of 220,000 U/mL.

1 g/mL of collagenase stock = 220,000 U/mL

10 aliquots of 1 mL working solution can be diluted to 10 mL containing HBSS medium to contain a concentration of 22,000 U/mL collagenase.

0.1% of 0.5% (w/v) = 1% w/v mg/ml - 5% mg/ml = 2.5 mL of collagenase/ mL (volume to be added into each well, as the 3D models have been grown in 24 well plates).

Stores aliquots in -20 °C.

2.6.2. Cell retrieval after tissue dissociation from 3D constructs for CIN studies

The cells grown in the 3D RAFT™ system were dissociated and retrieved to evaluate CIN by deploying the CBMN assay. This protocol was developed and modified at the University of

Westminster. Once the 3D models reached the desired growth conditions for 7 days (optimised conditions), cyt-B was added to the cell culture at a final concentration of 5 mg/mL. The cells were incubated at 37°C and 5% CO_2 for 24 hours before proceeding to 'tissue dissociation'. The 3D constructs were washed several times with HBSS containing calcium and magnesium. 500 µL HBSS with calcium and magnesium was used to submerge the 3D constructs. Collagenase, 50–200 U/mL, equivalent to 1 mg/mL-5mg/mL (w/v), was added as a working solution. 10 % v/v FBS was added into each well to 'neutralise' the collagen, and the cells were incubated at 37°C for 60 mins using a mid-speed rocker platform, 6. The collagen construct was transferred into a 15 mL Falcon tube, and the thin layer of collagen-embedded cells was further disassociated with a dropping pipette. To ensure no remaining collagen fragments were left, fresh collagenase solution was added and further incubated at 37°C for 5 minutes for further disassociation. This step was repeated if needed. The cells were washed once and pelleted by centrifugation at 1700 *x g* for 5 minutes at 37°C in HBSS without collagenase. Cells were counted using a haemocytometer. Hypotonic treatment was performed by adding KCL at 0.075 M dropwise, and the sample was gently swirled to prevent cell bursting. A volume between 5 and 7 mL was added. KCL was used as a hypotonic solution due to its lower solute concentration than the cytoplasm of a cell, resulting in water rushing into the cell through osmosis, which causes the cell to swell and improve visualisation of cells. Then, the cells were incubated for 7 minutes at 37°C and pelleted by centrifugation for 5 minutes at 1100 rpm.

The supernatant was discarded, and the pellet resuspended. This step was done several times to remove debris from the collagen or dead cells. A fixative solution (cold or kept on ice) was added to the resuspended cells using a 3:1 ratio of methanol to acetic acid. This was added dropwise for the first 2 mL, carefully swirling to achieve a final volume of 5 to 7 mL. Cells were pelleted and resuspended as before, and the fixative step was repeated. The cells were then centrifuged for 5 min at 1100 rpm. This step was repeated at least twice. A sample was taken by adding a drop to a microscope slide and viewed using light microscopy. The sample was frozen and used the next day by adding more fixative solution before cell staining.

2.7. Fluorescence In-Situ Hybridisation (FISH)

This tool is essential for investigating chromosomal behaviour in different biological and clinical contexts. The protocol followed was that of Salassidis *et al*. (1992). FISH was deployed on all four MDA-MB-231, BT-549, SKBR3 and MCF-7 to detect whether the observed MN in the different cell cultures were preferentially the result of aneugenic (defective kinetochore attachment) or clastogenic (double-strand break) effects. For this purpose, fixed cells were hybridised with the Human Centromere Probe (AHC; Ref KBI-20000G, Kreatech^{TM}), also known as Pan-centromeric probe, a combination of repetitive sequences found on all human chromosomes in 2X saline sodium citrate (SSC). A cover slip was added to the denatured area for 1 minute in a mixture solution prepared in 100 µL, consisting of 70 µL formamide, 20 µL dH_2O, and 10 µL 20X SCC. The coverslip was removed, and the slides were incubated for 5 minutes at 4°C in 70% v/v ethanol. Then, repeat at 90% v/v. The slides were allowed to dry before the next step. Then, a 10 µL probe was added to an Eppendorf tube after the slides had dried, and each slide was incubated for 10 minutes at 85°C. Immediately, the slides were transferred to ice to cool the separated double helix. Then, the probe was added at 37°C once the slides were dried. The slides were incubated for 48 hours after the coverslip was sealed, and the slide was fixed with Fixogum glue. After hybridisation of the cells, all coverslips were removed and washed for 2 minutes at room temperature with 100 mL of 2X SSC and 0.1% Tween 20. Then, the coverslips were washed with 0.4X SSC + 0.1% Tween 20 at 72 °C for 2 minutes, followed by a 2-minute wash with 2X SSC. For a 2X SCC working concentration, the formula is C1. V1 = C2. V2 was used to obtain a starting volume of 10 mL. For the 0.1% v/v Tween, 45 µL was added to 2X SSC. The cell slides were washed with 70% v/v ethanol, 90% v/v ethanol, and 100% v/v ethanol at room temperature for 4 minutes each and allowed to dry. A drop of VECTASHIELD antifade mounting medium with DAPI was added to the slide. A cover slip was added and stored at 4°C.

The formula below determines the percentage of MN1 centromere, a complex of proteins linked with the centromere of a chromosome in cell division. Scoring was deployed based on the presence of fluorochromes in the MN to evaluate clastogenic and aneugenic effects that lead to CIN.

$$\%\ MNi \text{ centromere} = \frac{Total\ number\ k-}{Total\ number\ MNi} \times 100$$

2.8. Imaging

hybridised Pancentromeric and HER2 amplification probes were imaged and captured using 100X fluorescence microscope magnification (model BX41TF, Olympus Corporation, Japan). A camera linked to CYTOCAM software v2 detected blue and green signals for pancentromeric sequences. HER2 amplification was carried out only on SKBR3 to indicate (blue, green, and red).

2.9. Statistical analysis

One-way ANOVA and a Chi-squared test were used, as appropriate, to determine the significance of the differences in the data generated in the laboratory experiments above. Microsoft Excel and GraphPad software were used for this purpose. P-value readings of <0.05 were considered significant.

Chapter 3

Glycosidase inhibition of breast cancer cells grown in 2D

One hypothesis suggests that altering the glycocalyx in cancer cells will enhance the penetration of chemotherapeutic agents.

Another hypothesis proposes that glycosidase inhibition will impact cell motility, reduce cell numbers, and affect the metabolic activity of breast cancer cell

3. Introduction

The research question for this chapter was to what extent does inhibiting glycosidase enzymes sensitise breast cancer cells to doxorubicin? Is there a synergistic effect when doxorubicin is combined with iminosugars, including DNJ? Does this inhibition have a greater effect on breast cancer cells if there is a synergistic effect? . The aims of this study intended to evaluate the effect on cell behaviour of inhibiting enzymes responsible for NLG trimming using breast cancer cells grown in 2D. The objectives were to assess the impact of glycosidase inhibition on the effectiveness of the chemotherapeutic drug, doxorubicin, and to assess the impact of glycosidase inhibition on cancer cell proliferation, migration and invasion in 2D.

This study aimed to evaluate the impact of glycosidase inhibition on cell migration and invasion, specifically in reducing metastatic traits and slowing the movement of breast cancer cells grown *in vitro*. It also examines the cytotoxic effects on cell viability and investigates whether alterations to the glycocalyx facilitate increased doxorubicin uptake. This study was concerned with the impact of treating four different human breast cancer cell lines (MCF-7, SKBR3, BT-549 and MDA-MB-231) with glycosidase inhibitors with and without doxorubicin. A range of assays was used to assess different aspects of cancer biology following the exposure of cells to glycosidase inhibitors at two concentrations (0.5 mM and 1 mM) over a 24-hour period.

Lectin fluorescence microscopy (shown in 3.1) was used to assess if there was a change in Con A, UEA-1 and WGA lectins binding after treatment with glycosidase inhibitors and to visualise glycan distribution on the cell surface (glycocalyx). The Alamar blue assay (shown in section 3.2) was deployed to measure the viability of treated cells by assessing cellular metabolic activity. This approach aimed to determine whether glycosidase inhibition was cytotoxic. To assess whether cell numbers decreased following exposure to glycosidase inhibitors, cells were stained with the nuclear dye DAPI to determine if there was a change in the number of nuclei (as a surrogate for cellular number), and particle counts were performed using ImageJ. The wound healing assay (shown in Section 3.4) was used to determine whether cell migration and movement were altered after treatment with the inhibitor compounds. The last assessment in this results section (shown in 3.5) was gene expression analysis using RT qPCR with markers of apoptosis, to determine if there were changes after treatment of TNBC cells (MDA-MB-231 and BT-549) with glycosidase inhibitors.

A schematic workflow representation of all experiments carried out (is shown in Fig. 3.1).

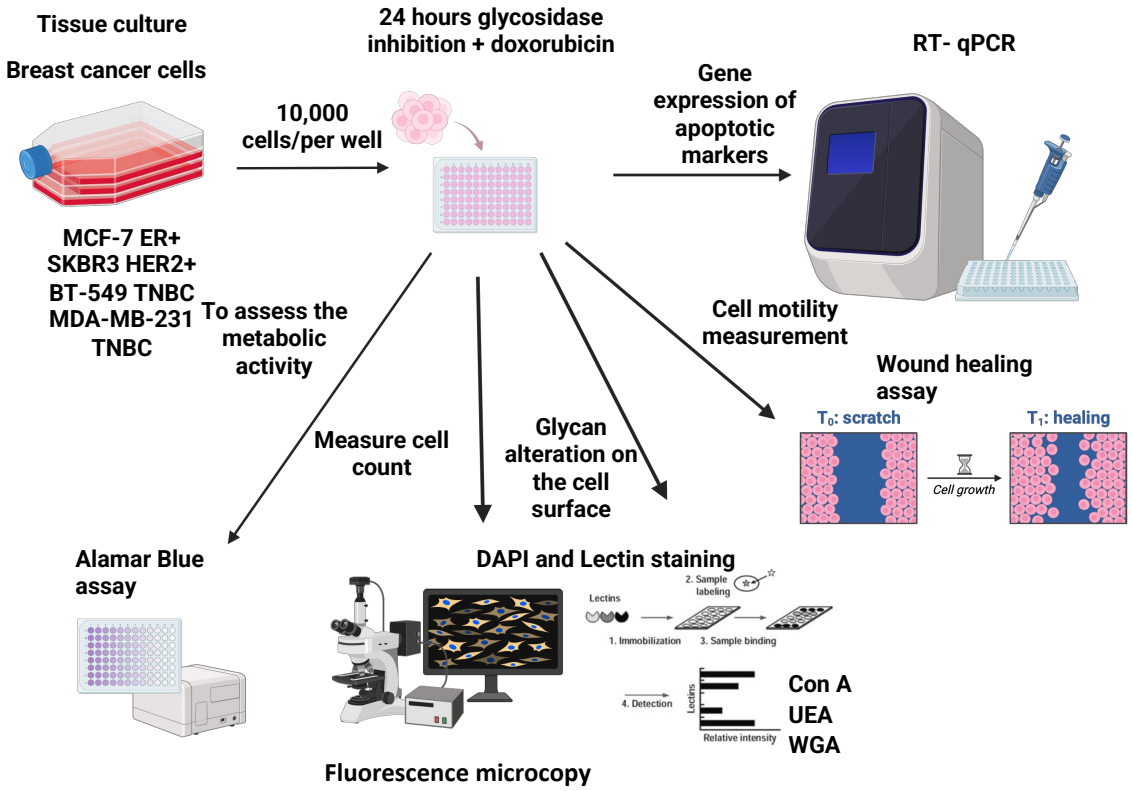

Figure 3.1. Schematic workflow representation of the glycosidase inhibition treatment involving different techniques to evaluate the effect of breast cancer cells.

The breast cancer cells treated with glycosidase inhibitors were evaluated in a lectin binding assay to assess whether alterations in glycans within the glycocalyx occurred, as shown below (section 3.1).

3.1. Lectin staining with Con A, UEA-1 and WGA following treatment with glycosidase inhibitors

Lectin labelling was performed as described in (Section 2.1.7). Lectins have been extensively used in glycobiology research to facilitate the analysis of alterations in the carbohydrate structures of glycoproteins (Pilobello & Mahal, 2007; Zhao *et al*., 2008).

Microscopy with fluorescently labelled carbohydrate-binding proteins, lectins, was employed to assess the effect of glycosidase inhibitor treatment on cellular glycosylation.
The four breast cancer cell lines, MCF-7, SKBR3, BT-549, and MDA-MB-231, were grown to 80% confluence and exposed to DNJ and three iminosugar compounds provided by the Phytoquest company (42, 44, and 255) at concentrations of 0.5 mM and 1 mM for 24 hours. This approach enabled the evaluation of changes in fluorescence intensity for each cell line following treatment. The fluorescence intensity was measured using ImageJ.

Multiple lectin staining studies are presented to demonstrate the statistical significance of the results among cells treated with glycosidase inhibitors. The single experiments were performed in triplicate, and the combined data are provided for repeated experiments for each treated cell line.

To assess the effect of glycosidase inhibition, the binding intensity of Con A, UEA, and WGA was assessed and compared with untreated cells. An example (is shown in Fig. 3.2). Image J was used as described in Chapter 2 (Section 2.1.10). In brief, this was accomplished by opening the binary processing, measuring the area, and tracing a square of the same size as all other treated and untreated areas. Measurements from the background areas were also taken, as shown in the figure below.

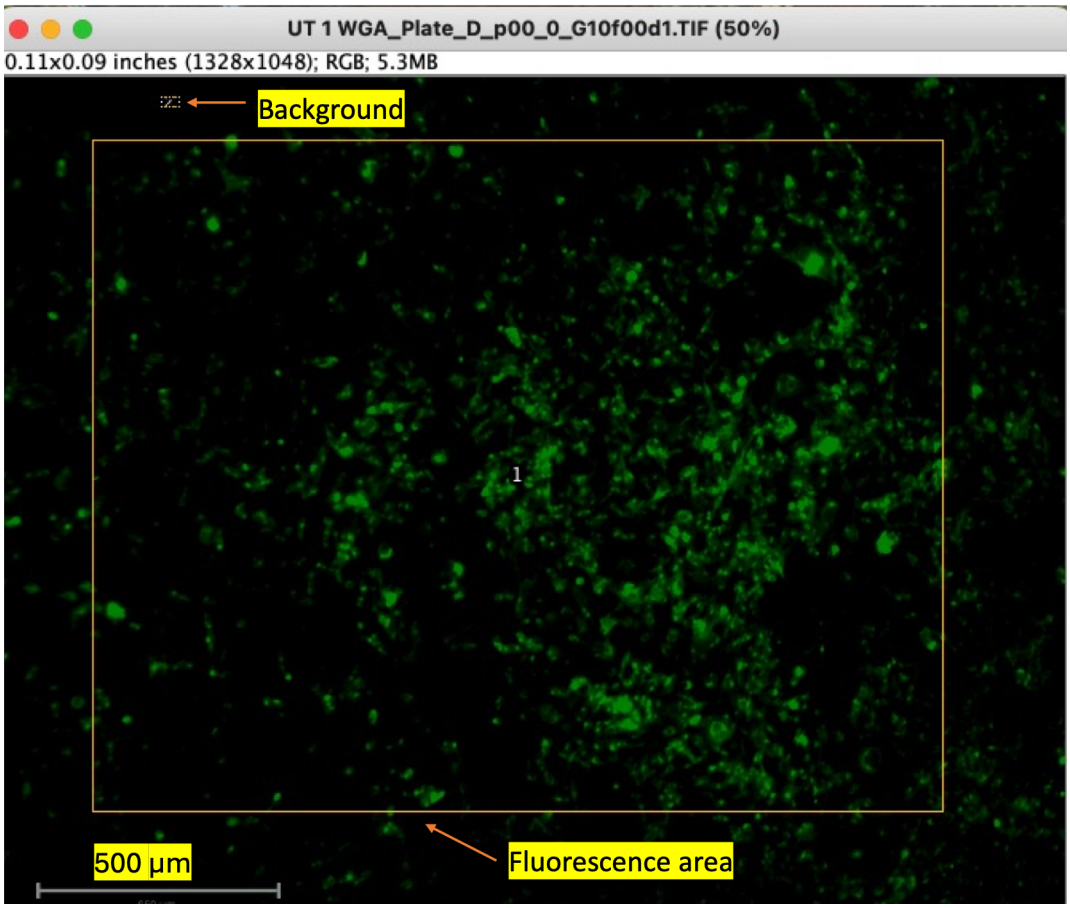

Figure 3.2. Con A lectin binding of untreated cells. The image J analysis of the example shows how the cellular fluorescence of each cell line was assessed. A square was drawn to mark the area of lectin staining to be evaluated, followed by a small square used to measure the background. This approach was carried out for all four breast cancer cell lines exposed to glycosidase inhibitors. The microscope was set to a total magnification of 100X, with a scale bar representing 500 µm.

The results of the effect of glycosidase inhibitors on breast cancer cells is presented below (Table 3.1). It highlights changes in Con A, UEA, and WGA lectin binding following treatment, resulting in varying changes in lectin binding intensity compared to untreated cells. This data is presented as an overview of four breast cancer cells treated with glycosidase at a concentration of 0.5 mM and subsequently stained with Con A, UEA-1, and WGA lectins. The results obtained from the breast cancer cell lines demonstrated the integrated density of the corrected fluorescence percentage across three experiments (N = 9).

This indicates that a small proportion of the treated cells displayed a huge increase in fluorescence. For example, SKBR3 cells showed a significant increase in DNJ when stained with Con A, compared to untreated cells. Compound 44 showed a significant increase in WGA fluorescence. Another cell line that showed a huge increase in Con A, including all inhibitor compounds, was the BT-549 cell line. While the other cell lines stayed the same or decreased.

Table 3.1. Corrected total cell fluorescence (CTCF) from the average of the integrated density percentage of the untreated vs cells treated with glycosidase inhibitors.

Condition	MCF-7 Average (%)	SKBR3 Average (%)	BT-549 Average (%)	MDA-MB-231 Average (%)
UT Con A	8.73	1.68	4.84	4.3
DNJ Con A	7.54	3.86	14.02	6.45
42 Con A	11.99	3.52	13.74	7.4
44 Con A	9.7	2.42	13.97	7.12
255 Con A	5.86	1.72	16.48	6.72
UT UEA	6.18	1.26	7.83	6.6
DNJ UEA	12.37	1.14	12.26	9.05
42 UEA	11.71	0.85	9	16.08
44 UEA	10.95	1.28	8.35	15.7
255 UEA	5.27	1.86	9.72	14.46
UT WGA	9.39	3.82	6.04	5.79
DNJ WGA	11.53	3.69	18.24	9.99
42 WGA	12.91	4.29	20.37	14.13
44 WGA	11.6	6.28	21.46	13.12
255 WGA	6.97	4.54	17.29	11.83

Note: UT: untreated; DNJ: 1-Deoxynojirimycin; Con A: Concanavalin A; UEA-1: *Ulex europaeus* agglutinin; WGA: wheat germ agglutinin.

Evaluation of the lectin experimental work conducted on MCF-7 cells is presented (in Fig. 3.3). MCF-7 cells treated with DNJ exhibited the highest increase in Con A lectin binding. Compounds inhibitors 42, 44, and 255 also showed a modest increase, but none was statistically significant. In UEA lectin binding, DNJ showed the highest increase, followed by compound inhibitors 42 and 44. Compound 255 showed a decrease instead. No significant difference was observed in the cells treated with any of the compound inhibitors.

In WGA lectin binding, a modest increase was shown in cells treated with compound inhibitors 42, DNJ and 44. In contrast, compound 255 showed a decrease in WGA staining. None of these results reached statistical significance: Con A (F (DFn, DFd) = 0.1482, P value= 0.9596), UEA-1 (F (DFn, DFd) = 0.4714, P value= 0.7560), and WGA (F (DFn, DFd) = 0.1034, P value= 0.9787).

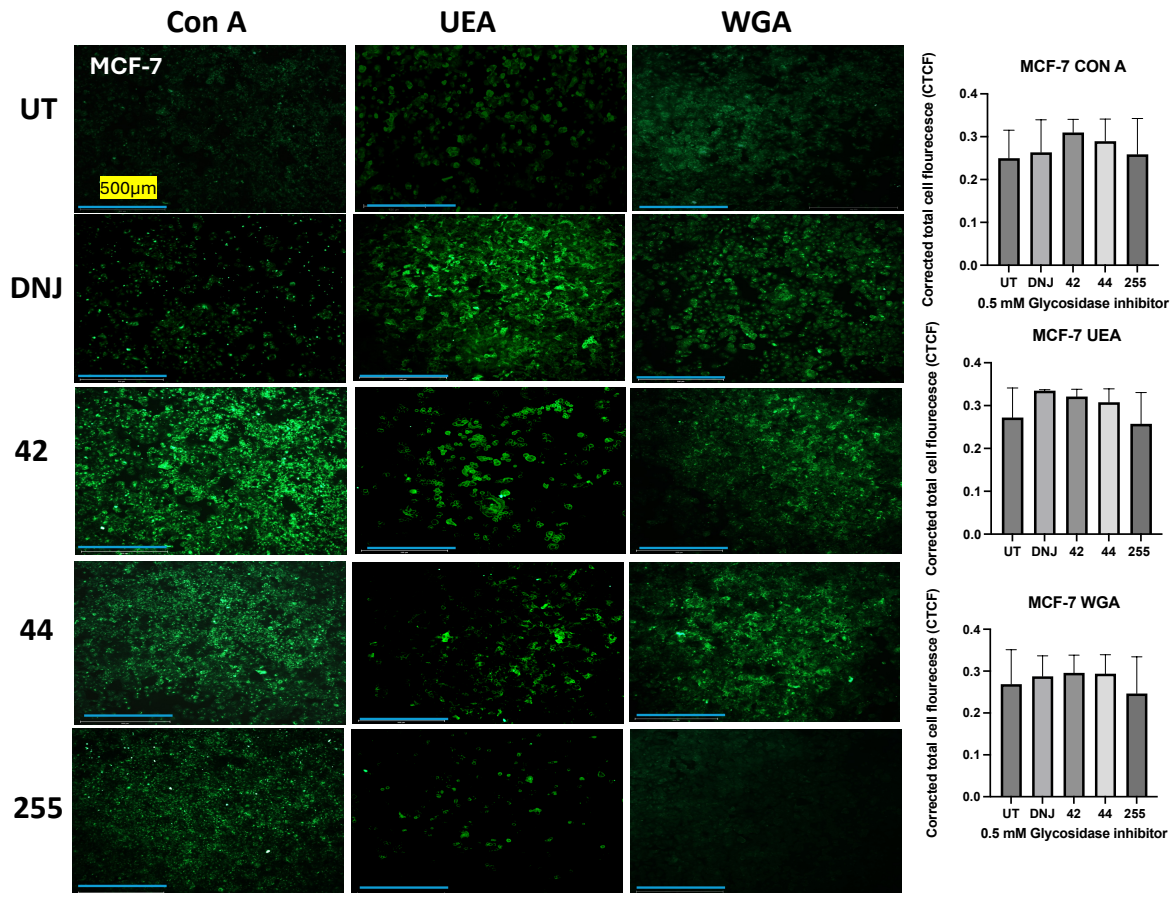

Figure 3.3. Fluorescence lectin microscopy of MCF-7 cells with/without exposure to glycosidase inhibitor compounds. Changes in lectin binding were observed, consistent with an accumulation of N-linked structures, increased (Con A, UEA-1, and WGA binding) following exposure of the cells to glycosidase inhibitor compounds at 0.5 mM for 24 hours. Left panel: Fluorescence microscopy images of MCF-7 cells stained with Con A (column 1), UEA-1 (column 2), and WGA (column 3), either untreated or treated (DNJ, 255, 42, and 44). The microscope was set to a total magnification of 100X, with a scale bar representing 500 µm. Right panel: Histogram depiction of the Image J data following analysis of the CTCF. The data were presented as mean values ± SE with N = 9. One-way ANOVA statistical analysis was performed. No significant difference was shown.

The lectin experimental work was conducted on SKBR3 cells presented in Fig. 3.4. SKBR3 cells treated with DNJ showed a statistically significant increase in Con A (F (DFn, DFd) = 3.984, P < 0.050, P value = 0.0347). Compound inhibitors 42 and 44 also resulted in an increase in Con A binding, whereas 255 had no effect compared to untreated cells, as no significant difference was observed. UEA lectin binding with cells treated with compound 255 exhibited a greater increase, although this difference did not reach statistical significance. There was a decrease in UEA binding following treatment in DNJ, 42 and 44, compared to the untreated cells. In

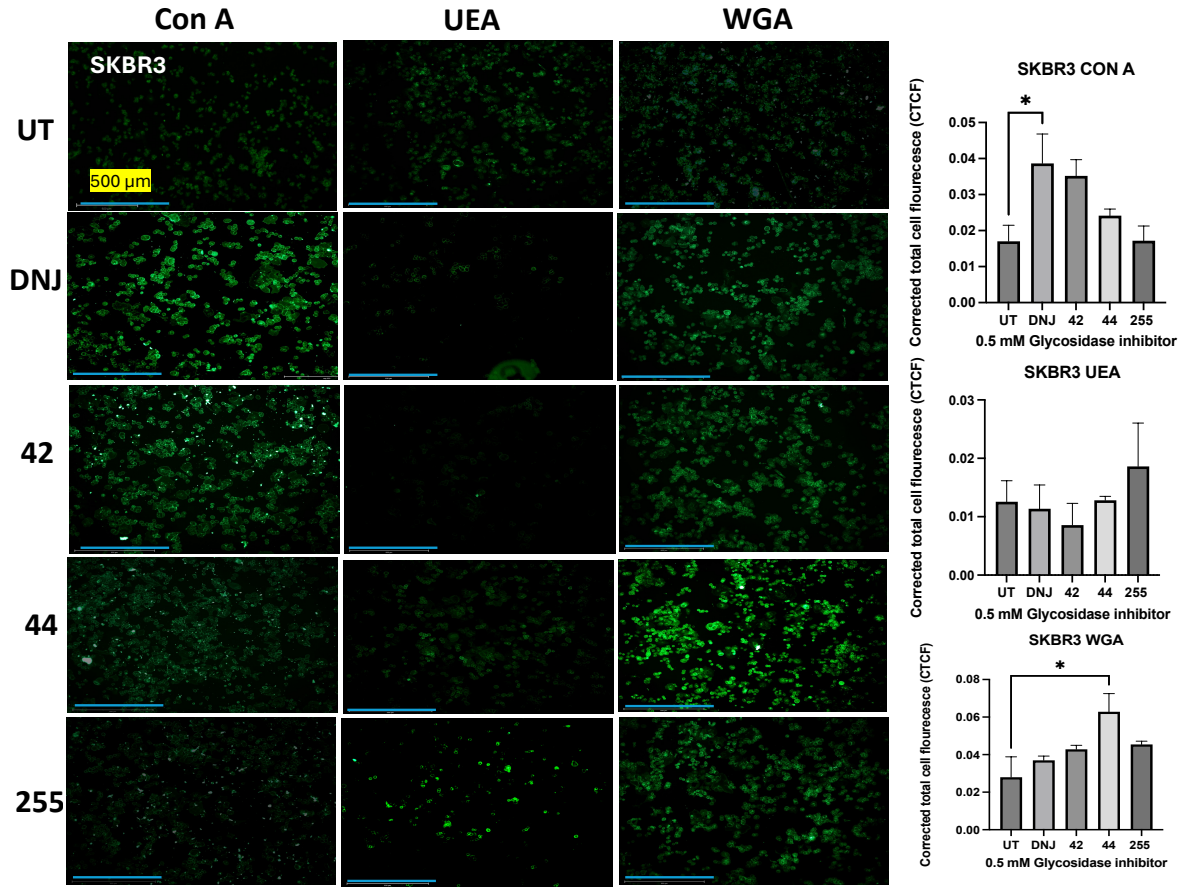

WGA lectin binding, the cells treated with the compound inhibitor showed a statistically significant increase. (F (DFn, DFd) =3.689, P=<0.050, P value=0.0428). While inhibitors, DNJ, 42, and 255 resulted in an increase, they did not reach a statistically significant difference.

Figure 3.4. Fluorescence lectin microscopy of SKBR3 cells with/without exposure to glycosidase inhibitor compounds. Changes in lectin binding were observed, consistent with the accumulation of N-linked structures (increased Con A, UEA-1, and WGA binding) following exposure of the cells to a glycosidase inhibitor compound at 0.5 mM for 24 hours. Left panel: Fluorescence microscopy images of SKBR3 cells stained with Con A (column 1), UEA-1 (column

2), and WGA (column 3), either untreated or treated (DNJ, 255, 42, and 44), The microscope was set to a total magnification of 100X, with a scale bar representing 500 µm. Right panel: Histogram depiction of the Image J data following analysis of the results CTCF. The data were presented as mean values ± SE, with N = 9. One-way ANOVA statistical analysis was performed. There was a significant difference on Con A * (DNJ, *p=<0.05) and UEA (42 inhibitor compound *p=<0.05), no significant difference in UEA.

The lectin experimental work conducted on BT-549 cells is presented in (Figure. 3.5.), BT-549 cells treated with DNJ, compound inhibitors 42,44 and 255 showed a statistically significant increase in Con A binding (F (DFn, DFd)= 4.461, P<0.050, P value 0.0251.

The most significant increase in UEA-1 binding was associated with DNJ, and inhibitors 255, 42, and 44; however, this did not reach statistical significance. The binding of WGA lectin revealed an increase following treatment of the cells with DNJ, compounds 42 and 255, with compound 44 having the highest increase; however, this was not statistically significant.

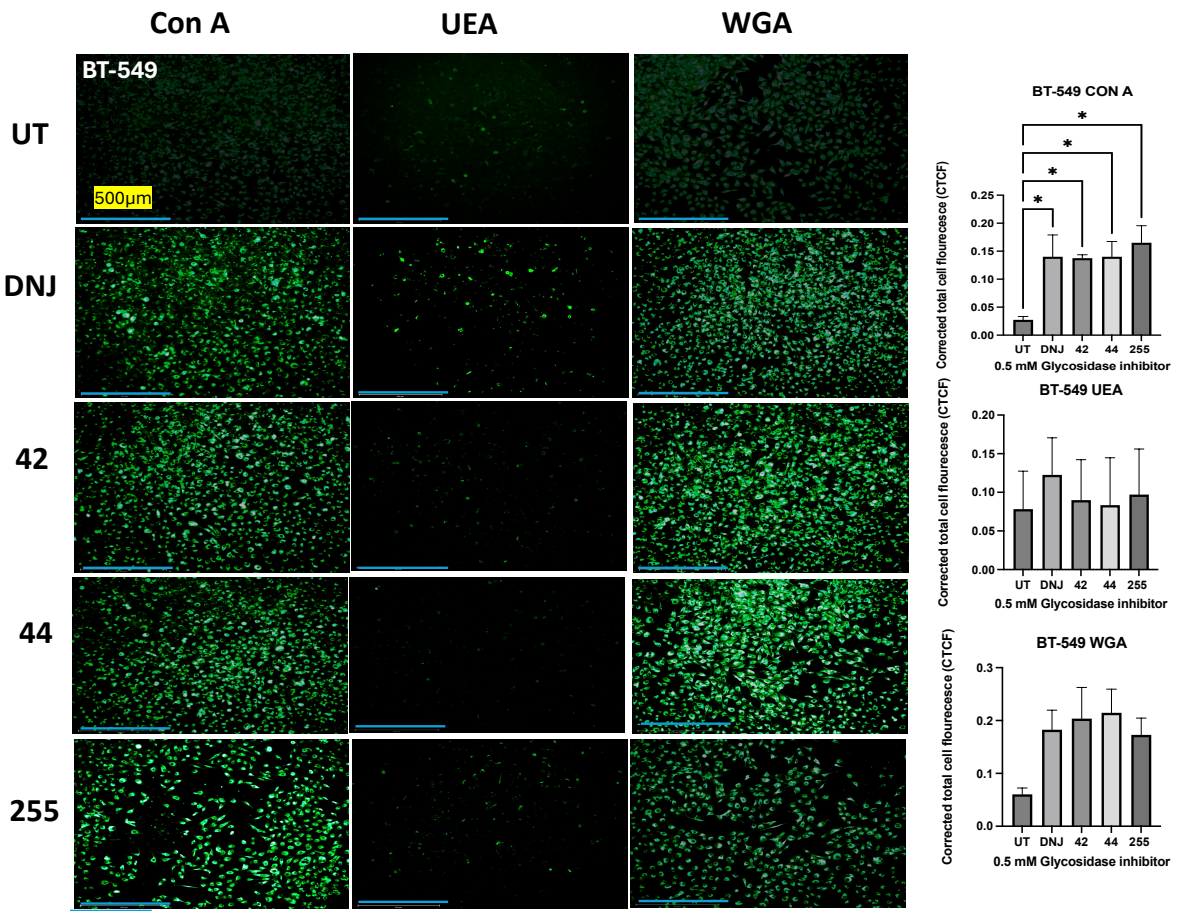

Figure 3.5. Fluorescence lectin microscopy of BT-549 cells with/without exposure to glycosidase inhibitor compounds. Changes in lectin binding were observed, consistent with an accumulation of N-linked structures (increased Con A, UEA-1 and WGA binding) following exposure of the cells to glycosidase inhibitor compound at 0.5 mM for 24 hours. Left panel: Fluorescence microscopy images of BT-549 cells stained with Con A (column 1), UEA-1 (column 2), and WGA (column 3), either untreated or treated (DNJ, 255, 42, and 44),), The microscope was set to a total magnification of 100X, with a scale bar representing 500 µm. Right panel: Histogram depiction of the Image J data following analysis of the results of CTCF. The data were presented as mean values ± SE, with N = 9. One-way ANOVA statistical analysis was performed. A significant difference was shown in Con A for all the compound inhibitors *P=<0.05. No significant difference in UEA and WGA was shown.

The lectin experimental work conducted on MDA-MB-231 cells is presented in (Fig. 3.6.) MDA-MB-231 cells treated with glycosidase inhibitors DNJ, 44 and 255 showed an increase in Con A lectin binding and compound 42 showed the highest increase. The most significant increase in UEA-1 binding was observed in cells treated with compound 42, followed by compounds 44 and 255, respectively. DNJ had the lowest increase. The binding of WGA lectin revealed an increase following treatment of the cells with DNJ, compounds 42 with the highest, followed by 44 and 255. None of these results from Con A, UEA and WGA reached statistical significance: Con A (F (DFn, DFd) = 0.5763, P=<0.050, P value= 0.6864), UEA-1 (F (DFn, DFd) =0.5383, P=<0.050, P value= 0.7113), and WGA (F (DFn, DFd) =0.2835, P=<0.050, P value= 0.8821).

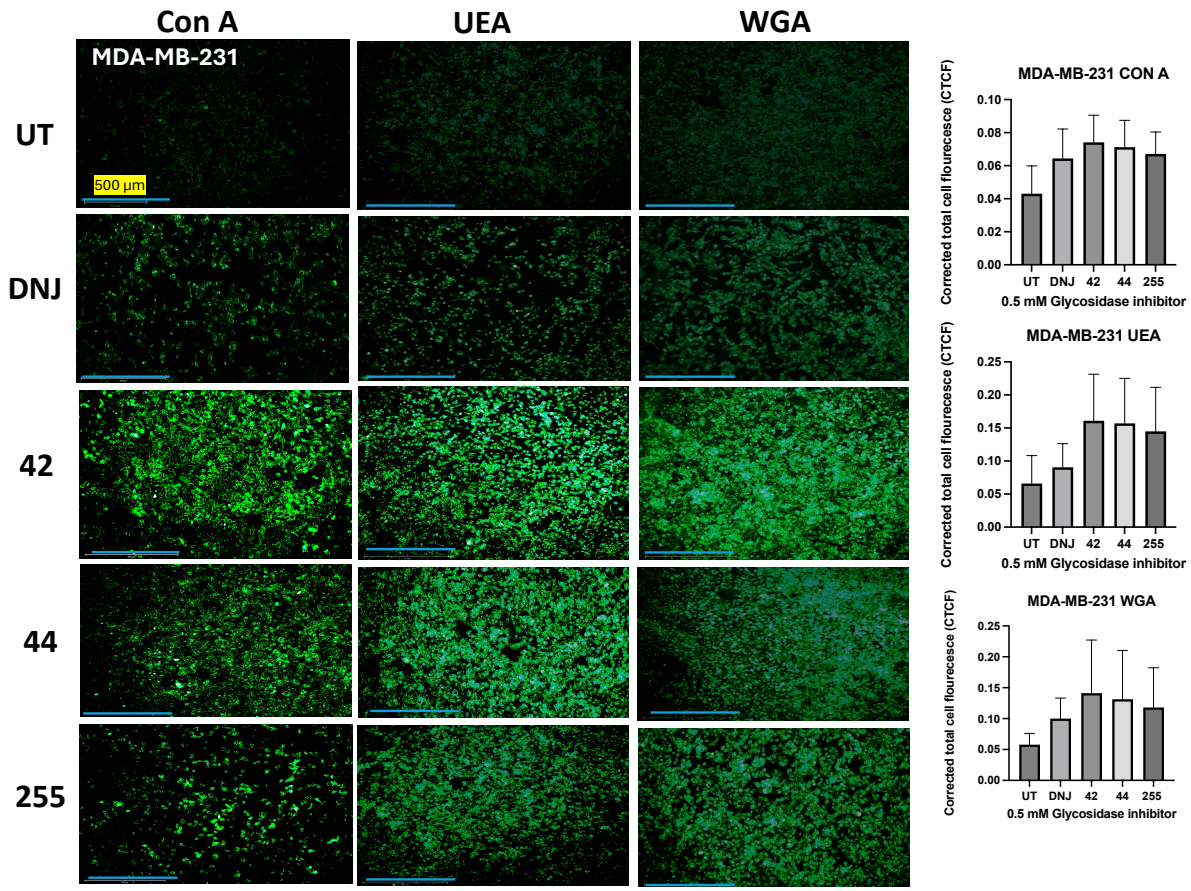

Figure 3.6. Fluorescence lectin microscopy of MDA-MB-231 cells with/without exposure to glycosidase inhibitor compounds. Changes in lectin binding were observed, consistent with an accumulation of N-linked structures (increased Con A, UEA-1 and WGA binding) following exposure of the cells to glycosidase inhibitor compound at 0.5 mM for 24 hours. Left panel: Fluorescence microscopy images of MDA-MB-231 cells stained with Con A (column 1), UEA-1 (column 2), and WGA (column 3), either untreated or treated (DNJ, 255, 42, and 44). The microscope was set to a total magnification of 100X, with a scale bar representing 500 µm. Right panel: Histogram depiction of the Image J data following analysis of the results of CTCF. The data were presented as mean values ± SE, with N = 9. One-way ANOVA statistical analysis was performed. No significant differences were shown.

The metabolic activity of the 4 breast cancer cells treated with glycosidase inhibitors is shown below (in Section 3.2)

3.2. Assessing the metabolic activity of breast cancer following glycosidase inhibition.

In this study, the Alamar blue assay was deployed as described in (Section 2.1.6) to evaluate the metabolic activity of treated cells with glycosidase inhibitors, including Deoxynojirimycin (DNJ) and Phytoquest compounds (42, 44, 255), by exposing cells to concentrations of 0.5 mM and 1 mM for 24 hours. 5 µM Doxorubicin concentration was also used to treat the cells alone or in combination with the compound inhibitors. These concentrations are supported by previous research (Azimi *et al*., 2020), with 0.5 mM and 1 mM of glycosidase inhibitors.
The assays were conducted in 96-well plates containing 10,000 cells per well, and data were collected from spectrophotometer readings across three replicates for each of the 3 experiments carried out (N = 9). This data was subsequently used for statistical analysis of the mean values +/-SD.

An overview of the metabolic activity of the four breast cancer cells after treatment with glycosidase inhibitors revealed different reduction percentages (Table 3.2). The data in yellow showed that breast cancer cell lines treated with glycosidase inhibitors exhibited the most significant effects, resulting in a reduction in metabolic activity, when combined with doxorubicin, compared to untreated cells.

Table 3. 2. Metabolic activity of breast cancer cells treated with glycosidase inhibition at concentrations of 0.5 mM and 1 mM by the compound inhibitors, DNJ, 42 44 and 255, as well as by doxorubicin at 5 µM in combination and used alone. The measurement employed was the percentage reduction in the Alamar Blue reagent. The values are the mean average of triplicates.

Cell Line & Concentration	Untreated	DNJ	DNJ + doxorubicin	42	42 + doxorubin	44	44 + doxorubicin	255	255 + doxorubicin	Doxorubicin (5 µM)
MCF-7										
0.5 mM	100	78	73*	81	74	85	84	70	74*	89
1.0 mM	100	87	72	75	66*	82	71	69	67*	89
SKBR3										
0.5 mM	100	98	82*	92	95	89	94	91	95	87
1.0 mM	100	77	66*	80	95	99	68	91	90	87
BT-549										
0.5 mM	100	79	68*	86	72	87	79	88	68*	86
1.0 mM	100	76	76	88	81	68*	76	75	77	86
MDA-MB-231										
0.5 mM	100	95	86	89	93	93	80	85	77*	90
1.0 mM	100	86	78	94	76	94	75*	90	84	90

Note: DNJ: 1-Deoxynojirimycin.

Experimental work for each cell line is presented, following the same order as the previous sections. The MCF-7, SKBR3, BT-459, and MDA-MB-231 cells treated with the compound inhibitors are displayed for all three experiments carried out (to demonstrate consistency across all three experiments). MCF-7 cells treated with glycosidase inhibitors and doxorubicin were analysed to assess cell viability, with three experiments conducted, each comprising three replicates. In (Fig. 3.7) presents three histograms illustrating the outcomes of each cell viability assay. In these assays, cells treated with the inhibitor compounds combined with doxorubicin exhibited variations in metabolic activity, revealing significant differences in the first and second experiments. Notable reductions were observed in the experiment when doxorubicin was combined with DNJ and compound inhibitor 42, respectively. Although reductions in metabolic activity occurred in the treated cells during experiment three, they were not statistically significant. In the cells treated with 1 mM, significant differences were observed in Experiment 1 when doxorubicin was combined with DNJ, 42, 255, and 44, respectively. Experiments 2 and 3 showed reductions in cells treated with glycosidase inhibitors; however, these were not statistically significant.

The total percentage reduction of Alamar Blue for all treated cells will be described in the following section. This analysis employed a statistical approach with a sample size of N = 9 to assess whether the combined results from all experiments demonstrated significant

differences. This aimed to provide a clearer understanding of the overall impact and variations among the experimental outcomes.

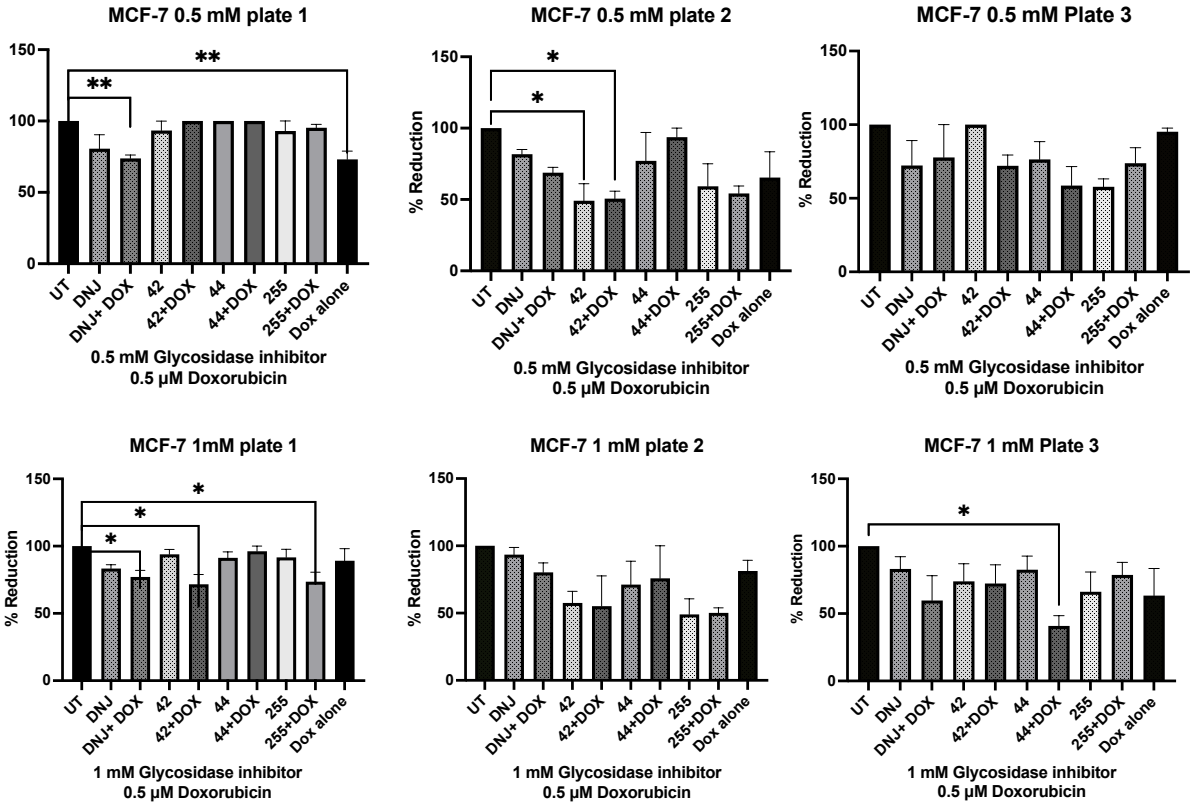

Figure 3.7. Cell viability results for MCF-7 cells subjected to 24-hour treatments with glycosidase inhibitors at concentrations of 0.5 mM (top panel) and 1 mM (bottom panel), with or without the addition of doxorubicin at 5 µM, are presented for each biological replicate. Each treatment involving glycosidase inhibitors was conducted in triplicate, resulting in a total of n = 9 for cell viability, which will be detailed in the following section. The data were presented as mean values ± SE, with N = 3. A one-way ANOVA statistical analysis was performed.

The following section (Fig. 3.8) displays histograms. MCF-7 cells treated with doxorubicin and glycosidase inhibitors exhibited reductions across all concentrations compared to the control group treated with doxorubicin alone. When cells were exposed solely to doxorubicin, a 10% decrease was noted. However, the combined treatment of the glycosidase inhibitor and doxorubicin showed a more pronounced effect at a concentration of 1 mM, resulting in a 34% reduction. This was followed by the combination of compound 255 and doxorubicin, which

resulted in a 33% reduction in Alamar Blue. Compound 44 and DNJ resulted in less reduction of metabolic activity. Although these reductions were observed, they were not statistically significant when treated cells were compared to those treated with doxorubicin.

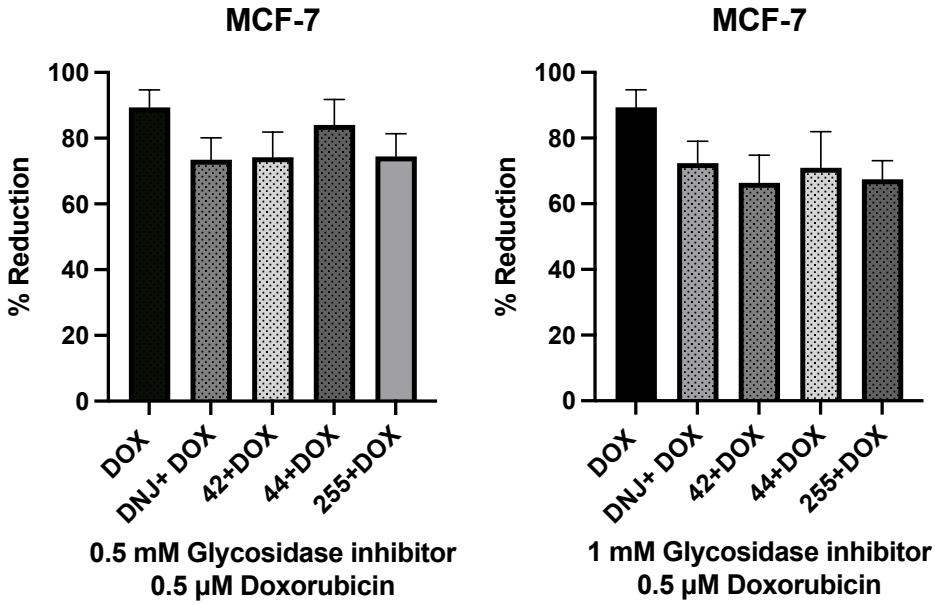

Figure 3.8. The cytotoxic effects on the MCF-7 ER+ breast cancer cell line were evaluated, focusing on glycosidase inhibitors with doxorubicin exposure, and compared to doxorubicin alone as a control at 5 µM. The left panel illustrates the reduction percentage at a concentration of 0.5 mM, while the right panel shows the reduction percentage at 1 mM. The data were presented as mean values ± standard error, with N=9. A one-way ANOVA statistical analysis was performed to assess the significance of the results. No significant differences were shown.

Histograms showing MCF-7 cells treated with glycosidase inhibitors compared to the untreated cells are (shown in Fig. 3.9). In the left panel, MCF-7 cells treated with the inhibitor compound 255 at 0.5 mM showed the biggest reduction, with 30%. DNJ, compounds 42 and 44 showed a slight reduction, but despite this, no significant difference was observed. In the right panel, cells treated with 1 mM showed a significant difference compared to cells treated with compound inhibitors 255 and 42, with reductions of 31% and 25%, respectively. 1.465, P= < 0.050, P value = 0.0245). (F(DFn, DFd) = F (9, 80) = 2.146, P < 0.050, P = 0.0147) . While

other compounds, DNJ and compound 44, exhibited similar reduction effects, they did not show significant differences in their effects.

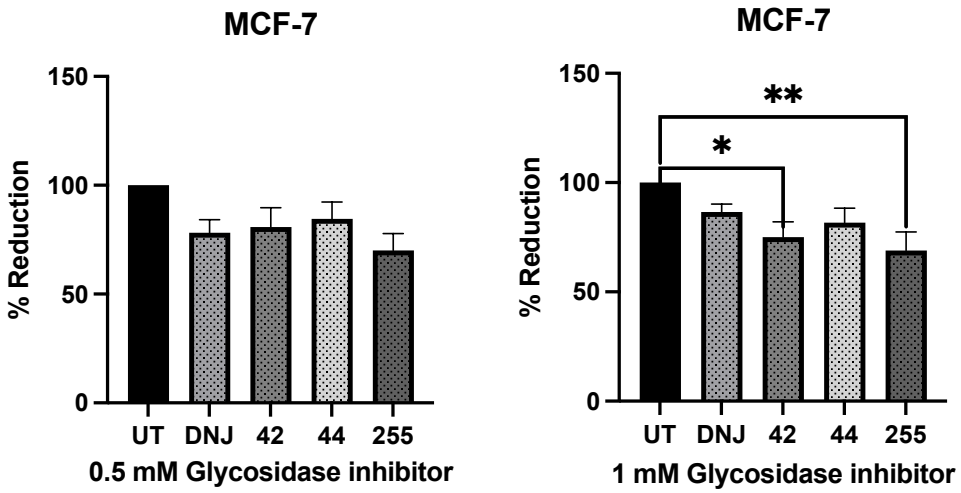

Figure 3.9. The cytotoxic effects on the MCF-7 ER+ breast cancer cell line were evaluated, focusing on glycosidase inhibitors with and without exposure to doxorubicin. The left panel illustrates the reduction percentage at a concentration of 0.5 mM, while the right panel shows the reduction percentage at 1 mM. Untreated (UT) MCF-7 cells were compared with those treated with glycosidase inhibitors. The data were presented as mean values ± standard error, with N=9. A one-way ANOVA statistical analysis was performed to assess the significance of the results. No significant differences were shown at 0.5 mM, while at 1 mM, it showed significant differences *p =< 0.050 (DNJ), **p =< 0.050 (255).

SKBR3 cells were treated with glycosidase inhibitors and doxorubicin to evaluate their metabolic activity, as shown below (Fig. 3.10). The top panel presents three histograms illustrating the outcomes of each cell viability assay. In these assays, cells treated with 0.5 mM of the inhibitor compounds combined with doxorubicin exhibited variations in metabolic activity, revealing a slight reduction but no significant difference in all three experiments. In the cells treated with 1 mM (Lower panel), statistically significant differences were observed in all three experiments, including DNJ and compound inhibitor 44 combined with doxorubicin, compared to the untreated cells.

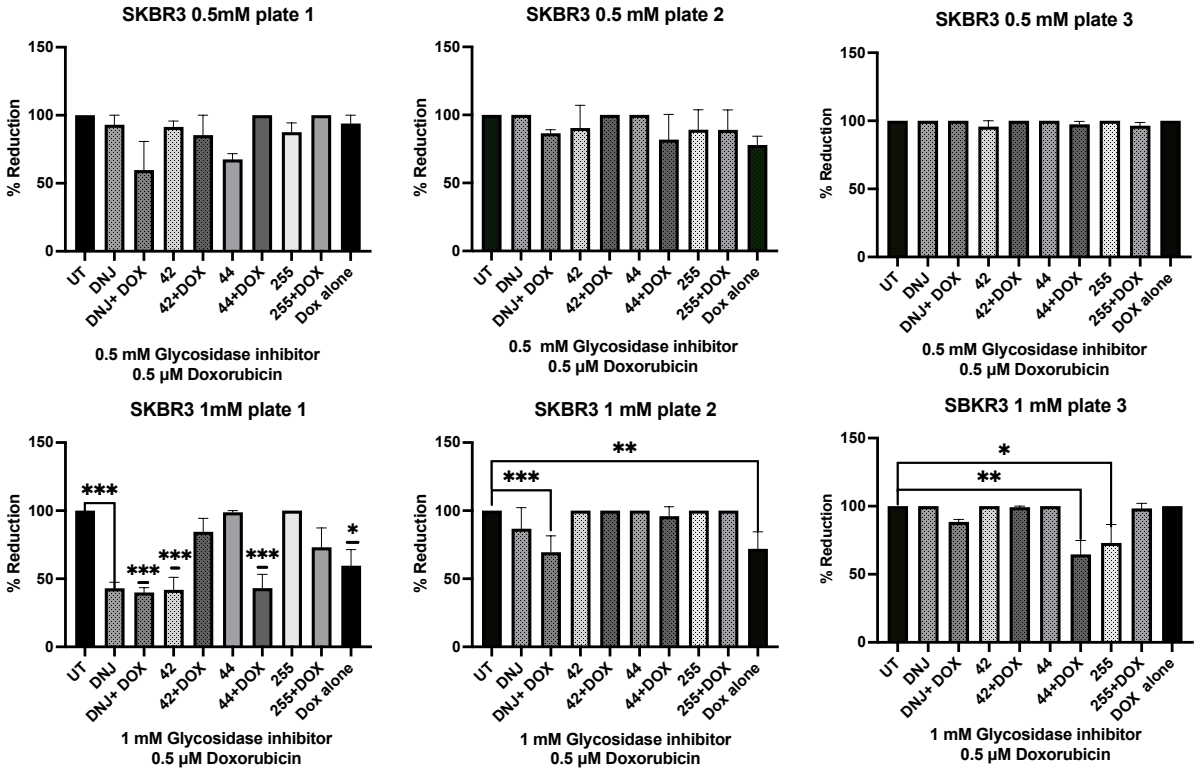

Figure 3.10. Cell viability results for SKBR3 HER2^{+} were subjected to 24-hour treatments with glycosidase inhibitors at concentrations of 0.5 mM (top panel) and 1 mM (bottom panel), with or without the addition of doxorubicin at 5 µM. They are presented for each biological replicate. Each treatment involving glycosidase inhibitors was conducted in triplicate, resulting in a total of N = 9 for cell viability, which will be detailed in the following section. The data are presented as mean values ± SE with N=3. A one-way ANOVA statistical analysis was performed.

The following section (Fig. 3.11) represents the main results obtained from the three experiments above, showing histograms of SKBR3 cells treated with doxorubicin alone as a control and compared with glycosidase inhibitors. In the left panel, SKBR3 cells were treated with DNJ and doxorubicin at a concentration of 0.5 µM, resulting in an 18% reduction in metabolic activity. The other treated cells with the compound inhibitors and doxorubicin showed an increase compared to doxorubicin alone, which had a 13% reduction. None of the treated cells resulted in a statistically significant difference.

In the right panel, SKBR3 cells treated with glycosidase inhibitors at a concentration of 1 mM, DNJ and doxorubicin, showed a 34% reduction in metabolic activity. Similarly, the inhibitor 44, combined with doxorubicin, resulted in a 32% reduction; however, this difference was not statistically significant. The combinations of doxorubicin with compound inhibitors 42 and 255 increased when compared to the cells treated with doxorubicin alone.

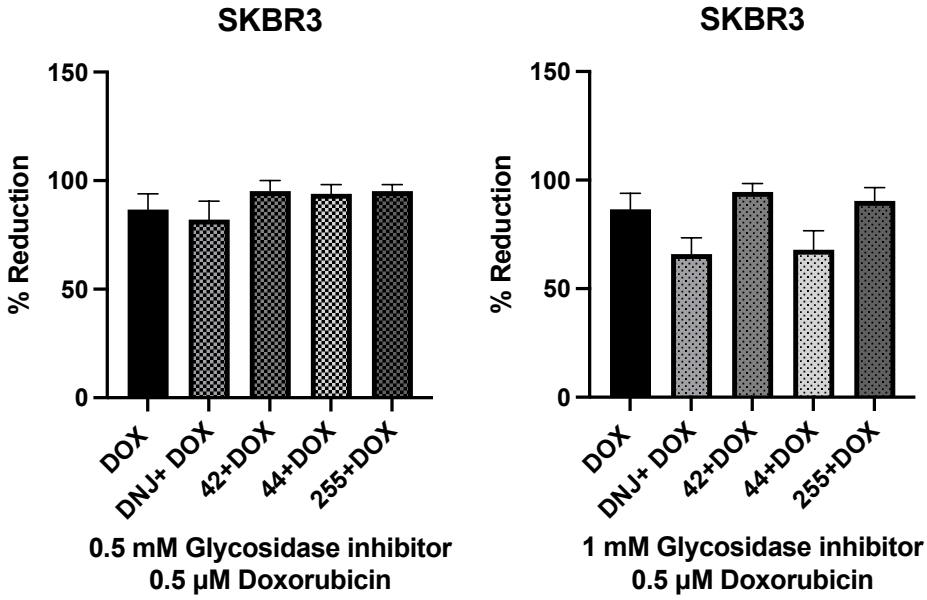

Figure 3.11. The cytotoxic effects on the SKBR3 HER^+ breast cancer cell line were evaluated, focusing on glycosidase inhibitors with doxorubicin exposure compared to doxorubicin alone as a control at 5 µM. The left panel illustrates the reduction percentage at a concentration of 0.5 mM, while the right panel shows the reduction percentage at 1 mM. The data were presented as mean values ± standard error, with N=9. A one-way ANOVA statistical analysis was performed to assess the significance of the results. No significant differences were shown.

Histograms showing SKBR3 cells treated with glycosidase inhibitors compared to the untreated cells are (shown in Fig. 3.12). In the left panel, SKBR3 cells treated with glycosidase inhibitors at concentrations of 0.5 mM showed modest reductions. In the right panel, cells treated with a 1 mM concentration showed greater reductions in all inhibitor compounds,

including DNJ and 42, with the highest reductions of 24% and 20%, respectively. Thus, no significant differences were shown.

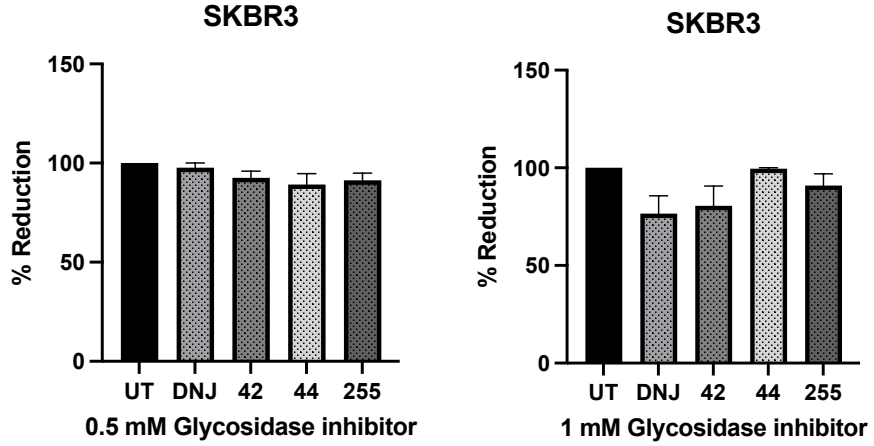

Figure 3.12. The cytotoxic effects on the SKBR3 HER2^{+} breast cancer cell line were evaluated, focusing on glycosidase inhibitor exposure. The left panel illustrates the reduction percentage at a concentration of 0.5 mM, while the right panel shows the reduction percentage at 1 mM. Untreated SKBR3 cells were compared with those treated with glycosidase inhibitors. The data were presented as mean values ± standard error, with N = 9. A one-way ANOVA statistical analysis was performed to assess the significance of the results. No significant differences were shown.

BT-549 cells treated with glycosidase inhibitors and doxorubicin were evaluated in terms of their metabolic activity, as shown below (Fig. 3.13), showing three histograms summarising the results of each cell viability assay. In these experiments, cells treated with the inhibitor compounds at 0.5 mM combined with doxorubicin showed variations in metabolic activity, with statistically significant differences evident in all three experiments. In the lower panel, cells treated at a 1 mM concentration showed significant differences in Experiments 2 and 3, although Experiment 1 did not result in statistical significant results despite a noted reduction in cell viability.

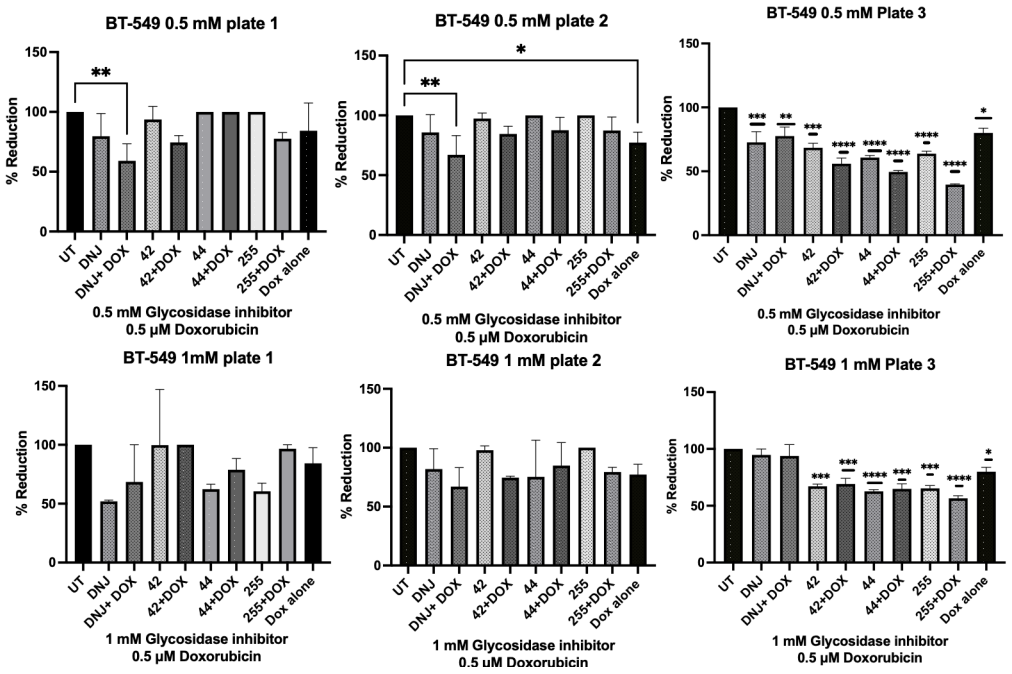

Figure 3.13. Cell viability results for the BT-549 TNBC line were subjected to 24-hour treatments with glycosidase inhibitors at concentrations of 0.5 mM (top panel) and 1 mM (bottom panel), with or without the addition of doxorubicin at 5 µM. They were presented for each biological replicate. Each treatment involving glycosidase inhibitors was conducted in triplicate, resulting in a total of n = 9 for cell viability, which will be detailed in the following section. The data were presented as mean values ± SE, with N = 3. A one-way ANOVA statistical analysis was performed.

The following section (Fig. 3.14) presents the main results obtained from the three experiments described in the preceding section. In the left panel, BT-549 cells treated with glycosidase inhibitors at 0.5 mM and doxorubicin exhibited a statistically significant difference compared to untreated cells. Specifically, the doxorubicin combination with DNJ, at doses of 42 and 255, respectively, resulted in reductions in cell viability of 32%, 28%, and 32%, respectively. Cells treated solely with doxorubicin showed a decrease in cell viability of 14%. However, these compounds did not result in a significant difference when compared to doxorubicin.

In the right panel, BT-549 cells were treated with glycosidase inhibitors at a concentration of 1 mM, along with doxorubicin at 0.5 µM, resulting in a modest reduction in cell viability for

the doxorubicin combination with DNJ and 44, respectively, both demonstrating a decrease of 24%, which was the highest reduction among the combined treatments. In comparison, doxorubicin with compound inhibitor 255 treatment resulted in a 23% decrease in tumour growth. However, despite the various treatments administered to BT-549 cells, no statistically significant differences were observed in the treated cells at 1mM ($F(DFn, DFd) = 1.380$, $P < 0.050$, P value = 0.2111).

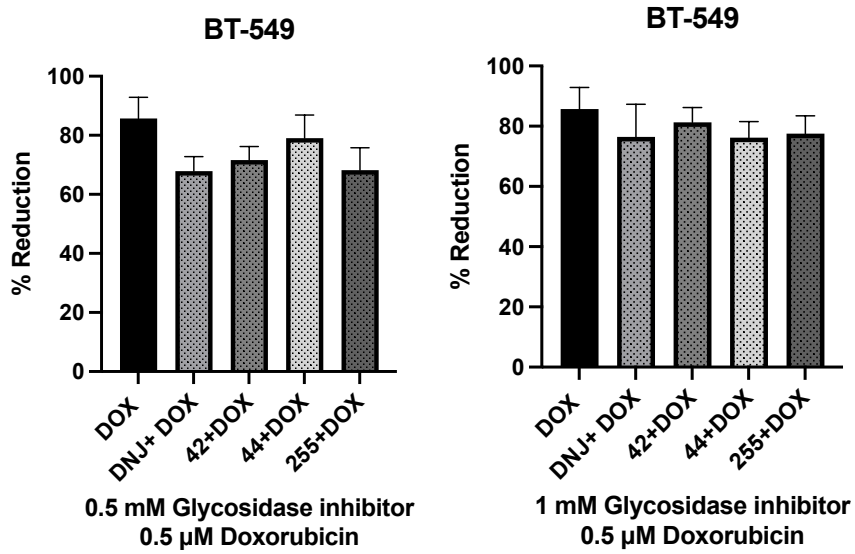

Figure 3.14. The cytotoxic effects on the BT-549 TNBC cell line were evaluated, focusing on glycosidase inhibitors with doxorubicin exposure compared to doxorubicin alone as a control at 5 µM. The left panel illustrates the reduction percentage at a concentration of 0.5 mM, while the right panel shows the reduction percentage at 1 mM. The data were presented as mean values ± standard error, with N=9. A one-way ANOVA statistical analysis was performed to assess the significance of the results. No significant differences were shown.

Histograms showing BT-549 cells treated with glycosidase inhibitors compared to the untreated cells are (shown in Fig. 3.15). BT-549 cells were treated with glycosidase inhibitors at a concentration of 0.5 mM, as shown in the left panel, which exhibited modest reductions in cell viability. DNJ showed the highest reduction, at 21%, resulting in a statistically significant difference. ($F (4, 40) = 2.123$ $P < 0.050$, P value = 0.0236). The other compound inhibitors, 42,

44, and 255, resulted in a 14%, 12%, and 13% reduction in metabolic activity, respectively, but these changes were not statistically significant.

In the right panel, cells subjected to treatment with the 1 mM concentration of inhibitor 44 exhibited a notable 34% reduction in cell viability, indicating a significant difference when compared to the untreated cells (F(DFn, DFd) = 1.380 (9,80), P =< 0.050, P = 0.0317). DNJ resulted in a 24% reduction, while the other inhibitors showed a minimal reduction, but none were statistically significant.

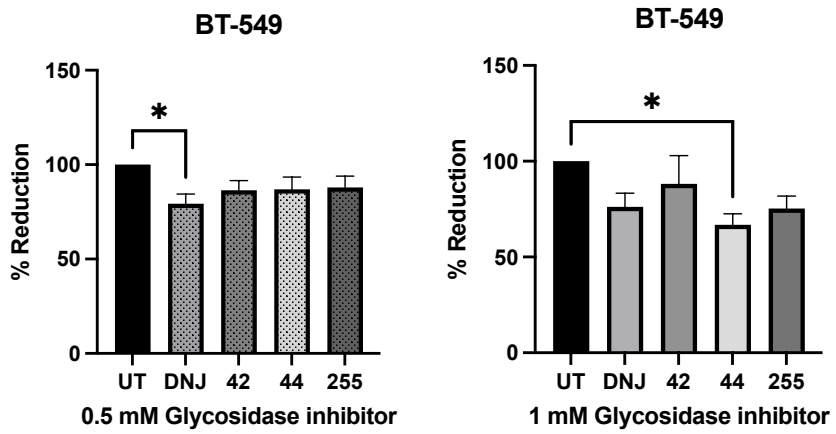

Figure 3.15. The cytotoxic effects on the BT-549 TNBC line were evaluated, focusing on the exposure to glycosidase inhibitors. The left panel illustrates the reduction percentage at a concentration of 0.5 mM, while the right panel shows the reduction percentage at 1 mM. Untreated BT-549 cells were compared with those treated with glycosidase inhibitors. The data were presented as mean values ± standard error, with N=9. A one-way ANOVA statistical analysis was performed to assess the significance of the results. Significant differences at 0.5 mM and 1mM were shown (DNJ) *p =< 0.050 , (44) * p =< 0.050.

MDA-MB-231 cells treated with glycosidase inhibitors and doxorubicin to evaluate their metabolic activity are (shown in Fig.3.16). The top panel displays MDA-MNB-231 cells on three histograms summarising the results of each cell viability assay. In these experiments, cells treated with the inhibitor compounds at a concentration of 0.5 mM combined with doxorubicin showed variations in metabolic activity, with statistically significant differences

evident in experiments 1 and 3. For cells treated at a concentration of 1 mM, significant differences were observed in Experiments 2 and 3, although Experiment 1 did not demonstrate statistical significance despite a noted reduction in cell viability.

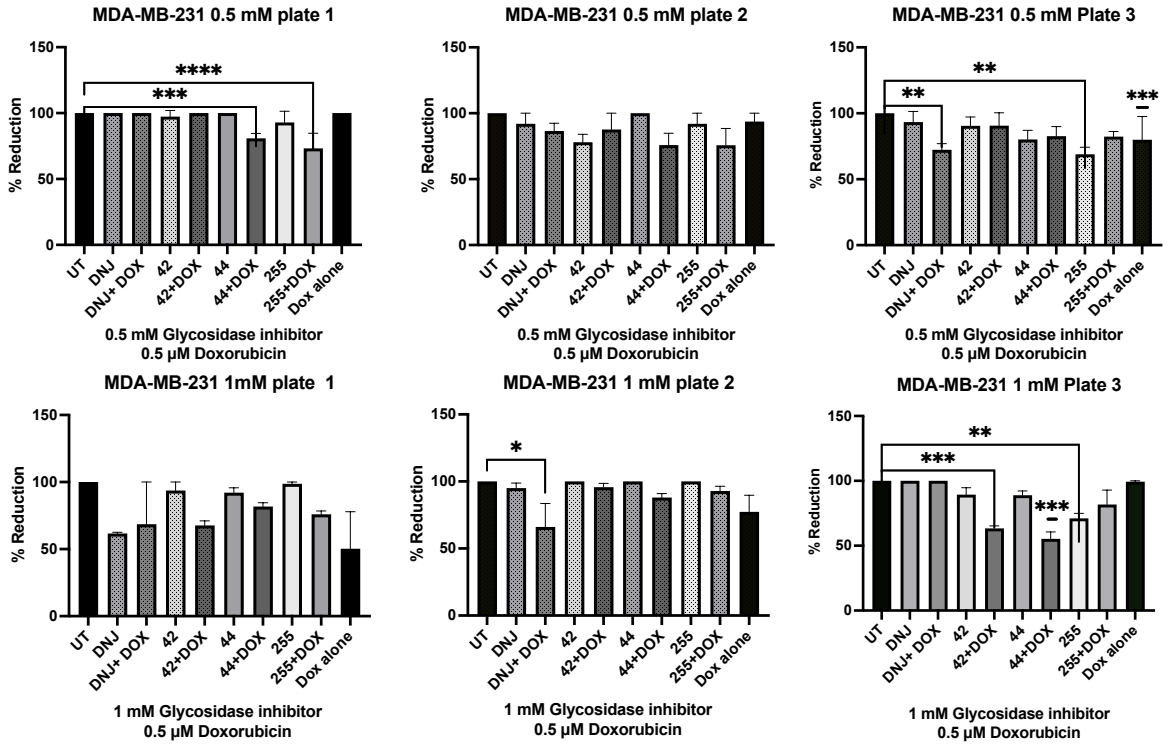

Figure 3.16. Cell viability results for the MDA-MB-231 TNBC line were subjected to 24-hour treatments with glycosidase inhibitors at concentrations of 0.5 mM (top panel) and 1 mM (bottom panel), with or without the addition of doxorubicin at 5 µM and are presented for each biological replicate. Each treatment involving glycosidase inhibitors was conducted in triplicate, resulting in a total of n = 9 for cell viability, which will be detailed in the following section. The data were presented as mean values ± SE, with N = 3. A one-way ANOVA statistical analysis was performed.

The following section (Fig. 3.17) represents the main results obtained from the three experiments from the above section. In the left panel, the combinations of doxorubicin with inhibitor compounds 44 and 255 resulted in the most substantial reductions in cell viability, showing reductions of 21% and 23%, respectively. Compound inhibitor 42 showed an

increase, while DNJ had no effect; however, no statistically significant difference was demonstrated in any of the treatments. In contrast, cells treated solely with doxorubicin experienced a modest decline in viability of 9%, with no statistically significant differences observed. In the right panel, MDA-MB-231 cells subjected to treatment with glycosidase inhibitors at a concentration of 1 mM, the combination of doxorubicin with compound inhibitor 44 showed a 24% reduction, representing the highest level of reduction among all the combined treatment groups. Cells were treated with doxorubicin and compound inhibitors 255 and DNJ, resulting in 16% and 22% reductions, respectively. Notably, the combination of doxorubicin and compound inhibitor 44 exhibited the least reduction in viability, at only 6%, as none of the other treatments reached statistical significance.

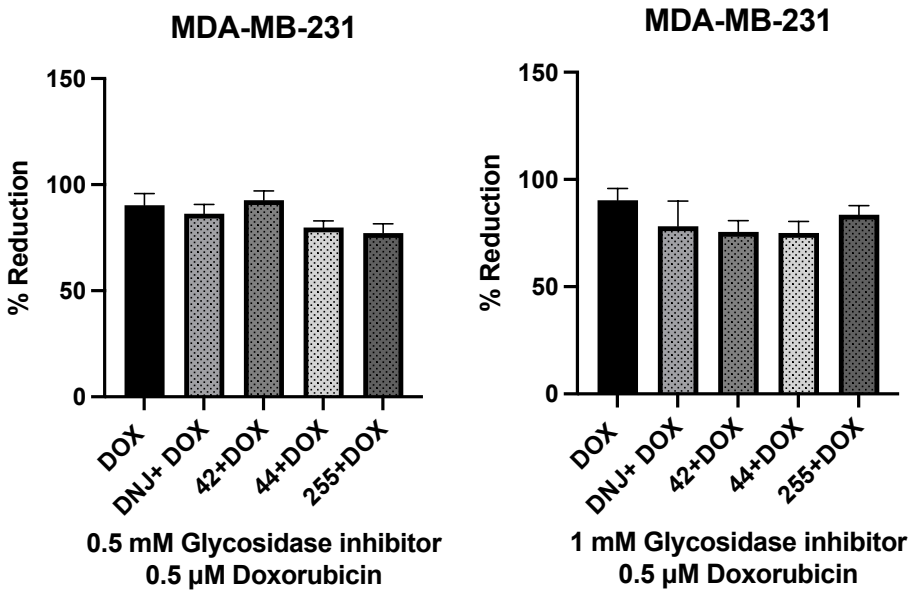

Figure 3.17. The cytotoxic effects on the BT-549 TNBC cell line were evaluated, focusing on glycosidase inhibitors with doxorubicin exposure compared to doxorubicin alone as a control at 5 µM. The left panel illustrates the reduction percentage at a concentration of 0.5 mM, while the right panel shows the reduction percentage at 1 mM. The data were presented as mean values ± standard error, with N = 9. A one-way ANOVA statistical analysis was performed to assess the significance of the results. No statistical differences were shown.

Histograms showing MDA-MB-231 cells treated with glycosidase inhibitors compared to the untreated cells are (shown in Fig. 3.18). In the left panel, MDA-MB-231 cells were treated at 0.5 mM with the compound inhibitors 255, resulting in a 15% reduction in cell viability compared to the untreated cells, showing a statistically significant difference (F(DFn, DFd) = 3.435 (9,80), P < 0.050, P value = 0.0381). Other inhibitors caused minor reductions in metabolic activity; however, these changes did not reach statistical significance. In the right panel, treatment with the 1 mM concentration of the inhibitor DNJ led to a 10% reduction, marking it as the most effective among the tested inhibitors, and showed a statistically significant difference when compared to the untreated cells (F(DFn, DFd) = 1.977 (9,80), P= < 0.050, P value = 0.0390).

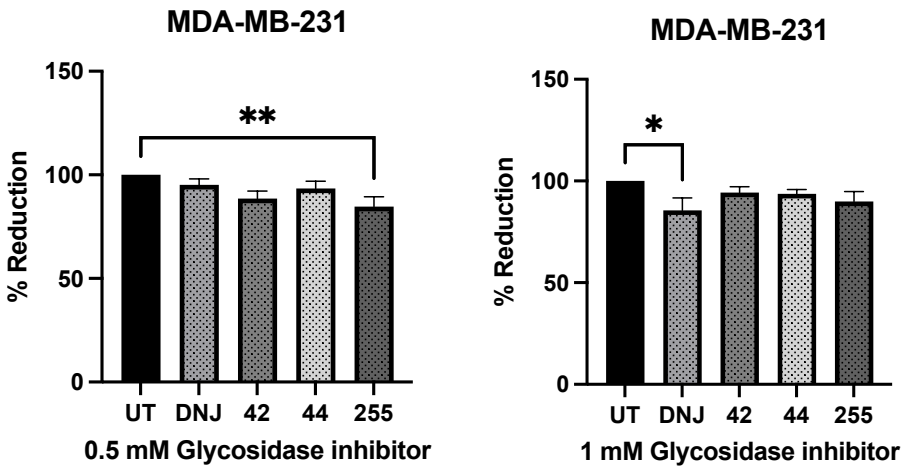

Figure 3.18. The cytotoxic effects on the MDA-MB-231 TNBC line were evaluated, focusing on the exposure to glycosidase inhibitors. The left panel illustrates the reduction percentage at a concentration of 0.5 mM, while the right panel shows the reduction percentage at 1 mM. Untreated MDA-MB-231 cells were compared with those treated with glycosidase inhibitors. The data were presented as mean values ± standard error, with N = 9. A one-way ANOVA statistical analysis was performed to assess the significance of the results. Statistical differences were shown at 0.5 mM and 1 mM concentrations, (255) **p =< 0.050, (DNJ) *p =< 0.050.

Examples of particle analysis measurements are shown below in (3.3) for changes in cell count detection by DAPI staining, which serves as a surrogate for nucleic growth profiles.

3.3. Nucleic particle analysis measurement

The cells treated with glycosidase inhibitors were stained with DAPI, which specifically binds to oligonucleotide in the nucleus (Kapuscinski, 1995), and was deployed as described in (Section 2.1.10) to serve as a surrogate in terms of nucleic count shown in (Fig. 3.19). To analyse, treated cells that were exposed to glycosidase inhibitors at a concentration of 0.5 mM for 24 hours. This analysis aimed to observe changes in cell count resulting from the treatment of cells with the glycosidase inhibitors. The particle analysis yielded valuable insights into the number of nuclei present.

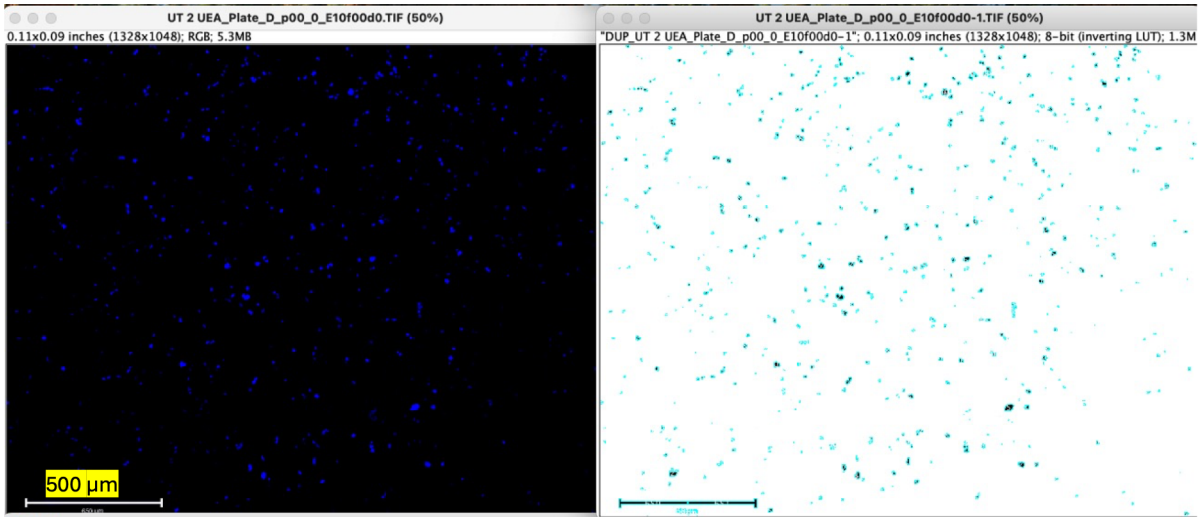

Figure 3.19. An example of applied image measurement, taken at 100X total magnification and scale bar representing 500 µm, in the particle analysis of the DNJ compound utilises ImageJ through a binary process of masking thresholds and the watershed tool to effectively separate cells that appear merged. Without this methodology, manually counting individual cells would be difficult and inaccurate.

MCF-7 cells (Fig. 3.20) treated with glycosidase inhibitors for 24 hours were stained with DAPI to evaluate the nuclei count as part of the growth profile. This assessment aimed to determine the effects of the various inhibitors and identify any changes in cell numbers. The upper panel showed the visualisation of cells treated with glycosidase inhibitors at a concentration of 0.5 mM, illustrating their impact on cell numbers. The data in the lower panel indicate that inhibitor 42 caused a significant increase in growth, resulting in approximately 500 more cells than the untreated group. Similarly, cells treated with inhibitor

compound 44 exhibited growth nearly equivalent to compound 42, showing increased cell numbers. Cells treated with DNJ showed a slight increase in growth, while those treated with compound 255 did not demonstrate any increase compared to the untreated cells. Overall, none of the cells treated with glycosidase inhibitors experienced a reduction in numbers; instead, they proliferated more aggressively. Thus, there was no statistically significant difference.

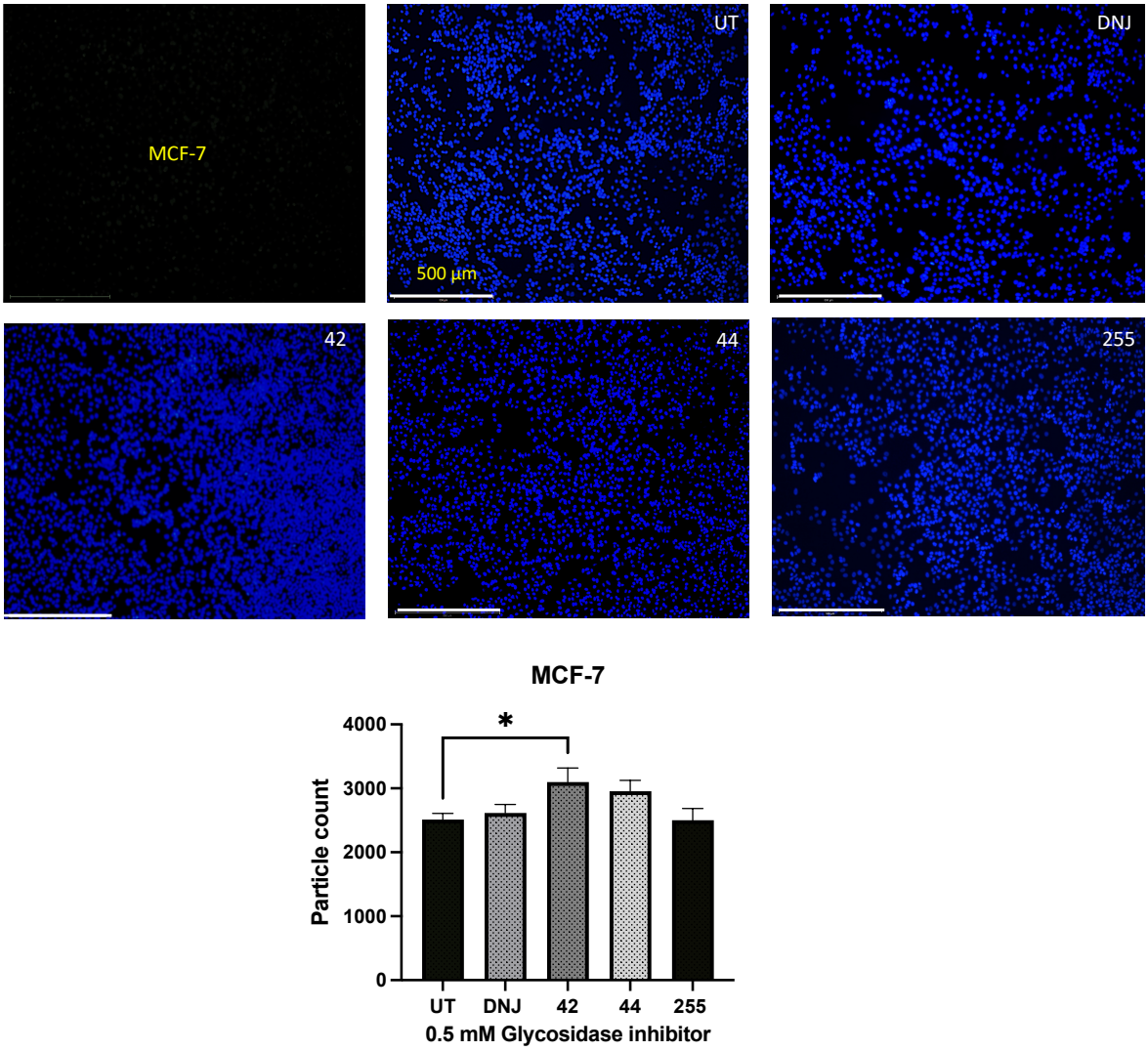

Figure 3.20. Upper Panel: Visualisation of DAPI fluorescence representing the nuclei of MCF-7 ER$^+$ breast cancer cells treated for 24 hours with glycosidase inhibitors, including DNJ and Phytoquest compounds (42, 44, and 255) at a concentration of 0.5 mM. Lower Panel: A histogram displaying particle analysis data from the glycosidase inhibition treatment using the ImageJ particle analysis program, with median values presented as ± SE with N = 27. The microscope was set to a total magnification of 100X, with a scale bar representing 500 µm. A one-way ANOVA statistical analysis was conducted on the non-parametric data to compare untreated and treated cells. No significant differences were shown in terms of reductions. It showed a statistical difference in the increase in cell numbers instead.

SKBR3 cells (Fig. 3.21) treated with glycosidase inhibitors for 24 hours were stained with DAPI to evaluate the nuclei count as part of the growth profile. The upper panel shows the

cells treated with glycosidase inhibitors at a concentration of 0.5 mM, illustrating their impact on cell quantities. Notably, a reduction in cell numbers was observed with the inhibitors DNJ and 255. The data presented in the lower panel aligns with the observations in the upper panel, indicating that the inhibitors DNJ and 255 resulted in the most significant decrease in cell numbers, with a statistically significant difference ($F(DFn, DFd) = 2.959$ (4, 130), $P = < 0.050$, P value= 0.0223). Cells treated with compound 42 also showed a decrease in cell numbers, while compound 44 had the least effect on the cells; however, the changes observed with these compounds were not statistically significant.

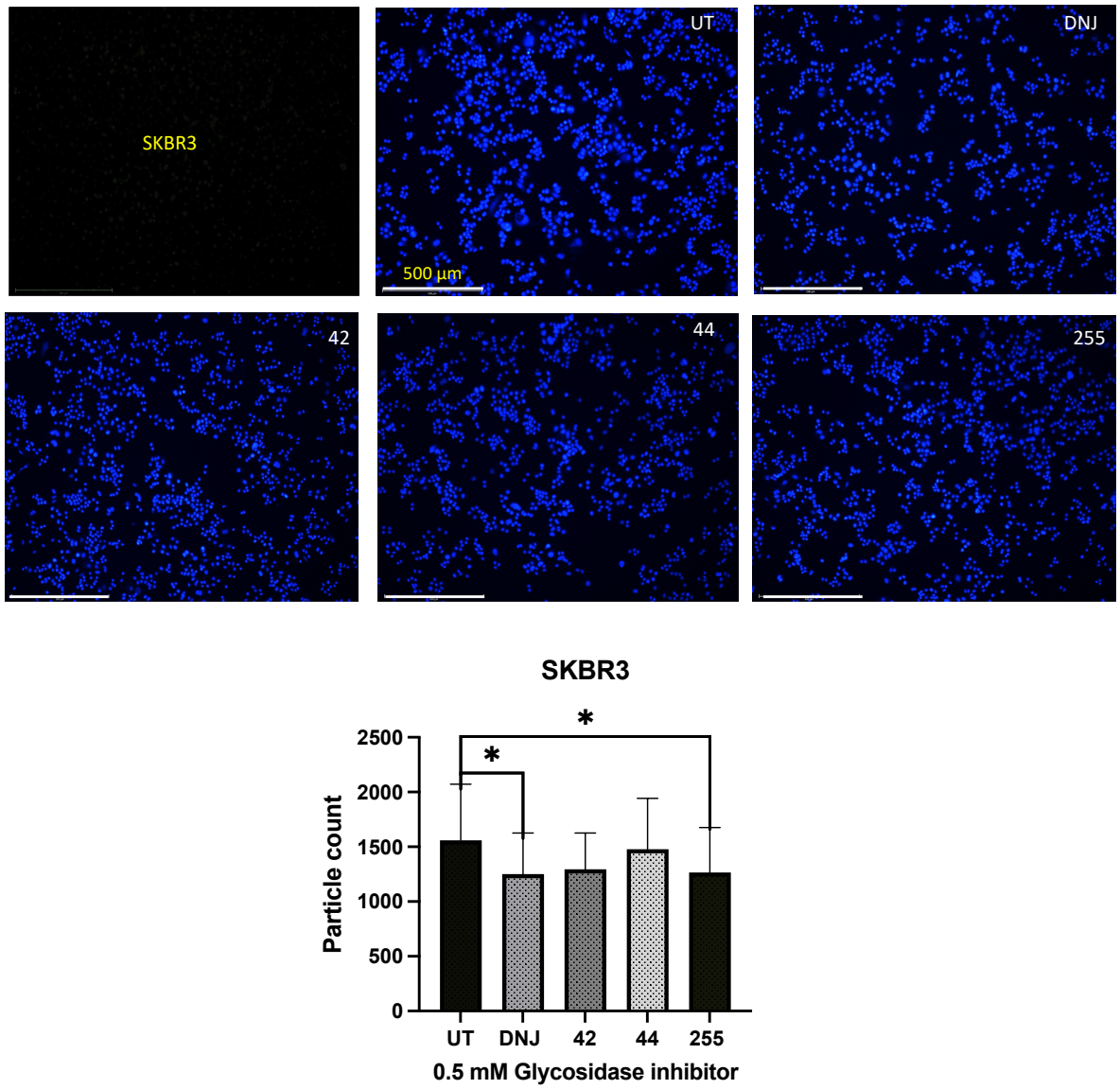

Figure 3.21. Upper Panel: Visualisation of DAPI fluorescence representing the nuclei of SKBR3 HER2^{+} breast cancer cells treated for 24 hours with glycosidase inhibitors, including DNJ and Phytoquest compounds (42, 44, and 255) at a concentration of 0.5 mM. Lower Panel: A histogram displaying particle analysis data from the glycosidase inhibition treatment using the ImageJ particle analysis program, with median values presented as ± SE with N = 27. The microscope was set to a total magnification of 100X, with a scale bar representing 500 µm. A one-way ANOVA statistical analysis was conducted on the non-parametric data to compare untreated and treated cells. A significant difference was shown on (DNJ) *p= < 0.050, and (255) *p =< 0.050. 44 and 44 compounds did not show significant differences.

BT-549 cells (Fig. 3.22) treated with glycosidase inhibitors for 24 hours were stained with DAPI to evaluate the nuclei count as part of the growth profile. BT-549 cells were treated with glycosidase inhibitors for 24 hours and stained with DAPI to evaluate the nuclei count as part of the growth profile. This assessment aimed to determine the effects of the various inhibitors and identify any changes in cell numbers.

The upper panel displays the visualisation of cells treated with glycosidase inhibitors at a concentration of 0.5 mM, illustrating the impact on cell numbers. The data in the lower panel indicate that all inhibitors caused an increase in growth, resulting in approximately 500 more cells than the untreated group. Similarly, cells treated with inhibitor compound 255 exhibited the least growth increase among all inhibitors. Overall, none of the cells treated with glycosidase inhibitors experienced a reduction in numbers; instead, they proliferated more aggressively. ($F(DFn, DFd) = 1.378$ (4, 130), $P =< 0.050$, P value= 0.2452).

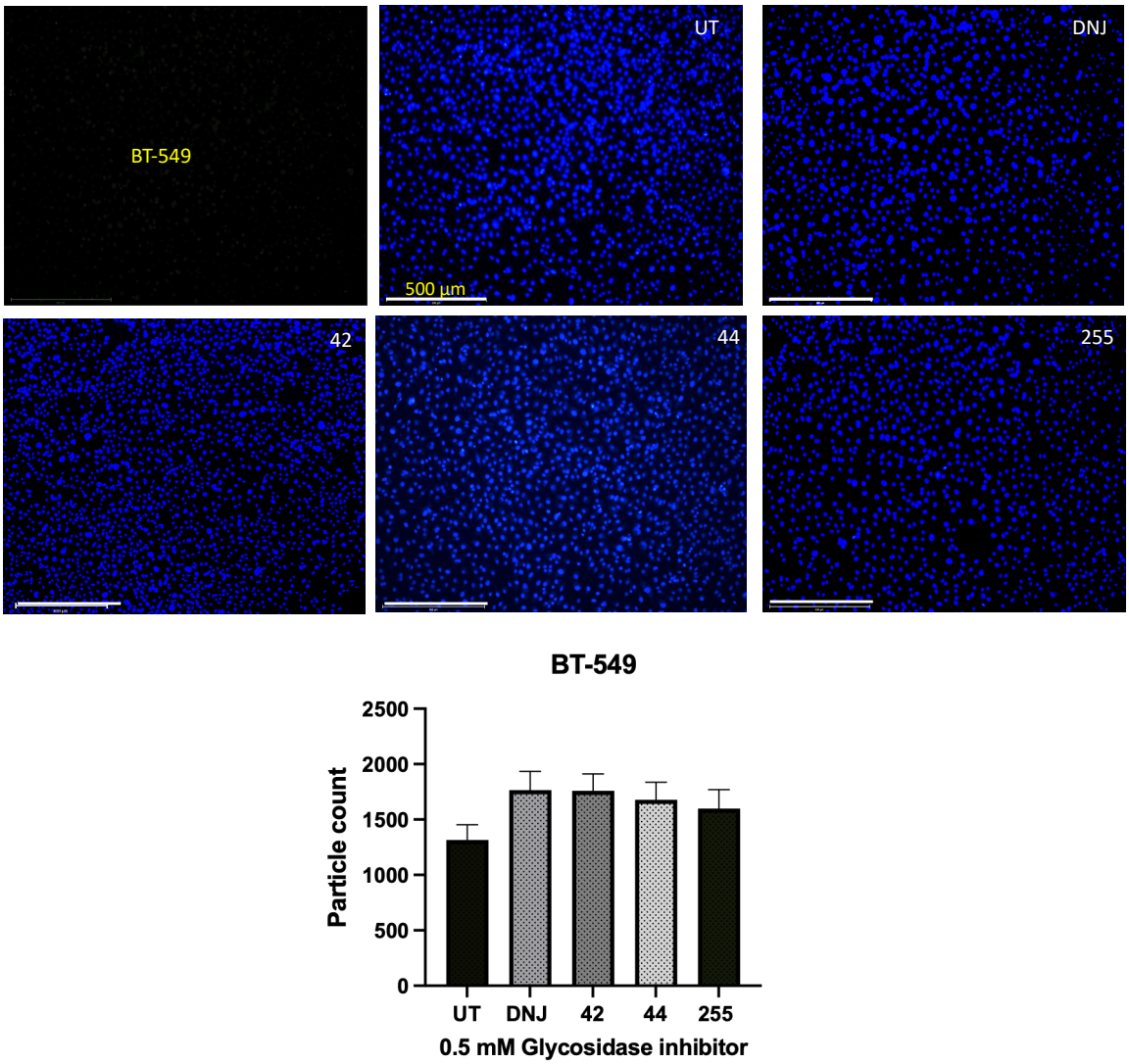

Figure 3.22. Upper Panel: Visualisation of DAPI fluorescence representing the nuclei of BT-549 TNBC cells treated for 24 hours with glycosidase inhibitors, including DNJ and Phytoquest compounds (42, 44, and 255) at a concentration of 0.5 mM. Lower Panel: A histogram displaying particle analysis data from the glycosidase inhibition treatment using the ImageJ particle analysis program, with median values presented as ± SE with N = 27. The microscope was set to a total magnification of 100X, with a scale bar representing 500 µm. A one-way ANOVA statistical analysis was conducted on the non-parametric data to compare untreated and treated cells. No significant differences were shown.

MDA-MB-231 cells (Fig. 3.23) treated with glycosidase inhibitors for 24 hours were stained with DAPI to evaluate the nuclei count as part of the growth profile. The upper panel visualises the cells treated with glycosidase inhibitors at a concentration of 0.5 mM, illustrating their

impact on cell quantities. Notably, there was a reduction in cell numbers, primarily observed with the inhibitors DNJ. The data presented in the lower panel aligns with the observations in the upper panel, indicating that the inhibitor DNJ resulted in the most significant decrease in cell numbers, with a statistically significant difference ($F(DFn, DFd) = 2.629$ (4, 130), $P =< 0.050$, P value = 0.0374). Cells treated with inhibitor compounds 44 AND 255 also showed a decrease in cell numbers, while compound 42 did not affect the cells compared to the untreated cells; however, the changes observed with these compounds were not statistically significant.

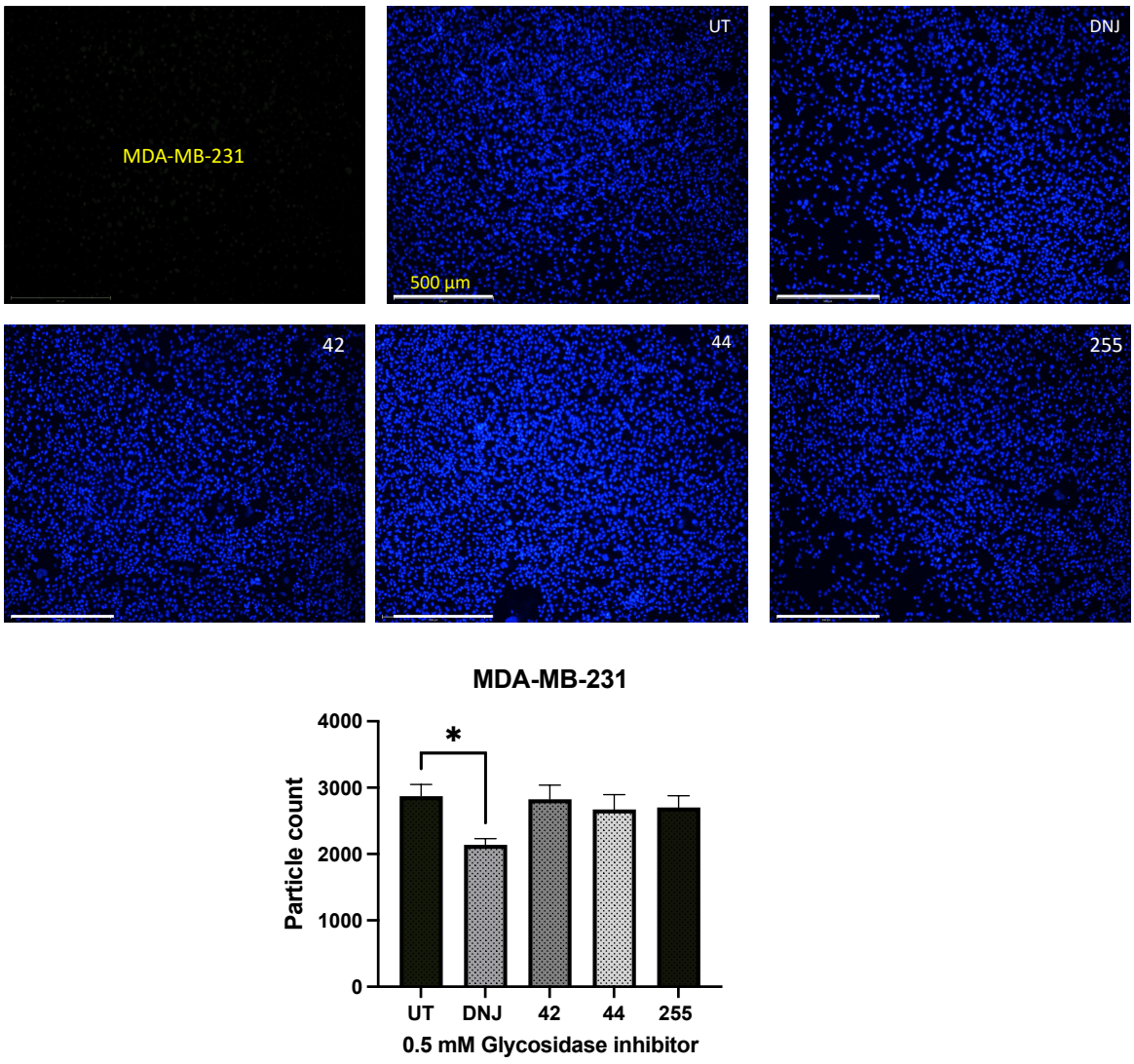

Figure 3.23. Upper Panel: Visualisation of DAPI fluorescence representing the nuclei of MDA-MB-231 TNBC cells treated for 24 hours with glycosidase inhibitors, including DNJ and Phytoquest compounds (42, 44, and 255) at a concentration of 0.5 mM. Lower Panel: A histogram displaying particle analysis data from the glycosidase inhibition treatment using the ImageJ particle analysis program, with median values presented as ± SE with N = 27. The microscope was set to a total magnification of 100X, with a scale bar representing 500 µm. A one-way ANOVA statistical analysis was conducted on the non-parametric data to compare untreated and treated cells. A significant difference was show on (DNJ) *p=< 0.050. No significant difference was shown in the ither compounds.

The statistical analysis of the four breast cancer cell lines to determine whether there is a significant difference is presented below (Table 3.3). This overview shows breast cancer cells treated with glycosidase inhibitors at 0.5 mM for 24 hours. The data generated in this analysis consisted of 9 replicates in each experiment for both untreated and treated cells with glycosidase inhibitors, conducted across 3 experiments, resulting in a total of N = 27.

Table 3. 3. One-way ANOVA statistical analysis of particle analyses of the four breast cancer cell lines used in this study.

	MCF-7	SKBR3	BT-549	MDA-MB-231
ANOVA summary				
F	2.692	2.959	1.378	2.629
P value	0.0339	0.0223	0.2452	0.0374
P value summary	*	*	ns	*
Significant diff. among means (P < 0.05)?	Yes	Yes	No	Yes
R squared	0.0765	0.08345	0.04067	0.07483

Measurements of cell migration were performed using the wound healing assay to evaluate cell motility among breast cancer cell lines treated with glycosidase inhibitors, as (shown below in Section 3.4).

3.4. Wound healing assay

The wound healing (or scratch) assay as described in (Section 2.1.11), was used to measure two-dimensional cell movement on cell lines treated with glycosidase inhibitors for 24 hours. An artificial gap was created on a confluent cell monolayer, and cell movement was tracked using microscopy. In the cell layer, the migration of surrounding cells to fill the gap was observed at different time points (0, 6, 12, and 24 hours). After 24 hours of treatment, most cells had restored the integrity of the cell layer. This assay provides valuable insights into cellular behaviours, particularly migration and cell motility. This study evaluated the impact of glycosidase inhibitors on the migratory capability of breast cancer cells. Glycosidase inhibitors are known to affect cell surface glycoproteins, which may influence cell migration. Images and statistical analysis of the wound healing assay were carried out on MCF-7 cells exposed to glycosidase inhibitors for 24 hours, as shown in the section below (Fig. 3.24) In the

upper panel, the illustration depicts MCF-7 cells treated with glycosidase inhibitors at 0 6, 12 and 24 hours, all groups show a gradual decrease in wound width Within 24 hours. The lower panel includes histograms displaying the percentage of wound closure at 6, 12, and 24 hours, corresponding to the illustrations in the upper panel. After 6 hours, the rate at which the scratch or wound area closed over time was measured. The cells treated with DNJ exhibited the highest closure percentage, at 6%, while the untreated cells had a closure percentage of 5%. In contrast, the cells treated with compound inhibitors 255 and 44 showed further widening of the wound gap, with negative closure values of -5% and -2%, respectively. Compound 42 resulted in a 2% closure gap. One-way ANOVA indicated no significant difference at the 6-hour time point.

At the 12-hour time point, untreated cells showed a 10% increase in wound closure. Cells treated with DNJ had an 8% closure rate, while those treated with inhibitor 42 showed a rate of around 6%. Cells treated with inhibitor 44 had a 2% closure. Notably, the cells treated with inhibitor 255 experienced a 9% decrease, indicating further widening of the wound gap. Statistical analysis revealed no significant differences in the one-way ANOVA. At the 24-hour time point, untreated cells exhibited approximately 30% gap closure. Cells treated with DNJ showed 22% closure, while those treated with inhibitors 42 and 44 had 15% and 16%, respectively. Conversely, cells treated with inhibitor 255 exhibited the least migration, with only a 3% gap closure; however, this difference was not statistically significant. The reason why there is negative gap closures on the cells exposed with compound inhibitor 44 and 255 in the first 12 hours, is because the cells were affected and seem to have opened the gap closure instead. Thus, affecting the proliferative rate of this cell line.

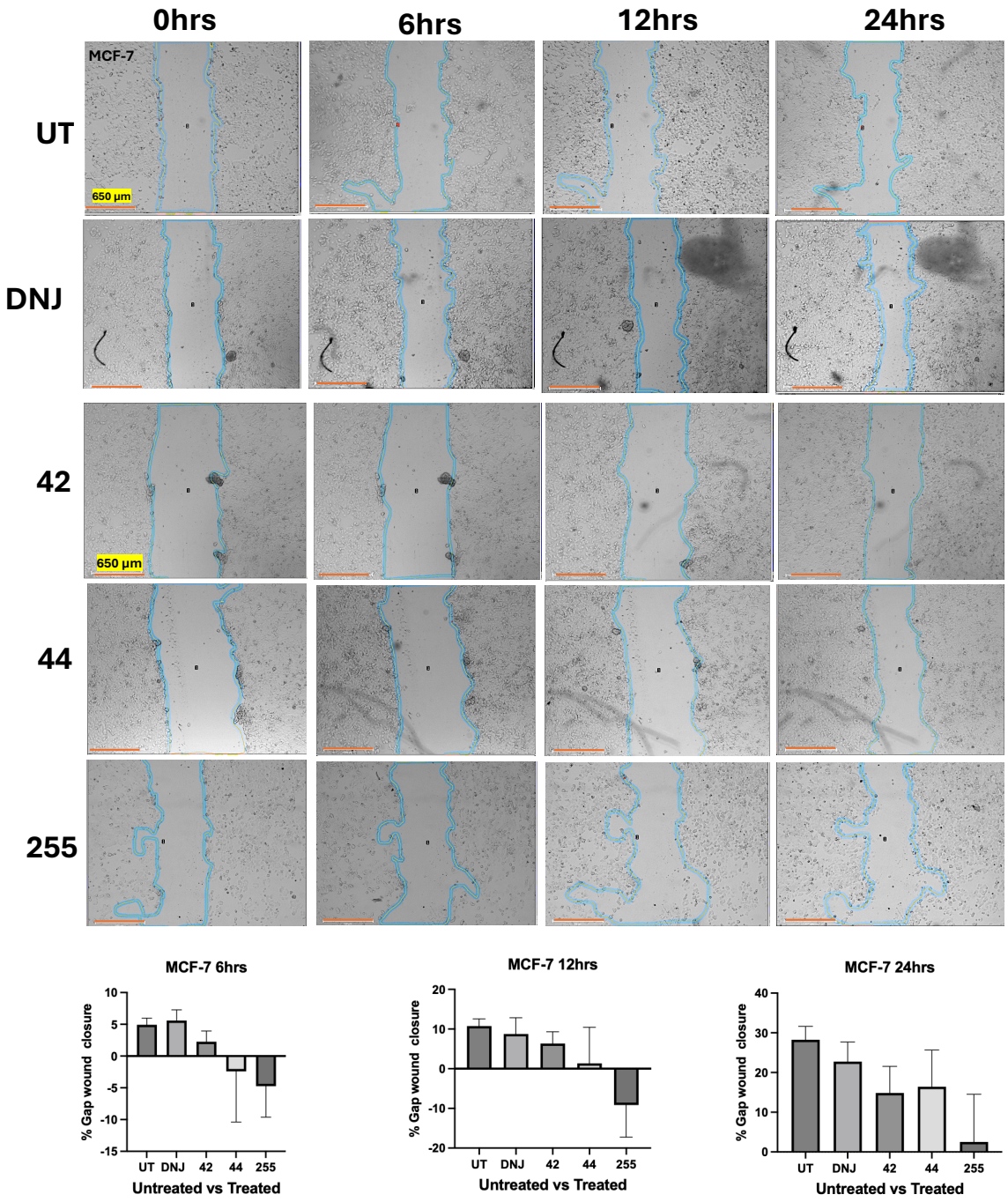

Figure 3.24. Time-course of wound healing in MCF-7 ER$^+$ breast cancer cells treated with glycosidase inhibitors at 0.5 mM for 24 hours. The upper panel illustrates images of MCF-7 cells in a scratch assay treated with DNJ, 42,44, and 255 inhibitor compounds at different time points, measured at 0, 6, 12, and 24 hours. Total magnification of X100, with a scale bar representing 650 µm. The lower panel shows the percentage gap wound closure at various time points of untreated vs treated cells with glycosidase inhibitors. The data are presented as mean values ± standard error, with a sample size of N = 12. A one-way ANOVA statistical analysis was performed. No significant differences were shown.

Statistical analysis (Table 3.4) was performed to determine whether there was a significant difference in the treated MCF-7 cells with the inhibitor compounds.

Table 3. 4. Scratch assay from One-way ANOVA statistical analysis of MCF-7 cells treated with glycosidase inhibitors.

ANOVA summary	6 hours	12 hours	24 hours
F	1.096	1.782	1.507
P value	0.3679	0.1456	0.2129
P value summary	ns	ns	ns
Significant diff. among means (P < 0.05)?	No	No	No
R squared	0.07381	0.1147	0.09875

Images and statistical analysis of the wound healing assay were performed on SKBR3 cells exposed to glycosidase inhibitors for 24 hours, as shown in the section below (Fig. 3.25). In the upper panel, the illustration depicts SKBR3 cells treated with glycosidase inhibitors at 0, 6, 12, and 24 hours. All groups show a gradual decrease in wound width within 24 hours. The lower panel includes histograms displaying the percentage of wound closure at 6, 12, and 24 hours, corresponding to the illustrations in the upper panel. After 6 hours, the rate at which the scratch or wound area closed over time was measured. The cells treated with DNJ exhibited the highest closure percentage at 5%, while the untreated cells had a closure percentage of 4.5%. In contrast, the cells treated with compound inhibitors 42 and 44 had 2% and 1% gap closure, respectively. Compound 255 resulted in a 1% closure gap.
One-way ANOVA revealed no significant difference at the 6-hour time point.

At the 12-hour time point, untreated cells exhibited a 7.5% gap in wound closure. Cells treated with DNJ demonstrated a 5% closure, while those treated with inhibitor 42 showed a 3% closure. Cells treated with inhibitor 44 had a 2% closure, and notably, the cells treated with inhibitor 255 experienced a decrease of -0.5% in wound closure, indicating a reduction in gap closure. Statistical analysis revealed significant differences concerning inhibitor 255 in the one-way ANOVA (F(DFn, DFd) = 2.047 (4, 55), P =< 0.050, P value= 0.0457).
At the 24-hour time point, untreated cells demonstrated approximately 12.5% gap closure. Cells treated with DNJ showed 9% closure, while those treated with inhibitors 42 and 44 had

closures of 5% and 6%, respectively. Although there was no statistically significant difference among these inhibitors, cells treated with inhibitor 255 exhibited the least migration, with a -0.5% decrease in gap closure. This result also indicated a significant difference in the ANOVA (F(DFn, DFd) = 2.288 (4, 55), P =< 0.050, P value= 0.0223.

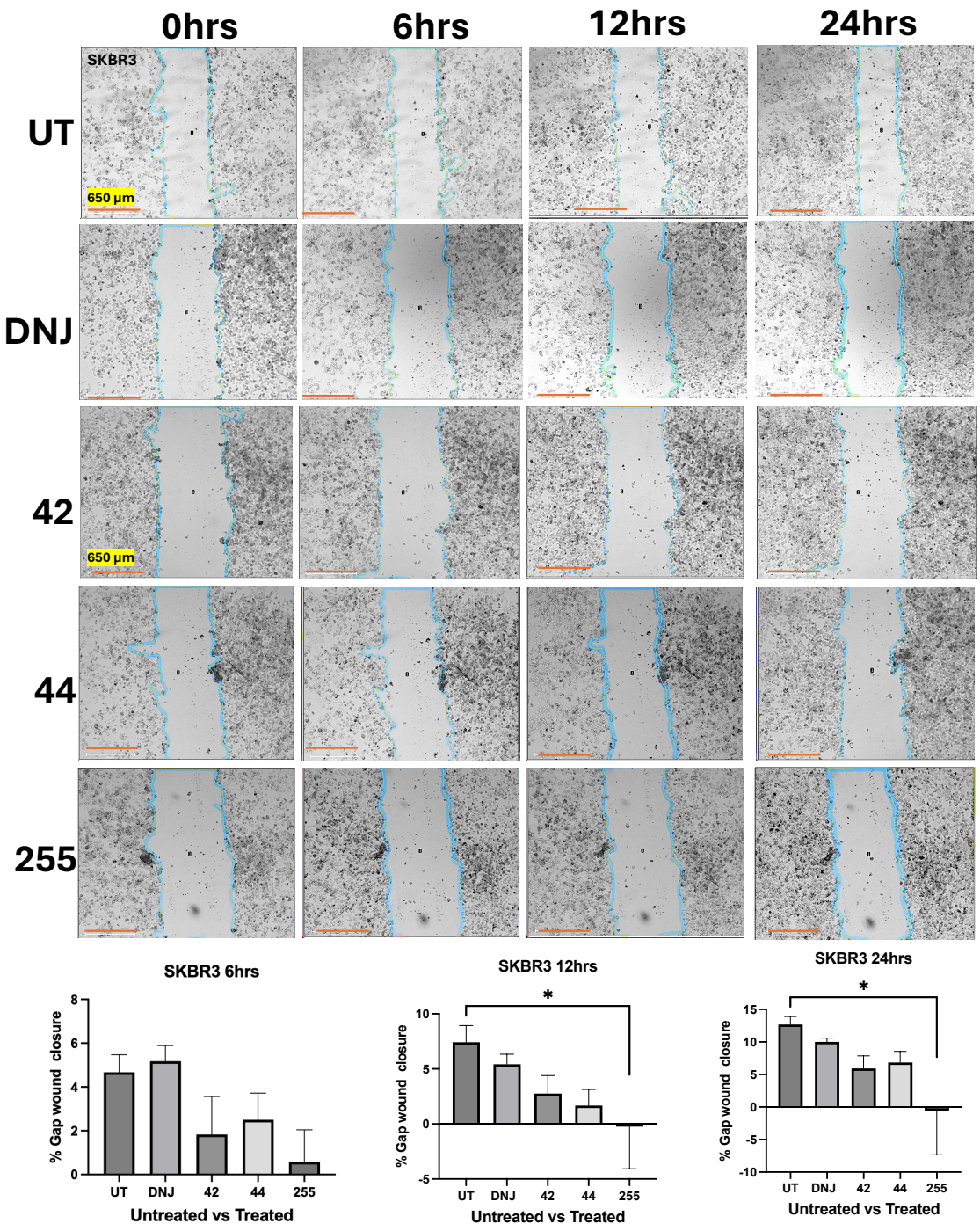

Figure 3.25. Time-course of wound healing in SKBR3 HER2^{+} breast cancer cells treated with glycosidase inhibitors at 0.5 mM for 24 hours. The upper panel illustrates images of SKBR3 cells in a scratch assay treated with DNJ, 42, 44, and 255 inhibitor compounds at different time points, measured at 0, 6, 12, and 24 hours. Total magnification of X100, with a scale bar representing 650 µm. The lower panel shows the percentage gap wound closure at various time points of untreated vs treated cells with glycosidase inhibitors. The data are presented as mean values ± standard error, with a sample size of N = 12. A one-way ANOVA statistical

analysis was performed to assess the significance of the results. A significance difference was shown on (255) *p=< 0.050 after 24 hours.

Statistical analysis (Table 3.5) was performed to determine whether there was a significant difference in the treated SKBR3 cells with the inhibitor compounds.

Table 3. 5. Scratch assay results from One-way ANOVA statistical analysis of SKBR3 cells treated with glycosidase inhibitors.

ANOVA summary	6 hours	12 hours	24 hours
F	2.398	2.047	2.288
P value	0.0611	0.1005	0.0714
P value summary	ns	ns	ns
Significant diff. among means (P < 0.05)?	No	No	No
R squared	0.1485	0.1296	0.1427

Images and statistical analysis of the wound healing assay performed on BT-549 cells exposed to glycosidase inhibitors for 24 hours are presented in the section below (Fig. 3.26). In the upper panel, the illustration depicts BT-549 cells treated with glycosidase inhibitors at 0, 6, 12, and 24 hours. All groups show a gradual decrease in wound width within 24 hours. The lower panel includes histograms displaying the percentage of wound closure at 6, 12, and 24 hours, corresponding to the illustrations in the upper panel. After 6 hours, the rate at which the scratch or wound area closed over time was measured. The cells treated with DNJ exhibited the highest closure percentage, at 25%, while the untreated cells had a closure percentage of 20%. In contrast, the cells treated with compound inhibitors 42 and 44 had 17% and 16% gap closure, respectively. Compound 255 resulted in a 24% reduction in the closure gap. One-way ANOVA indicated a significant difference at the 6-hour time point; F(DFn, DFd) = 2.557 (4, 55), P= < 0.050, P = 0.0457.

At the 12-hour time point, untreated cells exhibited a 37.5% gap in wound closure. Cells treated with DNJ demonstrated a 44% closure, while those treated with inhibitor 42 showed a 33% closure. Cells treated with inhibitor 44 had a 34% closure, and notably, the cells treated with inhibitor 255 resulting a 40% gap wound closure, indicating a greater increase in gap closure than untreated cells. Statistical analysis revealed no significant differences concerning all the inhibitors in the one-way ANOVA. At the 24-hour time point, untreated cells demonstrated approximately 70% gap closure. Cells treated with DNJ showed 75% closure, a bigger increase than untreated cells, while those treated with inhibitors 42 and 44 had closures of 5% and 6%, respectively. Although there was no statistically significant difference

among these inhibitors, cells treated with inhibitor 255 exhibited the least migration, with 70% in gap closure. This result also indicated no significant difference in the ANOVA (F(DFn, DFd) = 1.292 (4, 55), P =< 0.050, P value = 0.2891.

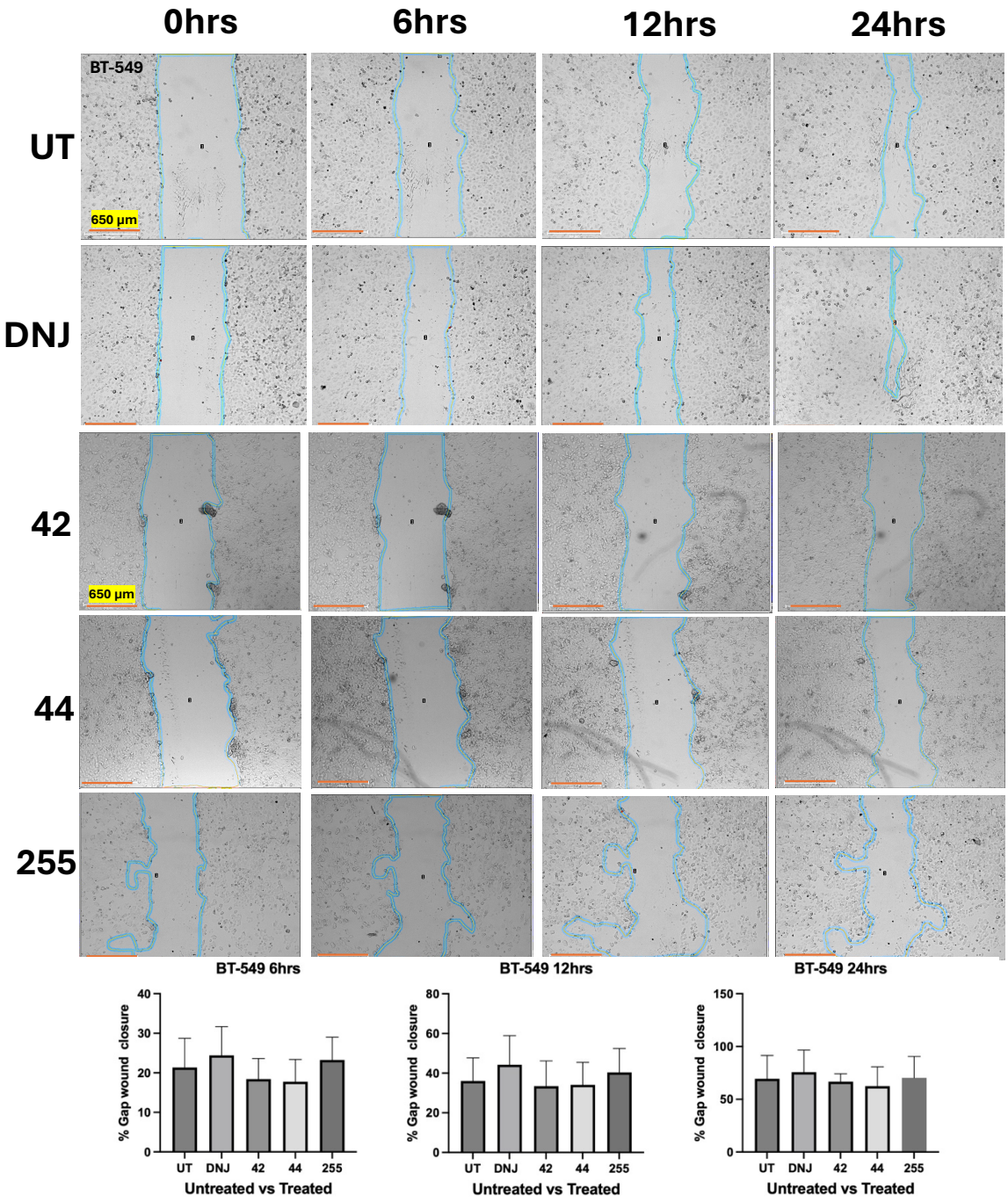

Figure 3.26. Time-course of wound healing in BT-549 TNBC cells treated with glycosidase inhibitors at 0.5 mM for 24 hours. The upper panel illustrates images of a BT-549 cell scratch assay treated with DNJ, 42, 44, and 255 inhibitor compounds at different time points, measured at 0, 6, 12, and 24 hours. Total magnification of X100, with a scale bar representing 650 µm. The lower panel shows the percentage gap wound closure at various time points of untreated vs treated cells with glycosidase inhibitors. The data are presented as mean values

± standard error, with a sample size of N = 12. A one-way ANOVA statistical analysis was performed to assess the significance of the results. No significant differences were shown.

Statistical analysis (Table 3.6) was performed to determine whether there was a significant difference in the treated BT-549 cells with the inhibitor compounds.

Table 3. 6. Scratch assay results from the One-way ANOVA test statistical analysis of BT-549 cells treated with glycosidase inhibitors.

ANOVA summary	6 hours	12 hours	24 hours
F	2.557	1.601	1.292
P value	0.0488	0.1872	0.2891
P value summary	*	ns	ns
Significant diff. among means (P < 0.05)?	Yes	No	No
R squared	0.1568	0.1043	0.08094

Images and statistical analysis of the wound healing assay were performed on MDA-MB-231 cells exposed to β-glycosidase inhibitors for 24 hours, as shown in the section below (Fig. 3.27). In the upper panel, the illustration depicts MDA-MB-231 cells treated with glycosidase inhibitors at 0, 6, 12, and 24 hours. All groups showed a gradual decrease in wound width within 24 hours. The untreated cells demonstrated greater wound closure than most treated cells, except for compound inhibitor 255, where the gap closure is wide. The lower panel includes histograms displaying the percentage of wound closure at 6, 12, and 24 hours, corresponding to the illustrations in the upper panel. After 6 hours of measuring the rate at which the scratch or wound area closes over time, the cells treated with DNJ and inhibitor 42 exhibited 30% gap closure, while the untreated cells had 35% gap closure. In contrast, the cells treated with compound inhibitors 44 and 255 had 10% and 0% gap closure, respectively, revealing a statistically significant difference compared to the untreated cells at 6 6-hour. One-way ANOVA data analysis showed significant difference; (F(DFn, DFd) = 8.769 (4, 55), P= < 0.050, P value = 0.001)

At the 12-hour mark, untreated cells exhibited a 40% gap in wound closure. Cells treated with DNJ demonstrated a 30% closure, while those treated with inhibitor 42 showed a 35% closure. Cells treated with inhibitor 44 had a 30% closure, and notably, the cells treated with inhibitor

255 experienced a decrease of -0.1% in wound closure, indicating a reduction in gap closure. Statistical analysis revealed significant differences for inhibitors 44 and 255. One-way ANOVA (F(DFn, DFd) = 13.89 (4, 55), P =< 0.050, P value = 0.0001).

At the 24-hour time point, untreated cells demonstrated approximately 70% gap closure. Cells treated with DNJ showed 62% closure, while those treated with inhibitors 42 and 44 had closures of 53% and 44%, respectively. However, there was no statistically significant difference among these inhibitors. However, cells treated with inhibitor 255 exhibited the least migration, with a -0.1% decrease rate in gap closure, indicating a significant difference in all three statistical tests: in one-way ANOVA F(DFn, DFd) = 9 (4, 55), P =< 0.050, P value = 0.0001).

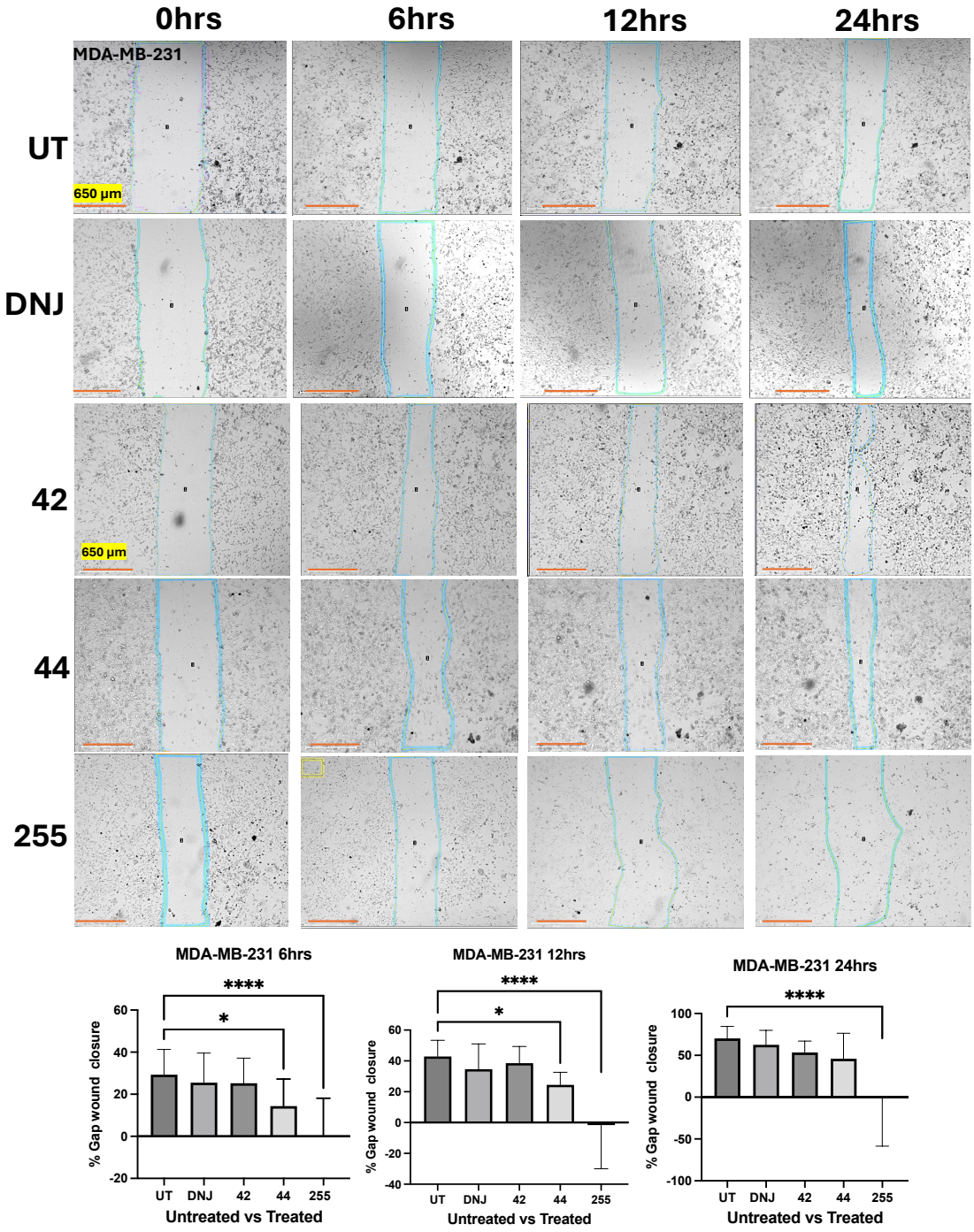

Figure 3.27. Time-course of wound healing in MDA-MB-231 TNBC cells treated with glycosidase inhibitors at 0.5 mM for 24 hours. The upper panel illustrates images of MDA-MB-231 cells in a scratch assay treated with DNJ, 42, 44, and 255 inhibitor compounds at different time points, measured at 0, 6, 12, and 24 hours. Total magnification of X100, with a scale bar representing 650 µm. The lower panel shows the percentage gap wound closure at various time points of untreated vs treated cells with glycosidase inhibitors. The data were presented as mean values ± standard error, with a sample size of N = 12. A one-way ANOVA statistical

analysis was performed to assess the significance of the results. A significant difference was shown on (255) ****p=< 0.050.

Statistical analysis (Table 3.7) was performed to determine whether there was a significant difference in the treated BT-549 cells with the inhibitor compounds.

Table 3. 7. Scratch assay results from One-way ANOVA statistical analysis of MDA-MB-231 cells treated with glycosidase inhibitors.

ANOVA summary	6 hours	12 hours	24 hours
F	8.769	13.89	9
P value	<0.0001	<0.0001	<0.0001
P value summary	****	****	****
Significant diff. among means (P < 0.05)?	Yes	Yes	Yes
R squared	0.3894	0.5025	0.3956

A statistical summary of breast cancer cells treated with glycosidase inhibitors for 24 hours showed that the time course of wound healing indicated reduced cell motility compared to untreated cells, as shown below (Fig. 3.28). The resulting variations in gap closure percentages were monitored at different time intervals, highlighting the varying effects of these treatments on cell migration. In the upper panel of the results, untreated MCF-7 and SKBR3 cells consistently demonstrated a high percentage of gap closure across all measured time points, indicating a robust rate of cell migration and movement, which is crucial for processes such as wound healing and metastasis. In stark contrast, the treated cells, subjected to glycosidase inhibitors DNJ, 42, 44, and 255, exhibited significantly reduced migratory capabilities. Among these inhibitors, DNJ proved to be the least effective, achieving the highest percentage of gap wound closure throughout the 24-hour treatment period. The other inhibitors, specifically 42 and 44, resulted in a more pronounced slowing of cell migration compared to untreated cells and those treated with DNJ. Inhibitor 255 showcased a unique pattern: in MCF-7 cells, there was an initial decline in gap closure during the first half of the treatment, showing reduced cellular activity. However, by the end of the 24 hours, the percentage of gap closure had reached approximately 3%. The state for SKBR3 cells treated with inhibitor 255 remained below 0%, indicating a complete halt in growth and cellular movement throughout the treatment. In the case of BT-549 cells, treatments with inhibitors

DNJ and 255 resulted in increased levels of gap wound closure, reaching approximately 71% and 76%, respectively, comparable to the untreated controls that exhibited about 70% closure. In contrast, inhibitors 42 and 44 underperformed, yielding approximately 60% closure, significantly less than the untreated benchmark.

Lastly, MDA-MB-231 untreated cells showed an approximate 70% gap closure, positioning them among the highest in cellular motility and migration. When treated with inhibitors, however, the cells' performance declined markedly. Specifically, DNJ and 42 reached only 50% and 40% gap closure, respectively, while compound 44 fell below 40%. Inhibitor 255 was particularly damaging to the cell, maintaining a gap closure percentage below 0% for the entire experiment, indicative of complete inactivity in growth and a significant reduction in cell migration.

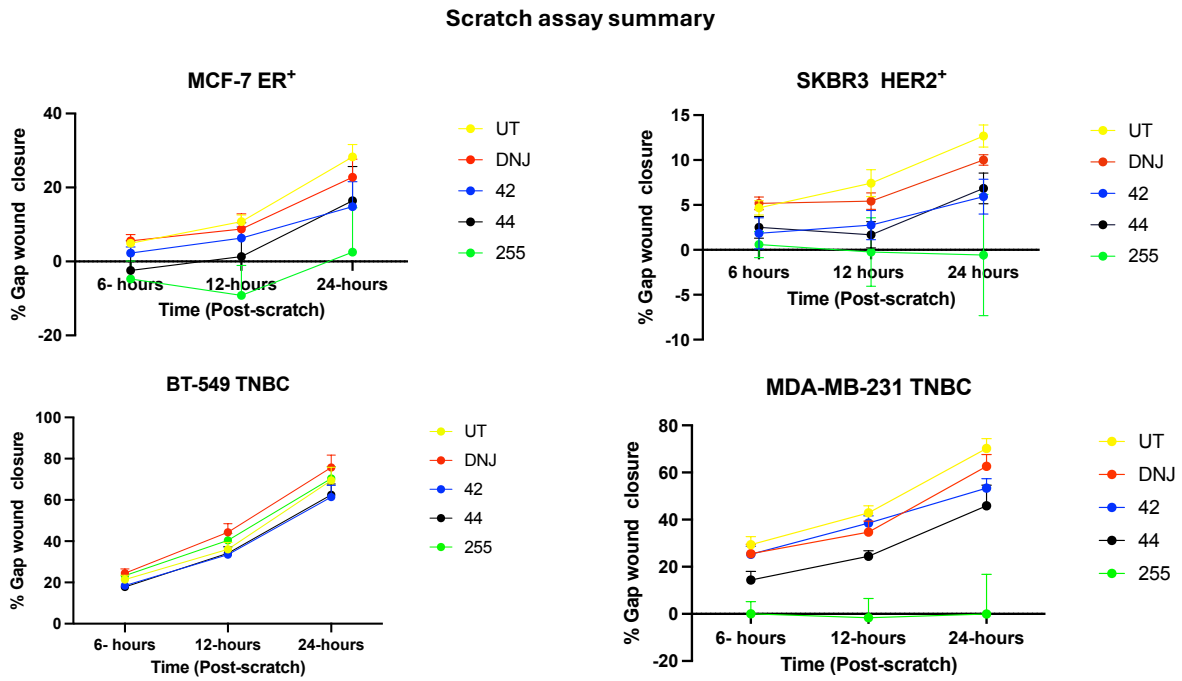

Figure 3.28. A summary of the glycosidase inhibition treatment at 0.5 mM for 24 hours showed the course of wound healing in the MCF-7, SKBR3 (upper panel), BT-549, and MDA-MB-231 (lower panel) breast cancer cell lines. The data were presented as mean values ± standard error, with a sample size of N = 12. A one-way ANOVA statistical analysis was performed to assess the significance of the results.

Overall, these results underscore the differential effects of glycosidase inhibitors on breast cancer cell lines, with significant implications for understanding how these compounds may influence tumour behaviour and response to treatment.

Gene expression analysis of the four breast cancer cells was carried out to evaluate the effect of glycosidase inhibitors and determine whether there was an upregulation or downregulation of apoptotic biomarkers *BCL2* and *CASP3*, as discussed (in section 3.5). Data analysis of MDA-MB-231 and BT-549 cells is presented in the appendix section, as these studies were conducted in preliminary investigations.

3.5. Expression analysis of *BCL2* and *CASP9* in MDA-MB-231

RNA extraction of replicate samples was prepared, followed by cDNA library preparation and real-time PCR analysis. The integrity and purity of the mRNA extracted from MDA-MB-231 were measured using the Nanodrop system. Apoptotic markers, *BCL2* and *CASP3*, were expressed using reverse transcriptase real-time polymerase chain reaction (RT qPCR) in MDA-MB-231 cells treated with glycosidase inhibitors for over 24 hours. MDA-MB-231 was selected for this study because of its aggressive nature as a TNBC cell line. It is particularly concerning due to the poor prognosis associated with this type of cancer. This cell line serves as an ideal model to test the effects of glycosidase inhibitors, especially since preliminary observations suggest that these inhibitors may reduce cell motility. Cells exposed to DNJ and compound inhibitors (255) for over 24 hours were analysed to assess the folding rate. Normalised gene expression of RNase II was used as an internal reference gene. Actual fold changes were calculated using the log2 formula to even out the scales of up-regulated and down-regulated values by dividing the treated value by the control value (untreated).

Histogram showing analysis on *BCL2* (Fig 3.29) gene expression on the left showed a significant difference between untreated and DNJ p value= 0.0045 (<0.05) and a 57-fold change resulting in upregulation. However, there was no significant difference between the untreated and compound 255; a slight upregulation of *BCL2* was observed. On the right histogram, the gene expression levels in *CASP3* showed a 3.4-fold change, with the treated compound 255 exhibiting downregulation at a 0.19-fold change compared to the untreated

sample. P-values show 0.4709 (<0.05), while DNJ showed upregulation; however, no statistically significant difference was observed between the two compound inhibitors. The analysis of relative gene expression data was generated by deploying Real-time quantitative PCR and the 2^-ΔΔCT method (Livak and Schmittgen, 2001).

.

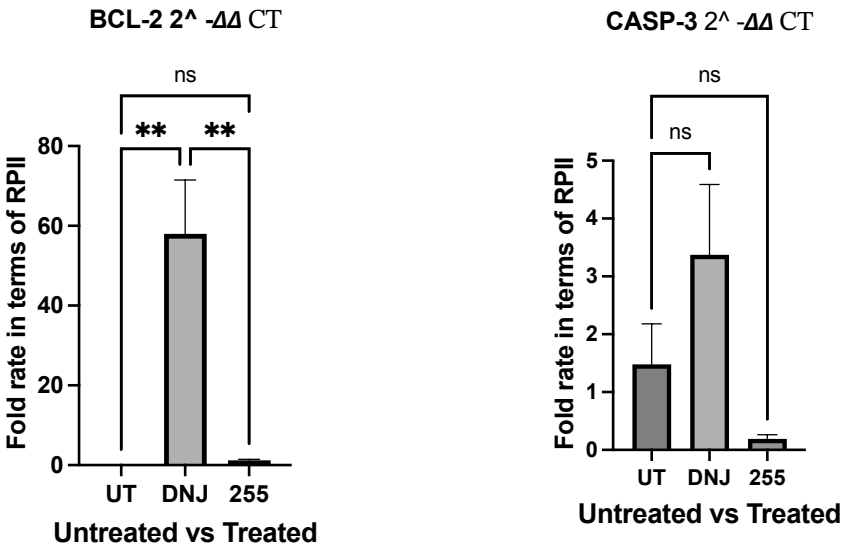

Figure 3.29. Quantifying *BCL-2* and *CASP-3* apoptotic markers in MDA-MB-231 Cells cultured in 2D was performed using RT-PCR. RPII expression was deployed as a normalised internal reference gene. The delta-delta cycle threshold (***ΔΔ*CT)** was calculated by deducting ***Δ***CT control from ***Δ***CT untreated, DNJ and compound 255 on glycosidase inhibition treatment over 24 hours. The gene expression of the apoptotic markers was analysed using the R2-ΔCT method, which relates to the fold change method. Statistical data were mean ± SD(n=6). A one-way ANOVA test analysis was conducted. A significant difference was shown on (DNJ) **p=< 0.050 (*BCL-2*). No significant difference was shown on compound inhibitor (255).

Gene expression statistical analysis of apoptotic markers is presented below, along with a One-Way ANOVA summary (Table 3.8).

Table 3. 8. One-way ANOVA statistical analysis of the level of gene expression of BCL2 and CASP3 fold-rate of MDA-MB-231 cells after glycosidase inhibition treatment over 24 hours.

ANOVA summary	***BCL2***	***CASP3***
F	18.19	3.887
P value	0.0028	0.0827
P value summary	**	ns
Significant diff. among means (P < 0.05)?	Yes	No
R squared	0.8584	0.5644
Are SDs significantly different (P < 0.05)?	No	No

3.6. Discussion

TNBC is a type of breast cancer lacking ER, PR and HER2 (Wolf *et al*., 2013) is characterised by its metastatic characteristics, in which the only available therapies are chemotherapy, radiotherapy and surgery, posing a health concern due to its poor prognosis and recurrence of cancer as a result of tumour resistance limiting the effectiveness of chemotherapy drugs like doxorubicin, commonly used for breast cancer treatment.

The underlying hypothesis tested in this first part of my study was that altering the glycocalyx in cancerous cells would facilitate greater chemotherapeutic penetration. This study aimed to evaluate the effects of glycosidase inhibition on breast cancer cells cultured in 2D. This was assessed by measuring cell viability and metabolic activity, as well as cell proliferation reduction, and observing changes in glycosylation and the ability of cells to migrate when exposed to the compound inhibitors. These factors may be indicators of a downregulation of the metastatic characteristics of a cancer cell.

The chemotherapeutic drug doxorubicin was previously used in combination with antibodies in other glycosylation studies conducted by the same research team to evaluate its effect on breast cancer cells and glycosidase inhibitors (Azimi *et al*., 2020). However, DNJ and novel compound inhibitors 255, 42, and 44 from the company Phytoquest were deployed to study

the effect and responsiveness of breast cancer cells grown *in vitro*, both alone and in combination with doxorubicin, which has been a novelty to discover the effects of the novel compound inhibitors, having a great impact for drug discovery and improving chemotherapy responsiveness. MDA-MB-231, MCF-7, SKBR3 and BT-549 breast cancer cell lines were studied as models for the different subtypes of breast cancer.

3.6.1. Exposure of breast cancer cells to doxorubicin

Doxorubicin alone did not result in a statistically significant difference on metabolic activity, although it had some effect on the cells. While doxorubicin may have some impact, it may not be sufficient to achieve substantial outcomes without the use of combinatorial therapies or higher dosages. While doxorubicin is highly effective for treating TNBC, its effectiveness can be compromised by the development of chemical resistance (Lian *et al*., 2023; Zeng *et al*., 2023). Particularly, doxorubicin alone often results in chemoresistance among breast cancer patients, particularly those with TNBC. However, the combined administration of doxorubicin and Doxil further improved therapeutic efficacy and reduced side effects on breast cancer (Ghahremanloo *et al*., 2025). In other studies, combining cannabidiol with high-dose doxorubicin in a mouse breast cancer model yielded a better antitumor effect and reduced doxorubicin's cardiotoxicity as the combination of this drug treatment could induce more apoptotic cells in breast tumors compared to doxorubicin or cannabidiol alone (Tabatabaei *et al*., 2024).

3.6.2. Synergistic effect of breast cancer cells

It was noted that glycosidase inhibition significantly sensitised breast cancer cells to doxorubicin. Both SKBR3 and MCF-7 cells demonstrated the most pronounced reduction in metabolic activity, with a 34% decrease compared to untreated cells at 1 mM when doxorubicin was administered in combination with DNJ and compound inhibitor 42. In contrast, MDA-MB-231 cells also exhibited a reduction in metabolic activity, with 23% when 255 was combined with doxorubicin at 0.5 mM and 25% at 1 mM, using the compound inhibitor 44 and doxorubicin. BT-549 cells, when subjected to 0.5 mM of doxorubicin combined with DNJ, showed a 32% reduction. Despite this outcome, no significant differences were observed when comparing doxorubicin as the control, which also had some reduction

in metabolic activity. However, when comparing this outcome with that of the untreated cells, a significant difference was observed.

Imino-sugars, as therapeutic agents, have significant potential for cancer glycobiology research, as these compounds inhibit the degradation of monosaccharide residues. All four cancer cells treated with glycosidase inhibitor compounds DNJ, 42, 44, and 255, combined with doxorubicin, showed some statistically significant reduction in metabolic activity, resulting in greater effects than when the cells were treated with doxorubicin alone.

The findings are consistent with those of previous studies (Azimi *et al*., 2020), which also reported the use of the Alamar Blue assay following exposure of MDA-MB-231 and SKBR3 cells to doxorubicin. In 2D monolayer cultures, MDA-MB231 cells exhibited a reduction in viability after treatment with doxorubicin. SKBR3 cells demonstrated a notable decrease in viability when subjected to concentrations of 0.5 μM doxorubicin or higher in 2D. Other similar studies have also implicated N-linked glycosidase inhibition in cellular glycosylation, which affects Herceptin binding and the sensitivity of breast cancer cells to doxorubicin and growth factors (Peiris *et al*., 2017).

The enhanced sensitivity to breast cancer cells observed when exposed to doxorubicin in combination with glycosidase inhibitors suggests a potential synergistic effect, possibly due to altered glycoprotein processing, which may impair cell survival pathways. This may be due to the possible inhibition of β-glucosidase, β-mannosidase, and β-fucosidase, which could alter the glycocalyx and facilitate better cellular penetration of doxorubicin. The disruption may be caused by the degradation of the glycocalyx's physical barrier by the effect inhibitors. By interfering with the synthesis and degradation of glycans in the cell, the dense meshwork of the glycocalyx can become degraded or thinned. This alteration allows doxorubicin to diffuse and penetrate the cell more effectively. This study lines similarly to other studies in which glycocalyx disruption reduced cancer invasiveness and increased nuclear damage in TNBC cells when exposed to TC and neuraminidase (Piplani *et al*., 2024). In terms of glycosylation pathways, early glycan processing is disrupted by glucosidase inhibition, which traps essential cell-surface structural proteins in a misfolded state in the ER (Oo *et al*., 2025). Without the branched scaffolds, structural hooks for terminal sialylation are absent. The capping stage fails, which removes the negative charge barrier (Bashian *et al*., 2026).

Additionally, inhibiting mannosidase prevents the removal of terminal mannose residues from newly formed N-linked glycans, which interrupts the glycoprotein folding process and leads to the accumulation of misfolded proteins (Avezov *et al*., 2008; Hosokawa et al., 2001). This accumulation activates the UPR and significant ER stress, which ultimately leads to a compromised and dysfunctional glycocalyx (Herbert *et al.*, 2005; Avezov *et al*., 2008).

These results indicated that the inhibitor compounds may have altered glycosylation pathways by blocking the degradation of oligosaccharide residues, such as glucose, mannose, fucose, or GlcNAc residues, leading to glycosidase inhibition in the ER and continuing through the Golgi apparatus, thereby altering the glycans on the cell surface and facilitating the more effective uptake of doxorubicin. Disruption of the glycocalyx may have occurred; however, the drug resistance and survival mechanisms of cancer cells could have mitigated the effect of these compounds, as the cancer cells were treated for a short time. This could be improved by developing 3D model systems and increasing doses and exposure over a longer period. Our findings are consistent with those of previous studies (Zhou *et al*., 2017), which also found that β-glucosidase inhibition sensitises breast cancer to chemotherapy. This increases the evidence of the potential involvement of β-glucosidase in cancer, which has been reported (Zhang *et al*., 2016), suggesting that the increased expression of β-glucosidase in hepatocellular carcinoma is associated with resistance to chemotherapy drugs (Milani *et al*., 2016). Other studies have previously examined this outcome (Baldini & Dwek, 2019).

3.6.3. Imino sugars alter cell metabolism

A significant reduction of metabolic activity was observed in most of the cells that were treated with glycosidase inhibitors, suggesting that there are changes and disruption of the glycosylation pathways, this could lead to glycoproteins not being properly folded and accumulating, causing ER stress and sending them to UPR if the adaptive mechanisms do not succeed in reestablishing protein-folding balance, the UPR signalling may remain active and eventually transition into different signalling pathways known as the terminal UPR leading to apoptosis (Shore *et al*., 2011).

The findings that natural and synthetic iminosugars affect cellular energy dynamics open up possibilities for their use in various applications, such as cancer therapy (Montebugnoli *et al.,*

2025). When breast cancer cells were exposed to these novel compounds from the Phytoquest company, the cells showed a reduction in metabolic activity. This study aligns with similar results investigating the impact of DNJ on colon cancer cells, finding that the compound disrupted energy metabolism and reduced cell viability (Montebugnoli *et al*., 2025), It also showed that these natural compounds can influence tumour bioenergetics, making DNJ a promising candidate as an adjunct therapy for colon cancer. Cell proliferation and growth are the most common factors in cancer development. Therefore, the effect of glycosidase inhibition on cancer cell metabolism, as a surrogate marker for cell proliferation, was significant. Targeting specific regions of the glycocalyx could block the degradation of cell-surface residues, potentially enhancing the effects of immunotherapies. Further details are described (page 46) in which studies were carried out in 2D and 3D.

3.6.4. Cellular growth decrease through exposure to a glycosidase inhibitor

The cells treated with glycosidase inhibitors resulted in a decrease in cell numbers. This was noted through the DAPI-stained assay, which served as a surrogate for nuclear count in terms of growth profile; however, it is currently unclear whether the fewer cells observed were due to cells undergoing apoptosis or whether the cells were lifting off the culture dish due to a change in glycosylation. This study also found that DAPI staining and Alamar blue correlated well with the metabolic activity of the treated cells. It also showed that the decreased number of cells correlates with all the analyses deployed and follows what has already been reported (Baldini & Dwek, 2019). It was found that SKBR3 cells exhibited a significant difference in cell number reduction with DNJ and the compound inhibitor 255. In contrast, in MDA-MB-231 cells, DNJ had the most important effect on reducing cell number.

3.6.5. Increase in lectin labelling as a result of glycosidase inhibition.

The lectin staining assay revealed that treatment with glycosidase inhibitors led to an increase in lectin labelling and a change in the glycosylation of all four breast cancer cell lines. Con A, UEA, and WGA were deployed to evaluate cells after exposure to the inhibitors, potentially

reflecting different glycosidase inhibitions occurring in the ER, Golgi apparatus, and alterations in the glycocalyx. Binding characteristics were summarised to assess the lectin recognition of the target glycans. For instance, Con A recognises α-D-glucosyl and α-D-mannosyl residues of glycoproteins and activated lymphocytes (Tiegs *et al.*, 1992). It was found that Con A binding was increased following exposure to glycosidase inhibitors, as evidenced by DNJ, 42, 44, and 255, which resulted in an increase in fluorescence intensity after treatment with all four cell lines. This means that it is likely that mannose, fucose, and GlcNAc residues accumulate. However, only SKBR3 and BT-549 showed statistically significant differences in Con A binding, with DNJ inhibiting mannosidase in SKBR3 cells and compounds 42, 44, and 255 in BT-549 cells, respectively. In the N-glycosylation pathways, the inhibition of mannosidase I and II, as well as glucosidase I and II, leads to the accumulation of high-mannose and hybrid N-glycans. Since the early trimming of glycans is blocked, the high-mannose chains remain exposed and not cleaved. This results in a significant increase in Con A binding (Kurhade *et al*., 2021).

UEA binding to fucose residues showed increased fluorescence, indicating fucose residues were accumulating according to the CTCF analysis. However, all four cell lines showed no significant difference. UEA binds selectively to terminal α-linked fucose residues 1,2 α-fucose modifications. Fucosylation occurs as a final modification carried out by fructosyltransferases within the Golgi apparatus, but it depends on a fully developed, trimmed complex glycan acceptor backbone. When early/intermediate glycosidases are inhibited, the pathway is blocked and the addition of fucose, is suppressed. A reduction or complete loss of UEA labelling would be observed (Yonezawa *et al*., 1982).

WGA binds GlcNAc and sialic acid in N-linked residues. It has also been reported that WGA-binding GlcNAc residues are associated with sialic-containing glycoconjugates and oligosaccharides (Ryva *et al*., 2019). Glucosidase inhibitors modify glycan processing, leading to decreased WGA binding on cell membranes. This is because WGA specifically targets terminal sialic acid and mature complex GlcNAc oligomers on the cell surface, inhibiting early trimming and thus reducing WGA binding (Spearman *et al*., 1987). The results suggested evidence of glycosidase inhibition in all four cell lines. Given the NLG biosynthetic pathway,

this aligns with the expected glycosidase inhibition of mannosidase and fucosidase. Impaired glycosylation frequently leads to issues with protein maturation and improper protein folding, triggering the unfolded protein response (UPR) within the ER (Amen *et al*., 2019; Wang *et al*., 2018). ER stress caused by UPR can trigger adaptive survival responses (Bhattarai *et al*., 2021) or cell death (Ricciardi & Gnudi, 2020). While some approaches rely on metrics like total integrated fluorescence or staining intensity, measuring the percentage of cells labelling positive offers distinct advantages, though it comes with its own limitations

Quantifying lectin labelling using the CTCF method had some limitations as weakly labelled cells can get lost in background noise, and measuring, For instance, the proportion of cells that show positive labelling has certain benefits, but it also has its drawbacks, as it is affected by gating thresholds and is sensitive to cells with weak labelling.

3.6.6. Glycosidase inhibition affects cell motility

It was found that all cell lines treated with glycosidase inhibitors were affected in their cell motility. However, treatment with inhibitor 255, which showed significant differences in SKBR3 and MDA-MB-231 cell lines, resulted in the most significant reduction in cell migration and invasion. The findings revealed that glycosidase inhibitors may play a crucial role in slowing the progression of metastasis. To determine their effect on migratory behaviour, all cells treated with glycosidase inhibitors were evaluated. This study showed that glycosidase inhibitors influence cell behaviour; they may do this by altering the glycoprotein composition on the glycocalyx, which can alter cell motility. Our findings are consistent with other studies by Ono and Hakomori (2003), indicating that glycosylation inhibits the motility and invasiveness of tumour cells generally supported by the inhibitory influence of GM3 on multiple human tumour cell lines, in addition to the LDLD cell line, which exhibits elevated levels of CD9 and integrin α3 expression, where CD9 and α3 create a stable complex in the presence of GM3. Thus, glucosidase inhibition can affect and reduce the levels of ganglioside GM3 (Dodge *et al*., 2022). Other studies indicate that high glucose levels in breast cancer cells lead to an increase in cell stiffness and contractility, which is associated with enhanced cell motility (Oh *et al*., 2023). This indicates that breast cancer cells treated with glycosidase inhibitors may significantly reduce cell motility and slow down metastasis.

3.6.7. Gene expression analysis

The gene expression analysis revealed a significant difference in the upregulation of *BCL2* and *CASP3* apoptotic markers in DNJ-treated cells, indicating that all MDA-MB-231 and BT-549 cells treated with this glucosidase inhibitor may have triggered the UPR and apoptosis.

Increased *BCL2* levels suggested that the cells became more resistant to apoptosis. This could potentially undermine the effectiveness of treatments as cancer cells could survive longer and resist drug-induced cell death (Qian *et al.*, 2022). Upregulation of *BCL2* may indicate a compensatory mechanism where the cells attempt to respond to the effects of glycosidase inhibition. This could be due to *BCL*-2 facilitating cell survival by disrupting the function of Bax/Bak proteins via the mitochondrial pathway (Du *et al*., 2017). These findings align with other studies, which indicate that overexpression of *BCL*-2 in 3T3 and C3H cell lines can increase G0 quiescence and delay entry into the S phase by stabilising *p27* (Greider *et al*., 2002).

In summary, the upregulation of *BCL2 may* serve as a protective response to the potential stress caused by glycosidase inhibition. However, this protective mechanism can be interchanged with decreased metabolic activity and slowed cell cycle progression, emphasising the intricate balance between survival strategies and metabolic stresses in cancer cells. An increase in *CASP3* levels typically correlated with an enhanced apoptotic response (Mcllwain *et al*., 2013). This suggests that the cells were primed for apoptosis, a process that could be beneficial in cancer treatment. Upregulation of *CASP3* might indicate that, despite the protective role of *BCL2*, the cells are still being driven towards apoptosis, possibly due to overwhelming pro-apoptotic signals from other pathways activated by glycosidase inhibition. The simultaneous upregulation of *BCL2* and *CASP3* might seem contradictory, but it reflects the complex regulatory networks within cancer cells. While *BCL2* attempts to inhibit apoptosis, the increase in *CASP3* suggests a strong apoptotic drive that could overcome *BCL2*'s protective effects under certain conditions.

The other compound inhibitor, 255, tested in MDA-MB-231 cells, showed a slight upregulation of *BCL2* and downregulation of *CASP3, a* marker of apoptosis. In contrast, BT-549 showed an upregulation of *CASP3* when DNJ, 255, and 44 were tested (only in preliminary studies), with no significant difference observed.

The downregulation of *CASP3* might seem inefficient because *CASP3* is typically associated with promoting apoptosis. However, this could indicate a complex regulatory mechanism in which the initial stages of apoptosis are controlled, or that alternative pathways compensate for *CASP3*'s reduced activity. It could also reflect a feedback mechanism where the cell adjusts caspase levels in response to changes in other apoptotic signals.

Glycosidase inhibition may be expected to affect various cellular processes, including cell adhesion and immune recognition. This is because cells typically attach to substrates through cell surface receptors that associate with proteins absorbed from the serum or secreted by cells themselves onto the surface of the substrate (Fung & Zaltsman, 1997). Other changes in glycosylation may occur due to cell adhesion to the plastic surface of the culture dish, as this could alter cell surface receptor glycosylation. In turn, other therapies that are used could be affected by this. For cell attachment, the plastic vessel used for growing cells in 2D, specifically hydrophobic polystyrene, must be modified to a more hydrophilic surface. This modification enables the attachment of vitronectin and fibronectin, which are present in the serum-containing medium, allowing the cells to spread and adhere to a more suitable surface (Brown *et al.*, 2021). Thus, cell adhesion could also alter glycosylation changes that occur when cells grow in plastic, which may lead to cell detachment.

The findings from this research underscore the potential of glycosidase inhibitors as a novel approach to enhance the efficacy of doxorubicin in treating breast cancer. The observed sensitisation of breast cancer cells to doxorubicin through the inhibition of glycosidases suggests a promising therapeutic strategy that could lead to improved treatment outcomes for patients. By altering glycoprotein processing and potentially disrupting cell survival pathways, glycosidase inhibitors may provide a valuable adjunct to standard chemotherapy.

The novelty of this study lies in its exploration of the specific mechanisms by which glycosidase inhibition impacts cancer cell metabolism, growth, and cell motility. While previous studies have indicated a connection between glycosylation and drug sensitivity, the current research expands upon this by demonstrating how glycosidase inhibitors can significantly reduce the metabolic activity of various breast cancer cell lines. This highlights

the importance of glycosylation pathways in cancer biology and offers a fresh perspective on how targeting these pathways can enhance the effectiveness of existing chemotherapeutics.

3.7. Summary

In conclusion, the investigation into the effects of doxorubicin in conjunction with glycosidase inhibitors on breast cancer cell lines reveals significant implications for the potential future treatment of TNBC cells. The enhanced sensitivity of TNBC cells to doxorubicin, attributed to alterations in glycoprotein processing and subsequent changes in glycosylation patterns, underscores the potential of targeting the glycocalyx as a therapeutic strategy. Additionally, cells treated with glycosidase inhibitors showed a reduction in cell motility, potentially slowing down the metastasis process. These findings not only contribute to a deeper understanding of the molecular mechanisms underlying TNBC but also pave the way for studies focused on investigating novel treatment approaches aimed at improving patient outcomes in this challenging subtype of breast cancer. This chapter will be further discussed in Chapter 6.

3. 8. Summary of findings and novelty

- Breast cancer cells showed significant effects when treated with glycosidase inhibitors, which inhibited mannosidase and glucosidase, thereby altering N-linked glycosylation pathways.
- Disruption of the glycocalyx in breast cancer cells allowed better chemotherapeutic uptake.
- Glycosidase inhibitors significantly reduced metabolic activity in treated cells.

- Glycosidase inhibitors reduced cell numbers in breast cancer cells.
- Glycosidase inhibitors significantly affected cell motility.
- Novel Aspects of This Chapter: Highlights the potential for glycosidase inhibitors to sensitise breast cancer cells to chemotherapy.

  Iminosugars can alter metabolic pathways, presenting new avenues for cancer treatment.
- Impact on how glycosylation modifications can affect cancer cell proliferation and survival, potentially opening new research topics.
- Glycosidase inhibition impacts cancer cell metabolism, growth, and cell motility.

Chapter 4

Glycosidase inhibition on 3D breast cancer tumoroid culture models

The hypothesis proposes that glycosidase inhibition will impact cell motility, reduce cell numbers, and affect the metabolic activity of breast cancer cells grown in 3D.

4. Introduction

The research question for this chapter: Does the inhibition of NLG trimming differentially suppress breast cancer cell proliferation, migration, and invasion on 3D tumoroid models? Does this glycosidase inhibition reduce metabolic activity on 3D tumoroid? The hypothesis proposes that glycosidase inhibition will impact cell motility, reduce cell numbers, and affect the metabolic activity of breast cancer cells grown in 3D. The aims of this study intended to evaluate the effect on cell behaviour of inhibiting enzymes responsible for NLG trimming using breast cancer cells grown in 3D. The objectives were to assess the impact of glycosidase inhibition on cancer cell proliferation, migration and invasion in 3D.

This chapter examined the impact of glycosidase inhibition on cell migration, specifically in terms of reducing metastatic traits and slowing the movement of breast cancer cells grown in 3D culture models.

In summary, section 4.1 and 4.2 show the optimisation studies of MCF-7 and MDA-MB-231 tumoroids and their metabolic activity over 11 days. The measurement of tumoroid invasive front analysis (Section 4.3) and cell migration (Section 4.4) was developed in this study to show the effect of glycosidase inhibitors DNJ, compound inhibitors 42, 44, and 255 on tumoroids. Particle analysis (Section 4.5) was also deployed to demonstrate the effect of glycosidase inhibitors.

In the workflow schematic depicted in (Fig. 4.1), various methodologies were outlined to facilitate comprehensive assessments of cell movement, migration, and particle analysis assays on the MDA-MB-231 and MCF-7 tumoroids. Upon completing the optimisation phase for both tumoroid types, we conducted detailed data analysis complemented by fluorescence and brightfield microscopy. These imaging techniques were instrumental in elucidating the growth profiles and behaviours of the cells.

Furthermore, a novel absorber technology was developed to create high-density collagen constructs, serving as critical scaffolds for tissue culture protocols, particularly in the context of the RAFT™ 3D model systems developed by Lonza. The process began with seeding an artificial cell mass (ACM) with 20,000 cells of MDA-MB-231 or MCF-7 in rat tail collagen type I. The tumoroids were subsequently assembled using an innovative "sandwich procedure," a technique pioneered at University College London (Pape *et al*., 2019), which enabled the

precise layering and structuring of the tumoroids. I collaborated with Professor Marilena Loizidou and actively participated in the Tumoroid Research Group at University College London, where I learned how to fabricate tumoroids. The work was carried out independently by me, from the fabrication of tumoroids and glycosidase inhibition treatment to metabolic activity (Alamar Blue assay), measurements, and statistical analysis. I was only supported by Professor Loizidou in sharing only how to fabricate the tumoroids and histology workshops of how the tumoroids were embedded in cassettes, when I then went to monthly meetings to update how my work was going by giving a summary and short presentations to the tumoroids group.

Also, information was shared on how the analysis workflow was developed based on the image capture of DAPI-stained tumoroids with the Evos microscope, shown in (Fig. 4 .6 and 4.7). Traditionally, researchers utilising 3D culture systems, such as tumoroids, have employed a time-consuming clock technique, which captures images from only a small fraction of the tumoroid. However, at the University of Westminster, this approach was developed using an automated setting on the EVOS fluorescent microscopy. This method enabled capturing 176 images from various regions of the tumoroid at X100 magnification, resulting in high-resolution visualisations of all the tumoroids in both brightfield and DAPI fluorescence.

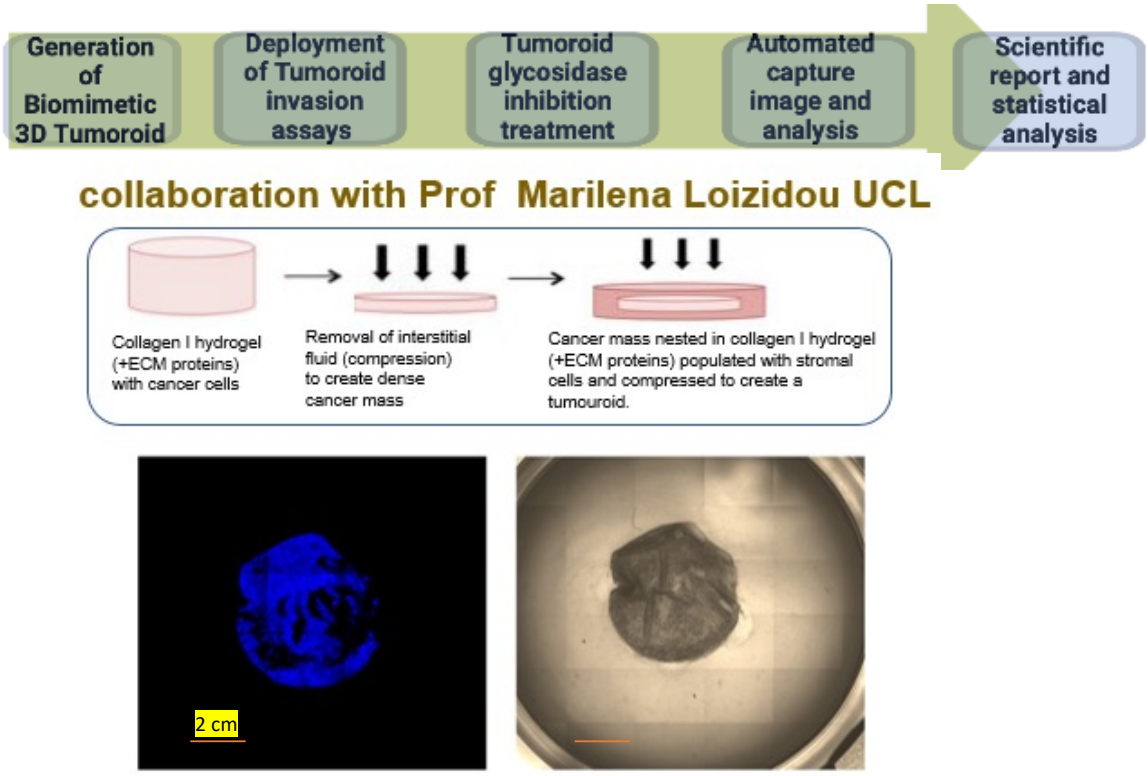

Figure 4.1. Schematic representation of A 3D RAFT^{TM} system fabrication of tumoroids with breast cancer cells exposed to inhibitors at 0.5mM, a collaboration with prof Marilena Loizidou, University College London. Below, a 24-well plate tumoroid can be observed through bright-field images, stained with DAPI using EVOS fluorescence at a 100x magnification with a bar scale representing 2 cm. With 2 × 10^4 cells seeded per 96-well plate. 176 images were completely stitched together using automated settings to have a view of the whole tumoroid and were established at the University of Westminster.

4.1. Tumoroid optimisation studies

In this study, a sophisticated biomimetic system was developed and designed to accurately reflect the complex behaviours of breast cancer. This 3D breast cancer model incorporated MDA-MB-231 and MCF-7 tumoroids, both types of breast cancer cell lines, and featured a central cancer mass surrounded by a non-cellular compartment. This design aimed to create a more realistic representation of tumour behaviour *in vivo*.

The primary objective of this research was to evaluate the invasive characteristics of cancer cells when subjected to various glycosidase inhibitors. To ensure the reliability and reproducibility of the results, a comprehensive 11-day optimisation protocol was implemented, specifically tailored to enhance the growth and structural integrity of the MDA-MB-231 and MCF-7 tumoroids before treatment with glycosidase inhibitor compounds. This phase involved careful optimisation of multiple parameters, including cell density, collagen matrix composition, and culture conditions, to establish optimal conditions for the tumoroids.

The subsequent phase of this study involved selecting between the MCF-7 and MDA-MB-231 tumoroids based on their aggressive and metastatic characteristics to be exposed to glycosidase inhibitors (DNJ, 42, 44, and 255) over 11 days, with a concentration of 0.5 mM for each treatment. For each glycosidase inhibition treatment, we utilised three tumoroids, ensuring that technical triplicates were obtained to enhance the robustness and validity of our findings. This structured approach allowed to gather substantial data on how glycosidase

inhibitors influence the invasive properties of these breast cancer cell lines, contributing valuable insights into potential therapeutic strategies.

Brightfield images of the MCF-7 (left) and MDA-MB-231(right) tumoroids growth profile over 11 days can be observed in (Fig. 4.2).

MDA-MB-231 tumoroid showed more cell density and invasion in the surrounding non-cellular compartments than MCF-7 tumoroid. Clusters of cells grew and migrated from the ACM into the stromal compartment, forming detached, invasive bodies.

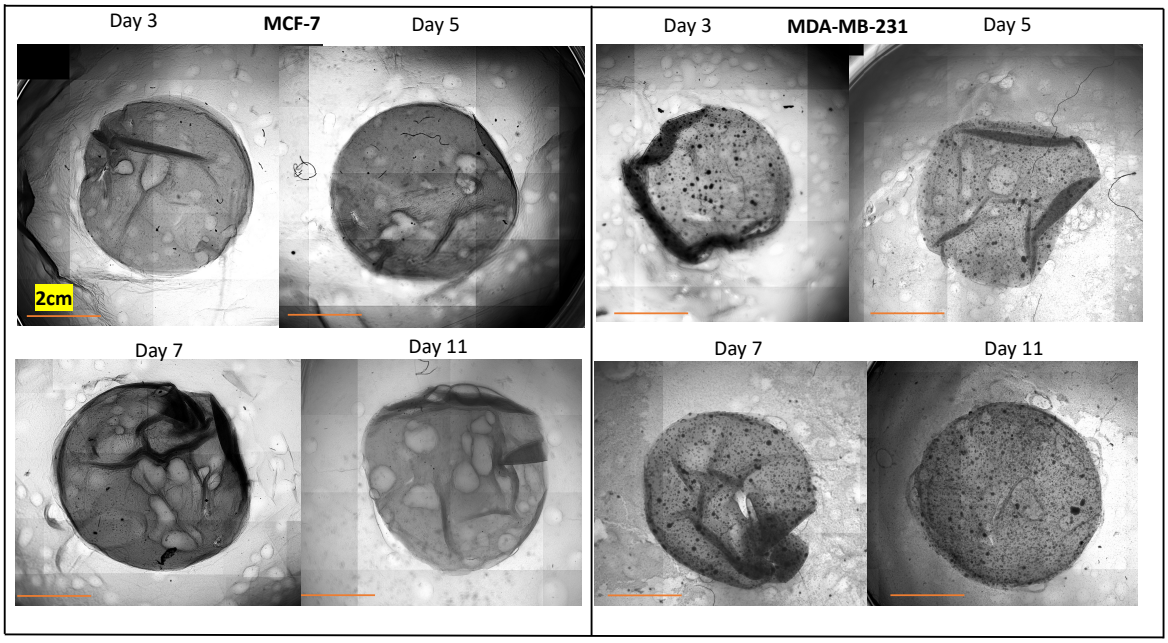

Figure 4.2. A total magnification of 100X with a scale bar representing 2 cm of brightfield images of MCF-7 cells (left panel) and MDA-231 tumoroids (right panel) were captured over 11 days, with the cells fixed accordingly.

Fluorescent-stained tumoroids with DAPI are shown below (Fig. 4.3). MFC-7 (left) and MDA-MB-231 tumoroids' growth profile of 11 days can be observed. The observed growth profile of the MDA-MB-231 tumoroids showed distinct changes over 10 days. By day 3, initial clumps of cells had formed, indicating the early stages of tumoroid development. By day 5, an increase in cellular density was noted, along with the emergence of cellular protrusions at the edges of the tumoroid, suggesting active growth and possible invasive behaviour. On day 7, larger clumps of cells within the central ACM were evident, signifying a robust increase in cell

proliferation and invasion into the ECM. By day 10, the tumoroids exhibited significant protrusions and invasive bodies, indicating a considerable depletion of the ECM due to extensive cell outgrowth.

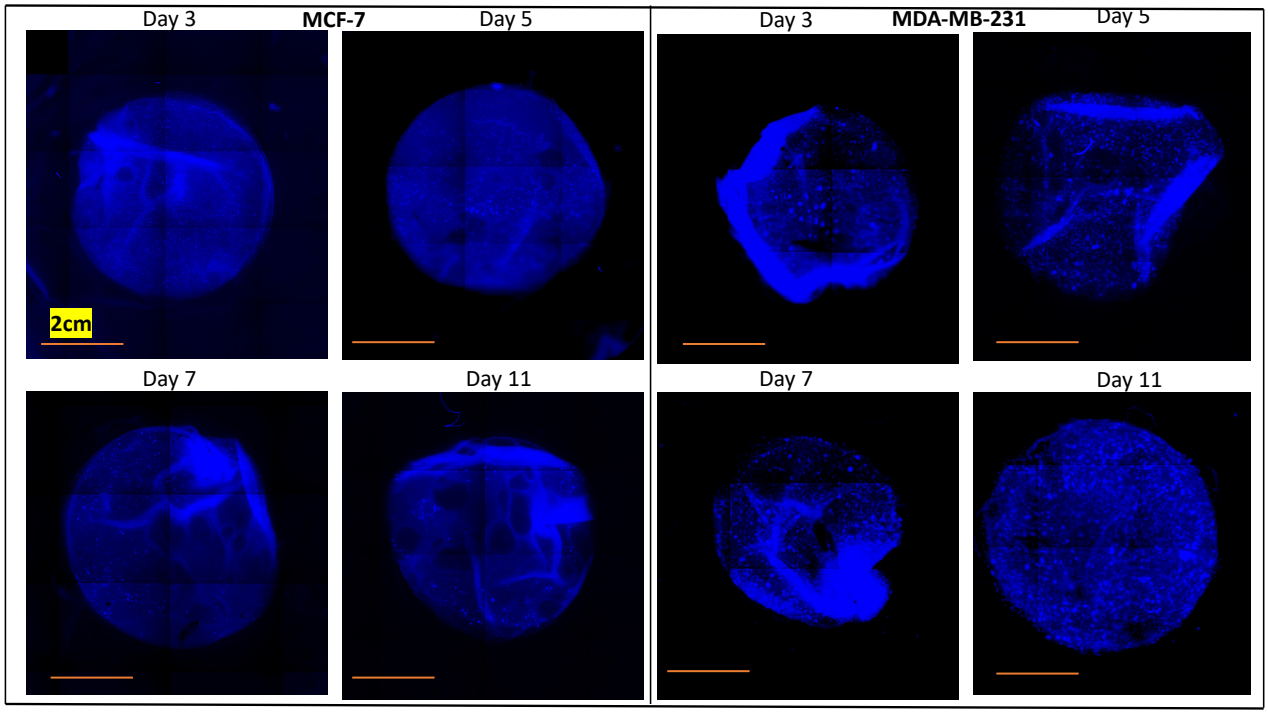

Figure 4.3. MCF-7 is shown in the left panel, while MDA-MB-231 tumoroids are depicted in the right panel Total magnification of X100, with a scale bar representing 2 cm DAPI-stained images in a 24-well plate, following an eleven-day incubation, the results from 176 multiple captures using Evos microscopy illustrate that an ACM (middle mass) nucleic stain indicates increased cell density at day 11, which is surrounded by a non-cellular compartment (Dark background): growth optimisation profiles for days 3, 5, 3,5,7, and 11.

This study aimed to evaluate the effect of glycosidase inhibition in the glycocalyx of breast cancer tumoroids to determine the impact of inhibition compounds. Growth profiles of the MDA-MB-231 and MCF-7 tumoroids were monitored, and samples were fixed at days 3, 5, 7, and 11 to assess changes in cellular density and invasive behaviour. This allowed for the determination of both the rate of invasive bodies and the extent of cell migration beyond the ACM into the surrounding non-cellular compartment.

Both tumoroids were evaluated for 11 days by deploying the Alamar Blue assay to determine their cell viability, shown below (Section 4.2)

4.2. Tumoroid metabolic activity

The Alamar Blue assay was deployed as described in (Section 2.1.6) to measure the metabolic activity of MCF-7 and MDA-MB-231 tumoroids, which were assessed to establish the optimal conditions to be exposed to inhibitor compounds.

The MDA-MB-231 tumoroids' growth profile showed, over 11 days, that their more aggressive characteristics were more suitable than those of MCF-7 tumoroids, despite a decrease in the first 7 days. However, by day 11, the metabolic activity increased is shown below in (Fig. 4.4) This led to the decision to treat MDA-MB-231 tumoroids with glycosidase inhibitors DNJ, 255, 42, and 5 after day 11 for fixation and DAPI analysis.

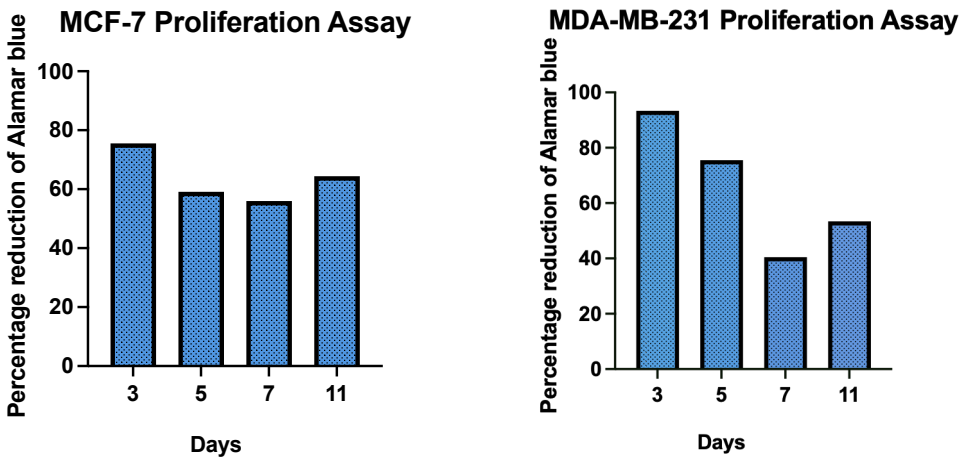

Figure 4.4. Alamar blue assay histogram of MCF-7 and MDA-MB-231 tumoroids cell viability measurements at days 3,5,7, and 11. Both showed an increase in cell proliferation at day 3. On days 5 and 7, cell viability decreased and increased on day 11. One tumoroid was deployed for each day with a total of 4 tumoroids for each cell line.

The optimisation of tumoroids involved a comprehensive analysis of the invading and growth profiles of MCF-7 and MDA-MB-231 tumoroids, which represent different subtypes of breast cancer, with MDA-MB-231 typically associated with a more aggressive phenotype. (Fig. 4.5) shows that by day 11, the cell density of MDA-MB-231 tumoroids significantly surpassed that of MCF-7 tumoroids. This distinct difference in growth patterns highlights the enhanced proliferative capacity and invasiveness of MDA-MB-231 cells compared to the more indolent MCF-7 subtype, emphasising the importance of cellular characteristics in tumour development and progression.

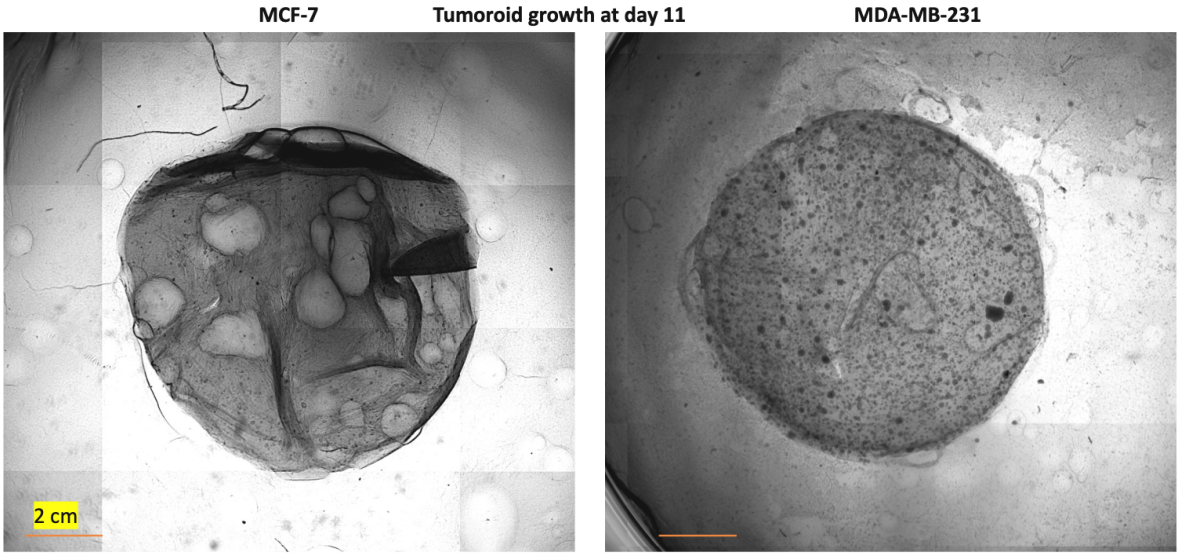

Figure 4.5. MCF-7 and MDA-MB-231 tumoroids were captured at with total magnification of X100, and a scale bar representing 2 cm brightfield images in a 24-well plate after a ten-day incubation, resulting from 176 multiple captures using Evos microscopy. This showed an ACM (middle mass) and a non-cellular compartment (external surrounding areas) on days 3, 5, 7, and 11, representing the growth optimisation profile.

The tumoroid front analysis was deployed to measure cell outgrowth into the acellular compartment, as shown below (Section 4.3).

4.3. 3D Tumoroid invasive front analysis

MC7 and MDA-MB-231 tumoroids were deployed as described in (Section 2.1.4) to measure invasive front as described in (Section 2.1.10). This investigation focused on enhancing the

understanding of cell behaviour within tumour microenvironments by integrating imaging analysis of DAPI nuclear staining and brightfield imaging techniques. The study specifically examined the growth and migration patterns of a clustered population of cells originating from the ACM. It was observed that these cells could penetrate and infiltrate the non-cellular compartments of MDA-MB-231 and MCF-7 tumoroids. This remarkable migratory capacity the formation of invasive, detached bodies, which raised essential implications for understanding tumour invasion and metastasis. Dual imaging methods provided a comprehensive view of these cellular dynamics, offering insights into the complex interactions between the tumour cells and their surrounding environment.

The diagrams from the top panel illustrate a cell invasion and migration assay used in cancer research to measure how breast cancer cells spread outward over an 11-day period (Fig.4.6). Left (Blue Image): Fluorescent staining (likely DAPI) highlighting the cell nuclei within the main cell cluster. Middle (Brightfield Image): Shows the physical mass of cells set into binary processing and converted into mask using ImageJ. The arrow points to Cell outgrowth, where individual cells are breaking away and migrating outward from the main centre (Cancer cell mass).Right (Traced Image): Demonstrates how the data is quantified. The software draws a yellow circle around the outer boundary (Measurement outgrowth area) to calculate the total surface area covered by the invading cells.

MCF-7 outgrowth showed a histogram in log2 (shown in Fig. 4.6) to quantify exponential growth rates, as very little growth occurred. Cells vary significantly in size. Taking the logarithm normalized this data, preventing a few large cells from skewing the results. A decrease was displayed after day 3. For days 5 and 7, there was no outgrowth or protrusions of cells into the non-cellular compartments. On day 11, there was a further decrease. The analysis revealed that as the histogram bar increased in height, the invaded area reduced its surface. A one-way ANOVA showed a significant difference, yielding a P-value of 0.0232 and an R-squared value of 0.6765. $F(3,8) = 5.578$, indicating the variance in the dependent variable that can be predicted by the growth model. This means that the growth profile model had a moderate to strong fit, which explains 67.65% of the variance in growth data for the MCF-7 tumoroids. In contrast, the histogram for MDA-MB-231 tumoroids was used to displayed an increase in area/µm after day three, continuing to grow exponentially until day 7. However,

by day 11, there was a decline in area, indicating a reduction in metabolic activity. Statistical analysis shows a P value (<0.0001), which is significantly different (P=< 0.05), and an R-squared of 0.9976 indicated an exceptionally strong, near perfect fit that was highly statistically significant as the model explains 99.76% of the variance in the growth data.

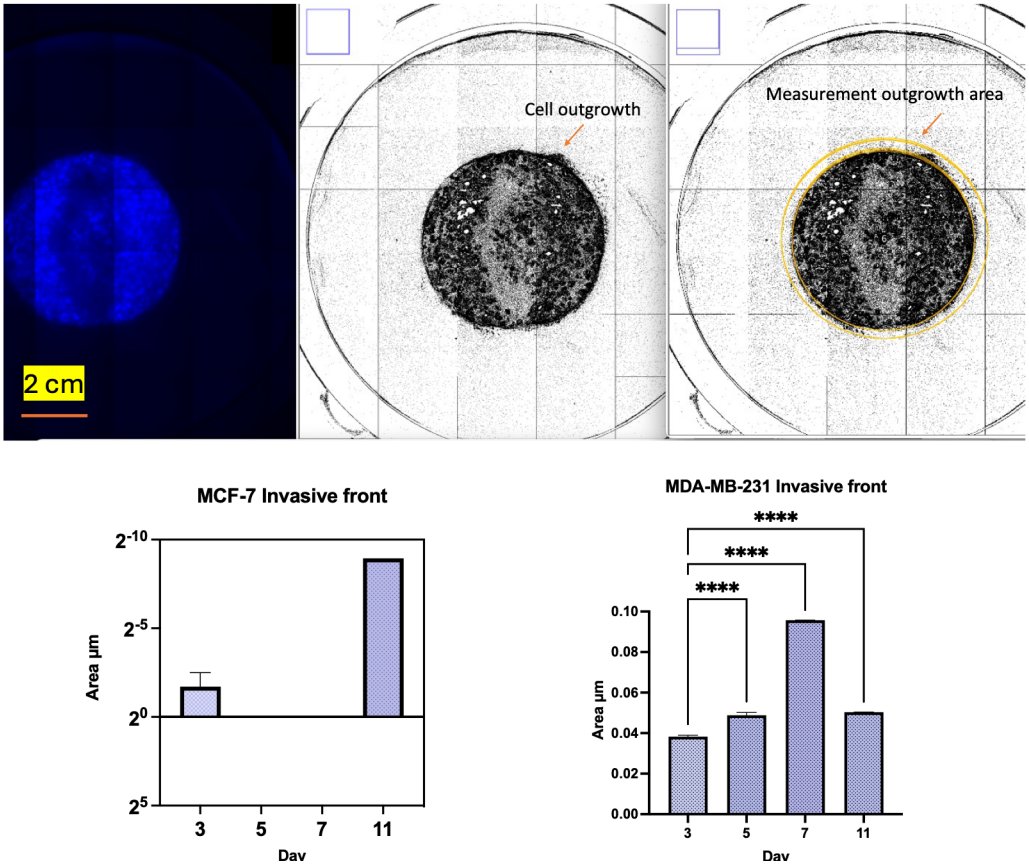

Figure 4. 6. In the upper panel, three images of the same tumoroids are displayed. The image on the left is stained with DAPI, while the middle image has undergone binary processing and converted into a mask. The DAPI image was captured at a total magnification of 100X, with a scale bar representing 2 cm. The image on the right illustrates the measurements taken from a yellow circle encircling the central cancer cell mass. The analysis results reveal the invasive front measurements of the cell protrusions that extend from the original ACM into the surrounding non-cellular collagen compartments. Lower panel: MDA-MB-231 tumoroids had a more significant overall outgrowth from the original ACM than MCF-7 tumoroids. One tumoroid for each day was produced with a total of 4 for each cell line. No significant differences were shown on MCF-7 tumoroid but in MDA-MB-231 tumoroids ****p=< 0.05.

Cell motility measurement was performed to evaluate cell movement, as shown below (in Section 4.7).

4.4. Cell motility measurement

MC7 and MDA-MB-231 tumoroid were deployed as described in (Section 2.1.4) to evaluate cell movement of invasive bodies was by measuring the number of clumps of cells as described in (Section 2.1.10) that invaded the non-cellular compartments shown below (Fig. 4.7)

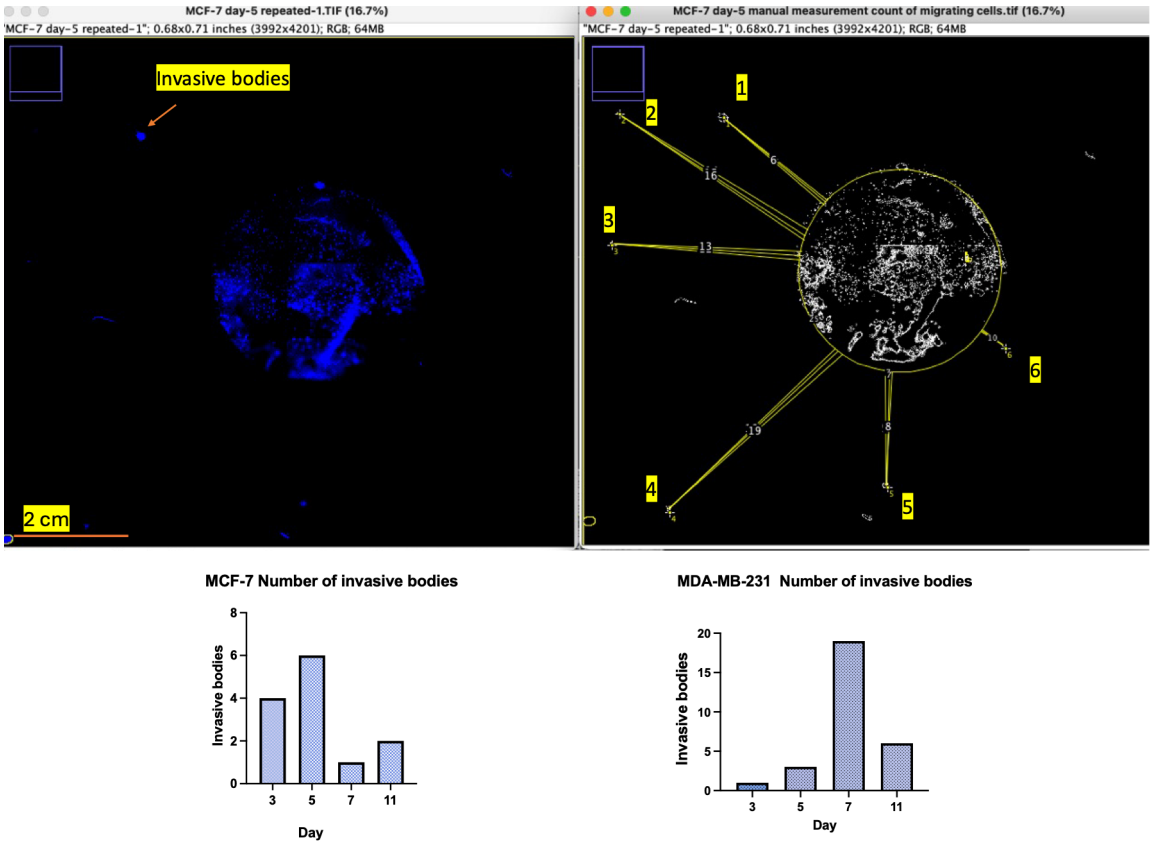

Figure 4.7. Upper panel: Example of an image J analysis of MCF-7 tumoroids captured at a total magnification of 100X, with a scale bar of 2 cm. DAPI stained images in a 24 well plate, following a ten-day incubation, resulted from 176 multiple captures using Evos microscopy shows an ACM (middle mass) image J analysis of nucleic stain DAPI analysis results show the distance migrated measurement and the number of invasive bodies from the original ACM into the non-cellular collagen compartments. Lower panel: MDA-MB-231 tumoroids indicated exponential growth from day 3 to day 7, and a decrease in several clumps was seen by day

11. MCF-7 tumoroids number of invasive bodies from day 3 to day 5 showed an increase, but again, it decreased by day 11—median values ± SE. One tumoroid was deployed for each day with a total of four tumoroids for each cell line. No significant differences were shown.

A cluster of cells migrated from the ACM into the non-cellular compartments (as shown in Fig. 4.8), forming detached, invasive bodies. MDA-MB-231 tumoroids' migrating distance shows a higher persistence of cell clump detachment than MCF-7 tumoroids. MCF-7 P value (0.7689) showed not significant difference ($P < 0.05$). F (0.3815) F value means that the value is well below 1.0, which shows that the variance between experimental groups is much smaller than the variance within the group. MDA-MB-231 tumoroids had no significant difference ($P < 0.05$), P value= 0.7597, and F (0.3917). This describes the rate of invasion from the ACM into the noncellular compartment of this 3D tumoroid model, which is determined by the aggressiveness of the cancer. This has led to the MDA-MB-231 optimised tumoroid, due to its aggressive nature in invading surrounding tissue, having more metastatic capabilities and will be deployed in the following study with glycosidase inhibition treatment.

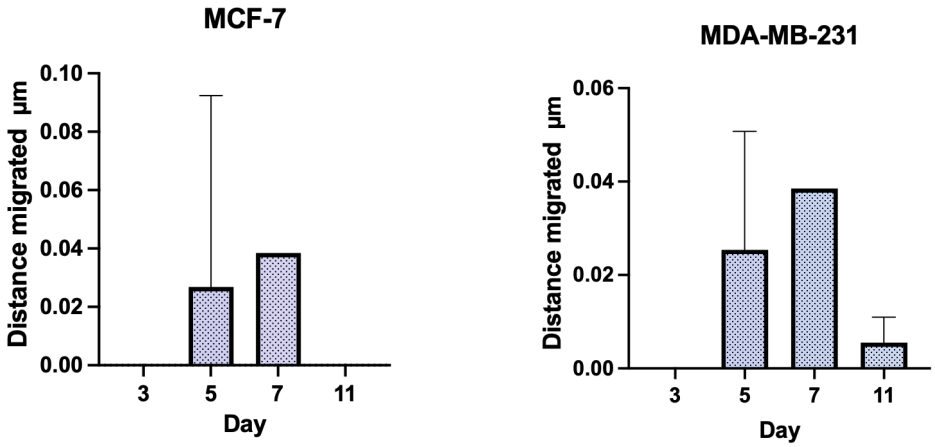

Figure 4.8. The histograms depicting the migration distances of MCF-7 and MDA-MB-231 tumoroids were analysed over an 11-day optimisation period. MCF-7 tumoroids exhibited a marked increase in migration distance between days 5 and 7; however, by day 11, no cell clumps were detected. In contrast, MDA-MB-231 tumoroids exhibited the most significant increase in migration distance on day 7, followed by a decrease by day 11. Median values ± SE. One-way ANOVA performed. No significant differences were shown. One tumoroid was deployed for each day with a total of 4 tumoroids for each cell line.

In the following section (4.5), the glycosidase inhibition treatment of MDA-MB-231 tumoroids was performed to evaluate the effects of compound inhibitors using the three developed methods for measuring cell reduction and motility.

4.5. 3D tumoroid glycosidase inhibition treatment

3D tumoroids were treated with glycosidase inhibitors as described in (Section 2.1.5).This study aimed to evaluate the characteristics of tumoroids when exposed to glycosidase inhibitor compounds and to gain a better understanding of how the glycocalyx responds to these treatments. Fifteen tumoroids were fabricated, with three replicates of each treatment: DNJ, inhibitor compounds from the Phytoquest company (255, 42, 44), and untreated tumoroids, for an 11-day time course. On day 2, 0.5 mM concentrations were added to each triplicate tumoroids sample every two days. The tumoroid's metabolic activity was also measured using the Alamar Blue assay on day 11, 24 hours after incubation.

The Alamar blue assay was carried out to measure the metabolic activity of MDA-MB-231 tumoroids after treatment with glycosidase inhibitors (Section .4.6)

4.6. Metabolic activity of the glycosidase inhibition treatment

Alamar blue assay was deployed as described in (Section 2.1.6) to measure the cell viability of the tumoroids after treatment with glycosidase inhibitors for 11 days. The Alamar blue assay was employed to assess the cell proliferation and metabolic activity of untreated and treated 3D MDA-MB-231 tumoroids, to determine whether these glycosidase inhibitors impacted the breast cancer glycocalyx. A significant difference resulted($P < 0.05$) between the untreated and the treated 3D tumoroids with DNJ, P value= 0.0041), and t-test value t= 15.48, df=2. It measured the size of the difference between the groups (treated vs untreated) relative to the variation within the data. A larger t-value means a larger, more significant difference. An extremely high value like (15.48) usually indicated an strong difference. (df = 2): This stands for degrees of freedom. It represented the amount of independent information used to estimate the data variance, which is directly tied to the sample size. Because the degrees of freedom are so small (df=2), the critical threshold for the t-score is higher.

However, a t-value of (15.48) is extraordinarily high. Even with only 2 degrees of freedom, this will result in a highly significant difference. Compound 255 (t=87.61, df=2, P value= 0.0001) showed the highest t-value and P value, indicating a greater significant difference. Compound 42 (t=8.342, df=2, P value=0.0141), compound 44 (t=6.221, df=2, P value=0.0249).

Evaluation of the cytotoxicity effect on MDA-MB-231 3D tumoroids exposed to glycosidase inhibitors alone (0.5 mM). Untreated 3D tumoroids were compared with those exposed to glycosidase inhibitors. MDA-MB-231 3D tumoroids were more sensitive to exposure to treated tumoroids with compound 255, exhibiting the most significant reduction in metabolic activity and cell viability, with a 30% decrease in cell viability. MDA-MB-231 3D tumoroids treated with compound 255 showed a statistically significant percentage reduction.

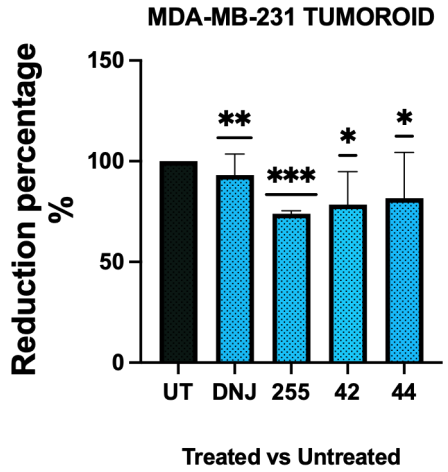

Figure 4.9. A histogram of MDA-MB-231 tumoroids cell viability measurements at day 11. This shows the percentage reduction of Alamar blue in the tumoroids after exposure to glycosidase inhibitor compounds DNJ, 255, 42, and 44 at days 2, 4, 6, 8, and 10. Tumoroids treated with *c*ompound 255 indicated the highest percentage reduction compared to the untreated tumoroid. Median values ± SE and *a t*-test was carried out. There was a significant difference in all treated groups (DNJ) **p=< 0.05, (255) ***p=< 0.05, (42) *p=< 0.05, (44) *p=< 0.05. N=3 technical replicates were deployed.

To further analyse the effects of glycosidase inhibitors on MDA-MB-231 tumoroids, particle analysis was carried out to evaluate whether there was a reduction in cellularity, as shown in (Section 4.7.)

4.7. MDA-MB-231 3D Tumoroids DAPI count particle analysis

Particles analysis was carried out as described in (Section 2.1.10) to measure cell numbers. MDA-MB-231 3D tumoroids were subjected to a fixation process, followed by nuclear staining with DAPI, to assess the impact of glycosidase inhibitors, specifically the DNJ, along with selected compounds numbered 255, 42, and 44 from the Phytoquest company. This evaluation was deployed over an 11-day *in vitro* treatment period, designed to monitor cellular responses and morphological changes in the tumoroids resulting from the glycosidase inhibition. The combination of fixation and DAPI staining allowed for precise visualisation of nuclei, facilitating detailed analysis of how these compounds influenced tumour cell behaviour and development over time, as shown below in how measurements were carried out (Fig. 4.10).

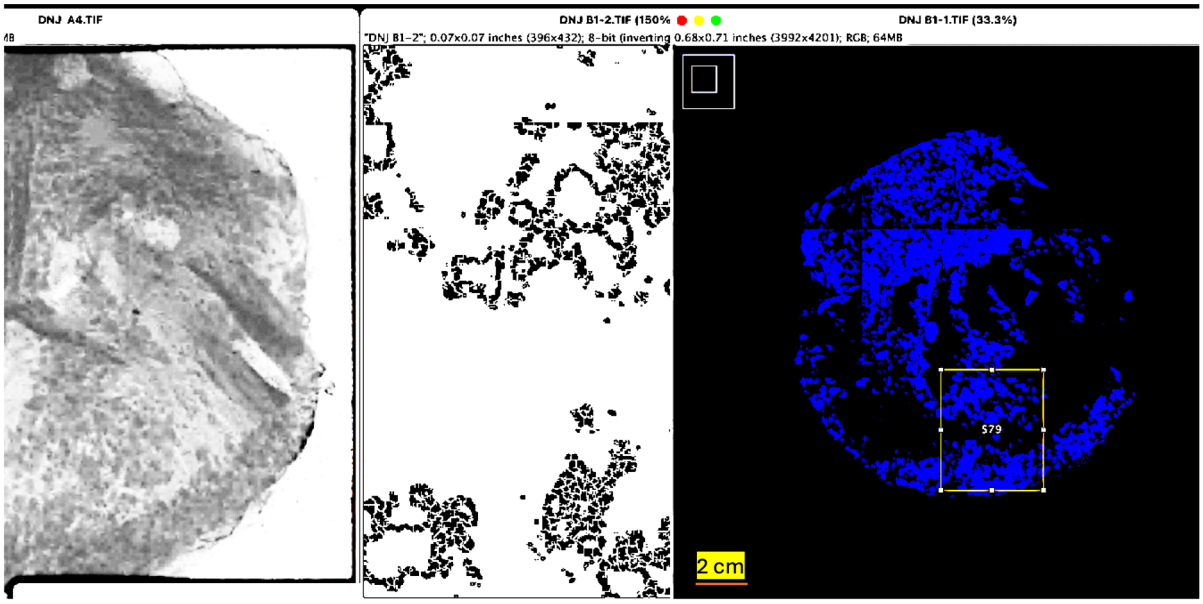

Figure 4.10. A brightfield image on the left, particle analysis measurements in the middle, and a whole tumoroid with DAPI-stained central cancer cell mass on the right, showing a selected area to be analysed. An example of an image J analysis of MDA-MB-231 tumoroids captured at a total magnification of 100X DAPI stained images, with a scale bar representing 2 cm. The images resulted from 176 multiple captures using Evos microscopy, analysis of nucleic stain

DAPI results shows particle analysis through binary processing, picture threshold RPG/B&W mask, watershed, particle analysis of tumoroids by choosing areas of 500 µm at high cell density to avoid folded collagen areas to interfere with the particle analysis. Data analysis was presented as median values ± SE.

Particle analysis was conducted to assess the effect of glycosidase inhibitors and determine whether cellular reduction occurred (Fig. 4.11). The statistical analysis performed using a one-way ANOVA test reveals a significant difference in the effects observed between the treated and untreated 3D tumoroids. With a p-value of 0.0001 ($P < 0.05$), indicating a strong statistical significance. Among the inhibitors evaluated in this study, compound 42 demonstrated the most significant decrease in metabolic activity, indicating its strong potential as an effective agent. This was followed closely by compounds 255 and 44, which showed notable reductions in cell numbers, although the reductions were slightly less pronounced. In contrast, DNJ exhibited the least reduction in cell viability among all the inhibitors tested. This observation suggests that DNJ may possess a relative lack of potency compared to the other compounds, making it less effective in targeting cell proliferation.

Specifically, all treated MDA-MB-231 tumoroids subjected to glycosidase inhibitors exhibited a pronounced reduction in cell density. This reduction in cell density is further corroborated by the particle analysis cell count histogram depicted in Figure 4.11, demonstrating a consistent trend across the experimental data. These findings suggest that the glycosidase inhibitors effectively enhance the anti-proliferative effects on the MDA-MB-231 tumoroids, providing valuable insights into potential therapeutic strategies for breast cancer treatment.

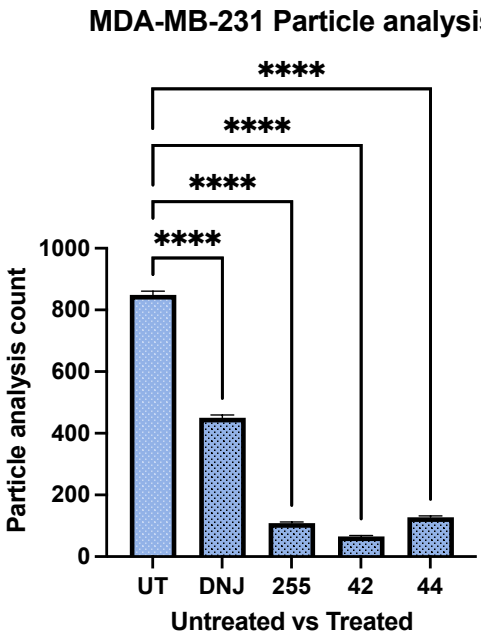

Figure 4.11. The MDA-MB-231 tumoroid histogram of particle analysis cell count, using ImageJ, showed a significant difference in all treated compounds, DNJ, 255, 42, and 44, compared to the untreated. The data were presented as median values ± standard error. A one-way ANOVA statistical analysis was performed to assess the significance of the results. A significant difference was shown in all treated cells. (DNJ) ****p= < 0.05, (255) ****p= < 0.05, (42) ****p= < 0.05, (44) ****p= < 0.05. N=3 was deployed.

Following the comprehensive particle analyses conducted on both the untreated and treated tumoroids, a one-way ANOVA statistical analysis was employed to assess whether there were significant differences among the various glycosidase inhibitors used in the study. The resulting statistical data analysis is presented below, highlighting key findings that contribute to our understanding of the impact of glycosidase inhibition on tumour biology (Table 4.1)

Table 4. 1. One-way ANOVA test statistical analysis comparing the untreated and treated 3D tumoroids, as analysed by particle analysis using ImageJ.

ANOVA summary	**MDA-MB-231**
F	460.3
P value	<0.0001
P value summary	****
Significant diff. Among means (P < 0.05)?	Yes

The treatment of MDA-MB-231 3D tumoroids with glycosidase inhibitors, specifically DNJ, compounds 255, 42, and 44, showed notable effects on cellular structure. As (shown in Fig. 4.12), cells were stained with DAPI, acting as a marker for cell count, revealing significant changes in cell area and density post-treatment. The treated tumoroids displayed a marked reduction in viable cells, although they often appeared grouped in clumps. This clustering made it challenging to count individual cells accurately, necessitating the assessment of cell populations by quantifying these aggregates. The untreated tumoroids exhibited a higher cellular density, indicating robust growth in the absence of inhibitory treatments.

Among the inhibitors studied, compound 42 resulted in the most pronounced decrease in cell number, followed closely by compound 255 and compound 44. Notably, DNJ exhibited the least reduction in viability among all the inhibitors tested, suggesting a relative lack of potency compared to the others. Overall, the observations indicate that the treated MDA-MB-231 3D tumoroids experienced a significant reduction in cell numbers or cell clumps compared to their untreated counterparts. This reduction aligns well with data from the cell viability assay, which demonstrated a consistent decrease in metabolic activity across all tumoroids treated with glycosidase inhibitors, further supporting the efficacy of these compounds in inhibiting tumour growth. There was a significant reduction of cell/clump numbers when the MDA-MB-231 tumoroids were treated with the glycosidase inhibitors for 11 days, resulting in a substantial difference with P values= 0.0001 ($P < 0.05$)

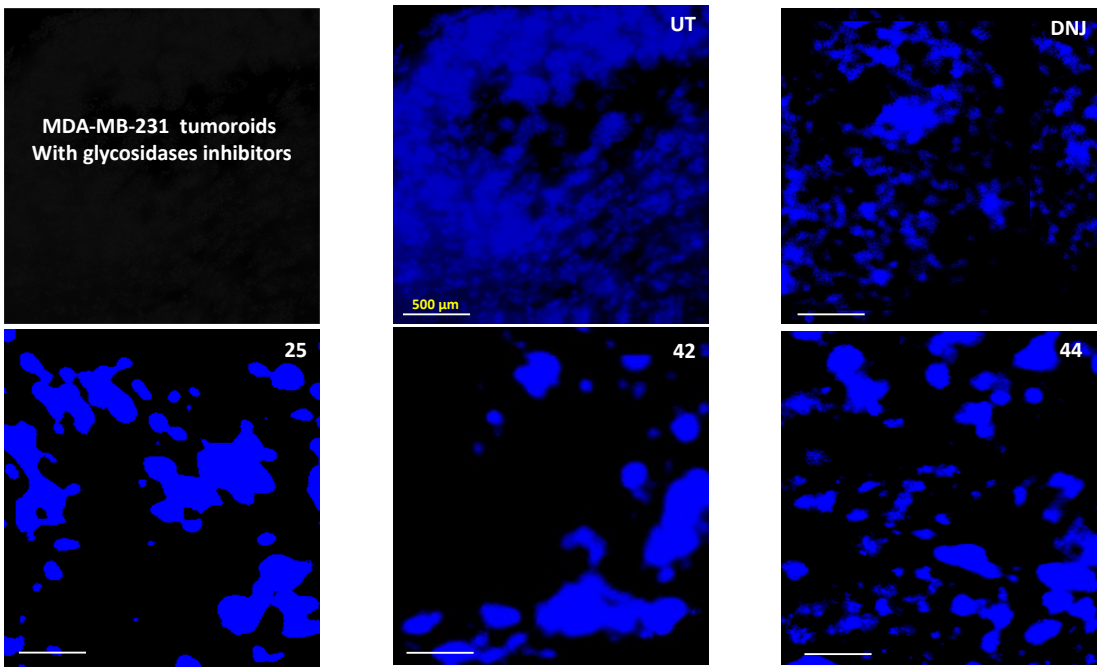

Figure 4.12. Visualisation of DAPI fluorescence of the MDA-MB-231 3D tumoroid nucleic particle analysis captured at total magnification of 200X, with a scale bar representing 500 µm. EVOS fluorescence microscopy showed a reduction in the cell numbers of the treated tumoroids, as the untreated tumoroid cell density is higher. Median values ± SE. These visualised images were sectioned and cut similarly to all 3D tumoroids, without interfering with folded collagen areas. An example is illustrated in Figure 4.10. A significant difference was shown in all treated cells **** p =< 0.05. N=3 was deployed.

Table 4.2 displayed the inhibition rates that these inhibitors compounds interfered and affected the proliferative mechanisms of the tumoroid mainly with glycoproteins that are influential in the development of cancer and metastasis. This study reflects the investigation deployed in 2D, where glycosidase inhibition treatment on four breast cancer cell lines showed a variable reduction in cell numbers due to their heterogeneity, resulting in different cells being less sensitive than others.

The mean difference showed the numerical difference between the average of the control group and the average of the treatment group. For example: The mean of the 42 group was 783.5 units higher than the mean of the UT group and thus had the strongest impact, followed by compound 255, 44 and DNJ which all had significant differences. The 95% confidence

interval difference was that all treated samples had true effects. All tested treatments elicited a statistically significant difference compared to the untreated cells ($p < 0.0001$). Treatment 42 demonstrated the strongest true effect, increasing the mean by (783.5) units 95% CI: 696.6 to 870.4). Treatments 255, 95% CI: 671. to 809.5 and 44 95% CI: 657.2 to 785.8 showed comparable high-magnitude effects, while DNJ produced a more moderate true effect 95% CI: 359.1 to 437.9.

Table 4. 2. Dunnett's multiple comparisons test between treated and untreated MDA-MB-231 tumoroids with glycosidase inhibitors DNJ, compounds 25, 42, and 44 from the Phytoquest company.

Dunnett's multiple comparisons test	Mean Diff.	95.00% CI of diff.	Below threshold?	Summary	Adjusted P Value
UT vs. DNJ	398.5	359.1 to 437.9	Yes	****	<0.0001
UT vs. 255	740.5	671.5 to 809.5	Yes	****	<0.0001
UT vs. 42	783.5	696.6 to 870.4	Yes	****	<0.0001
UT vs. 44	721.5	657.2 to 785.8	Yes	****	<0.0001

Further measurements were conducted, including outgrowth and the analysis of invasive clump numbers, as shown below (Fig. 4.13). Left Panel: The study indicated a noteworthy increase in invasive front tumoroids treated with compounds 42 and 44, suggesting a potential enhancement of invasive characteristics in these treatments. In contrast, the tumoroids treated with compound 255 exhibited a decrease in cell density area compared to their untreated counterparts, indicating a possible inhibitory effect on tumour growth or invasion. However, inhibitor 255 did not result in a statistically significant difference.

Right Panel: The counts of invasive cell clumps reveal that the tumoroid subjected to treatment with compound 42 displayed the highest number of invasive cell aggregates migrating into the non-cellular compartment of the ECM. This observation highlights the aggressive nature of these tumoroids and their capacity to invade surrounding tissues.

The ImageJ software was used to measure the invasive front, enabling the precise quantification of cell outgrowth from the ACM. Remarkably, the tumoroids treated with

compound 255 demonstrated no significant growth compared to the untreated tumoroids, reinforcing the notion that this compound may play a role in suppressing invasive behaviour.

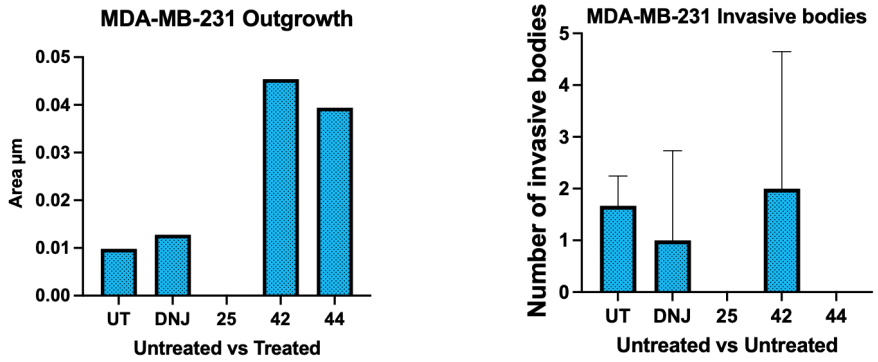

Figure 4.13. Histogram analysis of MDA-MB-231 3D tumoroid, the invasive front (left panel), and the invasive bodies count (right panel). The data were presented as median values ± standard error. A one-way ANOVA statistical analysis was performed to assess the significance of the results. N=3 technical replicates were deployed.

Whole MDA-MB-231 tumoroids were stained with DAPI and visualised below (Fig. 4.14); cellular reduction is observed due to the compound 255 inhibitors affecting cellularity compared to the untreated tumoroids. An 11-day glycosylation study was conducted using deployed glycosidase inhibitor compounds, including DNJ and Phytoquest compounds (42, 44, and 255), at a concentration of 0.5 mM. A comparative analysis of treated versus untreated MDA-MB-231 tumoroids observed significant differences in area reduction. Tumoroids were grown in 24-well plates and treated with compound 255, which exhibited the most pronounced decrease in size compared to other inhibitors tested. Specifically, the area reduction of these tumoroids highlights the compound's potency in inhibiting tumour growth. Additionally, tumoroids treated with compound 42 and 44 demonstrated a notable decrease in cell density when compared to untreated tumoroids, further underscoring the effectiveness of these compounds in targeting and reducing cancer cell proliferation. For clarity, it is essential to note that the cellular environment consisted of 20,000 cells seeded in an ACM and an acellular compartment grown in 24-well plates.

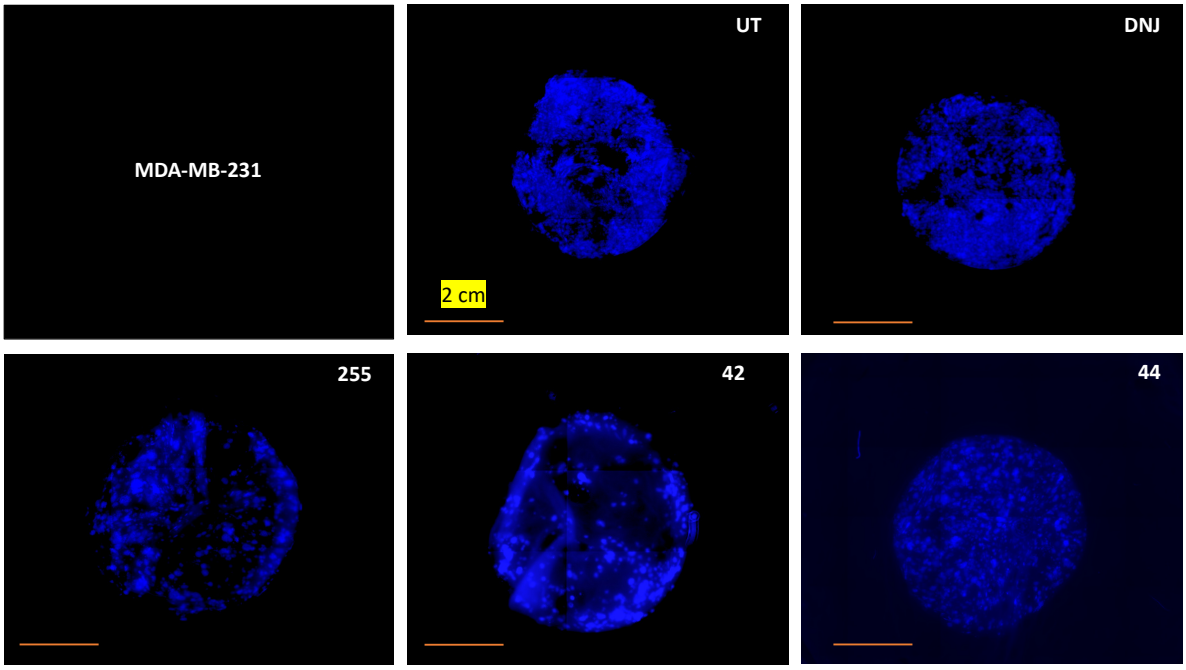

Figure 4.14. Visualisation of DAPI fluorescence of the MDA-MB-231 3D tumoroid nuclei representation following a ten-day incubation resulted from 176 multiple captures using Evos fluorescence microscopy at a total magnification of 100X, with a scale bar representing 2 cm. Data analysis was presented as median values ± SE. One-way ANOVA statistical analysis. Treatment of glycosidase inhibition on MDA-MB-231 tumoroids consisted of 3 tumoroids to generate technical triplicates for each treatment.

In the next section, MDA-MB-231 tumoroids were used in a second experiment with three replicates, similar to the previous experiment, focusing on glycosidase inhibition treatment. Due to their significant differences, only compound inhibitor 255 and DNJ were tested this time. While compound 42 showed the most significance, compound 255 and DNJ resulted in the most effective impact on breast cancer cells, as demonstrated in (section 4.6).

4.8. MDA-MB-231 tumoroids validation studies

In this investigation, MDA-MB-231 tumoroids were used to further validate findings from previous studies focused on glycosidase inhibition. This time, the analysis was restricted to testing two specific inhibitors: compound 255 and DNJ. The tumoroids were meticulously optimised for this study, specifically for the particle analysis measurements, with one notable

enhancement being the exclusion of any folded collagen during their production. This alteration was crucial, as folded collagen may significantly interfere with experimental accuracy and outcomes.

A whole-particle analysis was conducted to ensure a comprehensive evaluation of the tumoroid model, allowing for the capture and assessment of the cell population present within the tumoroids. Despite these refinements, the current study and prior investigations revealed a concerning trend: a marked decrease in cell density. This reduction prompts further exploration into the biological implications of glycosidase inhibition and its impact on tumoroid viability and growth dynamics.

Whole MDA-MB-231 tumoroids were stained with DAPI and visualised below. Cellular reduction is observed due to compound inhibitors, mainly compound 255, which affects cellularity compared to the untreated tumoroids (Fig. 4.15). A detailed statistical analysis was conducted in the lower panel, demonstrating a significant difference in particle analysis for the treated tumoroids. The results showed a strong effect of the glycosidase inhibitors, with an $F= 41.85$ (2, 6 degrees of freedom) and a p-value = 0.0003 ($P < 0.05$). This finding highlights the potential of DNJ and 255 to inhibit tumour growth at a statistically significant level, marking an essential advancement in the study of therapeutic agents for cancer treatment.

However, the histograms illustrating the invasive bodies in the acellular compartments and the treated tumoroids with glycosidase inhibitors did not reveal any statistically significant differences despite a decrease in invasive bodies compared to the untreated tumoroids. The final measurement indicated outgrowth from the ACM into the acellular compartment, where the inhibitor compound DNJ increased cell migration compared to the untreated tumoroids. In contrast, inhibitor 255 showed a decrease in migration. Nevertheless, these results were not statistically significant.

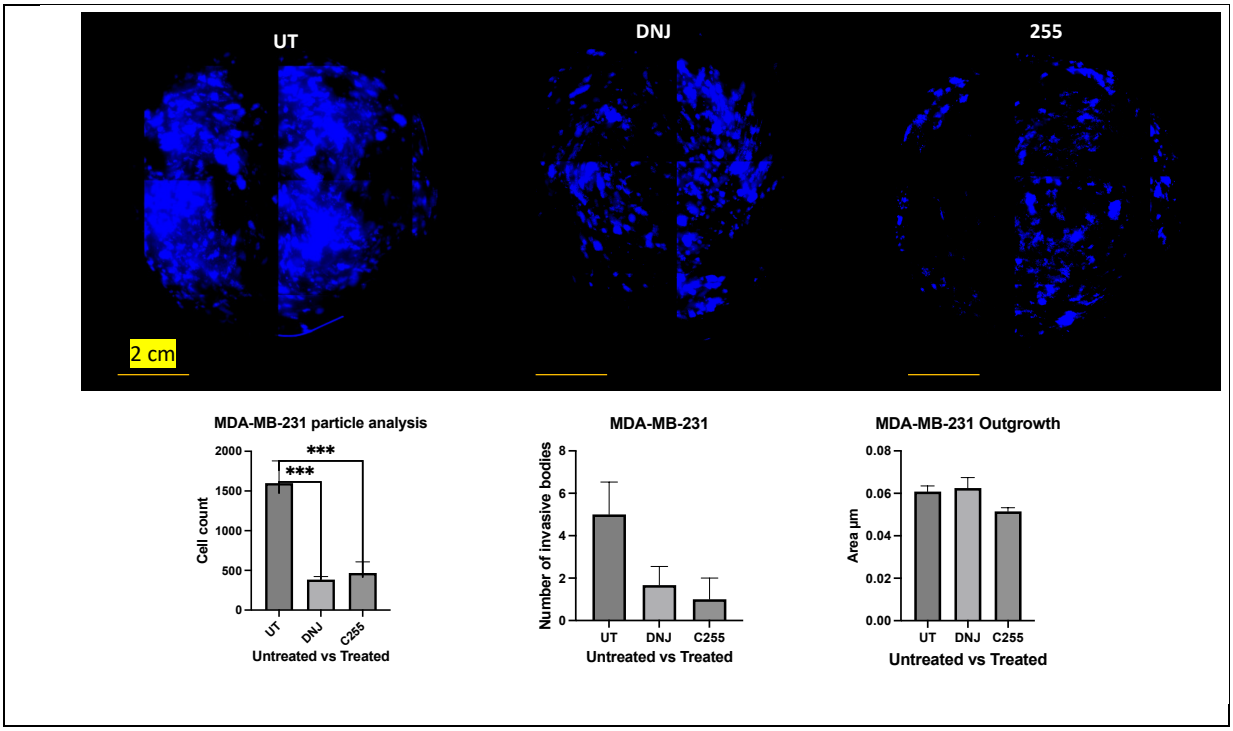

Figure 4.15. Upper panel: Visualisation of DAPI fluorescence of the MDA-MB-231 3D tumoroid nuclei representation following a ten-day incubation, resulting from 176 multiple captures using Evos fluorescence microscopy at a total magnification of X40, with a scale bar representing 2 cm. Lower panel: Statistical analysis from the particle analysis, measurement of invasive bodies and outgrowth. Data analysis was presented as Median values ± SE. One-way ANOVA statistical analysis. A significant difference was shown with both DNJ and 255 for particle analysis, *** p= < 0.05. No significant difference was shown on the number of invasive bodies and outgrowth. N=3 technical replicates were deployed.

In the upper panel, DAPI staining of MDA-MB-231 tumoroids revealed that those treated with the glycosidase inhibitors DNJ and 255 exhibited a notable reduction in cell viability compared to the untreated tumoroids. This suggests that the treatment effectively impairs cellular viability within these tumoroid models.

4.9. Discussion

ITH is a significant issue and an underlying cause of the failure of cancer treatments, which correlates with poor clinical outcomes (Landau, 2015; Kreso *et al.*, 2013). Drug penetration

into tissue is crucial for drug efficacy and can be effectively mimicked in 3D model screenings (Sirenko *et al.,* 2022). TNBC poses significant treatment challenges due to its aggressive nature and lack of targeted therapies. This study evaluated the effect of inhibiting enzymes responsible for NLG trimming on cell behaviour using breast cancer cells grown in 3D-optimised tumoroids. MDA-MB-231 3D tumoroids were developed to explore the impact of glycosidase inhibitors on tumour behaviour in a 3D environment. The development of MDA-MB-231 3D tumoroids represents a significant advancement in cancer research methodologies. Traditional 2D cell cultures often fail to replicate the complex interactions and behaviours of tumours *in vivo.* Investigating glycosidase inhibitors in 3D breast cancer models provides a highly translational approach to bridge the gap between *in vitro* research and clinical application. By comparing treated and untreated tumoroids, the aim was to gain insights into the effectiveness of specific compounds in reducing cell viability, proliferation, and motility, thereby enhancing our understanding of potential therapeutic strategies for TNBC. This confirms the findings from the 2D work in the previous chapter.

Cell density in untreated tumoroids was found to be significantly higher than that in those receiving treatment. Notably, DNJ, all compound inhibitors, and the Phytoquest compounds (255, 42, and 44) significantly reduced DAPI-stained nuclear areas, indicating decreased cell viability and proliferation relative to untreated controls. This highlights the effectiveness of these compounds in suppressing tumour growth within a 3D culture system. Moreover, more consistent exposure to glycosidase inhibitors may have influenced tumoroid cellularity, especially compared to cells treated with these inhibitors in 2D. The results of this study align with previous research on iminosugars, which evaluated colorectal cancer spheroids over a 13-day period to assess the effects of these compounds on growth and metabolism. Both natural iminosugars (such as D-fagomine and DNJ) and synthetic derivatives were examined. Two human colon cancer cell lines, representing early-stage (Caco-2) and late-stage (HCT-116) colon cancer, were cultured as spheroids for up to 13 days. Iminosugars were found to significantly decrease colon cancer cell viability. The late-stage (HCT-116) 3D tumor spheroids exhibited reduced mitochondrial reserves and increased lactate production, indicating a metabolic shift. Additionally, cells treated with specific derivatives, like NN-DNJ, showed a heightened dependence on lipids for energy (Montebugnoli *et al*., 2025). In other investigations, new inhibitors were designed to enhance the inhibition of mannosidases,

which forced immature N-glycans to the cell surface and disrupted cell-to-cell communication through molecular docking techniques. The researchers synthesized these derivatives and tested their ability to inhibit Golgi mannosidase at the cellular level and block the formation of 3D tumor spheroids. They discovered that the synthesized iminosugar derivatives effectively inhibited Golgi mannosidase in human malignant cells. One designated compound, AR524, demonstrated greater inhibitory activity against Golgi mannosidases than kifunensine. This designed inhibitor successfully suppressed the formation of 3D spheroids in culture. By disrupting the immature N-glycans, these compounds hindered the cell-to-cell communication necessary for spheroid formation, proving their potential as building blocks for future solid tumor chemotherapy (Koyama *et al*., 2020). There is much work done on iminosugars in 2D, but very little on 3D models related to this work. For instance, there is a lot of research done on 3D models testing chemotherapeutic drugs like doxorubicin alone, such as work involving MDA-MB-453, MDA-MB-231, and MCF-7 cell lines grown on chitosan scaffolds, which showed enhanced cell-extracellular matrix interactions. The 3D model effectively replicated the physical composition and dense growth patterns of real human breast tumours. Instead of testing with iminosugars, these models were tested with doxorubicin, as it showed resistance in breast cancer cells (Anil-Inevi *et al*., 2020). Even though iminosugars were not used, doxorubicin was evaluated on these models to determine if it had an effect on reducing cellularity, However, it did not result cellularity reduction.

This study reinforces the importance of utilising 3D tumoroid models to better understand tumour behaviour, particularly in relation to how glycosylation impacts cell viability and proliferation. This in-depth understanding can lead to improved modelling of tumour microenvironments. The current study introduces a novel approach to understanding the effects of NLG trimming on TNBC cells by utilising 3D tumoroid models. This method provides a more physiologically relevant environment compared to traditional 2D cultures, enabling a closer examination of tumour behaviour, cellular interactions, and treatment responses. The findings underscore the significance of 3D systems in capturing intra-tumoral heterogeneity, which is frequently overlooked in conventional models. By demonstrating the efficacy of glycosidase inhibitors, specifically DNJ and other compounds, in reducing cell viability and proliferation within 3D tumoroid systems, this research offers valuable insights into potential

therapeutic strategies for managing TNBC. The reduction in DAPI-stained nuclear areas in treated tumoroids underscores the effectiveness of these compounds in suppressing tumour growth, suggesting their promise as novel therapeutic agents.

Moreover, this study suggests that consistent exposure to glycosidase inhibitors may alter tumoroid cellularity more significantly than observed in 2D cultures, underscoring the need for further investigation of treatment dynamics in 3D environments. It reinforces the idea that the intricacies of extracellular matrix interactions and tumour microenvironments are better modelled in 3D systems, leading to more accurate predictions of drug efficacy and potential clinical outcomes.

The implications of this research extend beyond TNBC, potentially influencing the development of targeted therapies for various cancers by encouraging the adoption of 3D model systems in preclinical studies. This could pave the way for more effective treatment regimens and improved patient outcomes, addressing the pressing challenge of ITH in cancer therapy. There are studies where similar 3D tumour models were involved in the tumour biology and drug discovery, for instance, in a study where continuous flow and pressure to mimic the physical forces and interstitial fluid transport found in living tumors, researchers treated MDA-MB231 and SKBR3 cells with the chemotherapeutic agent doxorubicin to measure and compare cellular viability across 2D cultures, static 3D cultures, and 3D cultures under flow. They found cancer cells grown in 3D exhibited significantly reduced sensitivity to doxorubicin compared with standard 2D cultures. When physiological fluid flow and pressure were applied, this responsiveness was further reduced (Azimi *et al*., 2020).

In other studies, two breast cancer cell lines: MDA-MB-231 and MCF7 were cultured in 3D single-cell suspension, and 3D collagen-embedded multicellular spheroids. Researchers discovered that 3D spheroids demonstrated resistance to the drugs, closely mimicking the response of *in vivo* tumors to treatment. Administration of paclitaxel significantly elevated the cancer stem cell populations in all MDA-MB-231 models, indicating that this drug enhanced the presence of chemo resistant cancer stem cells regardless of tumor structure (Reynold *et al*., 2017).

4.9.1. Glycosidase inhibitors reduced metabolic activity

The findings indicated that compound DNJ initially showed promise in 2D models and exhibited a statistically significant difference in 3D tumoroid context in both replicated experiments. This research is consistent with other studies that evaluated the effects of natural iminosugars (e.g., D-fagomine and DNJ) and synthetic derivatives on colorectal cancer using 3D tumour spheroids. Findings showed that iminosugars significantly reduced cancer cell viability. In the late stages, the HCT-116 spheroids experienced a metabolic shift, which was characterized by reduced mitochondrial reserves and increased lactate production. Additionally, treatment with specific synthetic derivatives, such as NN-DNJ, led the cells to become highly dependent on lipids for their energy needs. As a result, there were changes in metabolic activity, including increased glycolysis and alterations in lipid and glycogen stores. DNJ reduced metabolic activity by exploiting the cancer cell's lack of mitochondrial reserves (Montebugnoli *et al*., 2025). (more information about this study is described in P46) Among the compounds tested, compounds DNJ, 42, and 44 caused effects in reducing metabolic activity. However, 255 emerged as the most effective with a greater decrease in cellular viability within the 3D models, which was also statistically significant in the particle analysis. These findings highlight the considerable potential of this agent as a therapeutic option for treating TNBC, warranting further investigation into its mechanisms of action and potential therapeutic applications.

The MDA-MB-231 cell line, grown in 2D, demonstrated greater resistance to therapy than in 3D tumoroids, which may contribute to cell heterogeneity and increased CIN. The ability of compound 255 to induce a statistically significant decrease in cellular viability in these more biologically relevant models may reveal new dimensions of tumour response to therapy, highlighting the relevance of tumour architecture in drug efficacy.

These findings not only underscore the therapeutic potential of DNJ and the Phytoquest compounds but also stimulate interest in exploring the mechanistic pathways through which these compounds exert their effects. Understanding these mechanisms could pave the way for developing tailored therapeutic strategies targeting specific cellular pathways unique to TNBC.

The findings from this research notably advance our understanding of glycosidase inhibitors, particularly compound 255, in the context of TNBC. The ability of this compound to

significantly reduce metabolic activity and cellular viability in 3D tumoroids, compared to conventional 2D models, highlights an innovative approach to assessing drug efficacy. This shift toward more biologically relevant models underscores the importance of tumour architecture in response to therapeutic agents. The novelty of this study lies in demonstrating that certain compounds, particularly DNJ and others from the Phytoquest library, can have a profound effect on TNBC cell viability, which encourages further exploration into their mechanisms of action. The identification of compound 255 as the most effective agent opens new avenues for targeted therapies. This emphasis on mechanisms of action can lead to the development of tailored treatment protocols that better address the unique challenges presented by TNBC.

4.9.2. Cell motility reduction

It was found that data generated through particle analysis using ImageJ supported these findings, revealing the formation of cell clumps within the acellular compartment. However, MDA-MB-231 tumoroids upon treatment with compounds DNJ, 42, and 42 showed no effect. 255 showed a reduction of protrusions, which have been identified as a cytotoxic agent with great potential for enhancing therapeutic strategies targeting TNBC. The measurement of the number of invasive bodies indicated a reduction in cell motility due to the inhibitor compounds DNJ and 255. Invasion assays conducted as part of this study provided compelling evidence that parameters such as the area occupied by invasive cells and the overall invasive capacity from the origination point in the ACM to adjacent regions. Despite 255 reducing the number of invasive bodies and the protrusion of cells into the acellular compartments, cell motility may have decreased, although there was no significant difference. Although 255 was effective in reducing the number of invasive bodies, the lack of a significant difference in overall cell motility indicates that further investigation is needed. This could mean that while some parameters improve, others may not be as responsive, emphasising the complexity of tumour behaviours and the need for a multifaceted approach in treatment.

To further explore the tumour microenvironment, this study employed the RAFT^{TM} 3D tumoroid system, which utilised specific absorbers to compress collagen, achieving a remarkable 40-fold increase in collagen density. The mechanical pressures exerted in these models, approximately 20 kPa, mimic the forces typically observed in actual tumours and

create a microenvironment comparable to the pathological hypoxia noted *in vivo* (Nyga *et al*., 2013). The tumoroid models exhibit significant relevance regarding collagen composition, which closely resembles that found in human tissues found highlighted by (Neuman & Logan, 1950). The ECM functions not only as a barrier that prevents drug penetration and the entry of immune cells, but also as a source of chemical signals and mechanical forces that influence cell shape, growth, movement, metabolism, and differentiation. Mechanical factors like compression, matrix stiffness, and fluid dynamics transmit positional and environmental cues to cells, triggering reactions that support tissue repair and maintenance until mechanical balance is achieved (Zhang & Zhang, 2025). Increased stiffness of the ECM activates cellular responses through mechanical signal transduction pathways, such as the Integrin/FAK and YAP/TAZ signaling pathways (Panciera *et al*., 2017). Higher stiffness of the ECM, especially in the liver, initiates the conversion of hepatic stellate cells into myofibroblasts, which boosts their ability to promote tumor growth and metastasis (Dou *et al*., 2018). Furthermore, heightened matrix stiffness triggers the expression of LOXL2, an enzyme that helps cross-link collagen and elastin in tumour cells via the integrin β1/α5/JNK/c-JUN signaling pathways. This process enhances the production of fibronectin and matrix metalloproteinase 9. These alterations not only change the physical characteristics of the TME but also facilitate the development of pre-metastatic niches (Wu *et al*., 2018).

This work highlights the crucial role of glycosylation and tumour microenvironment dynamics in developing practical therapeutic approaches against TNBC. Conventional monolayer cultures have helped elucidate fundamental cellular physiology; however, 3D models enable the study of multiple interactions between cells and the ECM to understand how signals from both cell-cell and cell-ECM interactions converge in a specific cell type. The N-linked glycosidase inhibition research in breast cancer conducted at the University of Westminster in 3D models aligns with other similar studies, in which the RAFT™ system was used as an appropriate 3D collagen framework for different cell types, such as pancreatic islets, thereby replicating the *in vivo* natural microenvironment. RAFT™ offers a sophisticated, standardised framework. The RAFT™ system with embedded cells delivers a strong technology suitable for automating semi-high-throughput or high-throughput assays in pharmacological applications (Szebeni *et al*., 2017). This evolution in 3D models marks a significant breakthrough in

understanding biological processes and optimising drug development strategiesA recent study using the RAFT™ system developed 3D tumour models to assess photodynamic therapy (PDT) with the photosensitizer TMPyP4, both alone and combined with doxorubicin, in breast and metastatic lung environments. Results indicated that PDT is more effective in metastatic lung tissue. MCF-7 tumours with metastatic stroma showed a 7.2-fold reduction in viability, while MDA-MB-231 showed only a 1.1-fold reduction. In MDA-MB-231 tumours with primary stroma, the combination of PDT and doxorubicin effectively reduced cancer cell viability and reversed tumour hypoxia, suggesting a promising strategy for treating aggressive TNBC.(Rafik *et al*., 2025). In another study, researchers developed 3D RAFT™ MCF-7 and MDA-MB-231 tumoroids to explore how different microenvironments affect the effectiveness of integrin-linked kinase (ILKI) inhibitors on breast cancer cells. They found that the stroma significantly influenced drug efficacy. For the invasive MDA-MB-231 cells, ILKI was 2.2 times more effective in primary breast tissue than in metastatic lung tissue. In contrast, for less invasive MCF-7 models, ILKI treatment was 1.4 times more effective in the lung metastasis area than in primary breast stroma. (Rafik *et al*., 2026).

4.10. Summary

In conclusion, this study underscores the significant advantages of employing 3D tumoroid models over traditional 2D cultures in investigating TNBC. The findings indicate that glycosidase inhibitors, particularly compound 255, effectively reduce cellularity and metabolic activity while also demonstrating potential in limiting cell motility. These results suggest that the 3D microenvironment reflects the *in vivo* conditions more accurately, enhancing the understanding of tumour behaviour and treatment responses. Further exploration of the mechanisms of action for these compounds is warranted, as they hold considerable promise as potential therapeutic agents for TNBC. This chapter will be further discussed in Chapter 6.

4.11. Summary of findings and novelty

- Glycosidase inhibitors significantly reduced metabolic activity in treated MDA-MB-231 tumoroids.
- Glycosidase inhibitors reduced cell numbers in MDA-MB-231 tumoroids.
- Glycosidase inhibitors had a small effect on cell motility.
- Novel Aspects of This Chapter:
- The novel aspect of this study lies in the use of 3D tumoroid models to investigate the impact of glycosidase inhibitors on TNBC cell behaviour in which 3D tumoroids more closely mimic *in vivo* conditions.
- Impact of glycosylation modifications on cancer cell proliferation and survival, potentially opening new research avenues.
- Glycosidase inhibition impacts cancer cell metabolism, growth, and cell motility in 3D tumoroids
- Development of cell migration and particle analysis assays deploying 3D tumoroids.

Chapter 5

Comparative studies of CIN in 2D and 3D models

The hypothesis for this study is that 3D cell cultures demonstrate lower levels of CIN compared to 2D systems. Inhibition of glycosidase activity in MDA-MB-231 cells will increase CIN levels.

5. Introduction

The research questions in this study were, was there more CIN in 2D than 3D and what was the relationship between glycosidase inhibition and CIN. The primary aim of this study was to investigate and compare the levels of CIN in 2D versus 3D cell culture models of breast cancer. A second aim was to explore the relationship between glycosidase inhibition and CIN, assessing how glycosidase inhibitors may influence chromosomal stability. The objectives were to deploy comparative assessment of CIN in 2D and 3D models and evaluation of the impact of glycosidase inhibitors on CIN.

This chapter presents the outcomes of a series of experiments designed to investigate intrinsic CIN in four breast cancer cell lines used as *in vitro* models in this research: MCF-7 (ER+), SKBR3 (HER+), BT-549 (TNBC), and MDA-MB-231 (TNBC). Due to the renowned effect of CIN on tumour resistance and its potential impact on compound testing, these experiments were designed to compare baseline CIN values in the four cell lines and identify model-specific CIN signatures related to pathobiological characteristics and different culture modalities (2D vs. 3D) (Sections 5.1 and 5.2). In addition, pancentromeric fluorescent in situ hybridisation (FISH) experiments, wherein a fluorescent DNA probe is used to visualise centromeric repetitive sequences common to all human chromosomes, were undertaken to establish the mechanistic origin of the observed CIN, whether caused by chromosomal mis-segregation during cell division (aneugenic) or caused by unrepaired double-strand breaks (clastogenic) (Section 5.2.2). This aspect is relevant in connection with the potential therapeutic exploitation of CIN. The outcomes of these initial investigations were used to inform subsequent research aimed at establishing the potential effects of glycosidase inhibitors on CIN (Section 5.3) as there might be a connection because this disruption of glycosidase inhibitors triggers ER stress, misfolded proteins, and cytoskeletal defects that lead to erroneous chromosome segregation and spindle formation during cell division.

The methodology applied to quantify and qualify CIN has been described in detail in the Materials and Methods (Section 2.3) and is exemplified in the workflow below (Fig. 5.1). Briefly, CIN in cell cultures was investigated using the CBMN Assay. This established genotoxicity assay enables quantification of cytological and nuclear anomalies in dividing cells (Fenech, 2007). Images were captured using a Zeiss AxioScanner2000 scanner, further

processed with QUPATH software, and then exported to ImageJ. Statistical analysis on scoring outcomes was performed using Excel, GraphPad, and one-way ANOVA. For Pancentromeric FISH, multicolour fluorescence imaging was performed using an Olympus (BX53) fluorescent microscope, and images were analysed with the Micropix software (Cytocam).

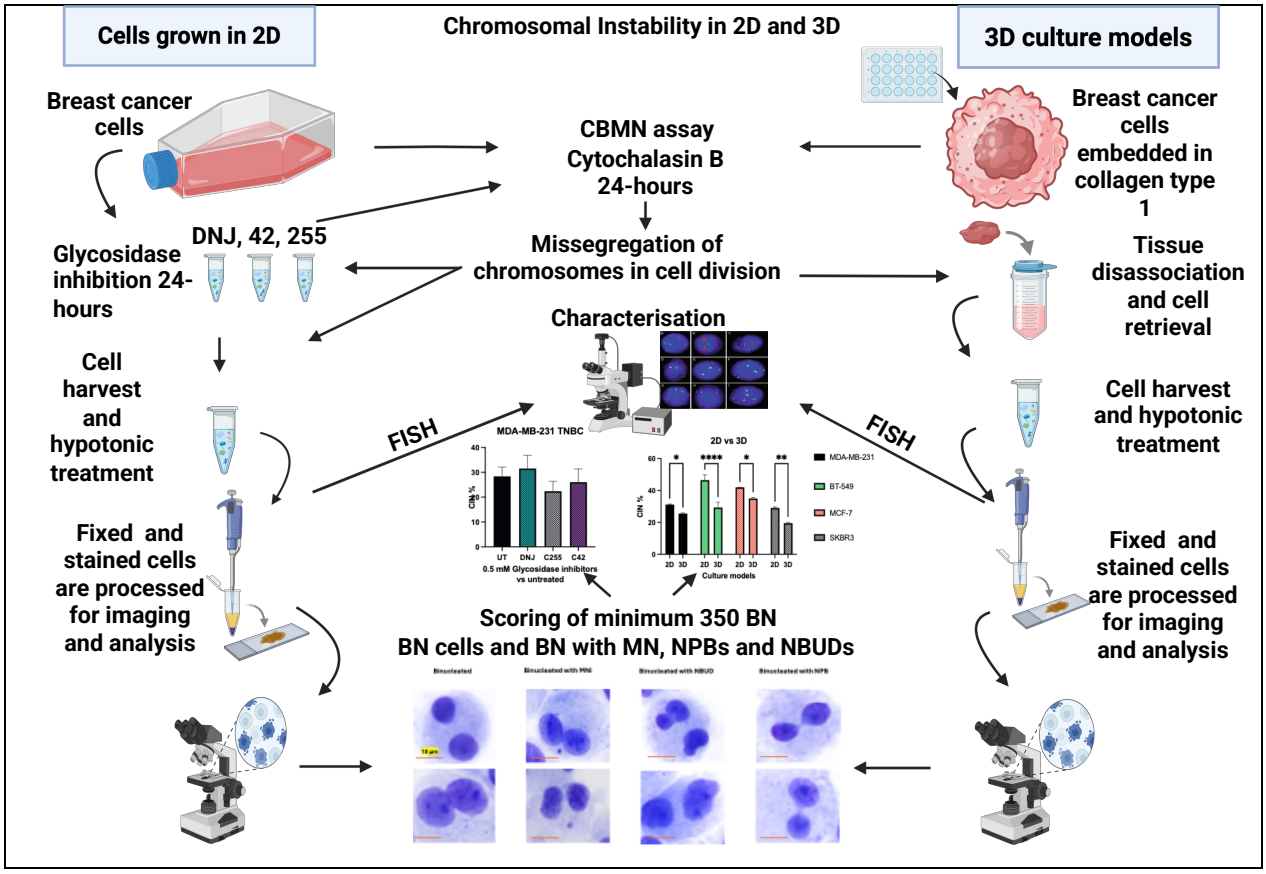

Figure 5.1. A schematic representation of the workflow for the evaluation of CIN in breast cancer cells cultured as 2D compared to 3D culture models. CIN levels were also assessed when the cells were exposed to glycosidase inhibitors in a 2D environment.

5.1. Evaluation of CIN in culture models

5.1.1. CIN in 2D

The CBMN assay was deployed as described in (Section 2.3) to establish baseline CIN values in routine 2D cultures. Semiconfluent cells were exposed to cyt-B for 24-48 hours. Cyt-B is an actin inhibitor that stops cytokinesis, causing actively dividing cells to be arrested in telophase and appear as BN. After the cyt-B treatment, cells were fixed and stained with Giemsa. A minimum of 300 BN cells were imaged and scored for each cell line in each experimental

condition. The purpose of the CBMN assay is to enable the accurate quantification of CIN by scoring a set of nuclear anomalies used as biomarkers of CIN, exclusively in cells that have undergone a round of cell division, albeit artificially interrupted by cyt-B treatment.

BN cells resulting from the cyt-B treatment were scored for the presence of nuclear abnormalities indicative of anomalies during cell division. Cells were annotated based on their morphological characteristics, which were subsequently organised and tabulated for detailed analysis. The presence of MN, NPBs, and NBUDs as markers of DNA damage provided evidence of CIN across the four distinct cell lines under investigation. MN are Small, extra nuclei that form when a piece of a chromosome or an entire chromosome fails to become incorporated into the main nucleus during cell division appear floating in the cytoplasm and contain either fragment or entire chromosomes. NPBs are visible, thread-like strands of DNA connecting two main nuclei. They occur when chromosomes fuse together incorrectly or struggle to separate during cell division. NBUDs are small nuclear protrusions emerging from the main nucleus that look similar to a micronucleus but remain physically connected to the main nucleus by a stalk, which also indicates DNA expulsion from the nucleus.

This research adhered strictly to the methodological guidelines established by Fenech in 2007, ensuring that the findings on CIN levels and associated indicators are reliable and contribute meaningfully to the broader understanding of genomic stability and its implications.

The table below (Table 5.1) presents the count and percentage of the four breast cancer cells grown in 2D to determine differences in scoring for CIN between BN cells with and without abnormalities. The data generated were tabulated using Excel and scored in a minimum of 300 BN cells each in two biological replicate experiments.

Table 5. 1. The data analysis from a Chi-square test reveals the differences between BN cells with and without CIN, based on a minimum of 300 BN cells grown in 2D.

Data analyzed	Binucleated cells with no biomarkers n, (%)	Binucleated cells with biomarkers n, (%)	Total
BT-549 2D	196 (53.41%)	171 (46.59%)	**367**
MDA-MB-231 2D	237 (68.50%)	109 (31.50%)	**346**
MCF-7 2D	223 (72.17%)	86 (27.83%)	**309**
SKBR3 2D	225 (70.98%)	92 (29.02%)	**317**

A pairwise Chi-square test was conducted to evaluate the overall differences in biomarker frequency across groups using a chi-square test for independence. Pairwise comparisons were performed using 2×2 Chi-square tests. Information on the cell line comparison and whether there is a significant difference among them is provided in below (Table 5.2).

Table 5. 2. The pairwise Chi-square test compares CIN in the breast cancer cell lines.

Pairwise comparison (Chi-square tests)			
Comparison	**χ^2, df**	***p*-value**	**Significance**
BT-549 vs MDA-MB-231	17.01, 2	0.0002	Significant
BT-549 vs MCF-7	25.06, 2	0.0001	Significant
BT-549 vs SKBR3	22.19, 2	0.0001	Significant
MDA-MB-231 vs MCF-7	1.052, 2	0.5909	Not significant
MDA-MB-231 vs SKBR3	0.4819, 2	0.7859	Not significant
MCF-7 vs SKBR3	0.1090, 2	0.947	Not significant

The CIN percentage was calculated from the data in the BN count, where BT-549 exhibited a 47% CIN. MDA-MB-231 cells showed 31% CIN, while MCF-7 and SKBR3 cell lines showed the lowest level of cumulative CIN with 28% and 29% respectively.

The results of the data analysis showed a pairwise Chi-square test statistical analysis that compared the cumulative CIN, where the data had proportions and variability due to the number of cells counted with and without CIN. This data determined whether there was a statistically significant difference among the cell lines grown in 2D. When comparing all four cell lines in 2D, the cumulative count of BN cells compared to BN cells with nuclear abnormalities showed that BT-549 cells had the highest level of cumulative CIN (all biomarkers), with a significant difference (< 0.05) P value= 0.0001 and 0.0002 when compared to MDA-MB-231, MCF-7 and SKBR3. Whereas no significant difference was observed among the other cell lines. These results are further shown below (Fig. 5.2) for further clarity and visualisation of the comparisons among the cell lines.

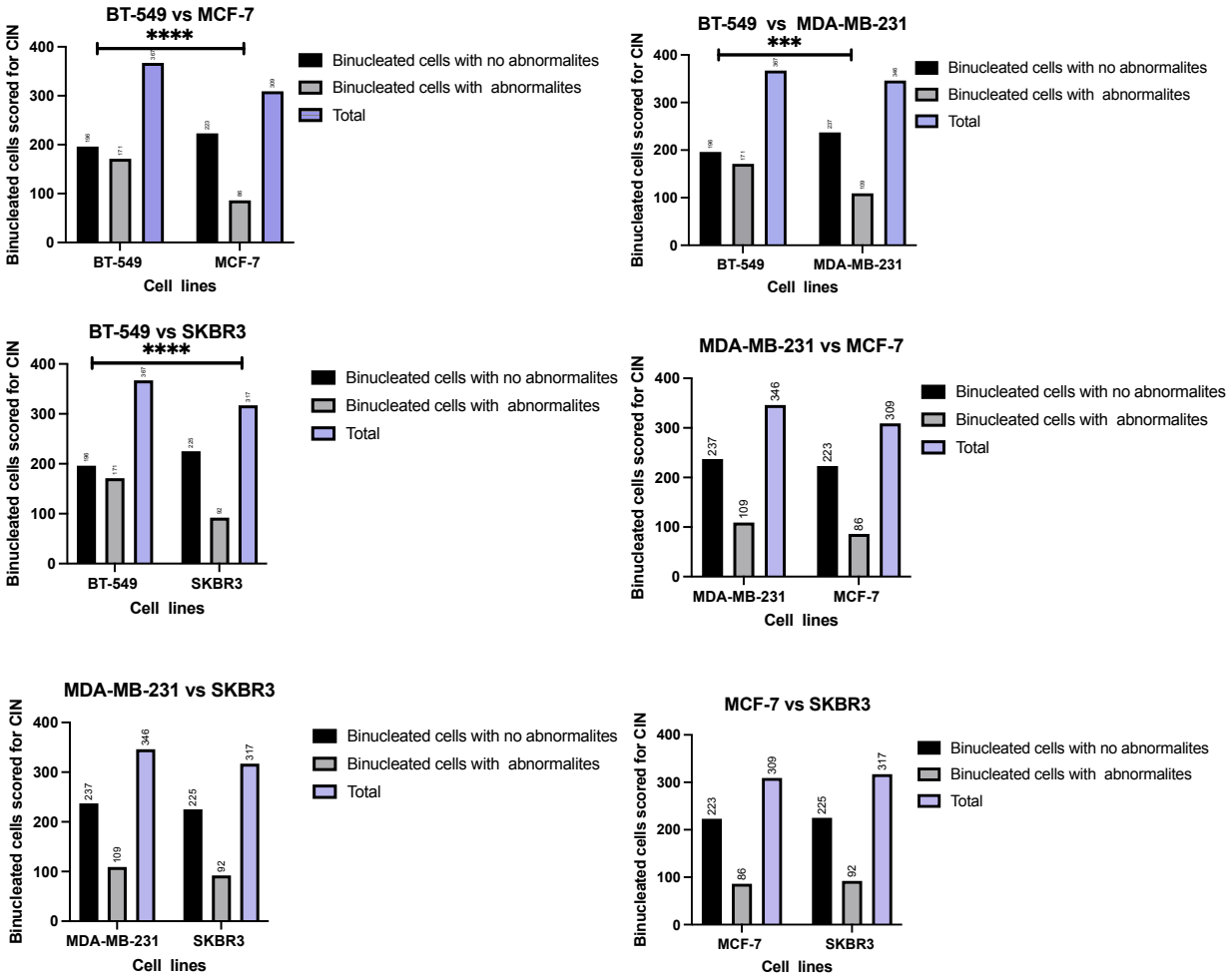

Figure 5.2. Cumulative CIN of BN cells with and without biomarkers from the four breast cancer cell lines grown in 2D. The top panel: BT-549 cells compared with MCF-7 and MDA-MB-231 cells. Middle panel: BT-549 cells were compared to SKBR3 cells and MDA-MB-231 to MCF-7 cells. Lower panel: MDA-MB-231 cells were compared to SKBR3 cells, and MCF-7 to SKBR3 cells. Data were presented as values from two replicate biological experiments. Data analysis was done using the pairwise Chi-square test. There was a significant difference on (BT-549 vs MCF-7) ****p= < 0.05, (BT-549 vs SKBR3) ****p= < 0.05, (BT-549 vs MDA-MB-231) ***p= < 0.05. There was no significant difference in the other comparisons.

5.2. Adaptation of CBMN in 3D

3D culture was carried out as described in (Section 2.1.3) to investigate CIN in 3D. The CBMN assay was deployed and adapted as described in (Section 2.6). Based on cell retrieval protocols recommended by the RAFT^{TM} manufacturer for flow-cytometry applications, cells were grown as 3D systems and treated with cyt-B, as described in (Section 2.6.2). Cells were then extracted from the collagen matrix by carrying out tissue disassociation before undergoing fixation in Carnoy's fixative (3:1 acetic acid/methanol). Fixed cells retrieved from the 3D cultures were then stained and imaged as described in (Section 2.3.1). Scoring of nuclear anomalies also followed the same methodology used in 2D cultures.

The process of creating 3D RAFT^{TM} system models for CIN studies was optimised, resulting in better yields when 5 × 10^5 cells were seeded and embedded in rat tail collagen per 24-well plate and grown for 7 days rather than 28 days. The longer culture period resulted in a decrease in cell yield upon harvesting. Automated cell count analysis indicated that approximately 1 million live cells were obtained after tissue dissociation.
The following section presents comparative studies of CIN in 2D and 3D models (Section 5.2.1).

5.2.1. Comparative studies of CIN in 2D and 3D culture models

This study aimed to investigate the hypothesis that 3D cell cultures exhibit lower levels of CIN compared to 2D systems. The investigation was conducted in parallel on the four breast cancer cell lines: MDA-MB-231, BT-549, MCF-7, and SKBR3. Comparing the rates of CIN between the 2D and 3D culture models can provide evidence on how culture conditions influence genomic stability in cancer cells, with implications for the suitability of different types of models in testing novel therapeutics.
The data obtained in this study were calculated using the same BN scoring for CIN carried in the four breast cancer cells in 2D (previous section). The table below presents a Chi-square test to assess the cumulative CIN in cells grown in 3D, comparing it to cells in 2D (Table 5.3), to determine which culture model exhibited more CIN.

Table 5. 3. A Chi-square test shows the differences between BN cells with and without CIN, based on cells grown in 3D.

Data analyzed	Binucleated cells with no biomarkers n, (%)	Binucleated cells with biomarkers n, (%)	Total
BT-549 3D	208 (70.08%)	89 (29.07%)	**297**
MDA-MB-231 3D	235 (75.03%)	78 (24.92%)	**313**
MCF-7 3D	222 (81.32%)	51 (18.68%)	**273**
SKBR3 3D	227 (80.50%)	55 (19.50%)	**282**

A pairwise Chi-square test was conducted to evaluate the overall differences in biomarker frequency across each cell line grown in 2D and compared to cells in 3D using a Chi-square test for independence. Pairwise comparisons were performed using 2×2 Chi-square tests. These results are provided (Table 5.4) and show P values to determine whether these cell lines had a significant difference between the two culture models.

Table 5. 4. The pairwise Chi-square test on the four breast cancer cell lines to compare cumulative CIN in 2D and 3D culture models.

Pairwise comparison (Chi-square tests)			
Comparison	**χ^2, df**	***p*-value**	**Significance**
BT-549 2D vs 3D	19.05, 1	0.0001	Significant
MDA-MB-231 2D vs 3D	3.504, 2	0.1734	Not significant
MCF-7 2D vs 3D	6.743, 2	0.0343	Significant
SKBR3 2D vs 3D	7.302, 2	0.026	Significant

In each of the cell lines, statistical analysis revealed higher levels of cumulative CIN in 2D cultures compared to 3D cultures. Specifically, in the BT-549 2D cultures, CIN, expressed as a percentage of BN cells exhibiting nuclear anomalies, was found to be 47%. In contrast, in 3D cultures of the same cell line, the total CIN rate was 29%. This difference presented the highest statistical significance among the cell lines, with a P value= 0.0001 ($P < 0.05$). The percentage of CIN in MDA-MB-231 TNBC cells was 31% in 2D cultures and 25% in 3D cultures, showing no statistically significant difference. For MCF-7 cells, the CIN percentage was 27% in 2D and 19% in 3D, demonstrating a statistically significant difference with a P value= 0.0389 ($P < 0.05$). In SKBR3 cells, the CIN percentage was 29% in 2D compared to 19% in 3D, reflecting a statistically significant difference with a P value= 0.026 ($P < 0.05$).

These results are further illustrated below (Fig. 5.3) for clarity and visualisation of the comparisons between 2D and 3D cell lines.

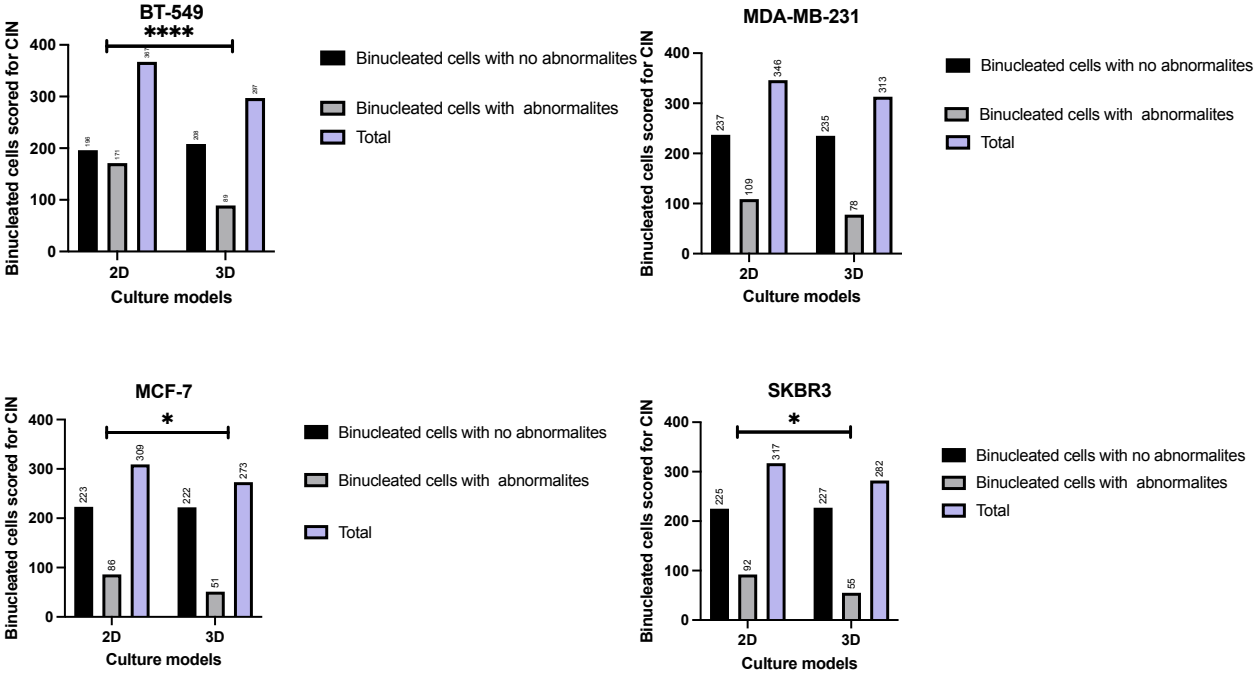

Figure 5.3. CIN Comparative studies in 2D and 3D showed the statistical analysis of CBMN assay scores from normal BN cells, and abnormalities such as MN, NBPs and NBUDs are indicators of chromosomal aberrations in CIN. Top panel: BT-549 and MDA-MB-231 were compared in 2D and 3D culture models. In the lower panel, MCF-7 and SKBR3 were compared between 2D and 3D conditions. Data were presented as two biological repeats, as data analysis was done using a pairwise Chi-square test. There was a significant difference on (BT-549) ****p= < 0.05, (MCF-7) *p= < 0.05 and, (SKBR3) *p= < 0.05. There was no significant difference on MDA-MB-231 cells.

MN contribution to CIN was also evaluated independently by comparing percentages of BN cells with MN in 2D vs 3D (Fig. 5.4). In accordance with cumulative CIN observations, MN were present at a higher rate in cells grown in 2D vs 3D, with BT-549 cells showing the most significant difference ($P < 0.05$) with a P value= 0.0001 and
15% in 2D and 6% CIN in 3D respectively. MCF-7 showed significant differences ($P < 0.05$) with a P value= 0.0001 with 11% CIN in 2D and 4% in 3D. MDA-MB-231 did not result in a significant

difference. SKBR3 cells showed a significant difference (P < 0.05) with a P value= 0.0336 with 7% CIN in 2D and 3% in 3D.

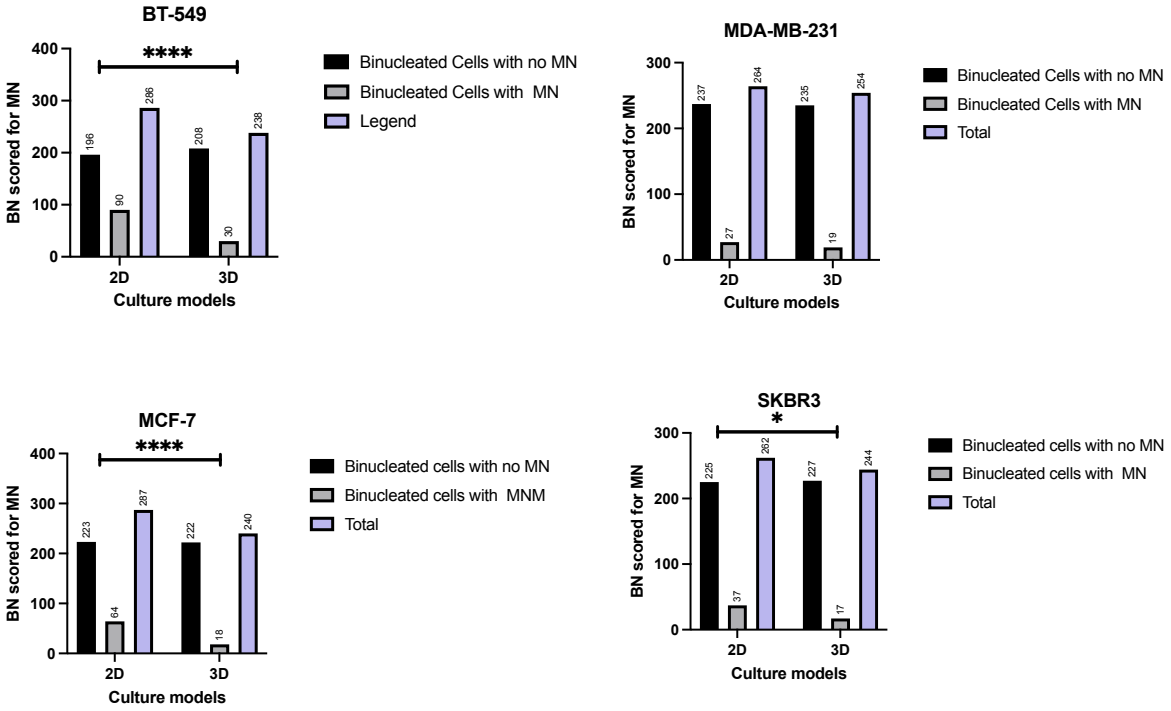

Figure 5.4. MN rates in 2D and 3D show the statistical analysis of CBMN assay scores as indicators of chromosomal aberrations in CIN. Top panel: BT-549 and MDA-MB-231 were compared in 2D and 3D culture models. In the lower panel, MCF-7 and SKBR3 were compared between 2D and 3D conditions. Data were presented as two biological repeats, as data analysis was done using a pairwise Chi-square test. There was a significant difference on (BT-549) ****p= < 0.05, (MCF-7) ****p= < 0.05 and, (SKBR3) *p= < 0.05. There was no significant difference on MDA-MB-231 cells.

The characterisation of the four cell lines was carried out to determine whether they are aneugenic and clastogenic, testing them with the FISH technique to identify the presence of centromeres, as shown below in (Section 5.2.2).

5.2.2. Pancentromeric FISH to differentiate between clastogenic and aneugenic CIN events

FISH with a pancentromeric probe, or a sequence recognising complementary sequences which are common to every single human chromosome, was conducted to differentiate between MN arising from aneugenic and clastogenic events. MN arising from aneugenic events or errors in chromosome segregation during cell division exhibit centromere-specific fluorescent hybridisation signals, indicating the presence of an entire chromosome. MN arising from a clastogenic event or defects in double-strand break repair would not present with fluorescent signals, suggesting the presence of part of a chromosome, not an entire chromosome. The outcome of clastogenic events is structural chromosomal aberrations, while the result of aneugenic events is numerical chromosomal aberrations.

The results showed a higher level of clastogenic events in 2D cultures than in 3D cultures. Aneugenic factors also arise as a combination of clastogenic and aneugenic events among all cell lines studied, resulting in variational effects. The DNA repeats at the centromere (Table 5.5) indicated the number of MN centromere-positive and -negative cells across the four breast cancer cell lines.

Table 5. 5. MN centromere testing on all four cell lines in 2D and 3D.

Cell line	MDA-MB-231		BT-549		MC-7		SKBR3	
	2D	3D	2D	3D	2D	3D	2D	3D
Number of cells	170	117	80	35	152	105	158	60
MN centromere+	7	5	3	2	12	4	5	1
MN centromere-	6	4	4	1	9	5	8	1

The data analysis of the cells scored for centromere testing, which determines the percentage of clastogenic and aneugenic sequences is shown below (Table 5.6.).

The study revealed that both aneugenic and clastogenic events occur during the process, indicating that both of these effects occurred across all four breast cancer cells studied in this investigation. However, no significant difference was observed in any of the cell lines. This illustrates that both aneugenic and clastogenic events occur in all cell types, attributed to chromosomal breakages and amplifications (EL-Zein *et al*., 2006).

Table 5. 6. The MN centromere test across all four cell lines in 2D and 3D.

Cell line	MDA-MB-231		BT-549		MCF-7		SKBR3	
	2D	3D	2D	3D	2D	3D	2D	3D
Centromere +	3.85%	2.75%	2.40%	1.60%	4.18%	1.39%	2.15%	0.43%
Centromere-	4.72%	3.15%	3.20%	0.80%	3.14%	1.74%	3.43%	0.43%

Additionally, $HER2^+$ sequences were analysed in SKBR3 cells to assess whether the visible nuclear anomalies or CIN were present. Biomarkers in those $HER2^+$ cells were the result of the physical amplification of the DNA sequence. The $HER2^+$ sequences in red are shown below to display their presence in the BN cell with MN.

These experiments were conducted solely with the SKBR3 cell line, as it is the only one of the four that exhibits HER2+ oncogene amplification. The rationale for these experiments is that blebs result from DNA amplification, suggesting that DNA amplification drives CIN.

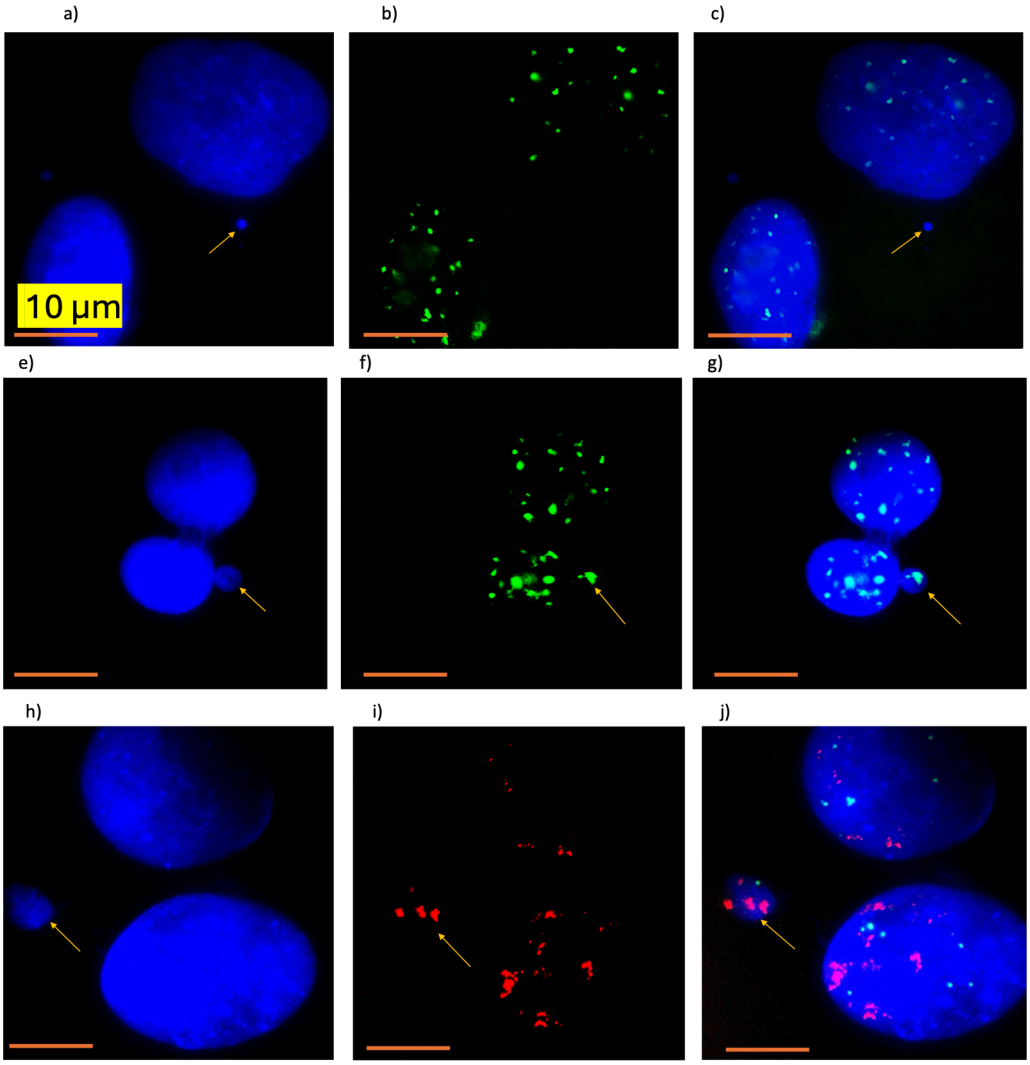

Figure 5.5. Examples of MN with and without centromeric signals: a) The DAPI channel shows a BN cell with an MN (arrow). B) In green, the pancentromeric sequences on nuclei. c) The merged image shows no green, fluorescent signal in the micronucleus, suggesting a lack of centromeric target DNA, which implies the content of the micronucleus is a fragment of a chromosome, not an entire chromosome (clastogenic event). d) A BN cell with MN stained with DAPI. f) The green channel showed BN cells, indicating pancentromeric signals in the MN. g) DAPI and green channels confirmed aneugenic characteristics. h) BN cells with MN DAPI channel. i) Red signals detected the presence of HER2 signals on the BN cell, and the arrow also indicated the presence of multiple copies of HER2 in the MNi. j) HER2 and PAN-C copies were detected in the MN, describing it as an eugenic event. Total magnification of X400, with a scale bar representing 10 µm.

The following section describes below (Section 5.3) CIN analysis conducted after 24 hours of exposure to glycosidase inhibitors in four breast cancer cell lines, aimed at evaluating the potential relationship between glycosidase inhibition and CIN.

5.3 The glycosidase inhibition and CIN

This study aimed to investigate the effect of glycosidase inhibition on CIN in the MDA-MB-231 cell line, which was selected for this study due to its metastatic capabilities, as it was chosen for the 3D glycosidase inhibition work in Chapter 4. This is because among all cell lines studied, MDA-MB-231 cells were more responsive to drug treatment than, for instance, the BT-549 cells, which are also a TNBC line. Prior research has established the baseline levels of CIN in MDA-MB-231 cells grown in both 2D and 3D cultures.

The CBMN assay was carried out on cells treated with DNJ and compound inhibitors 255 and 42, using the same approach as in the baseline 2D CIN work.

Hypothesis: Inhibition of glycosidase activity in MDA-MB-231 cells will increase CIN levels, as measured by the CBMN assay, due to the disruption of normal glycan structures that facilitate mitotic stability, given the effect of some glycoproteins on cytoskeletal organisation and the role of glycosylated adhesion molecules in cellular spatial orientation and the mitotic spindle alignment. Specifically, exposure to 0.5 mM concentrations of glycosidase inhibitors, such as DNJ, compound inhibitor 255, and compound inhibitor 42, is expected to result in an increase in CIN rates in TNBC cells.

The average results from the three experiments conducted to determine whether different compound inhibitors affect CIN in MDA-MB-231 cells (shown in Table 5.7). The data show the total number of BN cells with and without CIN, as well as the percentage of CIN among the treated and untreated cells. The untreated cells had 28% CIN, while the DNJ-treated cells had 31% CIN. In contrast, the other tested compounds, identified as 255 and 42, exhibited lower CIN levels than untreated cells; however, they did not show statistically significant differences in CIN. 255 had 22% CIN, and 42 had 26% CIN.

Table 5. 7. A Chi-square test was carried out on MDA-MB-231 between untreated cells and those treated with glycosidase inhibitors.

Sample	Binucleated cells with no biomarkers n, (%)	Binucleated cells with biomarkers n, (%)	Total
UT	227 (72%)	89 (28)%)	**316**
DNJ	200 (73%)	96 (33%)	**296**
C255	267 (78%)	76 (22%)	**342**
C42	201 (76%)	72 (26%)	**276**

The evaluation of CIN in MDA-MB-231 breast cancer cells in 3 experiments revealed that the treatment with the compound DNJ increased the level of CIN (shown in Table 5.8), suggesting that DNJ may disrupt chromosomal integrity in these cells. However, statistically, there was no significant difference.

Table 5. 8. A pairwise Chi-square test on MDA-MB-231 cells to show the cumulative CIN between untreated cells and those treated with glycosidase inhibitors.

Pairwise comparison (Chi-square tests)			
Comparison	**χ^2, df**	***p*-value**	**Significance**
UT vs DNJ	1.320, 2	0.5169	Not significant
UT vs C42	0.2452, 2	0.8846	Not significant
UT vs C255	3.163, 2	0.2057	Not significant

The (Fig.5.6 shown below) displays the results in histograms for clarity and visualisation of the comparisons between the untreated cells and the treated cells with glycosidase inhibitors.

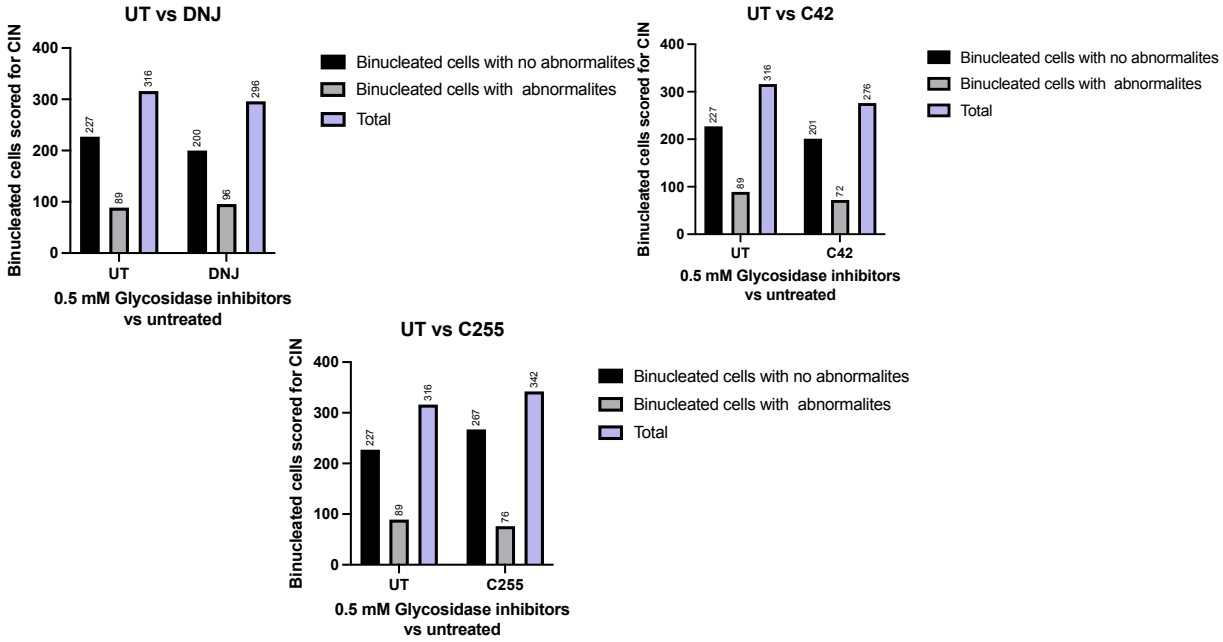

Figure 5.6. The level of CIN in treated MDA-MB-231 cells with glycosidase inhibitors at 0.5 mM for 24 hours showed that the statistical analysis of CBMN assay scores from normal BN cells and abnormalities such as MN (Fragmented chromosomes), NBPs(mis-repaired DNA or end-to-end chromosome fusions), and nuclear buds (amplified DNA or DNA complexes being eliminated) are indicators of chromosomal aberrations in CIN. The top panel showed the untreated cells compared to those treated with DNJ and compound inhibitor 255. The lower panel showed the untreated cells compared to the compound inhibitor 42. Data were presented as two biological repeats. Data analysis was done using a pairwise Chi-square test. No significant difference resulted.

The MN percentage was assessed to determine if these glycosidase inhibitors affect further chromosomal missegregation in MDA-MB-231 cells (Fig. 5.7).

DNJ and compound inhibitor 255 demonstrated an increase in CIN when evaluated in MN compared to untreated cells. This suggests that glycosidase inhibition impacts subsequent chromosome missegregation. In contrast, compound inhibitor 42 showed a slight decrease compared to the untreated cells. However, none of the treatments exhibited statistical significance.

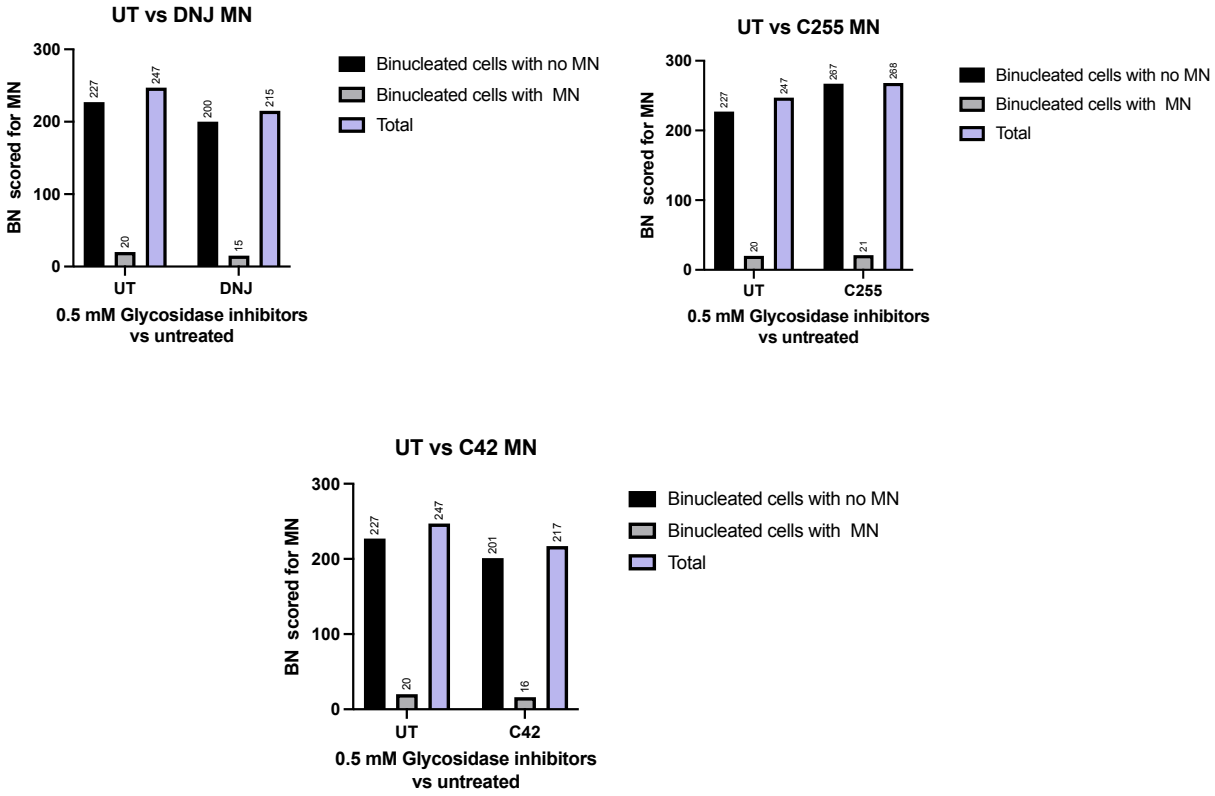

Figure 5.7. The level of CIN in treated MDA-MB-231 cells with glycosidase inhibitors at 0.5 mM for 24 hours was assessed using statistical analysis of CBMN assay scores, which included MN, serving as indicators of chromosomal aberrations in CIN. The top panel showed the untreated cells compared to those treated with DNJ and compound inhibitor 255. The lower panel showed the untreated cells compared to the compound inhibitor 42. Data were presented as two biological repeats. Data analysis was done using a pairwise Chi-square test. No significant difference resulted.

5.4. Discussion

Evidence supporting a critical role of CIN in enabling cancer has been growing steadily and has finally earned its validation as one of the 'new generation' hallmarks of cancer (Hanahan & Weinberg, 2011). The purpose of this study was to investigate whether culture conditions can affect the chromosomal stability of breast cancer cells *in vitro*.

5.4.1. CIN in 2D

The purpose of this part of the investigation was to analyse and compare the cumulative CIN percentages in and between different breast cancer cell lines grown in 2D. The study aimed to enhance understanding of the heterogeneity in breast cancer and how varying levels of CIN can influence tumour behaviour, progression, and treatment responses. From a pathobiological perspective, the findings regarding CIN in breast cancer cell lines suggest a significant correlation between CIN levels and cancer prognosis.

The findings of this study revealed significant differences in the cumulative CIN percentages across various breast cancer cell lines, with the BT-549 cell line being particularly notable. BT-549 TNBC cells exhibited a cumulative CIN percentage of 46%, which is significantly different when compared to other cell lines tested, such as MCF-7(27%), SKBR3 (29%), and MDA-MB-231 (31%), indicating that BT-549 may have inherent genetic alterations that contribute to a higher level of CIN. CIN's impact on the TME is expected to affect the progress of metastatic seeding. Additionally, CIN also has direct effects that enhance metastatic potential (Bakhoum et al., 2018; Li *et al*., 2023). Genetic heterogeneity caused by CIN allows cancer cells to develop traits that boost their invasive abilities, improve their survival in the CIN, which is a predominant characteristic of cancers that can influence metastasis and contribute to drug resistance. This instability can be induced by existing therapies such as paclitaxel and radiation, making it a focal point for innovative anticancer strategies. Therefore, gaining a comprehensive understanding of the mechanisms behind CIN in cancer is essential for optimising both current and emerging treatment options. Prior experiments have convincingly shown that lagging chromosomes are the primary source of CIN in non-transformed cells and in certain CIN-positive cancer cell lines, which do not display misaligned chromosomes at the onset of anaphase (Tucker *et al*.,2023). In a study, where single-cell

sequencing and laboratory experiments were deployed indicated that CIN enables cancer cells to rapidly alter their chromosome numbers in response to drug exposure including paclitaxel allowing tumor cells to survive therapeutic pressure, explaining why high CIN levels often lead to faster treatment failure. (Lukow *et al*., 2021). Other comparable studies employing various CIN-induction methods, different cell lines, and similar anti-cancer treatments, including paclitaxel and topotecan, also indicated that CIN can lead to drug resistance (Ippolito *et al*., 2020).

MDA-MB-231 cells displayed CIN of 31%, which, although lower than that of BT-549, still indicates a substantial CIN, a characteristic also associated with the TNBC phenotype and aggressive behaviour. Both BT-549 and MDA-MB-231 are TNBC cell lines, but they exhibit different levels of CIN. BT-549 cells have a higher CIN than MDA-MB-231 cells, primarily due to differences in their genetic profiles, including the tumour suppressor gene PTEN. MDA-MB-231 cells exhibit an intermediate loss of PTEN, resulting in lower CIN but increased resistance to certain drugs. In contrast, BT-549 cells exhibit complete PTEN loss, resulting in higher CIN (Rieckhoff *et al*., 2020). The presence of a notable CIN in MDA-MB-231 may contribute to its metastatic potential, making it a viable model for studying therapeutic resistance in TNBC. The elevated CIN in TNBC cells is due to a more aggressive phenotype, due to its basal-like subtype, which is often associated with poorer prognosis and greater treatment challenges compared to other subtypes (Cosar *et al*., 2022; Foulke *et al*.,2010) who have explored the tumor characteristics in various breast cancer subtypes.

The statistically significant differences, marked by P values of 0.0076, 0.0100, and 0.0163 when compared with MCF-7, SKBR3, and MDA-MB-231, respectively, confirm that these observations are not due to random variation or experimental error. The results strongly support the premise that BT-549 might evolve through mechanisms distinct from those of the luminal (MCF-7) and HER2-positive (SKBR3) subtypes. In contrast, both MCF-7 and SKBR3 showed lower cumulative CIN percentages. MCF-7 cells, categorised as luminal A subtype, typically exhibit more stable genomic characteristics, which aligns with their lower CIN percentage of approximately 27%. This stability is often associated with a better therapeutic response, particularly to hormone therapies like tamoxifen, by inducing apoptosis (Li *et al*.,

2017). Similarly, SKBR3 HER+ cells, while more aggressive than MCF-7 cells, showed lower CIN compared to BT-549.

The implications of these findings are numerous. Understanding the differences in CIN levels among these cell lines can deepen our knowledge of breast cancer biology, specifically how CIN correlates with clinical outcomes and treatment responses. Furthermore, this could pave the way for investigating novel treatment strategies that specifically target high levels CIN in cancers cell lines like BT-549 and MDA-MB-231, which may be more susceptible to specific therapeutic approaches, such as those that exploit DNA damage response pathways. Vargas-Rondón (2020) examined the cytotoxic effects of chemotherapy agents on breast cancer cell lines that exhibited different degrees of CIN and clonal diversity. Their findings indicated that cell lines with higher levels of CIN and greater clonal heterogeneity exhibited reduced responsiveness to chemotherapy drugs. This implies that CIN and clonal heterogeneity might significantly influence drug resistance and the failure of treatment in breast cancer (Tripathi *et al*, 2019).

Studies indicate that metastatic breast cancers exhibit higher levels of CIN when compared to corresponding primary tumours. This instability is mainly caused by an increase in misaligned chromosomes during cell division, rather than lagging chromosomes (Tucker *et al*., 2023).

All these previous studies align well with this study, which suggests TNBC have higher CIN than other subtypes. The CIN observed in TNBC cell lines like BT-549 is particularly concerning, as these cancers lack targeted therapies, making them harder to treat and associated with poorer clinical outcomes. Several studies have indicated that increased CIN correlates with a worse prognosis, as higher levels are often related to tumour heterogeneity (Bakhoum & Landau, 2017; Birback *et al*., 2011; Swanton, 2012).

This study investigated chromosomal mutational events using the CBMN assay as a comprehensive tool for genotoxicity assessment. The CBMN assay was significant in its ability to elucidate gene amplification, chromosomal breakage, and chromosomal reorganisation. The CBMN assay is widely recognised in *in vitro* studies and has promising potential for *in vivo* applications, as highlighted by Fenech (2020 a).

MN were particularly significant when observed in BN cells, as their presence indicated a failure of normal cytoplasmic division, which is a hallmark of cytogenetic assessments aimed at detecting chromosomal damage after genotoxic exposures. This finding aligns with the results of Fenech (2007), who emphasised the importance of MN as indicators of chromosomal damage and stability. Other biomarkers indicative of CIN, such as NPBs and NBUDs, were systematically measured. The deployment of cyt-B in the CBMN assay acted as a blocker, inhibiting cytoplasmic division. This intervention resulted in the formation of contractile microfilaments, which restricted cell movement and facilitated nuclear extrusion, as reported by Hwang *et al* (2013).

5.4.2. CIN in 2D vs 3D

Having established the presence of differences in CIN attributable to pathobiological characteristics and related to prognosis, this study explored whether cell culture conditions would have an effect. For this purpose, in each different cell line, CIN levels in cells grown in 2D were compared to CIN levels of cells in 3D. The adaptation of the CBMN assay to 3D breast cancer models represented a groundbreaking innovation, advancing the established 2D approach to new heights. This represents an element of novelty, as this work has not been done before in breast cancer research, highlighting a potential impact on enhancing the accuracy of the assay in assessing genetic damage and cellular responses, which can lead to more reliable results that inform therapeutic strategies and cancer research. The shift from 2D to 3D models signifies a significant step forward in understanding the dynamics of breast cancer and improving the development of targeted treatments.

The findings from adapting the CBMN assay to 3D breast cancer models represent a significant advancement in breast cancer research. By moving from traditional 2D models to 3D models, this innovative approach enhances the accuracy of assessing genetic damage and cellular responses. The novelty of this work is particularly noteworthy, as it addresses a gap in existing research and provides insights that can inform more effective therapeutic strategies. Comparing CIN in both 2D and 3D environments is crucial, as it can reveal differences in how breast cancer cells behave in a more physiologically relevant setting. This can lead to a better

understanding of tumour dynamics and facilitate the development of targeted treatments based on more reliable data. Overall, these findings may have a substantial impact on improving patient outcomes by informing more precise treatment options and advancing the field of cancer research as a whole.

Additionally, this work, which compares CIN in 2D and 3D, has not been previously conducted in breast cancer research. Similar work was carried out, but for the adaptation of 3D liver models for genotoxicity testing of engineered nanomaterials (Conway *et al.*, 2020).

The findings demonstrated a substantial alignment with the initial hypothesis, indicating that the data collected effectively support the proposed theory. This suggests that the 3D cell culture models resulted in lower levels of CIN than the 2D cell culture models, with statistically significant differences between 2D and 3D in each of the four breast cancer cell lines analysed. The BT-549 cell line showed a 17% difference in CIN levels between 2D (46%) and 3D (29%) cultures, which was particularly significant. The robust statistical significance (P = 0.0001) suggests that the dimensionality of the culture conditions has a profound impact on CIN. This finding raises the possibility that 3D cultures, which more closely mimic the *in vivo* environment, may promote cellular behaviours and genetic stability that are crucial for developing targeted therapies. Similarly, the MDA-MB-231, MCF-7, and SKBR3 cell lines also exhibit notable differences between the two culture conditions, albeit with varying degrees of statistical significance. The statistically significant changes in CIN levels for MDA-MB-231 (31% in 2D vs. 25% in 3D) and MCF-7 (42% in 2D vs. 35% in 3D) suggest that even slight variations in the cellular microenvironment can influence genetic stability. The variations observed in these cell lines could reflect different biological behaviours driven by their diverse molecular characteristics. For instance, the MDA-MB-231 cell line, known for its aggressive behaviour, may be more susceptible to alterations in culturing conditions compared to others. The statistical significance noted in SKBR3 cells (29% in 2D vs. 19% in 3D, P = 0.0041) further consolidates the argument that a 3D culture system favours genetic integrity, a crucial consideration in both basic research and therapeutic development. The degree of chromosomal anomalies not only influences cancer prognosis but also has potential ramifications for drug resistance, making it imperative to account for the dimensionality of culture in experimental designs. Moreover, while the study provides significant insights, it is

also essential to address potential limitations. For instance, the biological relevance of CIN levels may differ based on cell line characteristics and their native microenvironments.

In terms of tissue structure between 2D and 3D culture models, mechanical forces exerted by the extracellular matrix, as well as the specific nutrients in the culture medium, all influence the accuracy of chromosome segregation during cell division. Consequently, culture conditions play a significant role in chromosome segregation, as evidenced by the variations observed in cultured epithelial cells compared to their native tissue environments (Knouse *et al*., 2018). For instance, cells grown in a medium that lacks the complexity of their native environment lead to alterations in gene expression and protein interactions, ultimately affecting how chromosomes are distributed during cell division. 3D architecture of native tissues provides mechanical cues and spatial organisation that are often missing in two-dimensional culture systems. These factors can help guide the proper alignment and separation of chromosomes, reducing the risk of aneuploidy. Therefore, understanding the impact of culture conditions on chromosome segregation is essential for improving cell culture techniques (Knouse *et al*., 2018).

3D models can modify the mechanical and biochemical properties of their microenvironment, leading to changes in gene expression. Cells grown in 3D models typically exhibit slower growth compared to those in 2D cultures. Therefore, 3D models accurately resemble the characteristics of a real tumour. This is supported by another study (Costard *et al.*, 2021), in which cancer cell lines (MCF-7 and BT474) demonstrated a slower growth rate in collagen-based scaffolds than in 2D cultures, thus better simulating the behaviour of cancer cells found in xenografts. Another research study showed a reduction in cell proliferation in 3D cultures when comparing a decellularised tissue matrix to chitosan/gelatin and poly-L-lactic acid scaffolds used as 3D culturing substrates (Li *et al*.,2018). This suggests that culture systems provide a more stable and supportive environment that mitigates factors contributing to CIN, thereby enhancing our understanding of tumour biology and potential therapeutic responses. However, the 3D structure of tumour tissue frequently exhibits irregularities, variability, and a lack of organisation, potentially impacting the mechanical microenvironment (*Rafik et al*.,2025). The various architectural characteristics of tissues, such as their shape, confinement, and fluid dynamics, exert different mechanical pressures on cancer cells within

the tumour. These mechanical pressures play a crucial role in affecting the behaviour of cancer cells and their capacity to invade (Almagro *et al*.,2022).

The physical microenvironment of the tumour microenvironment (TME), characterised by increased stiffness or fibrosis linked to tumours, can influence the biochemical microenvironment in various ways. Changes in the matrix can alter the diffusion of cytokine and growth factor gradients, thereby affecting the sequestration of growth factors. Numerous studies using 3D tumour models have contributed to understanding the connections between these aspects of the TME (Rafik *et al*., 2025). For instance, cells cultured in plastic tissue culture plates provide a simplified version of the ECM. However, by integrating higher dimensionality, such as 3D structures, the ECM becomes more intricate, resembling the 3D TME. Consequently, this approach presents a more realistic option for cancer modelling. (Kim, 2005; Antoni *et al*., 2015). Additionally, cells grown in culture plastic flasks tend to lose key features of cancer cells, including abnormal cell growth, 3D shape, expression of genes typical of cancer stem cells, and the ability to form connections with other cells and the surrounding matrix (Rijal & Li, 2016).

A crucial signalling pathway that stimulates cell proliferation on rigid substrates is the Yes-associated protein (YAP)/transcriptional coactivator with PDZ-binding motif (TAZ) pathway. In this pathway, heightened cellular tension, resulting from the formation of focal adhesions and RhoA activity, leads to the movement of YAP/TAZ into the nucleus, which in turn triggers the expression of target genes (Young & Reinhart, 2023). Recent research has identified essential proteins that facilitate cell growth on stiffer ECM surfaces. When cells are grown on increasingly rigid matrices, the time taken for mitosis decreases, whereas softer substrates lead to delays in metaphase, resulting in longer mitotic durations (Belaadi *et al*., 2022). Furthermore, the protein SUN2, located in the inner nuclear membrane, has been found to have increased expression levels on rigid substrates. It plays a role in how the ECM rigidity affects mitosis by aiding the positioning of astral microtubules at the spindle poles after the nuclear envelope breakdown (Jones & Jones, 2024).

Biomechanical forces from the extracellular environment can be transformed into signals within cells, a process known as mechanotransduction. This intricate mechanism involves various signalling molecules and events that occur sequentially and simultaneously

(Nagelkerke *et al*., 2015). For instance, integrins and cadherins at adherent junctions are mechanosensitive molecules at the cell surface, RTKs, and ion channels mainly detect physical signals (Przybyla *et al*., 2016). Integrins, as transmembrane proteins, bind various ECM proteins, which interact with the extracellular environment (Yu & Weaver, 2011), detecting the mechanical characteristics of the ECM and transmitting these signals to focal adhesion kinase (FAK). This process reinforces focal adhesions and initiates subsequent intracellular signalling pathways (Liu *et al*., 2020). Another major mechanosensor in the detection and transmission of force is E-cadherin (Spill *et al*., 2016), another transmembrane protein.
3D environment with compressed rat tail I collagen embedded cells provided ideal functioning for cell-to-cell adhesion, ECM chemical interactions, as the cells may have reduced DNA damage as the indicators of CIN in BN cells; MNi, NDP and NBUDs indicated in both this study, which is why human cancer cells cultured in 3D had less CIN evidence compared to 2D. NPB and NBUD biomarkers showed a higher rate in 2D, which is generally expected in 2D due to their association with DNA MMR and the fusion of chromosomal ends.

The implications of model systems in 3D cell culture systems are that they more accurately replicate the architectural complexity of tumours found *in vivo*. This allows for a better understanding of tumour behaviour, mechanics, and growth patterns compared to 2D cultures, which can oversimplify cellular interactions and the microenvironment.
The cancer microenvironment is widely recognised as a crucial factor in the disease, which has led to the suggestion that 3D models could provide a viable alternative to overcome the limitations of 2D and animal models (Costard *et al*., 2021). The differences observed in CIN levels between 2D and 3D cultures highlight the role of the mechanical and biochemical properties of the microenvironment in influencing cancer cell behaviour.

This understanding can lead to more targeted therapies that consider the physical characteristics of tumours. In terms of whether these findings were expected or unexpected, the results largely align with the existing literature, which suggests that 3D cultures more accurately reflect the *in vivo* environment than 2D cultures. While the shift to 3D models was anticipated based on previous studies, the specific outcomes regarding CIN and tumour behaviour may still lead to new insights that challenge existing paradigms and necessitate

further investigation. The findings imply that the 3D culture models not only provide insights into the fundamental biology of breast cancer but also may point towards novel approaches for prognosis and treatment that consider the role of CIN in tumour behaviour.

5.4.3. Clastogenic and Aneugenic Effects in CIN

In this study, the *in vitro* micronucleus assay was employed as a genotoxicity test to identify MN in the cytoplasm of interphase cells from MDA-MB-231, BT-549, MCF-7, and SKBR3 cell lines, both in 2D and 3D cultures. The cells were treated with cyt-B for 24 hours to inhibit cytoplasmic division, resulting in aneugenic and clastogenic effects. These effects were characterised by structural and numerical chromosomal aberrations observed in the 2D and 3D RAFT™ systems.

Aneugenic and clastogenic events were observed in all examined cell lines, driven by mechanisms like chromosomal breakage and gene amplification (EL-Zein *et al*., 2006) indicated that the CBMN assay is a test for genotoxicity that offers simultaneous insights into various types of chromosomal damage, including chromosomal breakage, rearrangements, and gene amplification. Its straightforward, quick, and sensitive nature makes the CBMN test an essential resource for screening and potentially prioritising cases for the early detection of diseases.

In molecular epidemiology, the frequency of MN is a critical biomarker for assessing chromosomal damage within human populations exposed to genotoxic agents (Fenech *et al*., 1999). Specifically, a micronucleus without a pancentromeric signal indicates a clastogenic event, an instance of DNA damage that arises from double-strand breaks, which can occur at any location along the chromosome. This type of damage disrupts the integrity of the chromosomal structure, leading to the formation of MN that fail to undergo proper processing and repair. Conversely, the detection of a micronucleus containing a pancentromeric signal signifies the occurrence of an aneugenic event. This type of event is characterised by errors in chromosomal segregation, typically resulting from the improper attachment of chromosomes to the spindle apparatus during cell division. In these scenarios, the spindle checkpoint, which usually ensures correct chromosomal alignment and

segregation, fails to function correctly, allowing errors to propagate through the daughter cells (Decodier & Kirsch-Volders, 2013; Fucic *et al*., 2023).

In summary, the formation of MN can be attributed to two distinct but related processes: clastogenicity, which involves unhealed DNA breaks, and aneugenicity, wherein segregation errors go unchecked due to spindle checkpoint failures, as elucidated by Fenech *et al*. (2020). Understanding these mechanisms is essential for elucidating the underlying pathways of genotoxicity and its implications for human health.

5.5. CIN associated with glycosidase inhibition

CIN may also correlate with alterations in glycosylation, presenting an avenue for targeted therapeutic strategies utilising glycosidase inhibitors. If CIN marks an initial step in tumour cell growth and migration, it could also signify accompanying changes in glycosylation patterns. This study was a proof-of-principle research investigation into the potential association between TNBC cells and glycosidase inhibitors, which could serve as a link to CIN. The hypothesis was that glycosidase inhibition increased CIN in breast cancer cells. Although the findings do not support the hypothesis due to the lack of a significant difference, some alterations were observed. In essence, these were the expectations based on what is known; our data show no significance, most likely due to the limited sample size. Further research is needed.

This connection is supported in the understanding of how glycoproteins influence cytoskeletal organisation and the stability of mitotic processes, particularly in the context of TNBC. One of the key findings from this research is that treatment with DNJ appears to increase CIN from 28% in untreated cells to 31% in DNJ-treated cells. While the increase might suggest a small effect of DNJ on chromosomal integrity, the lack of statistical significance raises concerns about the robustness of this observation. An increase of only 3% is marginal, especially in a biological context where numerous factors can influence CIN. This limitation may reflect the need for a larger sample size or more sensitive methodologies to better discern the effects of such compounds. Conversely, the other glycosidase inhibitors, 255 and 42, showed lower CIN levels (22% and 26%, respectively), suggesting a different interaction with cellular processes; however, these differences were not statistically significant. The decline in CIN in these cases could imply that these inhibitors might stabilise genomic integrity or not significantly interfere

with glycan structures. However, the lack of statistical significance for these findings indicates that further research is essential to validate these trends. However, the MN test showed that all inhibitor compounds had a slight increase in CIN%, except for compound 42. This means that when MDA-MB-231 cells were treated with glycosidase inhibitors, the MN test showed some genotoxicity damage, indicating the drugs may have caused DNA damage either through breakage or improper segregation. These compounds could also play an essential role as genotoxicity biomarkers.

Additionally, while the research provides valuable insights into the role of glycosidase inhibitors in maintaining chromosomal stability, it is crucial to consider the underlying biochemical mechanisms involved. The relationship between glycan modifications and mitotic stability promises to be complex. It is possible that the concentrations used, such as 0.5 mM for the glycosidase inhibitors, may not fully capture the biological response, underscoring the need for dose-response studies to elucidate efficacy and effects more clearly. Moreover, future research should focus on a broader array of cellular assays and mechanisms to better understand the role of glycosylation in CIN. Assessing additional cellular pathways and employing long-term cultured models could provide a more comprehensive understanding of how these compounds affect chromosomal integrity over time and in more complex biological systems. In summary, while this proof-of-principle study opens the door to investigating glycosidase inhibitors as potential modulators of CIN in TNBC cells, the findings underscore the need for more comprehensive studies to further elucidate the role of these inhibitors. A closer examination of the biological implications and a refinement of methodologies would be advantageous in establishing a more definitive connection between glycosidase inhibition and CIN.

There may be a connection between CIN and glycosylation, particularly in relation to the role of integrins in cancer. Integrins, which facilitate cell adhesion, are vital for cell signalling and can be affected by glycosylation. Changes in glycosylation patterns, commonly observed in cancer cells, may influence the function and signalling of integrins, thereby affecting cell behaviour and contributing to CIN.

Our study aligns with other studies that indicate how the trimming and processing of N-linked oligosaccharides influence the cell surface expression of the melanoma vitronectin receptor, a member of the integrin family of cell adhesion receptors. Specific inhibitors for β-

glucosidases I and II, including castanospermine and N-methyldeoxynojirimycin, were employed. Their inhibition delayed the assembly of the vitronectin receptor's α / β chain heterodimer and the cleavage of the α chain, resulting in reduced receptor expression on the cell surface. Conversely, when mannosidase I and II inhibitors, such as DNJ and swainsonine, were used, the vitronectin receptor was transported normally to the cell surface with its α chain N-linked oligosaccharides remaining sensitive to endoglycosidase H (Spiro *et al*.,1989)

Inhibitors of mannosidase can influence integrins. For instance, blocking α-mannosidases, such as with DNJ, can alter the processing of N-linked oligosaccharides on integrins. This alteration may result in modifications to their expression and function on the cell surface, affecting integrin-related cell adhesion, migration, and signalling.

Recent studies indicate that integrin-mediated adhesion plays a crucial role in regulating cell division through the formation of the mitotic spindle during mitotic entry and the final separation of cells during cytokinesis at mitotic exit. Any failure in these processes directly affects the other during each cycle, impacting genomic integrity. Research conducted in a study by Rani *et al*. aimed to elucidate how integrin signals operate during cell cycle stages under normal conditions, as well as the safety mechanisms that may prevent the formation of aneuploid cells when integrin signalling is defective (Rani *et al*., 2022).

The sequence of events initiated by integrin activates FAK, Src, or integrin-linked kinase (ILK) signalling, which may lead to unchecked mitogenic activity and survival, or excessive actin assembly. This process regulates mitogenic signalling and associated gene expression, impacting cell survival, proliferation, migration, self-renewal, EMT, and the preservation of cellular stemness. (Rigiracciolo *et al*., 2021).

Moreover, the use of glycosidase inhibitors reveals a complex interplay between them. In contrast, some inhibitors reduce CIN, while others may exacerbate it due to their effects on cellular stress, leading to apoptosis and metabolic reprogramming that disrupt growth and survival by altering glucose metabolism. Notably, the modulation of integrin signals through altered glycosylation patterns can directly impact mitotic spindle formation and cytokinesis, further contributing to genomic instability. This connection underscores the need for further experimental validation to elucidate the precise mechanisms driving CIN and its relationship with glycosylation and integrin function in cancer progression.

Another important observation is that reducing ATP levels through glucosidase inhibition can influence KIF18A, as KIF18A's activity relies on ATP hydrolysis. Inhibiting β-glucosidase reduces the ATP supply in the cell, thereby diminishing the energy available for KIF18A to traverse microtubules and align chromosomes, and disrupting its typical function. Perhaps the concentration of glycosidase inhibitors could be increased to cause a more significant effect and further disrupt microtubules and chromosome alignment. Since the metabolic activity significantly decreased when breast cancer cells were exposed to glycosidase inhibitors for 24 hours, this could be a link between glycosidase inhibition and CIN, for which further studies are needed to determine the answer. In a study similar to this investigation, a potent ATP inhibitor, VLS-1272, interfered with KIF18A's motor activity, resulting in its relocation away from microtubule plus ends. This disruption resulted in reduced chromosome congression and mitotic arrest. Additionally, ongoing chromosome instability and an active mitotic checkpoint contributed to the anti-proliferative effect of VLS-1272 (Phillips *et al*., 2025).

5.6 Summary

This study underscores the critical role of the tumour microenvironment in influencing CIN across various breast cancer cell lines. The significant reduction of CIN observed in 3D RAFT™ culture models compared to traditional 2D cultures suggests that 3D systems may provide a more biologically relevant platform for studying cancer dynamics and therapeutic responses. The value of the CBMN assay and the novelty of developing this assay for deployment in 3D culture models pave the way for potential therapeutic strategies that could yield better results, as the 3D models resemble the characteristics of real tumours and minimise the use of animals in research. Additionally, the study highlights the potential therapeutic implications of targeting glycosidase pathways impacting CIN. Overall, continued exploration of these mechanisms and the application of advanced culture systems could lead to improved cancer treatment and better inform management strategies. Overall, the effect of integrins and KIF18A in breast cancer cells may suggest a link between glycosidase inhibition and CIN; however, further work will be necessary to establish direct evidence. This chapter will be further discussed in Chapter 6.

5.7. Findings and novelty

- BT-549 had the highest CIN among the four cell lines studied in 2D.
- There was more CIN in 2D than in 3D.
- The research suggested that although there were minor increases in CIN with certain glycosidase inhibitors (from 28% to 31% for DNJ-treated cells), these increases were not statistically significant. Other inhibitors resulted in lower CIN levels (22% and 26%).
- The study used a concentration of 0.5 mM for the glycosidase inhibitors, which may not have fully captured the biological response. This highlights the necessity for dose-response studies to better understand the relationship between glycosidase inhibition and CIN.
- The lack of statistically significant differences in CIN levels across treatments suggests that larger sample sizes or more sensitive methodologies may be required to yield clearer conclusions.
- Novelty: Research indicated that cells in 3D models exhibit lower CIN than 2D counterparts. This suggests that 3D models could provide a more specific understanding of how cellular and environmental factors contribute to CIN as they mimic the characteristics of a real human tumour.
- This research presents a novel approach to examining the potential role of glycosidase inhibitors in modulating CIN in TNBC cells, an area that has received limited attention thus far.
- The study advances understanding of how alterations in glycosylation might contribute to chromosomal instability, offering a new perspective on the mechanisms that underpin cancer progression.
- By linking CIN with glycosylation changes, the study opens possibilities for targeted therapeutic strategies using glycosidase inhibitors, potentially leading to innovative treatments for breast cancer.

Chapter 6

Discussion

6. Discussion

TNBC is characterised by the absence of ER, PR, and HER2 receptors (Wolf *et al*., 2013), which leads to a poor prognosis and limited treatment options, predominantly relying on chemotherapy, radiotherapy, and surgery. This study aimed to investigate the hypothesis that modifying the glycocalyx of cancer cells may enhance chemotherapeutic penetration, specifically focusing on the effects of glycosidase inhibition on breast cancer cells in 2D and 3D cultures, with an emphasis on reducing metabolic activity, cell proliferation, and cell motility.

6.1 Glycosidase inhibition in 2D and 3D

In the 2D studies, glycosidase inhibitors such as DNJ and compound inhibitors from the Phytoquest company (255, 42, and 44) were used, either alone or in combination with doxorubicin. Various breast cancer cell lines were analysed for cell viability, metabolic activity, and migration after treatment, including MDA-MB-231 and BT-549 (TNBC), MCF-7, and SKBR3. Key findings indicated that glycosidase inhibition significantly sensitised breast cancer cells to doxorubicin, including MCF-7, SKBR3, MDA-MB-231, and BT-549 cells, notably reducing their metabolic activity. The combination treatment of doxorubicin and glycosidase inhibitors showed an additive effect, suggesting that altered glycoprotein processing could enhance drug efficacy by impairing cell survival pathways. This means that the implications of combining doxorubicin with glycosidase inhibitors are significant for cancer therapy. The observed synergistic effect suggests that targeting glycoprotein processing may enhance the effectiveness of chemotherapy by disrupting the cell survival pathway. This research could pave the way for the development of new combination therapies. This contribution to knowledge presents a potential therapeutic strategy for developing more potent glycosidase inhibitor compounds than DNJ, such as 255 and 42, against breast cancer cells.

Iminosugars, which serve as competitive glycosidase inhibitors, represent a promising yet challenging therapeutic approach in oncology. Preclinical studies have shown that these compounds can interfere with tumour metabolism, reduce metastasis, and help combat immune evasion. However, achieving effective systemic treatment without significant toxicity

remains a major challenge. Systemic administration can burden internal filtration organs, presenting as severe tissue damage at high or prolonged doses (Zhang *et al*., 2024).

In a Phase I study of swainsonine for cancer patients, acute elevations in serum aspartate aminotransferase were identified as the dose-limiting toxicity, particularly among patients with existing liver metastases, but patients ultimately discontinued treatment due to disease progression and systemic toxicities (Goss *et al*., 1994). The use of glycosidase inhibitors in cancer patients is a promising approach. This approach is being explored through several methods, including glycosidase-activated prodrugs, glycosylation disruptors, and repurposed anti-diabetic medications. While the expected tolerability of these treatments varies, it is important to note that systemic inhibitors often lead to gastrointestinal distress. In contrast, targeted glycosidase inhibitors, such as prodrugs, provide high tumour specificity and excellent systemic tolerability (Martin *et al*., 2022).

The findings suggest that glycosidase inhibition has a potent effect on breast cancer cells, including MCF-7, SKBR3, MDA-MB-231, and BT-549. This is another contribution to knowledge that highlights the notable reduction in the metabolic activity of breast cancer cells, indicating that glycosidase inhibition may interfere with the cells' ability to sustain their growth and proliferation. This effect could have important implications for cancer therapy, as it suggests that targeting glycosidases may enhance the effectiveness of existing treatments or serve as a potential standalone approach in different breast cancer subtypes. Researchers evaluated the effects of DNJ on MCF-7 (ER^+) cells. The DNJ combined with kaempferol, a natural flavonoid polyphenol antioxidant, exhibited significant antiproliferative effects. They successfully inhibited cell migration and arrested the cell cycle at the S phase. The derivatives induced cell apoptosis via the mitochondria-mediated pathway, triggered the release of ROS, and downregulated COX-2 expression (Zhang *et al*., 2021). However, there is no clinical evidence for instance, that DNJ works to treat ER-positive breast cancer in humans. Although some early laboratory research indicates that DNJ may have an impact on breast cancer cells *in vitro*, it has never been approved for use or tested in human clinical trials for this condition. Furthermore, it cannot replace or replicate the established, life-saving effects of standard hormone therapies such as tamoxifen (Hlaing *et al*., 2022).

This study exclusively focused on TNBC because current treatment options for patients are limited to chemotherapy, surgery, radiotherapy, immune checkpoint inhibitors, and antibody-drug conjugates. Chemotherapy agents, particularly anthracyclines like doxorubicin, taxanes, and platinum compounds, remain the cornerstone of TNBC therapy (Wagle *et al*., 2025; Zhu et al., 2023).

Additionally, the diversity of the cell lines tested implies that this strategy could be applicable across different subtypes of breast cancer, which is critical given the heterogeneity of the disease. Further investigation would be essential to understand the underlying mechanisms by which glycosidase inhibition affects metabolic activity and to evaluate the potential for translating these findings into clinical applications. Overall, these results point toward a promising avenue for enhancing breast cancer treatment strategies.

Statistical analyses confirmed significant reductions in metabolic activity across all treated cell lines, indicating an impact of imino-sugars on cell metabolism. The glycosidase inhibitors significantly reduced metabolic activity in the various cell types, disrupting glycosylation pathways and leading to improper protein folding, ER stress, and potentially apoptosis. (Amen *et al*., 2019; Wang *et al*., 2018; Bhattarai *et al*., 2021; Ricciardi & Gnudi, 2020).

The assertion that imino-sugars significantly impact cell metabolism, cell viability and cell motility by disrupting glycosylation pathways and leading to improper protein folding, ER stress, and potentially apoptosis does reflect a level of interpretation based on the findings from the cited studies in which investigation from the effects of glycosidase inhibitors on various cancer cell lines, provided evidence that these inhibitors reduced metabolic activity and disrupted the glycosylation process, which is essential for proper protein functionality. The study suggested that targeting glycosidases could offer a therapeutic approach by inducing stress responses in tumor cells (Amen *et al*., 2019). Wang et al. built upon these findings, highlighting the implications of altered glycosylation in relation to cancer progression. Their research illustrated a clear connection between reduced glycosylation and increased rates of apoptosis in treated cells. This supports the idea that imino-sugars could trigger cell death pathways through metabolic interference (Wang *et al*., 2018), thereby emphasizing the therapeutic potential outlined in the current study.

Another investigation examined the broader impacts of carbohydrate metabolism on cell survival under stress conditions. Their results confirmed that glycosidase inhibitors led to significant metabolic reductions in both non-cancerous and cancerous cells. The cells experienced ER stress, indicating that correct glycosylation is crucial for maintaining cellular homeostasis (Bhattarai *et al*., 2021). Furthermore, another study provided insights into the mechanisms of ER stress induced by glycosidase inhibition. They discovered that dysregulated glycosylation pathways contribute to the activation of stress response pathways, including the UPR, leading to apoptosis in various cell types (Ricciardi & Gnudi, 2020). Notably, only the TNBC cell lines MDA-MB-231 and (BT-549 used only for preliminary gene expression studies) were chosen to be tested due to their aggressive nature.

This study aligns similarly with the synergistic effect of β-glucosidase inhibitors when combined with doxorubicin, which sensitised breast cancer cells to the chemotherapy drug. The researchers evaluated breast cancer cells that were depleted of β-glucosidase using Conduritol B Epoxide, a potent β-glucosidase inhibitor known for its high selectivity in targeting lysosomal β-glucosidase. They found that these breast cancer cells became more susceptible to chemotherapeutic agents like doxorubicin in both *in vitro* and *in vivo* models with mice. The study revealed that β-glucosidase expression and activity were significantly increased in breast cancer tissues. This overexpression activated the PI3K/Akt/mTOR signalling pathway, resulting in uncontrolled tumour growth. The researchers concluded that inhibiting β-glucosidase alone was sufficient to suppress cancer cell proliferation and induce apoptosis. Thus, they proposed that β-glucosidase acts as a tumour-promoting enzyme, and its inhibition presents a promising strategy to overcome chemotherapy resistance in breast cancer (Zhou *et al*., 2017).

These studies support the findings of this work done at the University of Westminster, in which the glycosidase inhibitors were observed to have had an affect on breast cancer cells by reducing metabolic activity, reducing cell numbers, reducing cell motility and a synergistic effect when doxorubicin was combined with most of the inhibitor compounds (DNJ, 255 and 42). Researchers have demonstrated that DNJ decreased the viability and survival of cancer cells, with a more pronounced effect on glioblastoma cells compared to gastric adenocarcinoma cells. The most significant finding was that DNJ did not cause significant

cytotoxicity in healthy MRC5 cells, indicating a promising therapeutic window (Fonseca *et al*., 2024). Researchers tested DNJ and related iminosugars on various cancer cell lines. They found these natural products, such as N-alkyl-1,5-dideoxy-1,5-imino-l-fucitols and N-(8-(3-ethynylphenoxy)octyl-1-deoxynojirimycin, exhibit strong cytotoxic and antiproliferative effects. The compounds inhibit tumor growth by blocking enzymes like α-glucosidase, restricting the cancer cells' glucose supply, inducing oxidative stress, and triggering apoptosis. The cytotoxic and antiproliferative effects of DNJ showed similar outcomes across different cancer cell lines such as lung, breast, colon, brain, cervical and leukaemia (Zhao *et al*., 2010; Zhou *et al*., 2019; Tang *et al*., 2020).

In another study on rat hepatocytes, researchers used three glucosidase inhibitors (DNJ, N-methyl-DNJ and castanospermine) to understand N-linked glycosylation pathways. They discovered that while all three inhibitors altered oligosaccharide processing, DNJ uniquely disrupted both trimming and initial de novo protein glycosylation. In the presence of the glucosidase inhibitors, glucosylated high-mannose-type oligosaccharides accumulated. whereas the others primarily affected later trimming steps, in which N-methyl-1-DNJ and castanospermine led to the accumulation of primarily triglucosylated oligosaccharides or complex glycoproteins (Gross *et al*., 1986).

Glycosidase inhibitors disrupt N-linked glycosylation by blocking the sequential trimming of glucose residues in the endoplasmic reticulum. By preventing correct glycoprotein folding, this mechanism induces severe ER stress and halts the maturation of crucial viral and cancer-promoting glycoproteins, offering significant therapeutic potential (reviewed by Oo *et al*., 2025).

The compound inhibitors from Phytoquest (specifically compounds 255 and 42) have not been previously explored, making this the first instance of testing these compounds on breast cancer cell lines. Based on existing literature, it is speculated that these compound inhibitors may affect glycosylation pathways. This speculation draws from the observed effects of DNJ on breast cancer cells. The results generated in this study support the interpretation of findings from the studies mentioned earlier.

The discovery of glycosidase inhibitors as agents that significantly reduce metabolic activity across different cell types presents a novel approach to understanding and manipulating glycosylation pathways. This research highlights the intricate relationship between glycosylation processes and protein homeostasis, revealing how disruptions can lead to improper protein folding, subsequent ER stress, and even initiation of apoptosis.

N-linked glycosylation in the ER is a critical cotranslational modification required for proper protein folding, stability, and solubility. Glycans serve as temporal and spatial indicators for glycoprotein quality control systems (such as the calnexin/calreticulin pathways), directing newly synthesised proteins toward their proper configurations (Cherepanova *et al*., 2016). When glycosylation is disrupted, proteins frequently fail to attain their correct 3D structures. This results in the buildup of misfolded or unfolded proteins within the lumen, a phenomenon referred to as ER stress. In response, the cell initially activates the UPR to restore proteostasis by increasing chaperone production and reducing translation (Malhotra & Kaufman, 2007). Thus, Inhibition of glycosidase activity acts as a direct structural barrier to proper protein folding, leading to rapid breakdown of proteostasis (protein homeostasis) and initiating apoptosis via the calnexin/calreticulin pathway (Wang and Wu, 2019).

The implications of these inhibitors provide a new avenue for therapeutic interventions in diseases characterised by glycosylation anomalies, underscoring their potential role in enhancing our understanding of cellular stress responses and in developing targeted strategies for disease treatment. Glycosidase inhibitors serve as critical therapeutic interventions for diseases involving altered glycosylation by preventing the formation of misfolded proteins, blocking viral entry, or acting as pharmacological chaperones to stabilise mutant enzymes (Asano 2003, Mehta *et al*., 1998). In lysosomal storage disorders, iminosugars (e.g., miglustat, isofagomine) act as pharmacological chaperones. They stabilise mutant lysosomal enzymes during protein folding, preventing the ER quality-control system from prematurely destroying them as the enzymes can safely reach the lysosomes to function (reviewed by Parenti *et al*., 2014).

Instead of replacing the missing enzymes causing the disease, Researchers have used substrate reduction therapy for Type 1 Gaucher disease by deploying iminosugars (like

miglustat) to partially block the enzyme that builds glycosphingolipids. This depletes harmful lipid buildup in preclinical models, and clinical trials confirm it successfully reduces liver and spleen volumes while improving blood parameters (Butters *et al*., 2005). A research study on late-onset Pompe disease, a lysosomal storage disorder, was conducted, in which N-butyl-DNJ was used in a phase III, double-blind, randomised clinical trial (NCT03729362) to assess the efficacy and safety of intravenous ATB200 co-administered with oral AT2221 (N-butyl-DNJ) in adults. They found that cipaglucosidase alfa (ATB200), combined with miglustat (AT2221), safely improved and stabilised motor and lung function in adults with Late-Onset Pompe disease. Long-term extension data demonstrate durable, clinically meaningful therapeutic benefits for patients (Schoser *et al*., 2021).

Viruses manipulate the machinery of host cells to heavily glycosylate their surface envelope proteins, which helps them evade the immune system. Enzyme inhibitors that target glucosidases in the endoplasmic reticulum (like castanospermine and DNJ) prevent the proper trimming of N-linked glycans. By interfering with the proper folding of viral envelope proteins, this disruption severely impairs the virus's capacity to assemble, infect, and replicate (reviewed by Wang *et al*., 2025). Additionally, glycosidase inhibitors like DNJ exhibit broad antiviral properties (Ji &Li, 2020; Dahiya *et al*., 2025), including both enveloped DNA viruses, as HBV and positive-strand RNA viruses, flaviviruses, such as bovine viral diarrhoea virus, dengue virus, and West Nile virus (Gu *et al*., 2007)

In a research study, miglustat, migalastat, miglitol, and swainsonine were utilized as lead compounds. The researchers also designed three types of glycosidase inhibitors α-glucosidase, α-galactosidase, and mannosidase—and conducted docking simulations to estimate their binding affinities. They identified two highly effective α -glucosidase inhibitors, with one compound being the most potent iminosugar-based anti-SARS-CoV-2 agent discovered so far, exhibiting an EC_90 value of 1.94 against the Omicron BA.1 variant in A549-ACE2 cells. While they observed that mannosidase inhibitors had some activity, they were excessively toxic, and α-galactosidase inhibitors displayed no antiviral properties. Consequently, the iminosugars hinder the function of host ER α -glucosidases, which prevents the virus from correctly folding its Spike proteins and disrupts viral replication (Ferjanci *et al*., 2024).

These findings suggest potential applications for iminosugars in cancer therapy. Furthermore, cells treated with glycosidase inhibitors resulted in decreased cell numbers, with uncertainties about whether this was due to apoptosis or changes in glycosylation. The study revealed a correlation between DAPI staining and metabolic activity affecting all breast cancer cell lines. alteration of glycans in lectin staining assays indicated altered glycosylation and increased accumulation of glycans on the surfaces of breast cancer cells, resulting from the inhibition of glycosidases. Various inhibitors showed significant differences in binding, correlating with increased glucose, mannose, and fucose residues. All cell lines treated with glycosidase inhibitors exhibited altered cell motility, with compound inhibitor 255 significantly reducing the motility of SKBR3 and MDA-MB-231 cells.

This may have altered glycocalyx composition, changing cell motility, which correlates with other research (Ono and Hakomori, 2003), in which glycosylation played a significant role in modulating the motility and invasiveness of tumour cells. This is supported by evidence that *GM3*, a type of glycosphingolipid, demonstrates inhibitory effects on various human tumour cell lines. Specifically, studies have noted that the LDLD cell line, which exhibits elevated CD9 integrin α3 levels, forms a stable complex with GM3. This interaction appears to enhance the inhibition of cell motility, suggesting that the glycosylation process can influence cellular dynamics and potentially limit tumour progression. The stable complex formed by CD9 and integrin α3 in the presence of GM3 further emphasises the importance of glycosylation in maintaining the structural integrity and function of cell surface proteins involved in tumour cell interactions and migration (Dodge *et al*., 2022). Overall, the data underscore the role of glycosidase inhibition in metabolic changes, glycoprotein accumulation, and the potential impact on cancer cell behaviour.

It has also been found that glycosidase inhibition impaired cell migration and movement. Research conducted elsewhere has demonstrated that this significantly reduces the glycosylation of CD147, disrupting its surface distribution at the leading edge and concurrently decreasing the expression of matrix metalloproteinase-9 (MMP-9), which results in reduced cell migration (Gonzales *et al*., 2020). This notable alteration, resulting from the inhibition, is also a potential therapeutic strategy. While MMP in cancer initially seemed promising, synthetic MMP inhibitors failed in Phase III clinical trials (Winer *et al*., 2018). The

unsatisfactory outcomes arose from widespread toxic effects, a lack of drug selectivity among MMP subtypes, and ineffective clinical trial designs that focused on late-stage disease rather than early metastasis (Fields, 2019).

This study further explored the effects of glycosidase inhibitors on TNBC cells using MDA-MB-231 3D tumoroids after they were optimised and adapted, which is a more accurate representation of tumour behaviour, and is crucial due to the aggressive nature of TNBC. Results showed that untreated tumoroids had significantly higher cell densities than treated ones, with compounds such as DNJ and all inhibitor compounds effectively reducing cell viability, proliferation, and motility. Among the tested compounds, 255 demonstrated the most substantial reduction in metabolic activity and cellular viability in 3D models, which correlates well with the 2D studies, highlighting its potential as a therapeutic agent for TNBC. Unlike in 2D models, MDA-MB-231 cells in 3D tumoroids displayed less resistance to therapy, indicating increased tumour heterogeneity and decreased CIN. Treatment with DNJ, 42, and 255 also reduced cell motility, with 255 showing promise as a cytotoxic agent. This approach yielded novelty and a contribution to knowledge, as these compound inhibitors demonstrated an effect on cells grown in both 2D and 3D, resulting in significant differences in metabolic activity and cellular reductions compared to untreated cells.

The study used the RAFT™ 3D tumoroid system to create a collagen-rich microenvironment that mimics real tumours, emphasising the critical role of glycosylation in tumour behaviour. This study aligns well with other studies, such as those by Azimi *et al.* (2019) and Montebugnoli *et al*. (2025) (described in detailed in page 159 and 46 accordingly) in which they deployed 3D models to test drugs that altered glycosylation in breast cancer cells. In cell migration studies, the compound inhibitor 255 had the greatest effect on reducing cellular outgrowth into the acellular compartment and the number of invasive bodies compared with untreated tumoroids. Despite this, no significant differences were observed.

All compound inhibitors showed promising results both in 2D and 3D. Still, compound 255 showed the most significant effect on cells treated with glycosidase inhibition, including most likely the inhibition of β-glucosidase and β-mannosidase, as well as glycosyltransferase

pathways. This paves the way for improved therapeutic strategies. This may inhibit the catalysis of the enzymes involved in the first steps of glycosylation, leading to the accumulation of mannosidase and GlcNAc residues in N-linked glycans.

Additionally, glycosidase inhibition could influence processes such as cell adhesion, which is mediated by changes in glycosylation, thereby affecting how cells interact with surfaces in culture. Modifying growth surfaces may enhance cell attachment, impacting experimental outcomes. Understanding glycoprocessing enzymes is crucial for drug development and therapeutic strategies, highlighting their role in fundamental biology and applied sciences.

The novelty of this research lies in demonstrating the effectiveness of these specific compounds in reducing cell density in tumoroids, which more closely mimics *in vivo* tumour behaviour than traditional 2D cell cultures. Additionally, the use of the Phytoquest compound adds a unique dimension to the study, highlighting the potential of natural compounds in cancer therapy. This emphasis on the structural and functional changes in tumoroids provides critical insights into the mechanisms of action of these treatments. It opens avenues for further exploration of their therapeutic roles.

The observed effectiveness of glycosidase inhibitors, such as DNJ and Phytoquest compounds, in reducing cell viability and proliferation offers promising avenues for new therapeutic strategies targeting TNBC. This could lead to the development of more effective treatments that specifically cater to the aggressive nature of TNBC. By demonstrating the differential effects of treatments in 3D models, the study provides a framework for the screening of new compounds that may enhance drug efficacy through improved drug penetration and cellular interactions. This could be particularly vital for developing targeted therapies that combat ITH.

The changes in glycoprotein profiles resulting from glycosidase inhibition may alter cell signalling related to growth, survival, and immune response (Stowell & Cummings, 2015). This disruption leads to decreased cancer cell proliferation and increased susceptibility to chemotherapeutic agents, thereby enhancing the effectiveness of cancer treatment. Inhibiting glycosidases causes RTKs to misfold, leading to their degradation. This directly downregulates vital downstream growth and proliferation networks, including the

PI3K/Akt/mTOR pathways (Zhou *et al*., 2017). In a study, researchers investigated how α -glucosidase II influences non-small cell lung cancer progression. They found that it acts as a key regulator of tumour growth by controlling the folding and secretion of specific oncogenic proteins, highlighting it as a potential therapeutic target. By knocking out this enzyme using CRISPR-Cas9, ER stress was induced while simultaneously slowing cancer cell growth enabling the secretion of specific factors (like lysyl hydroxylase 2, tissue Inhibitor of metalloproteinase, and TGF-β) that actively break down and remodel the tissue environment to support tumour growth (Wang *et al*, 2026).

A study found that prolonged chemotherapy activates the GBA1 gene in gastric cancer cells. Researchers successfully sensitised both treatment-sensitive and treatment -resistance cancer cell to 5-FU by using siRNA to silence the GBA1 gene. This knock down improve the effectiveness by inducing lysosomal induction. Inhibiting β-glucosidase made resistant gastric cancer cells more responsive to chemotherapy drugs such as (5-FU), resulting in a marked decrease in tumor growth and improved survival rates. This effect was attributed to the disruption of lysosomes. Blocking β-glucosidase by knocking down GBA1 gene via sRNA, the integrity and function of lysosomes were compromised, which is essential for the survival and waste management of cancer cells (Li *et al*., 2021).

There have been studies where glycosidase inhibition can alter immune responses in breast cancer cells. Researchers investigated the parent compound kifunensine along with new hydrophobic acylated derivatives aimed at improving cellular absorption. They treated both primary mouse and human B cells with kifunensine and its newly synthesised acylated derivatives, like JDW-II-004 and JDW-II-010. These specific inhibitors effectively blocked Type I mannosidases, leading to a dose-dependent rise in the production of high-mannose N-glycans. Remarkably, the acylated derivatives showed enhanced effectiveness compared to the original drug. The use of these inhibitors noticeably disrupted B-cell receptor signalling in primary mouse B cells. This disruption was associated with notable alterations in surface receptors, including increased CD79b and decreased CD19 levels (Huang *et al*., 2022). Kifunensine is used to promote the consistent production of high-mannose N-glycans. In oncology, it plays a crucial role in glycoengineering by helping develop afucosylated monoclonal antibodies (such as rituximab) that exhibit enhanced efficacy in destroying cancer

cells (Huang *et al*., 2022). A research study examined how kifunensine affects primary human NK cells and cultured YTS-CD16a cells. Kifunensine is a compound that disrupts the usual maturation of N-glycans, leading to the retention of simpler, oligomannose-type N-glycans on the surface of the cells. The researchers subsequently evaluated the treated NK cells to observe changes in their antibody-binding affinity and their capacity to induce ADCC. The inhibition of N-glycan processing enhanced the antibody-binding affinity of the CD16a receptor on the NK cell surface. Furthermore, the treated NK cells showed increased ADCC effector function (Rodriguez Benavente *et al*., 2023).

The comparison between this study's 2D and 3D culture systems reveals fundamental differences in cellular behaviour and responses to glycosidase inhibitors, particularly in breast cancer treatment. While glycosidase inhibitors were shown to affect metabolic activity in 2D, the implications of these changes are also consistent in 3D models. However, the potential for more complex signalling pathways and cellular interactions in 3D cultures might elucidate additional mechanisms by which glycosidase inhibition could affect cell motility and invasiveness, as indicated by alterations in glycocalyx composition. The work presented in this study aligns with other research in 2D and 3D (Montebugnoli *et al.,* 2025; Azimi *et al*., 2019). Described in detailed in page 46 and 159 accordingly.

The variability in treatment responses between 2D and 3D cultures emphasises the importance of using multiple models when studying cancer therapies. While 2D systems can provide valuable insights into specific molecular and cellular responses to drug treatments, they often fail to encapsulate the complexity of tumour interactions *in vivo*. The findings from this study suggest that integrating both culture systems can lead to a more comprehensive understanding of breast cancer dynamics and therapeutic strategies.

Overall, the discussion between the 2D and 3D work highlights the need for continued exploration of advanced culture systems to develop more effective cancer treatment approaches, recognising that the richer biological context provided by 3D models may offer critical insights into tumour biology that 2D systems may overlook.

The diagram (Figure 6.1) illustrates two divergent cellular pathways of N-glycan processing in the Golgi apparatus: a normal physiological pathway (upper site) that leads to functional

proteins, and an inhibited pathway that triggers apoptosis. The process begins with an immature high-mannose glycan chain (depicted with green circles representing mannose residues and blue squares representing GlcNAc. The enzyme Golgi mannosidase cleaves several terminal mannose residues from glycan branches. The enzyme Golgi mannosidase cleaves several terminal mannose residues from the glycan branches (Tu *et al*., 2017). The Golgi mannosidases MAN1A1, MAN1A2, and MAN1C1 degrade the mannose residues of Man8GlcNAc2 to Man5GlcNAc2 (Molinary, 2007). Oligosaccharide complexes are formed after Man5GlcNAc2 is further processed by specific enzymes in the medial and trans-Golgi compartments (Tu *et al*., 2017). Additional sugar residues (such as GlcNAc, galactose, and sialic acids, shown as blue squares, yellow circles, and purple diamonds) are attached to form hybrid glycan structures that are essential for proper protein trafficking, stability, and cell signalling (Li *et al*., 2017).

The Inhibited Pathway (lower site) occurs when Golgi mannosidase is blocked by glycosidase inhibitors, specifically DNJ or experimental compound inhibitors 255,42. The normal trimming mechanism is blocked. Glycan accumulation occurs, and the molecule remains structurally stuck as a high-mannose glycan, thus forming an unfolded glycan structures (Gonzales-Andrades *et al*., 2020). The UPR mechanism triggers the accumulation of misfolded proteins resulting from ER stress (Rab *et al*., 2007). When the UPR is unable to reestablish ER homeostasis because of intense or extended stress, it activates apoptosis to remove cells that are beyond repair (Fribley *et al*., 2009).

By disrupting the dense glycocalyx, tumours become physically softer, more permeable to chemotherapeutic drugs, and more vulnerable to immune system attacks. Disruption of the glycocalyx leads to decreased cancer invasiveness and increased nuclear damage (Piplani *et al*., 2024). Other previous studies mentioned in this discussion chapter have shown that inhibition of glycosidases sensitises breast cancer cells to chemotherapeutic drugs, including doxorubicin and 5-FU (Zhou *et al*., 2017; Li *et al*., 2021). Glycosidase inhibitors halt the growth of complex mucin sugars, causing the tumour's protective sugar-protein barrier to break down. This structural collapse strips away the dense, bulky mucins (such as MUC1 and MUC16), opening up the tumour and allowing cancer-killing drugs to penetrate deep into previously unreachable areas (Costa *et al*., 2020). Researchers investigating N-glycosylation

inhibitors (such as tunicamycin) and MGAT1 gene knockdowns reported a partial loss of cell-surface levels of both MUC1 and MUC16 (Taniguchi *et al*., 2017). In another study, researchers discovered that inhibiting Golgi mannosidases causes immature N-glycans to be transported to the cell surface. This disrupts the cell-cell communication that relies on mature N-glycans, preventing the outer structure of the tumour from holding together (Koyama *et al*., 2020).

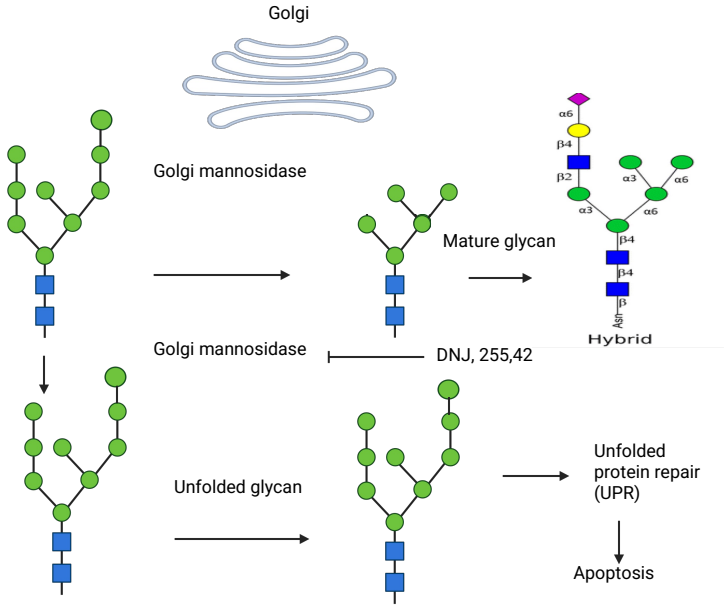

Figure 6.1. At the upper site, mannosidase trims the high-mannose glycoprotein, which then becomes a hybrid glycoprotein. At the lower site, Inhibition of Golgi α1,2-mannosidase I occurs with DNJ and a compound inhibitor (255, 42), potentially resulting in unfolded glycans being sent to the UPR and eventually leading to apoptosis.

The study introduces significant advancements in understanding the differential behaviours of breast cancer cells in 2D versus 3D culture systems, particularly in relation to glycosidase inhibitors. The novelty lies in the demonstration that glycosidase inhibition impacts metabolic activity across both culture types; however, the complexities inherent in 3D models reveal additional cellular signalling pathways and interactions that are not captured in 2D systems. This suggests that while traditional 2D cultures provide critical insights, they may not fully capture the dynamics of the tumour microenvironment.

The implications of these findings are substantial for cancer research and the development of cancer treatments. By highlighting the necessity of integrating both culture systems, the study

underscores the importance of a more nuanced understanding of tumour biology. This dual approach can enhance the predictive power of preclinical models, leading to more effective therapeutic strategies that consider the intricate behaviours and characteristics of tumours in a more biologically relevant context. Ultimately, this may lead to the development of more effective cancer treatments tailored to the complexities of human tumours, potentially improving patient outcomes. For example, Montebugnoli *et al*. (2025) found similar results in colorectal cancer cells treated with DNJ, noting decreases in cellularity and metabolic activity in 3D models. This finding aligns with the current study's results, which demonstrate that DNJ and other glycosidase inhibitors significantly reduce cell viability in TNBC tumoroids.

The similarities in glycosylation patterns across different cancer types suggest that insights gained from TNBC research may apply to other malignancies. For instance, many solid tumours, including pancreatic, colorectal, and ovarian cancers, exhibit alterations in NLG that correlate with tumour aggressiveness and poor patient outcomes. The therapeutic effects observed with glycosidase inhibitors in TNBC tumoroids may similarly impact these other cancers, particularly given that aberrant glycosylation often serves as a hallmark of malignant transformation. By targeting these common glycosylation pathways, similar strategies could be employed to enhance drug efficacy and patient survival across a variety of tumour types.

In other similar studies, the knockout of glucosidase II using CRISPR-Cas9 resulted in significantly decreased viability, migration, anchorage-independent growth, and RTK signalling activities in lung cancer cells (Khaodee *et al*., 2019). There is no doubt that the role of these compound inhibitors affecting β-glucosidase II was crucial in disrupting signalling pathways, resulting in a decrease in cell viability and migration. This study correlates well with the use of these inhibitors, mainly 255, which may affect other cancer cells.

Another aspect of this project is CIN in breast cancer models and the effect of culture conditions on CIN *in vitro*. CIN levels were evaluated using both 2D and optimised 3D RAFT^{TM} culture models. The findings indicated that 3D models presented statistically significantly lower levels of CIN compared to 2D models. This reduction could be attributed to the 3D environment, which may enable more efficient spindle functioning and partitioning of chromosomes during cellular division. Additionally, unlike 2D cultures, 3D environments

preserve key features of cancer cells and cell connectivity. The YAP/TAZ pathway is a significant signalling mechanism influencing cell proliferation on rigid substrates, with rigid matrices accelerating mitosis. (Belaadi *et al*., 2022). Lastly, the mechanotransduction allows cells to convert biomechanical signals from their environment into biological responses (Nagelkerke *et al*., 2015). Any disruption in these processes directly affects the others during each cycle, influencing genomic stability. A study by Rani *et al*. 2022 sought to clarify the functioning of integrin signals at various stages of the cell cycle under typical conditions, as well as the protective mechanisms that might avert the creation of aneuploid cells when integrin signalling is compromised (Rani *et al*., 2022).

The relationship between CIN and glycosylation, as explored in this study, serves as proof of principle, highlighting how glycosidase inhibitors can impact CIN. However, the observed effects were not statistically significant. Increased CIN in cells treated with specific inhibitors may have been linked to disrupted glycosylation, cell stress, altered cell cycle dynamics, and other factors that promote genomic instability. There may be a cause where integrins play crucial roles in the proper functioning of the mitotic spindle and glycosylation. However, further work on this topic needs to be explored, with a focus mainly on integrins by deploying biomarkers that indicate whether their levels are decreased due to glycosidase inhibition. This speculation aligns with other previous research demonstrating how glycosylation influences the expression of integrins, which are essential for cell adhesion and signalling (Rani *et al*., 2022). This indicates that specific glucosidase inhibitors were found to hinder the proper assembly of the melanoma vitronectin receptor, thereby affecting its cell surface expression. Conversely, inhibitors targeting mannosidases enhanced the transport of this receptor.

Inhibition of β-glucosidase can result in a reduction of integrin levels on the cell membrane. In particular, inhibiting β-glucosidase enzymes, which play a role in the processing of N-linked oligosaccharides, can disrupt the correct assembly and transport of integrin heterodimers, leading to a lower quantity of integrin present on the cell surface, as indicated by research (Spiro *et al*., 1989). This suggests that reducing the levels of specific integrins is generally seen as a beneficial strategy in cancer treatment, as elevated integrin expression is frequently associated with tumour growth, invasion, and metastasis (Liu *et al*., 2023).

Additionally, integrin-mediated adhesion plays a vital role in regulating cell division, and any disruption in this process can impact genomic integrity (Rigiracciolo *et al*., 2021). This study emphasises a complex interplay where some glycosidase inhibitors may reduce CIN, while others may exacerbate it due to their influence on cellular stress and metabolism. Further experimental validation is essential to understand these mechanisms and their implications.

Other observations regarding the interplay between ATP levels, β-glucosidase inhibition, and KIF18A activity present implications for understanding cell division and potential cancer therapies. The reliance of KIF18A on ATP hydrolysis underscores the crucial role of energy supply in cellular processes, such as chromosome alignment and microtubule dynamics. As noted, inhibiting β-glucosidase can diminish ATP availability, which likely leads to metabolic disruptions within the cell. This raises important questions about the extent to which manipulating energy levels in the mitochondria can impact mitotic processes, especially in cancer cells, which often exhibit altered metabolic profiles. The suggestion to increase the concentration of glycosidase inhibitors to achieve a more pronounced effect on microtubule dynamics warrants careful consideration. While this approach could amplify the initial findings, it is crucial to evaluate the potential for off-target effects and the overall biological consequences of such interventions. The observed decrease in metabolic activity when breast cancer cells are exposed to glycosidase inhibitors for 24 hours suggests a possible connection between glycosidase inhibition and CIN. However, further studies are necessary to determine whether this connection is causal or merely correlative. Determining the mechanisms underlying these effects could open new therapeutic avenues by targeting metabolic pathways in conjunction with traditional cancer treatments. The disruption of KIF18A's motor activity and its subsequent relocation from microtubule plus-ends, leading to reduced chromosome congression and mitotic arrest, underscores the critical relationship between energy metabolism and mitotic fidelity (Phillips *et al*., 2025). Further work is needed. Future research should aim to clarify the biological consequences of glycosidase inhibition, explore dose-response relationships, and determine the potential for combinatorial strategies that could enhance therapeutic efficacy while minimising adverse effects.

6.1. 2D limitations

2D cell culture has been the most common cell culture for decades. However, testing cells *in vitro* has limitations, as most treatments that are successful in 2D fail in clinical trials. Therefore, 3D culture models are more advantageous because they can more closely resemble the morphological characteristics of a human tumour (Kapalczynska *et al*., 2018). 3D culture models are expected to be more effective as they measure invasion and tumour interactions with the tissue microenvironment.

While four different breast cancer cell lines were used, each has unique characteristics and may not represent all subtypes of breast cancer. This limits the generalizability of the findings to other types of cancer or even other subtypes of breast cancer. While the study suggests alterations in glycoprotein processing due to glycosidase inhibition, the precise mechanisms behind these changes were not thoroughly examined. Further studies are needed to elucidate the pathways involved in the observed synergistic effects. The impact of glycosidase inhibitors may vary over time. The study may not have accounted for long-term effects or adaptations that cancer cells might develop in response to treatment.

6.2. 3D limitations

It is proposed that a thick glycocalyx serves as a protective shield, hindering the interaction between tumour cell ligands and the receptors on immune cells (Ghasempour & Freeman, 2023). By deploying a 3D synthetic bone matrix model, researchers found that the enhanced glycosylation of breast cancer cells led to a thicker glycocalyx surrounding the cancer cells. This thickening facilitated the cancer cells' ability to evade the cytotoxic effects of natural killer cells (Rafik *et al.,* 2025), while the study utilises 3D tumoroids to mimic human tumour conditions better, challenges remain in fully capturing the dynamic interactions and heterogeneity of tumour cells. As observed in various treatments, the differing responses to glycosidase inhibitors underscore the need for further investigation into the mechanisms of action and potential therapeutic applications to enhance efficacy in clinical settings. Additionally, the 3D structure of tumour tissue frequently exhibits irregularities, variability,

and a lack of organisation, potentially impacting the mechanical microenvironment (Rafik *et al*., 2025).

6.3. CIN Limitations

Further research incorporating a broader range of cell lines could provide more comprehensive insights into CIN across different cancer types. While the 2D and 3D culture models offer valuable insights, they may not wholly replicate the complex tumour microenvironment found *in vivo*. The lack of interactions with surrounding tissues and systemic factors could influence cellular behaviour and CIN levels. As the push for animal replacement continues, recreating *in vivo* conditions *in vitro* will become increasingly important.

Variability in the execution of the CBMN assay across different experimental setups could affect the reproducibility of results, necessitating standardisation of methodologies in future studies. Specifically, treating specific human breast cancer cell lines with cyt-B can lead to cytotoxic effects (Chang *et al*., 2016)

6.4 Future directions

Future research should focus on several key areas to build upon the findings of this study. Firstly, it is essential to conduct *in vivo* studies to validate the observed effects of glycosidase inhibitors and doxorubicin in a more clinically relevant environment, as results from *in vitro* models may not fully translate to human patients. Secondly, further investigation into the specific mechanisms by which glycosidase inhibition alters glycoprotein processing and cell survival pathways will provide insights into potential biomarkers for treatment response. Additionally, exploring combination therapies that integrate glycosidase inhibitors with immunotherapies or other chemotherapeutics could yield synergistic effects, thereby enhancing overall treatment efficacy. Lastly, the development of advanced 3D culture models and PDX could offer a more accurate representation of tumour biology and microenvironment interactions, ultimately improving the predictive power of preclinical studies.

We expect continued improvements in 3D tumoroid technology, leading to more sophisticated models that better mimic the *in vivo* tumour microenvironment. These advancements will enhance the accuracy of preclinical studies and facilitate the identification of effective therapeutic agents. As the field evolves, a shift towards personalised medicine in treating TNBC is foreseen. The ability to tailor glycosidase inhibitor therapies based on individual tumour characteristics and patient profiles will likely improve treatment outcomes and reduce adverse effects. With promising preclinical results, we anticipate that glycosidase inhibitors will progress towards clinical trials, with the expectation of gaining regulatory approvals for use in TNBC treatment. This would mark a significant milestone in expanding therapeutic options for patients. Future research is expected to integrate multi-omics approaches, including genomics, proteomics, and metabolomics, to provide a holistic view of the tumour biology. Such integration may uncover novel biomarkers for predicting treatment response and resistance.

As research continues to uncover the intricate mechanisms underlying these processes, it becomes clear how altered glycosylation patterns affect integrin and the disruption of KIF18A's motor activity that contribute to CIN. This could lead to a more nuanced understanding of the cellular pathways involved in cancer progression. Identifying specific glycosidase inhibitors that can either reduce or exacerbate CIN opens avenues for targeted therapies. These treatments could harness the effects of glycosylation modulation to promote genomic stability and impede tumour growth. Advanced genomic profiling and detailed cell cycle analysis will likely yield actionable insights into the relationship between CIN, cellular stress responses, and glycosylation. This integrative approach could help identify biomarkers for early detection and therapeutic response. Further exploration of integrin-mediated signalling roles during different cell cycle stages is expected. Understanding how integrins contribute to mitotic spindle formation and cytokinesis will clarify their potential as therapeutic targets for these processes. The complexity of CIN and glycosylation may lead to increased interdisciplinary collaborations among cancer biologists, biochemists, and medical researchers. Future studies may uncover additional regulatory and safety mechanisms that prevent aneuploidy when integrin signalling is impaired. This could provide insights into how cells maintain genomic integrity despite stress. Overall, the future of research in CIN and

glycosylation holds great promise, with the potential for significant advancements in the understanding and treatment of cancer.

Based on the findings regarding the impact of 3D cell culture models on CIN and tumour biology, several future expectations can be outlined, such as 3D culture models providing a more accurate representation of the TME. Future research will likely deepen our understanding of cancer cell behaviour, interaction dynamics, and the factors contributing to CIN. This could lead to the identification of specific molecular pathways and markers that are critical in cancer progression. Additionally, with a better understanding of the biophysical and biochemical interactions within the TME, researchers can develop more targeted therapeutic approaches. This includes the potential to discover novel drug candidates that more effectively treat different cancers by leveraging the characteristics observed in 3D models. Continued advancements in bioengineering are likely to enhance the complexity and functionality of 3D models, creating more biologically relevant systems that mimic aspects of *in vivo* tumour behaviour. This progression could improve the predictive power of preclinical studies. As 3D models gain acceptance in research and clinical applications, there may be an evolution in regulatory frameworks addressing their use. Ethical considerations surrounding the development and implementation of more personalised and effective cancer treatments using 3D models will also emerge. Overall, the future of cancer research holds exciting potential, driven by the advancements in 3D culture systems and a deeper understanding of the intricacies within the tumour microenvironment.

Future expectations in studying CIN and its relationship with glycosylation and integrin function in cancer are promising and multifaceted.

As research continues to uncover the intricate mechanisms underlying these processes, it becomes clear how altered glycosylation patterns affect integrin functionality and contribute to CIN. This could lead to a more nuanced understanding of the cellular pathways involved in cancer progression. Identifying specific glycosidase inhibitors that can either reduce or exacerbate CIN opens avenues for targeted therapies. These treatments could harness the effects of glycosylation modulation to promote genomic stability and impede tumour growth. Advanced genomic profiling and detailed cell cycle analysis will likely yield actionable insights into the relationship between CIN, cellular stress responses, and glycosylation. This integrative approach could help identify biomarkers for early detection and therapeutic

response. Further exploration of integrin-mediated signalling roles during different cell cycle stages is expected. Understanding how integrins contribute to mitotic spindle formation and cytokinesis will clarify their potential as therapeutic targets for these processes. The link between metabolic reprogramming, glycosylation, and CIN will likely gain traction.

Researching how cancer cells adapt their metabolic processes in response to altered glycosylation could reveal new therapeutic strategies. The complexity of CIN and glycosylation may lead to increased interdisciplinary collaborations among cancer biologists, biochemists, and medical researchers. Future studies may uncover additional regulatory and safety mechanisms that prevent aneuploidy when integrin signalling is impaired. This could provide insights into how cells maintain genomic integrity despite stress. Overall, the future of research in CIN and glycosylation holds great promise, with the potential for significant advancements in the understanding and treatment of cancer. On the other hand, further studies should investigate the downstream effects of reduced ATP levels on other mitotic proteins and processes to understand the broader implications of glycosidase inhibition on cell division and chromosome stability. This could encompass a comprehensive analysis of how KIF18A's impairment influences the dynamics of other molecular motors and may affect cancer cell proliferation.

Conclusion

In conclusion, this study highlights the promise of glycosidase inhibitors as a transformative approach in treating TNBC. By altering the glycocalyx of cancer cells, the iminosugars used in this study may enhance the sensitivity of tumours to chemotherapeutic agents, particularly doxorubicin, while also influencing key cellular processes such as metabolic activity and motility. The findings suggest that glycosidase inhibitors have the potential to alter metabolic activity, induce glycoprotein accumulation, impair cell migration, and modulate apoptosis pathways in breast cancer cells. The evidence supports further exploration of iminosugars as a promising addition to cancer treatment strategies, particularly in enhancing the efficacy of existing therapies and overcoming drug resistance. Understanding the intricate relationship between glycosylation, metabolic processes, and cell behaviour may lead to new

interventions that better target and manage breast cancer and possibly other malignancies characterised by glycosylation abnormalities.

3D models reveal significant insights into CIN and suggest that 3D cultures may mitigate factors contributing to CIN, enhancing our grasp of tumour biology and therapeutic responses. With the identification of MN as biomarkers, this study lays the groundwork for further investigation into glycosidase pathways as potential therapeutic targets, ultimately aiming to refine and improve treatment strategies for patients with this aggressive cancer type. This study highlights the importance of understanding how manipulating glycosidase activity affects chromosome alignment and cell division, potentially opening new avenues for therapeutic interventions targeting metabolic pathways. As we advance our knowledge of these mechanisms, it becomes clear that addressing CIN through innovative treatment strategies could enhance the efficacy of existing therapies while mitigating the risk of adverse effects. This highlights the crucial relationship between ATP regulation, glycosidase inhibition, and the potential impact on mitosis, suggesting that targeting these pathways could offer new approaches in cancer treatment. Further research will be necessary to validate these connections and explore potential therapeutic applications.

Novel contributions

- The disruption of N-linked glycosylation pathways by glycosidase inhibitors altered the glycocalyx of breast cancer cells, enhancing the uptake of chemotherapeutic agents such as doxorubicin.

- Iminosugars can alter metabolic pathways, presenting new avenues for cancer treatment.
- Impact of glycosylation modifications on cancer cell proliferation and survival in 2D and 3D culture models, potentially opening new research topics.
- Glycosidase inhibition impacts cancer cells in 2D by reducing metabolism, growth, and cell motility.
- Inhibition of glycosidases also affects MDA-MB-231 (TNBC) 3D tumoroids by decreasing metabolic activity, growth, and cell motility, thereby opening new possibilities for therapeutic treatments.
- The use of 3D tumoroid models to investigate the impact of glycosidase inhibitors on TNBC cell behaviour, in which 3D tumoroids more closely mimic *in vivo* conditions.
- Development of cell migration and particle analysis assays for 3D measurements.
- Adaptation of the CBMN in 3D culture models.
- 3D models exhibit lower CIN than 2D, suggesting that 3D models could provide a more specific understanding of how cellular and environmental factors contribute to CIN as they mimic the characteristics of a real human tumour.
- A proof of principle to examine the potential role of glycosidase inhibitors in modulating CIN in TNBC cells.
- The study advances understanding of how alterations in glycosylation might contribute to CIN, offering a new perspective on the mechanisms that underpin cancer progression.
- By associating CIN with glycosylation changes, the study opens the possibility of targeted therapeutic strategies using glycosidase inhibitors, potentially leading to innovative treatments for breast cancer cells.

References

Abraham, E., Sherman, H., Bergeron, A. (2020). Spheroids, Organoids Replacing Standard Cultures for Cell-Based Assays. Corning Life Sciences maintains that 3D cell cultures better capture *in vivo* conditions and are poised to improve drug screening. Vol 40, no 11. [Accessed

on 12 March 2021] Available from: https://www.genengnews.com/topics/drug-discovery/spheroids-organoids-replacing-standard-cultures-for-cell-based-assays/

Abu Samaan, T.M., Samec, M., Liskova, A., Kubatka, P. and Büsselberg, D., (2019). Paclitaxel's mechanistic and clinical effects on breast cancer. *Biomolecules*, *9*(12), p.789. Accessed on [21 October 2023]. Available from: https://www.mdpi.com/2218-273X/9/12/789

Adamczyk, B., Tharmalingam, T,. Rudd, P. (2012). Glycans as cancer biomarkers. Biochim Biophys Acta 2012, 1820:1347-1353 Accessed on [12 May 2021] Available from: http://dx.doi.org/10.1016/j.bbagen.2011.12.001.

Ahmed, S.A., Gogal Jr, R.M. and Walsh, J.E. (1994). A new rapid and simple non-radioactive assay to monitor and determine the proliferation of lymphocytes: an alternative to [3H] thymidine incorporation assay. *Journal of Immunological Methods*, *170*(2), pp.211-224. Accessed on [6 June 2025]. Available from: https://doi.org/10.1016/0022-1759(94)90396-4

Allen, A.K., Neuberger, A. and Sharon, N., (1973). The purification, composition and specificity of wheat-germ agglutinin. Biochemical Journal, 131(1), pp.155-162.

Almagro, J., Messal, H.A., Elosegui-Artola, A., van Rheenen, J. and Behrens, A. (2022). Tissue architecture in tumour initiation and progression. Trends in Cancer, 8(6), pp.494-505.

Al-Sohaily, S., Biankin, A., Leong, R., Kohonen-Corish, M, Warusavitarne, J. (2012). Molecular pathways in colorectal cancer. J Gastroenterol Hepatol; 27:1423–1431.

Al-Tassan, N., et al. (2002). Inherited variants of MYH associated with somatic G: C-->T: A mutation in colorectal tumours. Nat Genet; 30:227–232.

Al-Hajj, M., Wicha, M.S., Benito-Hernandez, A., Morrison, S.J. and Clarke, M.F., (2003). Prospective identification of tumorigenic breast cancer cells. Proceedings of the National Academy of Sciences, 100(7), pp.3983-3988.

Amado, M., Almeida, R., Schwientek, T. and Clausen, H. (1999). Identification and characterisation of large galactosyltransferase gene families: galactosyltransferases for all functions. *Biochimica et Biophysica Acta (BBA)-General Subjects*, *1473*(1), pp.35-53.

Ambros, R. A., & Kurman, R. J. (1993). Association of Ulex europaeus agglutinin I binding with invasion in endometrial carcinoma. *International journal of gynecological pathology: official journal of the International Society of Gynecological Pathologists*, *12*(4), 301–306 Assessed on [27 February 2025]. Available from: https://doi.org/10.1097/00004347-199310000-00004

Amen, O.M., Sarker, S.D., Ghildyal, R. and Arya, A. (2019). Endoplasmic reticulum stress activates unfolded protein response signaling and mediates inflammation, obesity, and cardiac dysfunction: therapeutic and molecular approach. *Frontiers in Pharmacology*, *10*, p.977. Accessed on [4 July 2025]. Available from: https://doi.org/10.3389/fphar.2019.00977

Amin, K., Tranchimand, S., Benvegnu, T., Abdel-Razzak, Z. and Chamieh, H. (2021). Glycoside hydrolases and glycosyltransferases from hyperthermophilic archaea: Insights on their characteristics and applications in biotechnology. *Biomolecules*, *11*(11), p.1557. Accessed on [22 June 2025]. Available from: https://doi.org/10.3390/biom11111557

Anderson, K.S. and Cresswell, P. (1994). A role for calnexin (IP90) in the assembly of class II MHC molecules. *The EMBO Journal*, *13*(3), pp.675-682. 306 Assessed on [27 February 2025]. Available from: https://doi.org/10.1002/j.1460-2075.1994.tb06306.x

Andrei, G. (2006). Three-dimensional culture models for human viral diseases and antiviral drug development. Antiviral Res, 71: 96–107.

Andrei, G., Duraffour, S., Van den Oord, J., Snoeck, R., (2010). Epithelial raft cultures for investigations of virus growth, pathogenesis, and efficacy of antiviral agents. Antiviral Res, 85: 431–449.

Anil-Inevi, M., Sağlam-Metiner, P., Kabak, E.C. and Gulce-Iz, S., (2020). Development and verification of a three-dimensional (3D) breast cancer tumor model composed of circulating tumor cell (CTC) subsets. Molecular Biology Reports, 47(1), pp.97-109.

Antoni, D., Burckel, H., Josset, E. and Noel, G. (2015). Three-dimensional cell culture: a breakthrough *in vivo*. International Journal of Molecular Sciences, 16(3), pp.5517-5527. Accessed on [10 July 2025]. Available from: https://doi.org/10.3390/ijms16035517

Apuri, S. (2017). Neoadjuvant and Adjuvant Therapies for Breast Cancer. Southern Medical Journal. 110(10):638–642. doi: 10.14423/smj.0000000000000703. PubMed PMID: 28973704; England.

Apweiler, R., Hermjakob, H., Sharon, N. (1999). The frequency of protein glycosylation, as deduced from analysis of the SWISS-PROTdatabase. Biochim Biophys Acta, 1473:4-8.

Arcamone, F., Cassinelli, G., Fantini, G., Grein, A., Orezzi, P., Pol, C., & Spalla, C. (1969). Adriamycin, 14-hydroxydaunomycin, a new antitumor antibiotic from S. peucetius var. caesius. *Biotechnology and Bioengineering*, *11*(6), 1101–1110. Accessed on: [10 June 2025]. Available from: https://doi.org/10.1002/bit.260110607

Arenas, M. I., Royuela, M., Fraile, B., Paniagua, R., Wilhelm, B., & Aumüller, G. (2001). Identification of N- and O-linked oligosaccharides in human seminal vesicles. Journal of andrology, 22(1), 79–87.

Arkesteijn, G.J.A., Erpelinck, S.L.A., Martens, A.C.M. and Hagenbeek, A., (1995). Chromosome specific DNA hybridization in suspension for flow cytometric detection of chimerism in bone marrow transplantation and leukemia. Cytometry: The Journal of the International Society for Analytical Cytology, 19(4), pp.353-360.

Arrowsmith, J.; Miller, P. (2013). Phase II, and Phase III attrition rates 2011–2012. Nat. Rev. Drug Discov. 12, 569. [Accessed on 24 March 2021]. Available from https://pubmed.ncbi.nlm.nih.gov/23903212/

Asano, N., (2003). Glycosidase inhibitors: update and perspectives on practical use. *Glycobiology*, *13*(10), pp.93R-104R. Accessed on [20 February 2024], available from: https://doi.org/10.1093/glycob/cwg090

Ashkenazi, A. and Dixit, V.M., (1999). Apoptosis control by death and decoy receptors. Current Opinion in Cell Biology, 11(2), pp.255-260. Accessed on [9th of January 2025]. Available from: https://doi.org/10.1016/S0955-0674(99)80034-9

Asselineau, D., Prunieras, M. (1984). Reconstruction of 'simplified' skin: control of fabrication. Br J Dermatol, 111 Suppl 27: 219–222

Attieh, Y. and Vignjevic, D.M., (2016). The hallmarks of CAFs in cancer invasion. European Journal of Cell Biology, 95(11), pp.493-502.

Augsten, M., (2014). Cancer-associated fibroblasts are another polarised cell type of the tumour microenvironment. Front. Oncol. 4,1–34

Aureli, M., Masilamani, A.P., Illuzzi, G., Loberto, N., Scandroglio, F., Prinetti, A., Chigorno, V. and Sonnino, S., (2009). Activity of plasma membrane β-galactosidase and β-glucosidase. *FEBS letters*, *583*(15), pp.2469-2473. Accessed on [26 June 2025]. Available from: https://doi.org/10.1016/j.febslet.2009.06.048

Avezov, E., Frenkel, Z., Ehrlich, M., Herscovics, A. and Lederkremer, G.Z., (2008). Endoplasmic reticulum (ER) mannosidase I is compartmentalized and required for N-glycan trimming to Man5–6GlcNAc2 in glycoprotein ER-associated degradation. Molecular biology of the Cell, 19(1), pp.216-225.

Ayyar, B.V., Arora, S. and O'Kennedy, R. (2016). Coming-of-age of antibodies in cancer therapeutics. Trends in Pharmacological Sciences, 37(12), pp.1009-1028.

Baldini, P., & Dwek, M. V. (2018). Glucosidase inhibitors change protein glycosylation in breast cancer cells and increase the binding of anti-HER2 antibodies. MSc thesis of the University of Westminster 1–38.

Bakhoum, S.F. and Landau, D.A., (2017). Chromosomal instability as a driver of tumor heterogeneity and evolution. Cold Spring Harbor perspectives in medicine, 7(6), p.a029611.

Bakhoum, S.F., Ngo, B., Laughney, A.M., Cavallo, J.A., Murphy, C.J., Ly, P., Shah, P., Sriram, R.K., Watkins, T.B., Taunk, N.K. and Duran, M., (2018). CIN drives metastasis through a cytosolic DNA response. *Nature*, *553*(7689), pp.467-472.

Banerjee, S., Ansari, A.A., Upadhyay, S.P., Mettman, D.J., Hibdon, J.R., Quadir, M., Ghosh, P., Kambhampati, A. and Banerjee, S.K. (2024). Benefits and pitfalls of a glycosylation inhibitor tunicamycin in the therapeutic implication of cancers. Cells, 13(5), p.395.

Bartsch, K., Knittler, K., Borowski, C., Rudnik, S., Damme, M., Aden, K., Spehlmann, M.E., Frey, N., Saftig, P., Chalaris, A. and Rabe, B., (2017). Absence of RNase H2 triggers generation of immunogenic micronuclei removed by autophagy. *Human Molecular Genetics*, *26*(20), pp.3960-3972. Accessed on [26 March 2024]. Available from: https://doi.org/10.1093/hmg/ddx283

Bashian, E.E., Paulson, J.C. and Wu, P., (2026). Sialic acids modulate immune responses in cancer: Therapeutic opportunities. Journal of Biological Chemistry, p.111245.

Bhatti, S., Kozlov, S., Farooqi, A., Naqi, A., Lavin, M., Khanna, K. (2011). ATM protein kinase: the linchpin of cellular defences to stress. Cell Mol Life Sci. 2011; 68:2977–3006.

Belaadi, N., Pernet, L., Aureille, J., Chadeuf, G., Rio, M., Vaillant, N., Vitiello, E., Lafanechère, L., Loirand, G. and Guilluy, C., (2022). SUN2 regulates mitotic duration in response to extracellular matrix rigidity. Proceedings of the National Academy of Sciences, 119(45), p.e2116167119. Accessed on [12 July 2025]. Available from: https://doi.org/10.1073/pnas.2116167119

Bendas, G., & Borsig, L. (2012). Cancer Cell Adhesion and Metastasis: Selectins, Integrins, and the Inhibitory Potential of Heparins. *International Journal of Cell Biology*, *2012*, 676731. https://doi.org/10.1155/2012/676731.

Bennett, E.P., Mandel, U., Clausen, H., Gerken, T.A., Fritz, T.A. and Tabak, L.A. (2012). Control of mucin-type O-glycosylation: a classification of the polypeptide GalNAc-transferase gene family. Glycobiology, 22(6), pp.736-756.

Bennett, E.P., Mandel, U., Clausen, H., Gerken, T.A., Fritz, T.A. and Tabak, L.A., (2012). Control of mucin-type O-glycosylation: a classification of the polypeptide GalNAc-transferase gene family. Glycobiology, 22(6), pp.736-756.

Bergeron, J.J., Brenner, M.B., Thomas, D.Y. and Williams, D.B., (1994). Calnexin: a membrane-bound chaperone of the endoplasmic reticulum. *Trends in biochemical sciences*, *19*(3), pp.124-128. Accessed on [22 June 2025]. Available from: https://doi.org/10.1016/0968-0004(94)90205-4

Beri, P.; Matte, B.F.; Fattet, L.; Kim, D.; Yang, J.; Engler, A.J. (2018). Biomaterials to model and measure epithelial cancers. Nat. Rev. Mater. 3, 418–430. Accessed on [10 April 2021] available on https://www.nature.com/articles/s41578-018-0051-6

Bernacki, R. J., Niedbala, M. J., & Korytnyk, W. (1985). Glycosidases in cancer and invasion. *Cancer Metastasis Reviews*, *4*(1), 81–101. Accessed on [17 June 2025]. Available from: https://doi.org/10.1007/BF00047738

Bhattarai, K.R., Riaz, T.A., Kim, H.R. and Chae, H.J., 2021. The aftermath of the interplay between the endoplasmic reticulum stress response and redox signalling. Experimental & Molecular Medicine, 53(2), pp.151-167. Accessed on [3 July 2025]. Available from: https://doi.org/10.1038/s12276-021-00560-8

Bishop, R., (2010). Applications of fluorescence in situ hybridisation (FISH) in detecting genetic aberrations of medical significance. *Bioscience Horizons*, *3*(1), pp.85-95.

Birkbak, N.J., Eklund, A.C., Li, Q., McClelland, S.E., Endesfelder, D., Tan, P., Tan, I.B., Richardson, A.L., Szallasi, Z. and Swanton, C., (2011). Paradoxical relationship between chromosomal instability and survival outcome in cancer. Cancer research, 71(10), pp.3447-3452.

Block, T.M., Deshmane, S., Masonis, J., Maggioncalda, J., Valyi-Nagi, T. and Fraser, N.W. (1993). An HSV LAT null mutant reactivates slowly from latent infection and makes small plaques on CV-1 monolayers. *Virology*, *192*(2), pp.618-630. Accessed on [June 22 2025]. Available from: https://doi.org/10.1006/viro.1993.1078

Boldescu, V., Behnam, M.A., Vasilakis, N. and Klein, C.D. (2017). Broad-spectrum agents for flaviviral infections: dengue, Zika and beyond. *Nature Reviews Drug Discovery*, *16*(8), pp.565-586. Accessed on [6 March 2025]. Available from: https://doi.org/10.1038/nrd.2017.33

Bonnet, D. and Dick, J.E., (1997). Human acute myeloid leukemia is organized as a hierarchy that originates from a primitive hematopoietic cell. Nature medicine, 3(7), pp.730-737.

Bordeaux, J., Orozco Bender, J., Vaupel, C., Geiss, G., Hinerfeld, D., & Balko, J. M. (2020). MEK activation modulates glycolysis and supports suppressive myeloid cells in TNBC. *JCI insight*, *5*(15), e134290. https://doi.org/10.1172/jci.insight.134290

Brancato, V., Gioiella, F., Imparato, G., Guarnieri, D., Urciuolo, F. and Netti, P.A., (2018). 3D breast cancer microtissue reveals the role of tumor microenvironment on the transport and efficacy of free-doxorubicin *in vitro*. Acta Biomaterialia, 75, pp.200-212.

Bray, F., Ferlay, J.; Soerjomataram, I.; Siegel, R.L.; Torre, L.A.; Jemal, A. (2018). Global cancer statistics 2018: GLOBOCAN estimates of incidence and mortality worldwide for 36 cancers in 185 countries. *CA Cancer J. Clin*, *68*, 394–424.

Breast Cancer Organization (2020). Triple-negative breast cancer. Breast Cancer Organization. [Accessed on 20 Feb 2021]. Available from: https://www.breastcancer.org/symptoms/diagnosis/trip_neg

Brien, C.O. and Murphy, P.V. (2011). Synthesis of 1-deoxynojirimycin derivatives from L-sorbose via wittig reactions. *Journal of Carbohydrate Chemistry*, *30*(7-9), pp.626-640. Assessed on [20 February 2024]. Available from: https://doi.org/10.1080/07328303.2011.619287

Brlek, P., Škaro, V., Hrvatin, N., Bulić, L., Petrović, A., Projić, P., Smolić, M., Shah, P. and Primorac, D., 2025. Advances in Precision Oncology: From Molecular Profiling to Regulatory-Approved Targeted Therapies. Cancers, 17(21), p.3500.

Brooks, S.A. and Leathem, A.J., (1991). Prediction of lymph node involvement in breast cancer by detection of altered glycosylation in the primary tumour. The Lancet, 338(8759), pp.71-74.

Brooks, S.A., (2000). Invited Reviews: The involvement of Helix pomatia lectin (HPA) binding N-acetylgalactosamine glycans in cancer progression. Histology and Histopathology, 15(1), pp.143-158.

Broustas, C.G. and Lieberman, H.B. (2014). *DNA Damage Response Genes and the Development of Cancer Metastasis.* Radiation Research Society. [Accessed on 30 September 2024]. Available from: https://doi.org/10.1667%2FRR13515.1

Brown, R.B., Hollingsworth, M.A. Schaffer, J.E. (2021). Protein Modifications | Mucin Family of Glycoproteins☆. In: Jez, J., (ed.) *Encyclopedia of Biological Chemistry III (Third Edition).* Oxford: Elsevier, 167-172.

Bull, C.F., Mayrhofer, G., Zeegers, D., Mun, G.L.K., Hande, M.P. and Fenech, M.F. (2012). Folate deficiency is associated with the formation of complex nuclear anomalies in the cytokinesis-block micronucleus cytome assay. *Environmental and molecular mutagenesis*, *53*(4), pp.311-323. Accessed on [27 March 2024]. Available from: https://doi.org/10.1002/em.21688

Butt, A.J., Firth, S.M. and Baxter, R.C., (1999). The IGF axis and programmed cell death. *Immunology and Cell Biology*, *77*(3), pp.256-262.

Butters, T.D., Dwek, R.A. and Platt, F.M., (2005). Imino sugar inhibitors for treating the lysosomal glycosphingolipidoses. Glycobiology, 15(10), pp.43R-52R.

Campos, D., Freitas, D., Gomes, J., Magalhaes, A., Steentoft, C., Gomes, C., ... & Reis, C. A. (2015). Probing the O-glycoproteome of gastric cancer cell lines for biomarker discovery. *Molecular & Cellular Proteomics*, *14*(6), 1616-1629. Accessed [28 June 2025]. Available from: https://doi.org/10.1074/mcp.M114.046862

Cantore, S.; Ballini, A.; Mori, G.; Dibello, V.; Marrelli, M.; Mirgaldi, R.; De Vito, D.; Tatullo, M. (2016). Anti-plaque and antimicrobial efficiency of different oral rinses in a 3-day plaque accumulation model. *J. Biol. Regul. Homeost Agent*, *30*, 1173–1178.

Carter, S.L., Eklund, A.C., Kohane, I.S., Harris, L.N. and Szallasi, Z., (2006). A signature of chromosomal instability inferred from gene expression profiles predicts clinical outcome in multiple human cancers. *Nature Genetics*, *38*(9), pp.1043-1048.

Cavo, M.; Caria, M.; Pulsoni, I.; Beltrame, F.; Fato, M.; Scaglione, S. (2018). A new cell-laden 3D Alginate-Matrigel hydrogel resembles human breast cancer cell malignant morphology, spread and invasion capability observed "*in vivo*". Sci. Rep. 2018, 8, 5333.

Cirri, P. & Chiarugi, P. (2012). Cancer-associated fibroblasts and tumour cells: a diabolic liaison driving cancer progression. Cancer Metastasis Rev. 31, 195–208.

Chaffer, C., L., & Weinberg, R., A., (2011). A perspective on cancer cell metastasis. Science 331, 1559–1564.

Chang, J., Guo, J. T., Du, Y., & Block, T. (2013). Imino sugar glucosidase inhibitors as broadly active anti-filovirus agents. *Emerging Microbes & Infections*, *2*(11), e77. Accessed on [17 June 2025]. Available from: https://doi.org/10.1038/emi.2013.77

Chang, J.M., Park, I.A., Lee, S.H., Kim, W.H., Bae, M.S., Koo, H.R., Yi, A., Kim, S.J., Cho, N. and Moon, W.K. (2013). Stiffness of tumours measured by shear-wave elastography correlated with subtypes of breast cancer. *European Radiology*, *23*, pp.2450-2458. Accessed on [23 March 2023]. Available from: https://doi.org/10.1007/s00330-013-2866-2

Chang, C. H., Qiu, J., O'Sullivan, D., Buck, M. D., Noguchi, T., Curtis, J. D. et al. (2015). Metabolic competition in the tumour microenvironment is a driver of cancer progression. Cell 162, 1229–1241.

Chang, H.T., Chou, C.T., Chen, I.S., Yu, C.C., Lu, T., Hsu, S.S., Shieh, P., Jan, C.R. and Liang, W.Z., (2016). Mechanisms underlying effect of the mycotoxin cytochalasin B on induction of cytotoxicity, modulation of cell cycle, Ca2+ homeostasis and ROS production in human breast cells. Toxicology, 370, pp.1-19. Accessed on [10 July 2025]. Available from: https://doi.org/10.1016/j.tox.2016.09.006

Chapel, C., Garcia, C., Bartosch, B., Roingeard, P., Zitzmann, N., Cosset, F.L., Dubuisson, J., Dwek, R.A., Trepo, C., Zoulim, F. and Durantel, D., (2007). Reduction of the infectivity of hepatitis C virus pseudoparticles by incorporation of misfolded glycoproteins induced by glucosidase inhibitors. *Journal of General Virology*, *88*(4), pp.1133-1143. Assessed on [20 February 2024]. Available from: https://doi.org/10.1099/vir.0.82465-0

Chavez, K.J., Garimella, S.V. and Lipkowitz, S., (2011). Triple negative breast cancer cell lines: one tool in the search for better treatment of triple negative breast cancer. *Breast Disease*, *32*(1-2), pp.35-48.

Chen, W., Hoffmann, A.D., Liu, H. *et al.* Organotropism: new insights into molecular mechanisms of breast cancer metastasis. *npj Precision Onc* 2, 4 (2018). https://doi.org/10.1038/s41698-018-0047-0.

Cherepanova, N., Shrimal, S. and Gilmore, R., (2016). N-linked glycosylation and homeostasis of the endoplasmic reticulum. Current opinion in cell biology, 41, pp.57-65.

Chojnowska, S., Kępka, A., Szajda, S.D., Waszkiewicz, N., Bierć, M. and Zwierz, K., (2011). Exoglycosidase Markers of Diseases. Accessed on [June 22 2025]. Available from: https://doi.org/10.1042/BST0390406

Christofori, G., Naik, P. and Hanahan, D., (1994). A second signal is supplied by insulin-like growth factor II in oncogene-induced tumorigenesis. *Nature*, *369*(6479), pp.414-418. Accessed on [10 January 2025]. Available from: https://doi.org/10.1038/369414a0

Cipolla, L., LAY, L., Nicotra, F., Pangrazio, C. and Panza, L., (1995). Synthesis of azasugars by Grignard reaction on glycosylamines. *Tetrahedron,* **51**(16), pp. 4679–4690. Accessed on [19 February 2025]. Available from: https://doi.org/10.1016/0040-4020(95)00151-W

Clevers, H. and Tuveson, D.A., (2019). Organoid models for cancer research. Annual Review of Cancer Biology, 3, pp.223-234.

Clevers, H., (2018). Organoids in cancer research. Nat Rev Cancer;18: pp. 407–18.

Cohen, E. (Ed.), (1974). Biomedical perspectives of agglutinins of invertebrate and plant origins. Ann. NY Acad. Sci. 234.

Compain, P. and Martin, O.R. eds., (2007). Iminosugars: From synthesis to therapeutic applications. John Wiley & Sons.

Contessa, J., N., B., M., S., Freeze, H., Ross, B., D., Rehemtulla, A., Lawrence, T.S. (2010). Molecular imaging of N-linked glycosylation suggests glycan biosynthesis is a novel target for cancer therapy. Clin Cancer Res, 16:3205-3214

Conway, G.E., Shah, U.K., Llewellyn, S., Cervena, T., Evans, S.J., Al Ali, A.S., Jenkins, G.J., Clift, M.J. and Doak, S.H., (2020). Adaptation of the *in vitro* micronucleus assay for genotoxicity testing using 3D liver models supporting longer-term exposure durations. *Mutagenesis*, *35*(4), pp.319-330.

Cosar, R., Sut, N., Ozen, A., Tastekin, E., Topaloglu, S., Cicin, I., Nurlu, D., Ozler, T., Demir, S., Yıldız, G. and Şenödeyici, E., (2022). Breast cancer subtypes and prognosis: Answers to subgroup classification questions, identifying the worst subgroup in our single-center series. *Breast Cancer: Targets and Therapy*, pp.259-280.

Costa, A.F., Campos, D., Reis, C.A. and Gomes, C., (2020). Targeting glycosylation: a new road for cancer drug discovery. *Trends in Cancer*, *6*(9), pp.757-766. Accessed on [28 June 2025]. Available from: https://doi.org/10.1016/j.trecan.2020.04.002

Costard, L.S., Hosn, R.R., Ramanayake, H., O'Brien, F.J. and Curtin, C.M., (2021). Influences of the 3D microenvironment on cancer cell behaviour and treatment responsiveness: A recent update on lung, breast and prostate cancer models. Acta Biomaterialia, 132, pp.360-378. Accessed on [10 July 2025]. Available from: https://doi.org/10.1016/j.actbio.2021.01.023

Crasta, K., Ganem, N.J., Dagher, R., Lantermann, A.B., Ivanova, E.V., Pan, Y., Nezi, L., Protopopov, A., Chowdhury, D. and Pellman, D., (2012). DNA breaks and chromosome pulverization from errors in mitosis. *Nature*, *482*(7383), pp.53-58. Accessed on [25 March 2024]. Available from: https://doi.org/10.1038/nature10802

Cristobal A, van den Toorn HW, van de Wetering M, Clevers H, Heck AJ, Mohammed S. (2017). Personalised Proteome Profiles of Healthy and Tumor Human Colon Organoids Reveal Both Individual Diversity and Basic Features of Colorectal Cancer. Cell Reports; 18:263-274.

Cummings, R.D. and Etzler, M.E., (2009). Antibodies and lectins in glycan analysis. Essentials of Glycobiology. 2nd edition.

Cytion, (2025). Breast cancer cell lines-BT-549. Assessed on [09 October 2025]. Available from: https://www.cytion.com/BT-549-Cells/300132

Dahiya, J., Kumar, G. and Narula, A.K., (2025). The multifaceted potential of azasugars: synthetic approaches, molecular interactions and therapeutic usage. Journal of Chemistry Letters, 6(2), pp.79-92.

Dashty, M., (2013). A quick look at biochemistry: carbohydrate metabolism. Clinical biochemistry, 46(15), pp.1339-1352. Accessed on [1 July 2025]. Available from: https://doi.org/10.1016/j.clinbiochem.2013.04.027

Davies, G.J., Gloster, T.M. and Henrissat, B., (2005). Recent structural insights into the expanding world of carbohydrate-active enzymes. *Current opinion in structural biology*, *15*(6),

pp.637-645. Accessed on [16 June 2025]. Available from: https://doi.org/10.1016/j.sbi.2005.10.008

Darby, I. A., Laverdet, B., Bonté, F. & Desmoulière, A. (2014). Fibroblasts and myofibroblasts in wound healing. Clin. Cosmet. Investig. Dermatol. 7, 301–311.

Davis, A., Gao, R., & Navin, N. (2017). Tumor evolution: linear, branching, neutral or punctuated? Biochim. Biophys. Acta Rev. Cancer 1867, 151–161.

De Angelis, M.L., Bruselles, A., Francescangeli, F., Pucilli, F., Vitale, S., Zeuner, A., Tartaglia, M. and Baiocchi, M., (2018). Colorectal cancer spheroid biobanks: multi-level approaches to drug sensitivity studies. *Cell Biology and Toxicology*, *34*, pp.459-469. Accessed on [20 February 2023]. Available from: https://doi.org/10.1007/s10565-018-9423-3

De Boer, J., Hoeijmakers, J., H. (2000). Nucleotide excision repair and human syndromes. Carcinogenesis. Mar;21(3):453-60. doi: 10.1093/carcin/21.3.453. PMID: 10688865.

Decordier, I. and Kirsch-Volders, M., (2013). Fluorescence in situ hybridization (FISH) technique for the micronucleus test. In Genotoxicity Assessment: Methods and Protocols (pp. 237-244). Totowa, NJ: Humana Press.

Dennis, J., W., Granovsky, M., Warren, C.E (1999). Glycoprotein glycosylation and cancer progression. Biochim Biophys Acta 1999, 1473:21-34.

Desgrosellier, J., S., and Cheresh, D., A. (2010). "Integrins in cancer: biological implications and therapeutic opportunities," *Nature Reviews Cancer*, vol. 10, no. 1, pp. 9–22.

Devine, M.J., Plun-Favreau, H. and Wood, N.W., (2011). Parkinson's disease and cancer: two wars, one front. *Nature Reviews Cancer*, *11*(11), pp.813-823. Accessed on [27 June 2025]. Available from: https://doi.org/10.1038/nrc3150

Dinur, T., Osiecki, K.M., Legler, G., Gatt, S., Desnick, R.J. and Grabowski, G.A., (1986). Human acid beta-glucosidase: isolation and amino acid sequence of a peptide containing the catalytic site. *Proceedings of the National Academy of Sciences*, *83*(6), pp.1660-1664. Accessed on [26 June 2025]. Available from: https://doi.org/10.1073/pnas.83.6.1660

Dittmer, J. and Leyh, B., (2015). The impact of tumour stroma on drug response in breast cancer. *Seminars in Cancer Biology* (Vol. 31, pp. 3-15). Academic Press. Accessed on [10 June 2025]. Available from: https://doi.org/10.1016/j.semcancer.2014.05.006

Dodge, J.C., Tamsett, T.J., Treleaven, C.M., Taksir, T.V., Piepenhagen, P., Sardi, S.P., Cheng, S.H. and Shihabuddin, L.S., (2022). Glucosylceramide synthase inhibition reduces ganglioside GM3 accumulation, alleviates amyloid neuropathology, and stabilises remote contextual memory in a mouse model of Alzheimer's disease. *Alzheimer's Research & Therapy*, *14*(1), p.19.

Dou, C., Liu, Z., Tu, K., Zhang, H., Chen, C., Yaqoob, U., Wang, Y., Wen, J., van Deursen, J., Sicard, D. and Tschumperlin, D., (2018). P300 acetyltransferase mediates stiffness-induced

activation of hepatic stellate cells into tumor-promoting myofibroblasts. Gastroenterology, 154(8), pp.2209-2221.

Downward, J., (1998). Mechanisms and consequences of activation of protein kinase B/Akt. *Current Opinion in Cell Biology*, *10*(2), pp.262-267. Accessed on [10 January 2025]. Available from: https://doi.org/10.1016/s0955-0674(98)80149-x

Drost, J., Van Boxtel, R., Blokzijl, F., Mizutani, T., Sasaki, N., Sasselli, V., de Ligt, J., Behjati, S., Grolleman, J.E., van Wezel, T. and Nik-Zainal, S., (2017). Use of CRISPR-modified human stem cell organoids to study the origin of mutational signatures in cancer. Science, 358(6360), pp.234-238.

Du, X., Fu, X., Yao, K., Lan, Z., Xu, H., Cui, Q. and Yang, E., (2017). Bcl-2 delays cell cycle through mitochondrial ATP and ROS. Cell Cycle, 16(7), pp.707-713. Accessed on [15 July 2025].Available from: https://doi.org/10.1080/15384101.2017.1295182

Duijf, P., G., Schultz, N., & Benezra, R., (2013). Cancer cells preferentially lose small chromosomes. Int. J. Cancer 132, 2316–2326.

Edelman, G.M., Cunningham, B.A., Reeke, G.N., Becker, J.W., Waxdal, M.J.,Wang, J.L., (1972). The covalent and three-dimensional structure of concanavalin A. Proc. Nat. Acad. Sci. U.S.A. 69, 4910–4919. Assessed on [26 February 2025]. Available from: https://doi.org/10.1073/pnas.69.9.2580

Efeyan, A., Garcia-Cao, I., Herranz, D., Velasco-Miguel, S., Serrano, M.,(2006). Tumour biology: Policing of oncogene activity by *p53*. Nature; 443:159.

Eger, A., Mikulits, W., (2005). Models of epithelial-mesenchymal transition. *Drug Discov. Today: Dis. Models*;**2**:57–63.

Elbein, Alan D. (1987). "Inhibitors of the biosynthesis and processing of N-linked oligosaccharide chains." Annual review of biochemistry 56, 497-534.

Elbein, A.D. (1991), Glycosidase inhibitors: inhibitors of N-linked oligosaccharide processing. The FASEB Journal, 5: 3055-3063. https://doi.org/10.1096/fasebj.5.15.1743438

Ellegren H. (2004). Microsatellites: simple sequences with complex evolution. Nat Rev Genet. 2004; 5:435–45. Assessed on [3 October 2024]. Available from: https://doi.org/10.1038/nrg1348

Elbein, A.D., (1987). Inhibitors of the biosynthesis and processing of N-linked oligosaccharide chains. Annual Review of Biochemistry, 56(1), pp.497-534.

El-Zein, R.A., Schabath, M.B., Etzel, C.J., Lopez, M.S., Franklin, J.D., and Spitz, M.R., (2006). Cytokinesis-blocked micronucleus assay as a novel biomarker for lung cancer risk. *Cancer Research*, *66*(12), pp.6449-6456. Accessed on [12 October 2023]. Available from: (https://doi.org/10.1158/0008-5472.CAN-06-0326).

Engbring, J., A., Kleinman, H., K.(2003). The basement membrane matrix in malignancy. J Pathol;200:465–70.

Evan, G. and Littlewood, T., (1998). A matter of life and cell death. *Science*, *281*(5381), pp.1317-1322. Accessed on [9th of January 2025]. Available from: https://doi.org/10.1126/science.281.5381.1317

Fan, C., Oh, D.S., Wessels, L., Weigelt, B., Nuyten, D.S., Nobel, A.B., Van't Veer, L.J. and Perou, C.M., (2006). Concordance among gene-expression–based predictors for breast cancer. New England Journal of Medicine, 355(6), pp.560-569.

Fang, L., Meyers, C., Budgeon LR, Howett MK (2006). Induction of productive human papillomavirus type 11 life cycle in epithelial cells grown in organotypic raft cultures. Virology, 347: pp. 28– 35.

Farquhar, M., (1983). Intracellular membrane traffic: pathways, carriers, and sorting devices. *Methods in Enzymology*, *98*, 1–13. Accessed on [16 June 2025]. Available from: https://doi.org/10.1016/0076-6879(83)98134-x

Fenech, M., and Morley, A.A., (1986). Cytokinesis-block micronucleus method in human lymphocytes: effect of *in vivo* ageing and low dose X-irradiation. *Mutation Research/Fundamental and Molecular Mechanisms of Mutagenesis*, *161*(2), pp.193-198. Accessed on [14 March 2024]. Available from: https://doi.org/10.1016/0027-5107(86)90010-2

Fenech, M., Holland, N., Chang, W.P., Zeiger, E. and Bonassi, S., (1999). The HUman MicroNucleus Project—an international collaborative study on the use of the micronucleus technique for measuring DNA damage in humans. Mutation Research/Fundamental and Molecular Mechanisms of Mutagenesis, 428(1-2), pp.271-283.

Fenech, M., (2000). A mathematical model of the *in vitro* micronucleus assay predicts false negative results if micronuclei are not specifically scored in binucleated cells or in cells that have completed one nuclear division. *Mutagenesis*, *15*(4), pp.329-336. Accessed on [13 of March 2024]. Available from: https://doi.org/10.1093/mutage/15.4.329

Fenech, M., (2000). The *in vitro* micronucleus technique. Mutat Res. 20;455(1-2):81-95. doi: 10.1016/s0027-5107(00)00065-8. PMID: 11113469

Fenech, M., (2010). The lymphocyte cytokinesis-block micronucleus cytome assay and its application in radiation biodosimetry. *Health physics*, *98*(2), pp.234-243. Accessed on [26 March 2024]. Available from: 10.1097/HP.0b013e3181b85044

Fenech, M., Kirsch-Volders, M., Natarajan, A.T., Surralles, J., Crott, J.W., Parry, J., Norppa, H., Eastmond, D.A., Tucker, J.D. and Thomas, P., (2011). Molecular mechanisms of micronucleus, nucleoplasmic bridge and nuclear bud formation in mammalian and human cells. *Mutagenesis*, *26*(1), pp.125-132. Accessed on [27 March 2024]. Available from: https://doi.org/10.1093/mutage/geq052

Fenech, M. (2020). Cytokinesis-Block Micronucleus Cytome Assay: Evolution into a More Comprehensive Method to Measure Chromosomal Instability. Genes (Basel). Oct 15;11(10):1203. doi: 10.3390/genes11101203

Fenech, M., Holland, N., Kirsch-Volders, M., Knudsen, L.E., Wagner, K.H., Stopper, H., Knasmueller, S., Bolognesi, C., El-Zein, R. and Bonassi, S., (2020). Micronuclei and disease–Report of HUMN project workshop at Rennes 2019 EEMGS conference. *Mutation Research/Genetic Toxicology and Environmental Mutagenesis*, *850*, p.503133. [Accessed on 23 October 2023]. Available from: https://www.sciencedirect.com/science/article/abs/pii/S1383571820300036

Fenech M, Holland N, Chang WP, Zeiger E, Bonassi S.(1999). The Human MicroNucleus Project-An international collaborative study on the use of the micronucleus technique for measuring DNA damage in humans. *Mutat Res*.;428(1-2):271-283. [Accessed on 16 October 2023]. Available from: https://pubmed.ncbi.nlm.nih.gov/10517999/

Fenlon, S., Ellis, I.O., Bell, J., Todd, J.H., Elston, C.W. and Blamey, R.W., (1987). Helix pomatia and Ulex europeus lectin binding in human breast carcinoma. *The Journal of Pathology*, *152*(3), pp.169-176. Assessed on [26 February 2025]. Available from: https://doi.org/10.1002/path.1711520305

Ferjancic, Z., Bihelovic, F., Vulovic, B., Matovic, R., Trmcic, M., Jankovic, A., Pavlovic, M., Djurkovic, F., Prodanovic, R., Djurdjevic Djelmas, A. and Kalicanin, N., (2024). Development of iminosugar-based glycosidase inhibitors as drug candidates for SARS-CoV-2 virus via molecular modelling and in vitro studies. Journal of Enzyme Inhibition and Medicinal Chemistry, 39(1), p.2289007.

Ferlay, J., Ervik, M., Lam, F., Colombet, M., Mery, L., Piñeros, M., Znaor, A., Soerjomataram, I. and Bray, F., (2020). Global cancer observatory: cancer today. Lyon: International Agency for Research on Cancer, 20182020.

Fields, R.D. and Lancaster, M.V., (1993). Dual-attribute continuous monitoring of cell proliferation/cytotoxicity. *American Biotechnology Laboratory*, *11*(4), pp.48-50. Accessed on [6 of June 2025]. Available from: https://europepmc.org/article/med/7763491

Fields, G.B., 2019. The rebirth of matrix metalloproteinase inhibitors: moving beyond the dogma. Cells, 8(9), p.984.

Fischer, P. B., Collin, M., Karlsson, G. B., James, W., Butters, T. D., Davis, S. J., Gordon, S., Dwek, R. A., & Platt, F. M. (1995). The alpha-glucosidase inhibitor N-butyldeoxynojirimycin inhibits human immunodeficiency virus entry at the level of post-CD4 binding. *Journal of Virology*, *69*(9), 5791–5797. Accessed on [23 October 2023]. Available from: https://doi.org/10.1128/JVI.69.9.5791-5797.1995

Fischer, D. and Kissel, T., (2001). Histochemical characterisation of primary capillary endothelial cells from porcine brains using monoclonal antibodies and fluorescein isothiocyanate-labelled lectins: implications for drug delivery. European Journal of Pharmaceutics and Biopharmaceutics, 52(1), pp.1-11. Assessed on [24 February 2025]. Available from: https://doi.org/10.1016/S0939-6411(01)00159-X

Fitzgerald, A. A., Li, E., & Weiner, L. M. (2021). 3D culture systems for exploring cancer immunology. *Cancers*, *13*(1), 1–19. https://doi.org/10.3390/cancers13010056

Flanagan, M. D., & Lin, S. (1980). Cytochalasins block actin filament elongation by binding to high affinity sites associated with F-actin. *The Journal of Biological Chemistry*, *255*(3), 835–838. Accessed on [28 March 2025]. Available from: https://pubmed.ncbi.nlm.nih.gov/7356663/

Florkin, M. and Stotz, E.H., (1973). Enzyme nomenclature: Recommendations (1972) of the Commission on Biochemical Nomenclature on the Nomenclature and Classification of Enzymes together with their Units and the Symbols of Enzyme Kinetics. Accessed on [16 June 2025]. Available from: https://cir.nii.ac.jp/crid/1130282272609705600

Fogh, J,M., Orfeo, T., (1977). One hundred and twenty-seven cultured human tumour cell lines producing tumours in nude mice. *J Natl Cancer Inst*. [Accessed on 15 October 2023]. Available from: https://pubmed.ncbi.nlm.nih.gov/327080/

Fonseca, C.L., Malaby, H.L., Sepaniac, L.A., Martin, W., Byers, C., Czechanski, A., Messinger, D., Tang, M., Ohi, R., Reinholdt, L.G. and Stumpff, J., (2019). Mitotic chromosome alignment ensures mitotic fidelity by promoting interchromosomal compaction during anaphase. *Journal of Cell Biology*, *218*(4), pp.1148-1163. Accessed on [26 Of March 2024]. Available from: https://doi.org/10.1083/jcb.201807228

Foulkes, W.D., Smith, I.E. and Reis-Filho, J.S., (2010). Triple-negative breast cancer. *New England Journal of Medicine*, *363*(20), pp.1938-1948.

Franklin, D.A., Sharick, J.T., Ericsson-Gonzalez, P.I., Sanchez, V., Dean, P.T., Opalenik, S.R., Cairo, S., Judde, J.G., Lewis, M.T., Chang, J.C. and Sanders, M.E., (2020). MEK activation modulates glycolysis and supports suppressive myeloid cells in TNBC. JCI Insight, 5(15), p.e134290.

Freeze, H., Kranz, C., (2010). Endoglycosidase and glycoamidase release of N-linked glycans. Curr Protoc Mol Biol. Accessed on [22 June 2025]. Available from: https://doi.org/10. 1002/ 04711 42735. im081 5s89

Freeze, H.H., Chong, J.X., Bamshad, M.J. and Ng, B.G., (2014). Solving glycosylation disorders: fundamental approaches reveal complicated pathways. The American Journal of Human Genetics, 94(2), pp.161-175.

Fribley, A., Zhang, K. and Kaufman, R.J., (2009). Regulation of apoptosis by the unfolded protein response. In Apoptosis: Methods and Protocols, Second Edition (pp. 191-204). Totowa, NJ: Humana Press.

Fried, P., Wolf, K. (2003). Tumour-cell invasion and migration: diversity and escape mechanisms. *Nat. Rev. Cancer.* 2003;**3**:362–374.

Fried, P., Hegerfeldt ,Y., Tusch ,M. (2004). Collective cell migration in morphogenesis and cancer. *Int. J. Dev. Biol*;**48**:441 449.

Fucic, A., Katic, J., Fthenou, E., Kogevinas, M., Plavec, D., Koppe, J., Batinic, D., Chalkiadaki, G., Chatzi, L., Lasan, R. and Kleinjans, J., (2013). Increased frequency of micronuclei in mononucleated lymphocytes and cytome analysis in healthy newborns as an early warning biomarkers of possible future health risks. Reproductive toxicology, 42, pp.110-115.

Fulford, L., G., Easton, D., F., Reis-Filho, J., S., Sofronis, A., Gillett, C., E, Lakhani, S., R., et al. (2006). Specific morphological features predictive for the basal phenotype in the breast's grade 3 invasive ductal carcinoma. Histopathology. 2006; 49: pp. 22–34.

Fung, L.K. and Saltzman, W.M., (1997). Polymeric implants for cancer chemotherapy. Advanced Drug Delivery Reviews, 26(2-3), pp.209-230.

Furmanski, P., Kirkland, W. L., Gargala, T., & Rich, M. A. (1981). Prognostic value of concanavalin A reactivity of primary human breast cancer cells. *Cancer Research*, *41*(10), 4087–4092. Assessed on [26 February 2025]. Available from: https://pubmed.ncbi.nlm.nih.gov/7026028/

Furlanetto, J. and Loibl, S., (2020). Optimal systemic treatment for early triple-negative breast cancer. Breast care, 15(3), pp.217-226.

Gallagher, J.T., Morris, A. and Dexter, T.M., (1985). Identification of two binding sites for wheat-germ agglutinin on polylactosamine-type oligosaccharides. Biochemical journal, 231(1), pp.115-122.

Gebeyehu, A., Surapaneni, S.K., Huang, J., Mondal, A., Wang, V.Z., Haruna, N.F., Bagde, A., Arthur, P., Kutlehria, S., Patel, N. and Rishi, A.K., (2021). Polysaccharide hydrogel based 3D printed tumor models for chemotherapeutic drug screening. Scientific Reports, 11(1), p.372.

Gerlinger, M., Rowan, A.J., Horswell, S., Larkin, J., Endesfelder, D., Gronroos, E., Martinez, P., Matthews, N., Stewart, A., Tarpey, P. and Varela, I., (2012). Intratumor heterogeneity and branched evolution revealed by multiregion sequencing. New England Journal of Medicine, 366(10), pp.883-892.

Geronimo, A. J. O., Bancual, M. E. J. F., Ko, K. A. L., Soliba, L. M. L., Ildefonso, J. J. C., Soriano, A. M. B., Tagalog, A. C. M. M., Acosta, N. E., Ang, V. S., Apigo, M. A., Buenconsejo, D. G. S., Chan, J. K. G., Gresh, C. B., Santos, C. B., Buñag, L. E. R., & Domantay, J. A. A. (2020). Free Radical Scavenging and *In vitro* Cytotoxic Activity of Bugnay (Antidesma bunius) Leaves Extract against A549 Human Lung Adenocarcinoma and HCT-116 Human Colorectal Cancer Cell Lines. https://doi.org/10.14499/indonesianjcanchemoprev11iss3pp124-133

Greaves, M.,(2015). Evolutionary determinants of cancer. Cancer Discov. 5, 806–821.

Greider, C., Chattopadhyay, A., Parkhurst, C. and Yang, E., (2002). BCL-xL and BCL2 delay Myc-induced cell cycle entry through elevation of p27 and inhibition of G1 cyclin-dependent kinases. Oncogene, 21(51), pp.7765-7775.

Girnita, L., Wang, M., Xie, Y., Nilsson, G., Dricu, A., Wejde, J. and Larsson, O., (2000). Inhibition of N-linked glycosylation down-regulates insulin-like growth factor-1 receptor at the cell surface and kills Ewing's sarcoma cells: therapeutic implications. *Anti-Cancer Drug Design*, *15*(1), pp.67-72

Gisselsson, D., Björk, J., Höglund, M., Mertens, F., Dal Cin, P., Åkerman, M. and Mandahl, N., (2001). Abnormal nuclear shape in solid tumours reflects mitotic instability. *The American Journal of Pathology*, *158*(1), pp.199-206. Accessed on [10 July 2005]. Available from: https://doi.org/10.1016/S0002-9440(10)63958-2

Ghahremanloo, A., Erfani, B., Asgharzadeh, F., Mansoori, S., Gheybi, F. and Hashemy, S.I., (2025). Reducing toxicity and enhancing efficacy of doxorubicin by liposomal doxorubicin and aprepitant in breast cancer. Scientific Reports, 15(1), p.9798.

Ghasempour, S. and Freeman, S.A., (2023). The glycocalyx and immune evasion in cancer. The FEBS Journal, 290(1), pp.55-65. Accessed on [11 July 2025]. Available from: https://doi.org/10.1111/febs.16236

Goldhirsch, A., Wood, W.C., Coates, A.S., Gelber, R.D., Thürlimann, B. and Senn, H.J., 2011. Strategies for subtypes—dealing with the diversity of breast cancer: highlights of the St Gallen International Expert Consensus on the Primary Therapy of Early Breast Cancer 2011. Annals of Oncology, 22(8), pp.1736-1747.

Goldhirsch, A., Winer, E.P., Coates, A.S., Gelber, R.D., Piccart-Gebhart, M., Thürlimann, B., Senn, H.J., Albain, K.S., André, F., Bergh, J. and Bonnefoi, H., (2013). Personalising the treatment of women with early breast cancer: highlights of the St Gallen International Expert Consensus on the Primary Therapy of Early Breast Cancer 2013. *Annals of Oncology*, *24*(9), pp.2206-2223.

Gonzalez-Noriega, A., Grubb, J. H., Talkad, V., & Sly, W. S. (1980). Chloroquine inhibits lysosomal enzyme pinocytosis and enhances lysosomal enzyme secretion by impairing receptor recycling. *The Journal of Cell Biology*, *85*(3), 839–852. Accessed on [16 June 2025]. Available from: https://doi.org/10.1083/jcb.85.3.839

Gonzalez-Andrades, M., Jalimarada, S.S., Rodriguez-Benavente, M., Feeley, M.N., Woodward, A.M., AbuSamra, D.B. and Argüeso, P., (2020). Golgi α1, 2-mannosidase I induces clustering and compartmentalisation of CD147 during epithelial cell migration. Cell Adhesion & Migration, 14(1), pp.96-105.

Goss, P.E., Baptiste, J., Fernandes, B., Baker, M. and Dennis, J.W., (1994). A phase I study of swainsonine in patients with advanced malignancies. Cancer Research, 54(6), pp.1450-1457.

Grabowski, G.A., Osiecki-Newman, K., Dinur, T., Fabbro, D., Legler, G., Gatt, S. and Desnick, R.J., (1986). Human acid beta-glucosidase. Use of conduritol B epoxide derivatives to investigate the catalytically active normal and Gaucher disease enzymes. *Journal of Biological Chemistry*, *261*(18), pp.8263-8269. Accessed on [26 June 2025]. Available from: https://doi.org/10.1016/S0021-9258(19)83905-4

Green, D.R. and Reed, J.C., (1998). Mitochondria and apoptosis. *science*, *281*(5381), pp.1309-1312. Accessed on [9th January 2025]. Available from: https://doi.org/10.1126/science.281.5381.1309

Gronroos, E. and López-García, C., (2018). Tolerance of chromosomal instability in cancer: mechanisms and therapeutic opportunities. *Cancer research*, *78*(23), pp.6529-6535.

Gross, V., Tran-Thi, T.A., Schwarz, R.T., Elbein, A.D., Decker, K. and Heinrich, P.C., (1986). Different effects of the glucosidase inhibitors 1-deoxynojirimycin, N-methyl-1-deoxynojirimycin and castanospermine on the glycosylation of rat α1-proteinase inhibitor and α1-acid glycoprotein. Biochemical Journal, 236(3), pp.853-860.

Gu, B., Mason, P., Wang, L., Norton, P., Bourne, N., Moriarty, R., Mehta, A., Despande, M., Shah, R. and Block, T., (2007). Antiviral profiles of novel iminocyclitol compounds against bovine viral diarrhea virus, West Nile virus, dengue virus and hepatitis B virus. Antiviral Chemistry and Chemotherapy, 18(1), pp.49-59.

Guha, P., Kaptan, E., Gade, P., Kalvakolanu, D.V. and Ahmed, H., (2017). Tunicamycin induced endoplasmic reticulum stress promotes apoptosis of prostate cancer cells by activating mTORC1. *Oncotarget*, *8*(40), p.68191.

Gupta, G.K., Collier, A.L., Lee, D., Hoefer, R.A., Zheleva, V., Siewertsz van Reesema, L.L., Tang-Tan, A.M., Guye, M.L., Chang, D.Z., Winston, J.S. and Samli, B., (2020). Perspectives on triple-negative breast cancer: current treatment strategies, unmet needs, and potential targets for future therapies. Cancers, 12(9), p.2392.

Haaf, T., Raderschall, E., Reddy, G., Ward, D.C., Radding, C.M. and Golub, E.I., (1999). Sequestration of mammalian Rad51-recombination protein into micronuclei. *Journal of Cell Biology*, *144*(1), pp.11-20. Accessed on [27 March 2027]. Available from: https://doi.org/10.1083/jcb.144.1.11

Hadley, M.,A., Byers, S.,W., Suarez-Quian, C.,A., Kleinman, H.,K., Dym, M., (1985). The extracellular matrix regulates Sertoli cell differentiation, tes- ticular cord formation and germ cell development. J Cell Biol;101:1511–22.

Haltiwanger, R., Stanley, P., (2002). Modulation of receptor signalling by glycosylation: fringe is an O-fucose-beta1,3-N- acetylglucosaminyltransferase. Biochim Biophys Acta, 1573:328-335

Hamid, R., Masood, A., Wani, I.H. and Rafiq, S., (2013). Lectins: proteins with diverse applications. Journal of Applied Pharmaceutical Science, 3(4,), pp.S93-S103. Accessed on [2 July 2025]. Available from: https://dx.doi.org/10.7324/JAPS.2013.34.S18

Hammond, C. and Helenius, A., (1994a). Folding of VSV G protein: sequential interaction with BiP and calnexin. *Science*, *266*(5184), pp.456-458. Accessed on [22 June 2025]. Available from: https://doi.org/10.1126/science.7939687

Hammond, C. and Helenius, A., (1994b). Quality control in the secretory pathway: retention of a misfolded viral membrane glycoprotein involves cycling between the ER, intermediate compartment, and Golgi apparatus. *The Journal of cell biology*, *126*(1), pp.41-52. Accessed on [22 June 2025]. Available from: https://doi.org/10.1083/jcb.126.1.41

Han, M., Oba, M., Nishiyama, N., Kano, M.R., Kizaka-Kondoh, S. and Kataoka, K., (2009). Enhanced percolation and gene expression in tumor hypoxia by PEGylated polyplex micelles. Molecular Therapy, 17(8), pp.1404-1410.

Han, X., Zhang, X., Li, H., Huang, S., Zhang, S., Wang, F. and Shi, Y., (2015). Tunicamycin enhances the antitumor activity of trastuzumab on breast cancer *in vitro* and *in vivo*. *Oncotarget*, *6*(36), p.38912.

Han, K., Pierce, S.E., Li, A., Spees, K., Anderson, G.R., Seoane, J.A., Lo, Y.H., Dubreuil, M., Olivas, M., Kamber, R.A. and Wainberg, M., (2020). CRISPR screens in cancer spheroids identify 3D growth-specific vulnerabilities. Nature, 580(7801), pp.136-141.

Hanahan, D., & Weinberg, R., A. (2011). Hallmarks of cancer: The next generation. *Cell*,*144*(5),646–674. https://doi.org/10.1016/j.cell.2011.02.013

Hanahan D, Coussens LM. (2012). Accessories to the crime: functions of cells recruited to the tumour microenvironment. Cancer Cell; 21:309-322.

Hanahan D. Hallmarks of Cancer: New Dimensions. Cancer Discov. (2022) Jan;12(1):31-46. Accessed on [10th January 2025]. Available from: https://doi.org/10.1158/2159-8290.CD-21-1059

Harbeck, N., Penault-Llorca, F.; Cortes, J.; Gnant, M. Houssami, N.; Poortmans, P.; Ruddy, K.; Tsang, J.; Cardoso, F. (2019). Breast Cancer. *Nat. Rev. Dis. Primers*, *5*, 66.

Hardman, K.D., Ainsworth, C.F., (1972). Biochemistry 11 (26), 4910–4919. Assessed on [26 February 2025]. Available from: https://doi.org/10.1021/bi00776a006

Harper, J.W. and Elledge, S.J., (2007). The DNA damage response: ten years after. *Molecular cell*, *28*(5), pp.739-745.

Harris, C.C., (1996). p53 Tumour suppressor gene: from the basic research laboratory to the clinic—an abridged historical perspective. Accessed on [10th of January 2025]. Available from: https://doi.org/10.1093/carcin/17.6.1187

Hatch, E.M., Fischer, A.H., Deerinck, T.J. and Hetzer, M.W., (2013). Catastrophic nuclear envelope collapse in cancer cell micronuclei. *Cell*, *154*(1), pp.47-60. Accessed on [24 March 2024]. Available from: https://doi.org/10.1016/j.cell.2013.06.007

Hebert, D.N., Foellmer, B. and Helenius, A., (1995). Glucose trimming and reglucosylation determine glycoprotein association with calnexin in the endoplasmic reticulum. *Cell*, *81*(3), pp.425-433. [accessed Jun 22, 2025]. Available from: https://www.cell.com/cell/pdf/0092-8674(95)90395-X.pdf

Hebert, D.N., Garman, S.C. and Molinari, M., (2005). The glycan code of the endoplasmic reticulum: asparagine-linked carbohydrates as protein maturation and quality-control tags. Trends in Cell Biology, 15(7), pp.364-370.

Hegde, S.M., Kumar, M.N., Kavya, K., Kumar, K.K., Nagesh, R., Patil, R.H., Babu, R.L., Ramesh, G.T. and Sharma, S.C. (2016). Interplay of nuclear receptors (ER, PR, and GR) and their steroid hormones in MCF-7 cells. *Molecular and Cellular Biochemistry*, *422*(1), pp.109-120.

Hennet, T.C.M.L.S., (2002). The galactosyltransferase family. *Cellular and Molecular Life Sciences CMLS*, *59*, pp.1081-1095. [Accessed on 1st of October 2024]. Available from: https://doi.org/10.1007/s00018-002-8489-4

Helenius, A. and Aebi, A.M., (2001). Intracellular functions of N-linked glycans. Science, 291(5512), pp.2364-2369.

Hering, K.W., Karaveg, K., Moremen, K.W. and Pearson, W.H., (2005). A practical synthesis of kifunensine analogues as inhibitors of endoplasmic reticulum α-mannosidase I. The Journal of Organic Chemistry, 70(24), pp.9892-9904.

Hlaing, M.T., Horimoto, Y., Denda-Nagai, K., Fujihira, H., Noji, M., Kaji, H., Tomioka, A., Ishizuka, Y., Saeki, H., Arakawa, A. and Saito, M., (2022). Tamoxifen-resistant breast cancer cells exhibit reactivity with Wisteria floribunda agglutinin. Plos one, 17(8), p.e0273513.

Ho, G.Y., Bierman, R., Beardsley, L., Walker, J., Wang, S., Schiffman, M., Castle, P., Schiffman, M., Wheeler, C., Solomon, D., Mitchell, M.F., Tortolero-Luna, G., Wright, T., Martin-Hirsch, Pl, Paraskevaidis, E., Kitchener, Lancet (2007). *Cervical human papillomavirus infection and intraepithelial neoplasia: a review*

Hohenschutz, L.D., Bell, E.A., Jewess, P.J., Leworthy, D.P., Pryce, R.J., Arnold, E. and Clardy, J., 1981. Castanospermine, a 1, 6, 7, 8-tetrahydroxyoctahydroindolizine alkaloid, from seeds of Castanospermum australe. Phytochemistry, 20(4), pp.811-814. act as potent and highly specific α-glucosidase inhibitors.

Holliday, D.L. and Speirs, V., (2011). Choosing the right cell line for breast cancer research. *Breast Cancer Research*, *13*, pp.1–7. Accessed on [21 October 2023] Available from: https://link.springer.com/article/10.1186/bcr2889

Homans, SW., Dwek, RA., (1987). Rademacher TW: Solution conformations of N-linked oligosaccharides. Biochemistry 1987, 26:6571-6578.

Hosokawa, N., Wada, I., Hasegawa, K., Yorihuzi, T., Tremblay, L.O., Herscovics, A. and Nagata, K., 2001. A novel ER α-mannosidase-like protein accelerates ER-associated degradation. The EMBO Reports, 2(5), pp.415-422.

Hossain, F. and Andreana, P.R., (2019). Developments in carbohydrate-based cancer therapeutics. Pharmaceuticals, 12(2), p.84. Accessed on [29 June 2025]. Available from: https://doi.org/10.3390/ph12020084

Hossler, P., Chumsae, C., Racicot, C., Ouellette, D., Ibraghimov, A., Serna, D., Mora, A., McDermott, S., Labkovsky, B., Scesney, S. and Grinnell, C., (2017). Arabinosylation of recombinant human immunoglobulin-based protein therapeutics. In MAbs (Vol. 9, No. 4, pp. 715-734). Taylor & Francis. Accessed on [28 June 2025]. Available from: https://doi.org/10.1080/19420862.2017.1294295

Hu, Z., Fan, C., Oh, D. S., Marron, J., He, X., Qaqish, B. F., et al. (2006). The molecular portraits of breast tumours are conserved across microarray platforms. *BMC Genomics* 7:96. doi: 10.1186/1471-2164-7-96

Huang, Z., Yu, P. and Tang, J. (2020). Characterisation of triple-negative breast cancer MDA-MB-231 cell spheroid model. *OncoTargets and Therapy*, *13*, p.5395. Accessed on [28 June 2025]. Available from: http://doi.org/10.2147/OTT.S249756

Huang, A., Kurhade, S.E., Ross, P., Apley, K.D., Griffin, J.D., Berkland, C.J. and Farrell, M.P., (2022). Disrupting N-glycosylation using type I mannosidase inhibitors alters B-cell receptor signaling. ACS Pharmacology & Translational Science, 5(11), pp.1062-1069.

Hudson, K.L.; Collins, F.S. (2013). Biospecimen policy: Family matters. Nature, 500, 141–142.

Hueber, A.O., Zornig, M., Lyon, D., Suda, T., Nagata, S. and Evan, G.I., (1997). Requirement for the CD95 receptor-ligand pathway in c-Myc-induced apoptosis. *Science*, *278*(5341), pp.1305-

1309. Accessed on [10 January 2025]. Available from: https://doi.org/10.1126/science.278.5341.1305

Hwang, J., Yi, M., Zhang, X., Xu, Y., Jung, J.H., & Kim, D. (2013). Cytochalasin B induces apoptosis through the mitochondrial apoptotic pathway in HeLa human cervical carcinoma cells. Oncology Reports, 30, 1929-1935. [Accessed on 16 October 2023] Available from: https://doi.org/10.3892/or.2013.2617

Hynes, R.O. (1976). Cell surface proteins and malignant transformation. *Biochimica et Biophysica Acta (BBA)-Reviews on Cancer*, *458*(1), pp.73-107. Accessed on [17 June 2025]. Available from: https://doi.org/10.1016/0304-419X(76)90015-9

Ippolito, M.R., Martis, V., Hong, C., Wardenaar, R., Zerbib, J., Spierings, D.C., Ben-David, U., Foijer, F. and Santaguida, S., (2020). Aneuploidy-driven genome instability triggers resistance to chemotherapy. Biorxiv, pp.2020-09.

Ishii, G., Ochiai, A. and Neri, S., (2016). Phenotypic and functional heterogeneity of cancer-associated fibroblast within the tumour microenvironment. *Advanced Drug Delivery Reviews*, *99*, pp.186-196.

Jackson, M.R., Cohen-Doyle, M.F., Peterson, P.A. and Williams, D.B. (1994). Regulation of MHC class I transport by the molecular chaperone, calnexin (p88, IP90). *Science*, *263*(5145), pp.384-387.

Jackson, S.P. and Bartek, J (2009). The DNA-damage response in human biology and disease. *Nature*, *461*(7267), pp.1071-1078.

Jaeken, J. and Péanne, R., (2017). What is new in CDG?. Journal of inherited metabolic disease, 40(4), pp.569-586.

James, N.D., Coker, R.J., Tomlinson, D., Harris, J.R.W., Gompels, M., Pinching, A.J. and Stewart, J.S.W. (1994). Liposomal doxorubicin (Doxil): an effective new treatment for Kaposi's sarcoma in AIDS. *Clinical oncology*, *6*(5), pp.294-296. Accessed on [10 June 2025]. Available from: https://doi.org/10.1016/s0936-6555(05)80269-9.

Jaroudi, S., Sengupta, S. (2007). DNA repair in mammalian embryos. Mutat Res; 635:53–77.

Ji, X. and Li, Z., (2020). Medicinal chemistry strategies toward host targeting antiviral agents. Medicinal Research Reviews, 40(5), pp.1519-1557.

Jiang, T., Munguia-Lopez, J.G., Gu, K., Bavoux, M.M., Flores-Torres, S., Kort-Mascort, J., Grant, J., Vijayakumar, S., De Leon-Rodriguez, A., Ehrlicher, A.J. and Kinsella, J.M., (2019). Engineering bioprintable alginate/gelatin composite hydrogels with tunable mechanical and cell adhesive properties to modulate tumor spheroid growth kinetics. Biofabrication, 12(1), p.015024.

Jing, X., Cui, X., Liang, H., Hao, C., Yang, Z., Li, X., Yang, X. and Han, C., (2018). CD24 is a potential biomarker for prognosis in human breast carcinoma. Cellular Physiology and Biochemistry, 48(1), pp.111-119.

Jitariu, A.A., Cimpean, A.M., Ribatti, D. and Raica, M., (2017). Triple negative breast cancer: the kiss of death. Oncotarget, 8(28), p.46652.Jones, D.B., and Johns, C.O. (1916). J. Biol. Chem. 28, 67–75.

Jones, M.J. and Jones, M.C., (2024). Cell cycle control by cell-matrix interactions. Current Opinion in Cell Biology, 86, p.102288. Accessed on [11 July 2025]. Available from: https://doi.org/10.1016/j.ceb.2023.102288

Jong, B. K. (2005). Three-dimensional tissue culture models in cancer biology. Seminars in Cancer Biology, 15(5 SPEC. ISS.), pp. 365–377. https://doi.org/10.1016/j.semcancer.2005.05.002

Jung, Y. H., Lim, E. J., Heo, J., Kwon, T. K., & Kim, Y. H. (2012). Tunicamycin sensitizes human prostate cells to TRAIL-induced apoptosis by upregulation of TRAIL receptors and downregulation of cIAP2. *International journal of oncology*, *40*(6), 1941-1948. Accessed on [28 June 2025]. Available from: https://doi.org/10.3892/ijo.2012.1402

Kalla, J., Pfneissl, J., Mair, T., Tran, L. and Egger, G., (2025). A systematic review on the culture methods and applications of 3D tumoroids for cancer research and personalized medicine. Cellular Oncology, 48(1), pp.1-26.

Kalluri, R. (2016). The biology and function of fibroblasts in cancer. Nat. Publ. Gr. 16, 582–598

Kalluri R, Weinberg RA. (2009). The basics of epithelial-mesenchymal transition. J Clin Invest; 119(6): 1420–1428. doi:10.1172/JCI39104

Kang, Y., and Massagué, J. (2004). Epithelial-mesenchymal transitions: Twist in development and metastasis. Cell, 118:277 279.

Kapałczyńska, M., Kolenda, T., Przybyła, W., Zajączkowska, M., Teresiak, A., Filas, V., Ibbs, M., Bliźniak, R., Łuczewski, Ł. and Lamperska, K., (2018). 2D and 3D cell cultures–a comparison of different types of cancer cell cultures. Archives of Medical Science, 14(4), pp.910-919.

Kaplan, A., Achord, D. T., & Sly, W. S. (1977). Phosphohexosyl components of a lysosomal enzyme are recognized by pinocytosis receptors on human fibroblasts. *Proceedings of the National Academy of Sciences of the United States of America*, *74*(5), 2026–2030. Accessed on [16 June 2025]. Available from: https://doi.org/10.1073/pnas.74.5.2026.

Kapuscinski, J., (1995). "DAPI: a DNA-specific fluorescent probe". *Biotech. Histochem*. **70** (5): 220–233.

Kerr, J.F., Wyllie, A.H. and Currie, A.R. (1972). Apoptosis: a basic biological phenomenon with wide-ranging implications in tissue kinetics. *British Journal of Cancer*, *26*(4), pp.239-257. Accessed on: [10 January 2025]. Available from: https://doi.org/10.1038/bjc.1972.33

Khaodee, W., Udomsom, S., Kunnaja, P. and Cressey, R. (2019). Knockout of glucosidase II beta subunit inhibits growth and metastatic potential of lung cancer cells by inhibiting receptor tyrosine kinase activities. Scientific Reports, 9(1), p.10394.

Kim, J.B., 2005, October. Three-dimensional tissue culture models in cancer biology. In *Seminars in cancer biology* (Vol. 15, No. 5, pp. 365-377). Academic Press.

Kim, M., Mun, H., Sung, C.O., Cho, E.J., Jeon, H.J., Chun, S.M., Jung, D.J., Shin, T.H., Jeong, G.S., Kim, D.K. and Choi, E.K., (2019). Patient-derived lung cancer organoids as *in vitro* cancer models for therapeutic screening. Nature communications, 10(1), p.3991.

Kitatani, K., Sheldon, K., Rajagopalan, V., Anelli, V., Jenkins, R.W., Sun, Y., Grabowski, G.A., Obeid, L.M. and Hannun, Y.A., (2009). Involvement of acid β-glucosidase 1 in the salvage pathway of ceramide formation. *Journal of Biological Chemistry*, *284*(19), pp.12972-12978. Accessed on [26 June 2025]. Available from: https://doi.org/10.1074/jbc.M802790200

Kleinman, H.K. and Martin, G.R. (2005). Matrigel: basement membrane matrix with biological activity. In *Seminars in Cancer Biology* (Vol. 15, No. 5, pp. 378-386). Academic Press.

Knouse, K.A., Lopez, K.E., Bachofner, M. and Amon, A. (2018). Chromosome segregation fidelity in epithelia requires tissue architecture. Cell, 175(1), pp.200-211. Assessed on [15 September 2025]. Available from: https://doi.org/10.1016/j.cell.2018.07.042

Kommineni, V., Markert, M., Ren, Z., Palle, S., Carrillo, B., Deng, J., Tejeda, A., Nandi, S., McDonald, K.A., Marcel, S. and Holtz, B., (2019). *In vivo* glycan engineering via the mannosidase I inhibitor (Kifunensine) improves efficacy of rituximab manufactured in Nicotiana benthamiana plants. International journal of Molecular Sciences, 20(1), p.194.

Korekane, H., Hasegawa, T., Matsumoto, A., Kinoshita, N, Miyoshi, E., Taniguchi, N (2012). Development of an antibody-lectin enzyme immunoassay for fucosylated a-fetoprotein. Biochim Biophys Acta, 1820:1405-1411 http://dx.doi.org/10.1016/j.bbagen.2011.12.015

Korsmeyer, S.J., (1992). Chromosomal translocations in lymphoid malignancies reveal novel proto-oncogenes. *Annual Review of Immunology*, *10*, pp.785-807. Accessed on [10th of January 2025]. Available from: https://doi.org/10.1146/annurev.iy.10.040192.004033

Koshland Jr, D.E. (1953). Stereochemistry and the mechanism of enzymatic reactions. *Biological Reviews*, *28*(4), pp.416-436. Accessed on [17 June 2025]. Available from: https://doi.org/10.1111/j.1469-185X.1953.tb01386.x

Koshkina, N. V., R.-B. K., Kleinerman, E. S. (2011). Effect of the histone deacetylase inhibitor SNDX-275 on Fas signalling in osteosarcoma cells and the feasibility of its topical application for the treatment of osteosarcoma lung metastases. Cancer;117:3457–3467. Accessed on [21 October 2023]. Available from: https://www.sciencedirect.com/science/article/abs/pii/B9781907568152500042

Koyama, R., Kano, Y., Kikushima, K., Mizutani, A., Soeda, Y., Miura, K., Hirano, T., Nishio, T. and Hakamata, W., (2020). A novel Golgi mannosidase inhibitor: molecular design, synthesis, enzyme inhibition, and inhibition of spheroid formation. Bioorganic & Medicinal Chemistry, 28(11), p.115492.

Kreso, A., O'Brien, C.A., Van Galen, P., Gan, O.I., Notta, F., Brown, A.M., Ng, K., Ma, J., Wienholds, E., Dunant, C. and Pollett, A. (2013). Variable clonal repopulation dynamics influence chemotherapy response in colorectal cancer. Science, 339(6119), pp.543-548.

Krishna, J.S., Bharathkumar, H., Nalla, S., Chirke, S.S., Basetty, S., Racha, V., Kumaraguru, T., Amanchy, R. and Rao, B.V. (2023). Synthesis, glycosidase inhibitory activity and computational studies of dideoxymethylnojirimycin and its derivatives. *Results in Chemistry*, *6*, p.101015. Assessed on [20 February 2024]. Available from: https://doi.org/10.1016/j.rechem.2023.101015

Kuhn, J. R., & Pollard, T. D. (2005). Real-time measurements of actin filament polymerization by total internal reflection fluorescence microscopy. *Biophysical Journal*, *88*(2), 1387–1402. Accessed on [28 March 2025]. Available from: https://doi.org/10.1529/biophysj.104.047399

Kurhade, S.E., Weiner, J.D., Gao, F.P. and Farrell, M.P., (2021). Functionalized High Mannose-Specific Lectins for the Discovery of Type I Mannosidase Inhibitors. Angewandte Chemie International Edition, 60(22), pp.12313-12318.

Kurosu, M., (2018). Inhibition of N-glycosylation towards novel anti-cancer chemotherapeutics. Journal of molecular pharmaceutics & organic process research, 6(1), p.141.

Lairson, L.L., Henrissat, B., Davies, G.J. and Withers, S.G. (2008). Glycosyltransferases: structures, functions, and mechanisms. *Annu. Rev. Biochem.*, *77*(1), pp.521-555. Accessed on [1st October 2024]. Available from: https://doi.org/10.1146/annurev.biochem.76.061005.092322

Lan, P.; Tonomura, N.; Shimizu, A.; Wang, S.; Yang, Y.G. (2006). Reconstitution of a functional human immune system in immunodeficient mice through combined human fetal thymus/liver and CD34+ cell transplantation. Blood, 108, 487–492. Accessed on [28 March 2021]. Available from https://doi.org/10.1182/blood-2005-11-4388

Landau, D.A., Tausch, E., Taylor-Weiner, A.N., Stewart, C., Reiter, J.G., Bahlo, J., Kluth, S., Bozic, I., Lawrence, M., Böttcher, S. and Carter, S.L., 2015. Mutations driving CLL and their evolution in progression and relapse. Nature, 526(7574), pp.525-530. Lane, D.P. (1992). p53, Guardian of the Genome. *Nature*, *358*(6381).

Lane, D. and Levine, A. (2010). p53 Research: the past thirty years and the next thirty years. *Cold Spring Harbor Perspectives in Biology*, *2*(12), p.a000893.

Lampreht Tratar, U., Horvat, S., & Cemazar, M. (2018). Transgenic Mouse Models in Cancer Research. *Frontiers in Oncology*, *8*, 268. https://doi.org/10.3389/fonc.2018.00268

Lasfargues, E.Y. and Ozzello, L., (1958). Cultivation of human breast carcinomas. Journal of the National Cancer Institute, 21(6), pp.1131-1147.

Lasfargues, E.Y., Coutinho, W.G. and Redfield, E.S. (1978). Isolation of two human tumor epithelial cell lines from solid breast carcinomas. *Journal of the National Cancer Institute*, *61*(4), pp.967-978.

Lasky, L.A. (1992). Selectins: interpreters of cell-specific carbohydrate information during inflammation. Science, 258:964-969.

Lavanya, V., Adil, M., Ahmed, N., Rishi, A.K. and Jamal, S. (2014). Small molecule inhibitors as emerging cancer therapeutics. *Integr. Cancer Sci. Ther*, *1*(3), pp.39-46.

Leathem A and Brooks S: (1987). Predictive value of lectin binding on breast-cancer recurrence and survival. Lancet 1: 1054-1056. Assessed on [26 February 2025]. Available from: https://doi.org/10.1016/s0140-6736(87)90482-x

Leimbacher, P.A., Jones, S.E., Shorrocks, A.M.K., de Marco Zompit, M., Day, M., Blaauwendraad, J., Bundschuh, D., Bonham, S., Fischer, R., Fink, D. and Kessler, B.M., (2019). MDC1 interacts with TOPBP1 to maintain chromosomal stability during mitosis. *Molecular cell*, *74*(3), pp.571-583. Accessed on [26 March 2024]. Available from: https://doi.org/10.1016/j.molcel.2019.02.014

Lehmann, J., M., Riethmüller, G., Johnson, J., P., (1989). MUC18, a marker of tumour progression in human melanoma, shows sequence similarity to the neural cell adhesion molecules of the immunoglobulin superfamily. Proc Natl Acad Sci USA 86:9891–9895.

Lehmann, B. D., Bauer, J. A., Chen, X., Sanders, M. E., Chakravarthy, A. B., Shyr, Y., Pietenpol, J. A. (2011). Identification of human triple-negative breast cancer subtypes and preclinical models for selection of targeted therapies. *The Journal of Clinical Investigation*, *121*(7), 2750–2767. https://doi.org/10.1172/JCI45014

Lengauer, C., Kinzler, K. W. & Vogelstein, B. (1997). Genetic instability in colorectal cancers. Nature 386, 623–627.

Letai, A. (2017). Functional precision cancer medicine—Moving beyond pure genomics. *Nat. Med.* **2017**, pp. *23*, 1028–1035.

Levine, A.J. (1997). p53, the cellular gatekeeper for growth and division. *Cell*, *88*(3), pp.323-331. Accessed on [10th of January 2025]. Available from: https://doi.org/10.1016/s0092-8674(00)81871-1

Li, M., Aggeler, J., Farson, D., A., Hatie, R. C., Hassell, J., Bissell, M. (1987).Influence of a reconstituted basement membrane and its components on casein gene expression and secretion in mouse mammary epithelial cells. Proc Natl Acad Sci;84:136 40.

Li, W., Shi, X., Xu, Y., Wan, J., Wei, S. and Zhu, R., (2017). Tamoxifen promotes apoptosis and inhibits invasion in estrogen-positive breast cancer MCF-7 cells. *Molecular Medicine Reports*, *16*(1), pp.478-484.

Li, W., Zhu, Z., Chen, W., Feng, Y. and Dimitrov, D.S., (2017). Crystallizable fragment glycoengineering for therapeutic antibodies development. Frontiers in Immunology, 8, p.1554.

Li, J., Zhou, Y., Chen, W., Yuan, Z., You, B., Liu, Y., Yang, S., Li, F., Qu, C. and Zhang, X., (2018). A novel 3D *in vitro* tumor model based on silk fibroin/chitosan scaffolds to mimic the tumor microenvironment. *ACS Applied Materials & Interfaces*, *10*(43), pp.36641-36651.

Li, L., Zheng, X., Zhou, Q., Villanueva, N., Nian, W., Liu, X. and Huan, T., (2020). Metabolomics-based discovery of molecular signatures for triple negative breast cancer in Asian female population. Scientific reports, 10(1), p.370.

Li, Z., Xu, D., Tong, X. and Shan, C. (2021). Inhibition of β-glucosidase overcomes gastric cancer chemoresistance through inducing lysosomal dysfunction. *Clinics and Research in Hepatology and Gastroenterology*, *45*(1), p.101456. Accessed on [28 June 2025]. Available from: https://doi.org/10.1016/j.clinre.2020.04.020

Li, J., Hubisz, M.J., Earlie, E.M., Duran, M.A., Hong, C., Varela, A.A., Lettera, E., Deyell, M., Tavora, B., Havel, J.J. and Phyu, S.M., (2023). Non-cell-autonomous cancer progression from chromosomal instability. Nature, 620(7976), pp.1080-1088.

Li, Y.X., Zhang, M., Shimadate, Y., Kato, A., Wang, J.Z., Jia, Y.M., Fleet, G.W. and Yu, C.Y., (2025). C-2 fluorinated castanospermines as potent and specific α-glucosidase inhibitors:

synthesis and structure–activity relationship study. Organic & Biomolecular Chemistry, 23(12), pp.2854-2877

Liang, Y., Wang, Y., Zhang, Y., Ye, F., Luo, D., Li, Y., Jin, Y., Han, D., Wang, Z., Chen, B. and Zhao, W., (2023). HSPB1 facilitates chemoresistance through inhibiting ferroptotic cancer cell death and regulating NF-κB signaling pathway in breast cancer. Cell Death & Disease, 14(7), p.434.

Lillelund V.H. Jensen H., Liang, X., Bols M., Chem. Rev. (2002), 102, 515–553; A. I. Meyers, C. J. Andres, J. E. Resek, C. C. Woodall, M. A. McLaughlin, P. H. Lee, D. A. Price, Tetrahedron, 1999, 55, 8931–8952. Accessed on [19 February 2025]. Available from: https://doi.org/10.1016/j.rechem.2023.101015

Lin, Y. and Lubman, D.M., (2024). The role of N-glycosylation in cancer. Acta Pharmaceutica Sinica B, 14(3), pp.1098-1110.

Lindahl, T., (1974). An N-glycosidase from Escherichia coli that releases free uracil from DNA containing deaminated cytosine residues. Proc Natl Acad Sci U S A. 1974;71:3649–3653.
Lis, H., Sharon, N. (1993). Protein glycosylation. Structural and functional aspects. Eur J Biochem, 218:1-27.

Livak, K.J. and Schmittgen, T.D. (2001). Analysis of Relative Gene Expression Data Using Real-Time Quantitative PCR and the 2−ΔΔCT Method. *Methods*, -12, vol. 25, no. 4, pp. 402 ISSN 1046-2023. DOI 10.1006/meth. 2001.1262.

Liu, B., Bian, H.J. and Bao, J.K. (2010). Plant lectins: potential antineoplastic drugs from bench to clinic. Cancer letters, 287(1), pp.1-12. Accessed on [2 July 2025]. Available from: https://doi.org/10.1016/j.canlet.2009.05.013

Liu, X.; Ory, V.; Chapman, S.; Yuan, H.; Albanese, C.; Kallakury, B.; Timofeeva, O.A.; Nealon, C.; Dakic, A.; Simic, V.; et al. (2012). ROCK inhibitor and feeder cells induce the conditional reprogramming of epithelial cells. Am. J. Pathol, 180, 599–607. Accessed on [9 January 2025]. Available from: https://pubmed.ncbi.nlm.nih.gov/22189618/

Liu, H., Zang, C., Fenner, M.H., Possinger, K. and Elstner, E. (2003). PPARγ ligands and ATRA inhibit the *in vitro* invasion of human breast cancer cells. *Breast cancer research and treatment*, *79*(1), pp.63-74.

Liu, F.; Huang, J.; Ning, B.; Liu, Z.; Chen, S.; Zhao, W., (2016). Drug Discovery via Human-Derived Stem Cell Organoids. *Front. Pharmacol; 7*, 334.

Liu, Q., Luo, Q., Ju, Y. and Song, G. (2020). Role of the mechanical microenvironment in cancer development and progression. Cancer Biology & Medicine, 17(2), pp.282-292.

Liu, F., Wu, Q., Dong, Z. and Liu, K. (2023). Integrins in cancer: Emerging mechanisms and therapeutic opportunities. Pharmacology & Therapeutics, 247, p.108458.

Liu, S., Batool, Z. and Hai, Y., (2026). Biosynthesis of the α-d-mannosidase inhibitor (−)-Swainsonine. Nature Chemical Biology, 22(2), pp.284-292.

Lo YH, Karlsson K, Kuo CJ.(2020). Applications of organoids for cancer biology and precision medicine. Nature Cancer; 1: 761–773.

Loeb, L., A., (2001). Mutator phenotype in cancer. Cancer Res. 2001; 61:3230–3239.

Lorea, P., Goldschmidt, D., Darro, F., Salmon, I., Bovin, N., Gabius, H.J., Kiss, R. and Danguy, A. (1997). *In vitro* characterization of lectin-induced alterations on the proliferative activity of three human melanoma cell lines. Melanoma research, 7(5), pp.353-363.Lotem, J. and Sachs, L. (1996). Control of apoptosis in hematopoiesis and leukaemia by cytokines, a tumor suppressor and oncogenes. *Leukaemia*, *10*(6), pp.925-931.

Lovitt, C.J., Shelper, T.B. and Avery, V.M. (2018). Doxorubicin resistance in breast cancer cells is mediated by extracellular matrix proteins. *BMC cancer*, *18*, pp.1-11. Accessed on [10 June 2025]. Available from: https://doi.org/10.1007/s00432-015-1950-1

Lu, H., Shi, C., Liu, X., Liang, C., Yang, C., Wan, X., Li, L. and Liu, Y. (2020). Identification of ZG16B as a prognostic biomarker in breast cancer. Open Medicine, Vol. 16 (Issue 1), pp. 1-13. Accessed on [12 May 2021]. Available from: doi.org/10.1515/med-2021-0004

Lu, X., & Kang, Y, (2007). Organotropism of breast cancer metastasis. J. Mammary Gland Biol. Neoplasia 12, 153–162.

Lukow, D.A., Sausville, E.L., Suri, P., Chunduri, N.K., Wieland, A., Leu, J., Smith, J.C., Girish, V., Kumar, A.A., Kendall, J. and Wang, Z., (2021). Chromosomal instability accelerates the evolution of resistance to anti-cancer therapies. Developmental cell, 56(17), pp.2427-2439.

Lupanova, T., Stefanova, N., Petkova, D., Staneva, G., Jordanova, A., Koumanov, K., Pankov, R. and Momchilova, A., (2010). Alterations in the content and physiological role of sphingomyelin in plasma membranes of cells cultured in a three-dimensional matrix. *Molecular and cellular biochemistry*, *340*, pp.215-222. Accessed on [8 June 2025]. Available from: https://doi.org/10.1007/s11010-010-0420-y

Lv, D., Hu, Z., Lu, L., Lu, H. and Xu, X., (2017). Three-dimensional cell culture: A powerful tool in tumor research and drug discovery. Oncology letters, 14(6), pp.6999-7010. Accessed on [9 July 2025]. Available from: https://doi.org/10.1016/j.biotechadv.2016.11.002

Ma, G., Liu, H., Du, M., Zhang, G., Lin, Y., Ge, Y., Wang, M., Jin, G., Zhao, Q., Chu, H. and Gong, W., (2019). A genetic variation in the CpG island of pseudogene GBAP1 promoter is associated with gastric cancer susceptibility. *Cancer*, *125*(14), pp.2465-2473. Accessed on [28 June 2025]. Available from: https://doi.org/10.1002/cncr.32081

MacLean-Fletcher, S.; Pollard, T.D. (1980). Mechanism of action of cytochalasin B on actin. *Cell, 20(2)*, 329-341. Accessed on [28 March 2025]. Available from: **https://doi.org/10.1016/0092-8674(80)90619-4**

Mackenzie, K.J., Carroll, P., Martin, C.A., Murina, O., Fluteau, A., Simpson, D.J., Olova, N., Sutcliffe, H., Rainger, J.K., Leitch, A. and Osborn, R.T., (2017). cGAS surveillance of micronuclei links genome instability to innate immunity. *Nature*, *548*(7668), pp.461-465. Accessed on [26 of March 2025]. Available from: https://doi.org/10.1038/nature23449

Magdeldin, T., López-Dávila, V., Pape, J., Cameron, G. W., Emberton, M., Loizidou, M., & Cheema, U. (2017). Engineering a vascularised 3D *in vitro* model of cancer

progression. *Scientific reports*, *7*, 44045. [Accessed on 3/10/2023]**.** Available from: https://doi.org/10.1038/srep44045

Magdeldin, T.; López-Dávila, V.; Pape, J.; Cameron, G.W.W.; Emberton, M.; Loizidou, M.; Cheema, U. (2017). Engineering a vascularised 3D *in vitro* model of cancer progression. Sci. Rep, Accessed on [28 March 2021]. Available from https://www.nature.com/articles/srep44045

Makki, J.(2015). Diversity of breast carcinoma: histological subtypes and clinical relevance. *Clin. Med Insights Pathol.* 8, 23–31.

Malaney, P., Nicosia. S., V., Davé, V., (2014). One mouse, one patient paradigm: New avatars of personalised cancer therapy. Cancer Lett. 2014 Mar 1;344(1):1-12. doi: 10.1016/j.canlet.2013.10.010.

Malhotra, J.D. and Kaufman, R.J., (2007). The endoplasmic reticulum and the unfolded protein response. In Seminars in cell & developmental biology (Vol. 18, No. 6, pp. 716-731). Academic Press.

Mani, S.A., Guo, W., Liao, M.J., Eaton, E.N., Ayyanan, A., Zhou, A.Y., Brooks, M., Reinhard, F., Zhang, C.C., Shipitsin, M. and Campbell, L.L., (2008). The epithelial-mesenchymal transition generates cells with properties of stem cells. Cell, 133(4), pp.704-715.Mantovani, A.,

Marchesi, F., Malesci, A., Laghi, L. & Allavena, P. (2017). Tumour-associated macrophages as treatment targets in oncology. Nat. Rev. Clin. Oncol. 14, 399–416.

Markiv, A., Rambaruth, N. D. S. and Dwek, M. V. (2012). 'Beyond the genome and proteome: Targeting protein modifications in cancer', Current Opinion in Pharmacology. Elsevier Ltd, 12(4), pp. 408–413. doi: 10.1016/j.coph.2012.04.003. Miller,

Martin, H., Lázaro, L.R., Gunnlaugsson, T. and Scanlan, E.M., (2022). Glycosidase activated prodrugs for targeted cancer therapy. Chemical Society Reviews, 51(23), pp.9694-9716.

Masso-Welch, P., Girald Berlingeri, S., King-Lyons, N.D., Mandell, L., Hu, J., Greene, C.J., Federowicz, M., Cao, P., Connell, T.D. and Heakal, Y., (2018). LT-IIc, a bacterial type II heat-labile enterotoxin, induces specific lethality in triple negative breast cancer cells by modulation of autophagy and induction of apoptosis and necroptosis. International Journal of Molecular Sciences, 20(1), p.85.

McDonnell, T.J. and Korsmeyer, S.J., (1991). Progression from lymphoid hyperplasia to high-grade malignant lymphoma in mice transgenic for the t (14; 18). *Nature*, *349*(6306), pp.254-256. Accessed on [10th of January]. Available from: https://doi.org/10.1038/349254a0

McIlwain, D.R., Berger, T. and Mak, T.W., (2013). Caspase functions in cell death and disease. Cold Spring Harbor perspectives in biology, 5(4), p.a008656.

Medhi, H., Khumukcham, S.S., Manavathi, B. and Paik, P., (2020). Effective in vitro delivery of paclitaxel by nanocargo of mesoporous polycaprolactone against triple negative breast cancer cells by minimalizing drug dose. RSC advances, 10(40), pp.24095-24107.

Mega, T. and Hase, S., (1991). Determination of lectin-sugar binding constants by microequilibrium dialysis coupled with high performance liquid chromatography. The Journal of Biochemistry, 109(4), pp.600-603.

Mehta, A., Zitzmann, N., Rudd, P.M., Block, T.M. and Dwek, R.A., (1998). α-Glucosidase inhibitors as potential broad based anti-viral agents. FEBS letters, 430(1-2), pp.17-22.

Mestas, J.; Hughes, C.C.W. (2004). Of Mice and Not Men: Differences between Mouse and Human Immunology. J. Immunol. 172, 2731–2738. [Accessed on 24 March 2021]. Available from https://pubmed.ncbi.nlm.nih.gov/14978070/

Meyers C, Frattini MG, Hudson JB, Laimins LA. (1992). Biosyn- thesis of human papillomavirus from a continuous cell line upon epithelial differentiation. Science, 257: pp. 971–973.

Milani, A., Geuna, E., Zucchini, G., Aversa, C., Martinello, R. and Montemurro, F., (2016). Breast Cancer in BRCA Mutation Carriers: Medical Treatment. *Minerva Ginecologica*, *68*(5), pp.557-565.

Mishra, A., Behura, A., Mawatwal, S., Kumar, A., Naik, L., Mohanty, S.S., Manna, D., Dokania, P., Mishra, A., Patra, S.K. and Dhiman, R., (2019). Structure-function and application of plant lectins in disease biology and immunity. *Food and Chemical Toxicology*, *134*, p.110827. Assessed on [24 february 2025]. Available from: https://doi.org/10.1016/j.fct.2019.110827

Mitchell BS, Schumacher U. (1999). The use of the lectin Helix pomatia agglutinin (HPA) as a prognostic indicator and as a tool in cancer research. Histopathol.;14(1):217–26

Mitelman, F., Johansson, B. & Mertens, F. Mitelman (2018). Database of Chromosome Aberrations and Gene Fusions in Cancer. (National Cancer Institute); http://cgap.nci.nih.gov/Chromosomes/Mitelman

Mo, Y. and Lim, L.Y., (2005). Paclitaxel-loaded PLGA nanoparticles: potentiation of anticancer activity by surface conjugation with wheat germ agglutinin. *Journal of Controlled Release*, *108*(2-3), pp.244-262. Assessed on [24 February 2025]. Available from: https://doi.org/10.1016/j.jconrel.2005.08.013

Mody, R., Antaram Joshi, S.H. and Chaney, W., (1995). Use of lectins as diagnostic and therapeutic tools for cancer. *Journal of Pharmacological and Toxicological Methods*, *33*(1), pp.1-10. Accessed on [3 July 2025]. Available from: https://doi.org/10.1016/1056-8719(94)00052-6

Molinari, M., (2007). N-glycan structure dictates extension of protein folding or onset of disposal. Nature chemical biology, 3(6), pp.313-320.

Montebugnoli, T., Grootaert, C., Bordoni, A., Rajković, A., Alderweireldt, E., Rombaut, J., De Maeseneire, S. L., Van Camp, J., & De Mol, M. L. (2025). Food Iminosugars and Related Synthetic Derivatives Shift Energy Metabolism and Induce Structural Changes in Colon Cancer Cell Lines. *Foods (Basel, Switzerland)*, *14*(10), 1713. Accessed on [2nd July 2025]. Available from: https://doi.org/10.3390/foods14101713

Moon, H.R., Ospina-Muñoz, N., Noe-Kim, V., Yang, Y., Elzey, B.D., Konieczny, S.F. and Han, B., (2020). Subtype-specific characterisation of breast cancer invasion using a microfluidic tumour platform. *PLoS One*, *15*(6), p.e0234012.

Morris, G.J., Naidu, S., Topham, A.K., Guiles, F., Xu, Y., McCue, P., Schwartz, G.F., Park, P.K., Rosenberg, A.L., Brill, K. and Mitchell, E.P., (2007). Differences in breast carcinoma characteristics in newly diagnosed African–American and Caucasian patients: A single-institution compilation compared with the National Cancer Institute's Surveillance, Epidemiology, and End Results database. Cancer: Interdisciplinary International Journal of the American Cancer Society, 110(4), pp.876-884.

Mostert, B., Sleijfer, S., Foekens, J., A., Gratama, J., W., (2009). Circulating tumour cells (CTCs): Detection methods and their clinical relevance in breast cancer. Cancer Treat Rev 35:463–474.

Motoyama, N. and Naka, K., (2004). DNA damage tumor suppressor genes and genomic instability. *Current opinion in genetics & development*, *14*(1), pp.11-16. Accessed [28 August 2025]. Available from: https://doi.org/10.1016/j.gde.2003.12.003

Muggia, F.M., Hainsworth, J.D., Jeffers, S., Miller, P., Groshen, S., Tan, M., Roman, L., Uziely, B., Muderspach, L., Garcia, A. and Burnett, A., (1997). Phase II study of liposomal doxorubicin in refractory ovarian cancer: antitumor activity and toxicity modification by liposomal encapsulation. *Journal of Clinical Oncology*, *15*(3), pp.987-993. Accessed on [10 June 2025]. Available from: https://doi.org/10.1200/JCO.1997.15.3.987

Nahta, R., Esteva, FJ., (2007). Trastuzumab: triumphs and tribulations. Oncogene.;26. doi: 10.1038/sj.onc.1210379.

Nagelkerke, A., Bussink, J., Rowan, A.E. and Span, P.N., (2015), December. The mechanical microenvironment in cancer: How physics affects tumours. In Seminars in cancer biology (Vol. 35, pp. 62-70). Academic Press.

Namba, Y., Sogawa, C., Okusha, Y., Kawai, H., Itagaki, M., Ono, K., Murakami, J., Aoyama, E., Ohyama, K., Asaumi, J.I. and Takigawa, M., (2018). Depletion of lipid efflux pump ABCG1 triggers the intracellular accumulation of extracellular vesicles and reduces aggregation and tumorigenesis of metastatic cancer cells. Frontiers in Oncology, 8, p.376.

Narimatsu, Y., Joshi, H.J., Nason, R., Van Coillie, J., Karlsson, R., Sun, L., Ye, Z., Chen, Y.H., Schjoldager, K.T., Steentoft, C. and Furukawa, S., (2019). An atlas of human glycosylation pathways enables display of the human glycome by gene engineered cells. *Molecular Cell*, *75*(2), pp.394-407.

Nash, R.J., Kato, A., Yu, C.Y. and Fleet, G.W., (2011). Iminosugars as therapeutic agents: recent advances and promising trends. Future Medicinal Chemistry, 3(12), pp.1513-1521.

Navin, N., E., (2014). Tumour evolution in response to chemotherapy: phenotype versus genotype. Cell Rep. 6, 417–419.

Neuman, R.E. and Logan, M.A., (1950). The determination of collagen and elastin in tissues. Journal of Biological Chemistry, 186(2), pp.549-556.

Nicolas, J.; Magli, S.; Rabbachin, L.; Sampaolesi, S.; Nicotra, F.; Russo, L.(2020). 3D Extracellular Matrix Mimics: Fundamental Concepts and Role of Materials Chemistry to Influence Stem Cell Fate. Biomacromolecules, 21, 1968–1994. Accessed on [10 April 2021]. Available on https://pubs.acs.org/doi/10.1021/acs.biomac.0c00045

Nicolau, M., Tibshirani, R., Borresen-Dale, A. L. & Jeffrey, S. S. (2007). Disease-specific genomic analysis: identifying the signature of pathologic biology. *Bioinformatics* **23**, 957–965.

Nishida, E., Ohta, Y., & Sakai, H. (1983). The regulation of actin polymerisation by the 88K protein/actin complex and cytochalasin B. *Journal of biochemistry*, *94*(5), 1671–1683. Accessed on [28 March 2025]. Available from: https://pubmed.ncbi.nlm.nih.gov/6654878/

Niwa, T., Ying, B.W., Saito, K., Jin, W., Takada, S., Ueda, T. and Taguchi, H., (2009). Bimodal protein solubility distribution revealed by an aggregation analysis of the entire ensemble of Escherichia coli proteins. *Proceedings of the National Academy of Sciences*, *106*(11), pp.4201-4206. Assessed on [20 February 2024]. Available from: https://doi.org/10.1073/pnas.0811922106

Noda, I., Fujieda, S., Seki, M., Tanaka, N., Sunaga, H., Ohtsubo, T., Tsuzuki, H., Fan, G.K. and Saito, H., (1999)). Inhibition of N-linked glycosylation by tunicamycin enhances sensitivity to

cisplatin in human head-and-neck carcinoma cells. *International journal of cancer*, *80*(2), pp.279-284.

Nouspikel, T., P., Hyka-Nouspikel, N., Hanawalt, P., C., (2006). Transcription domain-associated repair in human cells. Mol Cell Biol; 26:8722–8730

Nowell, P., C., (1976). The clonal evolution of tumour cell populations. Science; 194:23–28. [PubMed: 959840]

Nohara K, Wang F, Spiegel S. (1998).Glycosphingolipid composition of MDA-MB-231 and MCF-7 human breast cancer cell lines. Breast Cancer Res Treat. Mar;48(2):149-57. doi: 10.1023/a:1005986606010. PMID: 9596486.

Nyga,A., Loizidou,M., Emberton, M.& Cheema,U. (2013). A novel tissue-engineered three-dimensional in-vitro colorectal cancer model. *Acta Biomater.* **9**, 7917–7926 (2013). [Accessed on 23 October 2023]. Available from: https://pubmed.ncbi.nlm.nih.gov/23624217/

Nunes, A.S., Costa, E.C., Barros, A.S., de Melo-Diogo, D. and Correia, I.J., (2019). Establishment of 2D Cell Cultures Derived From 3D MCF-7 Spheroids Displaying a Doxorubicin Resistant Profile. Biotechnology journal, 14(4), p.1800268.

O'brien, J., Wilson, I., Orton, T. and Pognan, F., (2000). Investigation of the Alamar Blue (resazurin) fluorescent dye for the assessment of mammalian cell cytotoxicity. *European journal of biochemistry*, *267*(17), pp.5421-5426. Accessed on [7 June 2025]. Available from: https://doi.org/10.1046/j.1432-1327.2000.01606.x

O'Brien, C.A., Pollett, A., Gallinger, S. and Dick, J.E., (2007). A human colon cancer cell capable of initiating tumour growth in immunodeficient mice. Nature, 445(7123), pp.106-110.

Oh, M., Batty, S., Banerjee, N. and Kim, T.H., 2023. High extracellular glucose promotes cell motility by modulating cell deformability and contractility via the cAMP-RhoA-ROCK axis in human breast cancer cells. Molecular Biology of the Cell, 34(8), p.ar79.

Ohta Y, Sato T. (2014). Intestinal tumour in a dish. Frontiers in Medicine.; 1:14.

Ono, M. and Hakomori, S., (2003). Glycosylation defining cancer cell motility and invasiveness. Glycoconjugate journal, 20(1), pp.71-78.

Oo, T.Z.M., Wuttiin, Y., Choocheep, K., Kumsaiyai, W., Bunpo, P. and Cressey, R., (2025). Exploring Small-Molecule Inhibitors of Glucosidase II: Advances, Challenges, and Therapeutic Potential in Cancer and Viral Infection. International Journal of Molecular Sciences, 26(24), p.11867.

Oobatake, Y. and Shimizu, N., (2020). Double-strand breakage in the extrachromosomal double minutes triggers their aggregation in the nucleus, micronucleation, and morphological transformation. *Genes, Chromosomes and Cancer*, *59*(3), pp.133-143. Accessed on [27 March 2024]. Available from: https://doi.org/10.1002/gcc.22810

Ootani A, Li X, Sangiorgi E, Ho QT, Ueno H, Toda S, Sugihara H, Fujimoto K, Weissman IL, Capecchi MR, Kuo CJ. (2009). Sustained *in vitro* intestinal epithelial culture within a Wnt-dependent stem cell niche. Nature Medicine; 15:701-706.

Ovcaricek, T., Frkovic, S.G., Matos, E., Mozina, B. and Borstnar, S., (2011). Triple negative breast cancer-prognostic factors and survival. *Radiology and Oncology*, *45*(1).

Obidiro, O., Battogtokh, G. and Akala, E.O., (2023). Triple negative breast cancer treatment options and limitations: future outlook. Pharmaceutics, 15(7), p.1796.

Pal, M., Muinao, T., Boruah, H.P.D. and Mahindroo, N., (2022). Current advances in prognostic and diagnostic biomarkers for solid cancers: Detection techniques and future challenges. Biomedicine & Pharmacotherapy, 146, p.112488.

Palcic, M.M., (2011). Glycosyltransferases as biocatalysts. Current Opinion in Chemical Biology, 15(2), pp.226-233. Accessed on [29 June 2025]. Available from: https://doi.org/10.1016/j.cbpa.2010.11.022

Pallar, R.M., Pingle, S.K., Gaikwad, A.S., Yennam, N.S., Raju, N., Kumar, P., Adepu, V.K., Tumane, R.G., Veeranjaneyulu, C. and Matte, K., (2025). Lectin: a molecular tool in cancer diagnosis and therapy with special reference to reproductive cancers. Molecular Biotechnology, 67(2), pp.456-468. Accessed on [3 July 2025]. Available from: https://doi.org/10.1007/s12033-024-01086-w

Pan Y., Elbein A., (1995). How can N-linked glycosylation and processing inhibitors be used to study carbohydrate synthesis and function, in: J. Montreuil, J.F.G. Vliegenthart, H. Schachter (Eds.), Glycoproteins, Vol. 29a, Elsevier, Amsterdam, pp. 415^454. Accessed on [25 February 2024]. Available from: https://doi.org/10.1016/S0167-7306(08)60599-2

Panciera, T., Azzolin, L., Cordenonsi, M. and Piccolo, S., (2017). Mechanobiology of YAP and TAZ in physiology and disease. Nature reviews Molecular cell biology, 18(12), pp.758-770.

Pancione M, Giordano G, Remo A, Febbraro A, Sabatino L, Manfrin E, Ceccarelli M, Colantuoni V. (2014). Immune escape mechanisms in colorectal cancer pathogenesis and liver metastasis. Journal of Immunology Research:686879.

Parenti, G., Moracci, M., Fecarotta, S. and Andria, G., (2014). Pharmacological chaperone therapy for lysosomal storage diseases. Future medicinal chemistry, 6(9), pp.1031-1045.

Passaro, A., Al Bakir, M., Hamilton, E.G., Diehn, M., André, F., Roy-Chowdhuri, S., Mountzios, G., Wistuba, I.I., Swanton, C. and Peters, S., (2024). Cancer biomarkers: emerging trends and clinical implications for personalized treatment. *Cell*, *187*(7), pp.1617-1635. Accessed on [June 28 2025]. Available from: https://doi.org/10.1016/j.cell.2024.02.041

Pawar, V.S., Bhande, D., Pawar, S.D., Mudila, H., Kaushik, A. and Kumar, A., (2022). Investigating purification and activity analysis of urease enzyme extracted from jack bean source: A green chemistry approach. Analytical biochemistry, 659, p.114925.

Peiris, D., Spector, A. F., Lomax-Browne, H., Azimi, T., Ramesh, B., Loizidou, M., Welch, H., & Dwek, M. V. (2017). Cellular glycosylation affects Herceptin binding and sensitivity of breast cancer cells to doxorubicin and growth factors. *Scientific Reports*, *7*, 43006. Accessed on [10 June 2025]. Available from: https://doi.org/10.1038/srep43006

Pereira, M.E., Kisailus, E.C., Gruezo, F. and Kabat, E.A., (1978). Immunochemical studies on the combining site of the blood group H-specific lectin 1 from Ulex europeus seeds. Archives of Biochemistry and Biophysics, 185(1), pp.108-115.

Perou, C.M., Sørlie, T., Eisen, M.B., Van De Rijn, M., Jeffrey, S.S., Rees, C.A., Pollack, J.R., Ross, D.T., Johnsen, H., Akslen, L.A. and Fluge., (2000). Molecular portraits of human breast tumours. *Nature*, *406*(6797), pp.747-752. Accessed on [20 October 2023]. Available from: https://pubmed.ncbi.nlm.nih.gov/10963602/

Peck, B., Bland, P., Mavrommati, I., Muirhead, G., Cottom, H., Wai, P.T., Maguire, S.L., Barker, H.E., Morrison, E., Kriplani, D. and Yu, L., (2021). 3D Functional Genomics Screens Identify CREBBP as a Targetable Driver in Aggressive Triple-Negative Breast Cancer. *Cancer Research*, *81*(4), 847–859.https://doi.org/10.1158/0008-5472.can-20-1822

Persson, K., Ly, H.D., Dieckelmann, M., Wakarchuk, W.W., Withers, S.G. and Strynadka, N.C., (2001). Crystal structure of the retaining galactosyltransferase LgtC from Neisseria meningitidis in complex with donor and acceptor sugar analogues. Nature Structural Biology, 8(2), pp.166-175.

Pigman, W.W., (1944). Specificity, classification, and mechanism of action of the glycosidases. *Advances in Enzymology and Related Areas of Molecular Biology*, *4*, pp.41-74. Accessed on [16 June 2025]. Available from: https://onlinelibrary.wiley.com/doi/book/10.1002/9780470122495#page=48

Pinho, S.S. and Reis, C.A., (2015). Glycosylation in cancer: mechanisms and clinical implications. Nature Reviews Cancer, 15(9), pp.540-555.

Piplani, N., Roy, T., Saxena, N. and Sen, S., (2024). Bulky glycocalyx shields cancer cells from invasion-associated stresses. Translational Oncology, 39, p.101822.

Phelan, M; Lelkes, P; Swaroop, A. (2018). Mini and customised low-cost bioreactors for optimised high-throughput generation of tissue organoids. *Stem Cell Investigation*, *5*, 33–33, 10.21037/sci.2018.09.06

Pilobello, T,. Mahal LK. (2007). Lectin microarrays for glycoprotein analysis. Methods Mol Biol; 385:193–203. [PubMed: 18365713]

Phillips, A.F., Zhang, R., Jaffe, M., Schulz, R., Carty, M.C., Verma, A., Feinberg, T.Y., Arensman, M.D., Chiu, A., Letso, R. and Bosco, N., (2025). Targeting chromosomally unstable tumours with a selective KIF18A inhibitor. Nature Communications, 16(1), p.307.

Polo, S., E., Jackson, S., P. (2011). Dynamics of DNA damage response proteins at DNA breaks: a focus on protein modifications. Genes Dev. 2011;25:409–433

Przybyla, L., Muncie, J.M. and Weaver, V.M., (2016). Mechanical control of epithelial-to-mesenchymal transitions in development and cancer. Annual review of cell and developmental biology, 32(1), pp.527-554.

Qian, S., Wei, Z., Yang, W., Huang, J., Yang, Y. and Wang, J., (2022). The role of BCL-2 family proteins in regulating apoptosis and cancer therapy. Frontiers in oncology, 12, p.985363.

Rab, A., Bartoszewski, R., Jurkuvenaite, A., Wakefield, J., Collawn, J.F. and Bebok, Z., (2007). Endoplasmic reticulum stress and the unfolded protein response regulate genomic cystic fibrosis transmembrane conductance regulator expression. American Journal of Physiology-Cell Physiology, 292(2), pp.C756-C766.

Rafik, S.T., Bakkalci, D., MacRobert, A.J. and Cheema, U., (2025). Bioengineering facets of the tumor microenvironment in 3D tumor models: insights into cellular, biophysical and biochemical interactions. FEBS Open Bio. Accessed on [11 July 2025]. Available from: http/doi:10.1002/2211-5463.70018

Rafik, S.T., Ho, J., MacRobert, A.J. and Cheema, U., (2025). Engineering Complex Breast Tumor-Stroma Models: TMPyP4-Photodynamic Therapy Is More Effective at the Metastatic Site in Breast Tumors. ACS Biomaterials Science & Engineering, 12(1), pp.515-530.

Rafik, S.T., Upadhyay, A., MacRobert, A.J. and Cheema, U., (2026). Unlocking the Therapeutic Potential of Integrin-Linked Kinase Inhibitors in Bioengineered 3D Breast Tumor Stroma Models. The FASEB Journal, 40(2), p.e71390.

Rajagopalan, S., Xu, Y. and Brenner, M.B., (1994). Retention of unassembled components of integral membrane proteins by calnexin. *Science*, *263*(5145), pp.387-390. Accessed on [22 June 2025]. Available from: https://doi.org/10.1126/science.8278814

Rani, B., Gupta, D.K., Johansson, S. and Kamranvar, S.A., (2022). Contribution of integrin adhesion to cytokinetic abscission and genomic integrity. Frontiers in Cell and Developmental Biology, 10, p.1048717. Accessed on [12 July 2025]. Available from: https://doi.org/10.3389/fcell.2022.1048717

Rao, C.,V., Yamada, H.,Y., Yao, Y., Dai, W.(2009). Enhanced genomic instabilities caused by deregulated microtubule dynamics and chromosome segregation: a perspective from genetic studies in mice. Carcinogenesis. 2009; 30:1469–1474.

Reeke, G.N., Becker, J.W., Edelman, G.M., (1975). J. Biol. Chem. 250, 1525–1547. Assessed on [26 of February]. Available from: https://doi.org/10.1016/S0021-9258(19)41843-7

Reid, S.E., Kay, E.J., Neilson, L.J., Henze, A.T., Serneels, J., McGhee, E.J., Dhayade, S., Nixon, C., Mackey, J.B., Santi, A. and Swaminathan, K., (2017). Tumour matrix stiffness promotes metastatic cancer cell interaction with the endothelium. The EMBO Journal, 36(16), pp.2373-2389.

Reily, C., Stewart, T.J., Renfrow, M.B. and Novak, J., (2019). Glycosylation in health and disease. Nature Reviews Nephrology, 15(6), pp.346-366.

Reuten, R., Zendehroud, S., Nicolau, M., Fleischhauer, L., Laitala, A., Kiderlen, S., Nikodemus, D., Wullkopf, L., Nielsen, S.R., McNeilly, S. and Prein, C., (2021). Basement membrane stiffness determines metastasis formation. *Nature Materials*, *20*(6), pp.892-903.

Reynolds, D.S., Tevis, K.M., Blessing, W.A., Colson, Y.L., Zaman, M.H. and Grinstaff, M.W., (2017). Breast cancer spheroids reveal a differential cancer stem cell response to chemotherapeutic treatment. Scientific reports, 7(1), p.10382.

Ricci-Vitiani, L., Lombardi, D.G., Pilozzi, E., Biffoni, M., Todaro, M., Peschle, C. and De Maria, R., (2007). Identification and expansion of human colon-cancer-initiating cells. Nature, 445(7123), pp.111-115.

Ricciardi, C.A. and Gnudi, L. (2020). The endoplasmic reticulum stress and the unfolded protein response in kidney disease: Implications for vascular growth factors. Journal of cellular and molecular medicine, 24(22), pp.12910-12919.

Rieckhoff, J., Meyer, F., Classen, S., Zielinski, A., Riepen, B., Wikman, H., Petersen, C., Rothkamm, K., Borgmann, K. and Parplys, A.C., (2020). Exploiting chromosomal instability of PTEN-deficient triple-negative breast cancer cell lines for the sensitization against PARP1 inhibition in a replication-dependent manner. Cancers, 12(10), p.2809.

Rigiracciolo, D.C., Cirillo, F., Talia, M., Muglia, L., Gutkind, J.S., Maggiolini, M. and Lappano, R., (2021). Focal adhesion kinase fine tunes multifaced signals toward breast cancer progression. Cancers, 13(4), p.645. Accessed on [12 July 2025]. Available from: https://doi.org/10.3390/cancers13040645

Rijal, G. and Li, W., (2016). 3D scaffolds in breast cancer research. Biomaterials, 81, pp.135-156. Accessed on [11 July 2025]. Available from: https://doi.org/10.1016/j.biomaterials.2015.12.016

Rini, J.M., Moremen, K.W., Davis, B.G. and Esko, J.D., (2022). Glycosyltransferases and glycan-processing enzymes.

Rodriguez, L.G., Wu, X. and Guan, J.L., (2005). Wound-healing assay. In Cell migration: developmental methods and protocols (pp. 23-29). Totowa, NJ: Humana Press.

Rodríguez, C.E., Berardi, D.E., Abrigo, M., Todaro, L.B., Bal de Kier Joffe, E.D. and Fiszman, G.L., (2018). Breast cancer stem cells are involved in Trastuzumab resistance through the HER2 modulation in 3D culture. Journal of cellular biochemistry, 119(2), pp.1381-1391.

Rodriguez Benavente, M.C., Hughes, H.B., Kremer, P.G., Subedi, G.P. and Barb, A.W., (2023). Inhibiting N-glycan processing increases the antibody binding affinity and effector function of human natural killer cells. Immunology, 170(2), pp.202-213.

Roschke, A.,V., Kirsch, I.,R. (2010). Targeting karyotypic complexity and chromosomal instability of cancer cells. Curr Drug Targets; 11:1341–1350.

Rowley, R., Hudson, J. and Young, P.G., (1992). The wee1 protein kinase is required for radiation-induced mitotic delay. *Nature*, *356*(6367), pp.353-355.

Rülicke, T.H., Montagutelli, X., Pintado, B., Thon, R. and Hedrich, H.J., (2007). FELASA guidelines for the production and nomenclature of transgenic rodents. Laboratory animals, 41(3), pp.301-311.

Ryva, B., Zhang, K., Asthana, A., Wong, D., Vicioso, Y. and Parameswaran, R., (2019). Wheat germ agglutinin as a potential therapeutic agent for leukemia. Frontiers in Oncology, 9, p.100.

Salassidis, K., Huber, R., Zitzelsberger, H. and Bauchinger, M. (1992). Centromere detection in vinblastine-and radiation-induced micronuclei of cytokinesis-blocked mouse cells by using in situ hybridisation with a mouse gamma (Major) satellite DNA probe. *Environmental and molecular mutagenesis*, *19*(1), pp.1-6.

Samwer, M., Schneider, M.W., Hoefler, R., Schmalhorst, P.S., Jude, J.G., Zuber, J. and Gerlich, D.W., (2017). DNA cross-bridging shapes a single nucleus from a set of mitotic chromosomes. *Cell*, *170*(5), pp.956-972. Accessed on [27 March 2024]. Available from: https://doi.org/10.1016/j.cell.2017.07.038

Saraswathibhatla, A., Indana, D. and Chaudhuri, O., (2023). Cell–extracellular matrix mechanotransduction in 3D. Nature Reviews Molecular Cell Biology, 24(7), pp.495-516. Accessed on [10 July 2025]. Available from: https://doi.org/10.1038/s41580-023-00583-1

Savage, L. and Widener, A., (2008). Anthracyclines improve survival in HER2-positive breast cancer patients. JNCI: Journal of the National Cancer Institute, 100(1), pp.1-1.

Saul, R., Chambers, J. P., Molyneux, R. J., & Elbein, A. D. (1983). Castanospermine, a tetrahydroxylated alkaloid that inhibits β-glucosidase and β-glucocerebrosidase. Archives of Biochemistry and Biophysics, 221(2), 593-597

Saul, R., Ghidoni, J.J., Molyneux, R.J. and Elbein, A.D., (1985). Castanospermine inhibits alpha-glucosidase activities and alters glycogen distribution in animals. Proceedings of the National Academy of Sciences, 82(1), pp.93-97.Hohenschutz, L.D., Bell, E.A., Jewess, P.J., Leworthy,

Schachter H, Roseman S (1980). Mammalian glycosyltransferases: their role in the synthesis and function of complex carbohydrates and glycolipids. In: Lennarz WJ (ed) The biochemistry of glycoproteins and proteoglycans. Plenum Press, New York, 1980, pp 85--160. Accessed on [17 June 2025]. Available from: https://doi.org/10.1007/978-1-4684-1006-8_3

Schermuly, R., (2011). Mechanisms of disease: pulmonary arterial hypertension. *Nature Reviews Cardiology,* 8, 443–455

Schneeweiss, A., Chia, S., Hickish, T., Harvey, V., Eniu, A., Hegg, R., Tausch, C., Seo, J.H., Tsai, Y.F., Ratnayake, J. and McNally, V., (2013). Pertuzumab plus trastuzumab in combination with standard neoadjuvant anthracycline-containing and anthracycline-free chemotherapy regimens in patients with HER2-positive early breast cancer: a randomized phase II cardiac safety study Annals of Oncology, 24(9), pp.2278-2284.

Schoser, B., Roberts, M., Byrne, B.J., Sitaraman, S., Jiang, H., Laforêt, P., Toscano, A., Castelli, J., Díaz-Manera, J., Goldman, M. and Van der Ploeg, A.T., (2021). Safety and efficacy of cipaglucosidase alfa plus miglustat versus alglucosidase alfa plus placebo in late-onset Pompe disease (PROPEL): an international, randomised, double-blind, parallel-group, phase 3 trial. The Lancet Neurology, 20(12), pp.1027-1037.

Setaffy L, Langner C. (2015). Microsatellite instability in colorectal cancer: clinicopathological significance. Pol J Pathol. 66:203-18. [assessed on 3rd of October 2024]. Available from: https://doi.org/10.5114/pjp.2015.54953

Stanley P. (1984). Glycosylation mutants of animal cells. Annu Rev Genet; 18: 525–552. Accessed on [22 June 2025]. Available from: https://doi.org/10.1146/annurev.ge.18.120184.002521

Stanley, P., Caillibot, V. and Siminovitch, L., (1975). Selection and characterisation of eight phenotypically distinct lines of lectin-resistant Chinese hamster ovary cells. *Cell*, *6*(2), pp.121-128. [accessed Jun 22, 2025]. Available from: https://doi.org/10.1016/0092-8674(75)90002-1

Sharkey, R.M. and Goldenberg, D.M., (2006). Targeted therapy of cancer: new prospects for antibodies and immunoconjugates. *CA: a cancer journal for clinicians*, *56*(4), pp.226-243. Acessed on [28 June 2025]. Available from: https://doi.org/10.3322/canjclin.56.4.226

Shaw-Smith, C., Redon, R., Rickman, L., Rio, M., Willatt, L., Fiegler, H., Firth, H., Sanlaville, D., Winter, R., Colleaux, L. and Bobrow, M., (2004). Microarray based comparative genomic hybridisation (array-CGH) detects submicroscopic chromosomal deletions and duplications in patients with learning disability/mental retardation and dysmorphic features. *Journal of medical genetics*, *41*(4), pp.241-248.

Shiga, K., Hara, M., Nagasaki, T., Sato, T. & Takahashi, H (2015). Cancer-associated fibroblasts: their characteristics and their roles in tumour growth. Cancers 7, 2443–2458.

Shore, G.C., Papa, F.R. and Oakes, S.A., (2011). Signaling cell death from the endoplasmic reticulum stress response. *Current opinion in cell biology*, *23*(2), pp.143-149. Accessed on [12 July 2025]. Available from: https://doi.org/10.1016/j.ceb.2010.11.003

Simone, M.I., Mares, L.J., Eveleens, C.A., McCluskey, A., Pappin, B.B., Kiefel, M.J. and Houston, T.A., (2018). Back to (non-) Basics: an update on neutral and charge-balanced glycosidase inhibitors. *Mini-Reviews in Medicinal Chemistry*, *18*(10), 812–827. [Accessed on 22 October 2023]. Available from: https://pubmed.ncbi.nlm.nih.gov/28969552/

Sinha, S.J., Kumar, B., Prasad, C.P., Chauhan, S.S. and Kumar, M., (2025). Emerging research and future directions on doxorubicin: a snapshot. Asian Pacific journal of cancer prevention: APJCP, 26(1), p.5.

Singh, R., Bhatt, M.L.B., Singh, S.P., Kumar, V., Goel, M.M., Mishra, D.P. and Kumar, R., (2016). Evaluation of KiSS1 as a prognostic biomarker in North Indian breast cancer cases. Asian Pacific Journal of Cancer Prevention, 17(4), pp.1789-1795.

Singh, Y., Wang, T., & Demchenko, A. V. (2019). Direct Glycosidation of 2-Azido-2-deoxyglycosyl Nitrates. *European Journal of Organic Chemistry*, *2019*(37), 6413–6416. https://doi.org/10.1002/ejoc.201900748

Singh, S.K., Hawkins, C., Clarke, I.D., Squire, J.A., Bayani, J., Hide, T., Henkelman, R.M., Cusimano, M.D. and Dirks, P.B., (2004). Identification of human brain tumour initiating cells. Nature, 432(7015), pp.396-401.

Sinnott, M.L., (1990). Catalytic mechanism of enzymic glycosyl transfer. *Chemical Reviews*, *90*(7), pp.1171-1202. Accessed on [17 June 2025]. Available from: https://pubs.acs.org/doi/pdf/10.1021/cr00105a006

Sirenko, O., Brock, C.K., Lim, A., Macha, P., Nikolov, E., Olsen, C., McConnell, E.C., Wright, M., Collins-Burow, B.M., Cromwell, E.F. and Burow, M.E., (2022). Evaluating Drug Response in 3D Triple Negative Breast Cancer Tumoroids with High Content Imaging and Analysis.

Slamon, D., Eiermann, W., Robert, N., Pienkowski, T., Martin, M., Press, M., Mackey, J., Glaspy, J., Chan, A., Pawlicki, M. and Pinter, T., (2011). Adjuvant trastuzumab in HER2-positive breast cancer. New England Journal of Medicine, *365*(14), pp.1273-1283.

Smith, J., Tho, L.M., Xu, N. and Gillespie, D.A., (2010). The ATM–Chk2 and ATR–Chk1 pathways in DNA damage signaling and cancer. Advances in cancer research, 108, pp.73-112.

Sorlie, T., Perou, C., Tibshirani, R., Aas, T., Geisler, S. and Johnsen, H., Hastie T., Eisen MB, van de Rijn M, Jeffrey SS, Thorsen T., Quist H, Matese JC, Brown PO, Botstein D, Eystein P Lonning,

Borresen-Dale., (2001). AL Gene expression patterns of breast carcinomas distinguish tumour subclasses with clinical implications. *Proc Natl Acad Sci USA*, *98*, pp.10869–10874. Accessed on [20 October 2023]. Available from: https://pubmed.ncbi.nlm.nih.gov/11553815/

Soule, H.D., Vazquez, J., Long, A., Albert, S. and Brennan, M.J.J.O.T.N.C.I., (1973). A human cell line from a pleural effusion derived from a breast carcinoma. Journal of the National Cancer Institute, 51(5), pp.1409-1416.

Sparano, J.A., Malik, U., Rajdev, L., Sarta, C., Hopkins, U. and Wolff, A.C., (2001). Phase I trial of pegylated liposomal doxorubicin and docetaxel in advanced breast cancer. *Journal of clinical oncology*, *19*(12), pp.3117-3125. Accessed on [10 June 2025]. Available from: https://doi.org/10.1200/JCO.2001.19.12.3117

Spiro, R. C., Laufer, D. M., Perry, S. K., & Harper, J. R. (1989). Effect of inhibitors of N-linked oligosaccharide processing on the cell surface expression of a melanoma integrin. Journal of cellular biochemistry, 41(1), 37–45. Accessed [11 July 2025]. Available from: https://doi.org/10.1002/jcb.240410105

Stack, MS., Gray, R., D., Pizzo, S., V. (2004). Modulating murine B16F10 melanoma plasminogen activator production by a synthetic peptide derived from the laminin A chain. Cancer Res 1993; p. 53

Stamati, K., Redondo, P. A., Nyga, A., Neves, J. B., Tran, M. G. B., Emberton, M., Cheema, U., & Loizidou, M. (2020). The anti-angiogenic tyrosine kinase inhibitor Pazopanib kills cancer cells and disrupts endothelial networks in biomimetic three-dimensional renal tumouroids. *Journal of Tissue Engineering*, *11*.https://doi.org/10.1177/2041731420920597

Stanley P., Moremen KW., Lewis NE., Taniguchi N., Aebi M., (2022) N-Glycans. In: Varki A, Cummings RD, Esko JD, et al., editors. Essentials of Glycobiology [Internet]. 4th edition. Cold Spring Harbor (NY): Cold Spring Harbor Laboratory Press; 2022. Chapter 9. Available from: https://www.ncbi.nlm.nih.gov/books/NBK579964/

Stowell, S.R., Ju, T. and Cummings, R.D., (2015). Protein glycosylation in cancer. Annual Review of Pathology: Mechanisms of Disease, 10(1), pp.473-510.

Spill, F., Reynolds, D.S., Kamm, R.D. and Zaman, M.H., (2016). Impact of the physical microenvironment on tumor progression and metastasis. Current opinion in biotechnology, 40, pp.41-48.

Strasser, A., Harris, A.W., Bath, M.L. and Cory, S., (1990). Novel primitive lymphoid tumours induced in transgenic mice by cooperation between myc and bcl-2. *Nature*, *348*(6299), pp.331-333. Accessed on [10th of January 2025]. Available from: https://doi.org/10.1038/348331a0

Struck, D.K. and Lennarz, W.J., (1980). The function of saccharide-lipids in synthesis of glycoproteins. In *The biochemistry of glycoproteins and proteoglycans* (pp. 35-83). Boston, MA: Springer US. Accessed on [17 June 2025]. Available from: https://doi.org/10.1007/978-1-4684-1006-8_2

Sumner, J.B., (1919). J. Biol. Chem. 37, 137–144.

Sun, J., Wei, Q., Zhou, Y., Wang, J., Liu, Q. and Xu, H., (2017). A systematic analysis of FDA-approved anticancer drugs. *BMC systems biology*, *11*, pp.1-17. Accessed on: [10 June 2025]. Available from: https://doi.org/10.1186/s12918-017-0464-7

Sung, H., Ferlay, J., Siegel, R.L., Laversanne, M., Soerjomataram, I., Jemal, A. and Bray, F., (2021). Global cancer statistics 2020: GLOBOCAN estimates of incidence and mortality worldwide for 36 cancers in 185 countries. *CA: a cancer journal for clinicians*, *71*(3), pp.209-249.

Suzuki T., Cummings RD., Aebi M, and Parodi A., (2022). Glycans in Glycoprotein Quality Control. In: Varki A, Cummings RD, Esko JD, et al., editors. Essentials of Glycobiology [Internet]. 4th edition. Cold Spring Harbor (NY): Cold Spring Harbor Laboratory Press; 2022. Chapter 39.Available from: https://www.ncbi.nlm.nih.gov/books/NBK579973/ doi: 10.1101/glycobiology.4e.39

Swanton, C. (2012). Intratumor heterogeneity: evolution through space and time. Cancer Res. 72, 4875–4882.

Swain, S.M., Baselga, J., Kim, S.B., Ro, J., Semiglazov, V., Campone, M., Ciruelos, E., Ferrero, J.M., Schneeweiss, A., Heeson, S. and Clark, E., (2015). Pertuzumab, trastuzumab, and docetaxel in HER2-positive metastatic breast cancer. New England journal of medicine, 372(8), pp.724-734.

Symonds, H., Krall, L., Remington, L., Saenz-Robles, M., Lowe, S., Jacks, T. and Van Dyke, T., (1994). p53-dependent apoptosis suppresses tumor growth and progression *in vivo*. *Cell*, *78*(4), pp.703-711. Accessed on [10th January 2025]. Available from: https://doi.org/10.1016/0092-8674(94)90534-7

Szebeni, G.J., Tancos, Z., Feher, L.Z., Alfoldi, R., Kobolak, J., Dinnyes, A. and Puskas, L.G., (2017). Real architecture For 3D Tissue (RAFT™) culture system improves viability and maintains insulin and glucagon production of mouse pancreatic islet cells. Cytotechnology, 69(2), pp.359-369.

Tabatabaei, K., Moazzezi, S., Emamgholizadeh, M., Vaez, H., Baradaran, B. and Shokouhi, B., (2024). Improved therapeutic efficacy of doxorubicin chemotherapy with cannabidiol in 4T1 mice breast cancer model. Cancer Medicine, 13(21), p.e70395.

Tacar, O., Sriamornsak, P., & Dass, C. R. (2013). Doxorubicin: an update on anticancer molecular action, toxicity and novel drug delivery systems. *The Journal of pharmacy and pharmacology*, *65*(2), 157–170. Accessed on: [10 June 2025]. Available from: https://doi.org/10.1111/j.2042-7158.2012.01567.x

Takeichi, M., (1991). Cadherin cell adhesion receptors as a morphogenetic regulator. Science;251:1451–1455. doi: 10.1126/science.2006419.

Taniguchi, T., Woodward, A.M., Magnelli, P., McColgan, N.M., Lehoux, S., Jacobo, S.M.P., Mauris, J. and Argüeso, P., (2017). N-Glycosylation affects the stability and barrier function of the MUC16 mucin. Journal of Biological Chemistry, 292(26), pp.11079-11090.

Tang, Q., Xia, H., Liang, W., Huo, X. and Wei, X., (2020). Synthesis and characterization of zinc oxide nanoparticles from Morus nigra and its anticancer activity of AGS gastric cancer cells. Journal of Photochemistry and Photobiology B: Biology, 202, p.111698. Accessed on [1 July 2025]. Available from: https://doi.org/10.1016/j.jphotobiol.2019.111698

Tang, L., Xu, Y., He, J., Huang, G., Jiang, X., Li, Y., Li, H., Zhang, R. and Gui, Z., (2024). 1-Deoxynojirimycin derivative containing tegafur induced HCT-116 cell apoptosis through mitochondrial dysfunction and oxidative stress pathway. ACS Medicinal Chemistry Letters, 15(11), pp.1947-1952.

Tatullo, M., Marrelli, B., Benincasa, C., Aiello, E., Makeeva, I., Zavan, B., Ballini, A., De Vito, D. and Spagnuolo, G., (2020). Organoids in Translational Oncology. *Journal of Clinical Medicine*, *9*(9), p.2774.https://doi.org/10.3390/jcm9092774

Terrapon N., Henrissat B., Aoki-Kinoshita KF., Avadhesha S., and Stanley p., (2022). A Genomic View of Glycobiology. In: Varki A, Cummings RD, Esko JD, et al., editors. Essentials of Glycobiology [Internet]. 4th edition. Cold Spring Harbor (NY): Cold Spring Harbor Laboratory Press;. Accessed on [23 February 2024]. Chapter 8. Available from: https://www.ncbi.nlm.nih.gov/books/NBK579993/

Theodoropoulos, P. A., Gravanis, A., Tsapara, A., Margioris, A. N., Papadogiorgaki, E., Galanopoulos, V., & Stournaras, C. (1994). Cytochalasin B may shorten actin filaments by a mechanism independent of barbed end capping. *Biochemical pharmacology*, *47*(10), 1875–1881 Accessed on [28 March 2025]. Available from: https://doi.org/10.1016/0006-2952(94)90318-2

Thiery, J., P., Acloque, H., Huang, R., Y., Nieto, M., A., (2009). Epithelial-mesenchymal transitions in development and disease. Cell 139:871–890.

Thornberry, N.A. and Lazebnik, Y., 1998. Caspases: enemies within. *Science*, *281*(5381), pp.1312-1316. Accessed on [9th of January 2025]. Available from: https://doi.org/10.1126/science.281.5381.1312

Thomas, P., Umegaki, K. and Fenech, M., (2003). Nucleoplasmic bridges are a sensitive measure of chromosome rearrangement in the cytokinesis-block micronucleus assay. *Mutagenesis*, *18*(2), pp.187-194. Accessed on [27 March 2024]. Available from: https://doi.org/10.1093/mutage/18.2.187

Thompson, N. and Wakarchuk, W., (2022). O-glycosylation and its role in therapeutic proteins. Bioscience reports, 42(10), p.BSR20220094.

Tiegs, G., Hentschel, J. and Wendel, A., (1992). AT cell-dependent experimental liver injury in mice inducible by concanavalin A. The Journal of Clinical Investigation, *90*(1), pp.196-203.

Todaro, G.J., Lazar, G.K. and Green, H., (1965). The initiation of cell division in a contact-inhibited mammalian cell line. *Journal of Cellular and Comparative Physiology*, *66*(3), pp.325-333. Accessed on [9 June 2025]. Available from: https://doi.org/10.1002/jcp.1030660310

Tommelein, J., Verset, L., Boterberg, T., Demetter, P., Bracke, M. & De Wever, O (2015). Cancer-associated fibroblasts connect metastasis-promoting communication in colorectal cancer. Front. Oncol. 5,1–11.

Tolaney, S.M., Tarantino, P., Graham, N., Tayob, N., Parè, L., Villacampa, G., Dang, C.T., Yardley, D.A., Moy, B., Marcom, P.K. and Albain, K.S., (2023). Adjuvant paclitaxel and trastuzumab for node-negative, HER2-positive breast cancer: final 10-year analysis of the open-label, single-arm, phase 2 APT trial. The Lancet Oncology, 24(3), pp.273-285.

Tornaletti, S. and Hanawalt, P.C., (1999). Effect of DNA lesions on transcription elongation. Biochim, 81(1-2), pp.139-146.

Torres-Ruiz, R., Grazioso, T.P., Brandt, M., Martinez-Lage, M., Rodriguez-Perales, S. and Djouder, N., (2021). Detection of chromosome instability by interphase FISH in mouse and

human tissues. *STAR protocols*, *2*(3), p.100631. Assessed on [13 September 2025]. Available from: https://doi.org/10.1016/j.xpro.2021.100631

Tredan, O. et al. (2007). Drug resistance and the solid tumour microenvironment. J. Natl. Cancer Inst. 99, 1441–1454

Trempe, G. and Old, L.J. (1970). SKBR3 cell line. Trempe-Old Collection Memorial Sloan Kettering Cancer Center Archives, New York, NY. Available at: Memorial Sloan Kettering Cancer Center Archives (Accessed: 13 May 2026).

Trendowski M. (2015). Using cytochalasins to improve current chemotherapeutic approaches. *Anti-cancer agents in medicinal chemistry*, *15*(3), 327–335. Accessed on [29 March 2025]. Available from: https://doi.org/10.2174/1871520614666141016164335

Tricase, A.F., Cavalluzzi, M.M., Catalano, A., De Bellis, M., De Palma, A., Basile, G., Sinicropi, M.S. and Lentini, G., (2025). Insights into the activities and usefulness of deoxynojirimycin and Morus alba: a comprehensive review. Molecules, 30(15), p.3213.

Tsai, S., McOlash, L., Palen, K., Johnson, B., Duris, C., Yang, Q., Dwinell, M.B., Hunt, B., Evans, D.B., Gershan, J. and James, M.A., (2018). Development of primary human pancreatic cancer organoids, matched stromal and immune cells and 3D tumor microenvironment models. BMC cancer, 18(1), p.335.

Tsai, T.L., Wang, H.C., Hung, C.H., Lin, P.C., San Lee, Y., Chen, H.H. and Su, W.C., (2017). Wheat germ agglutinin-induced paraptosis-like cell death and protective autophagy is mediated by autophagy-linked FYVE inhibition. Oncotarget, 8(53), p.91209.

Tsai, S., McOlash, L., Palen, K., Johnson, B., Duris, C., Yang, Q., Dwinell, M.B., Hunt, B., Evans, D.B., Gershan, J. and James, M.A., (2018). Development of primary human pancreatic cancer organoids, matched stromal and immune cells and 3D tumor microenvironment models. BMC cancer, 18(1), p.335.

Tu, H.C., Hsiao, Y.C., Yang, W.Y., Tsai, S.L., Lin, H.K., Liao, C.Y., Lu, J.W., Chou, Y.T., Wang, H.D. and Yuh, C.H., (2017). Up-regulation of golgi α-mannosidase IA and down-regulation of golgi

α-mannosidase IC activates unfolded protein response during hepatocarcinogenesis. Hepatology communications, 1(3), pp.230-247.

Tuccillo, F.M., de Laurentiis, A., Palmieri, C., Fiume, G., Bonelli, P., Borrelli, A., Tassone, P., Scala, I., Buonaguro, F.M., Quinto, I. and Scala, G., (2014). Aberrant glycosylation as biomarker for cancer: focus on CD43. BioMed research international, (1), p.742831. Accessed on [3 July 2025].

Tulsiani, D.R., Harris, T.M. and Touster, O., (1982). Swainsonine inhibits the biosynthesis of complex glycoproteins by inhibition of Golgi mannosidase II. Journal of Biological Chemistry, 257(14), pp.7936-7939. Accessed on [29 June 2025]. Available from: https://doi.org/10.1016/S0021-9258(18)34274-1

Tucker, J.B., Bonema, S.C., García-Varela, R., Denu, R.A., Hu, Y., McGregor, S.M., Burkard, M.E. and Weaver, B.A., (2023). Misaligned chromosomes are a major source of chromosomal instability in breast cancer. Cancer research communications, 3(1), pp.54-65.

Utani, K.I., Okamoto, A. and Shimizu, N., (2011). Generation of micronuclei during interphase by coupling between cytoplasmic membrane blebbing and nuclear budding. *PloS one*, *6*(11), p.e27233. Accessed on [27 March 2024]. Available from: https://doi.org/10.1371/journal.pone.0027233

Van De Vijver, M.J., He, Y.D., Van't Veer, L.J., Dai, H., Hart, A.A., Voskuil, D.W., Schreiber, G.J., Peterse, J.L., Roberts, C., Marton, M.J. and Parrish, M., (2002). A gene-expression signature as a predictor of survival in breast cancer. New England Journal of Medicine, 347(25), pp.1999-2009.

Van Jaarsveld, R., H., & Kops, G., J. (2016). Difference makers: chromosomal instability versus aneuploidy in cancer. Trends Cancer 2, 561–571.

Varki, A. (2017). Biological roles of glycans. Glycobiology 27, 3–49

Vasiliu, D., Razi, N., Zhang, Y., Jacobsen, N., Allin, K., Liu, X., Hoffmann, J., Bohorov, O. and Blixt, O., (2006). Large-scale chemoenzymatic synthesis of blood group and tumor-associated

poly-N-acetyllactosamine antigens. *Carbohydrate research*, *341*(10), pp.1447-1457. [Assessed on 1st of October 2024]. Available from: https://doi.org/10.1016/j.carres.2006.03.04

Vasudevan, D., & Haltiwanger, R., S., (2014). Novel roles for O-linked glycans in protein folding. Glycoconj. J. 31, 417–426.

Vaux, D.L., Cory, S. and Adams, J.M., (1988). Bcl-2 gene promotes haemopoietic cell survival and cooperates with c-myc to immortalize pre-B cells. *Nature*, *335*(6189), pp.440-442. Accessed on [10th of January 2025]. Available from: https://doi.org/10.1038/335440a0

Vocadlo, D.J., Lowary, T.L., Bertozzi, C.R., Schnaar, R.L. and Esko, J.D., (2022). Chemical tools for inhibiting glycosylation. Accessed on [29 June 2025]. Available from: https://www.ncbi.nlm.nih.gov/books/NBK579965

Veltman, J.A., Schoenmakers, E.F., Eussen, B.H., Janssen, I., Merkx, G., van Cleef, B., van Ravenswaaij, C.M., Brunner, H.G., Smeets, D. and van Kessel, A.G., (2002). High-throughput analysis of subtelomeric chromosome rearrangements by use of array-based comparative genomic hybridization. *The American Journal of Human Genetics*, *70*(5), pp.1269-1276.

Vitale, I., Galassi, C. and Galluzzi, L., (2024). Chromosomal instability drives immunosuppression and metastatic dissemination. *Cell Research*, *34*(1), pp.7-8.

Wagle, N.S., Nogueira, L., Devasia, T.P., Mariotto, A.B., Yabroff, K.R., Islami, F., Jemal, A., Alteri, R., Ganz, P.A. and Siegel, R.L., (2025). Cancer treatment and survivorship statistics, 2025. CA: A cancer journal for clinicians, 75(4), pp.308-340.

Walsh, M., Watzlawick, H., Putnam, FW., Schmid, K., Brossmer, R., (1990). Effect of the carbohydrate moiety on the secondary structure of beta 2-glycoprotein. I. Implications for the biosynthesis and folding of glycoproteins. Biochemistry, 29:6250-6257

Wang, J.L., Cunningham, B.A., Edelman, G.M., (1971). Proc. Nat. Acad. Sci. U.S.A. 68, 1130–1134.

Wang, Y., Waters, J., Leung, M.L., Unruh, A., Roh, W., Shi, X., Chen, K., Scheet, P., Vattathil, S., Liang, H. and Multani, A., (2014). Clonal evolution in breast cancer revealed by single nucleus genome sequencing. Nature, 512(7513), pp.155-160.

Wang, X., Xiong, W. and Tang, Y., (2018). Tunicamycin suppresses breast cancer cell growth and metastasis via regulation of the protein kinase B/nuclear factor-κB signaling pathway. Oncology letters, 15(4), pp.4137-4142. Accessed on [28 June 2025]. Available from: https://doi.org/10.3892/ol.2018.7874

Wang, Y., Chen, Y., Zhou, Q., Xu, J., Qian, Q., Ni, P. and Qian, Y., (2018). Mild endoplasmic reticulum stress protects against lipopolysaccharide-induced astrocytic activation and blood-brain barrier hyperpermeability. Frontiers in Cellular Neuroscience, 12, p.222. Accessed on [4 July 2025]. Available from: https://doi.org/10.3389/fncel.2018.00222

Wang, X.; Sun, Q.; Pei, J. (2018). Microfluidic-based 3D engineered microvascular networks and their applications in vascularised microtumor models. Micromachines, 9, 493. [Accessed on 29 March 2021]. Available from https://www.mdpi.com/2072-666X/9/10/493

Wang, H. and Wu, Q., (2019). Glucosidase inhibition to study calnexin-assisted glycoprotein folding in cells. Bio-protocol, 9(11), pp.e3248-e3248.

Wang, Y., Qu, C., Di, Q., Zhang, J. and Na, L., (2025). 1-Deoxynojirimycin Combined with Theaflavins Targets PTGS2/MMP9 to Exert a Synergistic Hypoglycemic Effect. Nutrients, 18(1), p.99.

Wang, D., He, Z. and Chen, Z., (2025). Therapeutic Targeting of Viral N-Glycosylation Modification: From Molecular Mechanisms to Clinical Application Prospects. Infectious Diseases and Therapy, pp.1-22.

Wang, S., Ding, N., Chen, A., Cardin, D., Xu, Y., Grimley, K., Russell, W.K., Xu, J., Kurie, J.M., Xiao, G.Y. and Tan, X., (2026). Endoplasmic reticulum–resident α-glucosidase II drives non-small cell lung cancer progression via regulation of secretory glycoproteins. JCI insight, 11(11).

Warburg, O., (1956). On the origin of cancer cells. Science, 123(3191), pp.309-314.

Warren (1982). Editorial commentary. In: 'Membrane glyco-proteins in control and malignant cells', an Oncology Overview, prepared by International Research Data Bank Program of the National Cancer Institute, 1982.

Weeber F, van de Wetering M, Hoogstraat M, Dijkstra KK, Krijgsman O, Kuilman T, Gadellaa-van Hooijdonk CG, van der Velden DL, Peeper DS, Cuppen EP, Vries RG, Clevers H, Voest EE. (2015). Preserved genetic diversity in organoids cultured from biopsies of human colorectal cancer metastases. Proceedings of the National Academy of Sciences of the United States of America; 112:13308- 13311.

Weadge, J.T. and Palcic, M.M., (2008). Chemistry of glycosyltransferases. *Wiley Encyclopedia of Chemical Biology (Begley TP, ed) Vol*, *2*, pp.198-211. Accessed on [1st October 2024]. Available from: https://doi.org/10.1016%2Fj.copbio.2011.04.013

Wei, C., Cheng, J., Zhou, B., Zhu, L., Khan, M.A., He, T., Zhou, S., He, J., Lu, X., Chen, H. and Zhang, D., (2016). Tripartite motif containing 28 (TRIM28) promotes breast cancer metastasis by stabilizing TWIST1 protein. Scientific reports, 6(1), p.29822.

Weinert, T. and Hartwell, L., (1989). Control of G2 delay by the rad9 gene of Saccharomyces cerevisiae. *Journal of Cell Science*, *1989*(Supplement_12), pp.145-148.

Winer, A., Adams, S. and Mignatti, P., 2018. Matrix metalloproteinase inhibitors in cancer therapy: turning past failures into future successes. Molecular cancer therapeutics, 17(6), pp.1147-1155.

Witz, I., P. (2008). “The selectin-selectin ligand axis in tumour progression,” *Cancer and Metastasis Reviews*, vol. 27, no. 1, pp. 19–30, 2008.

Wojtowicz, K., Januchowski, R., Nowicki, M. and Zabel, M., (2015). Inhibition of protein glycosylation reverses the MDR phenotype of cancer cell lines. Biomedicine & Pharmacotherapy, 74, pp.49-56. Accessed on [13 March 2022]. Available from: https://doi.org/10.1016/j.biopha.2015.07.001

Wolff, A.C., Hammond, M.E.H., Hicks, D.G., Dowsett, M., McShane, L.M., Allison, K.H., Allred, D.C., Bartlett, J.M., Bilous, M., Fitzgibbons, P. and Hanna, W., (2013). Recommendations for human epidermal growth factor receptor 2 testing in breast cancer: American Society of Clinical Oncology/College of American Pathologists clinical practice guideline update. Journal of Clinical Oncology, 31(31), pp.3997-4013. Accessed on [15 February 2023]. Available from: https://doi.org/10.1200/JCO.2013.50.9984

Wu, B.B., Leung, K.T. and Poon, E.N.Y., (2022). Mitochondrial-targeted therapy for doxorubicin-induced cardiotoxicity. International Journal of Molecular Sciences, 23(3), p.1912.

World Health Organisation (WHO). (2025) Cancer. [Accessed: 29 December 2025].Available at: https://www.who.int/news-room/fact-sheets/detail/cancer

Wolf K., Wu, Y.I., Liu Y., Geiger J., Tam E., Overall C., Stack M.S., Friedl P. (2007). Multi-step pericellular proteolysis controls the transition from individual to collective cancer cell invasion. *Nat. Cell Biol.* 2007;**9**:893–904.

Wrodnigg, T.M., Steiner, A.J. and Ueberbacher, B.J., (2008). Natural and synthetic iminosugars as carbohydrate processing enzyme inhibitors for cancer therapy. Anti-Cancer Agents in Medicinal Chemistry (Formerly Current Medicinal Chemistry-Anti-Cancer Agents), 8(1), pp.77-85. Accessed on [29 June 2025]. Available from: https://doi.org/10.2174/187152008783330851

Wu, Y.M., Tang, J., Zhao, P., Chen, Z.N. and Jiang, J.L., (2009). Morphological changes and molecular expressions of hepatocellular carcinoma cells in three-dimensional culture model. *Experimental and molecular pathology*, *87*(2), pp.133-140. Accessed on [8 June 2025]. Available from: https://doi.org/10.1016/j.yexmp.2009.07.003

Wu, S., Zheng, Q., Xing, X., Dong, Y., Wang, Y., You, Y., Chen, R., Hu, C., Chen, J., Gao, D. and Zhao, Y., (2018). Matrix stiffness-upregulated LOXL2 promotes fibronectin production, MMP9 and CXCL12 expression and BMDCs recruitment to assist pre-metastatic niche formation. Journal of Experimental & Clinical Cancer Research, 37(1), p.99.

Wu, J., Chen, S., Liu, H., Zhang, Z., Ni, Z., Chen, J., Yang, Z., Nie, Y. and Fan, D., (2018). Tunicamycin specifically aggravates ER stress and overcomes chemoresistance in multidrug-resistant gastric cancer cells by inhibiting N-glycosylation. *Journal of Experimental & Clinical Cancer Research*, *37*, pp.1-12. Accessed on [29 June 2025]. Available from: https://doi.org/10.1186/s13046-018-0935-8

Wu, J., Fan, D., Shao, Z., Xu, B., Ren, G., Jiang, Z., Wang, Y., Jin, F., Zhang, J., Zhang, Q. and Ma, F., (2022). CACA guidelines for holistic integrative management of breast cancer. *Holistic Integrative Oncology*, *1*(1), p.7.

Wyllie AH, Kerr JF, Currie AR. (1980). Cell death: the significance of apoptosis. Int Rev Cytol. ;68:251-306.. Accessed on [13th January of 2025]. Available from: https://doi.org/10.1016/s0074-7696(08)62312-8

Xu, H., Lyu, X., Yi, M., Zhao, W., Song, Y. and Wu, K., (2018). Organoid technology and applications in cancer research. *Journal of hematology & oncology*, *11*, pp.1-15. Accessed on [23 May 2022]. Available from: https://doi.org/10.1186/s13045-018-0662-9

Xiong, Y., Li, Q., Kailemia, M.J., Lebrilla, C.B., Nandi, S. and McDonald, K.A., (2018). Glycoform modification of secreted recombinant glycoproteins through kifunensine addition during transient vacuum agroinfiltration. International journal of Molecular Sciences, 19(3), p.890.

Xu, K.; Wang, Z.; Copland, J.A.; Chakrabarti, R.; Florczyk, S. (2020). 3D porous chitosan-chondroitin sulfate scaffolds promote epithelial-to-mesenchymal transition in prostate cancer cells. Biomaterials, 254, 120126

Xu, R., Zhou, X., Wang, S. & Trinkle, C. (2020). Tumor organoid models in precision medicine and investigating cancer-stromal interactions. *Pharmacology & Therapeutics*, p.107668.

Xu, C., Zhang, M., Bian, L., Li, Y., Yao, Y. and Li, D., (2020). N-glycosylated SGK196 suppresses the metastasis of basal-like breast cancer cells. *Oncogenesis*, *9*(1), p.4. Accessed on [28 June 2025]. Available from: https://doi.org/10.1038/s41389-019-0188-1

Xu, H., Jiao, D., Liu, A. and Wu, K., (2022). Tumor organoids: applications in cancer modeling and potentials in precision medicine. Journal of hematology & oncology, 15(1), p.58.

Yamamoto H, Imai K. (2015). Microsatellite instability: An update. Arch Toxicol. 89:899–921. [Assessed on 3rd of October 2024]. Available from: https://doi.org/10.1007/s00204-015-1474-0

Yan, X., Lin, Y., Yang, D., Shen, Y., Yuan, M., Zhang, Z., Li, P., Xia, H., Li, L., Luo, D. and Liu, Q., (2003). A novel anti-CD146 monoclonal antibody, AA98, inhibits angiogenesis and tumor growth. Blood, 102(1), pp.184-191. Accessed on [September 18 2022]. Available from: https://doi.org/10.1182/blood-2002-04-1004

Yao, Y. and Dai, W., (2014). Genomic instability and cancer. Journal of carcinogenesis & mutagenesis, 5, p.1000165. Accessed [10 July 2025]. Available from: https://doi.org/10.4172/2157-2518.1000165

Yates, L.R., Knappskog, S., Wedge, D., Farmery, J.H., Gonzalez, S., Martincorena, I., Alexandrov, L.B., Van Loo, P., Haugland, H.K., Lilleng, P.K. and Gundem, G., (2017). Genomic evolution of breast cancer metastasis and relapse. Cancer cell, 32(2), pp.169-184. . Accessed on [August 22 2022]. Available from: https://doi.org/10.1016/j.ccell.2017.07.005

Yilmaz, M. and Christofori, G., (2009). EMT, the cytoskeleton, and cancer cell invasion. Cancer and metastasis reviews, 28, pp.15-33.

Yin, L., Duan, J.J., Bian, X.W. and Yu, S.C., (2020). Triple-negative breast cancer molecular subtyping and treatment progress. Breast Cancer Research, 22(1), p.61.

Yonezawa, S., Nakamura, T., Tanaka, S. and Sato, E., 1982. Glycoconjugate with Ulex europaeus agglutinin-I-binding sites in normal mucosa, adenoma, and carcinoma of the human large bowel. Journal of the National Cancer Institute, 69(4), pp.777-785.

Yong, K.M.A., Ulintz, P.J., Caceres, S., Cheng, X., Bao, L., Wu, Z., Jiagge, E.M. and Merajver, S.D., (2020). Heterogeneity at the invasion front of triple-negative breast cancer cells. *Scientific Reports*, *10*(1), pp.1-9.

Young, K.M. and Reinhart-King, C.A., (2023). Cellular mechanosignaling for sensing and transducing matrix rigidity. Current opinion in cell biology, 83, p.102208. Accessed on [11 July 2025]. Available from: https://doi.org/10.1016/j.ceb.2023.102208

Yu, Q., Zhang, K., Wang, X., Liu, X., Zhang, Z. (2010). Expression of transcription factors snail, slug, and twist in human bladder carcinoma. J Exp Clin Cancer Res. 2010 Sep 1;29(1):119. doi: 10.1186/1756-9966-29-119. PMID: 20809941; PMCID: PMC2942802.

Yu, H., Mouw, J.K. and Weaver, V.M., (2011). Forcing form and function: biomechanical regulation of tumour evolution. Trends in cell biology, 21(1), pp.47-56.

Zeng, Q., Li, W., Lu, D., Wu, Z., Duan, H., Luo, Y., Feng, J., Yang, D., Fu, L of., & Yan, X. (2012). CD146, an epithelial-mesenchymal transition inducer, is associated with triple-negative breast cancer. Proceedings of the National Academy of Sciences of the United States of America, 109(4), 1127–1132. https://doi.org/10.1073/pnas.1111053108

Zachara NE., Akimoto Y., Boyce M., and Hart GW., (2022). The O-GlcNAc Modification. In: Varki A, Cummings RD, Esko JD, et al., editors. Essentials of Glycobiology [Internet]. 4th edition. Cold Spring Harbor (NY): Cold Spring Harbor Laboratory Press. Chapter 19. Available from: https://www.ncbi.nlm.nih.gov/books/NBK579950/ doi: 10.1101/glycobiology 4e.19

Zechel, D.L. and Withers, S.G., (2000). Glycosidase mechanisms: anatomy of a finely tuned catalyst. *Accounts of Chemical Research*, *33*(1), pp.11-18. Accessed on [17 June 2025]. Available from: https://doi.org/10.1021/ar970172+

Zeng, W., Luo, Y., Gan, D., Zhang, Y., Deng, H. and Liu, G., 2023. Advances in Doxorubicin-based nano-drug delivery system in triple negative breast cancer. Frontiers in bioengineering and biotechnology, 11, p.1271420.

Zhang, C.Z., Spektor, A., Cornils, H., Francis, J.M., Jackson, E.K., Liu, S., Meyerson, M. and Pellman, D., (2015). Chromothripsis from DNA damage in micronuclei. *Nature*, *522*(7555), pp.179-184. Accessed on [24th March 2024]. Available from: https://doi.org/10.1038/nature14493

Zhang, X., P., L., F., Wang, W., (2011). Two-phase dynamics of p53 in the DNA damage response. Proc Natl Acad Sci U S A; 108:8990–8995.

Zhang, S.; Roche, K.; Nasheuer, H.P.; Lowndes, N.F. (2011). Modifying histones by sugar β-N-acetylglucosamine (GlcNAc) occurs on multiple residues, including histone H3 serine 10, and is cell cycle-regulated. *J. Biol. Chem.* , *286*, 37483–37495. Accessed on [23 October 2023] Available from: https://doi.org/10.1074/jbc.M111.284885

Zhang, Y., Zhu, K., Miao, X., Hu, X. and Wang, T., (2016). Identification of β-glucosidase 1 as a biomarker and its high expression in hepatocellular carcinoma is associated with resistance to chemotherapy drugs. *Biomarkers*, *21*(3), pp.249-256. Accessed on [12 July 2025]. Available from: https://doi.org/10.3109/1354750X.2015.1134662

Zhang, R., Zhang, Y., Xin, X., Huang, G., Zhang, N., Zeng, Q., Tang, L., Attaribo, T., Lee, K.S., Jin, B.R. and Gui, Z., (2021). Dual-targeting antiproliferation hybrids derived from 1-deoxynojirimycin and kaempferol induce MCF-7 Cell apoptosis through the mitochondria-mediated pathway. Journal of natural products, 84(5), pp.1534-1543.

Zhang, R., Cogan, D., Eng, C., Phillips, A., Carty, M.C., Feinberg, T., Verma, A., Tourdot, R., Swiston, A., Bettigole, S. and Drutman, S., (2022). Discovery of potent, orally active KIF18A inhibitors targeting CIN-high cancer cells.

Zhang, M. and Zhang, B., (2025). Extracellular matrix stiffness: mechanisms in tumor progression and therapeutic potential in cancer. Experimental Hematology & Oncology, 14(1), p.54.

Zhang, S., Zhang, Y., Yin, H., Liu, Y., Tang, L., Zhu, Y., Sun, P., Wu, K., Zhao, B. and Lu, H., (2024). Metabolomic analysis of swainsonine poisoning in renal tubular epithelial cells. Frontiers in Veterinary Science, 11, p.1387853.

Zhao, J., Patwa, H., Lubman, M., Simeone, M.(2008). Protein biomarkers in cancer: natural glycoprotein microarray approaches. Curr Opin Mol Ther. 2008; 10:602–610.

Zhao, H., Shen, J., Medico, L., Wang, D., Ambrosone, C.B., Liu, S.,(2010). A pilot study of circulating miRNAs as potential biomarkers of early-stage breast cancer. PLoS One. 5(10):e13735.

Zhao, Y., Liu, W., Zhou, Y., Zhang, X. and Murphy, P.V., (2010). N-(8-(3-ethynylphenoxy) octyl-1-deoxynojirimycin suppresses growth and migration of human lung cancer cells. Bioorganic & medicinal chemistry letters, 20(24), pp.7540-7543.

Zhou, X., Huang, Z., Yang, H., Jiang, Y., Wei, W., Li, Q., & Liu, J. (2017). β-Glucosidase inhibition sensitises breast cancer to chemotherapy. *Biomedicine & Pharmacotherapy*, *91*, 504-509. Accessed on [27 June 2025]. Available from: https://doi.org/10.1016/j.biopha.2017.04.113

Zhou, J., Negi, A., Mirallai, S.I., Warta, R., Herold-Mende, C., Carty, M.P., Ye, X.S. and Murphy, P.V., (2019). N-Alkyl-1, 5-dideoxy-1, 5-imino-l-fucitols as fucosidase inhibitors: Synthesis, molecular modelling and activity against cancer cell lines. Bio-organic Chemistry, 84, pp.418-433. Accessed on [1 July 2025]. Available from: https://doi.org/10.1016/j.bioorg.2018.12.003

Zhu, S., Wu, Y., Song, B., Yi, M., Yan, Y., Mei, Q. and Wu, K., 2023. Recent advances in targeted strategies for triple-negative breast cancer. Journal of hematology & oncology, 16(1), p.100.

Appendices

Appendix 1

Initial experimentation on glycosidase inhibition treatment on MDA-MB-231 and BT-549 TNBC cells on 2D over 24-hours. Inhibitors tested were DNJ and compound 00042.

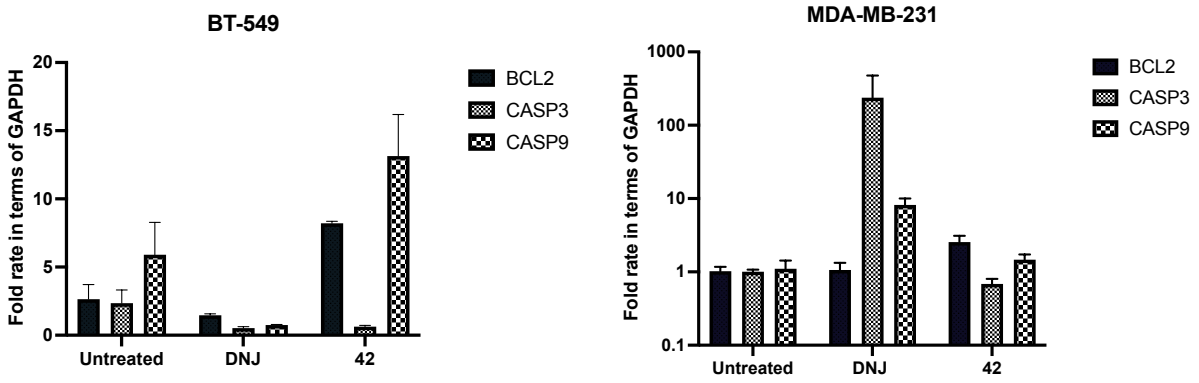

This is an initial set of experimental work deployed with the collaboration of MSc students, as they were supervised and guided them through their laboratory work, including tissue culture. PCR analysis shows MDA-MB-231 and BT-549 cells were treated with glycosidase inhibitors, and the deployment of apoptotic markers BCL2, CASP3 and CASP9 show the level of gene expression on untreated cells and cells exposed to DNJ and Phytoquest (42) inhibitors were analysed to assess the folding rate of the markers in terms of GAPDH expression. The average fold rate for each marker (BLC2, CASP3 and CASP9) and sample (Untreated).

in terms of normalised expression as internal reference gene, GAPDH was used.

PCR analysis of BT-549 in terms of BCL2, CASP3 and CASP9 expression on untreated cells and cells exposed to DNJ and Phytoquest (42) inhibitors were analysed to assess the folding rate of the markers in terms of GAPDH expression. The average fold rate for each marker (BLC2, CASP3 and CASP9) and sample (Untreated, DNJ, and Phytoquest (0042)) in terms of GAPDH expression is displayed in Figure 2. Regarding the untreated samples, DNJ was shown to report a reduced fold rate for each of the apoptotic

markers analysed. Phytoquest (0042) reported a reduced fold rate compared to the untreated sample for CASP3 at 0.3 the fold rate in terms of GAPDH expression. Meanwhile, for BCL2 and CASP9, Phytoquest (0042) showed a significantly increased fold rate at 3.39 and 2.60,

respectively. CASP3 expression reduced samples treated with DNJ and Phytoquest (0042) compared to the untreated samples.

Regarding the untreated samples on MDA-MB-231 cell, it was observed that DNJ showed a minimally increased fold rate for BCL2 at 1.06 compared with the untreated samples at 1.02. There was a significantly increased fold rate of CASP9 expression at 8.19-fold rate in terms of GAPDH compared with 1.1 for untreated. CASP3 was reported to be less than the fold rate for the untreated samples at 0.19. Phytoquest (0042) samples showed an increased fold rate for BCL2 at 2.56 and anBCL2 at9 at 1.47. In contrast, Phytoquest reported a reduced fold rate of CASP3 at 0.19. CASP3 expression was reduced in samples treated with both inhibitors compared to the untreated samples.

APPENDIX 2

RT-qPCR results from 24-hour glycosidase inhibition treatment on MDA-MB-231 cells with DNJ and compound 255 iminosugars.

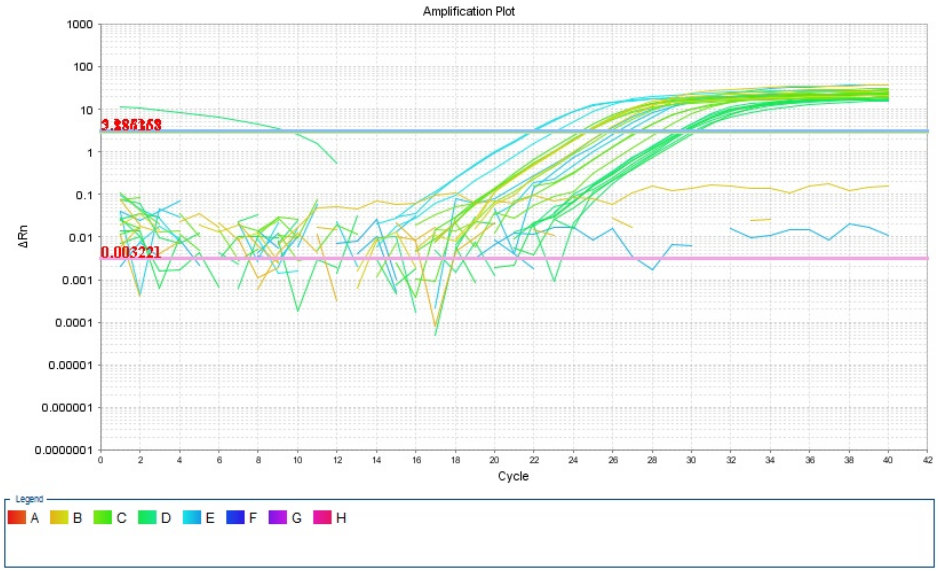

Amplification plot 1

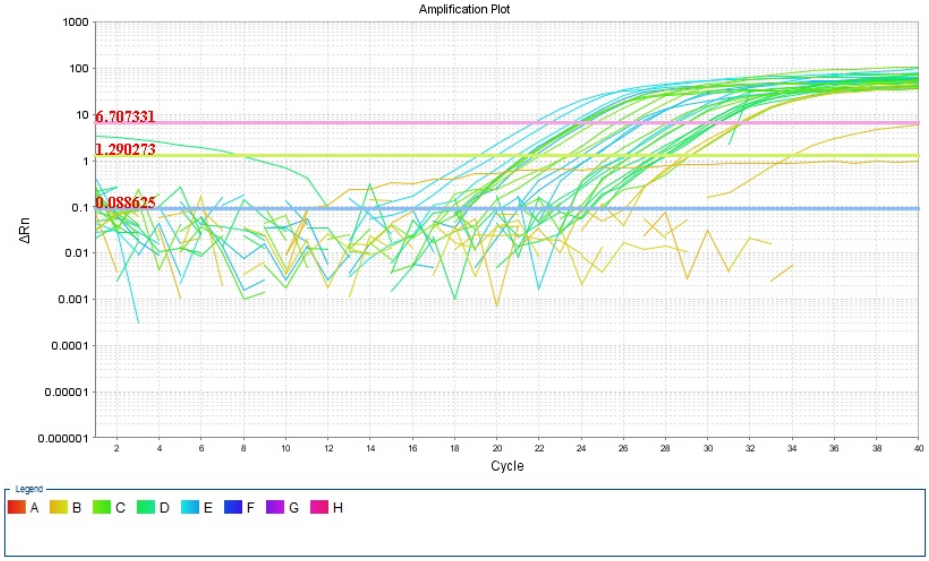

Amplification plot 2

Results from the RT-qPCR gene expression of BCL2 and Caspase 3 using RPII as a house-keeping gene

Treatment	RPII	Average	SEM	Gene	Average	SEM	Delta Ct	Average	SEM	Fold-difference	Average	SEM	
UT	25.96323			28.1491547			2.186			1.05636869			
	24.83773			27.1039219			2.266			0.99920058			
	24.83796	25.213	0.375	27.1809578	27.478	0.336	2.343	2.265	0.045	0.94739655	1.00098861	0.03147025	
DNJ	30.2947865			29.4969883			-0.798			8.35613773			
	29.5189915			29.6486664			0.130			4.39347719			
	29.5792809	29.7976863	0.24915869	29.9263077	29.691	0.126	0.347	-0.107	0.351	3.77901774	5.510	1.434	
C25	23.0964241			26.6253967			3.529			0.41640679			RPII TO BCL2
	21.8929729			25.5139503			3.621			0.39068038			
	21.9208832	22.303	0.397	26.0596199	26.066	0.321	4.139	3.763	0.190	0.27287297	0.360	0.044	

Treatment	RPII	Average	SEM	Gene	Average	SEM	Delta Ct	Average	SEM	Fold-difference	Average	SEM	
UT	25.96323			16.8047466			-9.158			1.24674895			
	24.83773			15.9427204			-8.895			1.03864109			
	24.83796	25.213	0.375	16.3705158	16.373	0.249	-8.467	-8.840	0.201	0.77224568	1.01921191	0.13732135	
DNJ	30.2947865			20.7425308			-9.552			1.63800896			
	29.5189915			20.7425308			-8.776			0.95670648			
	29.5792809	29.7976863	0.24915869	20.4754658	20.654	0.089	-9.104	-9.144	0.225	1.20038958	1.265	0.199	
C25	23.0964241			18.0309887			-5.065			0.07305481			
	21.8929729			16.1841393			-5.709			0.11411191			RPII TO CASP3
	21.9208832	22.303	0.397	16.9277058	17.048	0.536	-4.993	-5.256	0.227	0.06948595	0.086	0.014	

Table 2. Results from the RT-qPCR gene expression of BCL2 and Caspase 3 using RPII as a house-keeping gene

Treatment	RPII	Average	SEM	Gene	Average	SEM	Delta Ct	Average	SEM	Fold-difference	Average	SEM	
UT	16.9876652			29.3130798			12.325			0.00019484			
	18.6272602			26.4971066			7.870			0.00427504			
	17.8550911	17.823	0.474	25.5353603	27.115	1.133	7.680	9.292	1.518	0.00487538	0.00311509	0.00147037	
DNJ	24.3827724			28.1679382			3.785			45.4647851			BCL2
	24.3694038			27.2534714			2.884			84.9048981			
	24.0452614	24.2658126	0.11034309	27.8898735	27.770	0.271	3.845	3.505	0.311	43.6294775	58.000	13.463	
C25	17.2100258			26.0644665			8.854			1.35416424			
	15.9591475			24.6464577			8.687			1.5204867			
	14.1156111	15.762	0.899	24.0818272	24.931	0.590	9.966	9.169	0.401	0.62660463	1.167	0.274	

Treatment	RPII	Average	SEM	Gene	Average	SEM	Delta Ct	Average	SEM	Fold-difference	Average	SEM	
UT	16.9876652			25.7125473			8.725			0.24575514			
	18.6272602			23.9121304			5.285			2.667162			
	17.8550911	17.823	0.474	23.9458656	24.524	0.595	6.091	6.700	1.039	1.52562572	1.47951428	0.69938008	
DNJ	24.3827724			31.1628704			6.780			0.94610856			CASP3
	24.3694038			28.9254227			4.556			4.42033826			
	24.0452614	24.2658126	0.11034309	28.4965935	29.528	0.827	4.451	5.262	0.759	4.75301683	3.373	1.217	
C25	17.2100258			26.9634647			9.753			0.12046923			
	15.9591475			24.2511578			8.292			0.33174929			
	14.1156111	15.762	0.899	23.8112583	25.009	0.986	9.696	9.247	0.478	0.12539297	0.193	0.070	

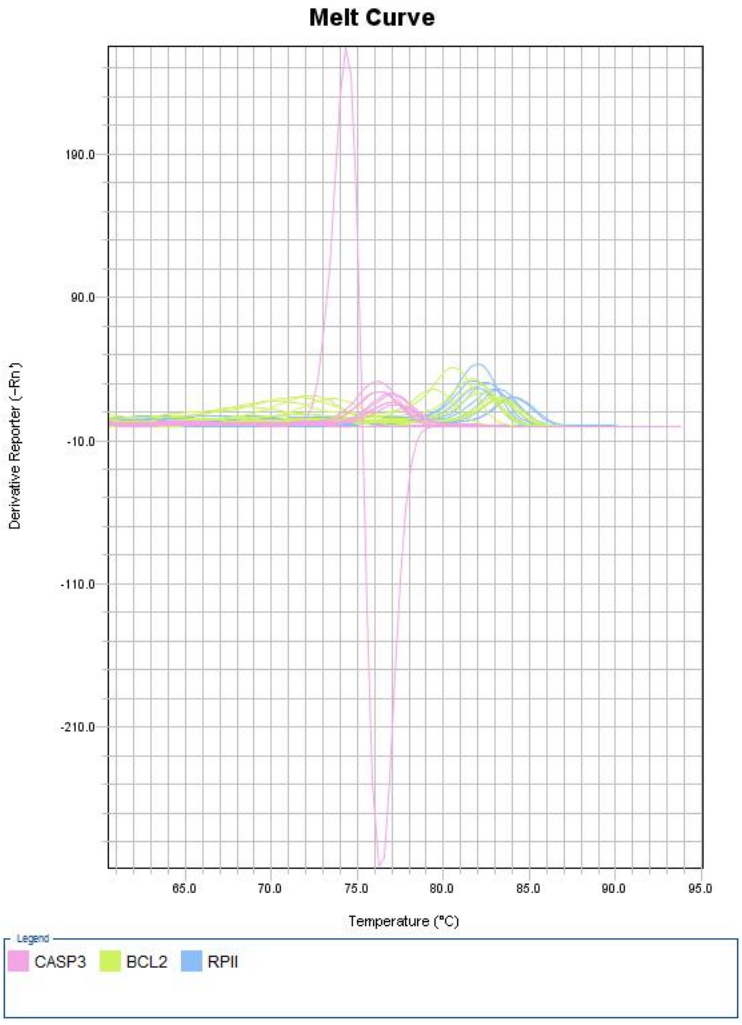
Melt Curve
190.0
90.0
-10.0
-110.0
-210.0
Derivative Reporter (-Rn')
65.0
70.0
75.0
80.0
85.0
90.0
95.0
Temperature (°C)
Legend
CASP3
BCL2
RPII

Appendix 3

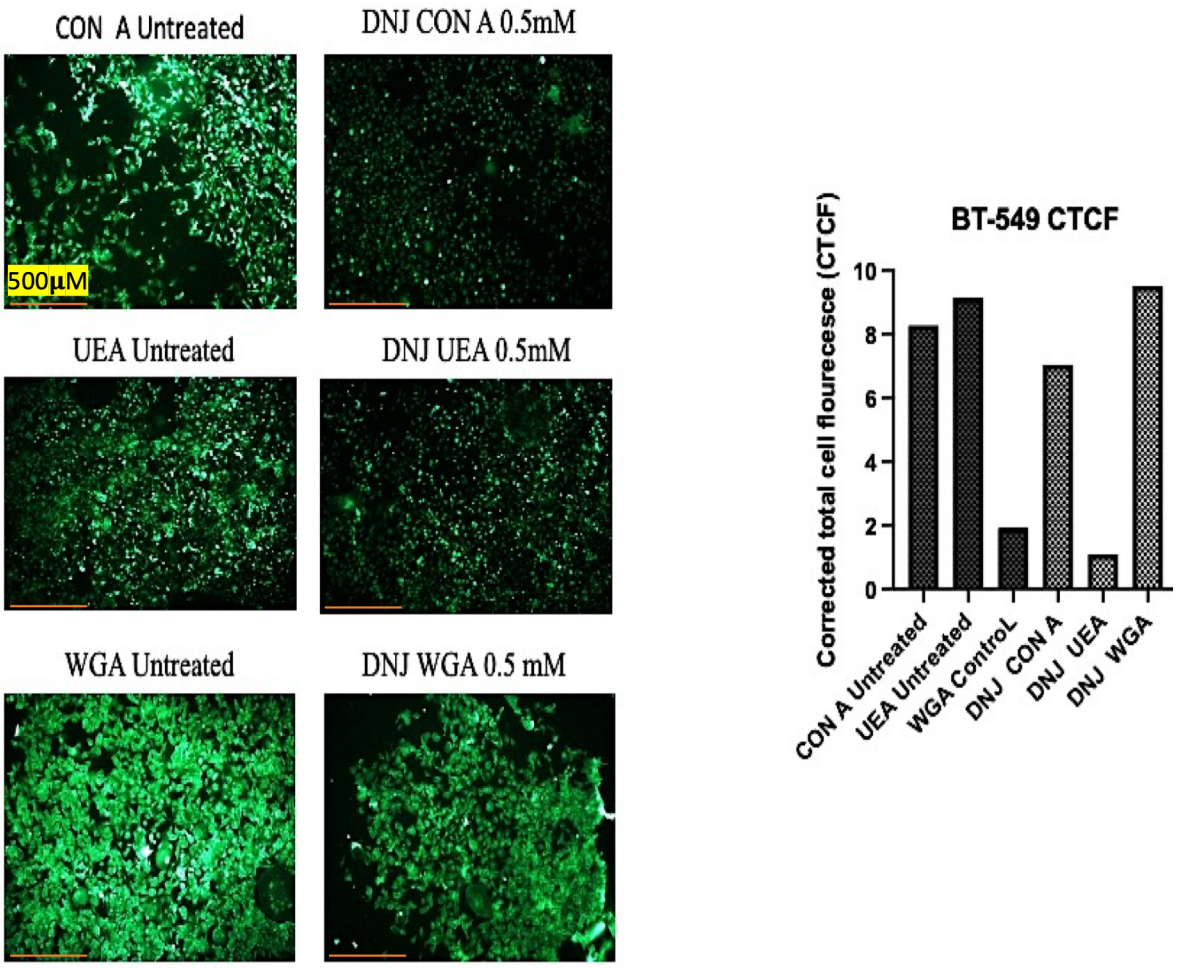

Figure 1. Left panel: BT-549 cells evaluated by lectin staining with Con A, UEA, and WGA showed different fluorescent intensities using ImageJ of the treated and untreated cells. Images were captured at 10X magnification using an Evos fluorescence microscope. Right panel: Analysis of the BT-549 untreated and treated cells showed the correlated total cell fluorescence (CTCF)—median values ± SE.

Lectin staining analysis of BT-549 cells with DNJ indicated that Con A and UEA showed the highest reduction of fluorescence intensity after treatment with an inhibitor compound. This light intensity reduction in the cells represents the absence of glycoprotein structures when treated with DNJ. This analysis correlated well with the Alamar blue and DAPI staining, in which the cells showed a more significant reduction when treated with DNJ. The histogram

in the right panel analyses the corrected total fluorescence (CTCF), which was calculated using ImageJ to analyse the selected area and measure, generating the mean, areas, and intensity readings. After using the formula CTCF = Integrated Density – (Area of selected cell X Mean fluorescence of background readings), the data was calculated using Excel and GraphPad.

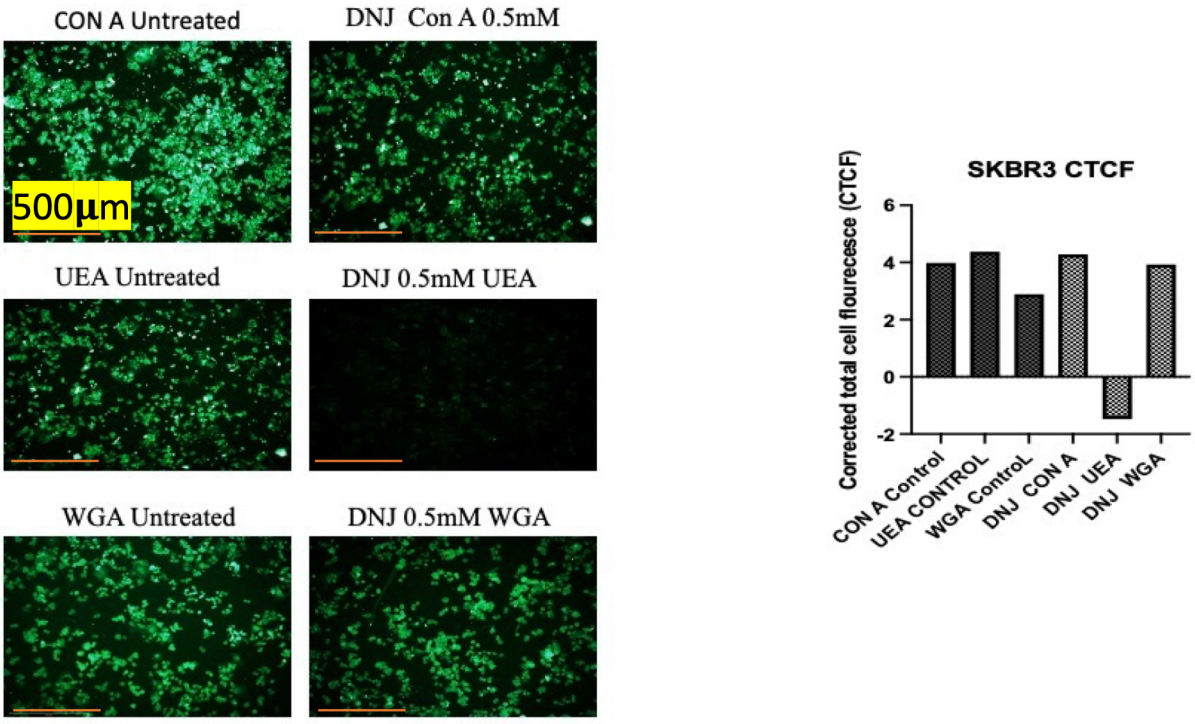

Figure 2. Left panel: SKBR3 cells evaluated by lectin staining with Con A, UEA, and WGA showed different fluorescent intensities using ImageJ of the treated and untreated cells. Images were captured at 10X magnification using an Evos fluorescence microscope. Right panel: Analysis of the SKBR3 treated and untreated cells showed the correlated total cell fluorescence (CTCF). Median values ± SE

The lectin staining of the SKBR3 cells treated with DNJ Con A indicated a high light intensity reduction due to a significant change in fluorescence compared to the untreated UEA. The histogram of the right panel shows that SKBR3, the CTCF, resulted in more reduction intensity with UEA than Con A treated cells.

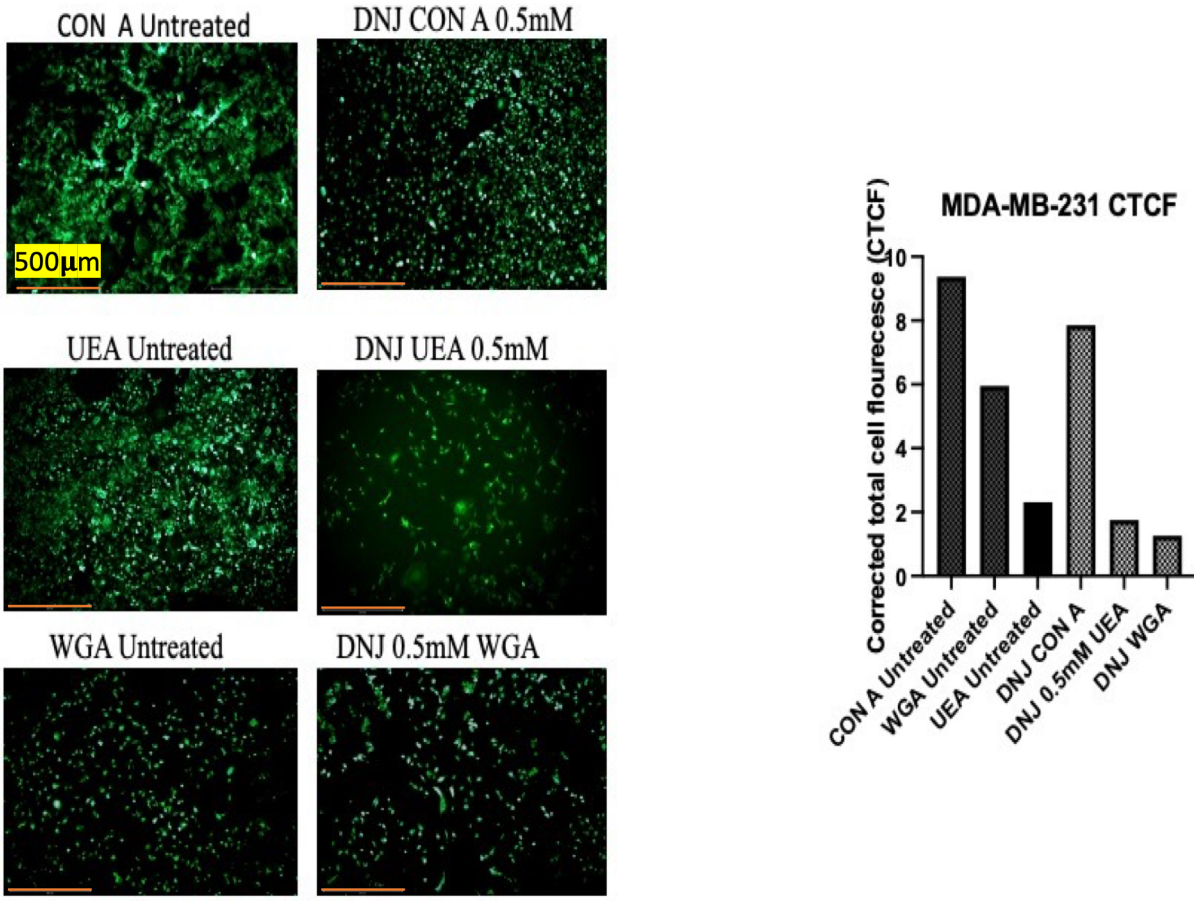

Figure 3. Left panel: MDA-MB-231 cells evaluated by lectin staining with Con A, UEA, and WGA showed different fluorescent intensities using ImageJ of the treated and untreated cells. Images were captured at 10X magnification using an Evos fluorescence microscope. Right panel: Analysis of the MDA-231-MB treated and untreated cells showed the correlated total cell fluorescence (CTCF). Median values ± SE

Treatment with DNJ on the MDA-MB-231 cells resulted in the most significant reduction of cell fluorescence intensity, as is observed in the images on the left panels. However, according to the CTCF, the data suggests that DNJ-treated cells reduced Con A, UEA, and WGA.

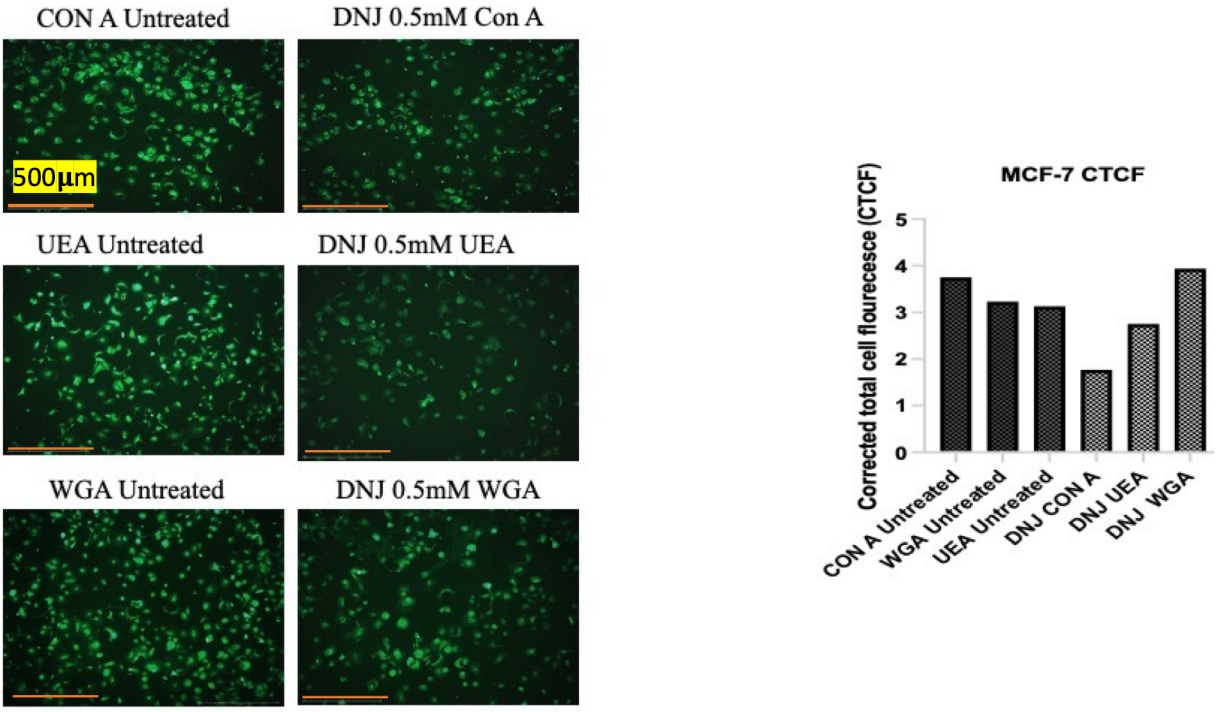

Figure 4. Left panel: MCF-7 cells evaluated by lectin staining with Con A, UEA, and WGA showed different fluorescent intensities using ImageJ of the treated and untreated cells. Images were captured at 10X magnification using an Evos fluorescence microscope. Right panel: Analysis of the MCF-7 treated and untreated cells showed the correlated total cell fluorescence (CTCF)—median values ± SE.

MCF-7 treated cells with DNJ UEA showed the most significant fluorescence intensity reduction, as observed in the left panel in Figure 15. Fluorescence intensity was calculated using image J (particle analysis; measure), and the CTCF was calculated, which indicates and confirms that treated cells with DNJ and UEA showed the most significant reduction in fluorescence intensity. The 24-hour treatment indicated that DNJ had more effect on the cells. This could result in DNJ UEA affecting the fucose levels in the cells after treatment. Therefore, there might be a more significant influence of glycosidase inhibitors reducing fucose levels than mannose or N-acetyl-glucosamine (GlcNAc)

The next stage for this study will be to determine whether there is a more significant effect on the cell when cultured in 3D rather than 2D culture. The next phase tests the cell response after 24-hour drug treatment of chemotherapy drugs and glycosidase inhibitors in 2D, using four breast cancer cell lines. These will be tested in 3D culture models and tumoroids to compare the reduction percentage these models will generate.

Table . One-way ANOVA and Brown-Forsythe statistical analysis show the different values of the particle analyses between the four breast cancer cell lines deployed in this study.

Table Analysed	SKBR3	MDA-MB-231	BT-549	MCF-7
ANOVA summary				
F	1.625	19.4	3.358	4.729
P value	0.2429	0.0001	0.0547	0.0211
P value summary	ns	***	ns	*
Significant diff. Among means (P < 0.05)?	No	Yes	No	Yes
R squared	0.3939	0.8858	0.5732	0.6542
Brown-Forsythe test				
F (DFn, DFd)	0.04405 (4, 10)	1.173 (4, 10)	0.1631 (4, 10)	1.680 (4, 10)
P value	0.9957	0.3794	0.9523	0.2304
P value summary	ns	ns	ns	ns
Are SDs significantly different (P < 0.05)?	No	No	No	No

Appendix 4

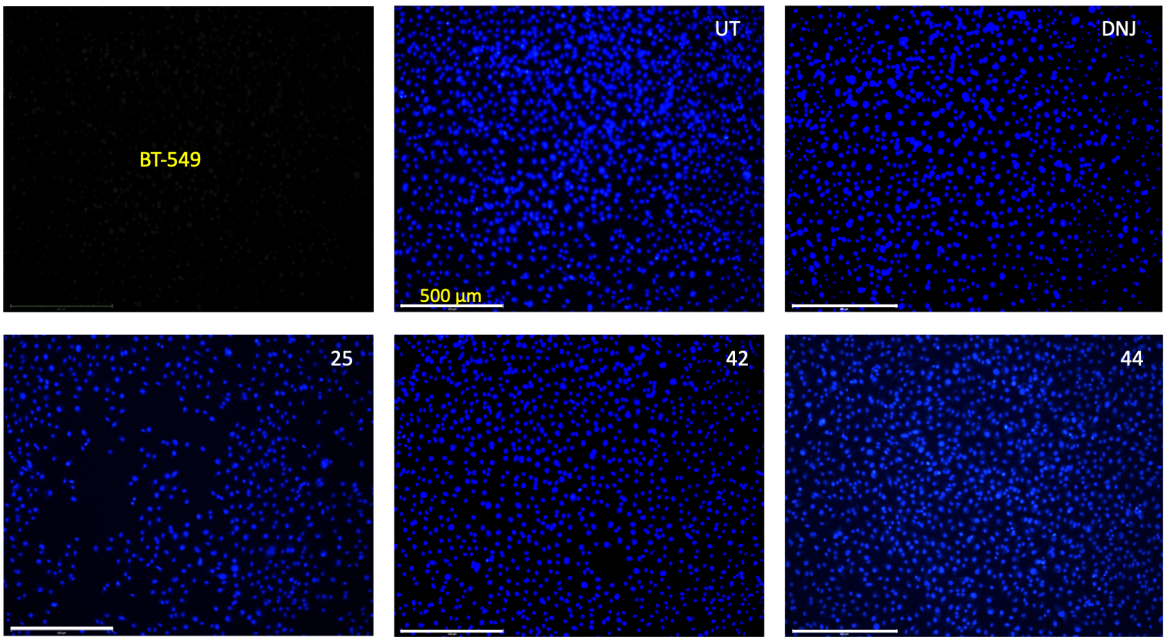

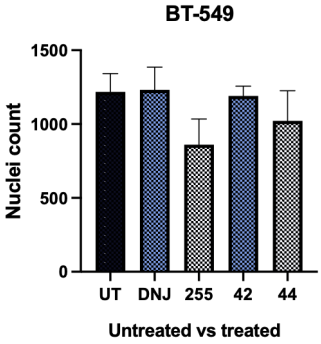

Figure 5. Upper panel: Visualisation of DAPI fluorescence of the BT-549 nuclei representation of the 24-hour drug treatment for the Glycosidase inhibitors including DNJ, Phytoquest compounds (42, 44 and 255) at concentrations of 0.5 mM. Treated BT-549 are more sensitive with both DNJ and 255 compounds, as they showed some reduction and seemed to cause an effect on growth inhibition. Lower panel: BT-549 Nucleic count histogram shows a significant difference on compound 255. Analysis was carried out using an EVOS microscope. Lower panel: Data analysis was generated using the ImageJ particle analysis program. Median values ± SE. Microscope magnification at 10X. One-way ANOVA statistical analysis was deployed for the non-parametrical data to compare the untreated vs the treated cells.

Treatment of the cells with DNJ and Phytoquest compound 44 resulted in the most significant reduction in the number of cells compared to untreated cells. As indicated below, a similar approach was taken with the remaining three cell lines, SKBR3, MDA-MB-231 and MCF-7.

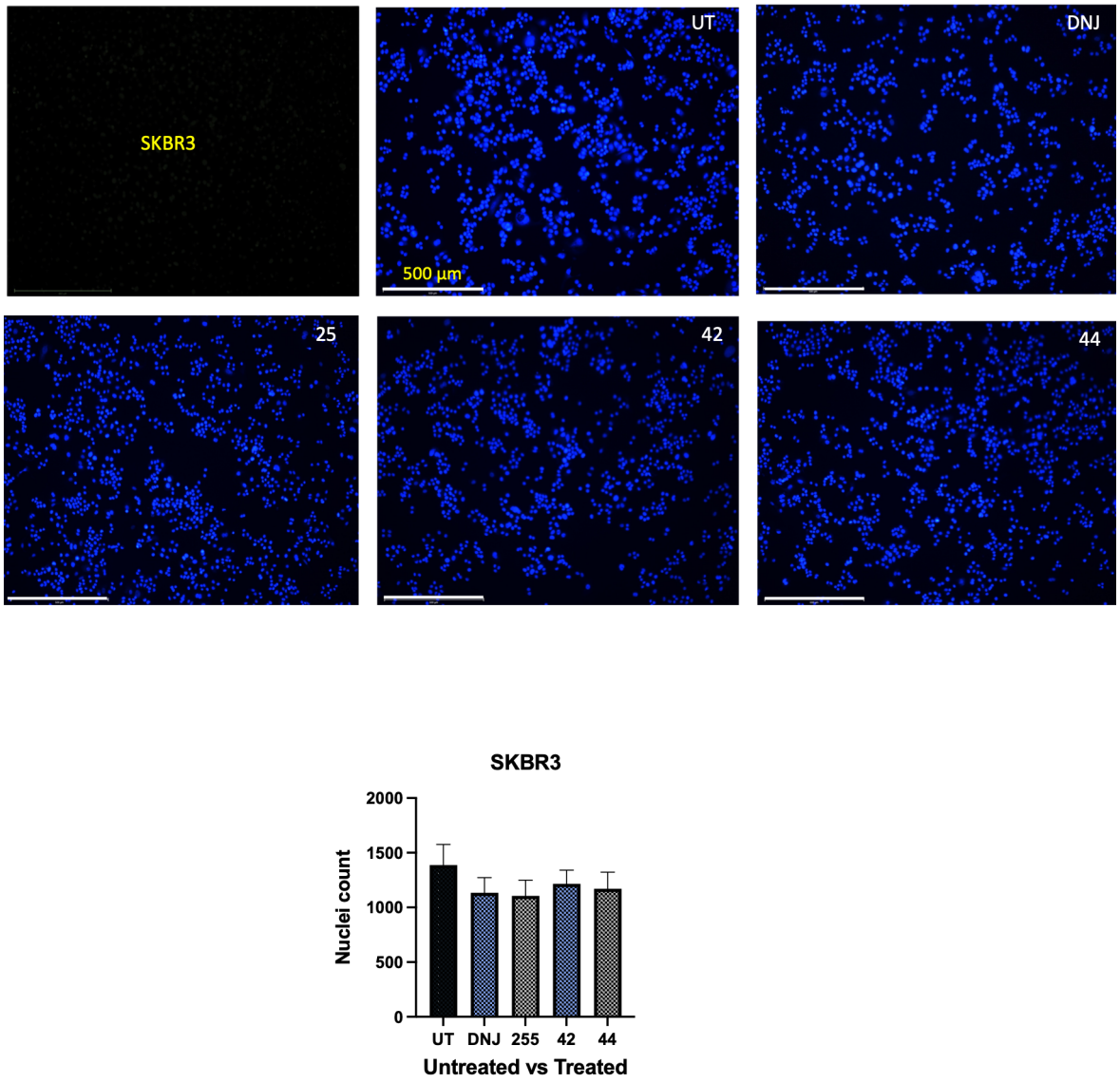

Figure 6. Upper panel: Visualisation of DAPI fluorescence of the SKBR3 nuclei representation of the 24-hour drug treatment for the Glycosidase inhibitors including DNJ, Phytoquest compounds (42, 44 and 255) at concentrations of 0.5mM. Treated SKBR3 are more sensitive to DNJ and 255 compounds as they seem to influence growth inhibition. Analysis was carried out using an EVOS microscope. Lower panel: SKBR3 Nucleic count histogram shows a significant difference on compound 255. Analysis was carried out using an EVOS microscope. Lower panel: Data analysis was generated using the ImageJ particle analysis program. Median

values ± SE. Microscope magnification at 10X. One way is that ANOVA statistical analysis was deployed for the non-parametric data to compare the untreated vs. the treated cells.

The analysis of SKBR3-treated cells indicated that DNJ showed the most significant effect as the number of cells decreased by more than 100 compared to the untreated cells.

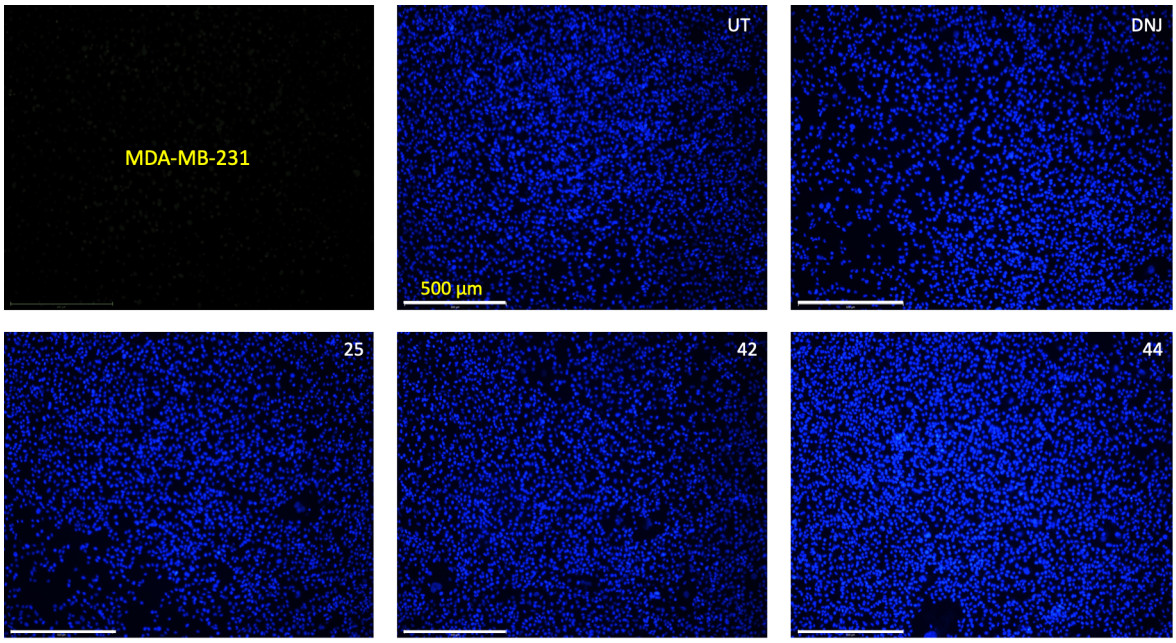

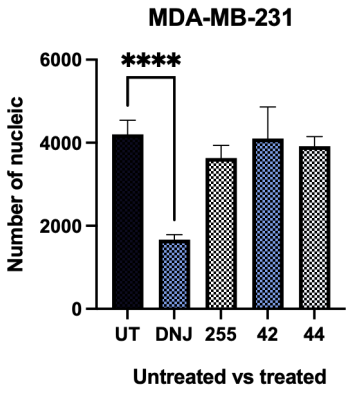

Figure 7. Upper panel: Visualisation of DAPI fluorescence of the MDA-MB-231 nuclei representation of the 24-hour drug treatment for the Glycosidase inhibitors including DNJ, Phytoquest compounds (42, 44 and 255) at concentrations of 0.5mM. Treated MDA-MB-231 cells are more sensitive to both DNJ and 255 compounds as they seem to affect growth inhibition. Analysis was carried out using an EVOS microscope. Lower panel:

MDA-MB-231 Nucleic count histogram shows a significant difference in compound DNJ. Analysis was carried out using an EVOS microscope. Lower panel: Data analysis was generated using the ImageJ particle analysis program. Median values ± SE. Microscope magnification at 10X. One-way ANOVA statistical analysis was deployed for the non-parametrical data to compare the untreated vs the treated cells. MDA-MB-231 cells treated with DNJ showed the most significant reduction in the number of cells compared to the other compounds, and the size area looks like the cells have gone apoptosis due to their reduction in area and size.

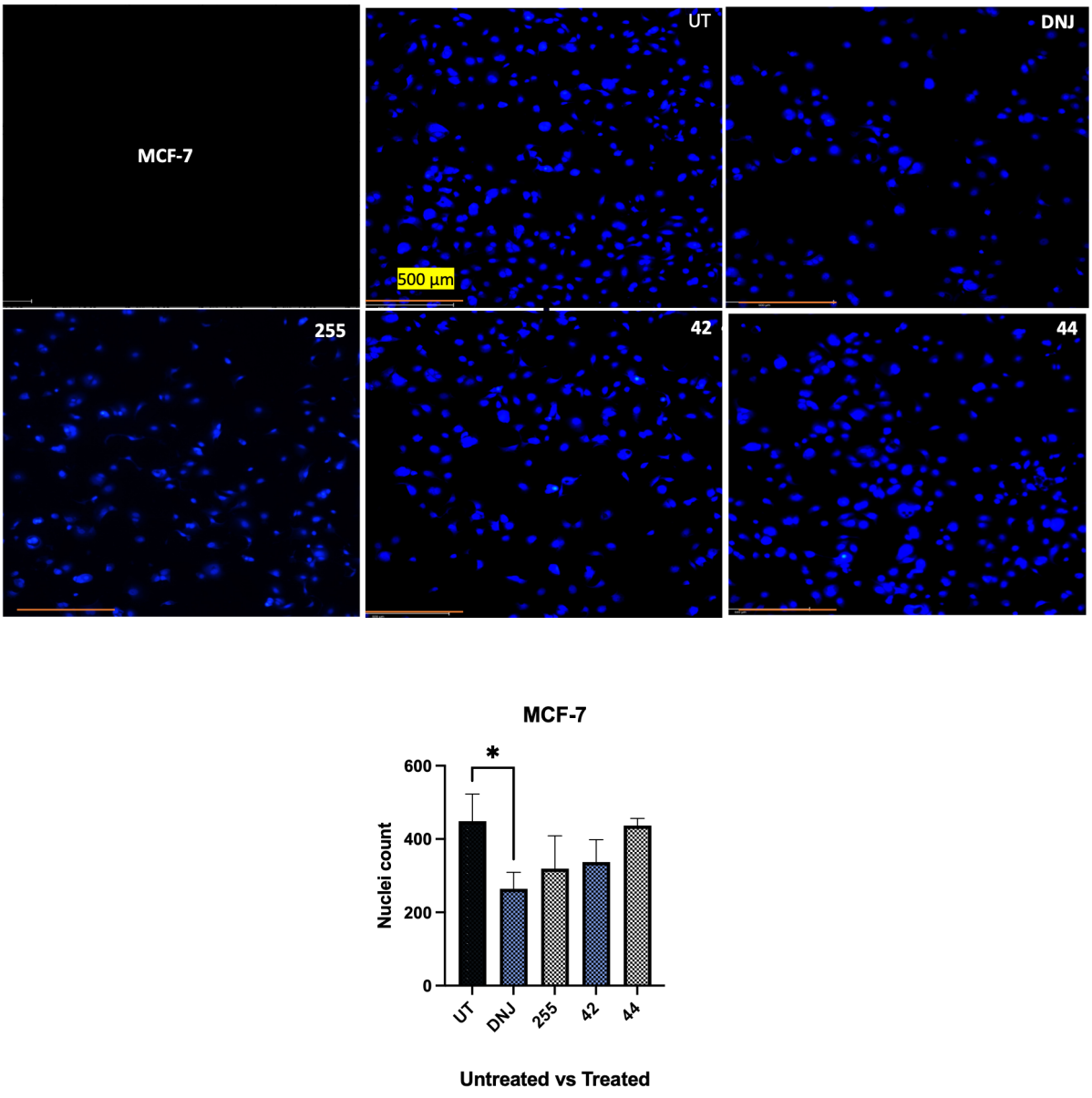

Figure 8. Upper panel: Visualisation of DAPI fluorescence of the MCF-7 nuclei representation of the 24-hour drug treatment for the Glycosidase inhibitors including DNJ, Phytoquest compounds (42, 44 and 255) at concentrations of 0.5mM. Treated MCF-7 are more sensitive

with both DNJ and 255 compounds as it seems to cause an effect on growth inhibition. Analysis was carried out using an EVOS microscope. Lower panel: MCF-7 Nucleic count histogram shows a significant difference in compound DNJ. Analysis was carried out using an EVOS microscope. Lower panel: Data analysis was generated using the ImageJ particle analysis program. Median values ± SE. Microscope magnification at 10X. One way is that ANOVA statistical analysis was deployed for the non-parametric data to compare the untreated vs. the treated cells. O

When the MCF-7 treated cells were stained with DAPI following glycosidase inhibitor treatment, DNJ resulted in the most significant reduction, with almost 50% compared to the untreated cells. The Phytoquest compounds also affected the cells like DNJ.

MCF-7 cells showed the most significant response regarding reduced cell numbers compared to MDA-MB-231, BT-549 and SKBR3 cell lines treated with DNJ, the glycosidase inhibitor with the highest response to treatment.

APPENDIX 5

The cyt-B was induced on breast cancer cells to inhibit the cytoplasmic division and cell movement of the cells by blocking the development of contractile microfilaments. A scoring system of 100 was deployed to determine the rate of CIN between the investigated breast cancer cells.

BT-549 cells grown in 3D exhibited different types of CINS, as shown in Figure 18, including NBUD, BN, MNi, and NPB.

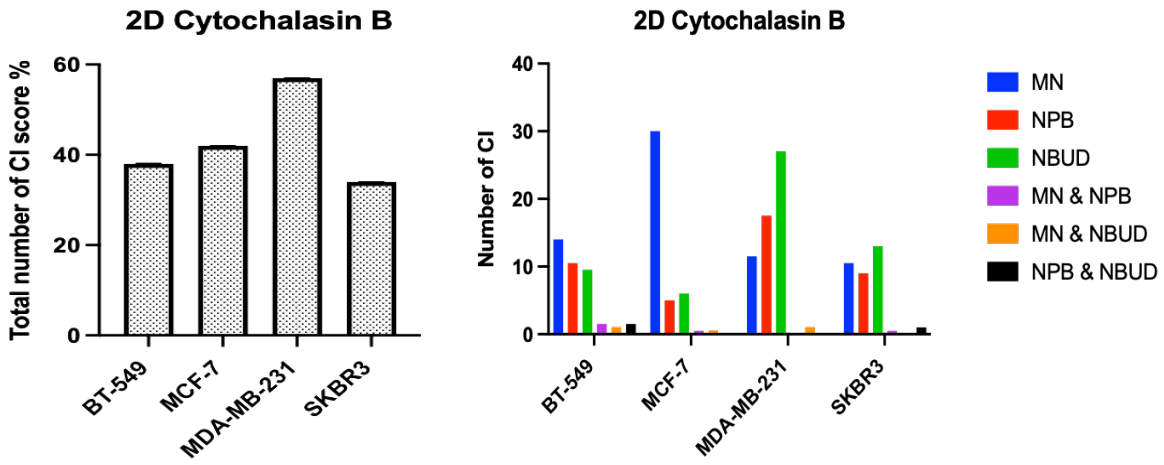

Figure 46. Left right panel: Histogram representation of the total CIN observed for the four cell lines BT-549, MCF-7, MDA-MB-231 and SKBR-3 grown in 2D cell culture shows the total number of CIN % in MDA-MB-231 with 57% and MCF-7, second with 45%. Right-hand panel: histogram representation of CIN baseline of the number of biomarkers CIN indicators (MN, NPB, NBUD, MN & NPB, MN & MBUD, NPD & NBUD) in which MCF-7 and MDA-MB-231 showed the highest CIN in 2D.

The different cell lines exhibited various types of CIN, with MN, NPD, and NBUD being the most frequently observed. Median values ± SE. In this study, figure 46 shows MDA-231-MB cells treated with cyt-B, indicating the percentage of CIN with 57% compared to all other cell

lines according to the total CI score %. The number of MNi found in binucleated cells in MDA-MB-231 was the highest compared to NPB and NBUD. The CI in MCF-7 cells had the second highest, with 42%.

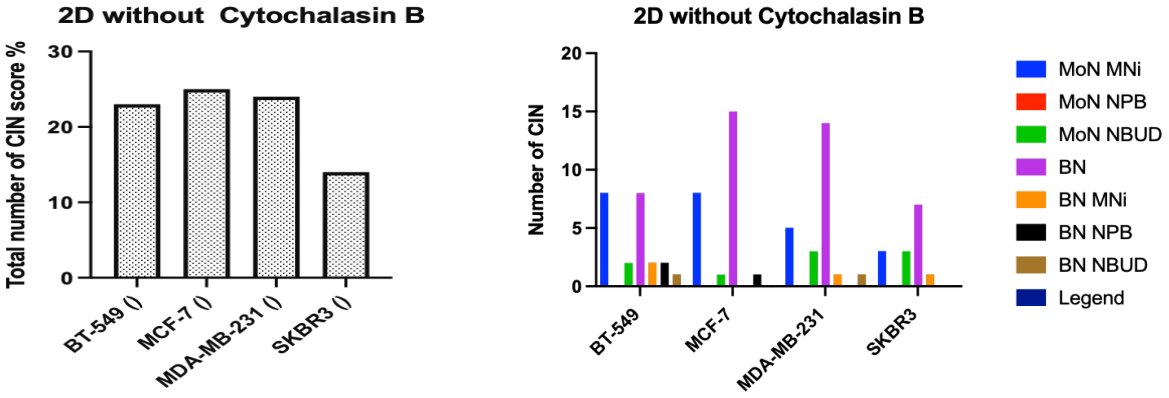

Figure 47. Left right panel: Histogram representation of the total CIN observed for the four cell lines BT-549, MCF-7, MDA-MB-231 and SKBR-3 grown in 2D cell culture. Right-hand panel: histogram representation of the different types of CIN observed for the four cell lines BT-549, MCF-7, MDA-MB-231 and SKBR-3 grown in 2D cell culture.

The cells were not exposed to cyt-B before analysis. In this treatment, mononucleated cells with 1 MNi appeared and were observed apart from BN cells.

In Figure 24, the cells grown in 2D and not treated with cyt-B showed that MCF-7 cells had the highest CIN evidence, 23%, compared to MDA-MB-231, the second highest with 22% CIN. The number of MN in BN cells was deficient compared to those treated with cyt-B. These naturally occurring events in cancer cells are common evidence of MI.

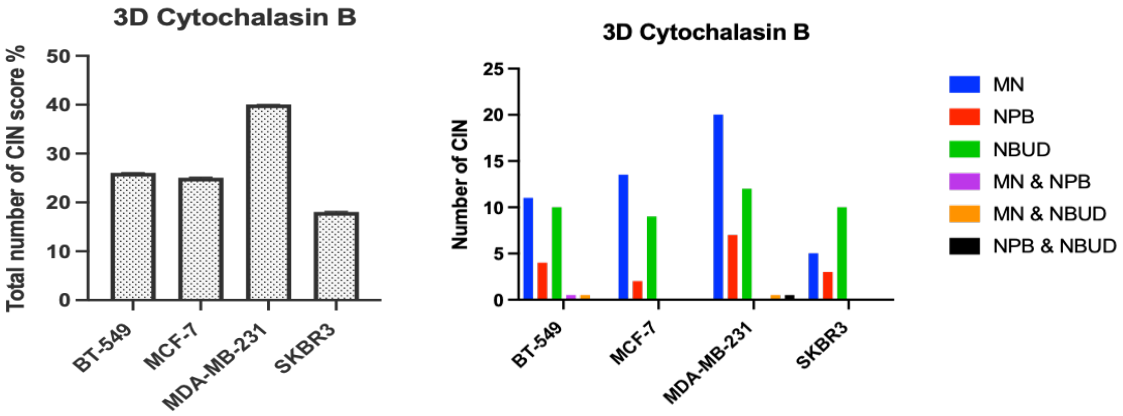

Figure 48. Histogram representation of the total number of CIN and CI score % of cells cultured in 3D treated with cyt-B.

MDA-MB-231 3D cells treated with cyt-B demonstrated a significantly elevated CIN rate compared to the other three cell lines analysed. This treatment not only increased the frequency of CIN, but it also resulted in the highest number of MN being observed in the BN cells.

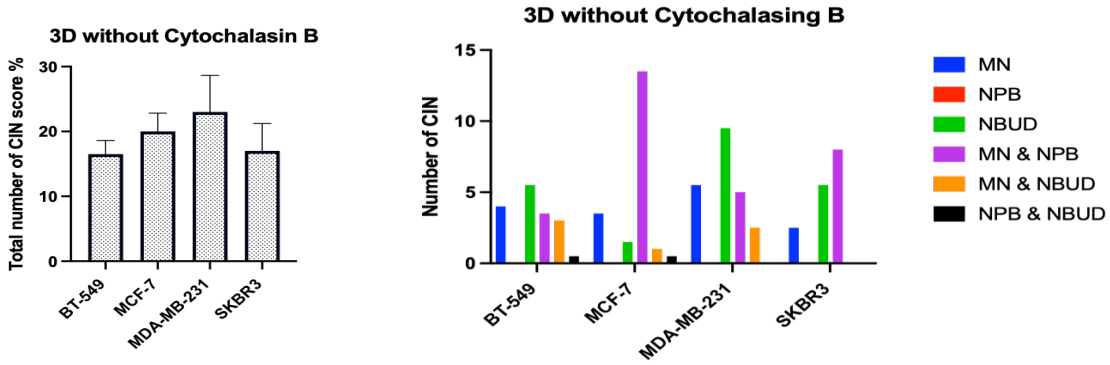

Figure 49. Histogram representation of the total number of CIN% and the number of CIN score % of cells cultured in 3D not exposed to cyt-B.

3D cells induced by cyt-B exhibited a reduction in CIN rates compared to 2D cells. Which was statistically significant according to the t-test deployed with P values 0.001 ***

($P < 0.05$)

Table 13. Comparative T-test statistical analysis shows the difference in CIN baseline values.

Table Analysed Paired T-test	**2D vs 3D**
Column B	**3D**
Vs.	**Vs.**
Column A	**2D**
P value	**0.001**
P value summary	*******
Significantly different (P < 0.05)?	**Yes**
One- or two-tailed P value?	**Two-tailed**
t, df	**t=13.02, df=3**
Number of pairs	**4**
How big is the difference?	
Mean of differences (B - A)	**-15.5**
SD of differences **2.38**	
SEM of differences	**1.19**
95% confidence interval	**-19.29 to -11.71**
R squared (partial eta squared)	**0.9826**

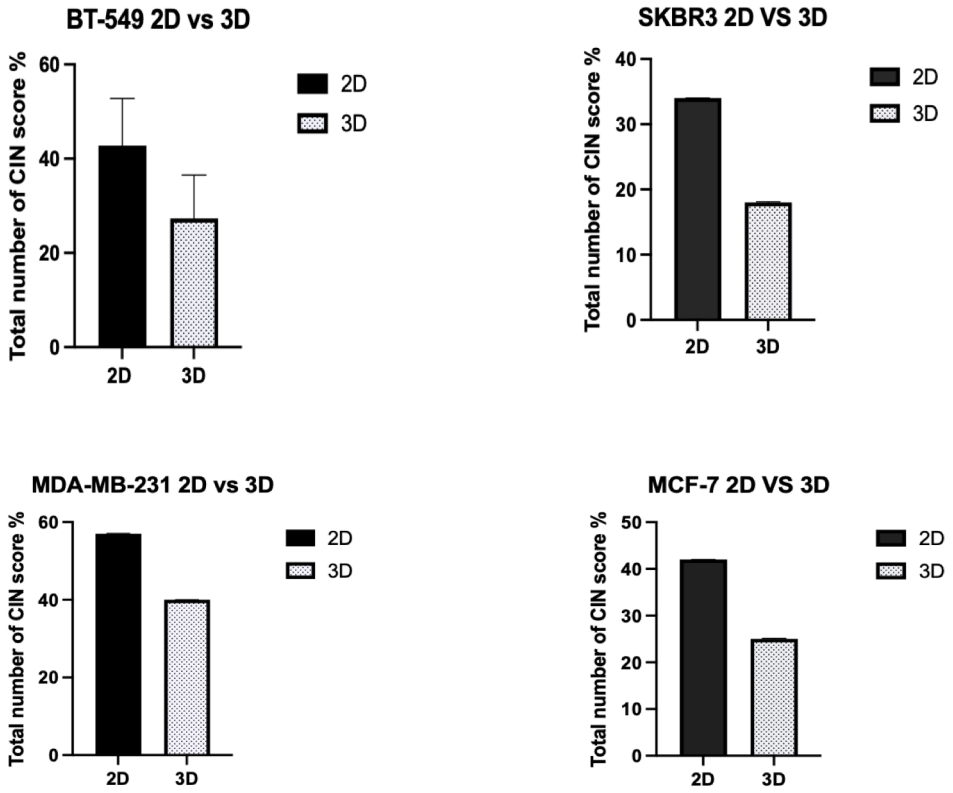

Figure 50. CIN Comparative studies show the statistical analysis of treated BT-549, SKBR3, MDA-MB-231 and MCF-7 cells with cyt-B, which were cultured in 2D and 3D. Cells grown in 2D exhibit the highest level of CIN compared to 3D models.

All four cell lines were evaluated in 2D and 3D after embedding in rat tail collagen type-1 and compressing using the RAFT system (Lonza). Cells grown in 2D were sampled when they had reached near-confluence. Cells grown in 3D were initially grown between 20 -28 days to allow the cells to fully occupy the collagen matrix before optimisation of the 3D model improved the yield of harvested fixative cells in 3D models grown for 7-8 days when all the cells were seeded at 5x10^5 in the embedded collagen. Figure 34 shows BT-549 cells grown in the 3D construct and evaluated after 4 and 12 days.